# HUMIDITY CELL TESTING OF MINE WASTES UNDER A $CO_2$ SUPPLEMENTED ATMOSPHERE

A thesis submitted for the degree of

**Doctor of Philosophy (Ph.D.)**

By

**Rhys John Savage BSc (Hons), MSc**

**June 2023**

**Cardiff University**

**School of Engineering**

# Acknowledgments

The author would firstly like to thank KESS 2 and Geochemic Ltd for financially supporting this PhD research project through the European regional funding office. This project would not have been possible without the support of individuals from Geochemic Ltd and Mine Environmental Management Ltd (MEM). I am grateful to Dr Andrew Barnes, Dr Mark Roberts, and Dr Ben Gersten for their unwavering support during the last 4 years. Without the support of the Geochemic team this project would have been near impossible in the face of the COVID-19 pandemic. The team continued to facilitate my experimental work when it seemed like it would be impossible, allowing me to produce results that were essential to this research study. I would also like to thank my PhD supervisor, Dr Devin Sapsford, who provided me with academic support throughout my studies, beyond what may be expected of a typical PhD supervisor. I would like to thank and acknowledge MEM Ltd and Boliden Mines who provided the mining wastes utilised in this study. I am grateful for the support of MEM Ltd and Boliden during my PhD, although neither party had a vested interest in this PhD project, they provided materials, support and technical input throughout.

I would lastly like to thank my family. Their support and encouragement throughout my time at university has been unbelievable. From my undergraduate degree in Swansea, to my MSc and PhD degrees in Cardiff, they have been the foundation that I have always depended upon. When things were hard and I questioned myself, my PhD, and my direction, they provided me with everything I needed to keep on moving forward.

Geochemic Ltd
Mining Geochemistry Services

kess 2
Ysgoloriaethau Sgiliau Economi Gwybodaeth
Knowledge Economy Skills Scholarships

UNDEB EWROPEAIDD
EUROPEAN UNION
Llywodraeth Cymru
Welsh Government
Cronfa Datblygu Rhanbarthol Ewrop
European Regional Development Fund

This projected was funded by the European Regional Development Fund as part of the Knowledge Economy Skills Scholarship (KESS) 2 program in partnership with Geochemic Ltd.

# Abstract

This doctoral research provides novel insights into the potential impact of an enhanced $CO_2$ atmosphere on the weathering of sulfidic mining wastes. This research project was undertaken with the overarching purpose of assessing the potential implications of enhanced $CO_2$ concentrations on mine waste geochemical development and acid rock drainage (ARD) classification and prediction.

Multiple studies have outlined seasonal and temporal variations in pore gas compositions within sulfidic mine waste storage facilities. To date no standardised kinetic or static characterisation tests have been developed to assess such conditions. Within this study a standardised kinetic leaching test method, commonly used within the mining industry, is modified with the purpose of assessing the drainage quality development and ARD onset potential of waste materials exposed to elevated $CO_2$ atmospheres.

A 60-week modified humidity cell test (HCT) protocol was undertaken to simulate a waste drainage environment enriched with 10% $CO_2$. Two sets of experiments were performed using wastes from distinct mine sites to test the robustness of the modified method. HCT cell sets were caried out at variable testing conditions to develop a more site-specific assessment of drainage quality prediction.

This study demonstrated that the introduction of an enhanced $CO_2$ atmosphere within the aeration system of a standard ASTM D5744 humidity cell test leads to variable weekly leaching characteristics. Key predictive parameters such as pH, sulfate, dissolved carbon species and metal leaching rates were shown to vary widely dependent on both the aeration system and temperature conditions.

The importance of this study stretches beyond traditional ARD characterisation and prediction, with silicate rich sulfidic waste materials viewed as a potential feedstock for large scale carbon dioxide removal technologies. The application of the findings presented within this study should aid in the environmental regulation of large-scale carbon mineralisation and enhanced weathering (EW) projects.

***"I didn't fail the test, I just found 100 ways to do it wrong".***

**Benjamin Franklin**

# Contents

# Abbreviations and Acronyms

| | |
|---|---|
| ABA | Acid Base Accounting |
| ABCC | Acid Buffering Characteristic Curves |
| ADL | Analytical Detection Limit |
| AMD | Acid Mine Drainage |
| AMIRA | Australian Mineral Industries Research Association |
| ANC | Acid Neutralizing Capacity |
| AP | Acid Production Potential |
| ARD | Acid Rock Drainage |
| ASTM | American Society for Testing and Materials |
| BECCS | Bioenergy with Carbon Capture and Storage |
| BSI | British Standards Institution |
| CCP | Carbon Capture Potential |
| CCS | Carbon Capture and Storage |
| CDR | Carbon Dioxide Removal |
| CEN | Comité Européen de Normalisation (European Committee for Standardization) |
| CLGB | Central Lapland Greenstone Belt |
| DACCS | Direct Air Capture with Carbon Storage |
| DIC | Dissolved Inorganic Carbon |
| EC | Electrical Conductivity |
| ED-XRF | Energy Dispersive X-Ray Fluorescence |
| EDS | Energy Dispersive Spectroscopy |
| EDX | Energy dispersive X-ray |
| EPA | Environmental Protection Agency |
| ETS | Emissions Trading System |
| EU | European Union |
| EW | Enhanced Weathering |
| GARD | Global Acid Rock Drainage |
| GGR | Greenhouse Gas Removal |
| GTK | Geologian Tutkimuskeskus (Geological Survey of Finland) |
| GWB | Geochemists Work Bench |

| | |
|---|---|
| HCL | Hydrochloric Acid |
| HCT | Humidity Cell Test |
| HDPE | High Density Polyethylene |
| ICP-OES | Inductively Coupled Plasma Optical Emission spectroscopy |
| INAP | International Network for Acid Prevention |
| IPCC | Intergovernmental Panel on Climate Change |
| ISO | International Organization for Standardization |
| L:S | Liquid to Solid Ratio |
| LOM | Life of Mine |
| MEM | Mine Environment Management |
| MEND | Mine Environment Neutral Drainage |
| ML | Metal Leaching |
| MPA | Maximum Potential Acidity |
| MRV | Monitoring, Reporting and Verification |
| Mt | Mega Tonnes |
| NAF | Non-Acid Forming |
| NAG | Net Acid Generation |
| NAPP | Net Acid Producing Potential |
| NASA | National Aeronautics and Space Administration |
| NDZ | Nautanen Deformation Zone |
| NMD | Neutral Mine Drainage |
| NNP | Net Neutralisation Potential |
| NP | Neutralizing Potential |
| NPR | Net-neutralizing Potential Ratio |
| OPEX | Operational Expenditure |
| ORP | Oxidation-Reduction Potential |
| PAF | Potentially Acid Forming |
| PAG | Potentially Acid Generating |
| PGE | Platinum Group Elements |
| PSD | Particle Size Distribution |
| QA | Quality Assurance |
| QC | Quality Control |
| RPD | Relative Percent Difference |

| | |
|---|---|
| SD | Saline Drainage |
| SEM | Scanning Electron Microscope |
| SOB | Sulfide Oxidising Bacteria |
| SRB | Sulfate Reducing Bacteria |
| STP | Standard Temperature and Pressure |
| UPT | Up Flow Percolation Test |
| USGS | United States Geological Survey |

# Lists of Figures, Tables and Equations

## *List of Figures*

## *List of Tables*



## *List of Equations*

# Chapter 1 Introduction

## 1.1 Research Rationale

This research looks to assess the potential implications of above atmospheric carbon dioxide concentrations on humidity cell test (HCT) leaching characteristics. Within this study ASTM standard HCT protocols are modified to provide an assessment of waste material geochemical development under an elevated $CO_2$ atmosphere (ASTM 2018a). The failure to predict acid rock drainage (ARD) accurately has the potential to lead to substantial environmental consequences (Parbhakar-Fox and Lottermoser 2015). An assessment of the leachate quality produced within modified kinetic testing protocols may allow for a more robust quantification of drainage quality under varied environmental conditions, when compared to current industrial standards.

To date no standardised kinetic or static tests have been developed to assess the potential environmental implications of above atmospheric $CO_2$ concentrations on sulfidic mine drainage quality. Herein above atmospheric levels of $CO_2$, >421ppm (NASA 2023), are referred to as enhanced for consistency. The potential environmental impacts of enhanced $CO_2$ concentrations and subsequent varied weathering of wastes is considered within this thesis. There is currently limited research that examines the environmental consequences of enhanced weathering or mineral carbonation, specifically related to the potential release of trace elements (Renforth 2019a). Within this study enhanced weathering (EW), refers to the accelerated weathering of mining wastes materials in the presence of above atmospheric $CO_2$ conditions, in line with the CDR Primer (Wilcox et al. 2021).

Multiple research studies have demonstrated elevated $CO_2$ concentrations within mining waste rock storage facilities (Lorca et al. 2016; Vriens et al. 2018; Vriens et al. 2019a). Such elevated $CO_2$ concentrations within waste rock dumps and tailings storage facilities are not currently considered as part of standardised kinetic testing methods utilised to assess drainage quality and prediction (AMIRA 2002; Price 2009; GARD 2014; ASTM 2018a).

The importance of this work stretches beyond the absence of consideration of enhanced $CO_2$ concentrations within mining waste facilities and the potential implications for mine drainage quality prediction. A joint report on greenhouse gas removal (GGR) by the Royal Society and the Royal Academy of Engineering, in 2018, outlined how enhanced weathering (EW) and mineral carbonation are two of the main avenues to reduce net carbon dioxide emissions globally, see Figure 1.

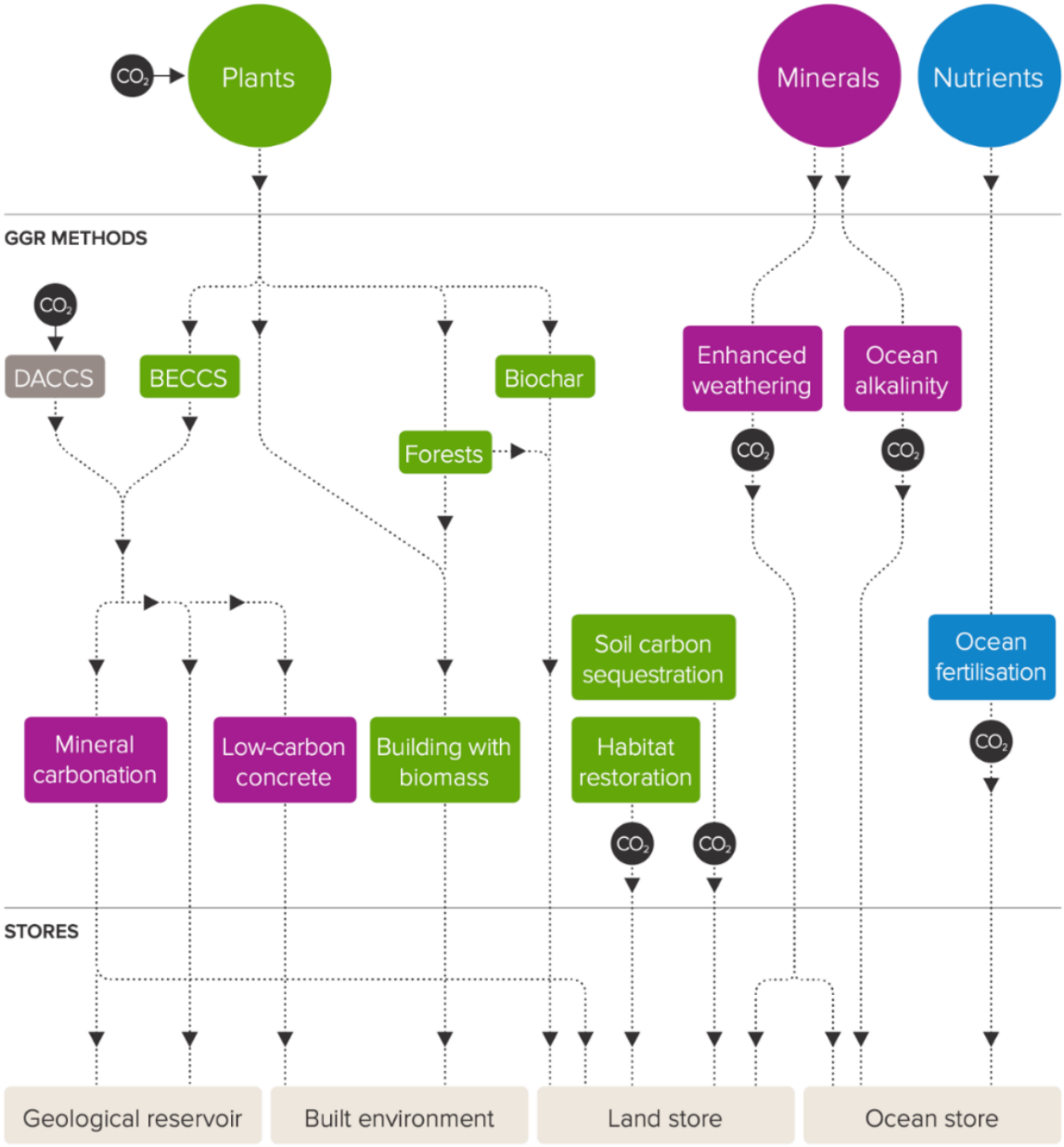


*Figure 1 – Carbon dioxide removal methods diagram* (Royal Society and Royal Academy of Engineering 2018) (BECCS refers to Bioenergy with Carbon Capture and Storage, DACCS refers to Direct Air Capture with Carbon Storage)

Due to the potential production of bicarbonate or stable carbonate minerals, mineral carbonation via enhanced weathering (EW) has a significant potential to sequester carbon dioxide securely, with geological longevity (IPCC 2005). It was outlined in the 2018 GGR report that the mining industry is particularly important in the implementation of large-scale carbon dioxide removal (CDR) approaches (Royal Society and Royal Academy of Engineering 2018).

This research feeds directly into recommendation 8 of the greenhouse gas removal (GGR) report (Royal Society and Royal Academy of Engineering 2018):

***"Establish international science- based standards for monitoring, reporting and verification (MRV) for GGR approaches, both of carbon sequestration and of environmental impacts. Standards currently exist for biomass and CCS, but not for GGR methods at large."***

This is prevalent as mine operators aim to reduce net operational emissions and move towards carbon 'neutral' mining practices (Power et al. 2014a). In 2017 the diamond mining operator De Beers outlined its goal to achieve carbon neutral mining at one of its mining operations within 10 years. De Beers has since been actively investing in its research and development project, Project Minera, which has looked to assess the potential for large scale sequestration of $CO_2$ via the mineralisation of kimberlite diamond wastes (Mervine et al. 2018). This movement towards utilising silicate mining wastes as a large scale-feedstock for carbon dioxide removal is being considered by several other mining operators. The BHP Group, Australia's largest mining and metals company, has actively been assessing the suitability of wastes from its Mount Keith Ni operation, with academic studies outlining the suitability of the operations tailings wastes for carbon mineralisation (Wilson et al. 2014a; BHP 2023).

The potential environmental implications of mineral carbonation and enhanced weathering practices in the presence of above atmospheric $CO_2$ concentrations are considered within this study. This research serves the dual purpose of assessing the potential environmental implications of enhanced weathering, while also assessing how such processes may impact mine waste drainage quality.

This research aims to assess the applicability of standard and modified kinetic and characterisation procedures to assess the environmental implications of enhanced $CO_2$ concentrations on mine waste weathering. At present standard techniques do not consider the potential presence of enhanced $CO_2$ concentrations within sulfidic mining wastes, which may impact mine drainage quality. Potential impacts must be quantified to improve current kinetic testing standards as well as aiding in the development of an understanding of how proposed enhanced weathering CDR schemes using mine waste materials may impact local environments.

The wider implications of enhanced $CO_2$ concentrations in waste storage facilities on ARD prediction and subsequent mine closure planning are considered. Figure 2 outlines evolving research questions and concepts considered in this study. This hypothesised concept map emphasises that to assess and understand the importance of considering elevated $CO_2$ in waste facilities a wider consideration of the operational and physiochemical aspects of ARD prediction and CDR must be considered.

It is noted that this concept map is simply conceptual and is designed to highlight potential connections between research themes. The concepts outlined in this figure will be discussed in more detail throughout this thesis.

Within this study waste rock materials from two separate Boliden AB mining operations are utilised within modified kinetic testing experiments. These mine wastes are known to demonstrate differing mineralogical and geochemical characteristics. The application of the modified testing protocol to mine wastes of varied composition allows an assessment of its suitability to predicting the ARD risks of differing sulfidic wastes materials.

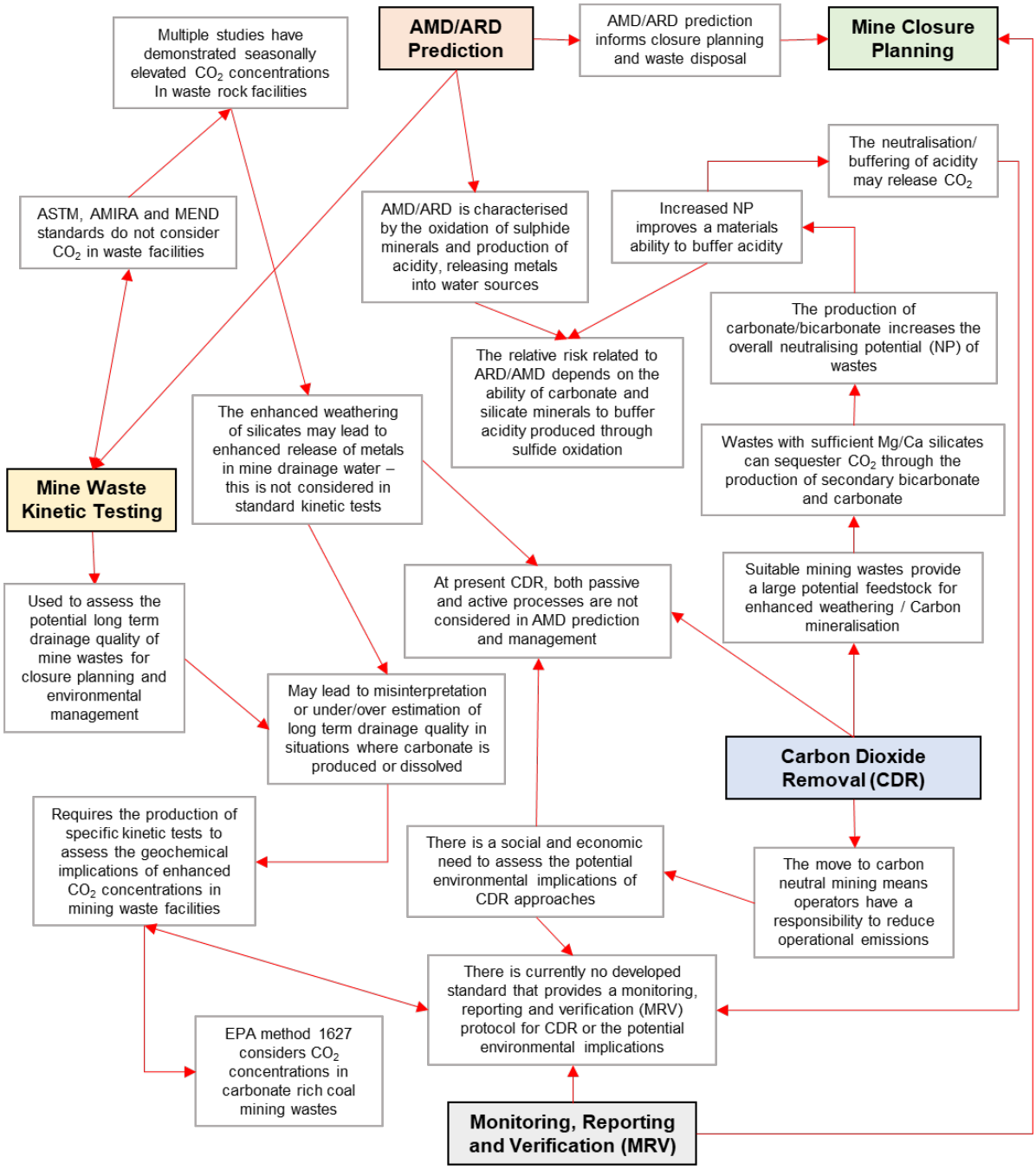


*Figure 2 – A hypothesised concept map of research themes considered.*

## 1.2 Thesis Aims, Hypothesis and Research Questions

**The following hypothesises were developed:**

- The presence of enhanced carbon dioxide concentrations within mining waste facilities has an impact on waste rock weathering.
- Current kinetic testing methods, specifically humidity cell testing (HCT), produce leaching characteristics that are not representative of environments in which above atmospheric carbon dioxide concentrations are present.

**Based on these research hypotheses the following thesis aims were developed:**

- To assess the potential implications of enhanced carbon dioxide concentrations on mine waste weathering.
- To determine whether running HCT's on aluminosilicate rich waste rocks under elevated $CO_2$ concentrations and varying temperatures impacts sulfide mineral oxidation rates and the quality of recovered cell leachates.
- To determine if alterations in waste geochemical and mineralogical characteristics have occurred between pre and post experimental testing.

**Research Questions**

1. What is the relationship between predicted ARD risk and $CO_2$ concentration?
2. How does host rock mineralogy and $CO_2$ concentration impact drainage quality?
3. Are altered humidity cell tests appropriate for assessing enhanced mine waste weathering in the presence of elevated $CO_2$?

**Humidity cell tests (HCT) specific research questions:**

- How does the introduction of 10% $CO_2$ into an ASTM standard HCT aeration cycle affect the leaching rates of key analytes and metals?
- How does the reduction in test temperature impact weekly leachate chemistry compared to standard temperature cells?

## 1.3 Organisation of Thesis

This thesis is organised into the following Chapters:

- **Chapter 2** outlines the study locations and wastes used within this research. This Chapter provides an overall summary of the characteristics of the two mining locations assessed within this study, including summaries of key mine waste geochemistry and closure planning considerations.
- **Chapter 3** reviews and describes the key components of mine drainage geochemistry, mining specific kinetic testing and waste facility pore gas compositions. This review Chapter outlines the current state of the research in this field and how the assessment of mine drainage geochemistry, enhanced weathering and CDR are systematically linked subjects.
- **Chapter 4** describes the methods and procedures utilised in this research project. This includes method statements for both the modified and standardised testing work undertaken as well as all characterisation methods.
- **Chapter 5** presents the results produced in this research project. This Chapter summaries key results factually to inform the research questions of the study.
- **Chapter 6** discusses the results of the tests carried out in this study. Results discussed include those generated through kinetic testing, static testing and characterisation analysis.
- **Chapter 7** presents the conclusions of this thesis and the implications for assessment of mine drainage quality and mine closure planning in scenarios where enhanced weathering may occur or engineered CDR systems are considered.

# Chapter 2 - Research Locations

## Introduction

Within this study materials collected from two Boliden AB mining operations have been utilised. The sites that have provided materials for this study are the Kevitsa open pit Ni-Cu-PGE mine, located in northern Finland, and the Aitik open pit Cu-Au-Ag mine, located in northern Sweden (Karlsson 2018; Berthet 2020).

These locations were chosen both due to the relative availability of the mine waste materials through this study's industrial partner, Geochemic Ltd, as well as the differing mineralogical and geochemical characteristics of each operations mine wastes. The differing geological, and subsequently mineralogical, characteristics of these mining operations allowed a quantification of the effectiveness of proposed testing protocols on mine wastes of differing geological origin.

The mine waste rock and tailings materials produced at the Kevitsa operation contain relatively high proportions of magnesium silicates, while displaying lower proportions of carbonate minerals and sulfide minerals, such as pyrite. The wastes recovered from the Aitik operation have much lower proportions of reactive silicates, with calcium silicates making up most of the silicate proportions. Compared to the Kevitsa operations wastes, Aitik also contains substantially more acid forming minerals.

The differing mineralogical compositions between the two Boliden AB operations provided the opportunity to assess the implications of enhanced carbon dioxide concentrations on mine waste weathering. The relative locational similarity of mines also merited the inclusion of two mining operations, as both sites lay within the Fennoscandian Shield, which encompasses parts of Finland, Sweden, and Norway (GTK 2018).

Within this Chapter the key characteristics of the two Boliden operations are outlined, with a focus on geological characteristics and potential mine waste compositions. Previously published studies carried out at these operations are described.

# 2.1 The Kevitsa Mining Operation

### 2.1.1 Location and climate

The Kevitsa mine is situated in northern Finland, approximately 140 kilometres north-northeast of Rovaniemi, the capital of Finnish Lapland, and 40 kilometres north of the town of Sodankylä (Luolavirta et al. 2018a). The location of the operation in relation to Sodankylä is shown in Figure 3. The mine is hosted within the Central Lapland Greenstone Belt (CLGB), which is an important metallogenic province in the Fennoscandian Shield (Vaasjoki 2001). Temperatures in the coldest month, January, average -13.4°C, while summer temperatures (June-August) average 10°C-25°C. The average annual precipitation is 544 mm. The location experiences an average of 180 days a year of snow cover (SRK 2019).

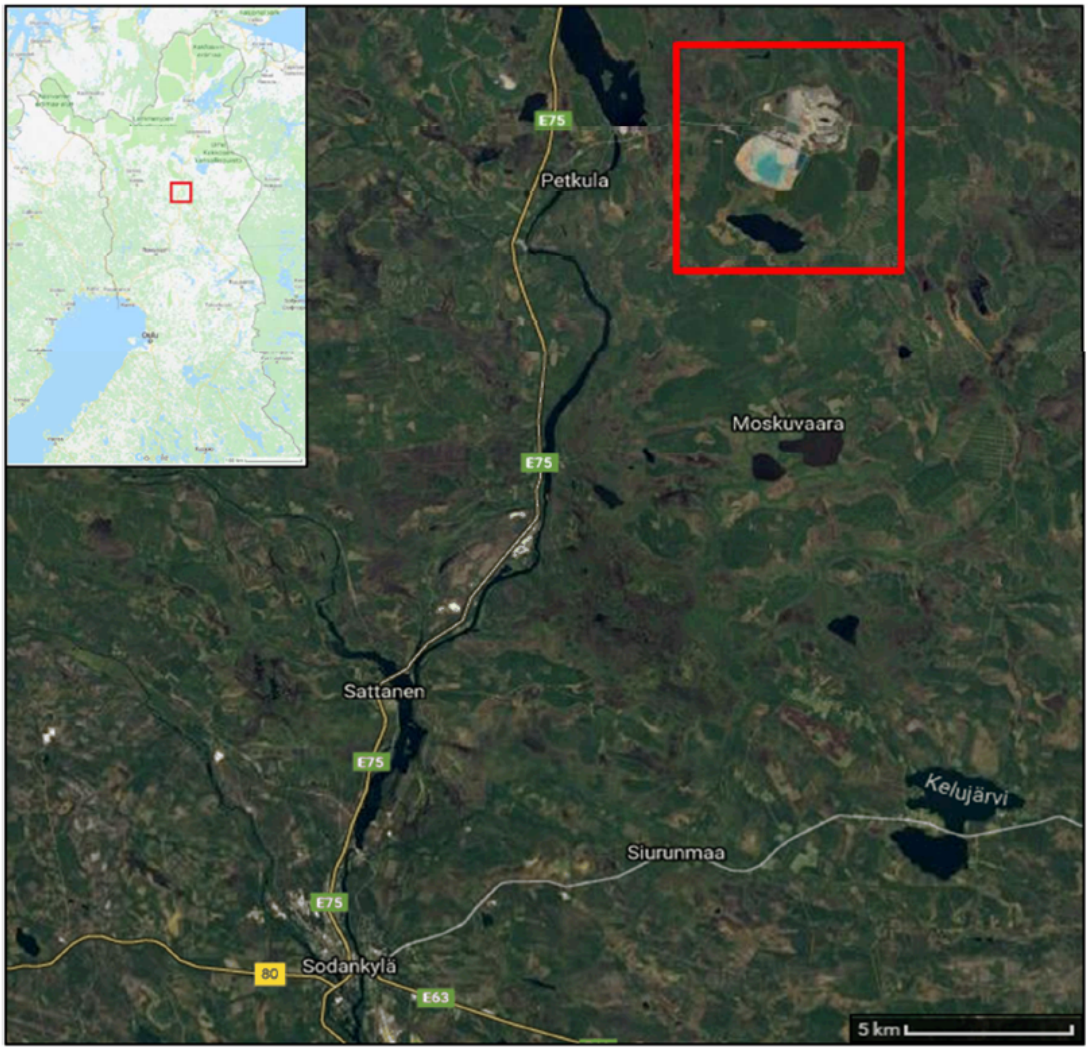


*Figure 3 - A location map of the Kevitsa operation, Sodankyla* (Berthet 2020).

### 2.1.2 Mine operations overview

The Kevitsa mine is a large open pit mine primarily producing Ni and Cu with additional by-products of Co, Au, and platinum group elements (PGEs) (Berthet 2020). The main Kevitsa mine operations are shown in Figure 4. The locations of the main operations at the mine, including the waste rock facilities, tailings storage facilities, processing plant and the operational open pit can be seen in this figure (O'Kane Consultants Ltd 2018b).

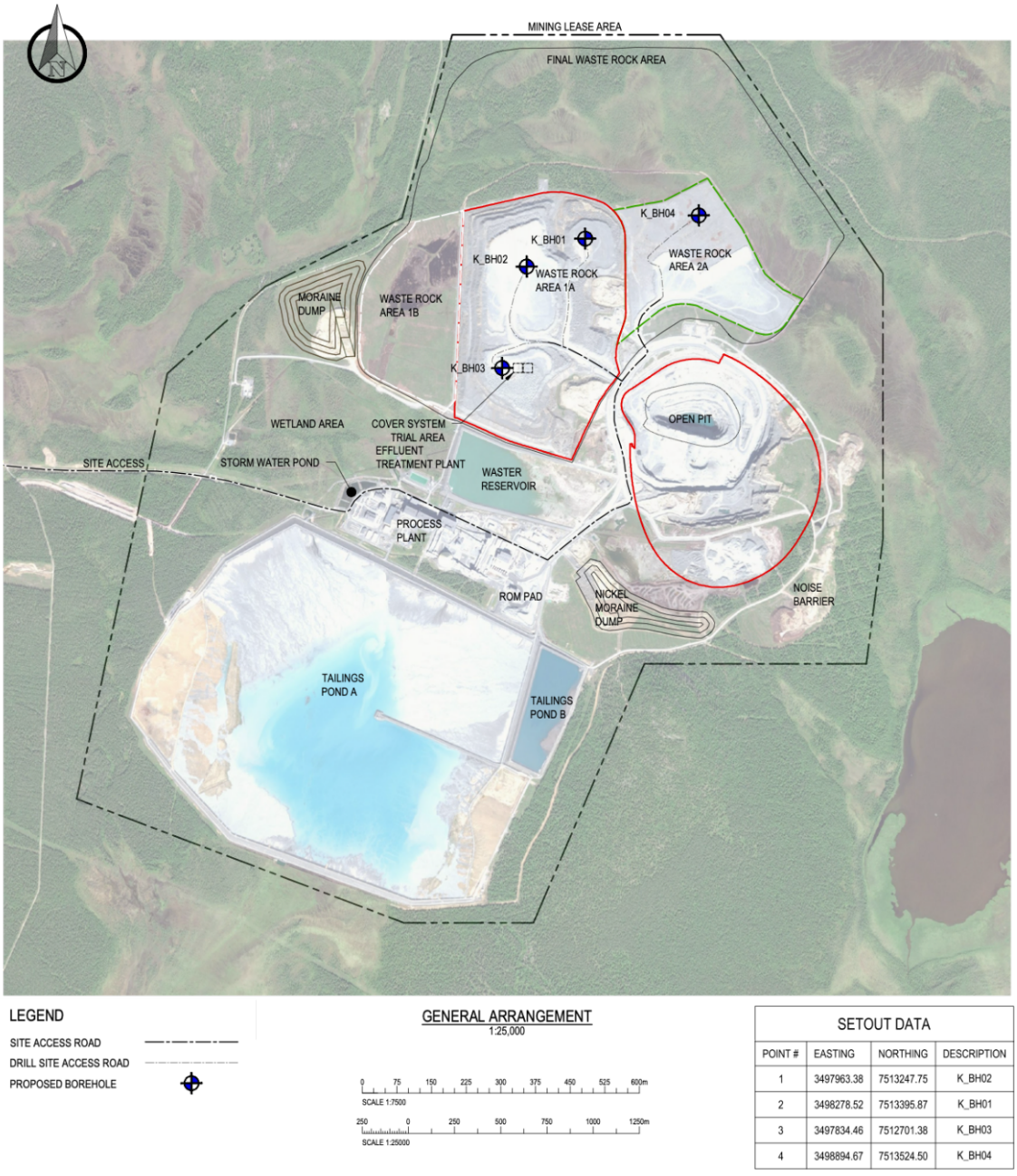


*Figure 4 - Kevitsa mine operational layout map (O'Kane Consultants Ltd 2018b).*

In 2020 mined out ore tonnage measured 9.4 Mt, with 30 Mt of waste produced (waste rock and tailings). Although Ni is produced as the main commodity at Kevitsa, Cu is the most valuable commodity accounting for 44.1% of revenue. Ni concentrate accounted for 32.1% of operational revenue, with other revenue generated through production of Au, Pd and Pt (Berthet 2020). Table 1 outlines the mineral resource and reserves for the Boliden Kevitsa mine deposit in 2019 and 2020.

*Table 1 - Mineral resources and mineral reserves for Boliden Kevitsa mine as of 31-12-2020 and 31-12-2019 for comparison* (Berthet 2020)

| Mineral resources for the year 2020 | | | | | | | |
|---|---|---|---|---|---|---|---|
| Classification | Mton | NiS | Cu | Au | Pd | Pt | CoS |
| | | % | % | % | % | % | % |
| Mineral Reserves | | | | | | | |
| Proved | 70 | 0.19 | 0.31 | 0.09 | 0.11 | 0.17 | 0.01 |
| Probable | 59 | 0.24 | 0.33 | 0.1 | 0.14 | 0.2 | 0.01 |
| Total | 128 | 0.21 | 0.32 | 0.09 | 0.12 | 0.18 | 0.01 |
| Mineral Resources | | | | | | | |
| Measured | 42 | 0.19 | 0.29 | 0.08 | 0.11 | 0.18 | 0.01 |
| Indicated | 132 | 0.23 | 0.34 | 0.07 | 0.07 | 0.13 | 0.01 |
| Total M&I | 175 | 0.22 | 0.33 | 0.07 | 0.08 | 0.14 | 0.01 |
| Inferred | 4 | 0.12 | 0.22 | 0.03 | 0.02 | 0.06 | 0.01 |
| Mineral resources for the year 2019 | | | | | | | |
| Classification | Mton | NiS | Cu | Au | Pd | Pt | CoS |
| | | % | % | % | % | % | % |
| Mineral Reserves | | | | | | | |
| Proved | 62 | 0.25 | 0.33 | 0.1 | 0.12 | 0.19 | 0.01 |
| Probable | 78 | 0.23 | 0.31 | 0.11 | 0.16 | 0.24 | 0.01 |
| Total | 140 | 0.24 | 0.32 | 0.1 | 0.14 | 0.21 | 0.01 |
| Mineral Resources | | | | | | | |
| Measured | 26 | 0.23 | 0.33 | 0.08 | 0.1 | 0.16 | 0.01 |
| Indicated | 113 | 0.23 | 0.34 | 0.08 | 0.09 | 0.14 | 0.01 |
| Total M&I | 139 | 0.23 | 0.34 | 0.08 | 0.09 | 0.15 | 0.01 |
| Inferred | 18 | 0.22 | 0.33 | 0.06 | 0.08 | 0.13 | 0.01 |

### 2.1.3 Geological setting – Kevitsa

#### *Regional geology*

The Kevitsa mine is located in the Fennoscandian Shield, which is the largest exposed part of the Baltic Shield, covering Finland, Sweden, and Norway (GTK 2018). The regional geology is dominated by the Central Lapland Greenstone Belt (CLGB), an Archean and Paleoproterozoic-aged terrain characterized by metamorphosed volcanic and sedimentary rocks (Berthet 2020). The Kevitsa intrusion itself is mafic-ultramafic, which is common within the region with large mafic layered intrusions dominating the surrounding CLGB, see Figure 5. The CLGB is one of the largest greenstone belts within the Fennoscandian shield (Luolavirta et al. 2018b).

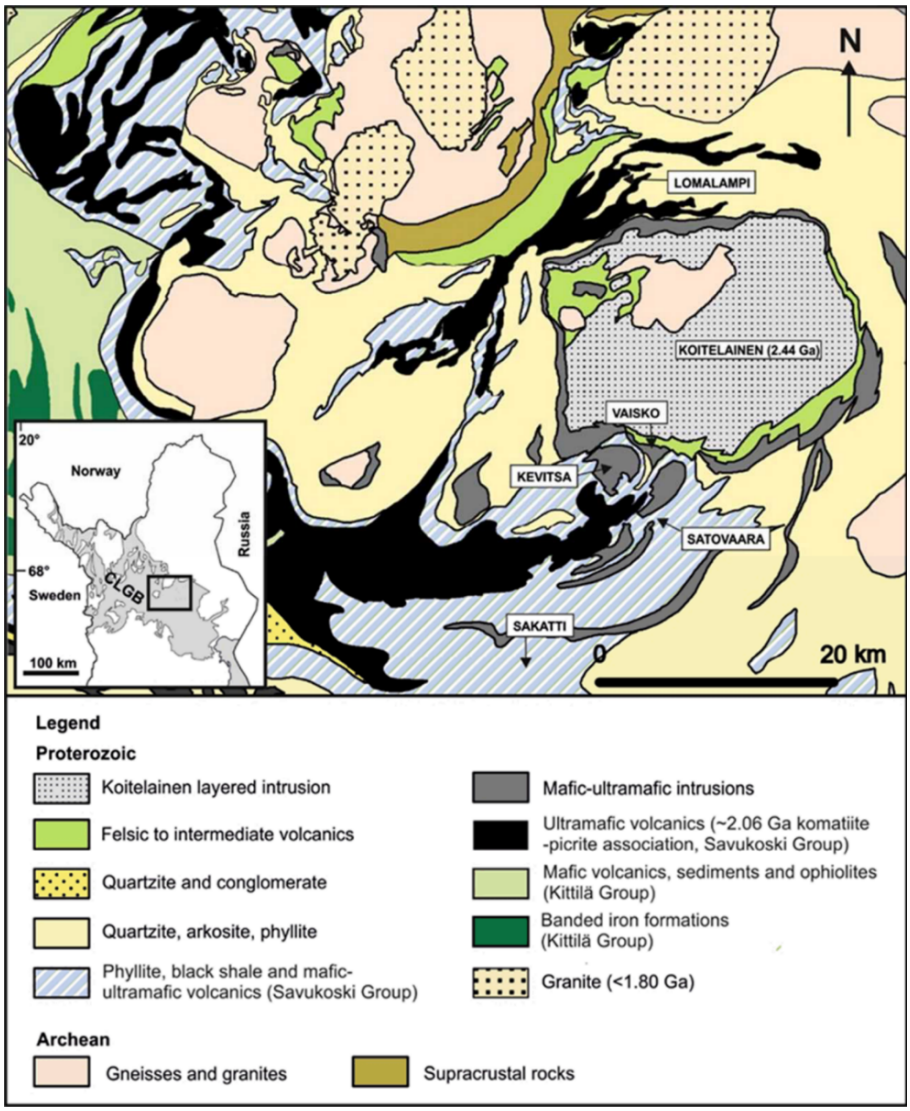


*Figure 5 - Regional geological map of the Kevitsa deposit* (Luolavirta et al. 2018b).

### *Local geology*

The local geology of the Kevitsa mine comprises mafic to ultramafic intrusions, volcanic rocks, and metasedimentary rocks (Maier et al. 2013). The Kevitsa intrusion, which hosts the deposit, is a layered mafic-ultramafic complex intruded into metavolcanic rocks and metasedimentary rocks of the CLGB. The intrusion is approximately 2.06 Ga old and has been affected by multiple deformation events, including folding and faulting (Makkonen et al. 2017; Jonsson et al. 2023). The lithology and location of the Kevitsa intrusion is shown in Figure 6.

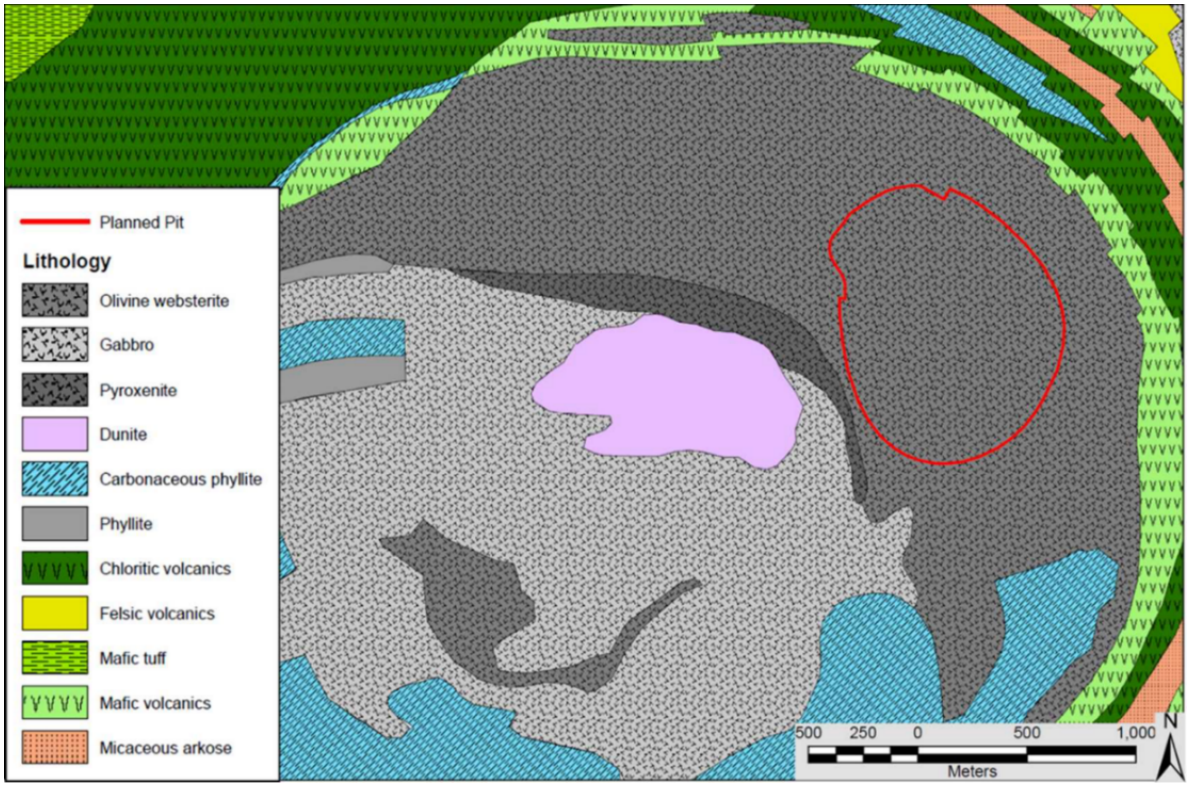


*Figure 6 - Local geological map of the Kevitsa intrusion* (Berthet 2020).

### *The Kevitsa deposit*

The Kevitsa deposit is classified as a Ni-Cu-PGE sulfide deposit associated with mafic-ultramafic intrusions. The host rocks are olivine pyroxenites, see Figure 6 (Ojala and Iljina 2008). The ore minerals include pentlandite, chalcopyrite, and pyrrhotite, with minor cobaltite, magnetite, and PGE-bearing minerals. The deposit is characterized by a disseminated to semi-massive sulfide mineralization, which is primarily controlled by the primary magmatic layering and structural features within the intrusion (Ojala and Iljina 2008; Makkonen et al. 2017). The main Kevitsa mineralisation is located within ultramafic intrusions, hosted by olivine websterite (Luolavirta et al. 2018b).

### 2.1.4 Mine waste composition and potential ARD/AMD sources

As of 2020, 233 Mt of waste (waste rock and tailings) had been produced at the Kevitsa operation, with waste rock and tailings stored on location in a tailings impoundment and waste rock storage facilities (Berthet 2020). The main sulphide minerals present within the Kevitsa ore are troilite, hexagonal pyrrhotite, pentlandite, and chalcopyrite (Ojala and Iljina 2008). The main economic minerals are chalcopyrite and pentlandite, although pyrrhotite is the most common sulfide mineral (Luolavirta et al. 2018a).The olivine pyroxenites are typically characterised as containing 20–25 wt% MgO, 10–20 wt% CaO, variable FeO of 4–16 wt% (Luolavirta et al. 2018b). Olivine minerals in the Kevitsa ore have been shown to contain up to 1.4 wt% Ni (Makkonen et al. 2017).

Specific geochemical characteristics of waste materials (waste rock and tailings) from the Kevitsa operation were assessed by Mine Environment Management Ltd (MEM) in 2019, on behalf of Boliden AB (MEM 2019). Summaries of the key mine waste compositional characteristics and ARD/AMD risks identified in this report are outlined as follows:

- The waste rock stored at the Kevitsa operation is dominated by the silicates tremolite, Ca-rich clinopyroxene, Mg-orthopyroxene and Mg-rich olivine.
- Sulfides within the waste rocks are present in the form of pyrrhotite, pentlandite and chalcopyrite. Pyrrhotite is the dominant sulfide mineral, posing the largest ARD/AMD risk of the sulfides present.
- The iron sulfides (pyrite and pyrrhotite) have been identified as the main potential acidity source within waste rock and tailings storage facilities.
- Carbonates are present in the form of calcite and dolomite. These carbonates are present in low concentrations (<0.3 wt%) but are considered to be the primary source of acid neutralising potential (NP).
- Metalliferous drainage potential at the Kevitsa operation is interpreted to not be dependent on the formation of acidic conditions. Laboratory testing and site measurements indicate that key metal species are released and mobile at circumneutral pH conditions (pH 6 to pH 7.8).
- The main source of sulfate and metal release into pore water and seepages has been identified as the dissolution of secondary Ca and Mg sulfate (gypsum and epsonite) mineral products that contain base metals (Ni, Co, Cu, Mn and Sr). These

sulfate minerals are formed as a direct result of the oxidation of Fe sulfides (pyrrhotite and pyrite) and base metal sulfides (pentlandite and chalcopyrite) and subsequent dissolution/buffering with carbonates (dolomite and calcite).

- The waste rock is rich in reactive Mg silicates (olivine and serpentine) which are proposed as a further source of metal release in the waste streams. The dissolution of these reactive silicate minerals may contribute to Ni, Mn and Co release. The coarse nature of the waste rocks means the relevant risk of the dissolution of these minerals is lower in comparison to sulfate sources at circum-neutral pH conditions.

### 2.1.5 Waste rock pore gas measurement

Between April 2019 and April 2020 Boliden mines undertook a series of pore gas measurements within the waste rock storage facilities at the Kevitsa operation. These measurements were taken within the four sonic drilling borehole locations, outlined in Figure 4. Pore gas measurements for $O_2$, $CO_2$ and $CH_4$ were taken as unspecified depths within the waste rock dumps. $CO_2$ concentrations were below the detection limits of the instruments used within the period of measurement, with the exception of the measurement taken on the 30/12/2019 when pore $CO_2$ gas concentrations were measured as 0.1% in borehole ports 1-3. Over the measurement period $O_2$ concentration was shown to vary between 19.6% and 21.4%, with little variation between borehole locations, see figure 7.

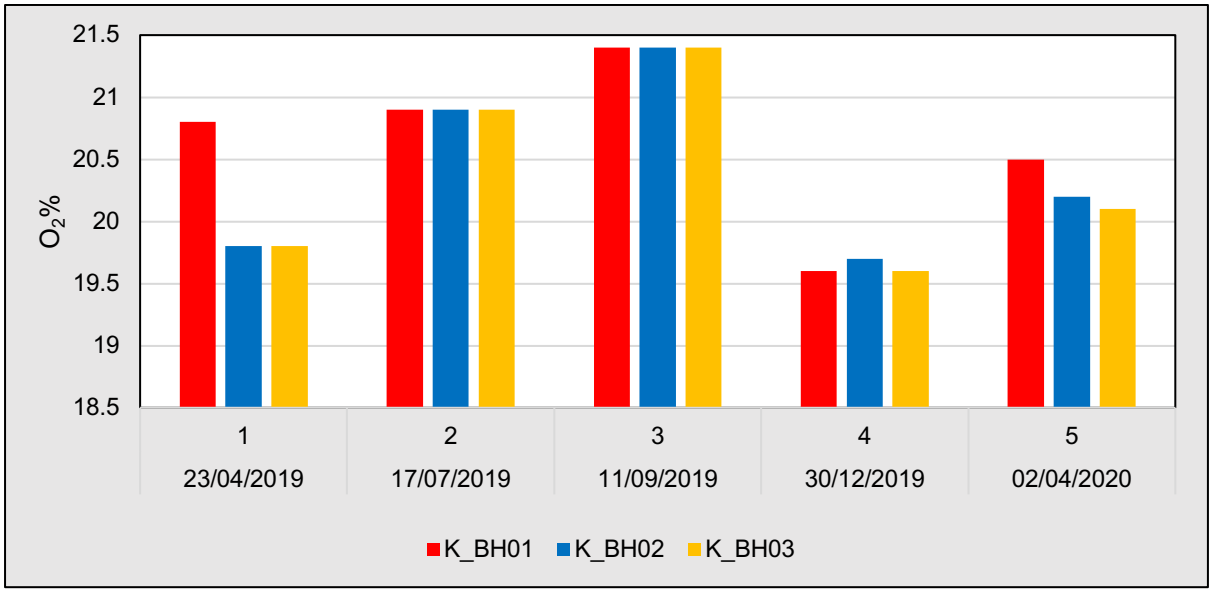


*Figure 7- Kevitsa waste rock $O_2$ (%) pore gas measurements (2019-2020)*

During this period a cover trial system was undertaken by Boliden at Kevitsa. This trial utilised waste rock material produced on site and allowed a quantification of potential pore gas composition change within Kevitsa waste rock facilities post closure if a cover was implemented to restrict $O_2$ ingress. Five port measurement locations were implemented in this trial, which provided $CO_2$ and $O_2$ measurements over the 12-month trial period. The data collected in this trial system is shown in Table 2.

*Table 2 – Kevitsa waste rock cover trial pore gas measurements. Data provided with permissions by Boliden Mines*

| | Date | | | | | | | | | |
|---|---|---|---|---|---|---|---|---|---|---|
| | 23/04/2019 | | 17/07/2019 | | 11/09/2019 | | 30/12/2019 | | 02/04/2020 | |
| Port | $O_2$ % | $CO_2$ % | $O_2$ % | $CO_2$ % | $O_2$ % | $CO_2$ % | $O_2$ % | $CO_2$ % | $O_2$ % | $CO_2$ % |
| 1 | 18.7 | 0.6 | 19.6 | 0.8 | 19.9 | 0.8 | 20.1 | 0.4 | 19.8 | 0.3 |
| 2 | 19.1 | 0.5 | 19.7 | 0.8 | 19.8 | 0.7 | 20.1 | 0.4 | 19.9 | 0.3 |
| 3 | 10.5 | 4.1 | 18.3 | 1.6 | 15.3 | 5.6 | 20.6 | 0 | 19.9 | 0.3 |
| 4 | 7.8 | 5.6 | 6.8 | 6.3 | 12.8 | 7.5 | 14.1 | 3.3 | 19.9 | 0.3 |
| 5 | 7.7 | 6.2 | 5.7 | 7.9 | 11.6 | 7.9 | 17.5 | 1.4 | 19.8 | 0.3 |

It can be seen in Table 2 that within the cover trial system $O_2$ concentrations were shown to diminish in line with increases in measured $CO_2$ concentrations. Over the course of the 12-month trial period $CO_2$ concentrations were measured above base line atmospheric concentrations. Data collected from measurement ports 3-5 demonstrated marked increases in pore gas $CO_2$ concentrations, peaking at 7.9% in July and August 2019 measurements. Distinct reductions in $O_2$ were also measured in these ports with $O_2$ dropping to 5.7% in July 2019.

The implications of these potential post closure conditions on mine waste geochemical development and the potential for ARD/AMD onset have not been assessed to date. The potential reduction in $O_2$ concentrations within closed waste facilities is likely to reduce sulfide oxidation rates (Vriens et al. 2018), although enhanced $CO_2$ pore gas concentrations are likely to cause enhanced weathering of reactive silicate minerals (Kemeny et al. 2021; Paulo et al. 2021a). The potential geochemical implications of these variations in pore gas in mine wastes are discussed in more detail in Chapter 3 of this thesis.

### 2.1.6 Measured Kevitsa operational emissions

$CO_2$ emissions data from the Boliden Kevitsa operation has been made available, collected in the period August 2016 to August 2018. The operational emissions from the mine and the mill at Kevitsa are shown in Figure 8. It can be seen in this figure that the majority of estimated $CO_2$ emissions from this operation can be attributed to the mining operation, with the mine mill also contributing a proportion of the overall emissions. Within this two-year measurement period the mining operations are estimated to have emitted 137,890 tonnes of $CO_2$. This can be compared to an estimated 12,838 tonnes of $CO_2$ from the mine mill. It is noted that the main sources of emitted $CO_2$ are attributed to burning of diesel and fuel oil for transportation and usage of explosives within the mine. The mill emissions can be mainly attributed to the burning of diesel for transportation, the burning of wood chips for heat production and the purchase of electricity and heat for the mill.

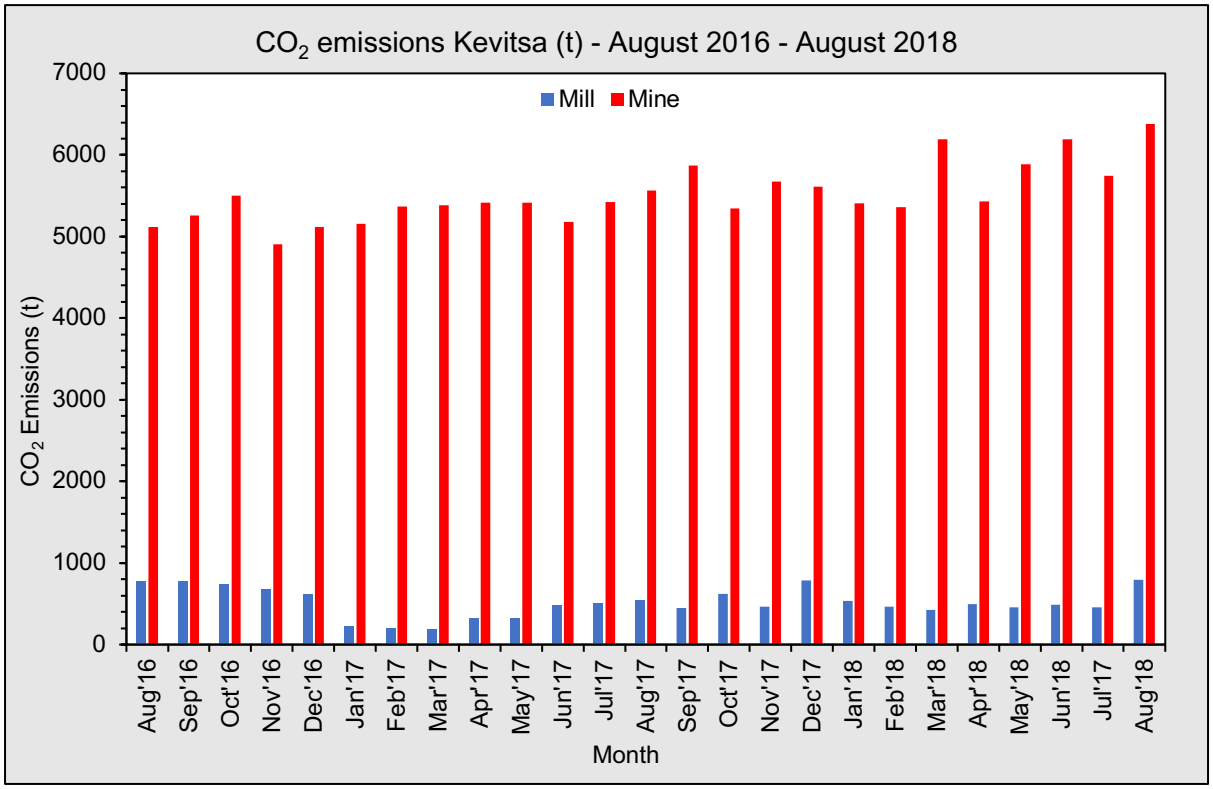


*Figure 8 - Operational $CO_2$ emissions estimations from the Kevitsa operation. Data provided with permissions by Boliden Mines.*

### 2.1.7 Previous CDR studies on Kevitsa waste materials

Previously to, and during, this research study the author, in collaboration with academic and industry partners, has undertaken smaller scale research projects that

have looked to assess the CDR potential of wastes generated at the Kevitsa mining operation. These studies have focused on the potential rate of mineral carbonation, geochemical changes to mine waste due to enhanced weathering and the potential implications for ARD prediction. These smaller scale projects have been published in the proceedings of three international conferences over the course of this PhD project. (Savage et al. 2019a; Savage et al. 2021; Savage et al. 2022). Relevant findings of these studies in relation to this research project have been summarised for context, with the full conference proceedings available in Appendixes 21-23.

A study was carried out in 2019 that presented a novel approach to assessing the rate of mineral carbonation within silicate rich mining waste rock and tailings facilities (Savage et al. 2019a). Within this study respirometry vessels and reactor column tests were undertaken to assess both the potential rate of carbonation within Kevitsa waste materials and the potential implications for ARD prediction and closure planning. Using the Renforth equation for carbon capture potential (CCP) (Renforth 2019a), it was estimated waste materials held an average CCP of ~300 kg of $CO_2$ per tonne of waste material. Broadly applying this to the life of mine (LOM) waste production estimations, the study estimated that wastes at Kevitsa could potentially sequester 57 Mt of $CO_2$. Characterisation of materials following short term reactor column testing displayed distinctive cementing and agglomeration of waste rock and tailings materials, potentially due to precipitation of stable carbonate phases. Static testing carried out after the reactor column had been decommissioned displayed distinct changes to total C% and parameters collected in standardised leach tests. The study concluded that there is the need for consideration of CDR strategies using suitable mine wastes in mine planning and closure considerations.

Building on the results of the 2019 study, a 2021 study looked to extend the experimental parameterisation of testing methods suggested in Savage et al., (2019). Within this study the experimental conditions within respirometry vessel tests were varied in relation to $CO_2$ gas compositions and test temperatures. Reactor column tests were carried out in the same nature as the 2019 study, but the testing length was extended, and a larger consideration was given to variable $CO_2$ concentrations and waste particle size. Within this study humidified $CO_2$ was cycled through a reactor column filled with either ‘fine’ waste rock, ‘coarse’ waste rock, tailings and a discrete

single waste rock sample that was known to contain a higher proportion of olivine group minerals than other samples. Columns were run in duplicate with one set carried out for 62 days, to provide comparison to the 2019 study, and another set carried out for ~12 months. The gas composition flushed through the systems was varied between 100% $CO_2$, 60% $CO_2$ and 30% $CO_2$, balanced with $N_2$ to isolate the reactions and avoid potential sulfide mineral oxidation in the presence of $O_2$.

The results shown within the referenced conference paper only contain the initial 62 days column results (Chmielarski 2019), with the paper published before the results of the 12-month reactor columns were available (Savage et al. 2021). To provide context to the geochemical results that may be generated within this research project some of the pre and post reactor column static testing results for total C%, carbonate neutralising potential (NP), total NP and net acid generation (NAG) pH have been demonstrated in Figures 9, 10, 11 and 12. Full experimental methods are outlined in Savage et al., (2021) and Chmielarski (2019).

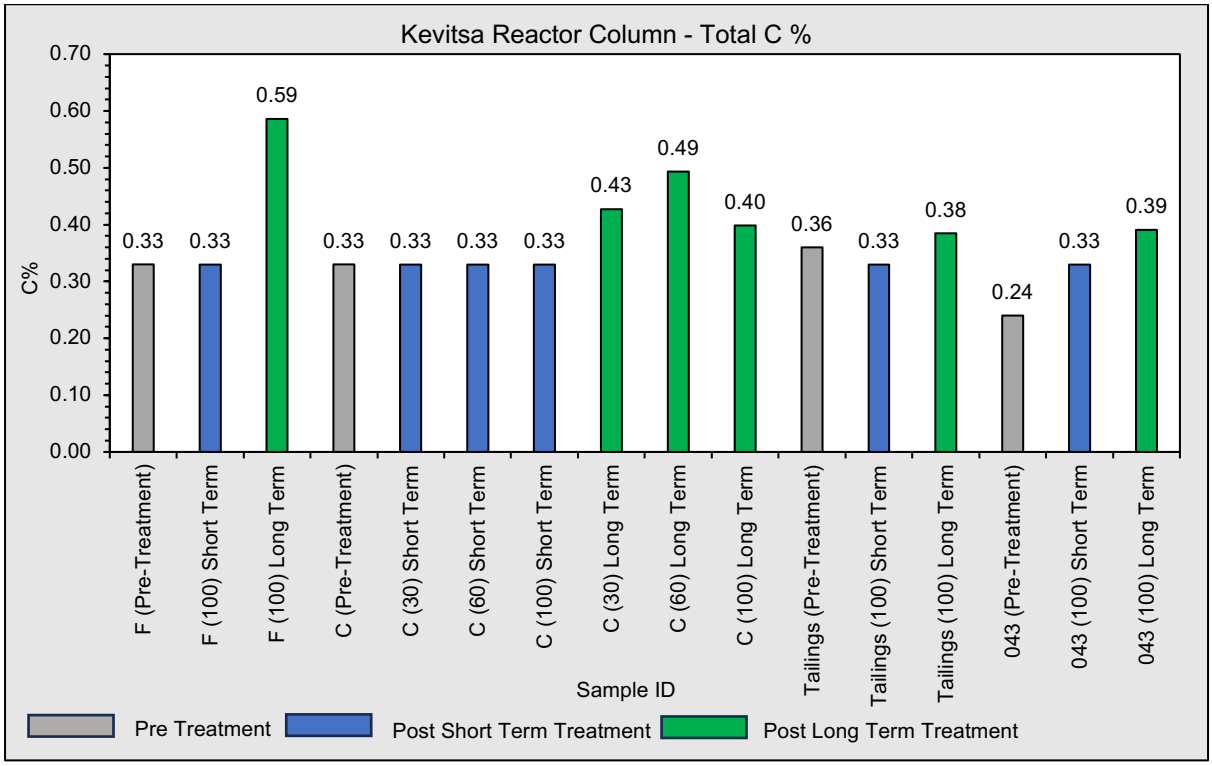


*Figure 9 - Pre and post reactor column total C% results.*

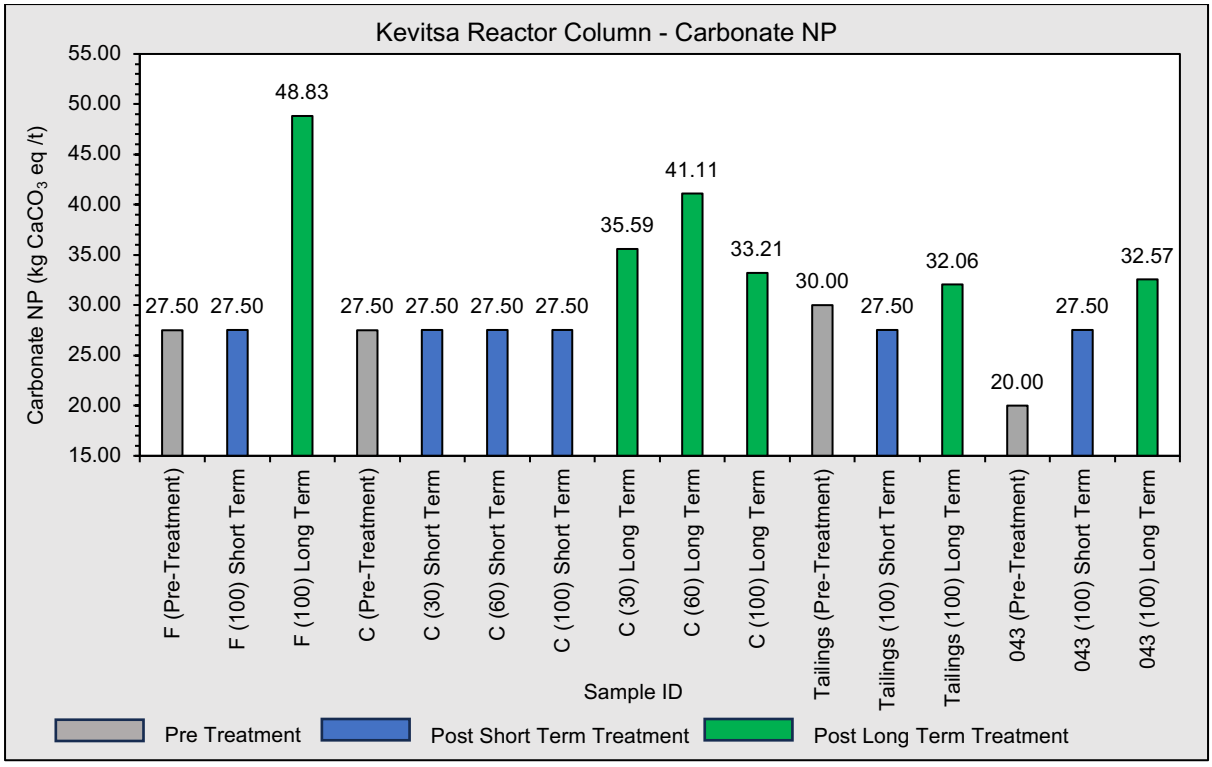


*Figure 10 - Pre and post reactor column Carbonate NP results.*

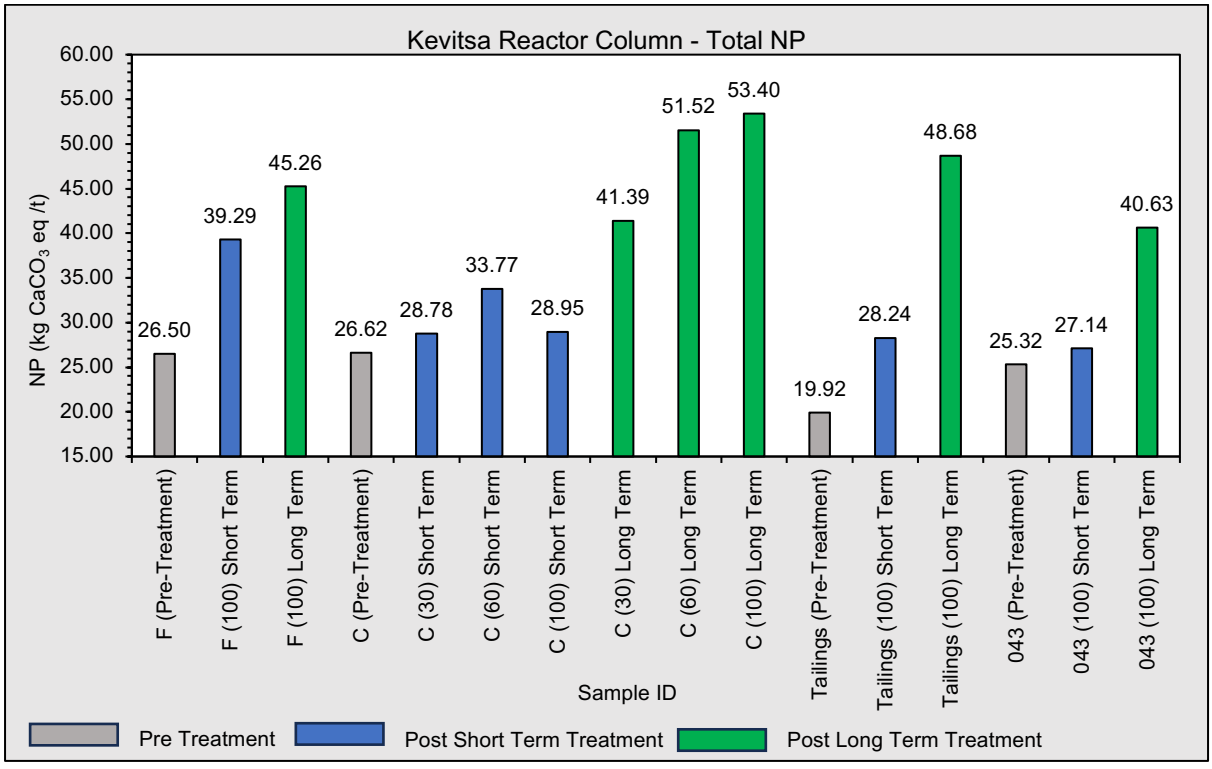


*Figure 11 - Pre and post reactor column Total NP results.*

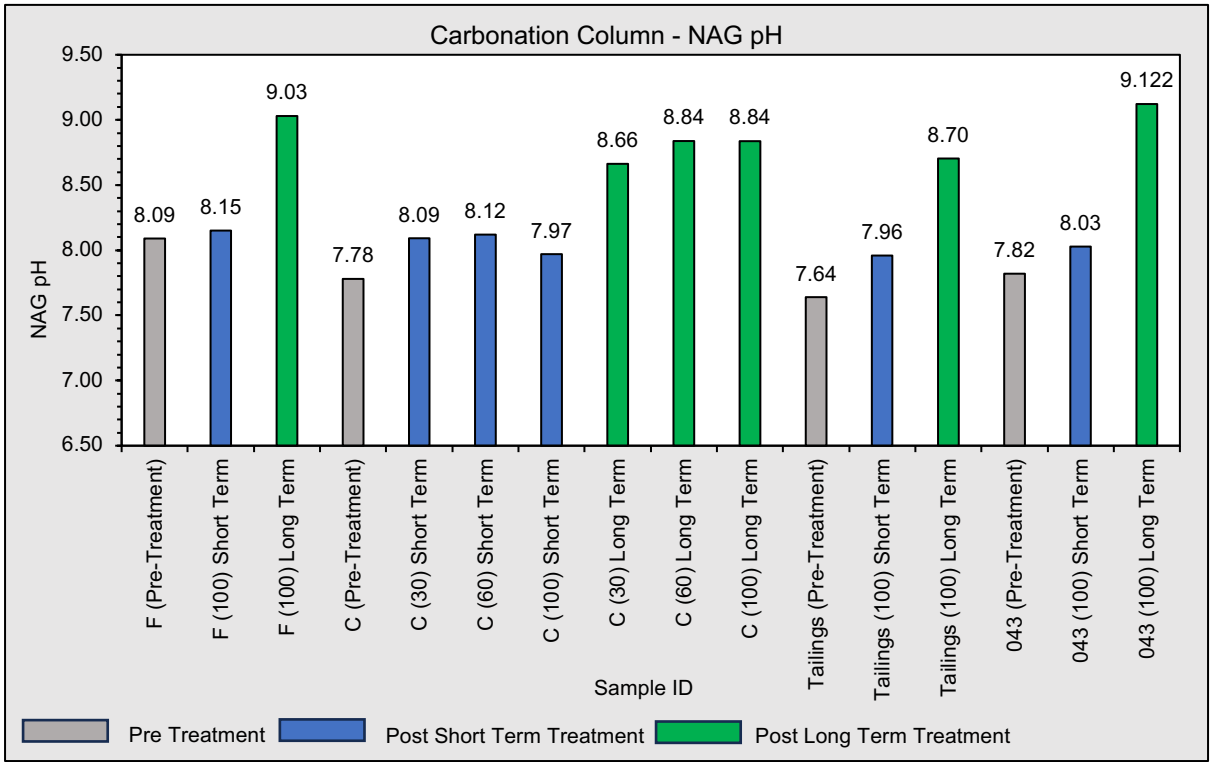


*Figure 12 - Pre and post reactor column NAG pH results.*

The static testing results presented in Figures 9-12 outline the importance of considering enhanced $CO_2$ concentrations in ARD prediction. The numbers within brackets in these figures denotes the $CO_2$ volume percentage within the aeration system. It can be seen in Figure 9 that after 62 days negligible differences were identified in material total C% results when compared to pre-treatment measurements. Comparatively measurements taken from the residues recovered from 12-month reactor columns displayed marked increases in total C% in all treated samples. Acid base accounting (ABA), testing in line with Price (2009) and BSI (2012), displayed complimentary results with noted increases in carbonate NP and total NP following the 12-month period.

It was theorised in Savage et al., 2021 that the enhanced weathering of silicates minerals within the tested materials would have led to the precipitation of stable carbonate phases. This theory would explain the increase in total C% and NP within longer term columns. NAG pH measurements are commonly used within ARD prediction to assess the ARD classification of a material (AMIRA 2002). It can be seen

in Figure 12 that a marked increase in NAG pH was noted in treated residues, with all materials classifiable as non-acid forming (NAF) (AMIRA 2002; Price 2009).

The importance of these results lies in the potential determination of ARD potential under varied atmospheric conditions. The results generated within the three referenced studies outline the potential for changes in waste geochemical composition in response to above atmospheric levels of $CO_2$ (Savage et al. 2019a; Savage et al. 2021; Savage et al. 2022). This is an importance consideration in the development and use of testing methods that are used within the prediction of ARD onset and metal leaching potential as the enhanced weathering of silicate mineral wastes may lead to the precipitation of secondary mineral phases and leaching of metal cations (Kandji et al. 2017a; McCutcheon et al. 2019; Lu et al. 2022).

It is noted that the results demonstrated in figures 9-12 are only partially published in conferences proceedings preceding the submission of this thesis. They have been provided and shown to give an indication of, and contextualise, the potential changes in ARD testing and classification parameters due to changes in $CO_2$ exposure.

## 2.2 The Aitik Mining Operation

### 2.2.1 Location and climate

The Aitik mine is located in northern Sweden, approximately 15 kilometres south of the town of Gällivare and 960 kilometres north of Stockholm, the capital of Sweden (Sammelin 2011; Karlsson 2018). The location of the Aitik mine within Sweden and the locality to Gällivare is shown in Figure 13. The mine is situated within the Paleoproterozoic Svecofennian Domain, which is characterized by granitoid intrusions, metavolcanic rocks, and metasedimentary rocks formed during multiple orogenic events (Kalinin and Kudryashov 2021).

The climate of the mine location is sub-arctic with an average temperature of 1$^{o}$C. The annual precipitation is dominated by snow fall, with average annual precipitation of 500mm. The variation in temperatures between summer highs and winter is great with summer temperatures reaching ~25$^{o}$C, while winter lows can drop to ~40$^{o}$C (Lindvall 2005).

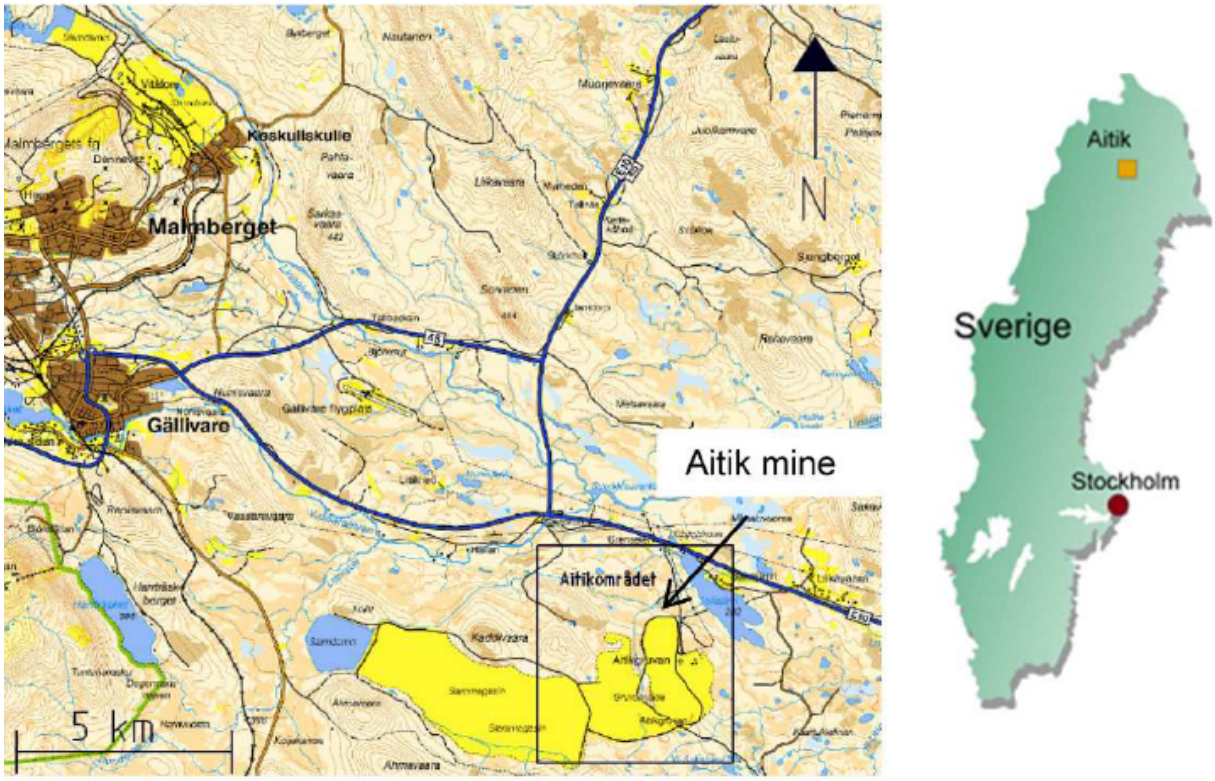


*Figure 13 - A location map of the Aitik mine within Sweden* (Karlsson 2018).

### 2.2.2 Mine operations overview

Aitik is a Cu-Au-Ag open pit mine consisting of two active pits: Salmijärvi and Aitik. The mining area consists of the two open pits, waste rock storage facilities, tailings storage facility, the industrial area and a transport terminal (Karlsson 2018). Aitik is the largest copper mine in Europe, occupying an area of ~50km$^2$ (Lindvall 2005). Copper (Cu) accounts for ~80% of the operations revenue stream, with gold (Au) and silver (Ag) accounting for ~15% and ~5%, respectively (Karlsson 2018). Operations started in 1968, with an initial ore capacity of 2 Mt annually. Multiple expansions have taken place since with ore production increased to over 36 Mt annually (Ojala and Iljina 2008). Over the operation period 1968-2018 total waste stripping (overburden and waste rock) is calculated as 784 Mt (Karlsson 2018).

### 2.2.3 Geological setting

#### *Regional geology*

The Aitik mine is situated within the Fennoscandian Shield, which encompasses parts of Finland, Sweden, and Norway (Kalinin and Kudryashov 2021). Located within the northern Norrbotten region of northern Sweden, the regional geology is dominated by

the Paleoproterozoic Svecofennian Domain, characterized by granitoid intrusions, metavolcanic rocks, and metasedimentary rocks (Sammelin 2011). The key regional and geological characteristics of the Aitik deposit are shown in Figure 14.

### *The Aitik deposit*

The Aitik deposit is a classic porphyry Cu-Au system, characterized by low-grade disseminated mineralization in altered granitoids and adjacent metavolcanic and metasedimentary rocks. The Aitik deposit is hosted within the Nautanen Deformation Zone (NDZ), a major structure that represents the contact between metavolcanic and metasedimentary rocks. The main ore minerals are chalcopyrite and pyrite, with minor amounts of molybdenite and gold (Wanhainen et al. 2003). In the Aitik Cu-Au deposit, sulfides are primarily found dispersed throughout and in the form of small veins, with the distribution of metals being uneven within the ore body (Sammelin 2011).

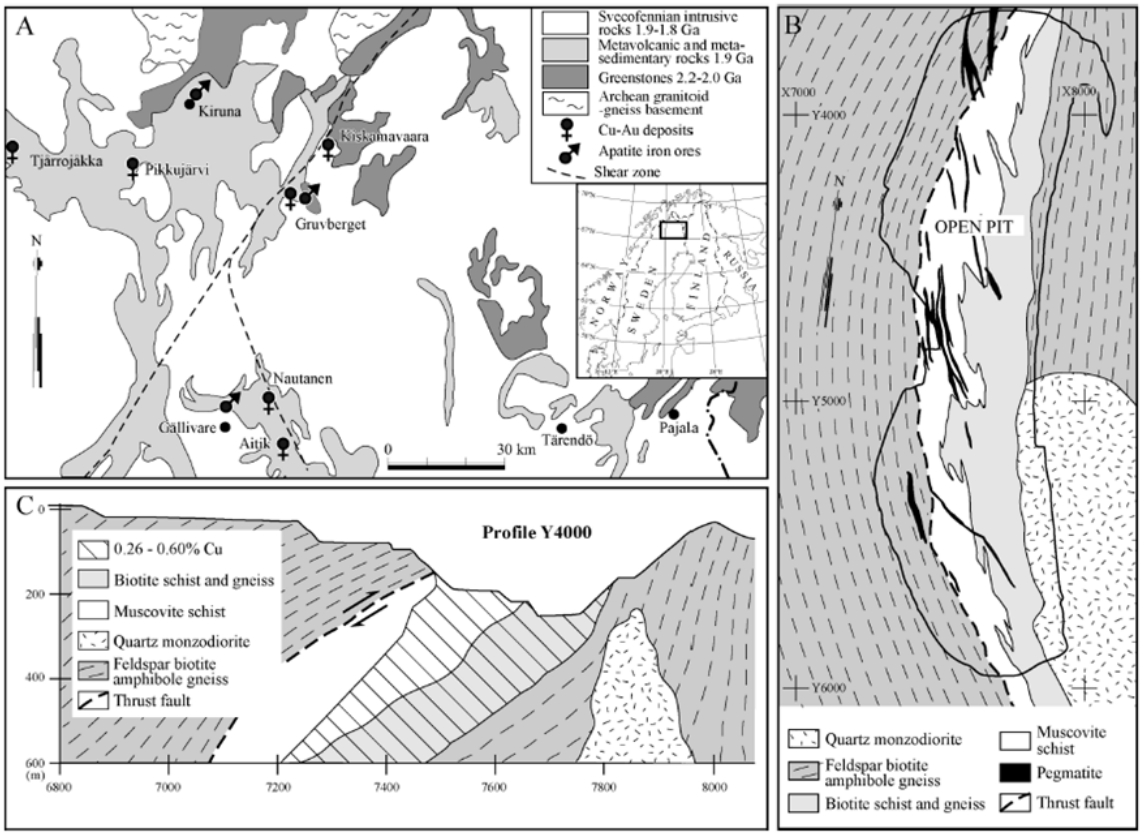


*Figure 14 - (A) The location of the Aitik deposit within the Norrbotten region of north Sweden. (B) The plan view of the main geological units of the Aitik deposit. (C) A W-E vertical cross section of the deposit* (Sammelin 2011).

### 2.2.4 Mine waste composition and potential ARD/AMD sources

As of 2018 waste stripping at the Boliden Aitik operation had produced 784 Mt of overburden and waste rock. Wastes categorised as potentially acid forming (PAF) and non-acid forming (NAF) are deposited and stored separately on site (Karlsson 2018). The waste rock produced is assumed to be heterogeneous in nature with uneven sulfide distribution within the deposit and host rocks (Sammelin 2011). The main sulfides of economic interest are chalcopyrite and pyrite, with minor pyrrhotite, these sulfides also present the main ARD/AMD risk within Aitik waste materials (Wanhainen et al. 2003; Karlsson 2018).

Multiple studies such as Lindvall (2005) and Stromberg and Banwart (1994) have assessed the geochemical characteristics and environmental risks of waste materials produced at the Boliden Aitik operation.

The study by Stromberg and Banwart (1994) created a kinetic model of the geochemical processes of waste rocks produced at the operation in northern Sweden. The study outlined a number of findings related to the characteristics of the waste rocks present at Aitik and the main sources of potential acid production (AP) and neutralising potential (NP). An assessment of water rock interactions found that sulfide minerals, pyrite and chalcopyrite, were the main potential sources of acidity and leaching of Cu into pore water. The relative absence of carbonates in the Aitik waste rock means that NP is dominated by weathering and dissolution of biotite and feldspar minerals, such as anorthite. Potential ARD/AMD onset, and subsequent metal release, was interpreted to be heavily dependent on the rate of sulfide oxidation and production of alkalinity through dissolution of reactive silicates. Waste rock internal temperatures were shown to vary considerably throughout the storage facility. Near surface temperatures were measured between -5$^{O}$C and 12$^{O}$C, while measurements at the base of waste facilities demonstrated temperatures between 0$^{O}$C and 3$^{O}$C. The exothermic nature of sulphide oxidation is cited as the main source of temperature variance.

The 2005 PhD thesis by Dr Manfred Lindvall outlined three published research journals that assessed strategies for remediation of the waste materials produced at the Aitik operation. This PhD thesis contains detailed waste characterisations for

waste rocks present at the operation, including a series of kinetic tests, in the form of humidity cell tests (HCT) and column tests. The kinetic testing in combination with a series of static tests, mineralogical analysis and geochemical modelling allowed the author to determine that ~20% of waste materials produced at Aitik are reactive and can be categorised as an ARD/AMD risk (Lindvall 2005). This could be explained by the highly heterogenous nature of the host rock and distribution of sulfide minerals identified in other studies of the deposit (Sammelin 2011). Similarly to the study by Stromberg and Banwart (1994), Lindvall (2005) identified the main acid buffering mineral sources within the waste materials as reactive silicates, including anorthite, albite, k-feldspar and biotite. Mineralogical analysis carried out within the multiple studies outlined in Lindvall (2005) identified plagioclase, K-feldspar, biotite, muscovite and quartz as major minerals, with minor proportions of garnet, chlorite tourmaline, calcite, magnetite, pyrite, pyrrhotite and chalcopyrite.

Restriction of $O_2$ ingress within waste rock facilities is a key ARD/AMD prevention method that is implemented at various mining operations around the world. At the Aitik waste rock facility waste rock storage facilities will be covered by compacted till and a vegetation layer, post closure. This cover system is intended to limit internal $O_2$ concentration to ~1%, reducing overall sulfide oxidation potential and subsequent ARD/AMD onset potential (Lindvall 2005).

### 2.2.5 Previous CDR studies on Aitik waste materials

At the time of submission, the only published work related to the CDR potential of waste materials produced at the Aitik mining operation was a conference paper published in 2022 by the thesis author and relevant partners (Savage et al. 2022). Within this conference paper the preliminary suitability of the waste rock materials produced at the Aitik operation for use in large scale CDR is discussed with reference to ARD implications.

# Chapter 3 - Technical Review

## Introduction

This technical literature review will outline and review the key concepts related to acid mine drainage (AMD) prediction, the interactions between carbon dioxide and mine waste weathering characteristics, carbon mineralisation and the geochemical characterisation of mining waste materials. The review aims to introduce each of the key themes of this research thesis and outline the current state of research, identifying key research gaps in existing scientific literature. Where extensive reviews exist for specific topics, reference will be given to such reviews.

This review is organised into distinctive sections. This provides a broader context to the importance and relevance of this research project. The following sections are defined as follows:

- **Section 1 – Mine Drainage Overview**
- **Section 2 – Drainage Characterisation and Prediction**
- **Section 3 – $CO_2$ Interactions with Sulfidic Mine Wastes**
- **Section 4 – Review Conclusions**

## 3.1 Section 1 – Mine Drainage Overview

Within this section the basic aspects of mine drainage are outlined to provide context to the overall subject area. Multiple books, journal papers, regulatory handbooks and review articles have outlined the subject area in general (EPA 1994; Morin and Hutt 2001; AMIRA 2002; Lottermoser 2010; Blowes et al. 2013; Parbhakar-Fox et al. 2013; GARD 2014; Simate and Ndlovu 2014; Parbhakar-Fox and Lottermoser 2015; Dold 2017; Karlsson 2022; Elghali et al. 2023).

Due to abundance of existing reviews and articles on the subject area, this section of the literature review will focus on outlining the basic chemistry and classification of mine waste drainage systems. Following sections will review specific topics related to this research study.

### 3.1.1 Mine drainage definitions and basic chemistry

Acid mine drainage (AMD) or acid rock drainage (ARD) typically refers to the release of acidic and metal-rich waters from mining wastes / storage facilities, primarily caused by the oxidation of sulfide minerals, such as pyrite ($FeS_2$) (Nordstrom and Alpers 1999; Lottermoser 2010; Blowes et al. 2013; GARD 2014; Parbhakar-Fox and Lottermoser 2015; Moodley et al. 2018). The oxidation of sulfide minerals, and subsequent ARD or metalliferous drainage onset, can occur in both waste rock and tailings materials produced at mining operations. Within this study waste rock and tailings are defined as follows (Lottermoser 2010; Blowes et al. 2013; GARD 2014):

- **Waste Rock** – Mined rock that is of insufficient value and falls below the cut-off grade. This material is removed before metallurgical processes and is often disposed of within a waste rock storage facility. These materials are usually heterogenous in natural, both geochemically and physically. Within a waste rock facility particle size can vary from sand sized particles, up to large boulder sized materials. Waste rock storage can vary depending on waste composition and closure planning objectives.
- **Tailings** – The solid product that is produced as a by-product of the mineral concentration of ore materials. These materials are separated from the commodity concentrate and are typically stored within a tailing's dam/impoundment. Tailings are typically much finer than waste rock materials, with particle sizes distributions varying from sand to clay sized. These materials are more homogeneous in nature and typically contain higher concentrations of remaining sulfides and metal products. As such these materials are typically stored in facilities designed to reduce oxidation reactions, this may include the inclusion of a water cover within a tailings pond.

It is noted that AMD and ARD are commonly used interchangeably within scientific literature, herein ARD is used when referencing acidified metalliferous mine drainage, directly or indirectly due to the oxidation of sulfide mineral bearing waste materials (Moodley et al. 2018). The definition and categorisation of mine drainage as 'acid mine drainage' (AMD) has led to misconceptions on the nature of overall mine drainage development. As evidenced in the Global Acid Rock Drainage (GARD) guide, developed by the International Network for Acid Prevention (INAP), mine drainage can

be characterised by the typical pH conditions of the assessed drainage system, which are not always acidic in nature, see Figure 15. It can be seen in this suggested scaling that ARD is characterised as drainage with a pH typically below pH 6, with drainage water with a pH >6 characterised as saline drainage (SD) or Neutral mine drainage (NMD). The guide suggests the use of the term AMD only in instances where acidic mine drainage onset is a direct results of mining activities alone (GARD 2014).

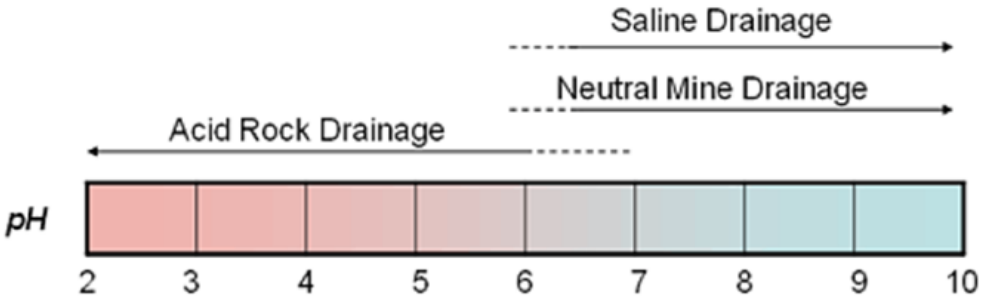


*Figure 15 - Typical mine drainage characterisation by pH* (GARD 2014).

ARD can have significant negative impacts on mine water discharge quality, aquatic life, and the surrounding environment, leading to long-term environmental and financial liabilities for mining operators (Morin and Hutt 2001; Parbhakar-Fox and Lottermoser 2015). Studies such as Parbhakar Fox et al., (2018) have stressed the importance of accurate prediction of drainage quality at the early stages of a mining operation.

***Basic sulfide mineral oxidation chemistry and ARD onset potential***

Under reducing environments sulfide minerals are chemically stable (Lottermoser 2010). The formation of ARD is primarily driven by the oxidation of sulfide minerals in the presence of water and oxygen. The formation of ARD is difficult to stop or mitigate once the process has formed as the oxidation of sulfide minerals will continue until one of the key reactants, sulfide minerals, oxygen or water, is fully consumed or exhausted (GARD 2014).The oxidation of sulfide minerals is covered extensively in Dunn (1997). The most common sulfide mineral associated with ARD is pyrite ($FeS_2$), but other sulfide minerals, such as chalcopyrite ($CuFeS_2$), pyrrhotite ($Fe_{(1-x)}S$) and sphalerite (ZnS), can also contribute to ARD generation (Dunn 1997; Nordstrom and Alpers 1999). The oxidation reaction of these minerals produces variable amounts of acidity ($H^+$), depending on the specific sulfide that has oxidised (GARD 2014). The production of acidity, in the form of sulfuric acid, leads to reduction in pore water pH,

which can then result in the dissolution of metal bearing minerals, subsequently releasing enhanced metal cations/anions into waste drainage systems (Morin and Hutt 2001; Lottermoser 2010; GARD 2014).

The oxidation of pyrite by atmospheric $O_2$ in the presence of water is shown in Equation 1, with sulfate ($SO_4^{2-}$) produced as a result of the dissociation of sulfuric acid ($H_2SO_4$) (GARD 2014). The reaction of pyrite in the presence of produced ferric ions ($Fe^{3+}$) is shown in Equation 2 (Dold 2017). These equations summarise the basic principle of 'run away' ARD production, where the oxidation products in the sulfide mineral oxidation reaction promotes further oxidation and acidity ($H^+$) production.

*Equation 1 - The oxidation of pyrite in the presence of oxygen and water*

$$FeS_2 + 7/2O_2 + H_2O \Rightarrow Fe^{2+} + 2SO_4^{2-} + 2H^+$$

*Equation 2 - The reaction of pyrite in the presence of ferric ions*

$$FeS_2 + 14Fe^{3+} + H_2O \Rightarrow 15Fe^{2+} + 2SO_4^{2-} + 16H^+$$

Although Pyrite oxidation is usually used as a base case in ARD, as the most abundant sulfide mineral, other sulfide minerals play a key role in the generation of ARD. The basic oxidation reactions of chalcopyrite and pyrrhotite are shown in Equations 3 and 4 (GARD 2014; Dold 2017).

*Equation 3 - The oxidation of chalcopyrite in the presence of oxygen and water*

$$CuFeS_2 + 4O_2 + 3H_2O \Longrightarrow Cu^{2+} + Fe(OH)_3 + 2SO_4^{2-} + 2H^+$$

*Equation 4 - The oxidation of pyrrhotite in the presence of oxygen and water*

$$Fe_{(0.9)}S + 2.175O_2 + 2.35H_2O \Longrightarrow 0.9Fe(OH)_3 + SO_4^{2-} + 2H^+$$

$$\text{Based on } Fe_{(1-x)}S \text{ and } x = 0.1$$

Although the oxidation of sulfide minerals produces acidity within a drainage system, the actual potential for ARD onset is dependent on the balance between acid producing oxidation reactions and neutralisation reactions taking place as a function

of time (Sherlock et al. 1995). This balance is dependent on the proportion and kinetic reactivity of acid producing (AP) minerals and minerals with neutralising potential (NP) (Sherlock et al. 1995; Price 2009; GARD 2014; Dold 2017). NP within mining wastes is primarily provided through carbonate minerals, with silicate minerals providing a secondary acid buffering source (Morin and Hutt 2001). As previously mentioned, metal leaching is a potential consequence of sulfide oxidation induced metal bearing mineral dissolution. If adequate NP is present within a waste material to neutralise produced acidity, metalliferous drainage may still occur as metal bearing NP minerals are dissolved (Price 2009; Lottermoser 2010; GARD 2014; Dold 2017) . The basic reaction of the carbonate mineral, calcite, in the presence of acidity can be seen in Equation 5 (Dold 2017). It can be seen in this equation that the reaction of calcium carbonate with acidity ($H^+$) leads to the release of free $Ca^{2+}$ cations and carbon dioxide ($CO_2$).

*Equation 5 - The basic reaction of calcium carbonate in the presence of acidity*

$$CaCO_3 + 2H^+ \Leftrightarrow Ca^{2+} + CO_2 + H_2O$$

The weathering of silicate minerals as a secondary source of NP is discussed in more detail later in sections 3.3.3 and 6.2.6 of this thesis.

### 3.1.2 The impact of bacteria on ARD and sulfide oxidation

It is widely accepted within the scientific literature that various bacteria species can impact the rate of sulfide oxidation and ARD onset. Iron oxidising bacteria, such as those within the acidithiobacillus genus, are well understood to increase the rate of metal sulfide oxidation (GARD 2014). The type of bacteria present within a drainage system is heavily influenced by environmental conditions, in particular temperature and pore gas composition (Jansen et al. 1984; Paul et al. 2017). It is noted that the impact of bacterial inoculation and specific bacterial species was minimally considered within this study. The GARD guide provides an in-depth review of various bacterial species and their impact on ARD onset, with referencing to both sulfide oxidising bacteria (SOB) and sulfate reducing bacteria (SRB) (GARD 2014).

## 3.2 Section 2 - Drainage Characterisation and Prediction

Within this review section the key aspects of mine waste and mine drainage characterisation and prediction are outlined. Multiple in-depth reviews, books, journal studies and research theses exist within the scientific literature that have covered the key aspects of mine drainage prediction and characterisation methods (Stewart et al. 2006; Price 2009; Parbhakar-Fox and Lottermoser 2015; Dold 2017; Moodley et al. 2018; Karlsson 2022; Pieretti et al. 2022; Elghali et al. 2023). As such the topic is not reviewed in detail within this thesis, with this review serving the purpose of informing the key aspects of the research study, with relevant studies that attribute to the research purpose and aims discussed. Chapter 4a of the Global Acid Rock Drainage (GARD) Guide provides an in-depth overview of ARD prediction and modelling methods.

Mine waste characterisation and ARD prediction methods can broadly be defined into 3 specific categories as follows (Morin and Hutt 2001):

1. Physical characterisation
2. Static testing methods
3. Kinetic testing methods

The individual tests and methods utilised within each of these categories are typically assessed in tandem, with kinetic testing usually carried out following static testing and physical characterisation (Morin and Hutt 1998; Morin and Hutt 2001; AMIRA 2002; Price 2009; GARD 2014; Parbhakar-Fox and Lottermoser 2015). Physical characterisation and static testing are not the key focus of this study, and as such are not reviewed in detail. The individualised static and characterisation testing methods undertaken within this study are outlined in detail in Chapter 4, section 4.4, with reference to parameter definitions.

Recent studies and review by authors such as Anita Parbhakar-Fox (University of Tasmania) have stressed the importance of site specific and tailored characterisation, static and kinetic test methods for sulfidic mine wastes (Parbhakar-Fox et al. 2013;

Parbhakar-Fox and Lottermoser 2015; Parbhakar-Fox et al. 2018b; Parbhakar-Fox et al. 2018a; Moyo et al. 2023).

### 3.2.1 Physical characterisation

Within this study physical characterisation refers to parameters that can be physically measured and are mainly descriptive in nature. Examples of physical characterisation include particle size distribution analysis (PSD), water content, specific gravity, and physical property descriptions (BSI 2012b; BSI 2015; BSI 2016b).

### 3.2.2 Static testing methods

Static testing methods provide geochemical data that is collected at one point in time and therefore provide a static measurement (Morin and Hutt 2001). Such testing protocols include acid base accounting (ABA), net acid generation (NAG), acid buffering characterisation curve (ABCC), paste pH and EC, single addition leach tests, total carbon, total sulfur, mineralogical abundance analysis and elemental abundance analysis (AMIRA 2002; BSI 2002a; Price 2009; BSI 2012a; GARD 2014). Assumptions are made based on the results of static testing that are then extrapolated over time, with kinetic testing employed to validate static testing parameters (Morin and Hutt 1998; Morin and Hutt 2001; Sapsford et al. 2008).

In a general sense the purpose of static testing is to assess the acid potential (AP) and neutralising potential (NP) of minerals within a waste material and their relative reactivity. AP, or maximum potential acidity (MPA), refers to the potential of a material to produce acidity, while NP, also referred to acid neutralising capacity (ANC), refers to the overall capacity of a material to neutralise produced acidity (AMIRA 2002; Price 2009; GARD 2014). AP is generally a product of sulfide mineral sources, while NP is provided carbonates, such as calcite, and silicate minerals (Sherlock et al. 1995).

Refined method descriptions and geochemical output parameters of static tests can be found within standards and ARD guides, such as MEND 1.20.1 manual, the AMIRA ARD handbook and the GARD guide (AMIRA 2002; Price 2009; GARD 2014). Specific method description and produced parameters relevant to this study are outlined in Chapter 4, sections 4.4.1 – 4.4.6.

### 3.2.3 Kinetic testing methods

Kinetic testing refers to testing methods that assess the geochemical parameters of a material over time and will typically produce results in the form of rates/loads of release, depletion or consumption of a specific mineral or element over the testing period (Sapsford et al. 2009a; Parbhakar-Fox et al. 2013; Parbhakar-Fox and Lottermoser 2015; Dold 2017). Kinetic testing methods are not as widely standardised, as static or physical characterisation methods, with the ASTM D5744 humidity cell test representing the only full standardised kinetic test for the assessment of sulfidic wastes.

Other testing methods, such as bulk leach columns, are suggested by various ARD manuals/handbooks, such as the free draining leach column test within Appendix F of the AMIRA ARD handbook (AMIRA 2002). The implementation of such tests varies widely regarding testing procedures and protocols.

Laboratory based kinetic test methods often aim to accelerate the weathering of material to estimate and predict the quality of produced leachate over time (Stromberg and Banwart 1994; Lapakko 2000a; Price 2009; ASTM 2018a). Specific attention to kinetic testing methods, in particular humidity cell tests, are outlined in sections 3.2.7 and 3.2.8 of this Chapter.

### 3.2.4 Mine drainage geochemical prediction

The prediction of mine drainage quality of any waste material is a complex process that involves the interpretation of multiple data sources. Wastes of differing geological and subsequently mineralogical composition can produce very different drainage. Subsequently a range of testing methods is needed to provide a reliable estimation of a wastes potential to produce drainage water that may pose environmental risk (Nordstrom and Alpers 1999; Maest and Nordstrom 2017).

A combination of field testing, onsite measurements, laboratory static and kinetic testing and mineralogical analysis is key in the holistic geochemical prediction of mine drainage (Parbhakar-Fox and Lottermoser 2015). Figure 16 outlines the wheel approach for the prediction of ARD risk outlined in Morin and Hutt (1998). Typical

industry utilised protocols and parameters used in the determination and prediction of mine waste drainage quality are outlined in this section, with direct reference to the appropriate standards that may be employed.

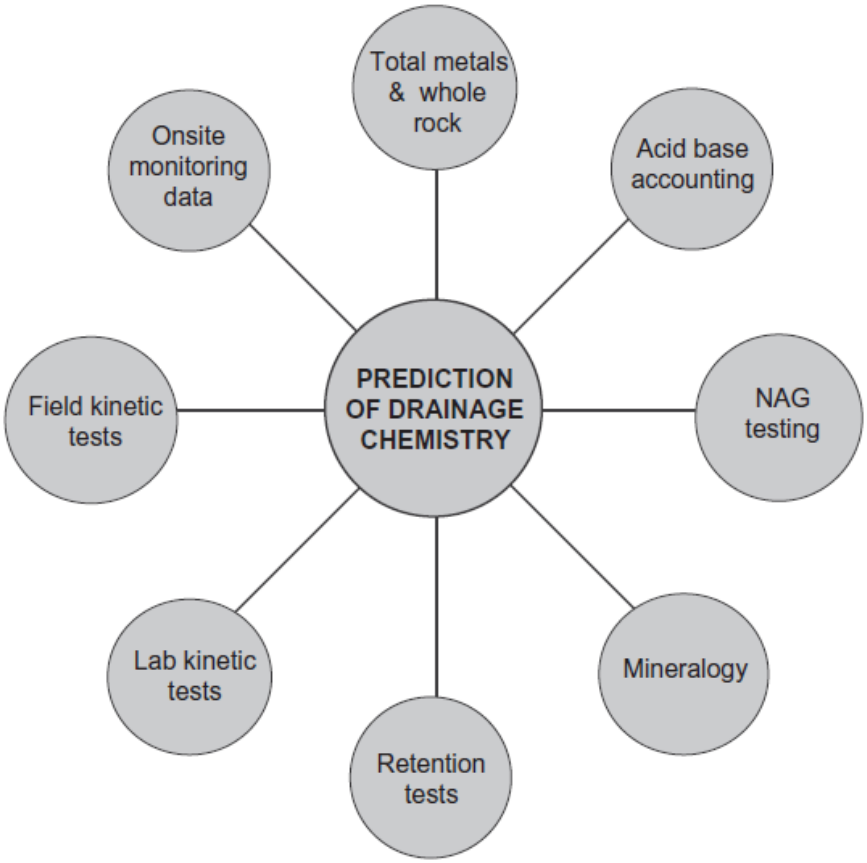


*Figure 16 - The wheel approach for the prediction of acid rock drainage (ARD) onset risk* (Parbhakar-Fox and Lottermoser 2015)

Assessments of kinetic and static testing methods in the prediction of ARD onset potential, including consideration of acid producing and acid neutralising minerals and their weathering properties has been covered in extensive detail. Key authors such as Werner Stumm, James Morgan, Kevin Morin, Nora Hutt, Keith Brady, Darrell Nordstrom, Andrew Sobek and Kim Lapakko have been instrumental in the development of current kinetic and static testing methods to assess the ARD potential of both sulfidic and coal bearing mining waste materials (Sobek et al. 1978; Lapakko 1988a; Stumm and Morgan 1995; Morin and Hutt 1998; Nordstrom and Alpers 1999; Lapakko 2000b; Morin and Hutt 2000a; Morin and Hutt 2001; Lapakko 2003; Brady and Scheetz 2005; Lapakko et al. 2006; Perry et al. 2009; Perry and Brady 2009; Maest and Nordstrom 2017; Morin 2017).

Morin and Hutt (2001) provided an in-depth review of the environmental geochemistry of mine site drainage, with practical consideration of prediction methods, with reference to specific case studies from various mining operations. More recent reviews by Parbhakar-Fox and Lottermoser (2015), and Dold (2017) have highlighted and reviewed recent development in ARD prediction. These reviews hold the commonality of expressing the inherent risk and limitations of ARD prediction methods, both static and kinetic, that are unrepresentative of field measurements (Parbhakar-Fox and Lottermoser 2015; Dold 2017).

Static and kinetic testing methods are used in coalition to characterise mine waste materials. Typically, materials are characterised using a suite of static and kinetic testing methods, in coalition with geological and mineralogical assessment (Morin and Hutt 1998; Lapakko 2000a; Morin and Hutt 2001; Perry and Brady 2009; Pieretti et al. 2022). Static testing is usually carried out first to provide key parameters, such as acid producing (AP) and neutralising potential (NP), at a single point in time, these single point values can then be validated through the undertaking of kinetic testing, allowing an estimation of drainage quality development over time (Morin and Hutt 2001). Characterisation testing methods are discussed in the following sections of this review Chapter as well as in sections 4.3, 4.4 and 4.5 of Chapter 4 within this thesis.

### 3.2.5 Industrial standards for mine waste drainage predication

Depending on the location of a mining operation around the world a range of standards, manuals and guides exist that provide information on methods of characterising, predicting, and managing mine drainage. These documents often overlap in content, but in some instances differentiate in their approach. The main internationally utilised methods, manuals and guides are outlined.

#### *MEND report 1.20.1*

The predictive manual for drainage chemistry from sulfidic geological materials (MEND Report 1.20.1) is a comprehensive manual designed to provide mining stakeholders with an understanding of methods utilised for the prediction of drainage chemistry. This manual was produced as part of the Mine Environment Neutral Drainage (MEND) program, on behalf of National Resources Canada, and is therefore

commonly utilised in North America as a guide for methods to characterise mine wastes of sulfidic composition and predict drainage quality of such materials (Price 2009).

***European standards (CEN)***

Unlike the MEND guidelines, standardised kinetic and static methods utilised within the UK and the European Union are based on individual standards for individualised testing methods. Therefore, a single document covering ARD prediction does not exist at present. Multiple standards cover various predictive testing methods, with individual countries having local regulatory versions of European standards (CEN). British standards are issued by the British Standards Institute (BSI). Selective standards utilised in the characterisation of mining waste materials include BS EN 15875:2011, which covers acid base accounting (ABA) testing, EN 12457 (1-4), which covers leach tests at variable liquid to solid ratios and CEN/TR 16365:2012, which covers the general characterisation of wastes produced in extractive industries (BSI 2002a; BSI 2002b; BSI 2012b; BSI 2012a).

***AMIRA ARD handbook***

The AMIRA test handbook, produced by the Ian Wark Research Institute, is a testing handbook developed to inform methods to predict ARD through kinetic and static testing methods. This handbook usually applied within Australasian counties and outlines a range of characterisation and predictive methods that are applied to sulfidic mine wastes. The terminology and units described within this guide differing from the MEND and European standards with NP and AP described as ANC and MPA, respectively. Unlike MEND and ASTM standards, AMIRA recommends the use of free draining leach columns as a standardised kinetic method for the prediction of waste geochemical evolution, in place of a humidity cell test (HCT).

***GARD guide (INAP)***

Unlike AMIRA and MEND, the Global Acid Rock Drainage (GARD) guide is not a regulatory document. The GARD guide was developed by the International Network for Acid Prevention (INAP) to provide a summary of the state of the art and best practices within international ARD prediction. The guide is based on best international

practises and methods, with direct reference to AMIRA, MEND, European, ASTM and EPA guides and standards. This extensive guide document also outlines the general aspects of mine drainage development, considering ARD onset mechanisms and remediation techniques (GARD 2014).

***EPA methods***

The United States environmental protection agency (EPA) has produced multiple standards related to static and kinetic testing within applications to sulfidic and coal wastes. The EPA has produced specific documents that provide an overview of ARD prediction and characterisation methods, such as EPA 530-R-94-036, as well as specific standards for the prediction of drainage quality produced from coal overburdens. Technical documents, including EPA 530-R-94-036, outline regulatory standards required within the United States of America (EPA 1994; EPA 2011).

***ASTM standards***

The American Society for Testing and Materials (ASTM) has produced several standard methods related to ARD predictive methods. Like BSI standards produced within the UK and CEN standards utilised within the European Union, ASTM standards are not predictive manuals or technical documents. ASTM standards are standalone method standards that are utilised within multiple regulatory regions. Examples of commonly used ASTM standards within ARD prediction include ASTM D5744, which outlines humidity cell testing (HCT) methods, in line with the findings and recommendations of Sobek et al., 1978 (ASTM 2018a).

### 3.2.6 Definition of ARD parameters utilized in static and kinetic testing methods

Within this study key ARD testing parameters are defined in line with the GARD guide with definitions quoted directly within the guides glossary. It is noted that the GARD guide is not exhaustive, with individual parameters covered in detail within regulatory documents and standards (AMIRA 2002; Price 2009; BSI 2012a; GARD 2014). The definition of individualised ARD parameters assessed within this study are defined within the individual test methodologies outlined in Chapter 4, sections 4.4 and 4.5.

### 3.2.7 Kinetic testing for mine waste

Kinetic testing, within the field of mine waste geochemical characterization, encompasses an array of laboratory and field-based tests tailored to simulate and monitor time-dependent reactions occurring in mine waste materials under various environmental condition (GARD 2014). The objective of these tests is to assess the potential for the onset of ARD as well as providing reaction rates of primary and secondary minerals, and subsequent metal leaching, thereby enhancing the understanding of the potential long-term environmental implications of mine waste disposal (Lapakko 1988b; EPA 1994; Lapakko 2000a; Hornberger et al. 2004; Perry et al. 2009). Common kinetic testing methods for sulfidic wastes are outlined in this section. Field based in-situ kinetic testing methods, such as lysimeters, are not considered as part of this review/study, as the research focus is on laboratory-based methods.

#### *Humidity cell tests (HCT)*

HCT's are laboratory-scale experiments that subject mine waste samples to periodic wet and dry aeration cycles under controlled humidity and temperature conditions, emulating/enhancing natural weathering processes (Morin and Hutt 2000a; Lapakko 2003; Sapsford et al. 2009a; GARD 2014; Maest and Nordstrom 2017).

Cells are typically leached on a weekly basis, with collected leachate analysed for pH, electrical conductivity (EC), metal leaching (ML) rates, total alkalinity, total acidity and various other analytes depending on the needs of the individual study (ASTM 2018a). Weekly analyte concentrations/ rates of release can then be interpreted to evaluate the waste material's leaching behaviour and geochemical development over time (Lapakko 2000b; Lapakko 2003).

Standard humidity cell tests are usually undertaken assuming unlimited oxygen availability over the course of the test (Sapsford et al. 2009a). There currently is no standardised method to interpret the data produced within HCT experiments, although suggested methods are shown in the MEND 1.20.1 manual and within the appendix of the ASTM D5744 standard (Price 2009; ASTM 2018a).

### *Column leach tests*

Bulk column leach tests usually involve placing waste material in a column and percolating water through it to simulate leaching under unsaturated or saturated conditions (Price 2009). The leachate generated within such tests is analysed for common analytes such as pH, oxygen redox potential (ORP) and leached metal concentrations. These parameters are then used to assess the waste material's potential long-term leaching behaviour (AMIRA 2002). These types of kinetic tests are commonly utilised within Australia (Parbhakar-Fox et al. 2013), with the AMIRA ARD handbook outlining a method within Appendix F (AMIRA 2002).

### *The use of HCT's in the mining industry*

Humidity cell testing (HCT) has become a widely adopted method for evaluating the acid-generating potential and leaching behaviour of wastes in the mining industry. The typical protocol involves subjecting mine waste samples to weekly humid and dry cycles, enhancing the weathering processes that occur in a natural environment (Price 2009; Sapsford et al. 2009a; GARD 2014). The fundamental purpose of a HCT is to obtain reaction rates of primary minerals though weekly rinsing (Morin and Hutt 2001).

The development of kinetic tests designed to assess the geochemical development of mine wastes and subsequent drainage quality prediction is documented back to the 1960's and continued through the 1970's. The basis of current humidity cell standards, as described in ASTM D5744−18 (ASTM 2018a) and MEND manuals (Price 2009), are based on the methods described in Sobek et al., (1978) (Sobek et al. 1978; Lapakko 2003).

Since the initial inception of the humidified and dry leaching cycles suggested in the Sobek method, various studies have refined this method to account for larger sample sizes and variable conditions to improve the applicability of the method (Morin and Hutt 2000b; Lapakko 2003; Price 2009; Sapsford et al. 2009a; EPA 2011; ASTM 2018a). Four primary refinements have been made that are reflected in most modern standardised protocols. These refinements, outlined in Morin and Hutt (2001), are as follows:

1. Sample size has increased to 1000g, compared to 200g in the Sobek method.
2. The volume of weekly rinse water has increased from 200ml to 500ml, reducing the L:S from 1:1 to 1:2.
3. Within fine grained samples, such as tailings, stirring is undertaken to ensure all particles are exposed to rinse water.
4. A perforated plate is commonly now used to suspend sample to improve the flow of humid and dry air within the humidity cell.

Although the applicability of current standardised HCT protocols has been questioned in various studies due to restrictive nature of the method, they still present a key industry wide standard for predicting primary reaction rates of soluble weathering products (Bouzahzah et al. 2010; Pieretti et al. 2022). Authors such as Kim Lapakko and Devin Sapsford have been instrumental in the assessment of the humidity cell test as an ARD predictive test method (Lapakko 2000b; Lapakko 2003; Lapakko et al. 2006; Lapakko and Antonson 2006; Sapsford et al. 2008; Sapsford et al. 2009a).

The review by Lapakko (2003) outlined the development in the HCT method and its potential applications. This review outlined issues related to the test length recommended in standard ASTM HCT standards, with 20 weeks not regarded as long enough to fully assess the ARD potential of some materials. The review suggests that cells should be undertaken until release rates of key analytes reach a ‘steady state’ for at least 5 weeks. The potential for misreporting sulfate release due to temperature variations in test methods was raised, with the author suggesting that there is the potential for alteration of testing temperatures from the standard to better reflect site-specific conditions (Lapakko 2003).

A study by Sapsford, Bowel and Williams (2009) assessed the testing protocols within humidity cells of varied design. This study included an assessment of common questions raised regarding humidity cell tests, such as test length, cell design, aeration regimes and bacterial inoculation. The authors stressed caution in the use of HCT cell results for the prediction of long-term drainage quality, with release of key analytes dependent on cell design and the exact nature of the intended weathering environment. It was argued that the usefulness of HCT cells as a predictive ARD testing method is heavily influenced by the purpose of the utilised protocol, with results

shown to vary by order of magnitudes for the same material depending on the test design (Sapsford et al. 2009a). Based on studies identified in this review, as well as existing reviews of standard HCT protocols, the potential advantages and disadvantages of current HCT standards are summarised in Table 3.

*Table 3 - Advantages and disadvantages of humidity cell testing (HCT).* (Morin and Hutt 2001; Lapakko 2003; Price 2009; Sapsford et al. 2009a; ASTM 2018a)

| Advantages | Disadvantages |
|---|---|
| Provide information on primary reaction rates of soluble weathering products. | The test is not intended to simulate the actual leaching behaviour of the material in the field or site-specific leaching conditions. |
| Standardisation and reproducible testing conditions allow comparisons of results between various mine operations and wastes. | Laboratory conditions and individual test conditions are not representative of typical humidified conditions on site. |
| Acidic producing and acid neutralising reactions can be assessed. | If secondary products do accumulate this may lead to misinterpretation of primary reaction rates |
| The main sulfide reaction rates and subsequent leachate quality can be assessed on regular intervals | The test is not designed to produce effluents that are in chemical equilibrium with the solid phase sample. |
| Multiple sample types can be tested simultaneously in multiple HCT arrays, allowing comparison of various types of waste rock/tailings that may be generated at a mining operation. | Crushing of waste rock materials may and lead to particle size distributions that vary greatly from in-situ conditions. |
| Testing apparatus can be amended to suit waste materials of differing physical characteristics. This would include broader cells for fine tailings materials. | Very high L/S ratio in order to enhance transport of weathering products (not intended to simulate field water:rock ratios), resulting in significant dilution of leachates compared to field conditions |
| | Preferential pathways may develop within the columns that can lead to heterogeneous oxidation |
| | Test length can vary depending on the mineral content of the sample assessed, this requires the initial purpose of the test to be identified. If the onset of acidity is specified as the end goal of the test, some waste materials with high carbonate content/fast reacting silicates (buffering source) and sufficient sulphides (source of acidity) may run for multi-year periods until buffering capacity of a material has been depleted. |

### 3.2.8 Kinetic testing standards for coal overburden

Significant research has been undertaken to development methods to predict mine drainage quality from coal wastes and overburden. Studies such as Perry and Brady (2009) and Brady and Hornberger (1989) have looked to develop methods to assess the ARD onset within coal wastes and predict the chemical composition of drainage produced from such wastes. The need for specific standards and methods for coal wastes is based on the abundance of carbonate minerals, compared to metal mine waste, combined with the potential for ARD onset through the oxidation of sulfide minerals (Brady and Hornberger 1989; Perry and Brady 2009).

The dissolution of abundant primary carbonates may lead to elevated $CO_2$ concentrations within the drainage system. A study of 140 coal mine discharges within the USA reported a median $pCO_2$ of 0.1 ATM (10%) within coal overburdens (Cravotta 2008). This finding led to the development of a kinetic column leach test by Perry and Brady (2009). Within this method the authors introduced 10% $CO_2$ within kinetic leach columns, filled with coal overburden, via a 6-day humidified aeration cycle. Analysis of weekly collected leachates demonstrated elevated levels of alkalinity and calcite super saturation. This study demonstrated representative drainage quality prediction, with leachates comparable to field data. The method developed in this study ultimately led to the creation of EPA standard 1627 (EPA 2011).

## 3.3 Section 3 – $CO_2$ Interactions with Sulfidic Mine Wastes

The presence of enhanced $CO_2$ concentrations within mining waste storage facilities is reviewed with specific reference to case studies and key researchers. Passive and active instances of elevated $CO_2$ pore gas compositions within waste storage facilities are considered, with specific reference to the potential implications for mine drainage quality and prediction.

Carbon sequestration is an umbrella turn used to describe various carbon dioxide removal (CDR) technologies and methodologies (USGS 2023). The CDR Primer book, published in 2021, outlines various technologies and methods that can be utilised to sequester carbon dioxide. This book was collaboratively authored by a number of the top cited authors, from academia and industry, within the field of CDR. Within this

publication an accumulation of two years of work is presented with reference to CDR technologies spanning geological, biological and ocean-based removal solutions (Wilcox et al. 2021). The glossary of this publication is used as a reference for CDR terminology used within this study.

Within this Chapter section CDR methods will be reviewed in the context of technologies that utilise mine waste materials, with a focus on carbon mineralisation and enhanced weathering (EW). A multitude of general carbon dioxide removal (CDR) /carbon capture and storage (CCS) reviews/books exist that cover various technologies within the academic literature, and therefore will not be reviewed in detail in this thesis (Reichle et al. 1997; Rackley 2017a; Sood and Vyas 2017; Kelemen et al. 2019; Raza et al. 2019; Baurov 2021; Wilberforce et al. 2021).

### 3.3.1 The potential for carbon dioxide emissions due to sulphide oxidation/ $CO_2$ gas flux in waste rock facilities (Case Studies)

Mineral reaction rates and subsequent leaching characteristics of mining waste rocks are difficult to determine and predict (Birkham et al. 2003). It is generally accepted that there is an inverse relationship between decreases in $O_2$ concentrations and $CO_2$ increases in waste rock facilities, but data sets related to internal gas compositions within waste facilities are usually limited to $O_2$, with little reference to other gases such as $CO_2$ and $N_2$ (Morin 2017).

A study by Morin (2017) outlined 17 years of pore gas data collected from the Equity Silver waste-rock pile, British Columbia. Data collection in this study produced 4000 data points for both $O_2$ and $CO_2$ within the waste rock pile, providing the largest continuous data that has been identified to date. Although this study raised questions over the complexity of the relationship between $O_2$ and $CO_2$, the study did demonstrate the expected inverse relationship over the 17-year test period. Figure 17, Figure 1-1 in Morin (2017), displays corresponding $CO_2$ and $O_2$ measurements from Equity Silver, plotted logarithmically. It can be seen in this figure that across the 5 collection points generally $CO_2$ increases as $O_2$ decreases.

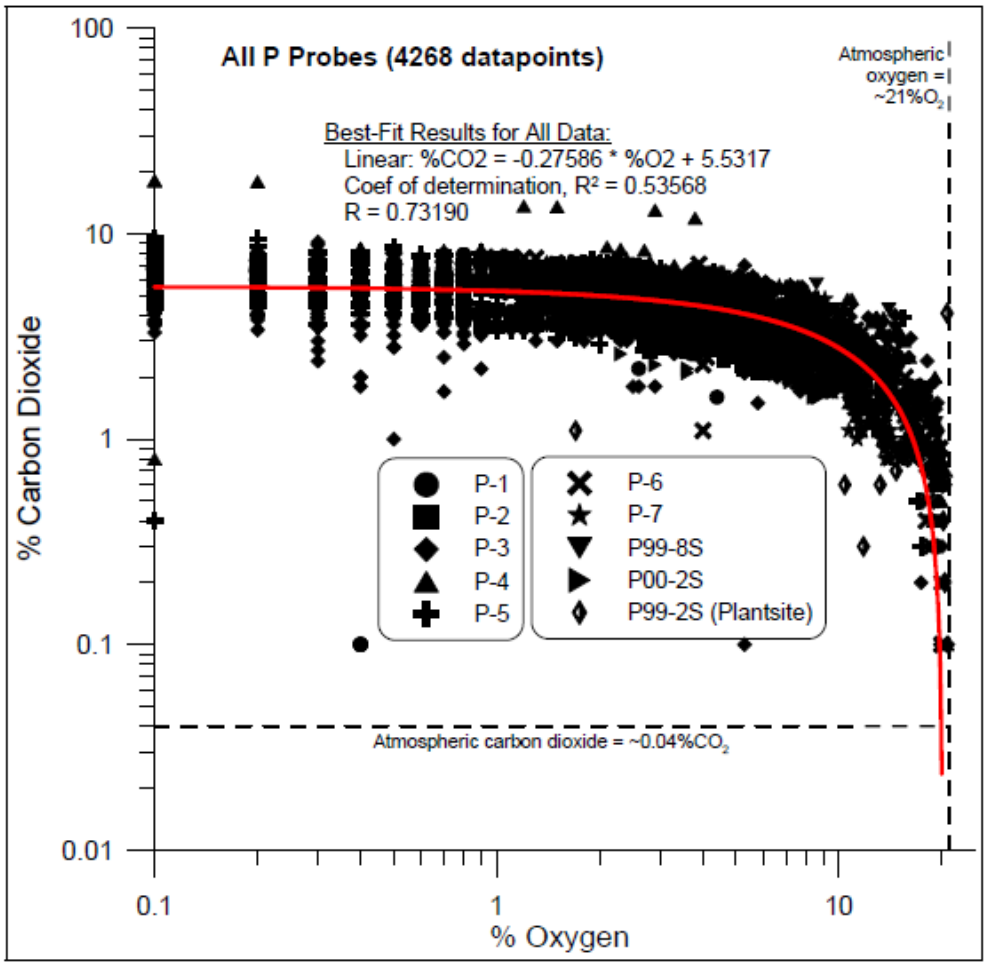


*Figure 17 - Pore-gas carbon dioxide ($CO_2$) vs oxygen ($O_2$)at locations and depths within the Equity Silver mine waste rock pile* (Morin 2017).

The trends identified in Morin (2017) are supported by multiple studies that have been carried out on waste rock facilities at the Antamina mine, Peru (Lorca et al. 2016; Vriens et al. 2018; Vriens et al. 2019a). Within these studies the spatial and temporal relationship between $CO_2$ and $O_2$ concentration within the waste rock storage facilities have been assessed. These studies build on the findings of the one published before it, all assessing multiyear data sets collected from a purpose-built waste rock facility, as well as full-scale operational waste rock piles.

Within Lorca et al., (2016) spatial and temporal changes in pore-gas compositions, temperature and moisture content were assessed. The study found that seasonally $CO_2$ and $O_2$ held intrinsic relationships, with wet season data sets displaying clear increases in $CO_2$ and decreases in $O_2$. It was shown that in during wet seasons $CO_2$ concentrations were shown to reach >2% (above the detection limit of the sensor used

in this study), well above atmospheric $CO_2$ concentrations. It was interpreted that enhanced volumetric water contents within the waste rock facility during the wet seasons restricted $O_2$ ingress, and subsequent oxidation of sulfides, and allowed ingress of $CO_2$ produced through carbonate dissolution (Lorca et al. 2016).

Although the study by Lorca et al., helped to expand the scientific understanding of waste rock internal pore gas compositions, reaction and transport limitations controlling sulfide oxidation remained poorly described at field scale (Vriens et al. 2018). The follow up studies by carried out at Antamina in 2018 and 2019 improved the experimental data set related to $CO_2$ and $O_2$ within the waste rock facilities, demonstrating clear intrinsic relationships between $CO_2$ and $O_2$ within bore hole measurements at various depths (Vriens et al. 2018; Vriens et al. 2019b). Figure 18 is amended from figure 4 of the 2018 study and shows $O_2$ and $CO_2$ content with depth with two pore gas sampling boreholes.

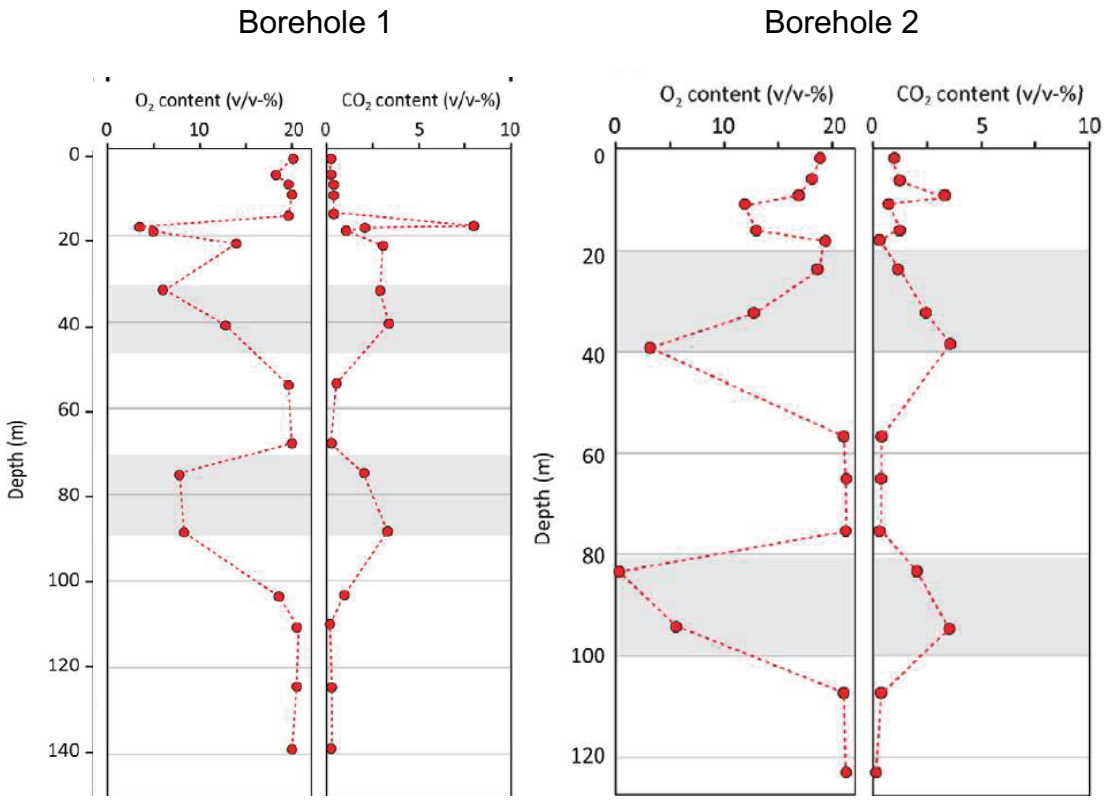


*Figure 18 - $O_2$ and $CO_2$ concentrations by depth from two boreholes within a waste rock dump trial at the Antamina mine, Peru* (Vriens et al. 2018)

Further research published by Vriens et al., (2019) assessed pore gas compositions in 5 large scale constructed waste rock piles (10,000 ± 2000$m^3$) with different types of waste rock. This study assessed different parameters that may influence spatial and temporal patterns in pore gas variations in different waste rock facilities. The study utilised three piles with coarse, low-S waste rock and two experimental piles with fine-grained, sulfide- and carbonate-rich wastes. The study demonstrated that the coarse low-S piles maintained near atmospheric levels of $CO_2$ and $O_2$, while the three sulfide and carbonate rich piles showed clear hotspots with varied temperatures, $O_2$ and $CO_2$ concentrations. $O_2$ concentrations were shown to drop to <15% while $CO_2$ concentrations measured above the detections limit of 2%. These trends were demonstrated with similar seasonal patterns as Lorca et al., (2016), with $O_2$ depletion and $CO_2$ production most pronounced during the wet seasons. This study linked the net-neutralizing potential ratio (NPR) of waste rock materials with the variations in $CO_2$, $O_2$ and temperature. It was shown that piles with similar acid production potential (AP) but differing carbonate content, and therefore neutralising potential (NP), demonstrated differing $CO_2$ concentrations. Piles with higher proportions of carbonate minerals demonstrated seasonally higher $CO_2$ production (Vriens et al. 2019a).

All four of the studies discussed in this section demonstrate a clear intrinsic relationship between sulfide oxidation and carbonate dissolution. It is noted that $O_2$ and $CO_2$ variations are likely influenced greatly within waste rock storage facilities by the oxidation of organic matter below waste materials in facilities, were underlying matter has not been managed (Birkham et al. 2003). Although the general trends observed in this study do support the outcomes demonstrated in the three studies carried out at the Antamina mine, Peru.

The importance of waste moisture content, PSD, geochemical characterisation, and permeability have been shown in temporal and spatial trends of $O_2$ and $CO_2$ (Lorca et al. 2016; Vriens et al. 2018; Vriens et al. 2019a). All of these studies outline the need for further research to understanding the mechanisms and consequences of varied pore gas compositions in sulfide rich mining wastes with both low and high relative carbonate contents.

### 3.3.2 Carbon mineralisation and enhanced weathering (EW)

Within this section the main aspects and mechanisms of carbon mineralisation and enhanced weathering of silicate minerals are outlined, with specific reference to key existing studies and authors. This section does not serve as a review of carbon mineralisation, but instead provides an overview of the key aspects and parameters that are essential for the topic in the context of this study. Carbon mineralisation has been reviewed and examined extensively within the scientific literature with multiple reviews outlining the technological readiness, basic chemistry, case pilot studies and economic feasibility as a CDR method (Herzog 2002; Fernández Bertos et al. 2004; Prigiobbe et al. 2009; Baciocchi et al. 2010; Olajire 2013; Power et al. 2013; Wilson et al. 2014b; Romanov et al. 2015; Matter et al. 2016; Rackley 2017b; Siegrist et al. 2017; Li and Hitch 2018; Mervine et al. 2018; Pogge von Strandmann et al. 2019; Hills et al. 2020; Kelemen et al. 2020; Snæbjörnsdóttir et al. 2020; Veetil and Hitch 2020; Gadikota 2021; Oskierski et al. 2021; Paulo et al. 2021a).

Key researchers that have contributed heavily to the scientific literature base on this field include authors such as Greg Dipple (University of British Columbia), Ian Power, (Trent University), Siobhan A. Wilson (University of Alberta), David Beerling (University of Sheffield), Phil Renforth (Heriot-Watt University), Peter B. Kelemen (Columbia University) and Michael Hitch (Curtin University) (Hitch et al. 2010; Renforth et al. 2011a; Hitch and Dipple 2012a; Renforth 2012; Harrison et al. 2013; Hartmann et al. 2013; Power et al. 2013; Harrison et al. 2015; Li and Hitch 2016; Montserrat et al. 2017; Beerling et al. 2018; Renforth 2019a; Beerling et al. 2020; Kelemen et al. 2020; McQueen et al. 2020; Power et al. 2020; Bullock et al. 2021; Puthiya Veetil et al. 2021; Eufrasio et al. 2022; Kantzas et al. 2022; Li et al. 2022; Lu et al. 2022). It is noted that these researchers have frequently collaborated on research projects and publications in this field, contributing greatly to the development and scientific knowledge related to enhanced weathering methods, carbon mineralisation and CDR in general.

### 3.3.3 Enhanced silicate weathering reactions

The production of carbonic acid following the dissolution of gaseous $CO_2$ into water leads to the production of acidity ($H^+$), through the dissociation of carbonic acid

($H_2CO_3$) (Stumm and Morgan 1995; Renforth et al. 2011a; Snæbjörnsdóttir et al. 2020). The acidity produced in this reaction causes the weathering of reactive silicate minerals. This is a natural process that occurs passively under atmospheric $CO_2$. Enhanced weathering (EW) refers specifically to the acceleration of this natural weathering process (Paulo et al. 2021a).

The dissolution of silicates promotes carbon mineralisation through (a) the consumption of protons, leading to the neutralisation of acidity, pushing up the pH and allowing carbonates to precipitate, and (b) the dissolution of silicates provides cations ($Mg^{2+}$ and $Ca^{2+}$) to an aqueous solution which can bond with the dissolved carbon species to form carbonates (Herzog 2002; Diedrich et al. 2014; Snæbjörnsdóttir et al. 2020). The precipitation of carbonate species is a function of pH (Hanrahan 2012a; Diedrich et al. 2014). The basic binding of MgO and CaO with $CO_2$ is represented in the binary oxide reactions shown in Equations 6 and 7 (Herzog 2002).

*Equation 6 - Binary Oxide reaction: CaO and $CO_2$*

$$\mathrm{CaO} + \mathrm{CO_2} \longrightarrow \mathrm{CaCO_3} + 179\mathrm{kJ/mole}$$

*Equation 7 - Binary Oxide reaction: MgO and $CO_2$*

$$\mathrm{MgO} + \mathrm{CO_2} \longrightarrow \mathrm{MgCO_3} + 118\mathrm{kJ/mole}$$

The precipitation of stable secondary carbonate phases is dependent on a solutions pH, which regulates the dominant dissolved carbon species (Stumm and Morgan 1995; Hanrahan 2012a). A solution with a pH <pH6 is likely to be dominated by carbonic acid, while an aqueous solution with a pH between pH 6 to pH 10 is likely dominated by bicarbonate ions. A more alkaline solution, with a pH between pH 8 to pH 14, is more likely to reach saturation in respect to carbonate phases, leading to carbonate precipitation (Manning 2001). Carbonate chemistry is discussed in more detail later in this thesis. Basic carbonation reactions involving common inosilicate and aluminosilicates minerals, including olivine, magnetite, serpentine, tremolite, enstatite and albite, are shown in Equations 8 to 13.

*Equation 8 - Olivine (Forsterite) carbonation reaction*

$$\mathrm{Mg_2SiO_4 + 2CO_2 \longrightarrow 2MgCO_3 + SiO_2}$$

*Equation 9 - Ca Clinopyroxene (Diopside) carbonation reaction*

$$\mathrm{CaMgSi_2O_6 + 2CO_2 \longrightarrow CaCO_3 + MgCO_3 + 2SiO_2}$$

*Equation 10 - Serpentine Carbonation Reaction*

$$\mathrm{Mg_3Si_2O_5(OH)_4 + 3CO_2 \longrightarrow 3MgCO_3 + 2SiO_2 + 2H_2O}$$

*Equation 11 - Tremolite Carbonation Reaction*

$$\mathrm{Ca_2Mg_5Si_8O_{22}(OH)_2 + 7CO_2 \longrightarrow 2CaCO_3 + 5MgCO_3 + 9SiO_2 + H_2O}$$

*Equation 12 - Orthopyroxene (Enstatite) Carbonation Reaction*

$$\mathrm{MgSiO_3 + CO_2 \longrightarrow MgCO_3 + SiO_2}$$

*Equation 13 - Albite (Feldspar member) Carbonation Reaction*

$$\mathrm{2Na(AlSi_3O_8) + CO_2 + 2H_2O \longrightarrow Na_2CO_3 + Al_2Si_2O_5(OH)_4 + 4SiO_2}$$

### 3.3.4 Carbon dioxide removal (CDR) and mine wastes

Mining wastes of varying compositions have been identified as a large potential feedstock for industrial scale CDR by multiple authors (Langman et al. 2014; Wilson et al. 2014b; Mervine et al. 2018; Renforth 2019b; Paulo et al. 2021a). Olivine, serpentine group, wollastonite, brucite and kimberlite rich wastes have been identified by multiple studies as waste materials that may have promise as CDR feedstocks, with the potential to offset large proportion of a mines operational emissions (Hitch and Dipple 2012a; Harrison et al. 2013; Harrison et al. 2015; Santos et al. 2015; Boschi et al. 2017; Mervine et al. 2018; Renforth 2019a; Power et al. 2020).

Carbon uptake has been measured at various mine sites as an unintended outcome of tailings management operations (Paulo et al. 2021b; Stubbs et al. 2022) The natural weathering process of silicate is typically kinetically limited by temperature and $CO_2$

availability (Power et al. 2020; Paulo et al. 2021a; Stubbs et al. 2022). Therefore, several studies have identified methods to accelerate this weathering process via enhanced weathering (Park et al. 2008; Kohler et al. 2010; Renforth 2012; Hartmann et al. 2013; Meysman and Montserrat 2017; Paulo et al. 2021a).

Studies such as Prigiobbe et al., (2009) have undertook various laboratory scale experiments to better understand the idealised conditions for the dissolution of reactive silicates. Within this study reactors were constructed to assess olivine dissolution at various temperatures and pressures. The study found that the rate of weathering is kinetically limited at standard temperature and pressure (STP) (Prigiobbe et al. 2009). Other authors have undertaken similar rate related studies specifically aimed at understanding the reaction kinetics of silicate minerals (Oelkers and Schott 1995; Harrison et al. 2013; Diedrich et al. 2014). As weathering rates are a function of surface areas studies have assessed enhancing reaction kinetics by increasing the mineral's surface area (Gerdemann et al. 2007). Multi-step approaches, where Mg, Ca and Fe cations are extracted from silicates before reacting with $CO_2$ have been undertaken (Sanna et al. 2014). These methods typically involve dissolution of silicates with an aqueous chemical, such as hydrochloric acid (HCl). The produced solution can then be regenerated via a pH swing or flushing with $CO_2$.

Several authors have reviewed the development of CDR using mining wastes via enhanced weathering and carbon mineralisation. A recent review by Veetil and Hitch (2020) outlined how the main challenges facing carbon mineralisation as a CDR include high operational expenditure (OPEX), energy input intensity and the efficiency of the mineralisation in conjunction with relatively slow reaction kinetics (Veetil and Hitch 2020). Snæbjörnsdóttir et al., (2020) argued in their review that the implementation and scalability of carbon mineralisation was still poorly defined, with most studies carried out in laboratory scale to date. This review outlined the need for advancements in carbon mineralisation methods and implementation strategies, with further assessment of the global applicability of the CDR technology, considering cost effectiveness (Snæbjörnsdóttir et al. 2020).

Table 4 outlines a summary of potential enhanced weathering methods that have been employed using suitable mining wastes in various studies.

*Table 4 - A summary of potential CDR methods that could be employed utilising mining waste materials. Based on the findings of* (Mayes et al. 2008; Renforth 2012; Mayes et al. 2018; National Academy of Sciences 2019; Renforth 2019b; Power et al. 2020).

| CDR Method | Targeted Materials | Method Details |
|---|---|---|
| Particle size reduction | Waste rock and additionally processed tailings | Most methods designed to accelerate carbonation rates will likely require mineral comminution if high degrees of carbon mineralisation efficiency is to be achieved. |
| Ex-situ mineral carbonation: direct | Tailings and waste rock | Ex-situ mineral carbonation is the direct reaction of carbon dioxide, water, and crushed silicate rock in high temperature 100 – 700°C reactors at >1-150 bar pressure of pure $CO_2$. The best conversion (up to 90%) have been demonstrated in serpentine group minerals, with the method also demonstrated using olivine and wollastonite minerals. |
| Ex-situ mineral carbonation: multi-step pH swing | All materials | Extraction of Ca and Mg from silicate minerals using acidic solutions (hydrochloric or sulphuric acid), and then reprecipitation of hydroxide or carbonate minerals with the addition of alkaline solutions and carbon dioxide. Primary limitation is the cost of recycling the extractants following each swing step. |
| Ex-situ mineral carbonation: chemical swing: ammonium sulphate | Mg silicate minerals. | Extraction of Mg from silicate minerals by solid-solid reaction at 400-500°C with ammonium sulphate to produce Mg-sulphate and ammonia gas. A low temperature reaction between condensed ammonia and Mg-sulphate produces Mg-hydroxide and ammonium sulphate. The Mg-hydroxide is amenable for reaction with $CO_2$ either rapidly in high temperature/pressure reactors or more slowly under flue gas or ambient conditions. Primary limitations are the energy requirements and the ability to efficiently recycle extractants. |
| Heap leaching – air sparging | Tailings and reprocessed waste rock. | The ambient reaction between mine waste and atmospheric $CO_2$ occurs passively in some mine tailing facilities. Only a small percentage of the material is exposed atmospheric $CO_2$ during deposition. If management practises were altered carbonation could be encouraged. There is very |

| | | |
|---|---|---|
| | | little experimental evidence testing different management protocols. Complete carbonation of feedstock materials may not be possible under these conditions but may potentially be of a high enough degree to offset mine emissions. |
| Heap leaching – microbial | All materials | Accelerated leaching of ore and waste heaps is routinely practiced in the mineral extraction sector in the beneficiation of metal resources. The same principle can be applied to extracting alkaline metals (Ca and Mg). The precipitation of carbonate minerals from the leachates has been demonstrated in small scale trials, but yet to be proven at scale. Complete carbonation may not be possible under these conditions, but potentially enough to offset mine operation emissions. |

### 3.3.5 The potential environmental implications of enhanced weathering

As it has been outlined within this review, there is a vast quantity of academic and industrial research that has assessed the potential of mining wastes as a feedstock for industrial scale CDR. To date limited studies have identified the potential environmental implications of EW on mine waste geochemical development post mine close and how this may affect the development or onset of ARD.

As it has been established within the previous sections that the EW of reactive silicate minerals within mining wastes may result in the release of metal cations into pore water (Nduagu et al. 2012; Duchesne et al. 2017; Lu et al. 2022). Although this is a key process in the carbon mineralisation process, as free Mg and Ca cations bond with bicarbonate and potentially precipitate stable carbonate, such processes are not currently considered as part of standardised regulatory frameworks for sulfidic mine waste storage. Commonly utilised sulfidic mine waste characterisation standards such as the MEND 1.20.1 manual, AMIRA handbook and GARD guide do not consider the EW of sulfidic mine wastes in the presence of above atmospheric $CO_2$ levels (AMIRA 2002; Price 2009; GARD 2014).

As previously outlined in Section 1 of this review mine waste drainage chemistry can be envisaged within three stages of reactions that involve primary and secondary minerals, see Figure 19 (Morin and Hutt 2001). The presence of enhanced $CO_2$ conditions, either passively or as part of an active EW process, within mine wastes will ultimately affect all three stages of reactions shown in this figure.

Sequestering $CO_2$ utilising mine wastes is achieved through the weathering of silicate minerals, resulting in the release of free metal cations and the subsequent precipitation of stable secondary carbonate minerals at certain pH conditions (Renforth et al. 2011a; Renforth 2012; Rackley 2017b; Renforth 2019a; Snæbjörnsdóttir et al. 2020). Through the application of this process ultimately the rate of primary mineral weathering is enhanced, while the addition of bicarbonate and precipitation of secondary stable carbonates adds buffering capacity and potentially alkalinity to a drainage system (Stumm and Morgan 1995; Morin and Hutt 2001; Lu et al. 2022).

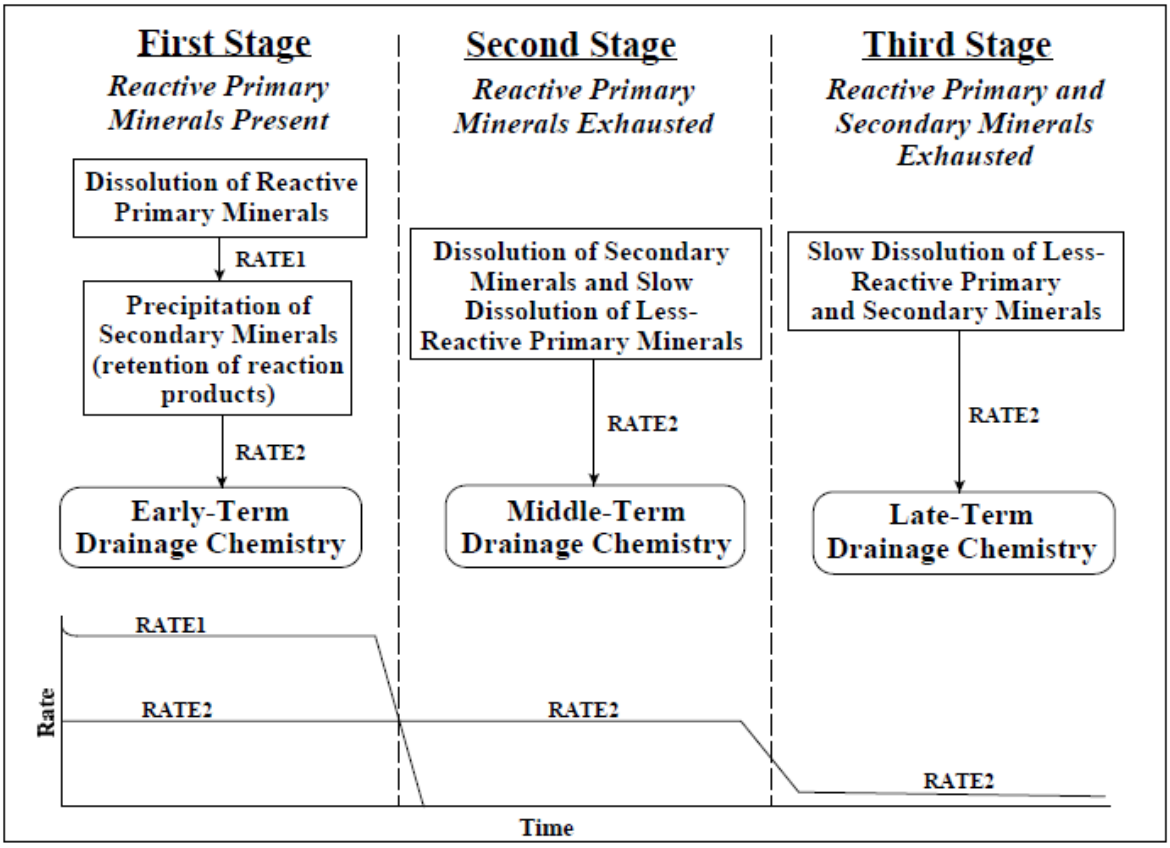


*Figure 19 - The three stages of mine drainage chemistry (Morin and Hutt 2001).*

Although the EW of silicate rich wastes as part of a CDR program may impact drainage quality, the EW of sulfidic wastes in the presence of passively enhanced $CO_2$ atmospheres also requires consideration. Within this study the terminology 'passively enhanced $CO_2$ concentrations/atmospheres' refers to temporal and seasonal variations in mining waste pore gas compositions. Such variations have been measured in active sulfidic waste rock facilities in Peru (Lorca et al. 2016; Vriens et al. 2018; Vriens et al. 2019a). The occurrence of these 'passively' variable pore gas compositions are outlined within section 3.3.1 of this review Chapter.

The impacts of enhanced $CO_2$ concentrations on coal mine waste (overburden) geochemistry and ARD onset have been considered in detail by authors such as Keith Brady and Roger Hornberger (Cravotta et al. 1994; Hornberger et al. 2004; Brady and Scheetz 2005; Perry et al. 2009; Perry and Brady 2009). The studies carried out by these authors and their various collaborating authors contributed to the creation of the EPA 1629 kinetic testing standard. This kinetic test aims to assess and predict the geochemical development of coal overburden in the presence of enhanced $CO_2$

concentrations, due to abundance and dissolution of reactive carbonate minerals within such wastes (EPA 2011).

No such standard exists for sulfidic mine wastes exposed to above atmospheric $CO_2$ concentrations, with standard kinetic tests, such as the ASTM D5744 humidity cell, assuming unlimited oxygen supply and atmospheric $CO_2$ levels (ASTM 2018a). As such, it can be theorised that sulfidic mine wastes exposed to variable pore gas compositions within waste facilities, such as those presented in Lorca et al., (2016) and Vriens et al., (2019), may be wrongly characterised in standardised kinetic and static testing protocols.

To date limited studies have actively assessed the ARD/drainage implications of EW in the presence of above atmospheric $CO_2$ concentration on sulfidic mine wastes. A study by Hamilton et al., (2018) looked to assess the fate of transition metals during passive carbonation. Within this study it was suggested that cations released during the weathering of silicates are immobilised within precipitated carbonate cements. The study outlines how the acceleration of carbon mineralisation within ultramafic wastes may reduce the environmental risks related to ARD, while the recovery of metals immobilised within carbonate cements could be of economic value (Hamilton et al. 2018a).

Researchers from the University of Quebec have published studies that have looked to assess the geochemical behaviours of ultramafic waste rock with carbon mineralisation potential (Duchesne et al. 2017; Kandji et al. 2017d; Kandji et al. 2017b). Within these studies the authors demonstrated, through leaching column testing, that the weathering of brucite rich mine wastes generated high Mg cation release and increased leachate pH readings. These studies demonstrated distinct cementing of waste materials within leaching columns post experimental protocols, with Scanning electron microscopy (SEM) and energy dispersive X-ray spectroscopy (EDS) (SEM-EDS) analysis demonstrating secondary carbonate precipitation on mineral surfaces. These studies have recommended that more kinetic testing that considers mineral carbonation reactions should be developed.

## 3.4 Section 4 – Review Conclusions

Based on the review of relevant literature within this study the following conclusions have been summarised in relation to ARD, ARD prediction, mine waste characterisation and carbon dioxide removal utilising mining wastes:

- There has to date been no tangible effort by regulatory or scientific bodies to create standards to assess the potential environmental implications of CDR, enhanced weathering, mineral carbonation using mining wastes.
- Research that has been carried out in this area has been limited in scope and has concentrated on the potential leaching of trace metals as a result of the EW of reactive silicates (Kandji et al. 2017a; Hamilton et al. 2018a).
- Current kinetic testing standards used within the mining industry, such as humidity cell tests (HCT), assume unlimited $O_2$ supply (ASTM 2018a). Studies conducted at various operational mining operations have demonstrated seasonally variable internal gas compositions within mining wastes storage facilities (Lorca et al. 2016; Vriens et al. 2018; Vriens et al. 2019a). This suggests that current kinetic testing standards, that are a regulatory requirement in many countries, may produce results that are neither representative nor site-specific. The pore gas assumptions within kinetic standards such as ASTM- D5744 may lead to wrongful estimations of sulfide oxidation and subsequent ARD onset.
- Various researchers have suggested the need for more site specific and targeted waste geochemical characterisation protocols that will allow a better estimation of long term mine drainage quality and allow for better mine closure, management, and rehabilitation (Stewart et al. 2006; Parbhakar-Fox and Lottermoser 2015; Karlsson 2022).
- Researchers and mining operators are actively assessing the potential for large-scale carbon dioxide removal (CDR) utilising mining wastes. Studies have shown physical, geochemical and mineralogical changes to waste composition as a result of both active and passive sequestration (Power et al. 2013; Wilson et al. 2014a; Harrison et al. 2015; Mervine et al. 2018; Kelemen et al. 2020; McQueen et al. 2020).

- Although ARD characterisation, classification and prediction are established research fields, the influence of EW of mine wastes in scalable CDR protocols is currently not considered in a demonstrated manor within the scientific research community.
- It is widely accepted that kinetic and static testing protocols often produce results that vary greatly from comparable results generated in situ (Morin and Hutt 1998; Morin and Hutt 2001). There is therefore the need for more site-specific testing procedures that can increase the reliability of laboratory based assessments of ARD to predict long-term mining waste drainage quality and waste geochemical evolution.
- Standards have been developed to assess enhanced $CO_2$ concentration in coal wastes, with EPA 1627 suggesting the application of 10% $CO_2$ within kinetic test aeration cycles (EPA 2011). It is theorised by the author that this consideration could be applied to sulfidic wastes, such as those demonstrated in Lorca et al., (2016), to provide a more site-specific assessment of ARD potential.

# Chapter 4 - Research Methodology

## Introduction

Within this Chapter the methodologies and testing standards utilised in this research project are outlined in detail. The key objective of the experimental work carried out was to assess the potential implications of enhanced $CO_2$ concentrations on mine waste geochemical development, metal leaching (ML) and physical characterisation.

This was achieved through implementation of $CO_2$ enhanced kinetic tests in conjunction with a static testing program. Kinetic tests undertaken were amended humidity cell tests (HCT), following the general protocols outlined within the ASTM standard commonly used within the mining industry (ASTM 2018a). Altering the ASTM HCT protocol, integrating enhanced $CO_2$ concentrations and reducing testing temperatures, allows an assessment of test suitability in predicting leachate quality from mining wastes exposed to pore gas/temporal conditions that vary from standard atmospheric conditions. This testing modification was made in line with the methods outlined in the EPA 1627 standard (EPA 2011).

A sample characterisation and static testing program was carried out to assess initial waste characteristics as well as any potential changes in wastes after planned experimental protocols. The waste characterisation protocols used within this research project are described in this Chapter with reference to the specific testing standards that have been utilised. Static testing used to characterise waste materials in this study followed the protocols utilised at the Geochemic Ltd laboratory. This study's objectives were achieved through assessment and investigation of the following criteria:

- The effect of differing gas compositions on cell metal leaching (ML) rates.
- The effect of differing testing temperatures on cell elemental leaching rates.
- The repeatability of leaching characteristics between triplicate cells.
- An assessment of pre and post HCT waste rock characteristics (geochemical, physical and mineralogical).

## 4.1 Research Design and Testing Parameters

Figure 20 outlines the key aspects of this project and the research rationale. This figure outlines the key aims, implementation strategies, intended outcomes and potential wider implications of this project.

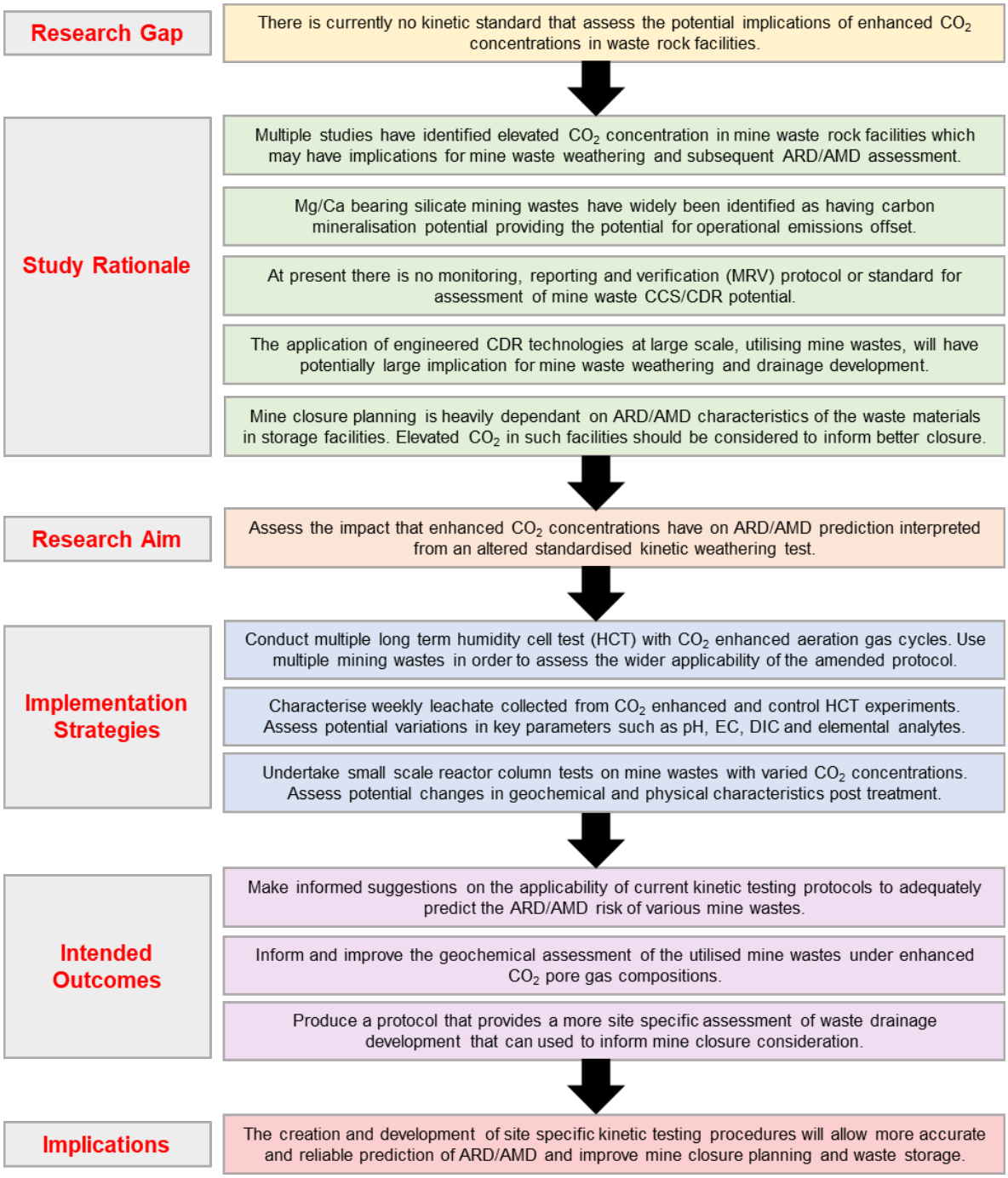


*Figure 20 - Research design flow diagram*

The methodologies utilised within this research project can be categorised into 5 main categories, as shown in Figure 21. Each of the methods and standard utilised within each of these categories is outlined in detail within this Chapter.

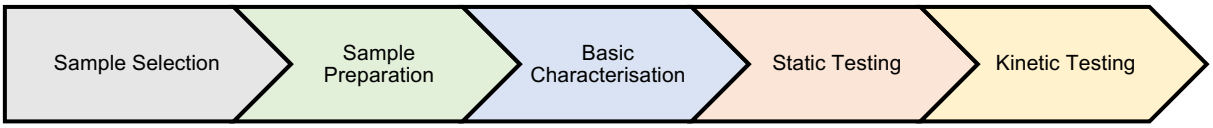


*Figure 21 - Research methodology categories*

The completion of tests and procedures within the 5 main method categories will result in data production. The parameters this data represents can be reported in a multitude of formats depending on the intended test output. Within this research project the following 3 parameter reporting types are used in most cases to describe and quantify amounts:

- **Concentrations** – Concentrations are used to quantify the amount of a parameter relative to the total amount of material tested. They can be expressed as a percentage of the parameter relative to the total, a weight relative to the weight of sample or a weight relative to the volume of liquid the sample was suspended in.
- **Reactivity equivalents** – these are generally used for parameters such as acid generation potential (AP) or acid neutralising potential (NP). Reactivity equivalents equate the reactivity of the material to that of an idealised compound, such as $H_2SO_4$ or $CaCO_3$.
- **Loads and Rates** – loads represent the total amount of a tested parameter released into a solution, as weight. This is calculated as the concentration (mg/L or µg/L) of a element or species multiplied by the volume of solution recovered per kg of sample. Within kinetic testing the load will be expressed in the context of release rates per unit time e.g. mg/kg/year or mg/kg/week.

Specific references to reported units for parameters in individual testing methods are outlined in the following sections of this thesis.

## 4.2 Preliminary Sample Selection and Preparation

Within these sections the sample selection and field sampling methodologies utilised are outlined.

### 4.2.1 Field sampling

Field sampling was not carried out by the author and was undertaken by specific operational staff, consultants, and operators prior to this research study. Information available on the specific field sampling techniques used in the acquisition of wastes from the Kevitsa or Aitik mining operations in this study has been outlined.

Waste rock sample collection from the Kevitsa and Aitik mining operations was undertaken by O'Kane consultants in 2017 and 2018, respectively. Kevitsa waste rock samples were collected through 4 sonic drill boreholes with depths ranging between 50-64.5 metres. Aitik waste rock materials were collected via 6 sonic drill boreholes with depths ranging from 40-70 metres. Sonic drilling was utilised for all boreholes at both mining operations. It is noted within the factual site drilling reports that as little water as possible was used during the drilling process to minimise changes in waste rock geochemistry (O'Kane Consultants Ltd 2018a; O'Kane Consultants Ltd 2018b).

Samples were provided to Geochemic Ltd on behalf of MEM consultants and Boliden AB for the purposes of waste characterisation and research within this study.

### 4.2.2 Sample preparation

Within this section sample preparation methods utilised within this study are outlined with specific reference to relevant standards and guidelines. Any amendments to suggested standards are discussed. Sample preparation, identification, sub-sampling and storage was undertaken in accordance with guidance related to extractive waste outline within the CEN/TR 16365:2012 standard (BSI 2012b).

### 4.2.3 Waste rock composite creation overview

Due to volume of homogeneous waste rock required to undertake kinetic testing, characterisation, and static testing a composite waste rock was created from individual waste material samples from each operation. At least ~15kg of composite waste rock

was required for each site, although composites of >50kg total were created in order to provide ample materials for re-runs and triplicate analysis.

Waste rock materials from both operations had been pre-screened for bulk particle sizes, with materials separated into <22 mm fractions and >22mm fraction (coarse rejects). >22 mm particle size fractions were selected for use in this study. Composite component samples were crushed utilising a jaw crusher to 85% passing a <6.3mm screen before being subsampled. Following subsampling individual samples were combined and homogenised through end over end drum tumbling. A simple homogeneity check of the created waste rock composites was undertaken through elemental analysis via energy dispersive X-ray fluorescence (ED-XRF) of composite splits. Information on specific subsampling, crushing, splitting and milling methods are outlined in sections 4.2.4 – 4.2.10 of this Chapter.

### 4.2.4 Subsampling procedures

At every stage of sample preparation subsampling of split and crushed materials was undertaken. Maintained samples were stored for future reference or re-evaluation. During splitting procedures, outlined in following sections, typically 1 split from each splitting round was maintained for reference and utilised for homogeneity checks and characterisation of key parameters measurements. Subsampling and storage was carried out in accordance with CEN/TR 16365:2012 sections 3.2-3.3.3 (BSI 2012b).

### 4.2.5 Size reduction procedures

Size reduction was carried out by either jaw crushing to 85% passing 6.3 mm or ball milling depending on the intended testing required. All utilised and characterised samples were crushed to <6.3mm before, with subsamples ball milled for selective characterisation tests. Prior to size reduction samples were dried at 60$^{o}$C to remove residual moisture.

### 4.2.6 Jaw crushing procedures

Primary size reduction was undertaken by mechanical comminution using a jaw crusher. The jaw crusher was set to a 6.3mm aperture. Individual samples that were chosen for use in either Kevitsa or Aitik waste rock composites were passed through

the jaw crusher. Multiple passes of material through the crusher were undertaken until 85% of materials were passing a 6.3 mm aperture sieve compliant with BS EN ISO 17892-4:2016 (BSI 2016b).

### 4.2.7 Ball milling procedures

Some of the characterisation and static testing carried out within this research study required further size reduction, this included acid base accounting (ABA), net acid generation (NAG) and acid buffering characterisation curve (ABCC) testing. In accordance with the size reduction needed subsamples from the initial pre composite samples and the combined composites were pulverised using a ball mill. This was carried out to reduce sample particle sizes to 95% <0.125mm (Price 2009). Some standards utilised, such as the AMIRA appendix G ABCC test, suggest pulverisation of samples to <75 µm (AMIRA 2002). Within this research project all pulverised samples were milled to 95% <0.125mm for consistency in reporting and interpretation.

### 4.2.8 Sample splitting procedures

Splitting of materials at various points of sample preparation and HCT decommissioning was necessary to reduce sample mass for use in kinetic testing as well as providing representative sample splits for characterisation and static testing which require less sample mass. Two distinct methods of sample splitting were utilised within this study: cone and quartering and riffle splitting (various riffle sizes depending on starting mass). A sample splitting and subsampling program was undertaken in line with the CEN/TR 16365:2012 and BS EN 932-2:1999 standards (BSI 2012b).

### 4.2.9 Cone and quartering procedures

Cone and quartering were used to split the large composite samples created following the crushing, combination, and homogenisation of individual samples. This was undertaken to representatively split the initial large composite volumes (~50-70 kg) into smaller secondary subsamples, which could then be riffle split down to required masses for testing. This was carried out following section 8.7 of the MEND 1.20.1 manual (Price 2009).

### 4.2.10 Riffle box splitting procedures

Following composite waste rock mass reduction further splitting was undertaken in the form of riffle box splitting, see Figure 22. Riffle box splitting was undertaken in 2 distinct stages following a sampling plan. Stage 1 involved the splitting of composite samples to 1kg splits for use in kinetic testing. This was undertaken with a larger riffle aperture of at least 3 times the largest particle size, following the CEN/TR 15310-3:2006 standard. Each composite was split into at least 12 distinct 1 kg splits. 9 splits of ~1kg mass from each operation were then utilised for kinetic testing, with 3 splits of ~1 kg mass maintained for characterisation and static testing. Stage 2 of riffling box splitting was undertaken in accordance with BS EN 932-2:1999. This stage involved the splitting of retained ~1kg masses of composite materials down to ~200g.

This procedure was carried out pre kinetic testing on maintained secondary samples from each composite as well as post kinetic testing on retained residues. 200g splits were checked for homogeneity through elemental characterisation. Each composite and post HCT residues were split to at least maintain two 200g splits. One split was used in test work requiring non pulverised materials, while the other was ball milled for testing that required pulverised materials of <0.125mm.

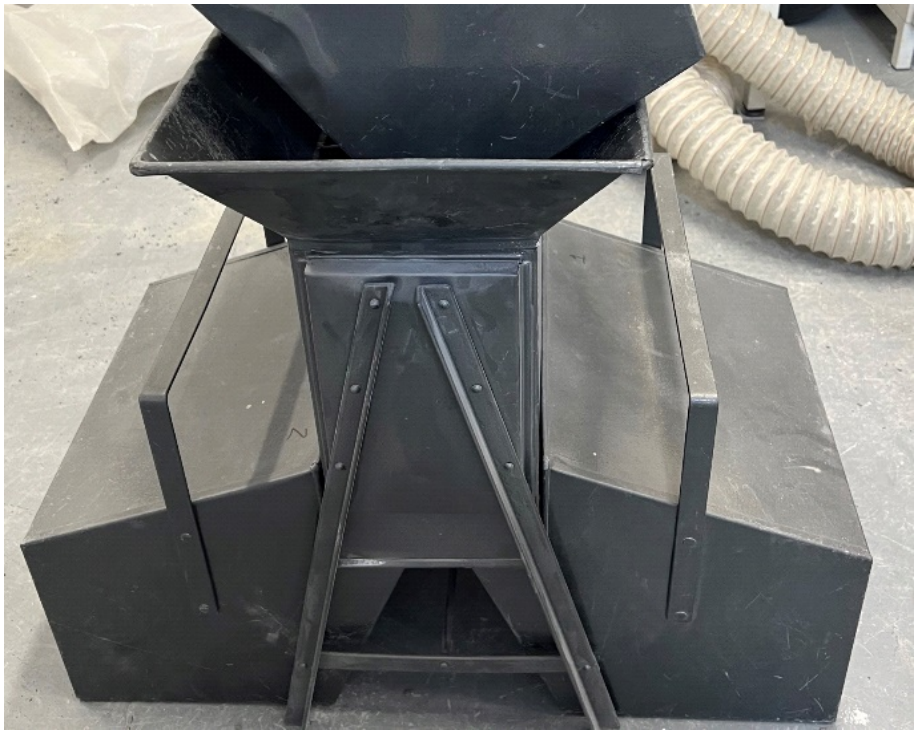

*Figure 22 - Riffle box splitter used in stage 1 splitting.*

## 4.3 Basic Material Characterisation

Following sample preparation, a series of basic characterisation methods were employed to assess key characteristics of composite materials from Kevitsa and Aitik. The characterisation program undertaken in this research study was carried out on pre and post kinetic testing composite materials from both operations, allowing an assessment of any changes to material characteristics due to testing regimes.

### 4.3.1 Visual material description procedures

At various points throughout this research projects descriptive material observations have been made in line with section 6 of British standard BS 5930:2015. Photographs of materials at set points were taken for comparative characterisation of material properties. This included period photos taken on individual HCT cell on a bi-weekly basis. This allowed for description of any visual physiological changes to materials as a result of testing protocols.

### 4.3.2 Moisture content and specific gravity procedures

Basic geotechnical characteristics were measured from all materials utilised within this study. This included an assessment of material moisture content/ water content and specific gravity ($G_s$). Moisture content was carried out via drying of samples at 105$^{O}$C. The weight of sample was measured pre and post drying which allowed calculation of total water content in accordance with BS 1377-2:2022 section 4 (BSI 2022). Specific gravity ($G_s$) was calculated for materials using the fluid pycnometer method outlined in BS EN ISO 17892-3:2015 (BSI 2015).

### 4.3.3 Particle size distribution (PSD) procedures

Material PSD was assessed through direct gravimetric separation of particle fractions through sieving. PSD analysis was carried out in accordance with the sieving and sedimentation standard, BS ISO 11277:2020. PSD is reported in the form of a PSD curve, which reflects the relative percentage of an initial material mass that passes a specific sieve size aperture. Within this study 6.3mm, 4mm, 2.36mm, 2mm, 1mm, 500 µm, 250 µm, 125 µm and 63 µm sieves were used. Material was passed through these sieves arranged in a shaking stack. After materials were passed through the sieve stack the individual sieves were weighed and cumulative percentage passing was

calculated relative to the material finer than the specific sieve size. The median size distribution value ($_d$50) is then calculated using the generated PSD curves.

### 4.3.4 Mineralogical characterisation procedures

Mineralogical characterisation was carried out to assess the initial mineralogical characteristics of waste materials used in this study, as well as any potential changes in bulk mineralogy after kinetic testing protocols. Waste rock samples from both operations were analysed at the Petrolab Ltd laboratory, an independent private mineralogy and petrography laboratory, based in Cornwall, United Kingdom. Bulk mineralogical composition was analysed via scanning electron microscopy-energy dispersive X-ray (SEM-EDX) analysis. Bulk mineral abundance is reported as the weight % of the sample that has been analysed. A detailed petrographic examination by optical microscopy was undertaken. The following mineralogical and petrographic analysis was carried out in this study:

- The submitted samples were examined and photographed as received and using a Nikon SMZ-U stereoscopic microscope with fibre optic illuminator. A macroscopic description based on visual and manual identification of the material characteristics at the scale of the sample provided was recorded.
- A petrographic thin section was prepared for selected samples. The sub sample used for thin section preparation was first impregnated with epoxy resin containing a yellow dye to aid identification of voids and cracks. A high resolution, low magnification digital image of each thin section was obtained using a film scanner.
- The thin sections were examined by conventional transmitted and reflected light polarising microscopy using a Nikon polarising microscope. A visual estimate of relative phase abundance was made. Digital photomicrographs were taken using a high-resolution digital camera attached to the trinocular head of the microscope.

Sample selection for mineralogic and petrographic analysis was limited by project budgets. As such a single pre-experimental subsample was analysed for each of the study locations, with one sample from each post HCT triplicate sets chosen for post-experimental analysis.

### 4.3.5 Elemental characterisation procedures

Elemental characterisation was carried out on all recovered post HCT materials after decommissioning as well as on pre HCT composite materials. This analysis was also used to check the homogeneity of split materials generated within the sample preparation stage of this research study. Analysis was carried out via a Panalytical MiniPal 4 DY683 energy-dispersive x-ray fluorescence (ED-XRF) at the Geochemic Ltd laboratory. Milled fractions of materials were loaded into SciMed 35mm XRF cup lined with TF-240 4µm gauge polypropylene x-ray film. Loaded samples were then loaded into the ED-XRF before the analysis chamber was flooded with helium to allow accurate measurement of light elements. Analysis was undertaken in line with BS ISO 18227:2014 (BSI 2014).

### 4.3.6 $CO_2$ sequestration capacity estimations

In order to assess the theoretical maximal enhanced weathering potential of waste materials used within this research study an adjusted version of the Steinour equation devised in Gunning, Hills and Carey (2010) was employed. The version of the equation presented in Equation 14 is based on the adjusted equation used in Renforth (2019). The equation uses bulk elemental oxide composition to estimate the maximum carbon capture potential (CCP), via enhanced weathering, of a waste material (Gunning et al. 2010). Elemental abundance data produced through ED-XRF analysis was used for these calculations.

*Equation 14 - Adjusted Steinour Maximum CCP Equation*

$$\left(\frac{1000}{100}\right)\cdot\left(\frac{CaO}{M_{W\ (CaO)}}+\frac{MgO}{M_{W\ (MgO)}}+\frac{Na_2O}{M_{W\ (Na_2O)}}+\frac{K_2O}{M_{W\ (K_2O)}}-\frac{SO_4}{M_{W\ (SO_4)}}-\frac{P_2O_5}{M_{W\ (P_2O_5)}}\right)\cdot M_{W\ (CO_2)}=CCP\left(\frac{kg_{CO_2}}{tonne_{(Mine\ waste)}}\right)$$

*Where $M_W$ (Oxide) is the molecular weight of the specific oxide*

The adjusted equation utilises elemental composition to Identify maximum carbon capture potential (CCP) based solely on bulk elemental analysis. The calculation output is in the form of kg of $CO_2$ per tonne of waste material and represents the quantitative hypothetical potential of the material to capture carbon dioxide as bicarbonate or carbonate. It must be noted that this equation does not take into consideration variables that effect carbonation and carbonation rates such as

temperature, known reaction rates, pressure, moisture content and PSD. The equation considers the presence of elemental sulphur (S) and phosphorus (P) as having a reducing effect on overall theoretical potential. This is due to two distinct rationales: (1) their dissolution has no implicit reaction with $CO_2$ directly and (2) they may become acid compounds, producing acidity which has implications on the carbonate system as $CO_2$ may be produced (Renforth 2019a).

## 4.4 Static Testing

Geochemical characterisation was carried out following a series of static testing protocols. This characterisation was carried out pre and post kinetic testing, in order to evaluate potential differentiations in sample geochemical development due to variable kinetic testing conditions. Table 5 outlines the static testing undertaken and the relevant testing standards that have been employed. Individual testing procedures are outlined in more detail later in this Chapter, with specific reference to any variations to standardised testing protocols.

*Table 5 - Static testing protocols and relevant standard references*

| Static Test | Standard Protocol | Reference |
|---|---|---|
| Acid Base Accounting (ABA) | BS EN 15875:2011 | (BSI 2012a) |
| Net Acid Generation (NAG) | AMIRA Handbook | (AMIRA 2002) |
| Acid Buffering Characterisation Curve (ABCC) | AMIRA Handbook | (AMIRA 2002) |
| Paste pH and EC | MEND Manual 1.20.1 | (Price 2009) |
| 24-Hour 2:1 (L:S) Leach test | EN 12457-1 | (BSI 2002a) |
| Total Carbon | EN 13137:2001 | (BSI 2001) |
| Total Sulfur | EN 14582:2016 | (BSI 2016a) |

Table 6 provides overview summaries of the static testing procedures undertaken within this research study with reference to specific sub-tests that were carried out within the main procedures used in the geochemical characterisation of waste rock materials.

*Table 6 - Static testing procedure summaries*

| Test | Sub-tests | Main Procedures |
|---|---|---|
| Total Carbon Analysis | N/A | Total carbon and sulfur analysis carried out using a Perkin and Elmer 2400 series II CHNS/O analyser. |
| 24-Hour 2:1 (L:S) Leach test | Initial Leach | Non-Pulverised, dried, column samples (50g) were leached with 100ml of de-ionised water (1:2) for 24 hours using a sample tumbler. Following the 24-hour period samples were filtered. |
| | pH and EC | A fraction (20ml) of the filtered sample was analysed for pH and EC using a Hach HQ30d flexi pH/EC meter. Samples were analysed 3 times each for data QA/QC purposes. |
| | DIC | Dissolved inorganic carbon (DIC) was analysed using a Sievers 820 portable TOC analyser. Approximately 10ml of sample was required. |
| | ICP-OES | 40ml of syringe filtered sample leachate was sent for ICP-OES aqueous elemental analysis at Cardiff Universities CLEER laboratory. The instrument used was a Perkin Elmer Optima 2100 DV ICP-OES. |
| Paste pH and EC | N/A | A 1:1 ratio of column pulverised waste rock material and de-ionised water was mixed by hand for 15 seconds. The solution was left to stand for 15 minutes and then analysed for pH and EC using a Hach HQ30d flexi pH/EC meter. |
| Acid buffering characterisation curve (ABCC) | N/A | Used a Metrohm 718 STAT Titrando titrator. Each sample was titrated with HCL while pH was monitored continuously. The buffering curve that is produced provides an indication of what proportion of the sample ANC is readily available for acid neutralising. |
| Acid Base Accounting (ABA) | N/A | ABA / acid neutralising capacity (ANC) testing was carried out in accordance with EN 15875. Involved the titration of a sample to pH 2.0 and pH 8.3 a provides information required for the calculation of ARD parameters including NP, AP/MPA, NNP and NPR. These parameters are used in the initial ARD classification of a material, in conjunction with other parameters, such as single addition NAG pH. |

### 4.4.1 Total carbon and sulfur procedures

Total C and S analysis was carried out in line with EN 13137:2001 and EN 14582:2016 (BSI 2001; BSI 2016a). Analysis was carried out on pulverised materials utilising combustion within a LECO induction furnace. Sample materials were combined with

a combustion catalyst material before being combusted at 1450ºC. Blanking and calibration was undertaken with LECO high and low C/S standards with samples ran in triplicate to assess repeatability of measurements. Analytical drift was assessed through the assessment of a blank and reference sample after every 10$^{th}$ sample combustion. Carbon and sulfur analysis is reported as total C% and total S%, representing the corresponding weight percentage of C/S.

### 4.4.2 Acid base accounting (ABA) testing procedures and calculations

Acid neutralising capacity (ANC) / Acid base accounting (ABA) tests were carried out on Kevitsa and Aitik materials pre and post HCT protocols to assess potential changes to acid base accounting (ABA) characteristics post kinetic testing. ABA testing has been carried out in accordance with the BS EN 15875:2011 standard (BSI 2012a). Terms and units commonly associated with ABA analysis can vary between northern hemisphere and southern hemisphere standards. Terms used within the MEND 1.20.1 manual, Amira AMD handbook and BS EN 15875:2011 are in some cases interchangeable (AMIRA 2002; Price 2009; BSI 2012a; GARD 2014). The test work carried out within this study follows European standard terminology, with the exception of AP which has been described as maximum potential acidity (MPA) within this study to avoid confusion with AP consumption calculations, discussed later in this section.

ABA parameters measured/calculated included neutralising potential (NP), carbonate NP ($CO_3$-NP), maximum potential acidity (MPA), net neutralisation potential (NNP) and neutralisation potential ratio (NPR). All of these ABA parameters, except NPR, are calculated in the units kg $CaCO_3$ eq /t. NPR is calculated as a ratio. Determination of a materials NP and AP/MPA allows for initial ARD classification screening of a material.

The parameters measured in ABA analysis allow for the assessment of a materials potential to produce acidic drainage, with the classifications such as potentially acid forming (PAF) or non-acid forming (NAF) commonly used. ABA parameters are often interpreted in line with results generated from other static tests as well as long term kinetic testing (Nordstrom and Alpers 1999; Sapsford et al. 2008; Price 2009; Sapsford et al. 2009a; Parbhakar-Fox and Lottermoser 2015).

### *ABA / ANC testing overview*

ABA testing is carried out on materials with a particle size of 95% <0.125 mm, therefore testing materials were pulverised with a ball mill before testing in this study. Utilised materials were dried at 40°C to remove residual moisture, without the onset of unwanted acid generating reactions. ANC/ABA testing methods outlined within BS EN 15875:2011, MEND 1.20.1 and the AMIRA ARD handbook are based on modified version of the Sobek method (Sobek et al. 1978). The ABA NP / ANC measurements are summarised as follows:

- 2.00g of pulverised material is measured into a beaker/test vessel.
- 90ml (+/- 5ml) of de-ionised water is added to the beaker and mixing is commenced.
- Sample is stirred for 15 minutes on a mechanical stirring plate before the pH is measured (pH at t = 0 hours). If pH at t = 0 is > pH 2 the test cannot be undertaken.
- After 15 minutes a predetermined volume and concentration of HCl is added to the sample based on carbonate rating (see Table 1 of BS EN 15875:2011).
- After initial HCl addition at t = 0 the sample is stirred continuously for 22 hours.
- At t = 22 hours the pH is measured (pH at t = 22). If the pH is below pH 2 the test is ended and initial HCl addition volume is reassessed.
- If the t = 22 pH is above pH 2.5 the sample is titrated to ~pH 2.0 with HCl.
- At t = 24 hours terminate the test, de-ionised water is added to the beaker/vessel to bring the total volume to ~125ml. Measure the pH and continue the test if within the desired pH range of pH 2.0 – pH 2.5. The test is decommissioned if outside this range.
- After additional de-ionised water addition, the sample is back titrated to pH 8.3 using NaOH. The volume of NaOH used is recorded.
- Titrations to pH 2.0 and back titrations to pH 8.3 are undertaken on an automated Metrohm Titrando titration system.

### *ABA parameter calculations*

Calculations and equations used for ABA testing within this research study follow the guidance outlined in BS EN 15875:2011, with explanations of relevant formulas outlined within Appendix D of this standard document (BSI 2012a).

### *Maximum potential acidity (MPA) calculations*

MPA/AP was calculated based on the total S% content of the test material, assuming all sulfur appear in the form of pyrite. MPA was calculated as $H^+$ (mol/kg) and kg $CaCO_3$ eq /t following Equations 15 and 16 respectively.

*Equation 15 - MPA calculation expressed as $H^+$ (mol/kg)*

$$MPA = 0.625 \times ws$$

Where:

MPA = Maximum Potential Acidity

0.625 = Conversion Factor (Assuming 1 mol of sulfur in pyrite creates 2 moles of $H^+$)

ws = Total S Content of Mass Fraction as a Percent (%)

*Equation 16 - MPA calculation expressed as kg $CaCO_3$ eq /t*

$$MPA = 31.25 \times ws$$

Where:

MPA = Maximum Potential Acidity

0.625 = Conversion Factor (ratio of molecular masses of $CaCO_3$ (100 g/mol) and S (32 g/mol))

ws = Total S Content of Mass Fraction as a Percent (%)

MPA assumes all sulfur occurs as pyrite as follows (AMIRA 2002):

$FeS_2 + 15/4\ O_2 + 7/2\ H_2O \Longrightarrow Fe(OH)_3 + 2H_2SO_4$

### *Neutralising potential (NP) calculations*

NP was calculated as both NP and Carbonate NP. Carbonate NP ($CO_3$-NP) has been calculated using measurements of total C% for each sample and represents the portion of neutralising potential (NP) available through weathering of carbonate sources in the presence of acidity (Price 2009) .

The calculation of $CO_3$-NP is outlined in Equation 17. NP was calculated using the titration data produced as part of the ANC test procedure and is calculated through use of the volumes and concentrations of HCl and NaOH used in titration and back titration to pH 2 and pH 8.3. The calculation of NP is outlined in Equation 18. Both NP and $CO_3$-NP are expressed as kg $CaCO_3$ eq /t.

*Equation 17 - Calculation of carbonate NP*

$$Carbonate\ NP\ (kg\ CaO_3eq/t) = (Total\ C\%)\ \times \left(\frac{100.09}{12.01}\right) \times 10$$

Where:

NP = Neutralising Potential

C% = Total Carbon percentage (%)

100.09 = Molar mass of $CaCO_3$

12.01 = Atomic mass of C

*Equation 18 - Calculation of neutralising potential (NP)*

$$NP\ (kg\ CaO_3eq/t) = 50\ \times \frac{c(HCl) \times\ V_A(HCl) - c(NaOH) \times V_B(NaOH)}{M_d}$$

Where:

NP = Neutralising potential

c(HCl) = The concentration of HCl in mol/l;

$V_A$(HCl) = The volume of HCl added (VA, t=0 + VA, t=22h) in ml;

c(NaOH) = The concentration of NaOH in mol/l;

$V_B$(NaOH) = The volume of NaOH used in back titration in ml;

$M_d$ = The dry mass of the test portion expressed in grams (g).

All NP is assumed to react like calcite in acidic conditions as follows:

$CaCO_3 + 2H+ \rightarrow Ca^{2+} + H_2CO_3^0$

### *Neutralisation potential ratio and net neutralisation potential calculations*

Neutralisation potential ratio (NPR) is used to anticipate if a material has enough neutralising capacity to neutralise potentially released acidity based on the results of MPA and NP calculations and measurements. An NPR <1 suggests a material does not contain enough neutralisation potential sources to adequately buffer potentially realised acidity (AMIRA 2002; Price 2009; BSI 2012a). NPR was calculated using Equation 19.

*Equation 19 - Calculation of neutralisation potential ratio (NPR)*

$$NPR = \frac{NP}{MPA}$$

Where:

$\mathrm{NPR} = \text{Neutralisation potential ratio}$

$\mathrm{NP} = \text{Neutralising potential}$

$\mathrm{MPA} = \text{Maximum potential acidity}$

Net neutralisation potential (NNP) represents the neutralisation potential (NP) minus the maximum potential acidity (MPA) and is expressed as kg $CaCO_3$ eq /t. An NNP value >0 may indicate a material is potentially acidy forming (PAF), while a NNP value <0 may indicate a material a material is non-acid forming (NAF). NNP requires quantification in line with other ABA parameters to be effectively used in ARD classification (Price 2009). NNP was calculated following Equation 20.

*Equation 20 - Calculation of net neutralisation potential (NNP)*

$$NNP = NP - MPA$$

Where:

$\mathrm{NNP} = \text{Net neutralisation potential}$

$\mathrm{NP} = \text{Neutralising potential}$

$\mathrm{MPA} = \text{Maximum potential acidity}$

### 4.4.3 Net acid generation test procedures

Single addition net acid generation (NAG) tests were carried out with line with guidance outlined in the AMIRA ARD handbook (AMIRA 2002). Single addition NAG tests are typically suitable for materials with a total S% of <1%. Within NAG testing a sample is reacted with hydrogen peroxide ($H_2O_2$) to rapidly oxidise sulfide minerals. During a NAG test acid generation and neutralisation reactions occur concurrently and therefore represents the net amount of acid generated by a material. NAG tests output 2 parameters in the form of total NAG estimation and NAG pH. Acidity is assessed through titration to pH 4.5 and pH 7. NAG pH is measured post boiling step and is used in conjunction with NNP values to classify a materials ARD potential. Simplified procedures are outlined as follows:

- 250 ml of 30% $H_2O_2$ is added to 2.50 g of material.
- Hydrogen peroxide is allowed to react overnight with the sample, while the solution is continuously stirred on a magnetic stirring plate.
- The following day the sample solution is gently heated on a boiling plate to accelerate oxidation of remaining sulfides.
- When sample reaches its boiling point it is allowed to boil for 2 minutes to decompose residual peroxide within the solution.
- Post boiling the sample is allowed to cool before the pH is measured (NAG pH).
- The sample solution is then assessed for acidity through titration to pH 4.5 and pH 7 on a Metrohm auto titration system. Total NAG is calculated using the titration volumes to the set pH points.

Total NAG/NAG capacity is expressed as kg $H_2SO_4$ eq/t. Total NAG was calculated following Equation 21. Total NAG and NAG pH is used in conjunction with NNP to categorise a samples potential for ARD generation.

*Equation 21 - Calculation of total NAG value*

$$Total\ NAG\ = \frac{49\ \times v\ \times m}{w}$$

Where:

Total NAG = Total net acid generation (kg $H_2SO_4$ eq/t)

v = volume of base NaOH titrated (mL)

m = molarity of base NaOH (moles/L)

w = weight of sample reacted (g)

### 4.4.4 Acid buffering characterisation curve test procedures

The acid buffering characterisation curve (ABCC) test provides an indication of the portion of neutralising potential (NP) of a material that is available for acid neutralisation at variable pH ranges (Price 2009; Gerson et al. 2019). The test involves the gradual titration of a pulverised material that has been mixed with de-ionised water to a set pH with hydrochloric acid (HCl). A buffering curve is produced which can be used to evaluate the neutralising characteristics of a material in conjunction with ABA and NAG testing, specifically for samples with a NAG pH of pH ~4.5 (Price 2009).

ABCC analysis carried out within this research study was undertaken in accordance with Appendix G of the AMIRA (2002) ARD Test Handbook 1 as follows:

- Accurately weigh 2.0g of pulverised (<75um) sample and place in a 250mL conical flask and add 100mL of deionised water.
- Titrate the sample to pH 2.5 with incremental additions of HCl. The acid strength and incremental acid addition volumes are defined within the AMIRA handbook.
- The sample is continuously stirred. After each incremental acid addition, 1000 seconds is allowed for the pH to equilibrate prior to the pH being recorded.
- ABCC tests were undertaken on an automated Metrohm 718 STAT Titrando titrator system.

### 4.4.5 Paste pH and EC procedures

Paste pH and EC results were derived following the near saturation paste pH analysis standard outlined in section 11.6.4 of the MEND 1.20.1 manual (Price 2009). The MEND manual suggests a 2:1 (L:S) for Paste pH measurements but within this research study the L:S was amended to 1:1. This was undertaken to avoid ponding of free water and achieve near saturation conditions. Paste pH and EC readings are used as a more representative measurement of sample solution pH and EC, due to resembling the L:S of pore water within wastes more so than other analytical techniques that employ higher L:S. Paste pH provides an indication of stored acidity that is readily available and is used to assess the acidification of weathered materials. Paste pH and EC analysis procedures are summarised as follows:

- 10g of dry pulverised material is transferred into a centrifuge tube.
- 10ml of de-ionised water is added and the generated sample solution is shaken and inverted for 30 seconds before being allowed to settle for 10 minutes.
- Following the 10-minute settlement period the pH and EC readings of the supernatant are measured.
- pH and EC electrodes are gently shaken to remove any water films that have accumulated on the probe surface.
- pH and EC probes are allowed to settle, and final Paste pH and EC measurements are taken once the electrode measurements are constant.

### 4.4.6 24-hour 2:1 (L:S) leach test procedures

One stage batch leach tests were carried out on pre and post HCT composite waste rock materials in accordance with the BS EN 12457-1:2002 standard (BSI 2002a). This leach test Is carried out to provide a quantification of readily soluble constitutes of a waste material.

This test assumes that equilibrium or near equilibrium has been achieved between liquid and solid phases. To avoid confusion within this research project the liquid portion added to a dry sample mass, in the form of de-ionised water, is referred to as the leachant, while the aqueous sample recovered after the leaching period is referred to as eluent. Within this test leachant is added to a dry sample mass (<4mm) at a liquid to solid ratio (L:S) of 2 parts leachant to 1-part dry sample mass (2:1). The resulting solution mixture is then agitated for 24 hours, followed by extraction of the liquid portion (eluent). Resultant eluent is then analysed for geochemical properties including pH, EC, ORP, DIC, sulfate and dissolved metal concentrations. This test provides an indication of the leaching properties of a waste material. Eluent is analysed in line with the aqueous sample analysis procedures outlined later in this Chapter. The test procedures have been summarised as follows:

- 50g of dry material mass <4mm (unpulverized) is added to a high-density polyethylene (HDPE) bottle with 100ml of de-ionised water added as a leachant.
- The mixed solution is then agitated over 24 hours using an end of end tumbler.
- After the agitation period the eluent is extracted from the mixed sample through filtration using a 0.45 µm syringe filter.
- Filtered eluent is then analysed for pH, ORP and EC on a Metrohm autosampler.
- Subsamples of the eluent are analysed for DIC and sulfate and dissolved metal concentrations.

## 4.5 Kinetic Testing Procedures

Kinetic testing was carried out within this research study in the form of humidity cell tests (HCT). The tests undertaken within this study were amended to assess the potential implications of enhanced carbon dioxide ($CO_2$) concentration on weekly leachate geochemical development and metal leaching (ML) rates over the testing

period. Table 7 outlines the main summary of the kinetic testing carried out within this study. Within this Chapter details on the designed kinetic testing protocol are outlined in detail with specific reference to amended test designs and test parameters.

*Table 7 – Amended HCT experimental summary.*

| Kinetic Test | Test Overview | Varied Test Parameters |
|---|---|---|
| Modified Humidity Cell Tests (HCT's) | An altered version of the ASTM D5744 standard was utilized for the HCT's within this study. Humidity cell tests (HCT's) are kinetic tests designed to allow assessment of mine waste weathering on a laboratory scale, allowing prediction of mine waste drainage quality. The tests within this study have increased the $CO_2$ concentrations within altered cells to allow assessment of potential enhanced weathering and subsequent changes to drainage quality. Control cells follow the standard ASTM procedure with a proportionally reduced $O_2$ atmosphere to match the $CO_2$ enhanced cells $O_2$ concentrations. | Cell gas composition – 90% air/10% $CO_2$, 90% air/10% $N_2$<br><br>Temperature – 20$^{O}$C and 10$^{O}$C |

### 4.5.1 Kinetic testing protocol summary

Within this study an amended version of the ASTM D5744 (Protocol 1) standard was carried out (ASTM 2018a). In accordance with ASTM D5744, cells underwent a 7-day aeration cycle of alternating dry and humid air flow, consisting of 3 days of dry air, 3 days of humid air flow (approximately 95% humidity), and a leaching day. The purpose of a humidity cell is to accelerate material weathering by promoting oxidation, allowing a quantification of primary mineral reaction rates and metal leaching (ML) characteristics (Price 2009; ASTM 2018a).

This study employed the ASTM D5744 recommended test apparatus and leaching procedures, which involved using 1kg of waste materials in each constructed cell, an initial deionized water leaching volume of 1000ml (1:1 L:S ratio) (Week 0), and weekly leaching of materials with 500ml of deionized water (1:2 L:S ratio). Geochemical characterization of the recovered leachates was conducted weekly to analyse key parameters/analytes, including pH, ORP, DIC, EC, sulfate, as well as major and trace elemental analysis. Further details on aqueous sample analysis are provided later in this Chapter.

As discussed In Chapter 3, section 3.3.1, pore gas $CO_2$ concentrations have been shown to vary from atmospheric levels in mine waste rock facilities (Lorca et al. 2016; Vriens et al. 2019a). At present standardised kinetic testing methods, including those for HCT's, do not account for potential changes in mine waste weathering due to variable concentrations of pore gas $CO_2$. Within this study a HCT protocol has been designed to allow an evaluation of the potential influence of enhanced $CO_2$ concentrations on weekly leachate quality within a HCT. Enhanced $CO_2$ concentrations, in accordance with procedures outlined in EPA method 1627, were used to achieve this assessed. This protocol was designed to assess the geochemical development of wastes produced at coal mining operations where the dissolution of carbonate minerals emits gaseous $CO_2$ (EPA 2011).

For each considered operation, nine (9) HCT cells were conducted, with all samples carried out in triplicate. Enhanced $CO_2$ cells contained 10% $CO_2$ / 90% air gas compositions, while control cells had proportionally reduced $O_2$ conditions to facilitate comparison without impacting leaching characteristics due to sulfide oxidation rate differences. To account for the colder climate conditions at the Kevitsa and Aitik sites, a triplicate set of enhanced $CO_2$ HCT cells were undertaken at reduced temperatures (10°C). This alteration was based on the recommendations of Lapakko (2003), which suggested the potential amendment to the HCT method, to consider site specific conditions. The sample identification system utilised within this study is outlined within the introduction portion Chapter 5 of this thesis.

### 4.5.2 Basic HCT procedures in this study

ASTM D5744 represents a standardized test method for evaluating solid materials' weathering in a laboratory setting using a humidity cell. This method is frequently applied to examine acid rock drainage potential and metal leaching from mining waste materials. The process aids in determining the pace and degree of weathering, as well as the release of contaminants under regulated conditions (ASTM 2018b). The basic methodology for conducting a humidity cell test in line with standard ASTM D5744 can be summarized in the following steps:

1. **Sample preparation:**

- Collect representative samples of the material to be tested.
- Crush and sieve the samples to the desired particle size, typically <6.3 mm.
- Determine the PSD, specific gravity, and total sulfur content of the sample.

2. **Humidity cell assembly:**

- Assemble the humidity cell apparatus, which usually consists of a column, gas inlet and outlet, water reservoir, and a sample holder.
- Place a pre-weighed amount of the prepared sample into the humidity cell. Use a filter or screen to prevent material from escaping the cell.
- Connect the gas inlet and outlet to a source of air or oxygen and a gas-collection system, respectively.
- Connect the water reservoir to the humidity cell for leachate collection and analysis.

3. **Humidity cell operation:**

- An initial leach should be carried out with a 1:1 (L:S), typically 1 litre of leachant to 1 kg of material, before cell commencement, with this initial leach referred to as week 0.
- Purge the humidity cell with dry/humidified air or oxygen to establish an oxidizing atmosphere. Humid and dry aeration should be alternated within 3-day cycles.
- Apply a controlled temperature and relative humidity to the cell, typically 25°C and 95-100% relative humidity.
- Maintain these conditions for the duration of the test, typically 20 weeks or longer.
- Periodically leach the humidity cell on a weekly basis with deionized water, at a 1:2 (L:S) leaching regime.

4. **Leachate collection and analysis:**

- Collect leachate samples from the collection vessel after each leaching event.

- Measure the pH, EC, ORP, and temperature of the leachate.
- Perform chemical analysis for relevant elements and compounds, such as DIC, sulfate, alkalinity/ acidity, metals, and metalloids.

5. **HCT decommissioning:**

- After the rates of metal/ analyte release and geochemical properties of produced leachates have reached a steady state the HCT should be decommissioned. This may occur after a set period of time irrelevant of steady state conditions.
- The cell should be disassembled, with the sample material prepared in line with ASTM D5744 and the initial preparation procedures utilized during setup.
- The post HCT residue material should be characterised for physical, mineralogical and geochemical properties in line with a predesignated static testing and characterisation program.

6. **Data interpretation and reporting:**

- Analyse the data to determine the concentrations of analytes, rates of weathering and metal leaching (ML) rates over the test period.
- Evaluate the potential for ARD onset and metal leaching based on the test results.
- Compare the characterisation and static testing results to evaluate changes to the material as a result of the kinetic testing protocol.

### 4.5.3 Weekly leachate analysis procedures

Collected leachates were analysed for each HCT cell on a weekly basis. Weekly collected leachates were analysed for pH, EC, ORP, Eh (SHE) (calculated), alkalinity and acidity by an automated Metrohm titration system. Leachate elemental concentration analysis was carried out on a weekly basis and metal leaching rates calculated, as well as cumulative release loads. Other analytes measured from leachates included sulfate, dissolved inorganic carbon (DIC). Further information on the analysis of aqueous solutions is provided in section 4.6 of this Chapter.

### 4.5.4 Alterations to HCT procedures

Following ASTM D5744 cells were exposed to a 7-day cycle of dry/humid air flow; 3 days of dry air, 3 days of humid air flow (~95% humidity), followed by a leaching day. According to the standard, the aim of a humidity cell is ultimately to accelerate the weathering rate of primary minerals within a material through the promotion of oxidation and precipitation of secondary minerals (ASTM 2018a).

ASTM standard D5744 recommended test apparatus and leaching procedures were used within this study. This included the use of 1kg of waste materials in each constructed cell, an initial de-ionised water leaching of 1000ml (1:1 L:S) in week 0, followed by weekly leaching of materials with 500ml of de-ionised water (week 1 onwards). Each week cells were leached, and leachates recovered for geochemical characterization following a set analytical regime. To implement test parameters that better represent site conditions enhanced $CO_2$ concentrations were utilized in line with EPA method 1627 (EPA 2011). This integration of different predictive standards allows site specific conditions to be better simulated. A 10% $CO_2$ to 90% air aeration gas composition was chosen, this allows compliance with the referenced EPA method, and is representative of the gas flux measurements identified within Kevitsa cover trial systems and the findings within other waste rock facilities, refer to section 3.3.1 (Lorca et al. 2016; Vriens et al. 2018; Vriens et al. 2019a).

Gas compositions within enhanced $CO_2$ cells were 10% $CO_2$ / 90% air, while control cells were run with proportionally reduced $O_2$ conditions, balanced with $N_2$. This allowed an assessment of variations in cell leachate geochemical development due to enhanced concentrations of $CO_2$ within aeration systems. Control cell aeration gas compositions were proportionally balanced with $N_2$ so that cell materials were exposed to the same $O_2$ concentrations as altered cells. This amendment to control cells minimized the differentiation in sulfide mineral oxidation rates due to potentially differing $O_2$ availability between cell sets. Due to the colder climate conditions at the assessed sites a set of triplicate samples cells were assessed under reduced temperatures ($10^{O}C$) for both Kevitsa and Aitik waste rock composite materials. A control cell set at reduced temperature conditions was not undertaken due to time and budgetary constraints.

### 4.5.5 HCT experimental design, schematics, and photos

The HCT design and aerations systems utilised are outlined within this section. The HCT experimental set ups within this research study utilised two distinct aeration systems. These systems are outlined as follows:

***System* 1** – This system was used for HCT with the identification codes K04, K05, K06, A04, A05 and A06 and serves as the control HCT system for Kevitsa and Aitik triplicate sets. Within this system a standard humidity cell aeration system, following ASTM-D5744, was employed with the only amendment related to a proportionally reduced $O_2$ gas content, balanced with $N_2$. This balance was undertaken in line with $O_2$ concentrations within the enhanced $CO_2$ HCT aeration system, system 2.

***System* 2** – This system was used for HCT's with the identification codes K01, K02, K03, K07, K08, K09, A01, A02, A03, A07, A08 and A09. This system was used to control the aeration cycles of enhanced $CO_2$ HCT's at both control temperature conditions (25$^o$C +/- 2$^o$C) and reduced temperature conditions (10$^o$C +/- 2$^o$C). Aeration cycle gas compositions within humid and dry cycles were amended from standard air to include 10% (by volume) $CO_2$. Balancing of gas compositions was undertaken with flow gauges, with aeration gas composition measured on a weekly basis with a Geotech G150 portable gas monitor. Any variations from the intended aeration gas mixture were noted on a weekly basis.

#### *HCT cell design and system schematics*

A simplified schematic of the HCT aeration system used within this study is shown in Figure 23 (a). Detachable pipe connectors were utilised to allow removal of the HCT cells from the system for weekly weight checks. Three-way values were utilised to allow gas flow through the cells during aeration cycles and isolation of gas pipelines during leaching procedures. Aeration gas feed was fed through up through the cell during aeration cycles with an outlet designed into the stop of the cell design. Three-way values were used to vary between dry and humid air cycles, allowing inflow gas to bypass the humidifier unit during dry air cycles. Figure 23 (b) shows the main components of the HCT cells that were used in this study. Tall cells were used in line with protocol 1 of the ASTM D5744 standard as this was more suited to coarser waste

rock materials (ASTM 2018a). A perforated plate and filter sheet was placed at the base of the HCT to minimise solid sample loss during the leaching procedures.

Control temperature and reduced temperature cells sets were run in distinct temperature control rooms at the Geochemic ltd laboratory. Figure 24 shows a schematic of the control temperature HCT array that was designed and implemented within this study. Separatory funnels were used to drip feed weekly leachant into the cells. This minimised uneven weathering of waste materials directly below the feed outlet and allowed control of feed rates between cells. One-way valves were used to avoid backflow of HCT within the air feed and humidifier system. Each cell was isolated with its own flow meter/gauge that allowed individual aeration adjustments so that cells received equal aeration throughout the leaching period.

Figure 25 shows a photo of the reduced temperature cell array and the aeration system that was utilised in system 2. The aerations systems gas mixer and humidifiers were kept within the distinct temperature-controlled rooms so that aeration gases/leachant feeds were in equilibrium with the testing conditions.

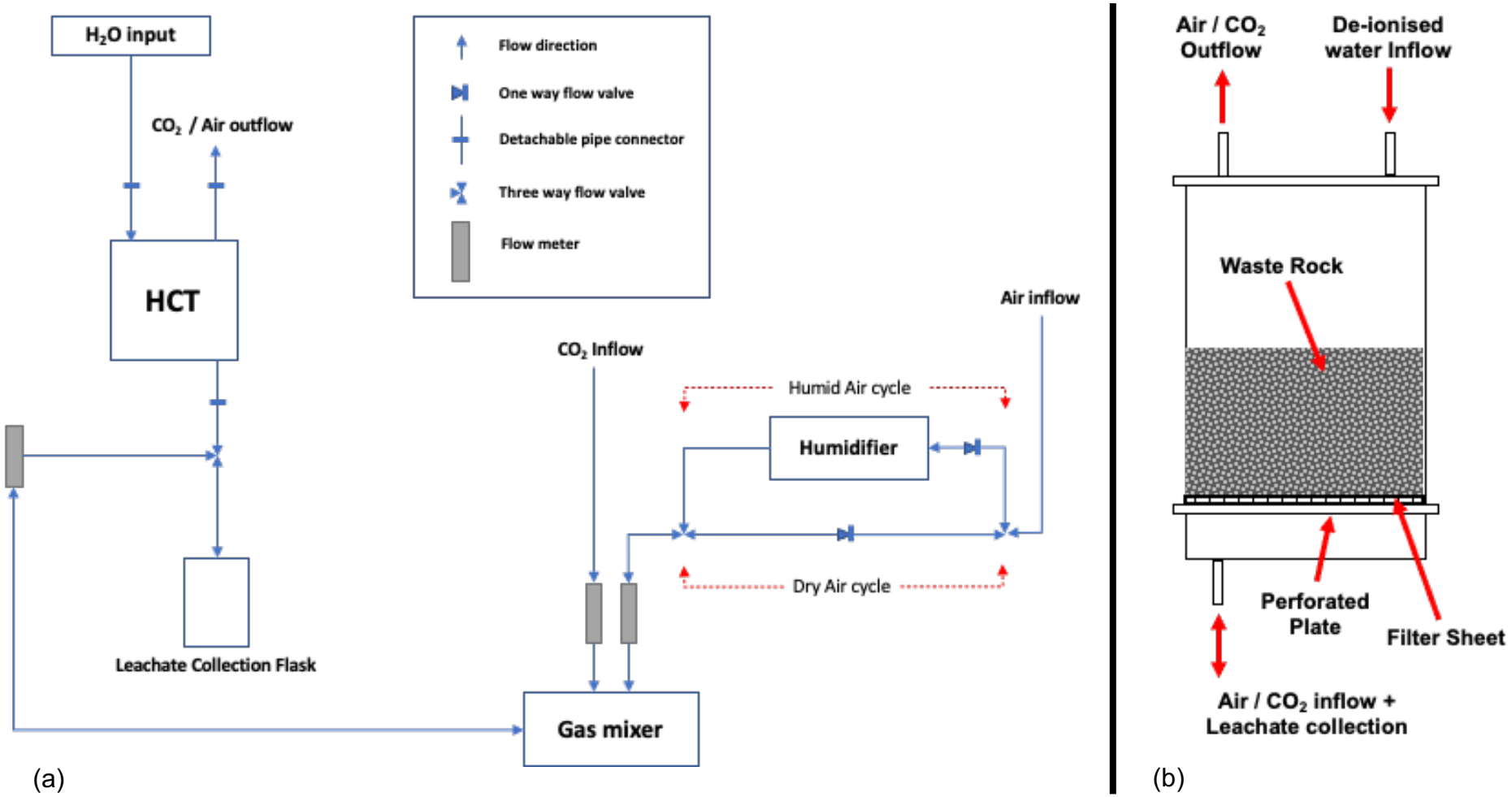


*Figure 23 – (a) Aeration system schematic and (b) utilised HCT design schematic.*

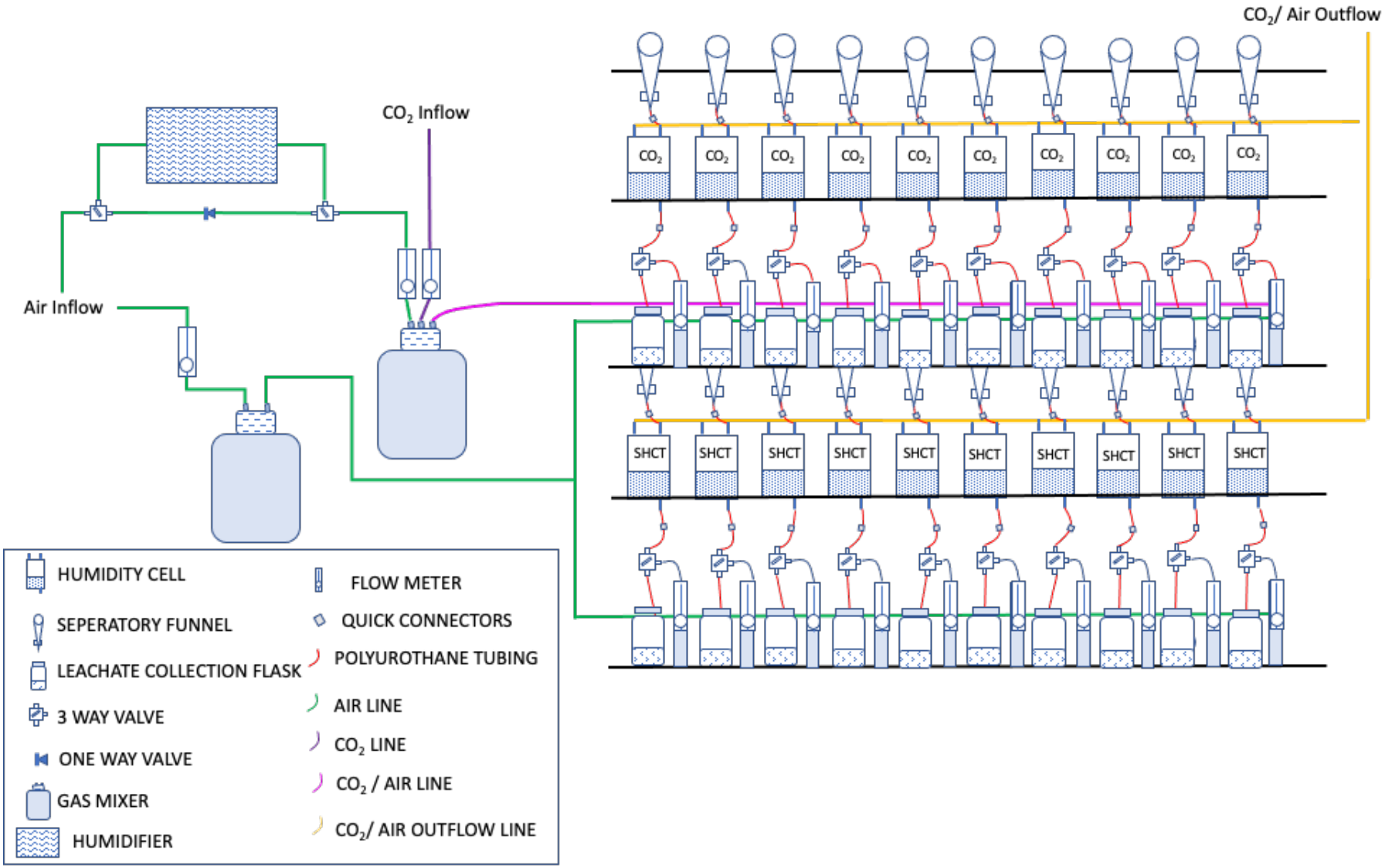


*Figure 24 - Humidity cell test (HCT) standard temperature set up schematic.*

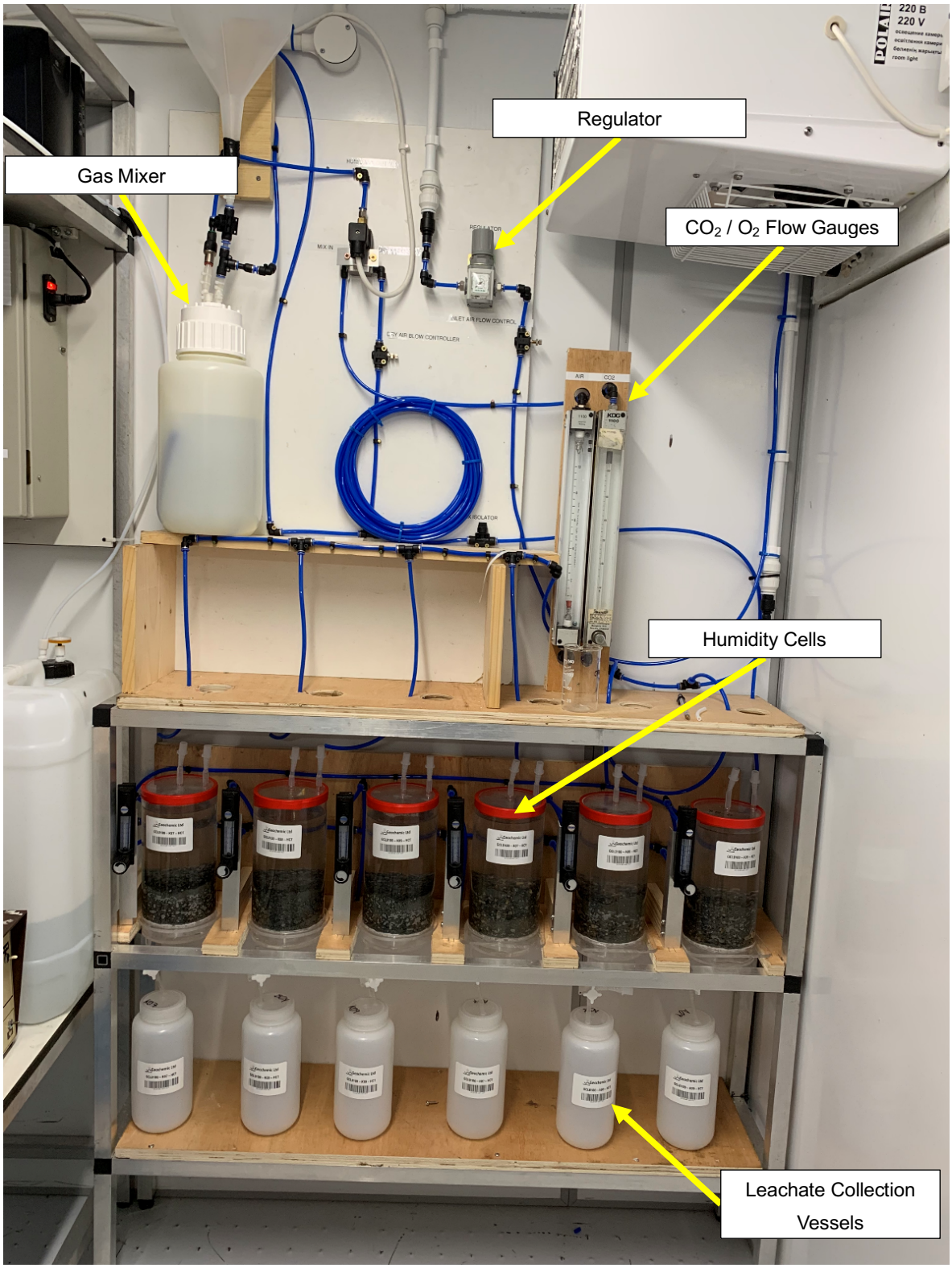


*Figure 25 - The humidity cell test (HCT) reduced temperature set array.*

## 4.6 Aqueous Sample Analysis

Aqueous samples collected from experimental protocols within this research study were analysed following the same suite of aqueous analysis. Leachate/eluent produced in kinetic testing and static testing procedures were all analysed for a standard suite of analytes. These analytes, reference methods/ standards, units and analytical detection limits (ADL) are outlines in Table 8 (Baird et al. 2015).

The analytes temperature, pH, EC, ORP, alkalinity and acidity were analysed in line with the methods recommended in Baird, Eaton and Rice (2015). Measurements of these analytes were undertaken using a Metrohm Titrando auto titration system. The auto sampling and titration system utilised Metrohm modules 855 (robotic titrosampler), 905 (auto titrator) and 814 (USB sample processor). This system used Metrohm 867 pH and 856 conductivity modules. All aqueous analysis was carried out on 50 ml of leachate which had been filtered through a 0.45 µm syringe filter.

Dissolved inorganic carbon (DIC) was analysed using an IO Analytics Aurora 1030W TOC analyser in line with BS EN 13137:2001 (BSI 2001). Sulfate analysis was carried out using ion chromatography analysis.

*Table 8 - Aqueous analysis analytical methods and units*

| Analyte | Method | Units | ADL |
|---|---|---|---|
| Temperature | APHA/AWWA/WEF 2550 | °C | - |
| pH | APHA/AWWA/WEF 4500-H+ | pH Units | - |
| Electrical conductivity (EC) @ 25°C | APHA/AWWA/WEF 2510B | µS/cm | 5 |
| Oxidation Reduction Potential (ORP) | APHA/AWWA/WEF 2580 | mV | - |
| Dissolved Inorganic Carbon (DIC) | IO Analytics Aurora 1030W TOC analyser | mg/L | 0.5 |
| Alkalinity to pH 8.3 | APHA/AWWA/WEF 2320B | mg/L as $CaCO_3$ to pH 8.3 | - |
| Alkalinity to pH 4.5 | | mg/L as $CaCO_3$ to pH 4.5 | - |
| pH post $H_2O_2$ addition | APHA/AWWA/WEF 2310 | pH post $H_2O_2$ addition | - |
| Acidity to pH 4.5 | | mg/L as $CaCO_3$ to pH 4.5 | - |
| Acidity to pH 8.3 | | mg/L as $CaCO_3$ to pH 8.3 | - |
| Sulfate (as $SO_4$) | Ion Chromatography | mg/L | |

### 4.6.1 Leachate alkalinity and acidity measurements

Leachates were analysed for alkalinity and acidity following basic chemical parameter measurements outlined in Baird, Eaton and Rice (2015). Alkalinity was determined via titration to pH 8.3 and pH 4.5. Total alkalinity was calculated using the total volume of acid added to reach pH 4.5 expressed as equivalent mg/L as $CaCO_3$ (Baird et al. 2015).

Following alkalinity titrations, 2 mL of 30% hydrogen peroxide ($H_2O_2$) was added to the 50mL leachate sample and heated on a hot plate to boiling for 2 minutes. This process oxidises dissolved reduced species (e.g. thiosalts, and ferrous iron). Following boiling the sample is allowed to cool (and topped up to 50mL with de-ionised water) before the solution is then titrated with 0.1M NaOH first to pH 4.5 and then to pH 8.3. The actual acidity is calculated from the moles of base added to reach pH 8.3 minus the moles of acid added during the alkalinity titration.

The post $H_2O_2$ addition pH was measured as an indication of the amount of reduced species that may potentially contribute to the total acidity. If the pH drops below 4.5 then this likely indicates that the oxidation step results in a reduction in the pH from that attained in the alkalinity titration.

The net alkalinity / acidity was calculated from the actual alkalinity minus the actual acidity. A positive value indicates that the solution is net alkaline and there is sufficient alkalinity present in the solution to resist pH change from any latent acidity. A negative value indicates that the solution is either already acidic, or that there is insufficient alkalinity to resist the pH change posed by solutes that may oxidise in the solution (e.g. thiosalts and ferrous iron) 'latent acidity' resulting in potential solution acidification (Baird et al. 2015).

### 4.6.2 Leachate elemental/ metal concentration analysis

Elemental analysis was carried out through ICP-OES analysis of leachates using a Perkin Elmer Optima 2100 DV Inductively Coupled Plasma Optical Emission spectroscopy (ICP-OES). Analysis of weekly leachate samples via ICP-OES was carried out at Cardiff University. Major anions, cations and trace elements were

measured over the kinetic testing 60-week leaching period as well as on sample eluents recovered from static leach tests. The following elements were measured throughout this research project: Al, Si, As, Ba, Cd, Cr, Co, Cu, Li, Mn, Mo, Ni, Sr, V, Zn, Na, Mg, K, Ca and Fe. Calibration protocols were carried out before weekly ICP-OES runs, with reference standards and sample blanks added to each run set.

### 4.6.3 Acid potential, neutralising potential and AP/NP consumption

The relative rates of acid potential generation, sulfate production, acid neutralisation, NP consumption and metal leaching rates were calculated in line with Chapter 18 of the MEND 1.20.1 guide (Price 2009). These values can be used in the interpretation of humidity cell and kinetic testing data outputs. AP and NP consumption rates vary depending on the available NP minerals within a material and if a system is open or closed to carbon dioxide ($CO_2$).

#### *Neutralisation potential (NP) consumption calculations*

NP consumption has been calculated as theoretical NP consumption at pH 6 and empirical open system NP consumption at ~pH 7. NP consumption refers to the depletion of a materials NP over time as a result of NP consumption in the presence of acidity (Price 2009). Theoretical NP consumption and empirical open system NP consumption rates are calculated following Equations 22 and 23, respectively. Cumulative NP consumption is calculated in line with equation 24.

*Equation 22 - Theoretical NP consumption at pH 6*

$$Theoretical\ NP\ Consumption\ at\ pH\ 6\ \ (mg\ CaCO_3/kg/week)\ = Sulphate\ Release\ Rate\ (mg\ SO_4/kg/week)\ \times 100.09\ /\ 96.06$$

Based on (1):

(1) $2H^{+}SO_4^{2-}+CaCO_{3(s)} \Leftrightarrow Ca^{2+}+ SO_4^{2-}+H_2CO_3^{0}$

*Equation 23 - Empirical Open System NP consumption around Neutral pH*

$$Empirical\ Open\ system\ NP\ Consumption\ around\ Neutral\ pH\ (mg\ CaCO_3/kg/week) = Theoretical\ NP\ Consumption\ (mg/kg/week) + Alkalinity\ Production\ Rate\ (mg/kg/week) - Acidity\ Production\ Rate\ (mg/kg/week)$$

Based on (1) and (2):

(1) $2H^+SO_4^{2-} + CaCO_{3(s)} \Leftrightarrow Ca^{2+} + SO_4^{2-} + H_2CO_3^0$

(2) $H_2CO_3^0 + CaCO_{3(s)} \Leftrightarrow Ca^{2+} + 2HCO_3^-$

*Equation 24 - Cumulative NP Consumption Calculation*

$$Cumulative\ NP\ Consumption\ (kg\ CaCO3\ eq\ /\ t) = Empirical\ Open\ system\ NP\ Consumption\ (mg/kg)\ /\ 1000$$

### *Acid potential (AP) consumption calculations*

Acid potential (AP) is a measure of the potential acidity that a material could generate when exposed to idealised conditions, such as unlimited oxygen supply and water. AP consumption refers to the reduction of AP over time as AP mineral sources, primarily sulfides, react with oxygen and water to produce acidity. The consumption of AP is a dynamic process and will continue until all the AP source minerals are exhausted or isolated from the reactive environment. AP consumption is calculated through measurement of sulfate ($SO_4$) release within this study. Cumulative AP consumption over time has been calculated following equation 25. This calculation provides an estimation of the consumption of acidity that could be produced if all the sulfur present were to oxidize to sulfuric acid ($H_2SO_4$). An AP constant is used within this calculation based on the oxidation of pyrite ($FeS_2$).

As all sulfur is assumed to be present as pyrite, the oxidation of one mole of pyrite produces two moles of sulfuric acid ($H_2SO_4$). If we consider the molecular weight of S (~32 g/mol) and the molecular weight of $CaCO_3$ (~100 g/mol), a conversion factor can be calculated as (2 * 100) / 32 = 31.25, allowing the expression of AP as $CaCO_3$ equivalent (Stumm and Morgan 1995).

*Equation 25 - Cumulative AP Consumption Calculation*

$$Cumulative\ AP\ Consumption\ (kg\ CaCO3\ eq\ /\ t)\ = Cumulative\ Sulfate\ (SO_4)\ Release\ (mg/kg)\ /\ 10000\ \times 31.25\ /\ (96/32)$$

Where:

$31.25 =$ AP Constant

$96 =$ Sulfuric Acid Constant

$32 =$ Molecular Weight of Sulfur (g/mol)

### 4.6.4 Analyte release rate calculations

Aqueous analyte concentrations (sulfate, DIC and dissolved metals) measured in mg/L were converted to rates of release (mg/kg/week) and cumulative release loads (mg/kg). Conversion of concentration to release rates follow Equation 26. This release rate calculation has been used for all analytes expressed as rates of release, by weight over time.

*Equation 26 - Analyte release rate calculation*

$$Analyte\ Release\ Rate\ (mg/kg/week)\ = Analyte\ Concentration\ (mg/L)\ \times Volume\ Leachate\ Collected\ (L)\ /\ Sample\ Weight\ (kg)$$

## 4.7 Quality Assurance and Quality Control (QA/QC)

QA/QC was carried out through both the implementation of duplicates/ triplicate sampling throughout this study and the application of statistical checks on the repeatability of these duplicate and triplicate sets.

### 4.7.1 Sample selection and composite homogeneity checks

It is well established that waste rock materials produced at mining operations can be heterogeneous in nature, with wastes deposited within the same waste facilities displaying variable mineralogical and geochemical characteristics (Lottermoser 2010). As a large volume of waste rock material was required for multiple kinetic tests a composite waste rock material was created for each site, composed of available discrete waste rock samples from each waste storage facility. The creation of a large, composited waste rock material for each operation allowed homogenisation of the

utilised materials, reducing potential variability in kinetic and static testing results. The homogeneity of the created composites was tested through an assessment of elemental abundance via ED-XRF analysis.

### 4.7.2 Duplicate and triplicate testing

Throughout this study analytical duplicates and triplicates have been employed to check the robustness of the testing methods and the repeatability of produced results/measurements. Due to potential variability in kinetic testing over an extended period, humidity cell testing procedures were employed in triplicates for both assessed operations waste sets. Similarly, within characterisation and static testing procedures duplicates were utilised to check to potential variability of result sets. Weekly leachate analysis employed a duplicate of a varied cells leachate to check the analytical results generated for key parameters.

### 4.7.3 Relative percentage difference (RPD) checks

To assess the potential variation between duplicate and triplicate samples/ measurements relative percentage difference (RPD) calculations were undertaken.

RPD was calculated in line with section 9.3.3 of the EPA 1627 standard (EPA 2011), with averaged RPD amended from ASTM-D5744 (ASTM 2018a). A lower RPD percentage suggests greater reliability and repeatability between results. An RPD of <20% is generally considered acceptable, while RPD values >50% suggest potential issues in test repeatability and therefore require further quantification (BCFSM 2013). The RPD calculation used within this study is shown in Equation 27.

*Equation 27 - RPD between duplicate samples*

$$RPD = \frac{(C1 - C2)}{(C1 + C2)/2} \times 100\%$$

*Where:*

$C1 = Concentration\ in\ primary\ sample$

$C2 = Concentration\ in\ duplicate\ sample$

### 4.7.4 Correlation analysis

To assess the repeatability of and correlation between HCT triplicate results correlation analysis was undertaken. Correlation analysis was carried out on the weekly leaching data measured from all cells over the HCT protocol. This analysis was carried out to assess the relationship between two variables through the measurement of their correlation coefficient (*r*). This correlation coefficient is a linear coefficient (Pearson), with *r* = 1 and *r* = -1 indicating the variables have either a positive linear (*r* = 1) or negative linear (*r* = -1) relationship. It is noted that correlation does not demonstrate causation or statistical significance, it is rather a demonstration of correlation strength. The equation used to calculate correlation coefficient is shown in Equation 28, with *r* values reported to 4 decimal points (McCarroll 2016). The outputs of this test are presented in the form of a correlation coefficient matrix that is used to display correlations between corresponding sample measurements, as well as potentially associated parameters within a produced data set. Correlation analysis was carried out in line with McCarroll (2016).

*Equation 28 - Correlation coefficient of two variables*

$$r\,(X,Y) = \frac{\Sigma(x-\bar{x})(y-\bar{y})}{\sqrt{\Sigma\,(x-\bar{x})^2\Sigma\,(y-\bar{y})^2}}$$

*Where:*

$r$ = *correlation coefficient*

$X$ = *variable 1*

$Y$ = *variable 2*

$\bar{x}$ = *mean of variable 1 values*

$\bar{y}$ = *mean of variable 2 values*

# Chapter 5 – Research Results

## Introduction

This Chapter summarises the results of the Kevitsa and Aitik HCT leaching experiments, further discussion, and interpretation of these results in presented in Chapter 6. The results of pre and post characterisation are also outlined where relevant to the objectives of the research study. Additional results including raw leaching data and characterisation data can be found in the Appendix of this thesis. Throughout this Chapter the following labelling system is employed to differentiate between the 3 triplicate sample sets employed with both Kevitsa and Aitik waste rock materials:

**Kevitsa Triplicates:**

- **Kevitsa Test Conditions 1 (K-TC1): K01, K02, K03** – Control Temperature (25°C), Enhanced $CO_2$ HCT (10% $CO_2$ by volume)
- **Kevitsa Test Conditions 2 (K-TC2): K04, K05, K06** – Control Temperature (25°C), Control Aeration HCT (10% $N_2$ to balance $CO_2$ by volume)
- **Kevitsa Test Conditions 3 (K-TC3): K07, K08, K09** – Reduced Temperature (10°C), Enhanced $CO_2$ HCT (10% $CO_2$ by volume)

**Aitik Triplicates:**

- **Aitik Test Conditions 1 (A-TC1): A01, A02, A03** – Control Temperature (25°C), Enhanced $CO_2$ HCT (10% $CO_2$ by volume)
- **Aitik Test Conditions 2 (A-TC2): A04, A05, A06** – Control Temperature (25°C), Control Aeration HCT (10% $N_2$ to balance $CO_2$ by volume)
- **Aitik Test Conditions 3 (A-TC3): A07, A08, A09** – Reduced Temperature (10°C), Enhanced $CO_2$ HCT (10% $CO_2$ by volume)

To assess any physical, geochemical, or mineralogical changes to waste rock materials as a result of 60 weeks of kinetic testing, pre-kinetic testing samples were subjected to the same characterisation program as post-kinetic testing samples. Within this Chapter pre-kinetic testing waste rock samples are labelled as K-Pre and A-Pre, representing comparable composited waste rocks from Kevitsa and Aitik, respectively.

## 5.1 Basic Sample Characterisation Results

Prior to kinetic testing waste rock composite samples from Kevitsa and Aitik were subjected to a series of basic characterisation tests and procedures. Testing procedures used within this study are outlined in detail within Chapter 4, section 4.3. The same tests were then carried out post HCT materials following decommissioning. The following characterisation data is presented in this section:

- Particle size distribution (PSD).
- Mineralogical characterisation (SEM-EDX).
- Elemental Characterisation (ED-XRF).
- Empirical carbon capture potential (CCP) (Steinour Equation).

### 5.1.1 Particle size distribution (PSD) Results

PSD analysis was carried out via gravimetric dry sieving. The PSD gravimetric dry sieving methods used within this study are outlined in detail in section 4.3.3 of this thesis.

***Kevitsa HCT PSD curves***

The PSD percentage passing results for Kevitsa cells are shown in Figure 26. Within triplicate set K-TC1 72.55%, 74.82%, and 74.95% of the initial mass passed through the 4mm sieve for cells K01, K02, and K03, respectively. Notably, for the 63 µm sieve size, K01 had 5.30% of the initial mass passing, while K02 had 1.29% and K03 had 5.11%. K-TC2 cells, A04, A05 and A06 measured 75.93%, 78.03%, and 77.78% of initial mass passing 4mm. These cells measured 4.87%, 6.13%, and 4.71% of the mass passing the 63 µm sieve. The final Kevitsa triplicate set of K07, K08 and K09 measured 77.45%, 75.54%, and 75.81% of the initial mass passing through the 4mm sieve, respectively. As with the previous triplicates, the mass passing reduces with decreasing sieve sizes, culminating in 5.60%, 5.15%, and 5.25% of the initial mass passing through the 63 µm sieve for K07, K08, and K09, respectively. The d50 for all samples within these sets was ~2-2.5mm.

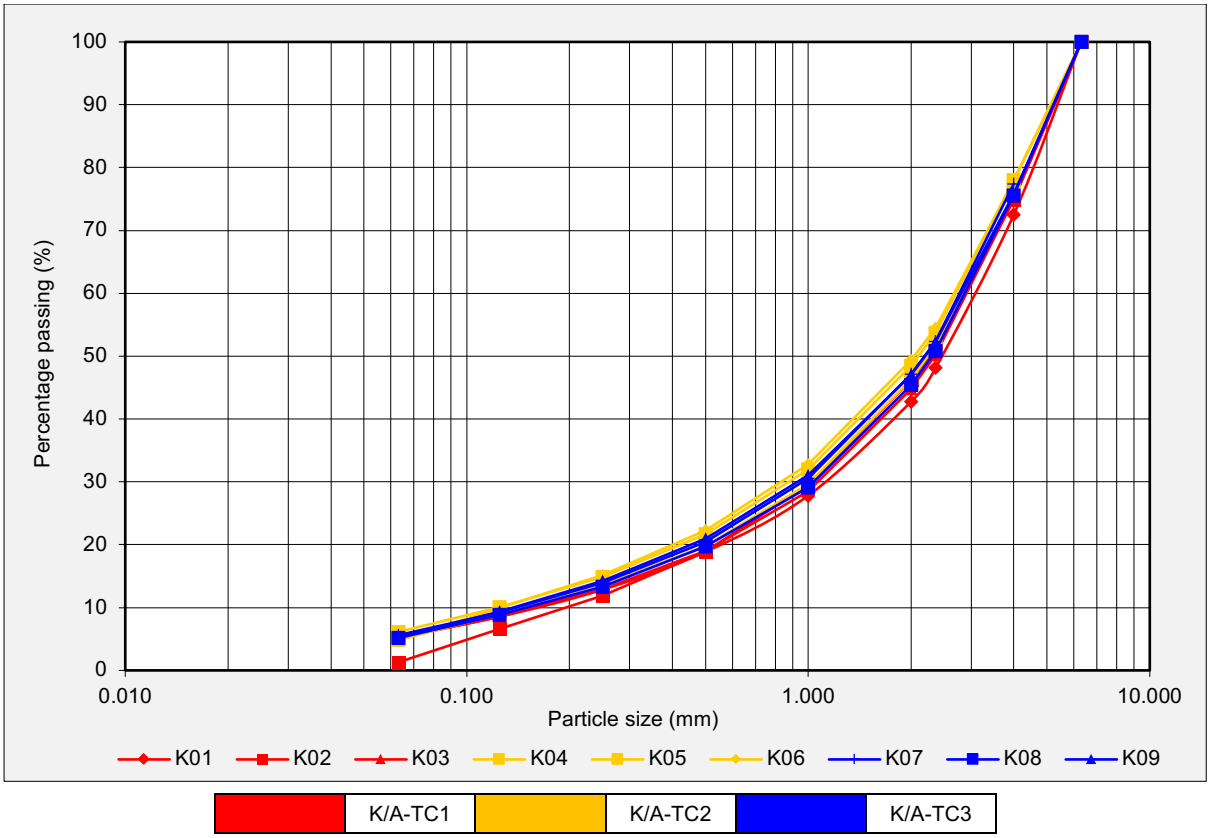


*Figure 26 - Kevitsa HCT particle size distribution curves, presented as % passing.*

### *Aitik HCT PSD curves*

The PSD percentage passing results for Aitik cells are shown in Figure 27. Within triplicate A-TC1 70.28%, 77.65%, and 70.71% of the material from cells A01, A02 and A03 passed the 4mm sieve respectively. This decreased consistently as the sieve size reduced, with 4.53%, 7.75%, and 4.30% of the material passing a 63 µm sieve. The data indicates that A02 contained a slightly higher proportion of finer particles compared to A01 and A03. It is noted that following drying protocols sample A02 was dropped post HCT decommissioning and around 50% of the total sample mass was recovered. This would potentially explain the differentiation in post HCT PSD displayed in Figure 27.

Within triplicate set A-TC2 a slightly lower proportion of samples A04, A05 and A06 passed the 4mm sieve, when compared to A-TC1, with 70.49%, 69.52%, and 66.83% passing, respectively. 4.48%, 4.21%, and 4.08% of materials from cells A04, A05 and A06 passed the 63 µm sieve. This group generally had slightly fewer finer particles than the A-TC1 group. A-TC3 cells, comprising samples A07, A08, and A09) measured 4mm sieve passing percentages of 66.56%, 70.99%, and 69.22%,

respectively. 3.65%, 4.81%, and 4.41% of samples A07, A08 and A09 passed the 63 µm sieve, respectively. All Aitik samples, except for A02, held d50 values ~2.5mm, while A02 held a d50 value of ~1.8mm.

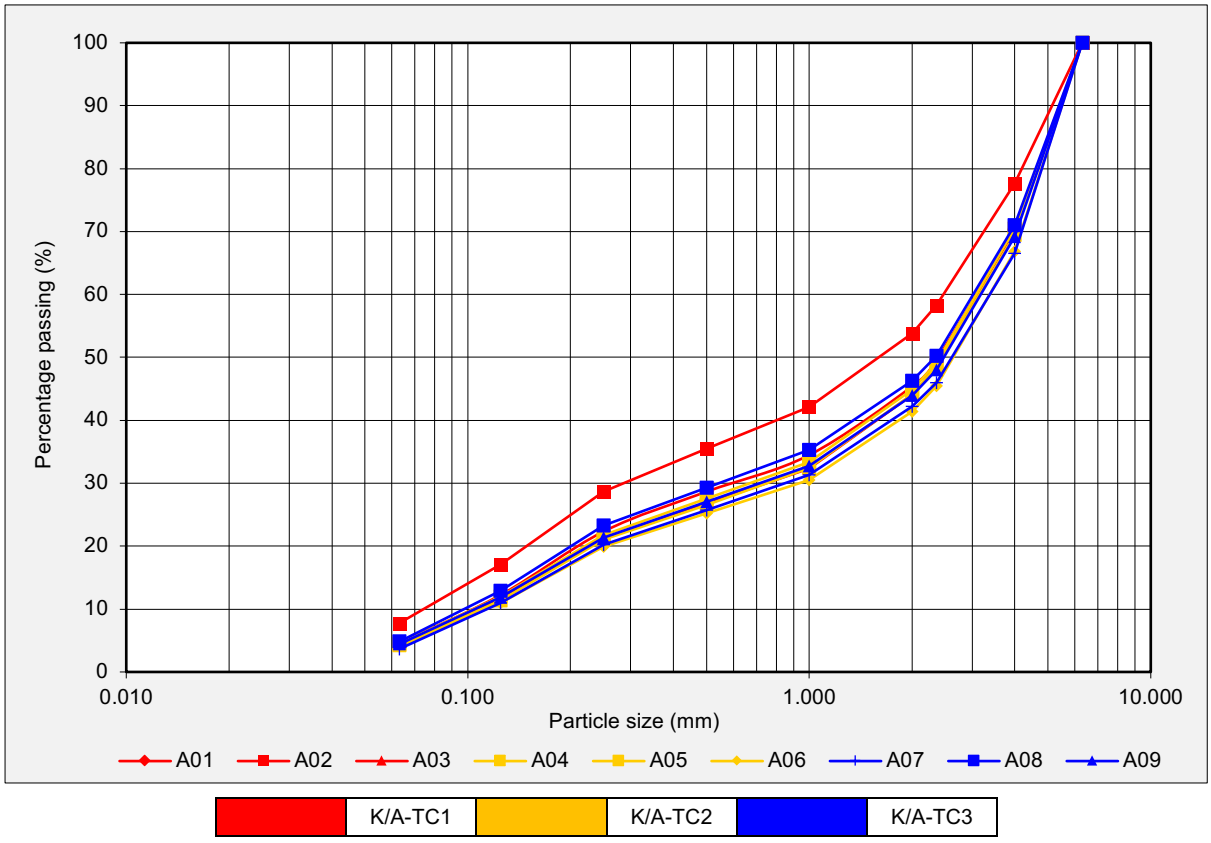


*Figure 27 - Aitik HCT particle size distribution curves, presented as % passing.*

## 5.1.2 Mineralogical and petrographic analysis results

Twenty samples, collectively, were analysed for mineral abundance, including one pre-leach composite for each operation (A-Pre & K-Pre) and 9 subsequent post leach composites from each sample set. Mineralogical method descriptions can be found in Chapter 4, section 4.3.4, of this thesis.

### *Bulk mineral abundance*

The bulk mineral abundances of Kevitsa and Aitik samples, pre and post HCT, are shown in Figures 28 and 29, respectively. Bulk mineral abundances are displayed as mineral groups and are measured by total sample weight percentage (%). Differences between individual minerals within mineral groups, such as amphibole group minerals, are described in within the next section of this thesis and in Appendix 3.

### *Kevitsa bulk mineralogy results*

The bulk mineral abundance of Kevitsa HCT materials, pre and post, are shown in Figure 28. It can be seen in this Figure that pre and post HCT materials were dominated by silicate group minerals, including clinopyroxene, amphibole and orthopyroxene group minerals. Cumulatively these inosilicate group minerals account for >76 wt % of all Kevitsa HCT samples by weight, both pre and post, irrelevant of triplicate grouping. Clinopyroxene group and amphibole group minerals typically represented between 28-42 wt % of the bulk mineral composition of Kevitsa waste rock composite samples. Major sulfide minerals included pyrrhotite, pyrite and chalcopyrite with these minerals constituting between 0.5-1.4 wt %, 0-0.3 wt % and 0.1-0.4 wt % of Kevitsa materials, respectively. Tremolite was the silicate mineral with the highest individual bulk abundance of individually distinguishable minerals, with weight percentage of between 5.6-10.6 wt % reported within these cells. Minor phases identified within Kevitsa materials included albite (0.1-22 wt %), goethite (1-1.6 wt %) and serpentine minerals (0.9-1 wt %).

### *Aitik bulk mineralogy results*

The bulk mineral abundance of Aitik HCT materials, pre and post, are shown in Figure 29. It can be seen in this figure that albite and quartz dominate the bulk mineral composition of Aitik HCT materials in all 10 samples. Within the sample set albite, feldspar aluminosilicate mineral, account for between 23.4 wt% and 36.3 wt % of Aitik HCT materials. Quartz, the second most abundant mineral, accounts for 17.6-25.8 wt% of assessed materials. Plagioclase feldspar group mineral, anorthite, is the third most abundant mineral within Aitik pre sample, A-Pre. This mineral displays a mineral abundance of between 6.9 wt% and 13.5 wt % within this group. There is a marked reduction in bulk abundance of anorthite in post HCT samples, with post HCT samples A01-A09 displaying anorthite weight percentages of between 6.9 wt % to 8.5 wt %. The main distinguishable sulfide minerals include pyrite (0.5-3.4 wt %) and minor abundances of pyrrhotite (0.1-0.7 wt %) and chalcopyrite (0-0.5 wt %). Calcium carbonate mineral, calcite, is noted to represent 0.3-0.7 wt % of Aitik samples within this bulk mineral abundance assessment.

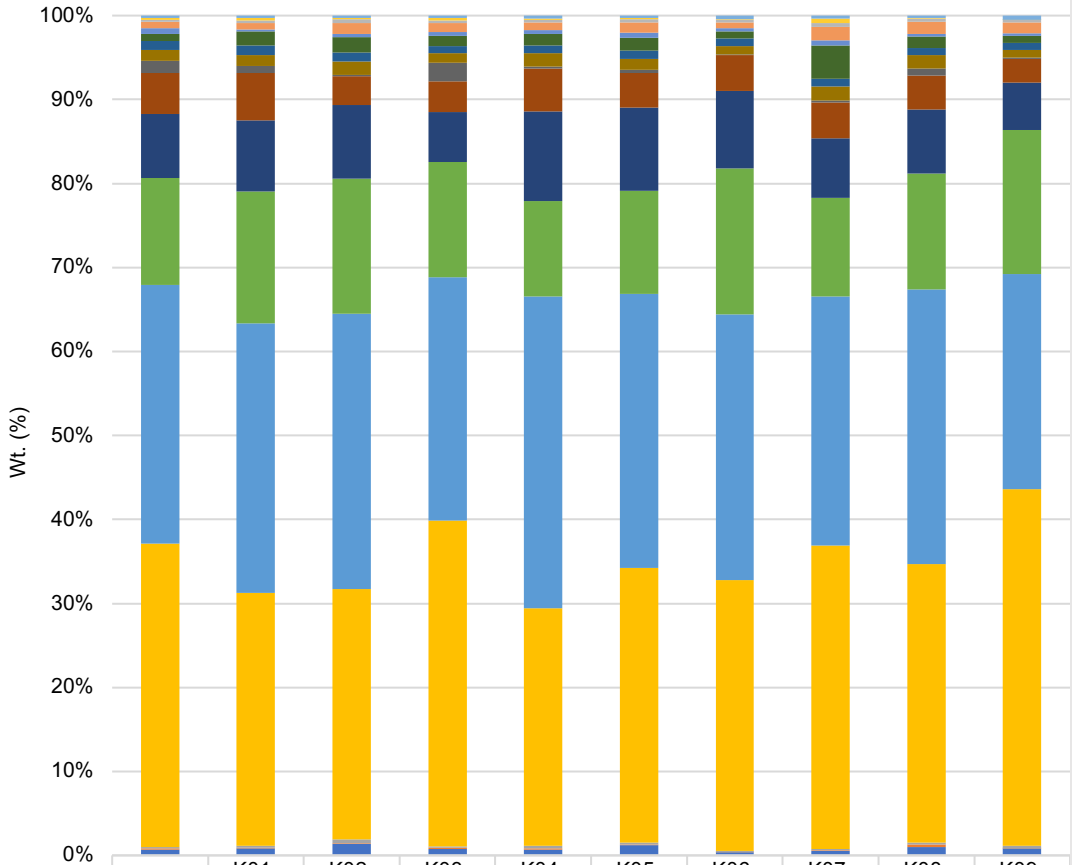


| | K-PRE | K01-POST | K02-POST | K03-POST | K04-POST | K05-POST | K06-POST | K07-POST | K08-POST | K09-POST |
|---|---|---|---|---|---|---|---|---|---|---|
| Chrome-magnetite | 0.2 | 0.3 | 0.3 | 0.3 | 0.3 | 0.3 | 0.5 | 0.4 | 0.3 | 0.5 |
| Quartz | 0.3 | 0.3 | 0.1 | 0.3 | 0.2 | 0.1 | 0.1 | 0.5 | 0.1 | 0.1 |
| Hematite | 0.3 | 0.3 | 0.5 | 0.3 | 0.3 | 0.4 | 0.3 | 0.5 | 0.4 | 0.2 |
| Anorthite | 0.7 | 0.7 | 1.3 | 1.1 | 0.9 | 1.2 | 0.7 | 1.6 | 1.4 | 1.3 |
| Biotite | 0.7 | 0.2 | 0.4 | 0.4 | 0.4 | 0.6 | 0.3 | 0.6 | 0.3 | 0.3 |
| Magnetite | 0.9 | 1.7 | 1.8 | 1.2 | 1.3 | 1.5 | 0.9 | 3.9 | 1.3 | 0.8 |
| Serpentine | 1.0 | 1.1 | 1.0 | 0.9 | 0.9 | 1.0 | 0.9 | 0.9 | 0.9 | 0.9 |
| Goethite | 1.3 | 1.3 | 1.6 | 1.1 | 1.6 | 1.3 | 1.0 | 1.6 | 1.5 | 0.9 |
| Albite | 1.5 | 0.8 | 0.2 | 2.2 | 0.3 | 0.3 | 0.1 | 0.2 | 0.9 | 0.2 |
| Chlorite | 4.8 | 5.6 | 3.4 | 3.6 | 5.0 | 4.1 | 4.2 | 4.2 | 4.0 | 2.8 |
| Tremolite | 7.5 | 8.4 | 8.8 | 5.9 | 10.6 | 9.8 | 9.2 | 7.0 | 7.6 | 5.6 |
| Orthopyroxene | 12.6 | 15.5 | 15.9 | 13.6 | 11.2 | 12.1 | 17.2 | 11.7 | 13.7 | 17.0 |
| Amphibole | 30.6 | 31.7 | 32.5 | 28.8 | 36.7 | 32.4 | 31.4 | 29.4 | 32.4 | 25.5 |
| Clinopyroxene | 35.8 | 29.8 | 29.6 | 38.6 | 28.0 | 32.4 | 31.9 | 35.8 | 32.9 | 42.2 |
| Chalcopyrite | 0.1 | 0.2 | 0.4 | 0.1 | 0.4 | 0.3 | 0.2 | 0.2 | 0.2 | 0.3 |
| Pyrite | 0.2 | 0.1 | 0.1 | 0.2 | 0.1 | 0.1 | 0.0 | 0.0 | 0.3 | 0.0 |
| Pyrrhotite | 0.7 | 0.8 | 1.4 | 0.7 | 0.7 | 1.2 | 0.4 | 0.5 | 1.0 | 0.8 |

*Figure 28 – Bulk mineral classifications for Kevitsa waste rock samples.*

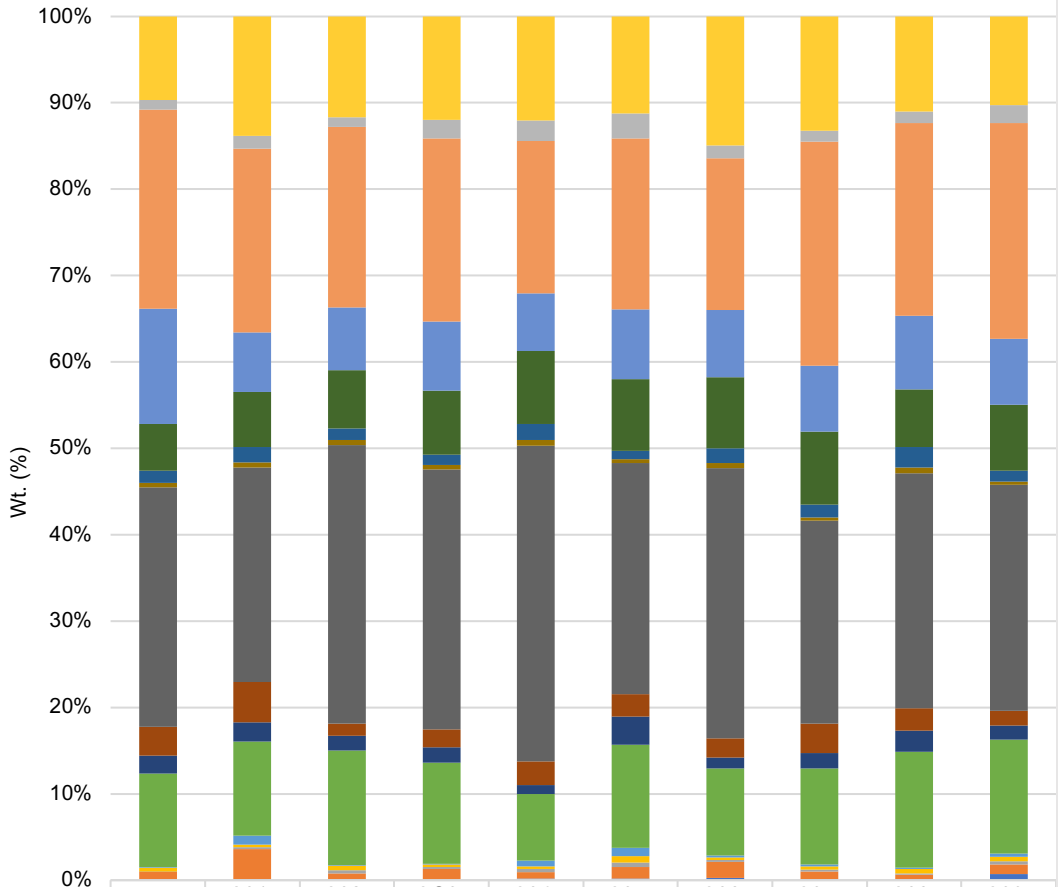


| | A-PRE | A01-POST | A02-POST | AO3-POST | A04-POST | A05-POST | A06-POST | A07-POST | A08-POST | A09-POST |
|---|---|---|---|---|---|---|---|---|---|---|
| Muscovite | 9.6 | 13.7 | 11.6 | 11.9 | 12.0 | 11.2 | 14.9 | 13.2 | 10.9 | 10.3 |
| Accessory Phases | 1.1 | 1.5 | 1.1 | 2.2 | 2.4 | 2.9 | 1.5 | 1.3 | 1.4 | 2.1 |
| Quartz | 22.9 | 21.2 | 20.9 | 21.1 | 17.6 | 19.7 | 17.4 | 25.8 | 22.2 | 24.9 |
| Anorthite | 13.3 | 6.9 | 7.2 | 8.0 | 6.6 | 8.0 | 7.8 | 7.6 | 8.5 | 7.6 |
| Biotite | 5.4 | 6.4 | 6.7 | 7.4 | 8.4 | 8.3 | 8.2 | 8.4 | 6.6 | 7.6 |
| Magnetite | 1.4 | 1.8 | 1.3 | 1.2 | 1.8 | 1.0 | 1.7 | 1.5 | 2.4 | 1.2 |
| Goethite | 0.5 | 0.6 | 0.6 | 0.5 | 0.7 | 0.4 | 0.6 | 0.4 | 0.7 | 0.4 |
| Albite | 27.6 | 24.7 | 32.1 | 30.0 | 36.3 | 26.7 | 31.2 | 23.4 | 27.0 | 26.1 |
| Chlorite | 3.3 | 4.6 | 1.5 | 2.1 | 2.8 | 2.6 | 2.2 | 3.4 | 2.6 | 1.7 |
| Tremolite | 2.1 | 2.2 | 1.6 | 1.8 | 1.0 | 3.3 | 1.3 | 1.7 | 2.4 | 1.7 |
| Amphibole | 10.8 | 10.8 | 13.2 | 11.7 | 7.7 | 11.9 | 10.1 | 11.1 | 13.3 | 13.2 |
| Clinopyroxene | 0.1 | 1.0 | 0.1 | 0.1 | 0.6 | 0.9 | 0.2 | 0.2 | 0.1 | 0.4 |
| Calcite | 0.4 | 0.3 | 0.5 | 0.3 | 0.3 | 0.7 | 0.3 | 0.4 | 0.5 | 0.5 |
| Chalcopyrite | 0.0 | 0.2 | 0.4 | 0.2 | 0.4 | 0.5 | 0.2 | 0.3 | 0.2 | 0.3 |
| Pyrite | 0.8 | 3.4 | 0.7 | 1.3 | 0.7 | 1.3 | 1.9 | 0.8 | 0.5 | 1.1 |
| Pyrrhotite | 0.1 | 0.1 | 0.1 | 0.1 | 0.2 | 0.2 | 0.3 | 0.1 | 0.1 | 0.7 |

*Figure 29 – Bulk mineral classifications for Aitik waste rock samples.*

***Petrographic thin sections***

One post HCT sample was analysed from each of the triplicate sets as well as pre HCT materials from Kevitsa and Aitik. The following samples were analysed A-Pre, K-Pre, K02, K05, K08, A02, A05 and A08. Each sample was photographed as received, followed by the collection of multiple petrographic images including: a low magnification of image taken under white cathode light, a general thin section image taken under plane polarised transmitted light (x25), a cross polarised transmitted light image (x25) and a reflected light image taken under plane polarised reflective light (x25). Utilised methods are outlined in detail in Chapter 4, section 4.3.4, of this thesis.

Petrographic thin section analysis displayed minimal differences in mineralogical characteristics between pre and post HCT residues. A summary of the observed results is presented in this section. All images taken of pre and post HCT residue materials, as well as detailed textural descriptions are included in Appendix 3 of this thesis.

Petrographic thin section analysis of pre and post HCT residues confirmed the bulk mineral abundance results demonstrated in Figures 28 and 29. Kevitsa samples were predominantly composed of gabbroic fragments (websterite to olivine websterite in composition) containing abundant clinopyroxene. Trace amounts of olivine group minerals were observed within petrographic thin sections, which had been readily altered to serpentine. Sulfide mineral within Kevitsa samples were confirmed to be present in the form of pyrrhotite, pyrite, chalcopyrite and traces of pentlandite. Sulfides and silicate mineral textures were not shown to greatly alter in response to HCT testing, with minimal alteration present between materials exposed to differing testing conditions.

Anorthite was shown to represent 13.1% of the Aitik pretesting composite. Similarly to the Kevitsa thin sections, Aitik post HCT residues displayed minimal change in response to the 60-week kinetic testing protocol. Identified sulfides included pyrite and pyrrhotite which were commonly coarse, euhedral and liberated.

Example images of cross polarised thin sections collected as part of this study are shown in Figures 30 and 31 for samples K-Pre and A-Pre, respectively.

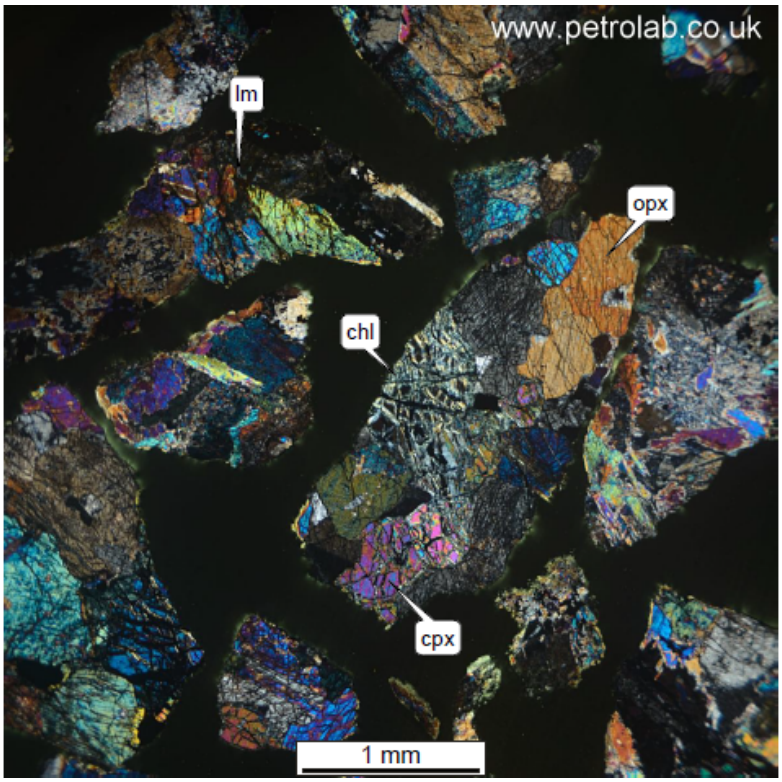


*Figure 30 - Cross polarised light thin section image of sample K-Pre.*

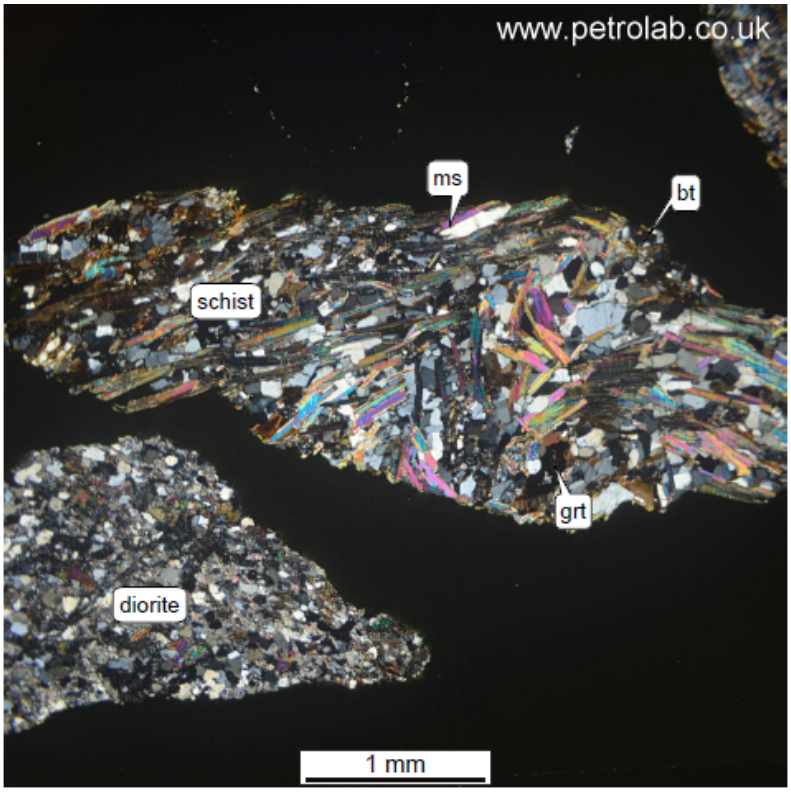


*Figure 31 - Cross polarised light thin section image of sample A-Pre.*

***Kevitsa and Aitik pre and post HCT elemental abundance results***

Elemental characterisation was carried out via solid ED-XRF analysis. The elemental characterisation results of Kevitsa and Aitik pre and post HCT cell samples are shown in Tables 9 and 10, respectively. The following elements were analysed: Al, Ca, Fe, Mg, Na S, Ba Si, Cr, Cu, Mn, Ni, Sr, V and Zn. Methods utilised in elemental analysis have been described in Chapter 4, section 4.3.5. Elements of interest have been displayed for both operations waste rock materials within these tables. Complete elemental analysis carried out via ED-XRF can be found in Appendix 19 of this thesis. Elemental composition is presented in either % or mg/kg, with specific elemental analytical detection limits shown within this table.

It can be seen in Table 9 that following humidity cell testing the elemental composition of Kevitsa waste rock materials displayed minimal changes when compared to results obtained from the pre HCT composite sample (K-Pre). Calcium concentrations were shown to slightly increase in all Kevitsa post HCT samples, although this change was in the relatively small range of between 0.3-0.4%. Iron content was shown to stay consistent between pre and post HCT samples, with a K-Pre holding an Fe content of 7.2%, while post samples held Fe contents between 6.8-7.2%. No clear pattern in elemental concentration change was observed for major or minor elements analysed via ED-XRF between pre and post HCT testing for Kevitsa samples. Sulfur concentrations displayed slight variations between pre and post samples, although the measured concentrations were close to the analytical detection limits (ADL).

It can be seen in Table 10 that post HCT testing that the elemental concentration of aluminium increased in all cells compared to the pre HCT Aitik material. Analysis of calcium, iron, potassium, magnesium, manganese and strontium showed little distinguishable changes in elemental concentrations post HCT in any of the 9 Aitik cells. Sulfur content was consistent within pre and post HCT samples, holding elemental concentration values ~0.4% (+/- 20%). Sodium concentrations within all post HCT cell samples was noted in these results. Within samples A-Pre the Na content was measured as 1.18%, while post HCT concentrations were shown to range between 1.87-2.52%. No distinguishable patterns between elemental concentration change and specific Aitik HCT triplicate set were noted within these results.

*Table 9 - Pre and post Kevitsa HCT elemental compositional data*

| Element | Al | Ca | Fe | Mg | S | Si | Cr | Cu | Mn | Ni | Sr | V | Zn |
|---|---|---|---|---|---|---|---|---|---|---|---|---|---|
| Unit | % | % | % | % | % | % | mg/kg | mg/kg | mg/kg | mg/kg | mg/kg | mg/kg | mg/kg |
| ADL | 0.3 | 1 | 0.1 | 0.5 | 0.2 | 1.5 | 200 | 50 | 150 | 200 | 10 | 100 | 25 |
| K-PRE | 1.55 | 8.13 | 7.2 | 11.5 | 0.28 | 19.2 | 2281 | 756 | 1282 | 920 | 15.1 | 120 | 46 |
| K-TC1 Post-HCT Samples | | | | | | | | | | | | | |
| K01 | 1.83 | 8.41 | 7.1 | 11.7 | 0.32 | 20.7 | 2342 | 747 | 1294 | 857 | 24.9 | 123.1 | 49.6 |
| K02 | 1.66 | 8.44 | 7.1 | 12.0 | 0.32 | 20.5 | 2395 | 764 | 1269 | 900 | 16.3 | 124.8 | 42.3 |
| K03 | 1.62 | 8.53 | 7.1 | 11.8 | 0.27 | 20.4 | 2393 | 738 | 1300 | 910 | 13.3 | 120.5 | 47.2 |
| K-TC2 Post-HCT Samples | | | | | | | | | | | | | |
| K04 | 1.54 | 8.46 | 7.1 | 11.4 | 0.29 | 19.6 | 2389 | 705 | 1251 | 865 | 15.6 | 136.1 | 51.5 |
| K05 | 1.68 | 8.34 | 6.8 | 11.6 | 0.26 | 20.2 | 2291 | 688 | 1275 | 843 | 20.2 | 116.7 | 48.7 |
| K06 | 1.58 | 8.57 | 7.2 | 11.8 | 0.33 | 20.3 | 2442 | 790 | 1284 | 879 | 18.6 | 128 | 48.5 |
| K-TC3 Post-HCT Samples | | | | | | | | | | | | | |
| K07 | 1.71 | 8.37 | 7.2 | 12.3 | 0.31 | 21.0 | 2383 | 728 | 1287 | 847 | 15.8 | 124.5 | 48.4 |
| K08 | 1.64 | 8.37 | 7.1 | 12.3 | 0.33 | 20.4 | 2350 | 789 | 1234 | 852 | 13.9 | 124.2 | 46.1 |
| K09 | 1.59 | 8.52 | 7.0 | 11.8 | 0.28 | 20.8 | 2400 | 707 | 1256 | 856 | 14.7 | 128.9 | 44.6 |

*Table 10 - Pre and post Aitik HCT elemental compositional data*

| Element | Al | Ca | Fe | K | Mg | Na | S | Si | Ba | Cu | Mn | Sr | Zn |
|---|---|---|---|---|---|---|---|---|---|---|---|---|---|
| Unit | % | % | % | % | % | % | % | % | mg/kg | mg/kg | mg/kg | mg/kg | mg/kg |
| ADL | 0.3 | 1 | 0.1 | 0.2 | 0.5 | 1 | 0.2 | 1.5 | 300 | 50 | 150 | 10 | 25 |
| A-PRE | 6.73 | 2.41 | 4.3 | 3.33 | 1.27 | 1.18 | 0.44 | 23.7 | 2428 | 738 | 2252 | 350.6 | 70.8 |
| A-TC1 Post-HCT Samples | | | | | | | | | | | | | |
| A01 | 7.17 | 2.51 | 4.2 | 3.24 | 1.16 | 1.96 | 0.36 | 25.4 | 2359 | 738 | 2119 | 355.1 | 73 |
| A02 | 7.64 | 2.5 | 4.4 | 3.22 | 1.24 | 2.2 | 0.4 | 27.6 | 2198 | 867 | 2084 | 350.2 | 63.7 |
| A03 | 7.58 | 2.46 | 4.4 | 3.42 | 1.2 | 2.01 | 0.36 | 26.8 | 2782 | 898 | 2066 | 383.4 | 70 |
| A-TC2 Post-HCT Samples | | | | | | | | | | | | | |
| A04 | 7.54 | 2.38 | 4.4 | 3.34 | 1.18 | 2.37 | 0.47 | 27.2 | 2438 | 849 | 2412 | 348.1 | 64.9 |
| A05 | 7.62 | 2.42 | 4.3 | 3.32 | 1.22 | 1.97 | 0.4 | 27.1 | 2552 | 969 | 2182 | 349.2 | 71.3 |
| A06 | 7.76 | 2.54 | 4.2 | 3.24 | 1.25 | 2.26 | 0.43 | 27.2 | 2293 | 915 | 2037 | 335.3 | 68 |
| A-TC3 Post-HCT Samples | | | | | | | | | | | | | |
| A07 | 7.85 | 2.5 | 4.4 | 3.23 | 1.34 | 2.52 | 0.45 | 27.7 | 2353 | 901 | 2111 | 327.1 | 64.4 |
| A08 | 7.54 | 2.53 | 4.4 | 3.23 | 1.25 | 1.87 | 0.44 | 26.8 | 2749 | 906 | 2382 | 361.5 | 69.5 |
| A09 | 7.73 | 2.42 | 4.3 | 3.29 | 1.28 | 2.43 | 0.4 | 27.7 | 2543 | 786 | 2311 | 356.1 | 72.1 |

**Empirical carbon capture potential (CCP)**

Utilizing the elemental composition data collected via ED-XRF analysis, empirical maximal carbon capture potential (CCP) has been calculated using the adjusted Steinour equation outlined in Chapter 4 of this thesis, see Equation 14. CCP represents the maximal potential of a material to sequester $CO_2$, based purely on elemental composition and without consideration of environmental or experimental conditions. CCP values are presented as kilograms of $CO_2$ that could be sequestered per tonne of material (kg/t $CO_2$). The CCP estimations for pre and post Kevitsa and Aitik HCT materials is presented in Figure 32. K-Pre composite material held a CCP value of 295 (kg/t $CO_2$), with post HCT values ranging from 295-312 (kg/t $CO_2$). Pre HCT Aitik material, A-Pre, held a CCP of 73 (kg/t $CO_2$), while post HCT CCP values ranged from 80-87 (kg/t $CO_2$). The lack of variation in CCP amongst all cells in this study reflects the minimal change in elemental composition.

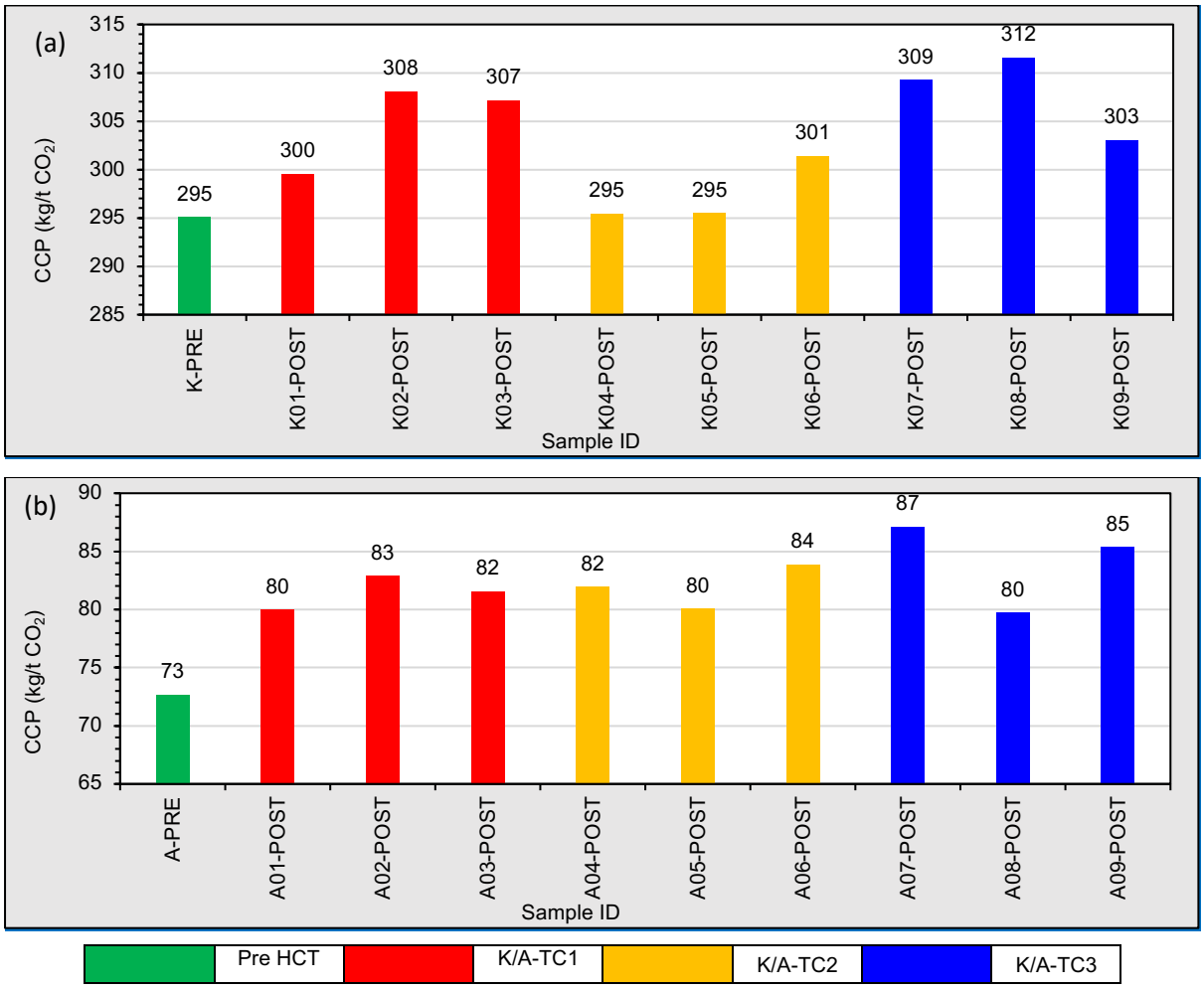


*Figure 32 – Kevitsa (a) and Aitik (b) pre and post HCT CCP values*

## 5.2 Static Testing Results

The results of the static testing program undertaken in this study are outlined within this section. The procedures, standards and any relevant deviations from standards used within this program are outlined in Chapter 4, section 4.4, of this thesis.

### 5.2.1 Total C and S results

Total C was measured following the EN 13137:2001 standard, while total S assessment followed EN 14582. Detailed method descriptions are outlined in section 4.4.1 of this thesis.

***Kevitsa total carbon and sulfur analysis results***

It can be seen in Figure 33 (a) that the composite waste rock material utilised in Kevitsa HCT cells comprised a total C% content of 0.09%, with the K-Pre duplicate also comprising 0.09% C. Post HCT cell triplicate cells showed minimal alteration after the 60-week HCT protocol. K-TC1 cell all measured a C% content of 0.07% after decommissioning. K-TC2 cells displayed C contents of 0.08% for cell K04, with cells K05 and K06 measuring 0.073%. Reduced temperature cells, K07, K08 and K08, displayed post HCT total C% of 0.074%, 0.066% and 0.07%, respectively. Post testing all HCT cell materials displayed marginally reduced total S% content compared to K-Pre, see Figure 33 (b). K-TC1, K-TC2 and K-TC3 cells held mean total S% contents of 0.43%, 0.41% and 0.42% respectively, with K-Pre measuring a total S% of 0.47%.

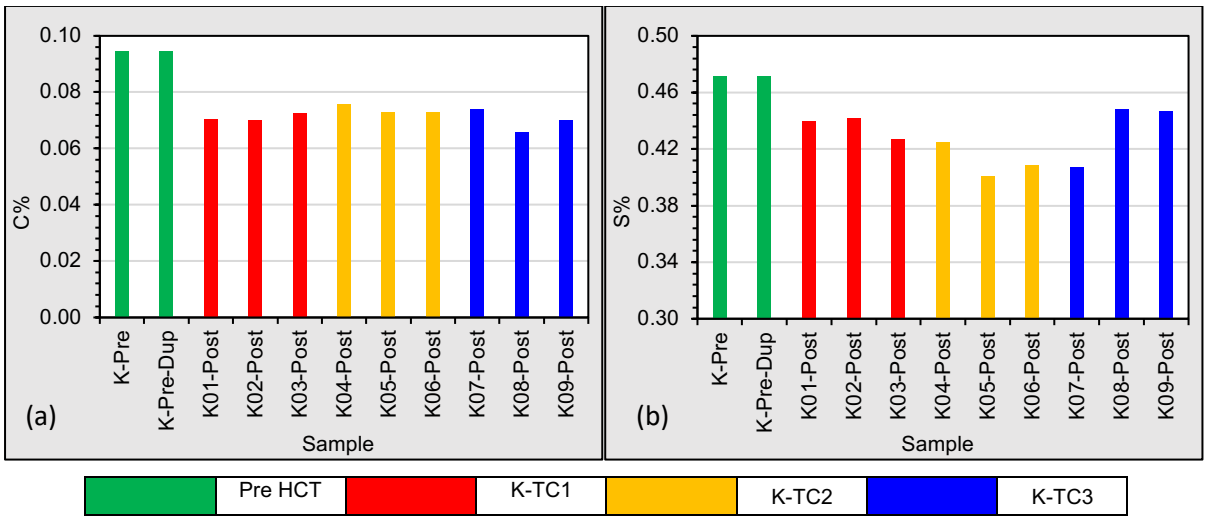


*Figure 33 - Kevitsa pre/post HCT total carbon (a) and sulfur (b) results*

***Aitik total carbon and sulfur analysis results***

A-Pre material measured a total C% content of 0.03%, see Figure 34 (a). Post HCT cells displayed marginal, but consistent, increases in total C% across all Aitik triplicate sets. A-TC1 cells, A01, A02 and A03, held post HCT C% contents of 0.038%, 0.037% and 0.037% respectively. Similarly, A-TC2 cells displayed increased C% contents of 0.040% for cells A04 and A05, with cell A06 having a C% content of 0.043%. Cells within A-TC3 demonstrated similar C% content to A-TC1 with A07, A08 and A09 holding post HCT values of 0.043%, 0.037% and 0.035% respectively.

Post HCT total S% values were shown to decrease in all Aitik triplicate samples, compared to A-Pre with 0.85% sulfur. A-TC1 cells A01 and A02 displayed the greatest reduction in total S% with measured values of 0.628% and 0.688%. Cell A03 is an outlier within this triplicate, with a post HCT total S% content of 0.818%. Control cells in A-TC2 held measured total S% contents of 0.706%, 0.736 and 0.733%, respectively, while it can be seen in Figure 34 (b) that A-TC3 cells measured values of 0.711%, 0.785% and 0.698% in cells A07, A08 and A09.

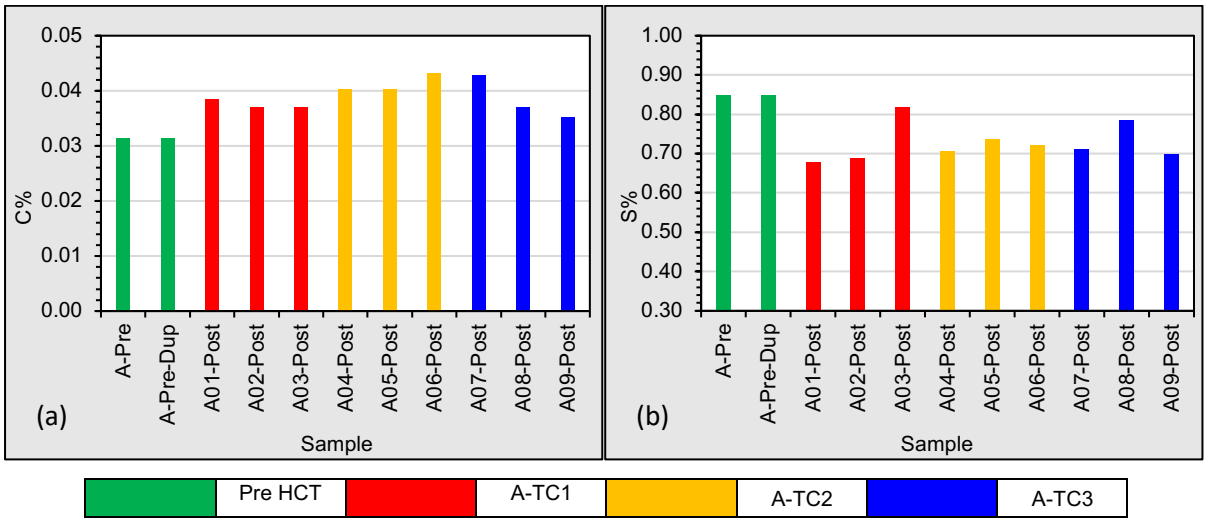


*Figure 34 – Aitik pre/post HCT total carbon (a) and sulfur (b) results*

### 5.2.2 ANC and ABA results

Acid neutralising capacity (ANC) tests were carried out on Kevitsa and Aitik materials pre and post HCT protocols to assess potential changes to acid base accounting (ABA) characteristics post kinetic testing. Assessment of ABA parameters including neutralising potential (NP), carbonate NP ($CO_3$-NP), maximum potential acidity (MPA), net neutralisation potential (NNP) and neutralisation potential ratio (NPR) has been

carried out. ABA procedures within this study followed the BS EN 15875:2011 standard, with more method details available in section 4.4.2 of Chapter 4.

ANC and ABA experimental outputs and parameter comparison graphs can be found in Appendix 16 of this thesis.

***Kevitsa ABA results***

The main ABA results obtained through ANC testing for Kevitsa pre and post HCT samples are outlined in Table 11. The pre HCT Kevitsa composite samples, K-Pre, held an NP values of 24.63 kg $CaCO_3$ eq /t and 24.19 kg $CaCO_3$ eq /t (duplicate). It was demonstrated that NP increased in all post HCT Kevitsa cell samples. K-TC1, K-TC2 and K-TC3 triplicate cells held mean average NP values of 29.61 kg $CaCO_3$ eq /t, 28.95 kg $CaCO_3$ eq /t and 28.48 kg $CaCO_3$ eq /t, demonstrating little variation between post HCT sample NP. Carbonate NP was shown to decrease in all Kevitsa HCT samples, which would be expected due to reduced total C% contents identified in Figure 33 (a).

MPA values were shown to decrease in all post HCT samples (~10-20%), this would also be expected due to small reduction in total S% contents in corresponding samples. As NP has increased and MPA has decreased in all analysed samples, NNP has also increased. Pre HCT NNP values were 9.91 kg $CaCO_3$ eq /t, 9.47 kg $CaCO_3$ eq /t in the duplicate, indicating the sample is classifiable as non-potentially acid generating (non-PAG). NPR values are >1 in all analysed samples indicating sufficient NP is available to neutralise potential acidity.

*Table 11 - Kevitsa pre and post HCT ABA parameter results*

| Kevitsa Acid Base Accounting (ABA) Parameters | | | | | |
|---|---|---|---|---|---|
| Sample ID | NP | Carbonate NP | MPA | NNP | NPR |
| | (kg CaCO3 eq /t) | (kg CaCO3 eq /t) | kg CaCO3 eq /t | kg CaCO3 eq /t | |
| K-Pre | 24.63 | 7.87 | 14.72 | 9.91 | 1.67 |
| K-Pre-Dup | 24.19 | 7.87 | 14.72 | 9.47 | 1.64 |
| K-TC1 Post HCT Samples | | | | | |
| K01-Post | 29.01 | 5.87 | 13.73 | 15.28 | 2.11 |
| K02-Post | 30.31 | 5.85 | 13.80 | 16.51 | 2.20 |
| K03-Post | 29.52 | 6.04 | 13.33 | 16.19 | 2.21 |
| K-TC2 Post HCT Samples | | | | | |
| K04-Post | 29.88 | 6.32 | 13.28 | 16.59 | 2.25 |
| K05-Post | 29.66 | 6.08 | 12.53 | 17.13 | 2.37 |
| K06-Post | 27.32 | 6.07 | 12.78 | 14.54 | 2.14 |
| K-TC3 Post HCT Samples | | | | | |
| K07-Post | 27.85 | 6.16 | 12.72 | 15.13 | 2.19 |
| K08-Post | 28.38 | 5.48 | 14.00 | 14.37 | 2.03 |
| K09-Post | 29.21 | 5.84 | 13.97 | 15.24 | 2.09 |

### *Aitik ABA results*

The main ABA results obtained through ANC testing for Aitik pre and post HCT samples are outlined in Table 12. It can be seen in Table 12 that pre-HCT the Aitik composite sample measured an NP of 7.76 kg $CaCO_3$ eq /t, 7.11 $CaCO_3$ eq /t in sample duplicate. Variable NP results were observed following HCT protocols in all Aitik samples. A-TC1 samples, A01, A02 and A03, held NP values of 6.63 $CaCO_3$ eq /t, 6.92 $CaCO_3$ eq /t and 7.66 $CaCO_3$ eq /t post testing. Control Aitik cells, A-TC2, displayed similarly variable post HCT NP results with values of 6.87 $CaCO_3$ eq /t, 7.88 $CaCO_3$ eq /t and 6.69 $CaCO_3$ eq /t measured in A04, A05 and A06 materials. Aitik reduced temperature cells, A-TC3, displayed a more pronounced and consistent increases in post HCT NP with cells A07, A08 and A09 demonstrating NP values of 9.16 $CaCO_3$ eq /t, 10.11 $CaCO_3$ eq /t and 9.52 $CaCO_3$ eq /t, respectively. Carbonate NP was shown to increase after the 60-week leaching period, which is due to the observed increase in total C% content in all cells.

MPA was shown to decrease from ~26.5 $CaCO_3$ eq /t in A-Pre duplicates to between 21.1 $CaCO_3$ eq /t to 25.5 $CaCO_3$ eq /t in post HCT materials. Pre and post Aitik HCT samples are classified as potentially acid forming (PAG), with all samples holding NNP values <0 $CaCO_3$ eq /t and NPR values <1. Increases in NNP and NPR was noted in

all cells post HCT protocols, due to the reduction in total S% content noted in Figure 47(a). No distinguishable differentiations in ARD classification are noted in Aitik HCT materials following the experimental testing period.

*Table 12 - Aitik pre and post HCT ABA parameter results*

| Aitik Acid Base Accounting (ABA) Parameters | | | | | |
|---|---|---|---|---|---|
| Sample ID | NP | Carbonate NP | MPA | NNP | NPR |
| | (kg CaCO3 eq /t) | (kg CaCO3 eq /t) | kg CaCO3 eq /t | kg CaCO3 eq /t | |
| A-Pre | 7.76 | 2.61 | 26.47 | -18.71 | 0.29 |
| A-Pre-DUP | 7.11 | 2.61 | 26.78 | -19.67 | 0.27 |
| A-TC1 Post HCT Samples | | | | | |
| A01-Post | 6.63 | 3.20 | 21.18 | -14.55 | 0.31 |
| A02-Post | 6.92 | 3.09 | 21.49 | -14.58 | 0.32 |
| A03-Post | 7.66 | 3.09 | 25.58 | -17.91 | 0.30 |
| A-TC2 Post HCT Samples | | | | | |
| A04-Post | 6.87 | 3.35 | 22.07 | -15.20 | 0.31 |
| A05-Post | 7.88 | 3.35 | 23.00 | -15.12 | 0.34 |
| A06-Post | 6.69 | 3.59 | 22.56 | -15.86 | 0.30 |
| A-TC3 Post HCT Samples | | | | | |
| A07-Post | 9.16 | 3.57 | 22.21 | -13.04 | 0.41 |
| A08-Post | 10.11 | 3.07 | 24.53 | -14.42 | 0.41 |
| A09-Post | 9.52 | 2.93 | 21.81 | -12.29 | 0.44 |

### 5.2.3 NAG test results

Net acid generation (NAG) testing undertaken in this study followed the single addition net acid generation (NAG) test outlined in the AMIRA ARD handbook (AMIRA 2002), refer to section 4.4.3 of this thesis. NAG tests differ from ABA assessments as they provide a direct measurement of overall sample reactivity (Charles et al. 2015). Results obtained in this test, in conjunction with NNP, can be used to classify the acid generating potential of a material. Total NAG results are presented in kg $H_2SO_4$ eq/t, in line with the utilised AMIRA test method. NAG pH is noted as the pH measured post hydrogen peroxide ($H_2O_2$) addition and boiling seps of the single addition NAG test.

#### *Kevitsa NAG results*

The NAG pH results obtained for pre and post Kevitsa HCT materials are shown in Figure 35. It can be seen in this Figure that pre HCT Kevitsa composite material demonstrated a NAG pH of ~pH 7.3. All post HCT samples, irrelevant of triplicate set, displayed increased NAG pH post 60-week HCT protocols. It is noted that this is likely

due to the notable reduction in total S% shown in Figure 33 (a). All Kevitsa materials measured NAG pH values above pH 4.5 and pH 7, therefore no titration was required to reach these pH values. As such no distinguishable total NAG value could be calculated for these materials. Sequential or kinetic NAG tests may be required to adequately determine NAG potential of these materials (AMIRA 2002).

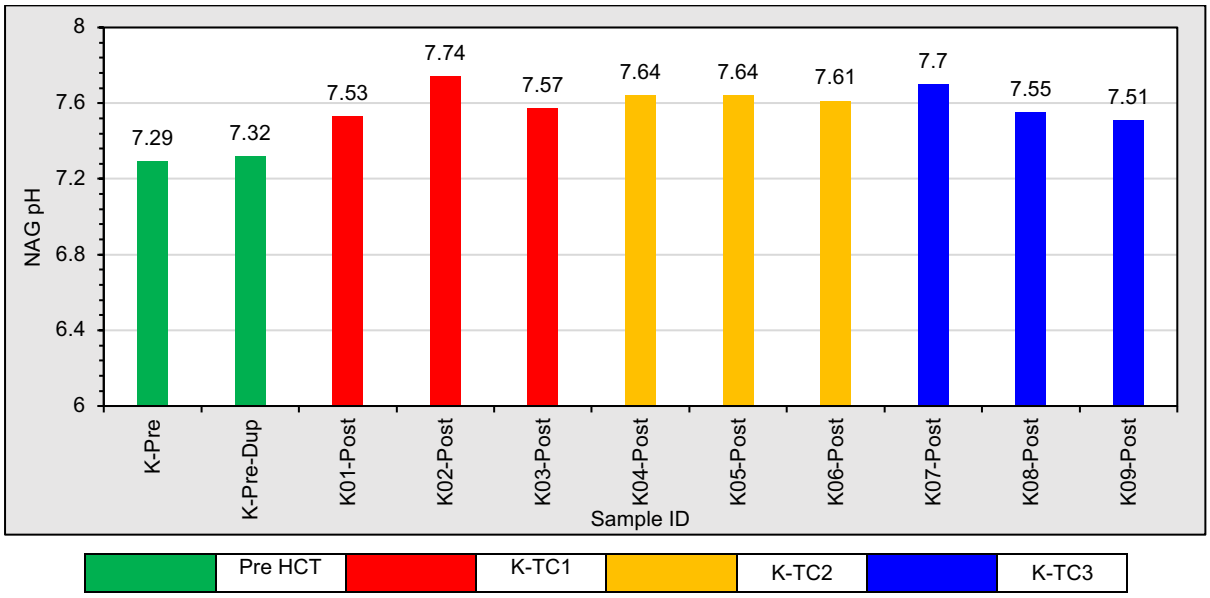


*Figure 35 - Kevitsa pre and post HCT NAG pH results*

***Aitik NAG results***

The NAG pH results obtained from single addition NAG tests caried out on pre and post Aitik HCT samples are shown in Figure 36 (a). Following $H_2O_2$ addition and boiling, pre HCT Aitik materials demonstrated NAG pH values of pH 3.37 and pH 3.23 between duplicates. Post HCT materials demonstrated a consistent increase in NAG pH amongst all Aitik triplicate sets. No distinguishable differentiation in NAG pH is apparent between A-TC1, A-TC2 and A-TC3 cell sets, with values within the range of pH 4.04 and pH 4.16. Purely based on NAG pH, all Aitik samples may be considered potentially acid forming (PAF) / potentially acid generating (PAG), as all sample hold a NAG pH of <4.5.

As all Aitik materials, both pre and post HCT, held NAG pH values below pH 4.5, total NAG could be calculated through titration to pH 4.5 and pH 7. It can be seen in Figure 36 (b) that the pre HCT Aitik composite material held total NAG values of 6.56 $H_2SO_4$ eq/t and 6.75 $H_2SO_4$ eq/t amongst sample duplicates. Variations amongst post HCT

sample total NAG values were observed within triplicate sets. Within A-TC1 all samples displayed a reduction in total NAG, with cells A01, A02 and A03 measuring values of 5.29 $H_2SO_4$ eq/t, 6.27 $H_2SO_4$ eq/t and 5.88 $H_2SO_4$ eq/t, respectively. Control cells A05 and A06 displayed reduced total NAG values of 5.29 $H_2SO_4$ eq/t and 5.48 $H_2SO_4$ eq/t, while cell A06 held a total NAG value of 6.66 $H_2SO_4$ eq/t, sitting between the pre HCT duplicate values. A-TC3 cells displayed similar levels of variation in total NAG with values between 5.88 $H_2SO_4$ eq/t and 7.05 $H_2SO_4$ eq/t measured. These results do not present distinguishable patterns between total NAG result and test conditions.

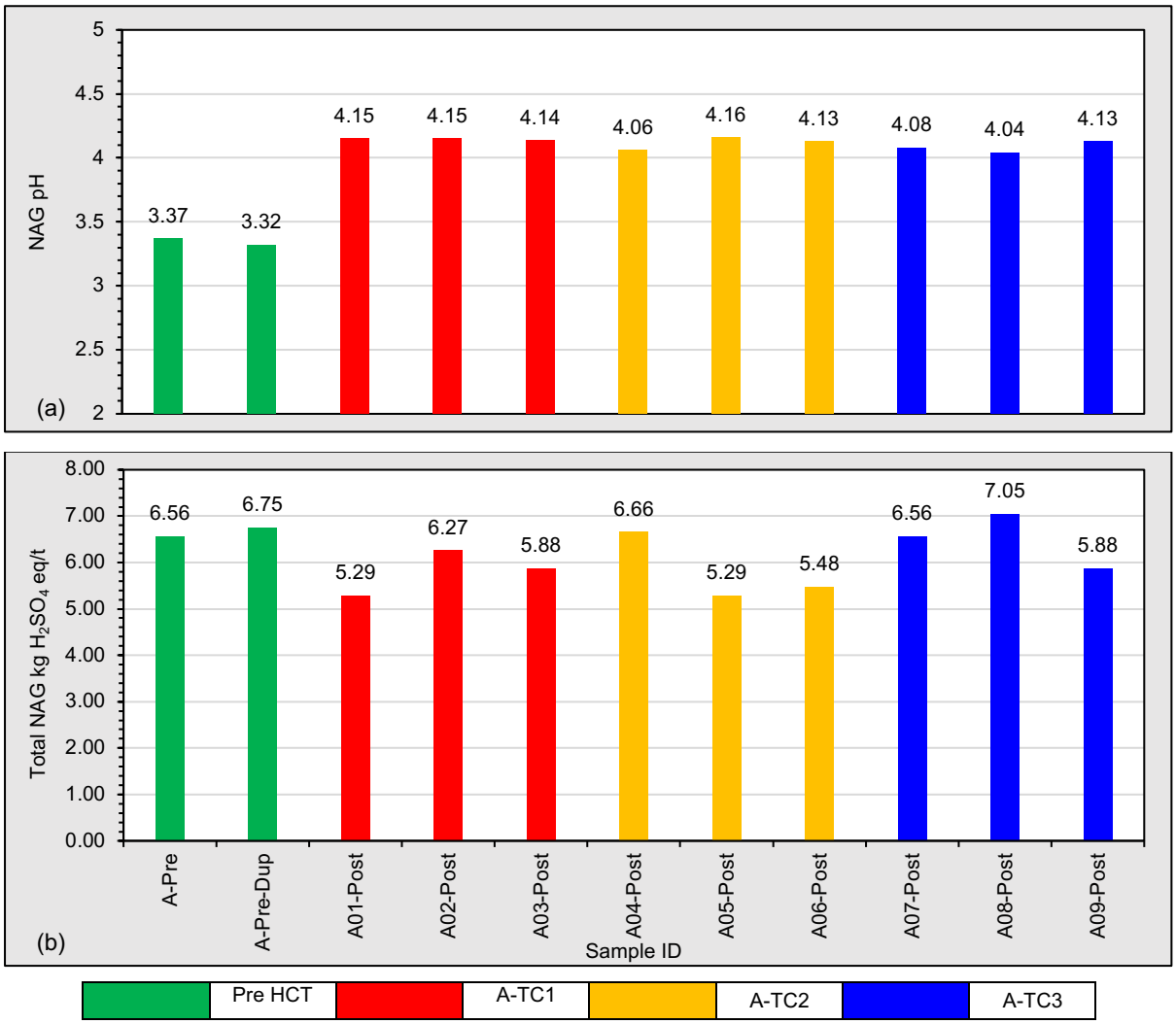


*Figure 36 - Aitik pre and post HCT (a) NAG pH and (b) total NAG results*

### 5.2.4 ABCC test results

ABCC testing was carried out was undertaken in accordance with Appendix G of the AMIRA (2002) ARD Test Handbook (AMIRA 2002), refer to section 4.4.4 of Chapter 4. Pre HCT composite samples, used in both the Kevitsa and Aitik HCT triplicate sets, were tested as well as the post HCT residues. Due to time and budgetary constraints one post HCT sample was tested from each of the three triplicate sets for both Kevitsa and Aitik HCT's. HCl additions to reach the end pH of pH 2.5 have been converted to $H_2SO_4$ eq kg/t in line with the AMIRA guidance.

#### *Kevitsa ABCC curves*

The results of ABCC testing on pre and post Kevitsa HCT samples are shown in Figure 37. Out of the nine post HCT samples available K02, K05 and K08 were selected for ABCC testing, allowing for analysis of one post HCT samples from the three Kevitsa triplicates sets. It can be seen in this figure that K-Pre and K-Pre-DUP required the addition of 22.76 $H_2SO_4$ eq kg/t and 26.23 $H_2SO_4$ eq kg/t to reach pH 2.5. Comparatively K-TC1 and K-TC3 cells K02 and K08 required the addition of 21.78 $H_2SO_4$ eq kg/t and 19.66 $H_2SO_4$ eq kg/t, respectively to reach pH 2.5. Control cell, K05, required 29.86 $H_2SO_4$ eq kg/t to reach pH 2.5 and displayed a distinctly different buffering curve than the K-Pre, K-TC1 and K-TC3 samples.

The shape of the buffering curves shown in Figure 37 suggest a slight decrease in readily available NP in K-TC1 and K-TC3 cells, compared to K-Pre, while K05 displays more readily available NP. Samples K02, K05 and K08 hold comparable ABA based NP values (30.31 kg $CaCO_3$ eq /t, 29.66 $CaCO_3$ eq /t and 28.38 $CaCO_3$ eq /t), therefore these results suggest that NP is more readily available in post HCT sample K05.

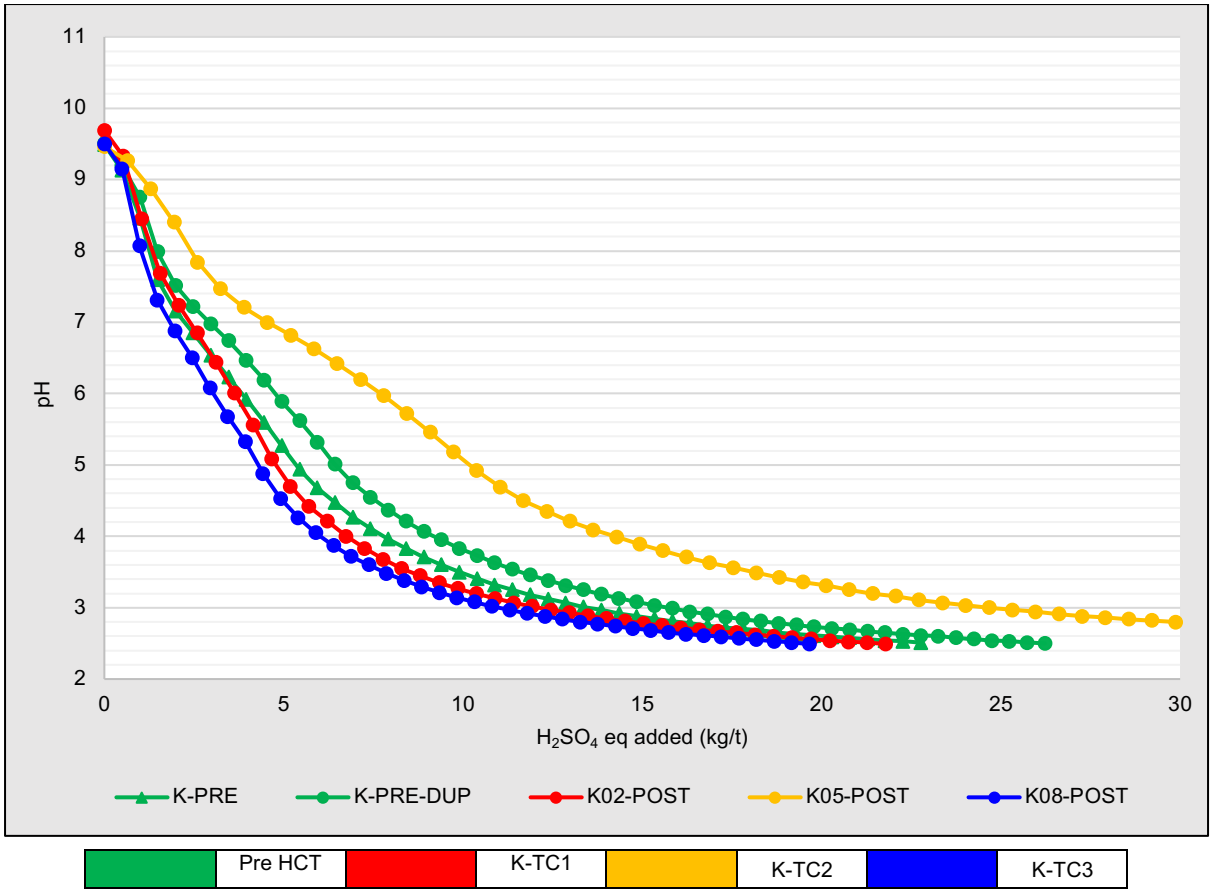


*Figure 37 - Kevitsa pre and post HCT ABCC curves*

### *Aitik ABCC curves*

The results of ABCC testing on pre and post Aitik HCT samples are shown in Figure 38. Out of the nine post HCT samples available A02, A05 and A08 were selected for ABCC testing, allowing for analysis of one post HCT samples from the three Aitik triplicates sets. It can be seen in Figure 38 that pre HCT Aitik material duplicates required the addition of 14.84 $H_2SO_4$ eq kg/t and 18.70 $H_2SO_4$ eq kg/t to reach pH 2.5. A-TC1 and A-TC3 cell samples, A02 and A08, required 24.10 $H_2SO_4$ eq kg/t and 21.14 $H_2SO_4$ eq kg/t to reach pH 2.5, suggesting a slight increase in available buffering capacity. Conversely to the results displayed for Kevitsa post HCT ABCC results, A-TC2 cell, A05, required a lower addition volume, 17.66 $H_2SO_4$ eq kg/t, to reach pH 2.5. The buffering curves display a distinct lack of readily available NP in all Aitik materials.

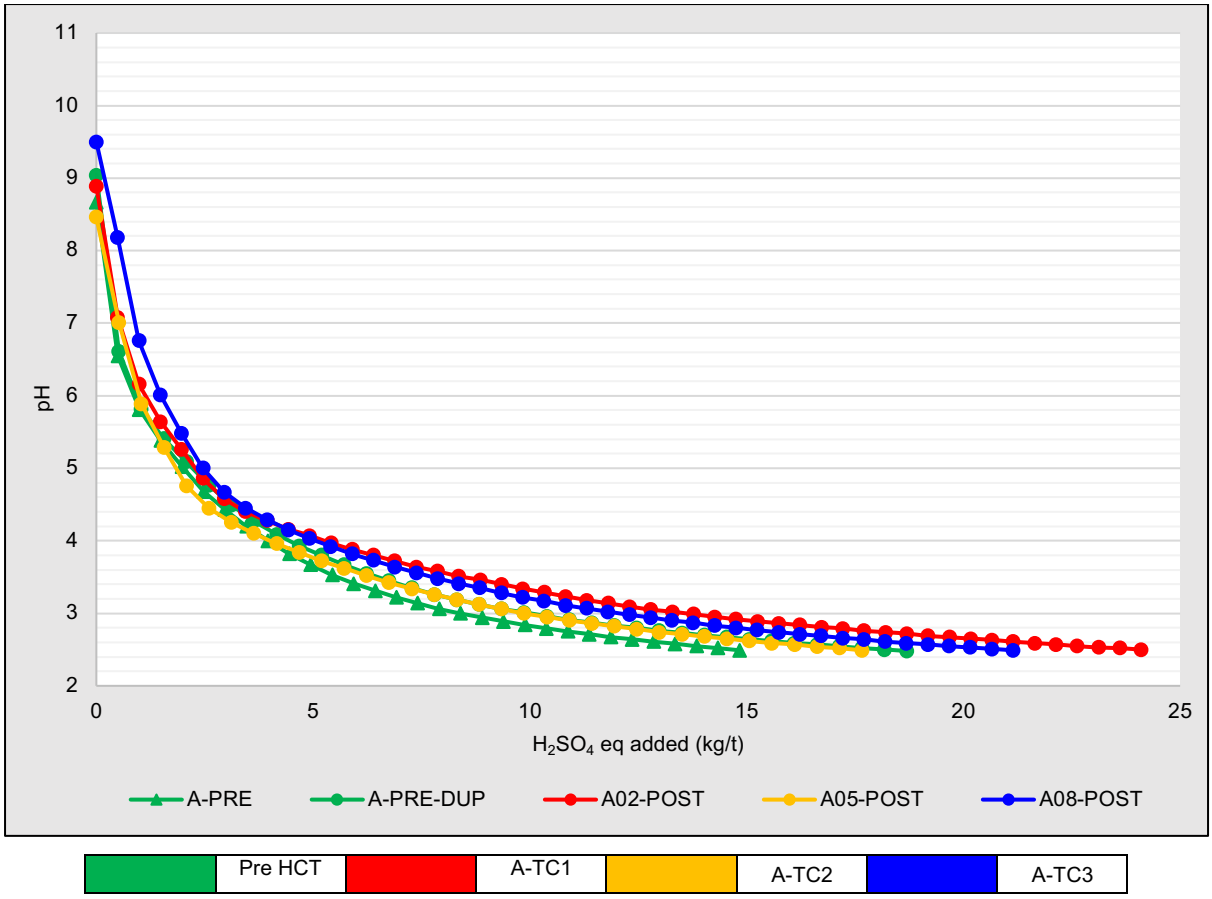


*Figure 38 - Aitik pre and post HCT ABCC curves*

### 5.2.5 Paste pH and EC test results

Paste pH and EC results were derived following the near saturation paste pH analysis standard outlined in section 11.6.4 of the MEND 1.20.1 manual (Price 2009). The standard has been amended from a 1:2 liquid to solid ratio, to a 1:1 liquid to solid ratio, refer to section 4.4.5 of Chapter 4. Paste pH presents a potentially more accurate representation of pore water conditions within waste and subsequently is used to assess potential acidification of weathered materials.

It can be seen in Figure 39 (a) that pre HCT material from Kevitsa, K-Pre, held a paste pH value of pH 8.9. Post HCT samples from all Kevitsa triplicate sets displayed minimal alteration to paste pH, irrelevant of triplicate set, with values within the narrow range of pH 8.82 to pH 8.81. K-Pre held a paste EC value of 735 µS/cm, while EC values were shown to variably drop in post HCT samples. This would be expected due to flushing of soluble salts during HCT leaching.

Aitik samples displayed clearly changes in paste pH and EC following variable HCT protocols. It can be seen in Figure 39 (b) that pH was shown to rise in all post HCT samples, from ~pH 8 in A-Pre, to > pH8.2 in all cell samples. A-TC3 displayed the largest increase in paste pH with sample A08 reaching pH 8.73. This increase in paste pH is seemingly coupled with distinct reduction in paste EC as sample A08 measured an EC of 524 µS/cm, compared to the EC reading of 986 µS/cm measured in A-Pre duplicate samples.

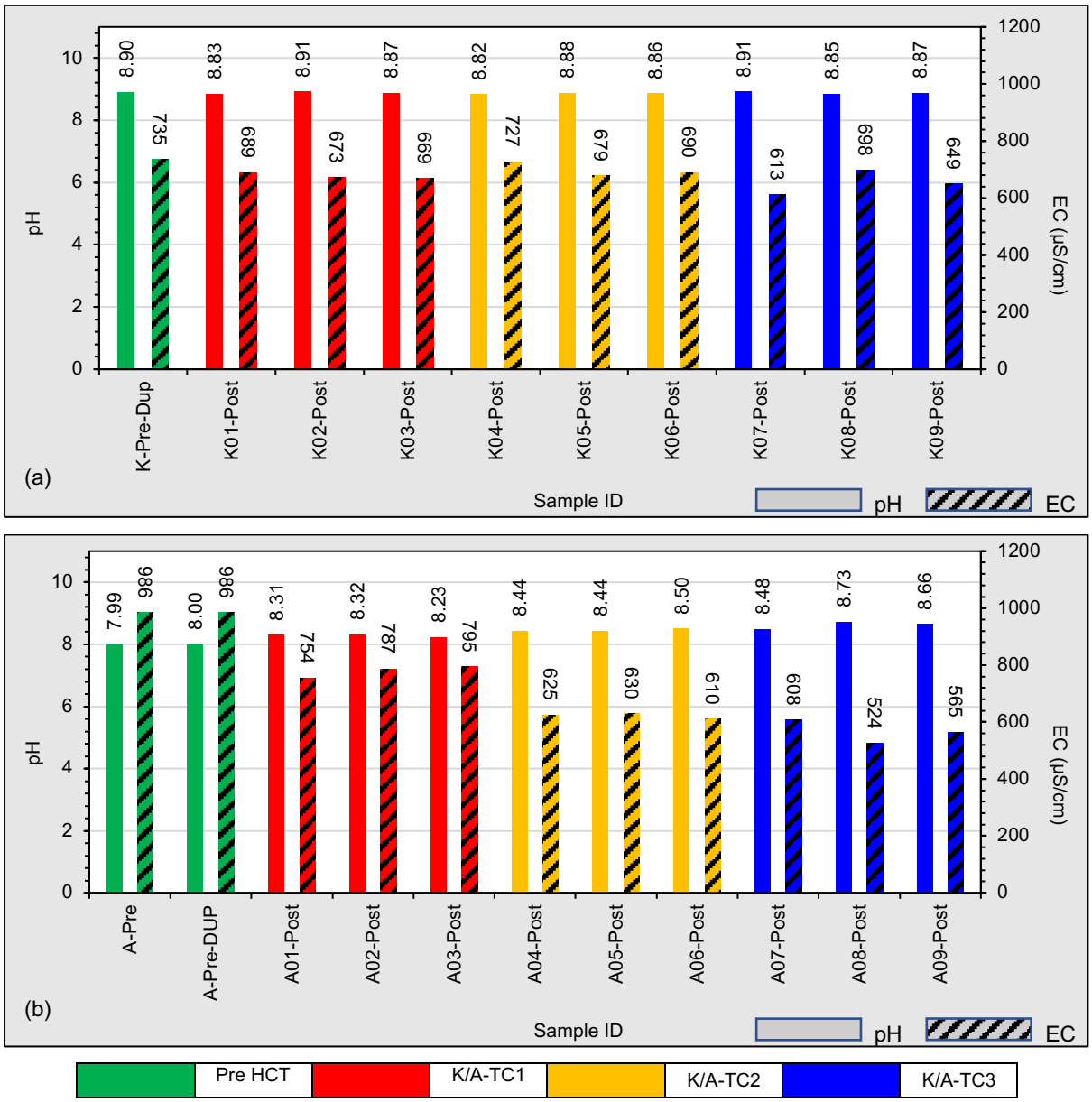


*Figure 39 - Pre and Post HCT Kevitsa (a) and Aitik (b) paste pH and EC Results*

### 5.2.6 24 hour 2:1 leach test results

A single stage 24 hour 2:1 (L:S) batch leach test was carried out on pre and post HCT materials from both Kevitsa and Aitik. This test followed an amended version of the CEN-EN 12457-1 standard (BSI 2002a). Full method details and amendments are outlined in section 4.4.6 of Chapter 4. Following the 24-hour leaching period cell sample eluent from both Kevitsa and Aitik pre and post HCT materials were subjected to aqueous elemental analysis via ICP-OES. Basic chemical parameters were also measured including eluent pH, EC, ORP, DIC and sulfate.

#### *Kevitsa leach test results*

Basic chemistry measurements and elemental analysis was undertaken on post leach eluent recovered from leach tests carried out on samples K-Pre, K01-K03 (K-TC1), K04-K06 (K-TC2) and K07-K09 (K-TC3). Elements presented include Ca, K, Mg, Na, S, Si and Ni. Other elemental results obtained in this test can be found in Appendix 8.

The basic chemical characteristics of recovered leach eluent from Kevitsa materials tests are shown in Figure 40. It can be seen in Figure 40 (a) that post leach pH increased for all post HCT cell materials. K-Pre held a post leach pH's of pH 9.62 and pH 9.6 between duplicate tests runs. Post HCT materials recovered from K-TC1 cells, K01, K02 and K03, held comparable post leach pH measurements of pH 9.78, pH 9.73 and pH 8.82. Control Kevitsa cell materials demonstrated the greatest increase in post leach pH of all Kevitsa triplicates with cells K04, K05 and K06 measuring eluent pH values of pH 9.88, pH 9.93 and pH 9.86. K-TC3 cells held the lowest post leach pH results of Kevitsa post HCT materials, with eluent pH's of pH 9.73, pH 9.75 and pH 9.73 measured from cells K07, K08 and K09, respectively.

As was expected following a 60-week leaching protocol, all post HCT materials from Kevitsa demonstrated marked decreases in eluent EC when compared to K-Pre. K-Pre and K-Pre-DUP held post leach EC measurements of 386.6 µS/cm and 387.6 µS/cm, respectively. Comparatively, post HCT triplicate sets K-TC1, K-TC2 and K-TC3 held mean average post leach EC values of 244.9 µS/cm, 217.6 and 284.6 µS/cm, respectively.

These results indicate that alterations to HCT testing parameters in K-TC1 and K-TC3 cells may have led to a marginal retention of soluble salts when compared to control cells in K-TC2.

Post leach DIC eluent concentrations were variable within post HCT samples. Sample K-pre displayed DIC concentrations of 5.92 mg/L and 6.01 mg/L between duplicates. Post leach DIC concentrations from K-TC1 cells ranged from 5.1 mg/L to 6.54 mg/L. Results obtained from K-TC2 post leach eluents demonstrated similar variable DIC concentrations with cells K04, K05 and K06 measuring 5.73 mg/L, 6.53 mg/L and 6.76 mg/L, respectively. The highest DIC concentration increase was noted in the post leach eluent of cell K07, which measured 6.94 mg/L. Eluents collected from cells K08 and K08 measured DIC concentrations of 6.2 mg/L and 6.08 mg/L, respectively.

It can be seen in Figure 40 (d) that K-Pre held a post leach sulfate concentration of ~106 mg/L. Post HCT samples demonstrated clear reductions in available leached sulfate post testing. K-TC1, K-TC2 and K-TC3 cells held mean average sulfate concentrations of 43.8 mg/L, 34.8 mg/L and 58 mg/L, respectively.

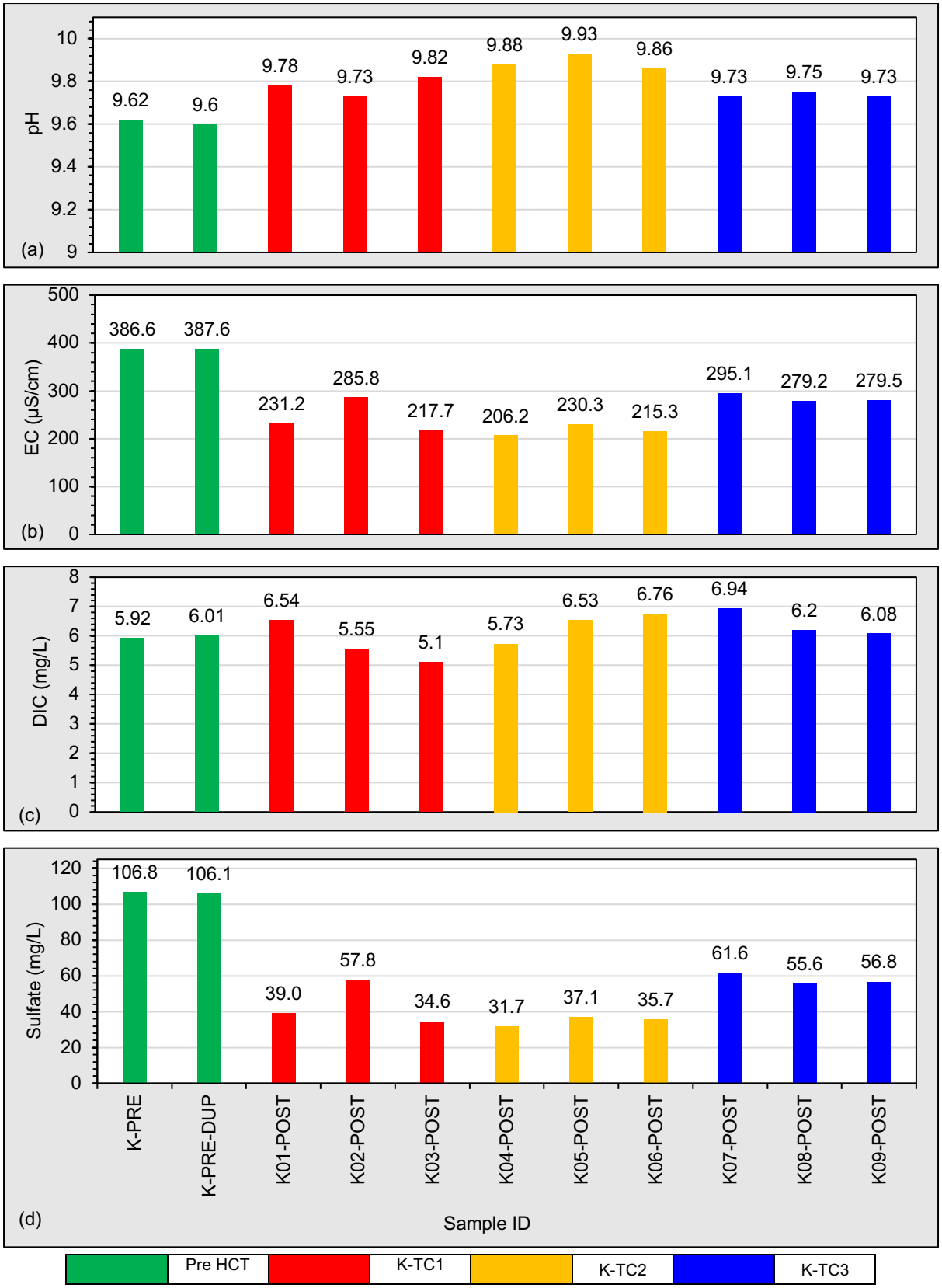


*Figure 40 - Kevitsa HCT 2:1 24-hour leach test basic chemistry results. (a) pH, (b) EC, (c) DIC and (d) sulfate.*

Selective elemental concentrations measured from pre and post Kevitsa HCT material 24-hour leach eluents are shown in Table 13. It can be seen in this table that Mg concentrations measured in post leach eluents was reduced for all HCT samples, irrelevant of triplicate set. Pre HCT composite material, K-Pre, held a measured Mg concentration of ~25.6 mg/L, compared to concentrations of between 7.2-7.9 mg/L within post HCT control set K-TC2. The concentrations of Mg in post leach eluents from K-TC1 and K-TC3 cells displayed a less pronounced reduction when compared to K-TC2. Cells K01 and K03 held Mg concentrations of 10.0 mg/L and 9.6 mg/L, while cells K02 demonstrated a higher Mg concentration of 16.7 mg/L. K-TC3 cells measured a mean average post leach Mg concentration of 12.1 mg/L.

Post leach measurements of all displayed elemental concentrations within cell K02 were notably higher than cells K01 and K03, with a S concentration ~100% higher than these comparable cells. This variation is unlikely to be pH dependent with post leach pH measurements consistent with the K-TC1 triplicate set. Si concentrations were notably higher in post HCT leach eluents with K-TC1 and K-TC2 displaying marginally higher concentrations than K-TC2 control cells. Excluding the questionable S concentration noted in cell A02 post leach eluent, S concentrations were higher on average within K-TC3 cells than K-TC1 and K-TC3 cells. K-TC3 held a mean S concentration of 35.8 mg/L, compared to 23.7 mg/L in KTC-2 cells and 21.8 mg/L (excluding cell A02) in K-TC1 cells. This may suggest a higher proportion of remaining available S sources in K-TC3 cells post HCT testing compared to control cells and K-TC1 cells.

*Table 13 - Kevitsa 24-hour leach eluent elemental concentrations*

| Kevitsa pre and post HCT 24-hour 2:1 leach test elemental concentrations | | | | | | | |
|---|---|---|---|---|---|---|---|
| Element | Ca | K | Mg | Na | S | Si | Ni |
| Unit | mg/L | mg/L | mg/L | mg/L | mg/L | mg/L | µg/L |
| ADL | 0.1 | 0.1 | 0.1 | 0.1 | 1 | 0.1 | 1 |
| K-Pre | 23.2 | 19.3 | 25.6 | 6.8 | 49.4 | 9.2 | 4.0 |
| K-Pre-DUP | 23.1 | 19.4 | 25.4 | 6.7 | 49.6 | 9.2 | 3.9 |
| K-TC1 Post HCT Samples | | | | | | | |
| K01 | 16.6 | 6.8 | 10.0 | 2.4 | 22.5 | 13.5 | 2.1 |
| K02 | 26.4 | 10.6 | 16.7 | 3.3 | 41.3 | 17.8 | 2.1 |
| K03 | 16.3 | 6.4 | 9.6 | 2.5 | 21.2 | 15.1 | 1.9 |
| K-TC1 Post HCT Samples | | | | | | | |
| K04 | 16.5 | 8.6 | 7.2 | 2.6 | 18.4 | 12.8 | 1.9 |
| K05 | 18.9 | 7.5 | 7.7 | 2.9 | 28.5 | 13.1 | 1.5 |
| K06 | 17.3 | 7.0 | 7.9 | 2.5 | 24.2 | 12.6 | 1.9 |
| K-TC1 Post HCT Samples | | | | | | | |
| K07 | 23.1 | 7.6 | 12.9 | 2.4 | 43.1 | 12.5 | 2.1 |
| K08 | 21.8 | 8.1 | 11.8 | 2.3 | 28.7 | 14.1 | 1.9 |
| K09 | 21.2 | 8.5 | 11.7 | 2.3 | 35.6 | 12.8 | 2.5 |

### *Aitik leach test results*

Basic chemistry measurements and elemental analysis was undertaken on post leach eluent recovered from leach tests carried out on all Aitik post HCT triplicate samples and the Aitik pre HCT composite sample. Elements presented include Ca, K, Mg, Na, S, Si and Mn. Other elemental results measured can be found in Appendix 8.

Post leach eluent pH, EC, DIC and sulfate measurements from pre and post Aitik HCT materials are shown in Figure 41 parts (a), (b), (c) and (d), respectively. Post leach eluent pH measurements were variable in cell set A-TC1, with an eluent pH range of pH 7.76-8.08. This is compared to A-Pre duplicate leaches which measured post leach eluent pH readings of pH 8.07 and pH 8.13. A-TC2 control cells showed less variation in post leach eluent pH with cells A04, A05 and A06 measuring pH's of pH 7.95, pH 8.08 and pH 7.99, respectively. Of the three post HCT triplicate sets, A-TC3 showed the closest range of post leach eluent pH measurements, reporting pH's of pH 7.88, pH 7.87 and pH 7.9 in cells A07, A08 and A09. Electrical conductivity (EC) measurements within Aitik pre HCT duplicates were 341.3 µS/cm and 344.5 µS/cm.

EC was shown to drop by >60% in all post HCT materials recovered from Aitik cells. A-TC1, A-TC2 and A-TC3 held mean average EC measurements of 123.5 µS/cm, 118.4 µS/cm and 101.8 µS/cm, respectively. Cell A03 displayed the highest EC of post HCT leached samples with an EC of 148.5 µS/cm.

All post leach eluents recovered from post HCT samples, apart from A03, displayed DIC values <6 mg/L, compared to ~9.23 mg/L within A-Pre. Eluent recovered from cell A03 displayed the highest post HCT DIC measurement of all cells with a DIC concentration of 8.65 mg/L. Excluding this erroneous value, A-TC1, A-TC2 and A-TC3 held mean average DIC concentrations of 4.7 mg/L, 5.75 mg/L and 4.08 mg/L.

Pre HCT Aitik materials displayed a post leach sulfate concentration of 98.8 mg/L. All post HCT leach eluent sulfate concentrations were shown to decrease within a consistent range across all post HCT cells, irrelevant of triplicate set. It can be seen in Figure 41 (d) that post HCT leach eluent sulfate measurements ranged between 15.9 mg/L (cell A09) and 19.8 mg/L (cell A01). A-TC3 was shown to have the marginally lower average sulfate concentration of all Aitik cell sets.

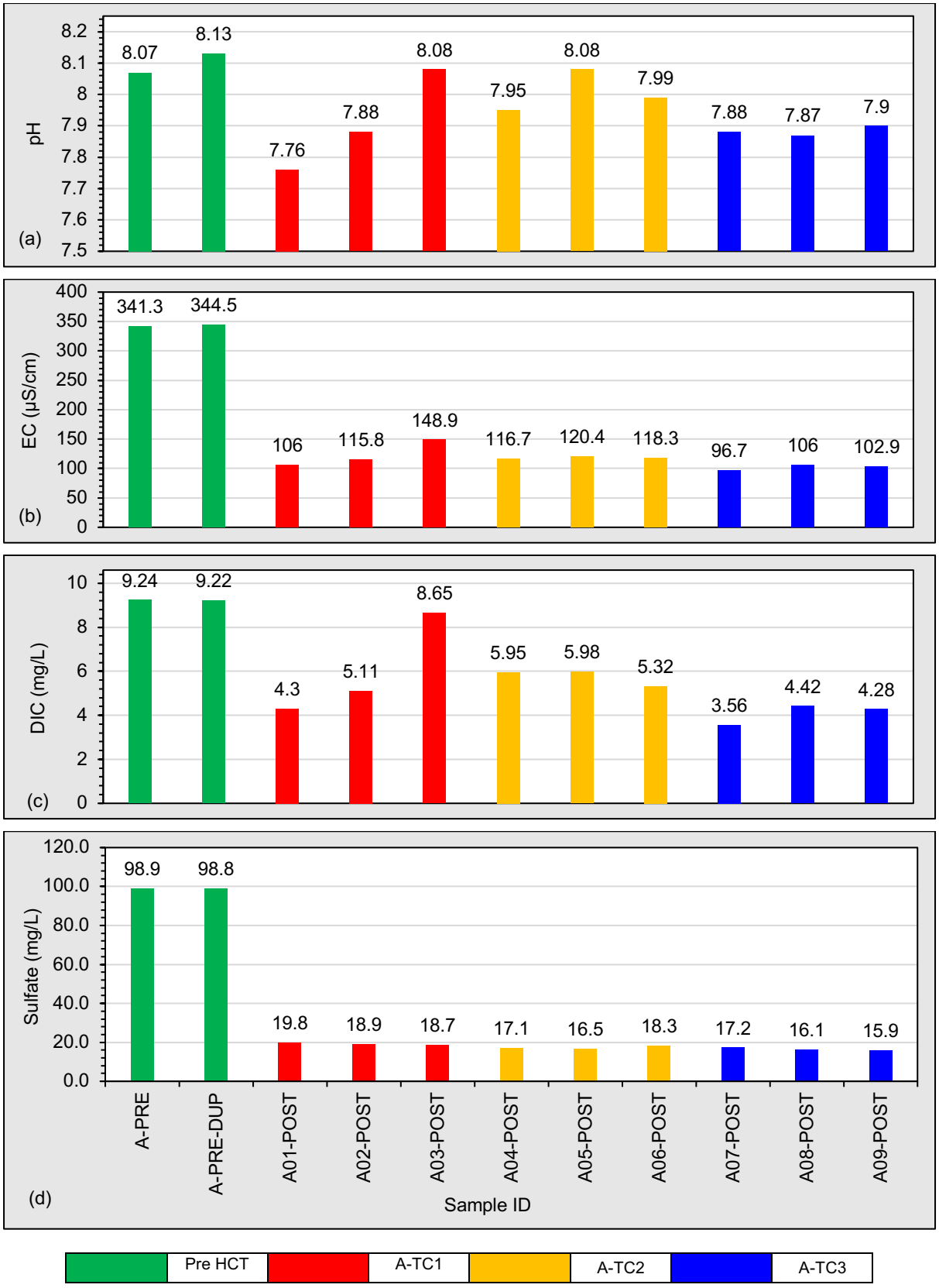


*Figure 41 - Aitik HCT 2:1 24-hour leach test basic chemistry results. (a) pH, (b) EC), (c) DIC and (d) sulfate.*

Selective elemental concentrations measured from pre and post Aitik HCT material 24-hour leach eluents are shown in Table 14. It is noted that elemental analysis was not available for post leach eluents recovered from sample cell A05.

The Aitik triplicate sets A-TC2 and A-TC3 displayed reasonably consistent Ca, K, Mg, Na, S and Si concentration across cells within each triplicate. Similarly, cells A01 and A02 displayed consistent concentrations of these analysed elements. In line with erroneous chemistry results noted in Figure 41, cell A03 displayed variable elemental results when compared to other cells within its triplicate. Cell A03 measured Ca, K and Mn concentrations of 12.6 mg/L, 23.2 mg/L and 10.8 µg/L, respectively. This is compared to A01 and A02 which displayed comparable Ca, K and Mn concentrations of 5.2/7.2 mg/L, 21.6/21.0 mg/L and 51.0/32.5 µg/L. It is theorised that the notably higher pH and DIC within cell A03 post leach eluent, with a pH 8.08 and DIC concentration of 8.65 mg/L, lead to a decrease in the solubility of Mn with increased eluent alkalinity (Buamah 2009).

Generally, post HCT concentrations of all displayed elements decreased in comparison to pre HCT leach eluent concentrations. A notable increase in Si concentrations between pre and post HCT eluents was noted in cells A01, A07, A08 and A09, with these cells measuring Si concentrations >3.5 mg/L, compared to 2.2 mg/L within A-pre post leach duplicates.

*Table 14 - Aitik 24-hour leach eluent elemental concentrations*

| Aitik pre and post HCT 24-hour 2:1 leach test elemental concentrations | | | | | | | |
|---|---|---|---|---|---|---|---|
| Element | Ca | K | Mg | Na | S | Si | Mn |
| Unit | mg/L | mg/L | mg/L | mg/L | mg/L | mg/L | µg/L |
| ADL | 0.1 | 0.1 | 0.1 | 0.1 | 1 | 0.1 | 1 |
| A-Pre | 37.5 | 32.2 | 5.8 | 6.9 | 35.2 | 2.2 | 112.5 |
| A-Pre-DUP | 38.0 | 32.7 | 6.0 | 7.1 | 34.9 | 2.2 | 114.0 |
| A-TC1 Post HCT Samples | | | | | | | |
| A01 | 5.2 | 21.6 | 0.8 | 3.6 | 8.8 | 4.0 | 51.0 |
| A02 | 7.2 | 21.0 | 0.8 | 3.1 | 8.4 | 2.8 | 32.5 |
| A03 | 12.6 | 23.2 | 0.8 | 3.4 | 9.1 | 2.1 | 10.8 |
| A-TC1 Post HCT Samples | | | | | | | |
| A04 | 7.7 | 22.2 | 0.7 | 3.3 | 8.7 | 2.2 | 17.0 |
| A06 | 7.1 | 22.6 | 0.8 | 4.2 | 9.3 | 2.9 | 24.4 |
| A-TC1 Post HCT Samples | | | | | | | |
| A07 | 3.9 | 21.7 | 0.8 | 4.2 | 8.3 | 4.9 | 54.4 |
| A08 | 5.1 | 21.4 | 0.7 | 4.2 | 8.2 | 3.6 | 30.6 |
| A09 | 4.9 | 21.5 | 0.7 | 3.6 | 9.2 | 4.5 | 44.4 |

## 5.3 Kinetic Testing Results

Within this subsection the main weekly leachate results of the altered humidity cell testing (HCT) undertaken in this study are outlined. Results are described factually in this Chapter with interpretation of trends and conclusions drawn in Chapters 7 and 8 respectively. Extended data sets and result descriptions not displayed in this thesis can be found in Appendixes 18 and 21, respectively. Methods utilised within this project are described in Chapter 4, sections 4.5 and 4.6.

### 5.3.1 Weekly HCT leachate volumes and retention rates

Within this section the weekly leachate volumes and water retention rates for all HCT carried out in this study are described. It is noted that all cells were leached with 1000ml (1 Litre) of de-ionised water in the initial leach, designated as week 0 within this results Chapter, representing a 1:1 liquid to solid ratio. Between weeks 1-60 all HCT's were leached with 500ml (0.5 Litre) of deionised water (1:2 L:S), in line with the ASTM-D5744 HCT standard. As a result of the high initial L:S water retention rates are expected to be highest within week 0.

***Kevitsa weekly leachate volumes and retention rates***

Figure 42 (a) displays the weekly leachate volumes for all of the nine (9) Kevitsa HCT, while part (b) shows the measured water retention rates of the corresponding cells over the 60-week leaching period.

The first set of triplicates set K-TC1 (Cells K01, K02, and K03) displays variability in water retention rates over the 60-week leaching period. K01 showed a fluctuating trend across the 60 weeks, with water retention volumes peaking at 101.9 ml in week 0 and dropping to a low of -23.05 ml in week 7. The mean and median water retention volumes were 55.27 ml and 54.95 ml, respectively. Cell K02 was similar with its maximum water retention volume of 104.1 ml occurring in week 0 and the minimum of 6.45 ml in week 38. The mean and median retention volumes for cell K02 were 42.38 ml and 41.85 ml, respectively. Cell K03 followed a slightly different trend. Its highest retention volume was 98.2 ml at week 0, while its lowest was 7.65 ml in week 3. The mean retention volume for this cell was 58.57 ml, and the median was 60.55 ml.

Within the K-TC2 cell set, K04 displayed a relatively steady trend, with a maximum water retention volume of 80.55 ml in week 0 and a minimum of 20.45 ml in week 53. The mean and median retention volumes were 61.41 ml and 63.8 ml, respectively. Cell K05, on the other hand, peaked at 124.9 ml in week 0, falling to a low of 24.39 ml in week 17. The mean and median volumes for this cell were 48.99 ml and 45.95 ml, respectively. Cell K06 measured a maximum water retention volume of 109.35 ml in week 0 and a minimum water retention volume of 33.9 ml in week 26. The mean and median volumes for this cell were calculated as 59.49 ml and 59.45 ml, respectively.

K-TC3 group showed a distinct set of trends compared to other Kevitsa cells. Cell K07 reached a maximum of 97.8 ml in week 0 and a minimum of 2.55 ml in week 40. The mean and median water retention volumes for this cell were 18.86 ml and 15.5 ml, respectively. K08 had its highest volume at 107.2 ml in week 0 and its lowest at 3.8 ml in week 40. The mean and median volumes were 21.26 ml and 19.2 ml, respectively. Cell K09 measured its peak volume of 104.85 ml in week 0 and its lowest volume of 2.8 ml in week 18. The mean and median volumes were 22.76 ml and 20.6 ml, respectively.

In comparing the triplicate groups, K-TC1 and K-TC2 had similar mean and median volumes, with K-TC2 demonstrating slightly higher stability. K-TC3 showed a distinct lower average water retention volume. It is noted that condensation was noted within reduced temperature cells between flushing cycles.

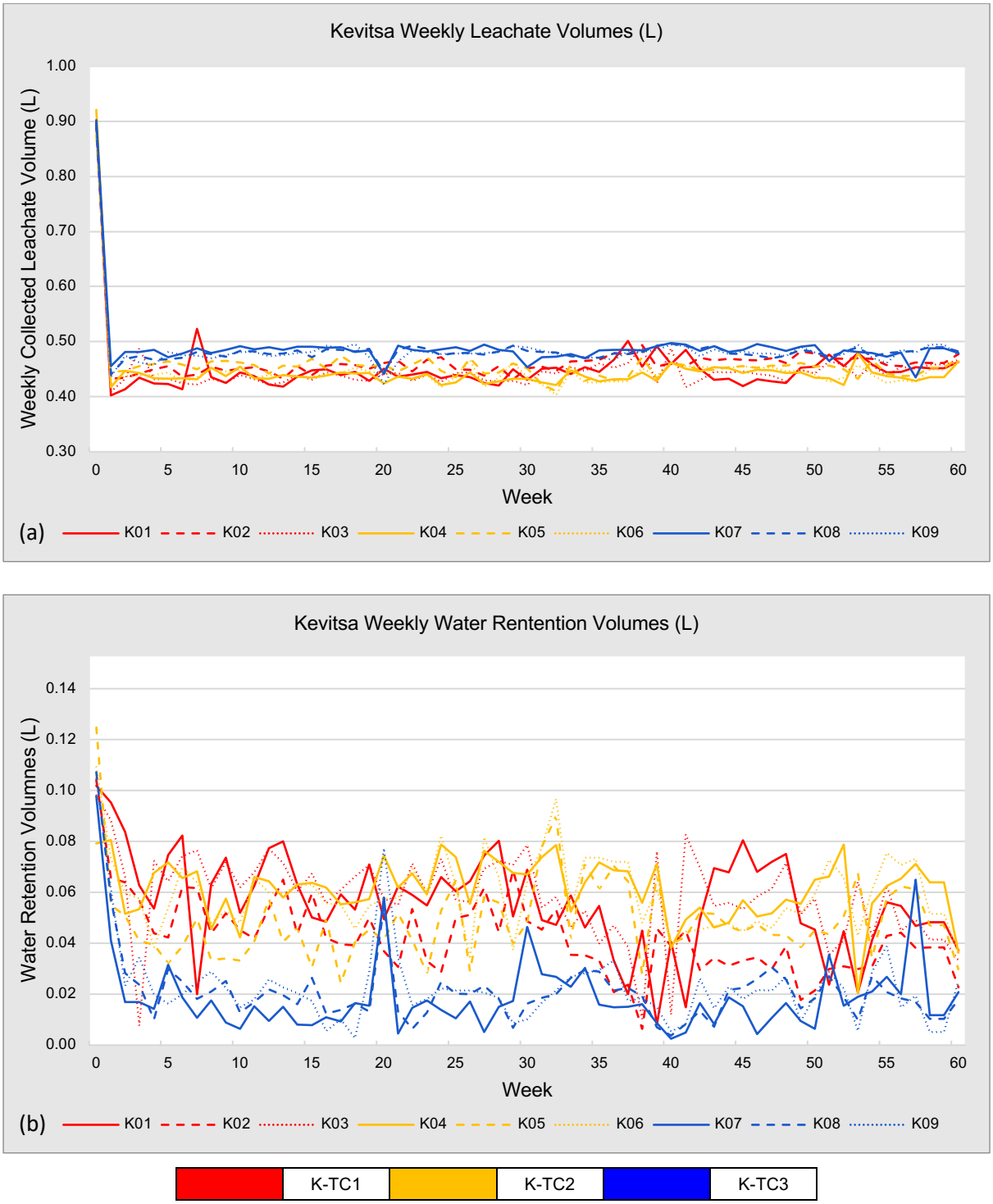


*Figure 42 - (a) Weekly Kevitsa HCT leachate volumes and (b) weekly Kevitsa HCT water retention volumes. All volumes are presented as litres (L).*

***Aitik weekly leachate volumes and retention rates***

Figure 43 (a) displays the weekly leachate volumes for all the nine (9) Aitik HCT, while part (b) shows the measured water retention rates of the corresponding cells over the 60-week leaching period. Cell A01 measured an initial water retention volume of 125.05 ml (week 0), while this cells week 60 water retention volume was 26.1 ml. The mean retention volume for A01 was 45.53 ml, while the median was 43.45 ml, with a minimum value of 19.75 ml at week 54. Cell A02 retained 125.2 ml following the initial leach. The mean retention volume for cell A02 was 45.32 ml, with a median of 42.6 ml across the 60 weeks. The cell demonstrated its minimum retention volume of 3.8 ml at week 1. The final A-TC1 cell, A03 retained 121.55 ml of de-ionised water following week 0 and measured mean and median retention volumes of 47.6 ml and 44.7 ml, respectively. This cell recorded the lowest value of 14.45 ml at week 41.

Cells within A-TC2 demonstrated the highest mean and median water retention volumes amongst Aitik cells. The cell A04 also exhibited the highest maximum water retention volume at week 32 with a value of 138.45 ml. The median values across this triplicate set were less consistent than A-TC1, indicating a more varied water retention volume over time. The minimum water retention volumes occurred in week 60 for all cells within this triplicate set.

A-TC3 triplicate cells A07, A08 and A09 demonstrated the lowest mean and median water retention volumes of the three triplicate sets. The HCT set also demonstrated the lowest maximum water retention volumes. The minimum water retention volumes occurred at different weeks within this triplicate set: week 50 for A07 (-0.9 ml), week 40 for A08 (-3.1 ml), and week 23 for A09 (-6.6 ml). Negative values in these cells may indicate drying of cells during the prior aeration cycle, causing a reduction in sample moisture content prior to leaching.

Water retention trends were comparable between Aitik and Kevitsa triplicate sets exposed to same testing conditions. Reduced temperature cells from both operations displayed distinctly lower mean average retention rates than standard temperature cells. The potential implications of this on leachate quality are discussed in Chapter 6.

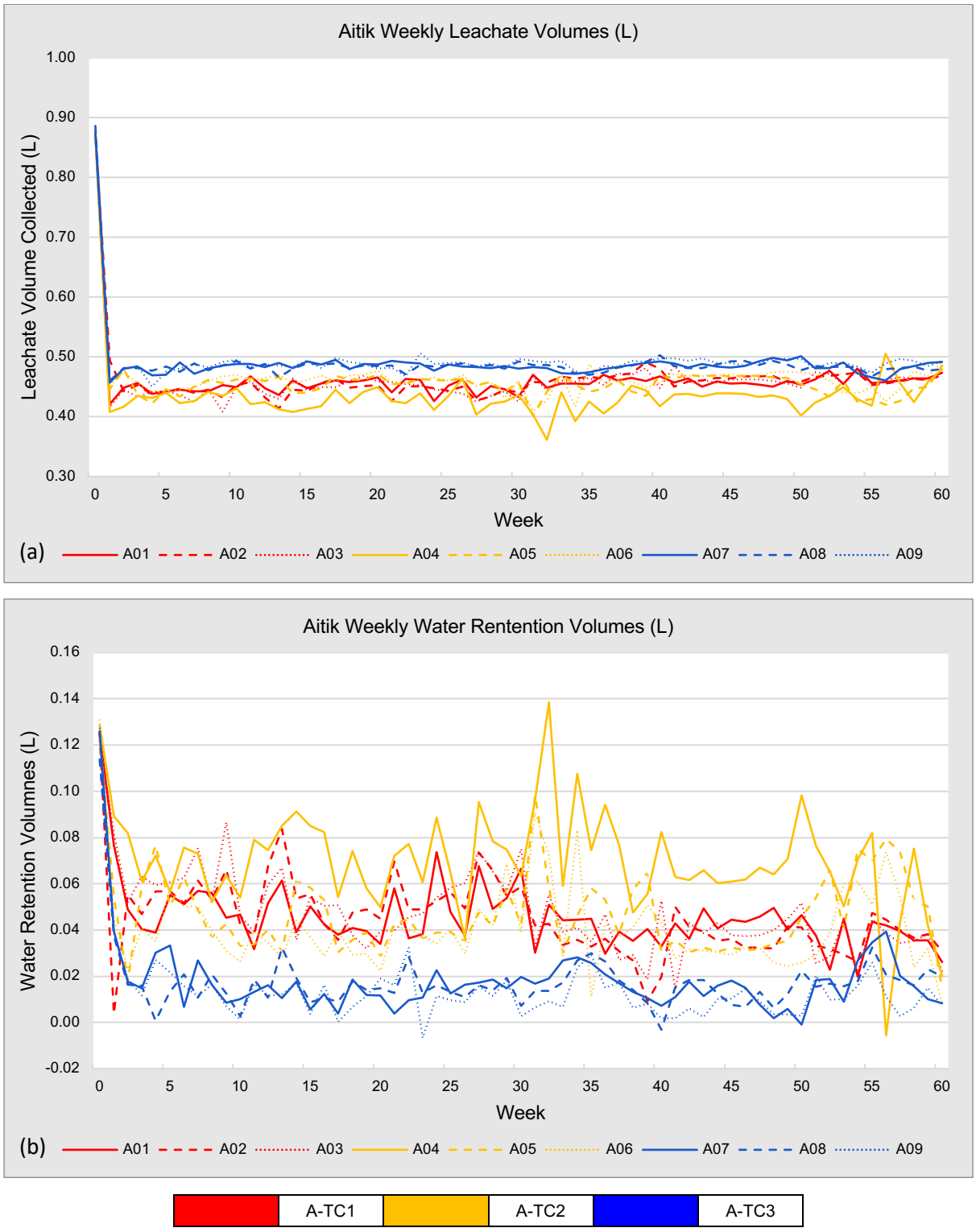


*Figure 43 - (a) Weekly Aitik HCT leachate volumes and (b) Weekly Aitik HCT water retention volumes. All volumes are presented as litres (L).*

### 5.3.2 Weekly HCT leachate basic chemistry results

Within this section analytical results obtained through weekly analysis of HCT leachates for both Kevitsa and Aitik HCT sets are outlined. Within this section basic chemistry results are described, including pH, electrical conductivity (EC), Eh (calculated), dissolved inorganic carbon (DIC), measured alkalinity (via titration) and acidity (via titration). General trends and variations between testing triplicates are outlined. Detailed data trend descriptions for EC and Eh can be found in Appendix 20.

#### *Weekly leachate pH results*

Leachate pH results for Kevitsa are shown in Figure 44, while pH results measured from Aitik HCT leachates are shown in Figure 45.

#### *Kevitsa HCT pH results*

Within Figure 44 it is demonstrated that cell K01 measured a maximum pH value of pH 8.3 in week 2 and a minimum pH of pH 6.85 in the initial flush (week 0). Over the 60-week period, the mean pH value for this cell is approximately pH 7.48. In parallel, cell K02 experiences an initial pH spike of pH 8.95 during week 2 (highest pH value amongst the set), with the lowest pH of pH 6.56 measured in week 10. Cell K02 held a mean pH value over the test duration of approximately 7.43. Lastly, cell K03 demonstrates a slightly different leachate pH progression, with an initial drop to pH 6.22 in week 1, followed by a peak pH measurement of 8.81 in week 2. The mean pH value for cell K03 is pH 7.44.

K-TC2 triplicate cells, K04- K06, generally display less variation in their pH levels compared to K-TC1 triplicate cells. Cell K04 reaches a maximum pH of pH 7.35 in week 2 and a minimum pH of pH 6.43 in week 43. The mean pH value across the 60-week period for cell K04 is pH 7.11. Cell K05 recorded the highest pH value of the K-TC2 triplicate set at pH 7.46 in week 15, while the lowest pH for this cell was pH 6.26 (week 1). The mean pH value for cell K05 is pH 7.11. Cell K06 measured a maximum pH of pH 7.46 in week 15 and a minimum pH of pH 6.26 at week 1. Cell K06 had a mean pH value of pH 7.04 over the 60-week testing period.

Cell K07 measured a maximum pH value of pH 7.98 in week 2 and a minimum pH of pH 6.35 in week 43. The mean pH value for K07 is pH 7.37. Cell K08 exhibits a maximum pH of pH 8.06 in week 2 and a minimum of pH 6.37 in week 43. The mean pH value of this cell over the 60-week period is pH 7.41. Lastly, cell K09 registers a peak pH value of 8.12 at week 2 (the set's peak), while the lowest pH is pH 6.51 at week 43. The mean pH value for K09 is pH 7.44.

Noticeable drops in K-TC3 leachate pH readings are noted in weeks 39 and 43, which aligns with noted drops in $CO_2$ within cell aeration systems during these weeks. Generally, over the 60-week leaching period K-TC1 and K-TC3 cells held higher leachate pH readings than control triplicate cells in K-TC2. K-TC1 and K-TC3 cells showed marked increases in leachate pH during the last 10 leaching weeks.

***Aitik HCT pH results***

Aitik HCT leachate pH measurements are displayed in Figure 45. Within A-TC1 triplicate HCT's there's a general upward trend in collected leachate pH over time. Cells A01 and A02 display a similar pattern in pH changes, with initial flush (week 0) pH readings of pH 6.35, showing fluctuations within the leaching weeks, but eventually rising to pH 7.13 and pH 7.07 respectively in week 60. A03 holds a slightly higher initial leachate pH of pH 6.47, with a final week leachate pH of pH 7.23, displaying the most significant pH increase within this triplicate over the leaching period. Although these cells showed gradual pH increases over the 60-week period the maximal pH readings for cells A01 (pH 7.86) and A02 (pH 7.71) and were measured in week 1, while cell A03 (pH 7.58) held its highest pH in week 24.

A-TC2 cells displayed a generally steadier trend over the leaching period. Each of the cells within this set held initial leachate pH values between pH 6.2-6.52, with distinct fluctuations during the initial and middle weeks, with a slight increase to pH 6.78 (A04), pH 6.67 (A05), and pH 6.62 (A06) by week 60. The variations in this triplicate set are relatively lower than those displayed in triplicate sets A-TC1 and A-TC3.

Of the three Aitik triplicate sets A-TC3 displayed the most dynamic changes in cell leachate pH over the testing period. Cells A07 and A08 show the greatest overall

increase in pH levels, with initial leach pH measurements of pH 6.06 and 7.51, respectively, and reaching pH 6.8 and pH 7.18 by the final week. Cell A09 held an initial pH of pH 6.33, increases to a peak pH in week 53 (pH 7.81), with a decline to pH 6.92 by the 60th leaching week. The relatively high initial leachate pH of cell A08 was noticeably higher than cells A07 and A09, with consistently higher leachate pH readings until week 18, after this leach following leachate pH readings from A08 were more consistent with the rest of the A-TC3 triplicate.

A-TC1 and A-TC3 cells displayed a gradual overall upward leachate pH trend, while A-TC2 displayed a more stable trend over the leaching period. Cell leachate pH was more variable in A-TC1 and A-TC3 cells with pronounced drops in cell pH readings in week 39 and 43. These pH outlier readings align with noted drops in $CO_2$ within cell aeration systems during these weeks.

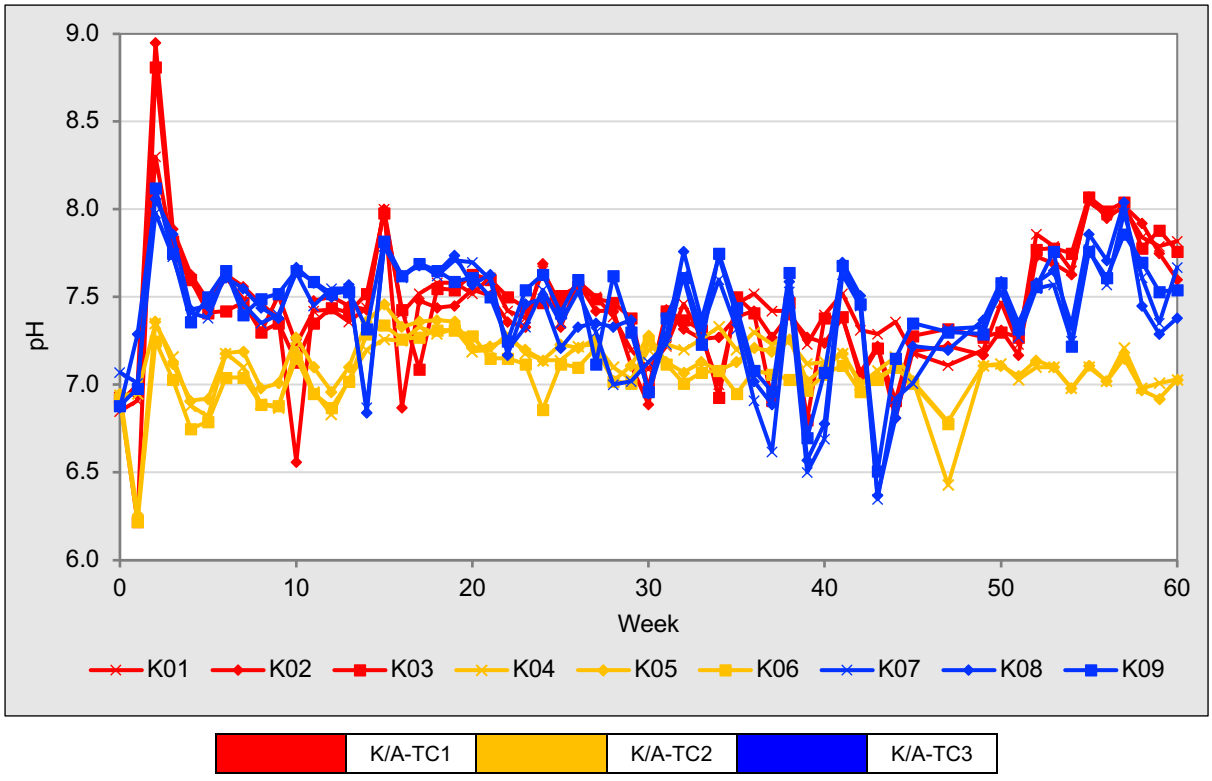


*Figure 44 - Kevitsa mine waste humidity cell tests (HCT) pH results measured from leachates collected over the 60-week testing period.*

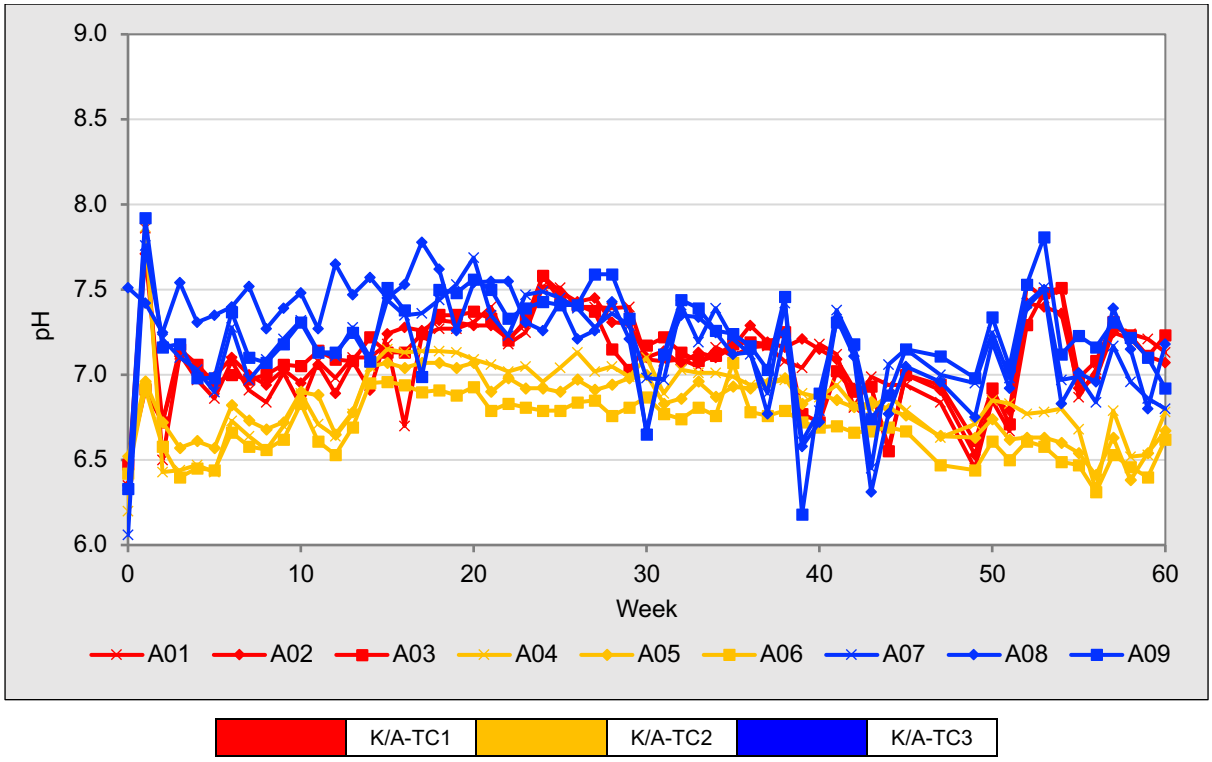


*Figure 45 – Aitik mine waste humidity cell tests (HCT) pH results measured from leachates collected over the 60-week testing period.*

***Weekly leachate electrical conductivity (EC) results***

Leachate EC (µS/cm) collected for both Kevitsa and Aitik HCT sets displayed minimal variations between control and altered cell conditions over the 60-week testing period. Kevitsa and Aitik cell sets displayed initial fluctuations in EC over the first 15 weeks of leaching, with the highest EC readings recorded for all cells in week 1. Cell K03 demonstrated the highest overall EC measurement amongst Kevitsa cells, with 657.24 µS/cm measured in week 1. Following week 15, Kevitsa cell EC measurements displayed general stabilisation, with readings generally between 100-200 µS/cm over the remaining weeks of testing. Aitik cells displayed a comparable level of stabilisation with EC measurements general recorded between 75-200 µS/cm. Anomalously high EC readings were measured in weeks 13 (all cell sets), 43 (TC3 cells) and 59 (A-TC3 cells), which aligned with higher pH readings in corresponding leaching weeks.

Figures (A20.1 and A20.2) and detailed descriptions of Kevitsa and Aitik cell leachate EC measurements over the 60-week leaching period can be found in Appendix 20 of this thesis.

### *Weekly leachate Eh results*

Leachate redox potential (Eh) (mV) measurements for Kevitsa and Aitik cells over the 60-week period displayed high levels of variability for all cell sets. There were noticeable fluctuations in the readings throughout the 60-week period, with a distinct 'consistent' period of lower Eh values between weeks 18 and 40, demonstrated for all triplicate sets in this study. Following week 40 both Kevitsa and Aitik cells displayed a general uptrend in Eh measurements, although a high level of week-by-week fluctuation in readings was observed. Both Kevitsa and Aitik cell sets displayed similar trends in Eh measurements, irrelevant of the cell condition set over the 60-week testing period.

Figures (A20.3 and A20.4) and detailed descriptions of Kevitsa and Aitik cell leachate Eh measurements over the 60-week leaching period can be found in Appendix 20 of this thesis.

### *Weekly leachate dissolved inorganic carbon (DIC) results*

Leachate total dissolved inorganic carbon (DIC) (mg/kg/week) results for Kevitsa are shown in Figure 46, while DIC results measured from Aitik HCT leachates are shown in Figure 47. Cumulative DIC release for Kevitsa and Aitik triplicate HCT sets are displayed in Figure 48 and 49, respectively.

### *Kevitsa HCT DIC results*

Over the 60-week leaching period K-TC1 triplicate cells, K01, K02 and K03, held mean DIC release rates of 7.23 mg/kg/week, 7.46 mg/kg/week, and 7.22 mg/kg/week, respectively. These cells held median DIC release rates of 6.55 mg/kg/week, 6.94 mg/kg/week, and 6.44 mg/kg/week, while the minimum and maximum releases ranged from 0.75 mg/kg/week to 19.04 mg/kg/week. The K-TC1 cell set presents a wide variability in weekly DIC release rates, with readings fluctuating considerably after week 30. K01 and K02 demonstrate similar trends, with a sharp increase in readings in week 1, a gradual decline thereafter, and periodic spikes in weeks 6, 7, 8, 10, 16, 17, 18, and 30. K03, while showing similar overall trends, exhibiting their maximal readings in weeks 3 and 6. Cumulative DIC release from K-TC1 cells was measured

as 440 mg/kg, 440 mg/kg and 425 mg/kg over the 60 weeks of leaching in cells K01, K02 and K03, respectively.

For the K-TC2 triplicate cell set the mean DIC release rates were 1.25 mg/kg/week, 1.06 mg/kg/week, and 0.92 mg/kg/week for cells K04, K05 and K06, respectively. The median release rates for these cells were 0.97 mg/kg/week, 0.83 mg/kg/week, and 0.75 mg/kg/week respectively, while the minimum values fall to as low as 0.08 mg/kg/week. The K-TC2 DIC release rates are much more consistent than K-TC1 and K-TC3 cells over the leaching period and show less variability, generally measuring below 2 mg/kg/week. There's a clear outlier in week 55 for K04 with a relatively high DIC release, in the context of the triplicate, of 9.45 mg/kg/week. Cumulative DIC release from K-TC2 cells was measured as 73 mg/kg, 62 mg/kg and 54 mg/kg over the 60 weeks of leaching in cells K04, K05 and K06, respectively.

Cells K07, K08, K09 held mean DIC release rates of 9.41 mg/kg/week, 10.07 mg/kg/week, and 9.03 mg/kg/week, respectively, during this testing regime. Their median release rates were 7.21 mg/kg/week, 7.40 mg/kg/week, and 7.08 mg/kg/week, while the minimum and maximum values range from 1.10 mg/kg/week to 63.08 mg/kg/week. The K-TC3 cell set exhibits considerable fluctuations in DIC release, specifically in the later leaching weeks. Particularly noticeable are the extreme spikes in weeks 39 and 43. The trends for K07, K08, and K09 are similar, with all three cells demonstrating significant increases in readings in the aforementioned weeks. It is noted that the distinguishable spikes in K-TC3 cell DIC release coincide with HCT aeration variability during these weeks. Due to issues with $CO_2$ and air mixing in later weeks, erratically high levels of $CO_2$ within humid cycles in some weeks was recorded. During weeks 39 and 43 K-TC3 aeration gas compositions reached >50% $CO_2$. Other triplicate cells were not affected by this aeration malfunction as K-TC1, K-TC2, A-TC1 and A-TC2 cells ran through separate aeration systems during the experimental period. The noted jump in DIC can clearly be seen within cumulative DIC release results presented in Figure 48. Cumulative DIC release from K-TC3 cells was measured as 554 mg/kg, 594 mg/kg and 533 mg/kg over the 60 weeks of leaching in cells K07, K08 and K09, respectively.

It can be seen in Figure 48 that cumulative DIC release results demonstrated a close visual association between K-TC1 and K-TC2 cells until week 39. Over the initial 39 weeks these triplicates demonstrated little variation. It is noted that without aeration system malfunctions that K-TC3 cell cumulative DIC release rates would likely be near in line with K-TC1 cells.

***Aitik HCT DIC results***

A-TC1 cells, A01, A02, and A03, demonstrated mean DIC release rates of 4.07 mg/kg/week, 3.88 mg/kg/week, and 3.92 mg/kg/week, respectively over the 60-week leaching period. The median DIC release rates for cells A01, A02, and A03 were calculated as 3.89 mg/kg/week, 3.74 mg/kg/week, and 3.65 mg/kg/week, respectively. These cells measured minimum DIC release rates of 0.33 mg/kg/week, 0.36 mg/kg/week, and 0.34 mg/kg/week, respectively, with minimal release rates all recorded in week 49. A-TC1 cells demonstrated maximal DIC releases of 11.06 mg/kg/week, 8.52 mg/kg/week, and 12.18 mg/kg/week, in weeks week 10 for cells A01 and A02 and in week 6 for cell A03. DIC release rates of A-TC1 cells exhibited variability over the course of the 60 weeks, with A03 periodically demonstrating higher DIC concentrations compared to cells A01 and A02. Cells A01, A02 and A03 released cumulative DIC concentrations of 240, 236 and 239 mg/kg, respectively.

Aitik control cells (A-TC2) A04, A05, and A06, held mean DIC release rates over the 60-week leaching period of 0.63 mg/kg/week, 0.67 mg/kg/week, and 0.53 mg/kg/week, respectively. The median DIC release value for cells A04, A05, and A06 were 0.60 mg/kg/week, 0.60 mg/kg/week, and 0.57 mg/kg/week, respectively. The minimum DIC concentration release cells for A04, A05, and A06 was 0.21 mg/kg/week, 0.33 mg/kg/week, and 0.23 mg/kg/week, respectively. These occurred at week 51 for cells A04 and A05, and at week 4 for cell A06. The maximum DIC values for A04, A05, and A06 were 1.45 mg/kg/week, 2.51 mg/kg/week, and 2.03 mg/kg/week, respectively. These occurred at week 0 for all three cells. A-TC2 cells released 38 mg/kg, 40mg/kg and 32 mg/kg of DIC cumulatively during this testing.

Similarly, to results demonstrated within comparable Kevitsa HCT's, A-TC3 cells demonstrated the highest overall DIC release of Aitik cells during this testing period,

with the most erratic leaching characteristics of the three triplicates. Cells A07, A08, and A09, averaged mean DIC release rates of 5.52 mg/kg/week, 7.48 mg/kg/week, and 4.87 mg/kg/week, respectively. The minimum DIC release rates for these cells were 0.73 mg/kg/week, 0.62 mg/kg/week, and 0.68 mg/kg/week. These minimal release rates occurred in week 51 for all three cells. The maximum DIC release rates for cells A07, A08, and A09 were measured as 24.43 mg/kg/week, 26.49 mg/kg/week, and 19.04 mg/kg/week, respectively. These occurred at week 43 for A07 and A08, and at week 39 for A09. A-TC3 cells, A07, A08 and A09, released 38 mg/kg, 40mg/kg and 32 mg/kg of DIC cumulatively during this testing.

Both Kevitsa and Aitik reduced temperature HCT triplicate sets, K-TC3 and A-TC3, demonstrated highly visually variable DIC release rates in coinciding leaching weeks. As previously discussed, this was due to a malfunction in the HCT aeration system for these cells during select weeks. This has led to notable differences between the triplicate cells, with significant deviation in cumulative DIC releases, particularly in later leaching weeks.

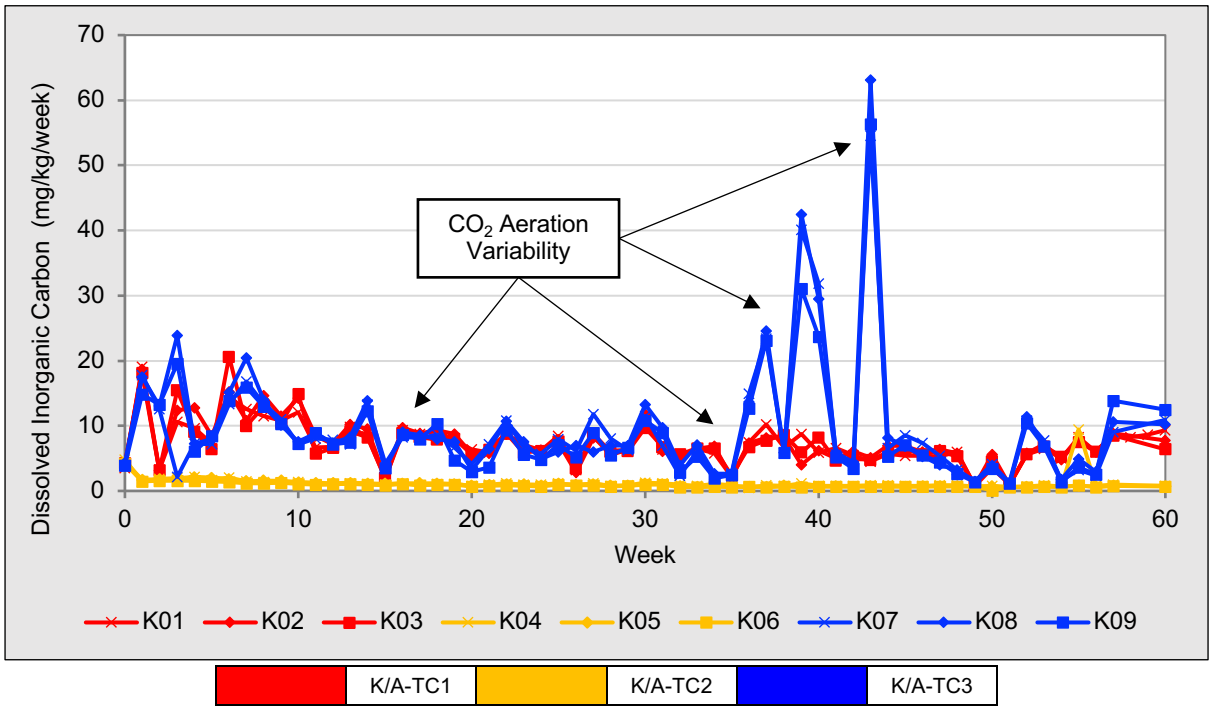


*Figure 46 - Kevitsa mine waste humidity cell tests (HCT) Dissolved Inorganic Carbon (DIC) results measured from leachates collected over the 60-week testing period.*

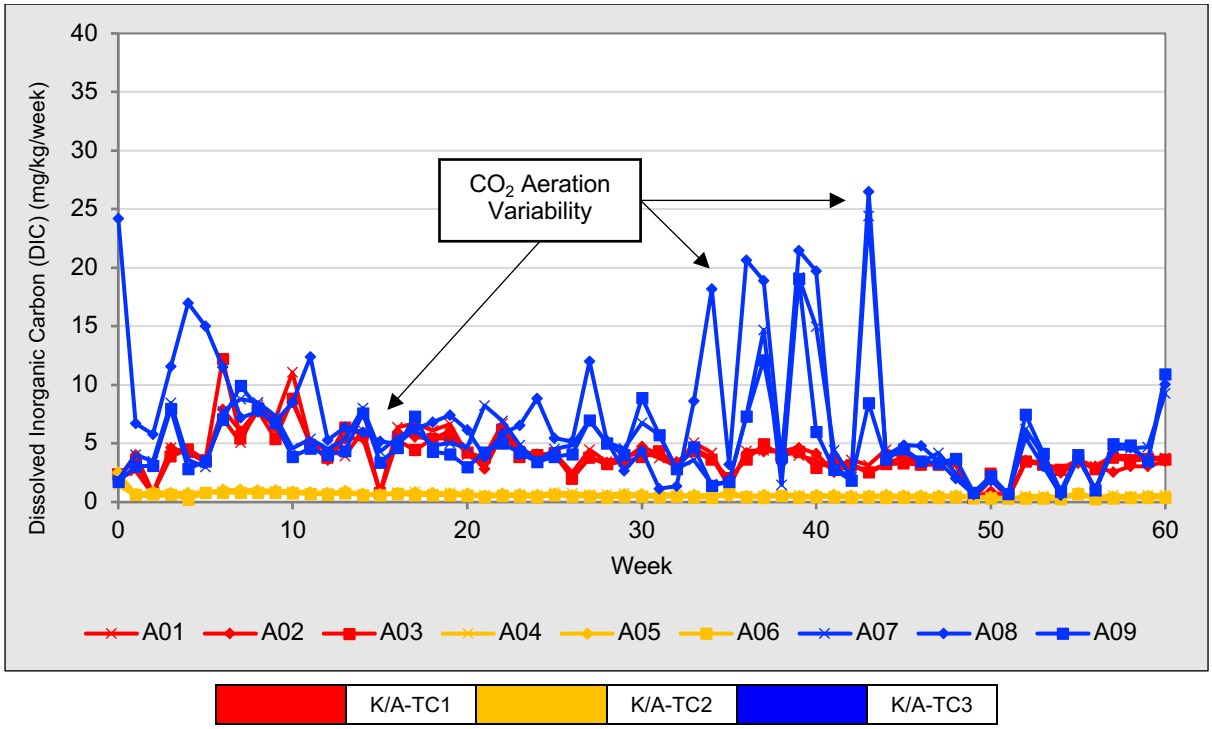


*Figure 47 - Aitik mine waste humidity cell tests (HCT) Dissolved Inorganic Carbon (DIC) results measured from leachates collected over the 60-week testing period.*

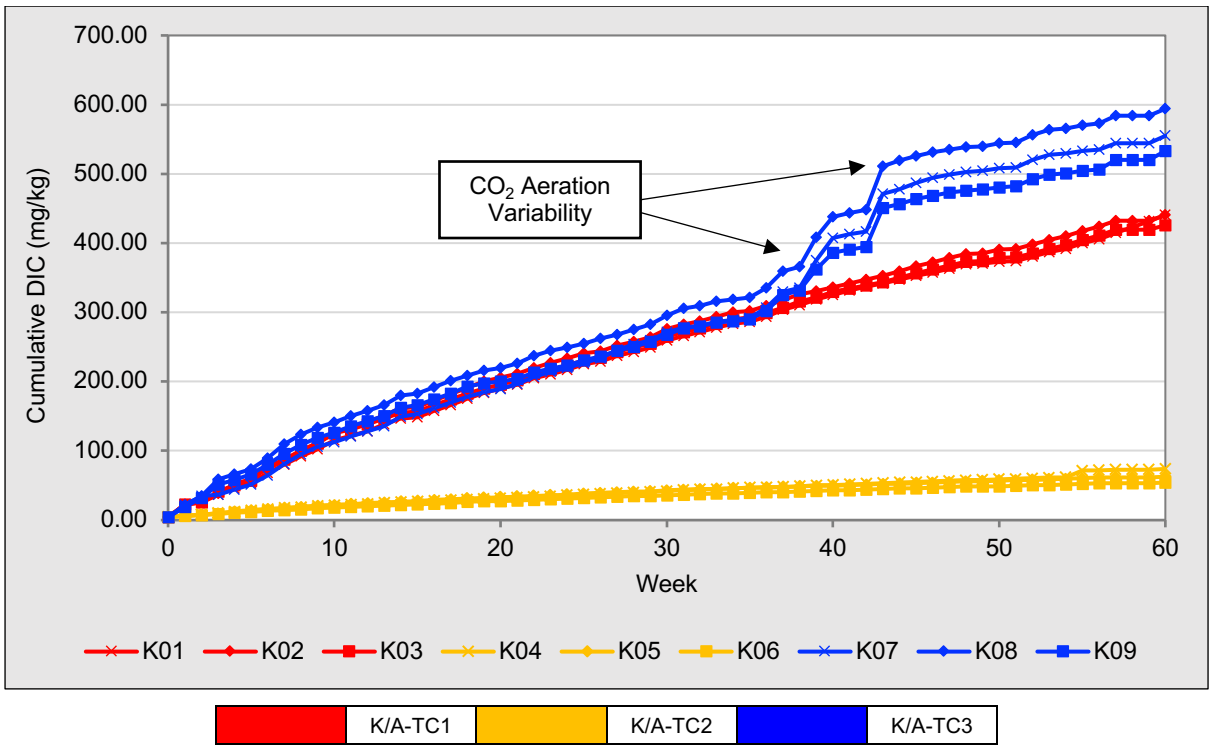


*Figure 48 – Kevitsa mine waste humidity cell tests (HCT) cumulative DIC results measured from leachates collected over the 60-week testing period.*

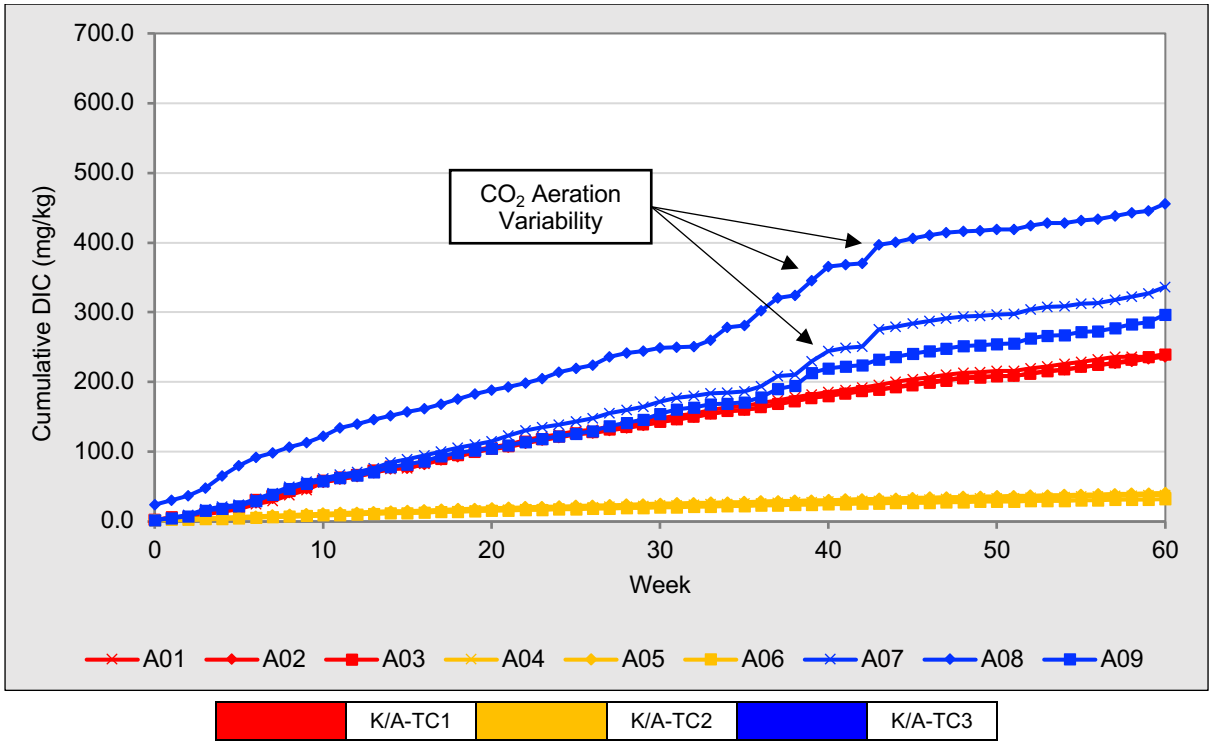


*Figure 49 – Aitik mine waste humidity cell tests (HCT) cumulative DIC results measured from leachates collected over the 60-week testing period.*

***Weekly leachate alkalinity and acidity results***

Within this section weekly HCT leachate Total Alkalinity, Post Hydrogen peroxide ($H_2O_2$) addition pH and Total Acidity results for Kevitsa and Aitik HCT triplicate sets are outlined. These results are displayed and discussed together within this section due to related methods utilised during measurement, with alkalinity, post $H_2O_2$ pH and acidity measurements carried out in sequence. These methods are outlined in detail within Chapter 4, section 4.6, of this thesis.

Leachate Total Alkalinity and Total Acidity results for Kevitsa HCT triplicates are shown in Figures 50 and 52, while the results of those parameters are shown in Figures 51 and 53 for Aitik HCT triplicates. Alkalinity and Acidity are expressed as mg/L as calcium carbonate ($CaCO_3$) within this results section. pH measurements were taken post hydrogen peroxide addition, providing an indication of reduced species that may potentially contribute to the total acidity of the aqueous sample. Results for these parameters were available in week 0 to week 45 of his 60-week experimental study. This was due to experimental constraints and laboratory restrictions. Results obtained within the 45 weeks of leachate analysis are presented.

Post hydrogen peroxide ($H_2O_2$) pH measurements for Kevitsa and Aitik cell sets are not displayed or described in detail within this thesis as minimal alteration was shown between cell sets over the testing period. Generally, all cells displayed their lowest post $H_2O_2$ pH measurements within the preliminary weeks (0-8) of the leaching program. Following this period both Kevitsa and Aitik cell sets displayed generally consistent post $H_2O_2$ pH measurements between pH 4 and pH 4.7. Figures (A20.5 and A20.6) and detailed descriptions of Kevitsa and Aitik cell leachate post $H_2O_2$ pH measurements can be found in Appendix 20 of this thesis.

***Kevitsa HCT alkalinity and acidity results***

Within K-TC1 triplicate cell K01 leachate alkalinity measurements ranged from a minimum of 16 mg/L as $CaCO_3$ to a maximum of 173 mg/L as $CaCO_3$, with minimum and maximal measurement occurring in the initial leach (week 0) and week 1. Over the 60-week period the mean alkalinity measurement was 57.92 mg/L as $CaCO_3$, while the median was 53.25 mg/L as $CaCO_3$. The second K-TC1 cell, K02, measured minimal and maximal alkalinity readings of 15.5 mg/L as $CaCO_3$ (week 35) and 156 mg/L as $CaCO_3$ (week 1), respectively. The mean alkalinity measurement of this cell was 55.68 mg/L as $CaCO_3$, with a median of 48.75 mg/L as $CaCO_3$. Similarly to cells K01 and K02, cell K03 measured its maximal alkalinity measurement, 163 mg/L as $CaCO_3$ within leaching week 1. This cell measured a minimum alkalinity of 18.5 mg/L as $CaCO_3$ within week 15. Cell K02 held mean and median alkalinity measurements of 55.85 mg/L as $CaCO_3$ and 48.5 mg/L as $CaCO_3$, respectively.

K-TC2 cells displayed noticeably lower alkalinity measurements over the 45 weeks of leaching data available when compared to K-TC1 cells. Cell K04 measured a minimum alkalinity measurement of 5.5 mg/L as $CaCO_3$ and a maximal value of 21 mg/L as $CaCO_3$, within the initial leach (week 0). This cell held a mean alkalinity of 9.5 mg/L as $CaCO_3$. K-TC2 cells K05 and K06 demonstrated the same alkalinity trend as cell K04 over the leaching period, with consistently lower alkalinity measurements than K-TC1 and K-TC3 cells. Cells K05 and K05 demonstrated maximal alkalinity measurements over the 45-week period of 20.5 mg/L as $CaCO_3$ and 19 mg/L as $CaCO_3$, both of which were measured within in the initial leach leachates of these cells. These cells held

mean alkalinity measurements of 9.16 mg/L as $CaCO_3$ and 8.13 mg/L as $CaCO_3$, respectively.

Throughout the first 35 weeks of leaching K-TC3 cells displayed closely visually associated alkalinity measurements with corresponding K-TC1 HCT cells. Between weeks 35 and 45 reduced temperature triplicate cells in this set demonstrated distinct peaks in weekly leachate alkalinity measurements. Over 45 weeks of leaching cell K07 held minimum and maximum alkalinity measurements of 7 mg/L as $CaCO_3$ (week 0) and 139 mg/L as $CaCO_3$ (week 1), respectively, with a mean of 58.16 mg/L as $CaCO_3$ and a median is 50.75 mg/L as $CaCO_3$. Cell K08 measured its minimum alkalinity measurement of 6.5 mg/L as $CaCO_3$ in week 4, proceeding this cell maximum measurement of 165.5 mg/L as $CaCO_3$ within the previous week (week 3). Similarly, to cell K07, cell K08 showed a clear differentiation between mean (62.90 mg/L as $CaCO_3$) and median (56 mg/L as $CaCO_3$) alkalinity measurement, displaying a skewness in measurements over this period. Cell K09 measured its maximal alkalinity measurement within the later period of leaching with 142.5 mg/L as $CaCO_3$ measured in week 43.

It can be seen in Figure 50 that K-TC1 and K-TC3 cells displayed visually significant spikes in alkalinity in the early weeks of leaching, after which they fluctuate with a general downward trend until week 35. The K-TC3 triplicate displays the highest mean and maximum alkalinity measurements among the triplicate sets. K-TC3 cells display variability in alkalinity measurements in weeks 35 – 45 with distinctly higher measurements in weeks 39, 40 and 43. These peaks align with noted peaks in DIC demonstrated in Figures 46-49, noted as a result of erratic and variable conditions within the K-TC3 and A-TC3 aeration systems within these weeks.

Total acidity measured from Kevitsa HCT leachates is displayed in Figure 52. It can be seen in this figure that K-TC2 control cells measured consistently higher total acidity, calculated as mg/L as $CaCO_3$, than K-TC1 and K-TC3 triplicate cells over the 45-weeks of leaching data available. All 9 Kevitsa cells measured a total acidity measurement within the initial leach (week 0), but in subsequent leaches K-TC1 and K-TC3 cells measured distinguishable total acidity in only 12 measurements across 6 cells over the 45-week period. K-TC2 control Kevitsa HCT cells displayed consistently

measurable total acidity throughout the 45-week period available. K04 started with an acidity level of 4 mg/L as $CaCO_3$ in week 0, increased to a maximum of 25 mg/L as $CaCO_3$. Cell K04 held a mean total acidity of 11.11957 mg/L as $CaCO_3$, with a median total acidity of 10.75 mg/L as $CaCO_3$. Cell K05 demonstrated a distinctly high maximum total acidity of 44.5 mg/L as $CaCO_3$ in week 37, with mean and median values of 11.70652 mg/L as $CaCO_3$ and 10.75 mg/L as $CaCO_3$, respectively. Cell K06 measured a maximum total acidity of 33 mg/L as $CaCO_3$ in week 7, with a minimum measurement of 3.5 mg/L as $CaCO_3$ and a mean total acidity of 12.27 mg/L as $CaCO_3$.

***Aitik HCT alkalinity and acidity results***

A-TC1 cells exhibit similar trends in total alkalinity across the 45-week period of data available for Aitik HCT. Cell A01 measured a minimum alkalinity level of 4.5 mg/L as $CaCO_3$ in week 45, a maximum of 44 mg/L as $CaCO_3$ in week 8, a mean of 25.14 mg/L as $CaCO_3$. The minimal alkalinity of cell A02 was slightly higher than cell A01 with minimum alkalinity measurement of 5.5 mg/L as $CaCO_3$. This cells maximal alkalinity measurement was 44.5 mg/L as $CaCO_3$, measured in week 8, while demonstrating a mean alkalinity of 25.25 mg/L. A03 had the highest maximum measured alkalinity of the triplicate set at 55.5 mg/L as $CaCO_3$ (week 6).

A-TC2 cells demonstrated relatively stable alkalinity measurements across the 45-week period, with minor fluctuations. Cell A04's alkalinity ranged from a minimum of 3 mg/L as $CaCO_3$ in weeks 40-42 to a maximum of 8 mg/L as $CaCO_3$ in weeks 9 and 35. This cell held a mean alkalinity over the period of 5.12 mg/L as $CaCO_3$, with a median value of 5.5 mg/L as $CaCO_3$. Similarly to cell A04, cell A05 presented a minimum alkalinity value of 3 mg/L as $CaCO_3$ in weeks 40-42, while its maximum alkalinity measurement of 10 mg/L as $CaCO_3$ was within the initial leach (week 0). Cell K05 held a mean alkalinity measurement of 5.25 mg/L as $CaCO_3$ across 45 weeks of leaching. Cell A06 measured the lowest minimum alkalinity of the set at 2.5 mg/L as $CaCO_3$ between weeks 40-45, with a maximum of 8 mg/L as $CaCO_3$ in week 0. This cell held the lowest mean and median alkalinity levels of the triplicate with 4.27 mg/L as $CaCO_3$ and 4 mg/L as $CaCO_3$, respectively.

A-TC3 cells demonstrated more variability in their alkalinity levels compared to the other Aitik triplicate sets. A07 had a minimum alkalinity of 4.5 mg/L as $CaCO_3$ in week 0, a maximum of 54.5 mg/L as $CaCO_3$ in week 43, a mean of 32.59 mg/L as $CaCO_3$. A08 presented the highest alkalinity measurement in the triplicate set, with a maximum of 99.5 mg/L as $CaCO_3$ in week 4, a mean of 41.63 mg/L as $CaCO_3$, a median of 41.25 mg/L as $CaCO_3$, and a minimum alkalinity of 8.5 mg/L as $CaCO_3$ in week 34. A09's Alkalinity ranged from a minimum of 6 mg/L as $CaCO_3$ in week 0 to a maximum of 56 mg/L as $CaCO_3$ in week 27, with a mean alkalinity of 29.55 mg/L as $CaCO_3$ and a median of 28.75 mg/L as $CaCO_3$. Unlike the Kevitsa reduced temperature triplicate set, K-TC3, the comparable Aitik set, A-TC3, did not show distinguishable alkalinity peaks in line with increases in DIC. Over the 45-week period Aitik triplicates showed more consistency in alkalinity, with less distinct period of high alkalinity, when compared to comparable Kevitsa HCT sets.

Total acidity measurements, calculated as mg/L as $CaCO_3$, for Aitik HCT's are shown in Figure 53. Over the 45-wek period A-TC2 cells generally displayed higher calculated total acidity than A-TC1 and A-TC3 cells during the same leaching weeks. More variability in variable parameter cell sets, A-TC1 and A-TC3, are displayed for Aitik cells when compared to comparable trends in Kevitsa triplicates over the same leaching period. Over the 45-week period A-TC1 cells held mean calculated acidity measurements of 3.41 mg/L as $CaCO_3$, 1.66 mg/L as $CaCO_3$, and 2.23 mg/L as $CaCO_3$ for cells A01, A02 and A03, respectively. This is compared to A-TC3 cells, A07, A08 and A09, which held mean values of 2.03 mg/L as $CaCO_3$, 1.44 mg/L as $CaCO_3$ and 2.38 mg/L as $CaCO_3$. Significant peaks of total acidity were noted at various points throughout the leaching period for cells within A-TC1 and A-TC3 triplicate sets. These include cell A01's total calculated acidity of 59.50 mg/L as $CaCO_3$ in week 32, which was considerably higher than the cells median value of 0 mg/L as $CaCO_3$. Similarly, cell A09 measured a total acidity of 57.00 mg/L as $CaCO_3$ in week 4, compared to the samples mean total acidity of 2.38 mg/L as $CaCO_3$.

A-TC2 cells demonstrated the highest mean total acidity measurements over the 45-week leaching period. Cells A04, A05 and A05, held mean calculated total acidity measurements of 16.22 mg/L as $CaCO_3$, 17.66 mg/L as $CaCO_3$ and 17.27 mg/L as $CaCO_3$, respectively during this testing period.

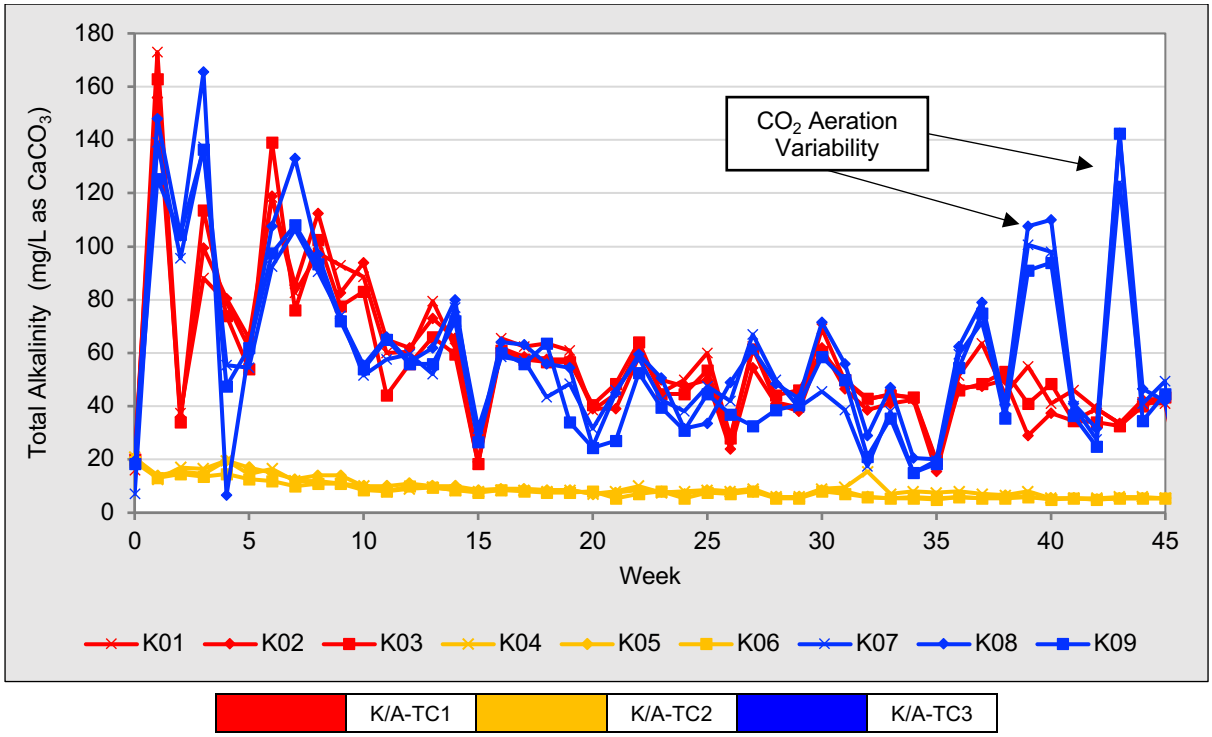


*Figure 50 – Kevitsa mine waste humidity cell tests (HCT) total alkalinity results measured from leachates collected over the 60-week testing period.*

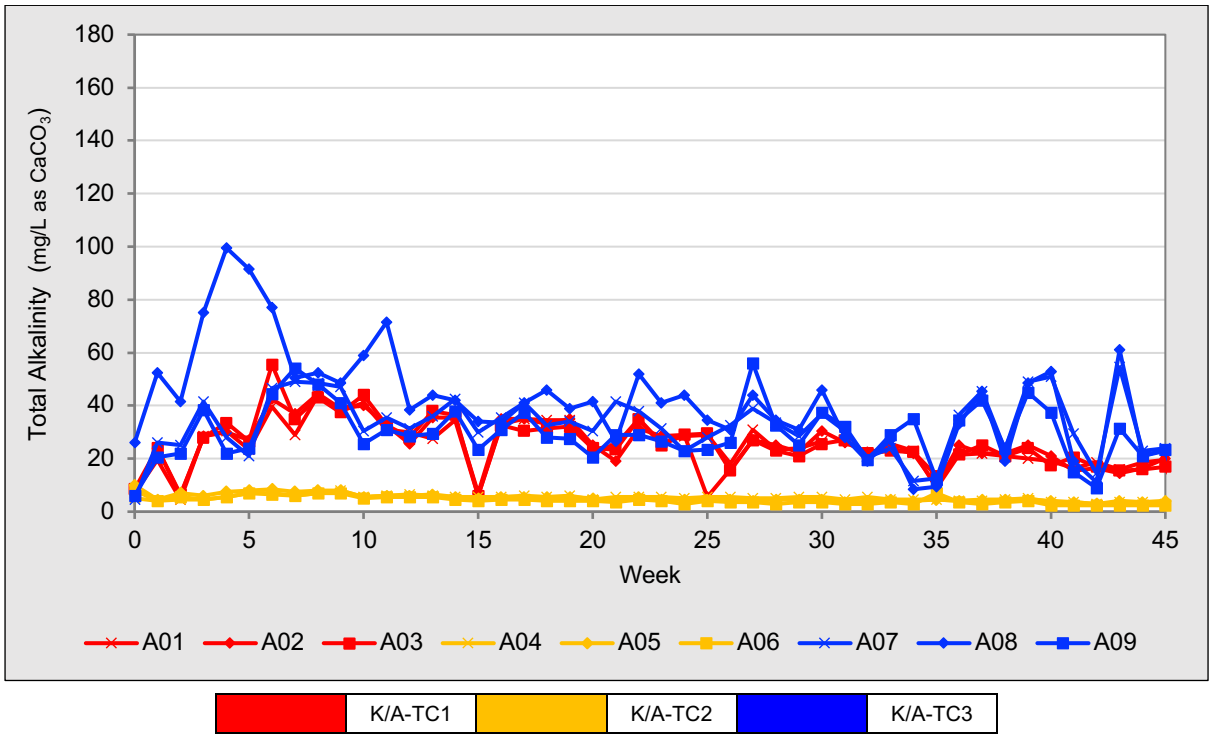


*Figure 51 – Aitik mine waste humidity cell tests (HCT) total alkalinity results measured from leachates collected over the 60-week testing period.*

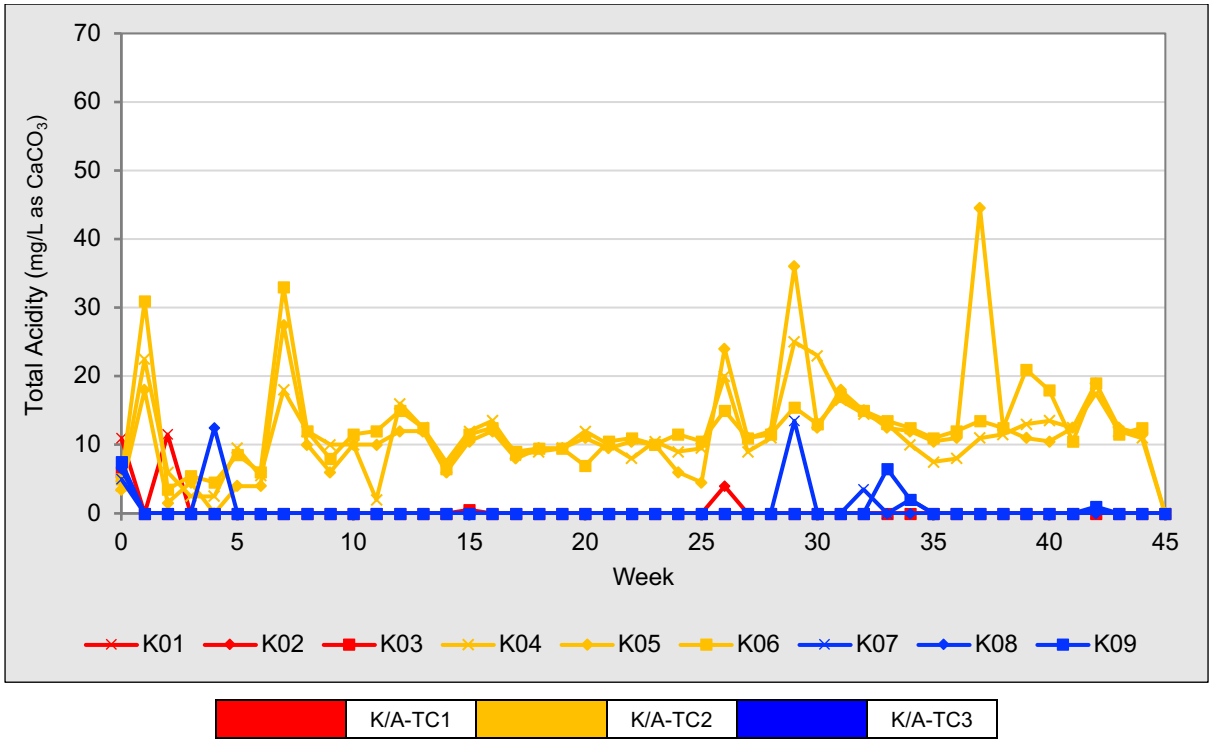


*Figure 52 – Kevitsa mine waste humidity cell tests (HCT) total acidity results measured from leachates collected over the 60-week testing period.*

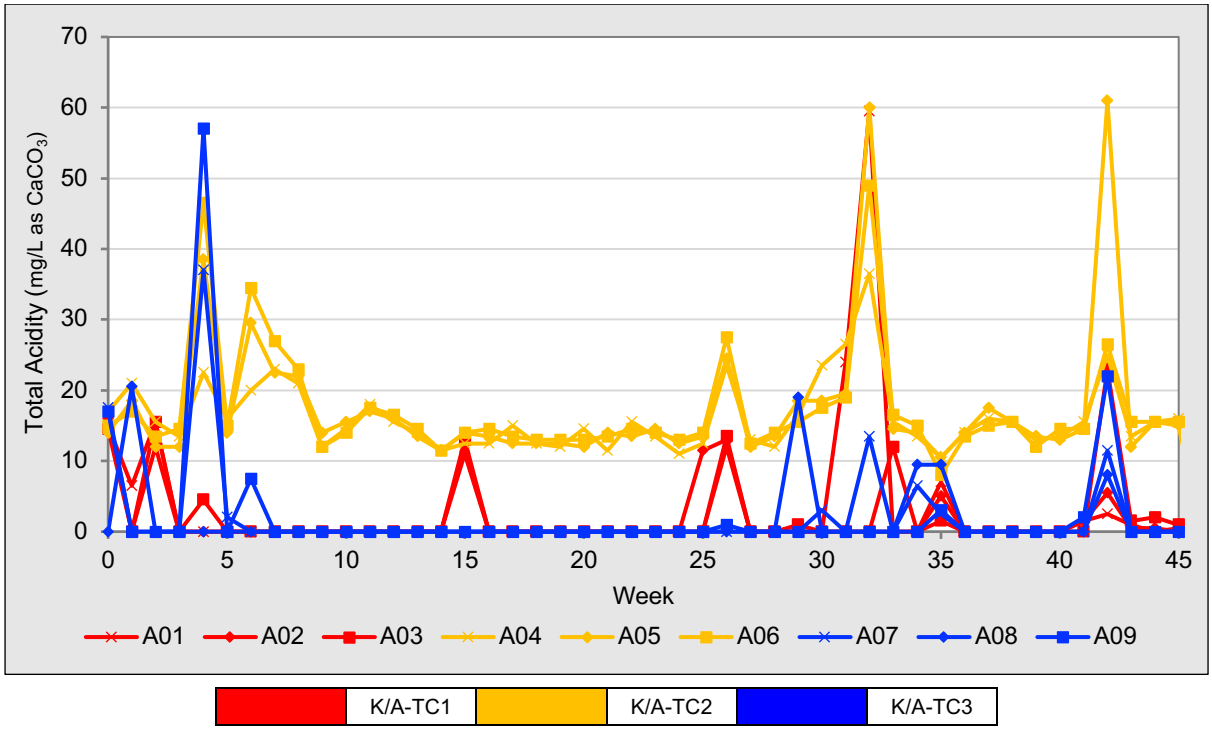


*Figure 53 – Aitik mine waste humidity cell tests (HCT) total acidity results measured from leachates collected over the 60-week testing period.*

***Weekly leachate sulfate results***

Leached sulfate ($SO_4$) release results measured for Kevitsa HCT's are shown in Figure 54, while sulfate results measured from Aitik HCT leachates are shown in Figure 55.

***Kevitsa HCT sulfate results***

It can be seen in Figure 54 that K-TC1 cells generally exhibit a decreasing trend in sulfate release over the 60-week leaching period. Within this set the maximum Sulfate release values were observed in the initial weeks, with cells K01, K02 and K03 measuring peak concentration releases of 211.63 mg/kg/week, 178.36 mg/kg/week and 207.54 mg/kg/week in week 1 of leaching. The minimum values for K01, K02, and K03 were 0.68 mg/kg/week (Week 57), 15.91 mg/kg/week (Week 48), and 13.992 mg/kg/week (Week 38), respectively. The mean sulfate release concentrations for these cells were 35.31 mg/kg/week, 35.75 mg/kg/week, and 36.45 mg/kg/week, respectively, while their median release values were 24.52 mg/kg/week, 25.64 mg/kg/week, and 26.95 mg/kg/week.

Similarly to A-TC1 cells, cells within A-TC2 displayed a sharp decrease in weekly sulfate concentration release between week 0 to week 10. It is generally noted that after week 10 all cells displayed less fluctuations in weekly sulfate concentration. The maximum sulfate release concentrations for cells K04, K05, and K06 occurred in the first leach week, with measured values of 163.58 mg/kg/week, 127.87 mg/kg/week, and 158.37 mg/kg/week, respectively. The minimum measured release rates for these cells were 19.26 mg/kg/week (Week 48) for K04, 21.12 mg/kg/week (Week 48) for K05, and 22.19 mg/kg/week (Week 48) for K06. K-TC2 cells held mean sulfate release rates of 45.61 mg/kg/week for K04, 44.29 mg/kg/week for K05, and 50.16 mg/kg/week for K06, while their respective median sulfate release rates were 37 mg/kg/week, 38.75 mg/kg/week, and 45.31 mg/kg/week.

K-TC3 triplicate cells (K07, K08, and K09) measured the lowest sulfate release of the three Kevitsa triplicate sets over the 60-week leaching period. The peak sulfate releases for K07, K08, and K09 all occurred in week 1 with release rates of 129.26 mg/kg/week, 123.50 mg/kg/week and 131.328 mg/kg/week, respectively. The

minimum sulfate concentrations for these cells occurred at Week 43 for K07 (5.532 mg/kg/week) and week 48 for K08 (4.819 mg/kg/week) and K09 (3.541 mg/kg/week). The mean sulfate release rates for K07, K08, and K09 were 18.79 mg/kg/week, 18.12 mg/kg/week, and 18.54 mg/kg/week, respectively, while their median release values were 10.57 mg/kg/week, 10.36 mg/kg/week, and 11.13 mg/kg/week.

All Kevitsa HCT cells from triplicate sets K-TC1, K-TC2, and K-TC3 showed a consistent decrease in sulfate concentrations over the 60-week period. The highest sulfate concentrations were observed in the initial weeks for all cells. The cells within the same set showed similar behaviour and sulfate concentration ranges, but there are variations in mean and median sulfate concentrations between the sets. The control set, K-TC, demonstrated the highest mean and median sulfate release rates compared to K-TC1 and K-TC3 cells. Reduced temperature cell set, K-TC3, demonstrated the lowest overall sulfate release over across all cells. This would be expected due to reduced sulfide mineral oxidation kinetics with reduced temperatures.

Over the 60-week leaching period K-TC1 cells (K01, K02 and K03) cumulatively released 943 mg/kg, 976 mg/kg and 959 mg/kg, respectively. Comparatively Kevitsa control cells, K04, K05 and K06, released 1183 mg/kg, 1194 mg/kg and 1315 mg/kg of sulfate over the same period. Reduced temperature cells, K07, K08 and K09, had cumulative sulfate releases of 477 mg/kg, 533 mg/kg and 545 mg/kg, representing a >60% reduction in sulfate release when compared to control Kevitsa HCT cells.

***Aitik HCT sulfate results***

It is demonstrated in Figure 55 that A-TC1 cells (A01, A02, A03) initially reported high Sulfate readings, peaking within the initial leach (week 0) with maximum sulfate release rates of 142.01 mg/kg/week, 126.15 mg/kg/week, and 113.90 mg/kg/week, respectively. Over the first 6 weeks sulfate release rates declined sharply, before settling into more of a steady state of release for the remaining leaching weeks. The minimum sulfate release rates were measured in weeks 27, 23, and 48 for cells A01, A02 and A03, respectively. These sulfate release rates were measured as 6.09 mg/kg/week, 0.41 mg/kg/week and 6.73 mg/kg/week. The mean release rates over the period for cells A01, A02 and A02 were 18.59 mg/kg/week, 18.91 mg/kg/week,

and 18.92 mg/kg/week, while these cells had median release rates of 10.92 mg/kg/week, 11.19 mg/kg/week, and 11.87 mg/kg/week. The relatively large difference between the mean and median release rates within this triplicate of HCT's can be attributed to the initial high rates of sulfate release within early leaching weeks creating a skewness in the average rates of release.

The A-TC2 triplicate cells displayed similar trends to A-TC1, although it can be seen in Figure 54 that these cells displayed a slightly lower rate of sulfate release compared to control Aitik HCT cells over the 60-week period. The highest recorded values were in week 0 for all A-TC2 cells (A01, A02 and A03) with sulfate release rates of 161.52 mg/kg/week, 131.54 mg/kg/week, and 129.16 mg/kg/week respectively. The cells measured their lowest sulfate release rates in weeks 24, 49, and 49 with readings of 11.19 mg/kg/week, 9.35 mg/kg/week, and 9.50 mg/kg/week, respectively. The mean sulfate release rates for A-TC2 cells over the 60-week leaching period were 25.34 mg/kg/week, 22.75 mg/kg/week, and 22.54 mg/kg/week, while these cells held median release rates of 17.20 mg/kg/week, 16.00 mg/kg/week, and 16.458 mg/kg/week.

Over the 60-week leaching period A-TC3 cells measured the lowest rates of sulfate release of the three Aitik HCT triplicates sets. Similar to A-TC1 and A-TC2 cells, the highest rates of sulfate release were measured within the initial leach (week 0) with readings of 110.30 mg/kg/week, 113.85 mg/kg/week, and 115.38 mg/kg/week for cells A07, A08, and A09, respectively. The lowest rate of sulfate release for cell A07 was observed in week 43 (2.09 mg/kg/week), while cells A08 and A09 both experienced their lowest release rates in week 23 (0.75 mg/kg/week and 0.581 mg/kg/week). The mean sulfate release rates for these cells were calculated as 11.70 mg/kg/week, 9.57 mg/kg/week, and 10.88 mg/kg/week, while these cells held corresponding median sulfate release rates of 4.96 mg/kg/week, 3.82 mg/kg/week, and 4.37 mg/kg/week.

All Aitik HCT cells experienced their highest sulfate release rates within the initial HCT leach (week 0). All cells reached a relatively consistent steady state of release after the first 5-7 weeks, however of the leaching period A-TC2 cells demonstrated higher mean and median sulfate release rates compared to the A-TC1 and A-TC3 cell sets.
Over the 60-week leaching period there was clear differentiation in cumulative sulfate release between the differing HCT triplicate sets. A-TC1 cells (A01, A02 and A03)

cumulatively released 522 mg/kg, 546 mg/kg and 537 mg/kg of sulfate during this kinetic testing protocol. Over the same period control Aitik cells (A-TC2) measured cumulative releases of sulfate of 659 mg/kg, 655 mg/kg and 656 mg/kg across the triplicate set (A04, A05 and A06). The ~20% reduction in released sulfate between A-TC1 cells and control cells (A-TC2) demonstrates sulfate release suppression, potentially due to reduced rates of sulfide mineral oxidation. The greatest differentiation in sulfate release between control cells and altered cells was demonstrated in A-TC3 cells. Cells A07, A08 and A09 cumulatively release 354 mg/kg, 301 mg/kg and 337 mg/kg of sulfate, representing an ~50% reduction in sulfate compared to A-TC2 cells over the same leaching period.

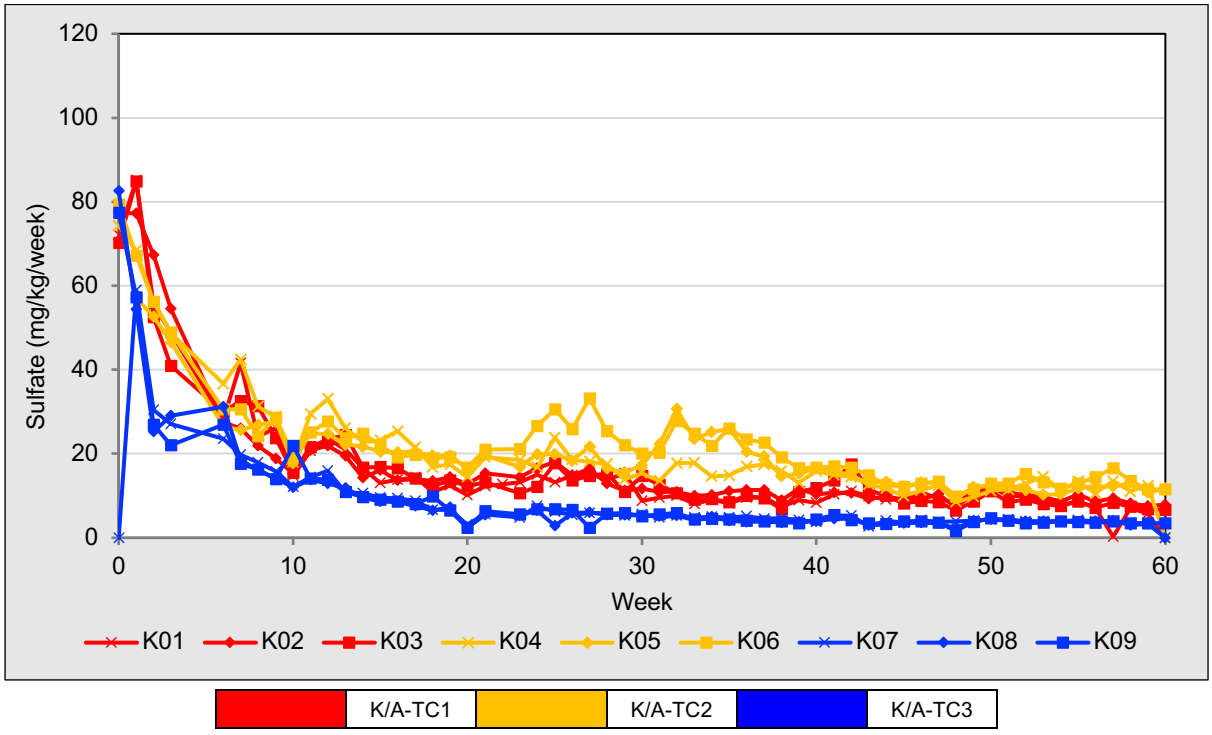


*Figure 54 – Kevitsa mine waste humidity cell tests (HCT) sulfate results measured from leachates collected over the 60-week testing period.*

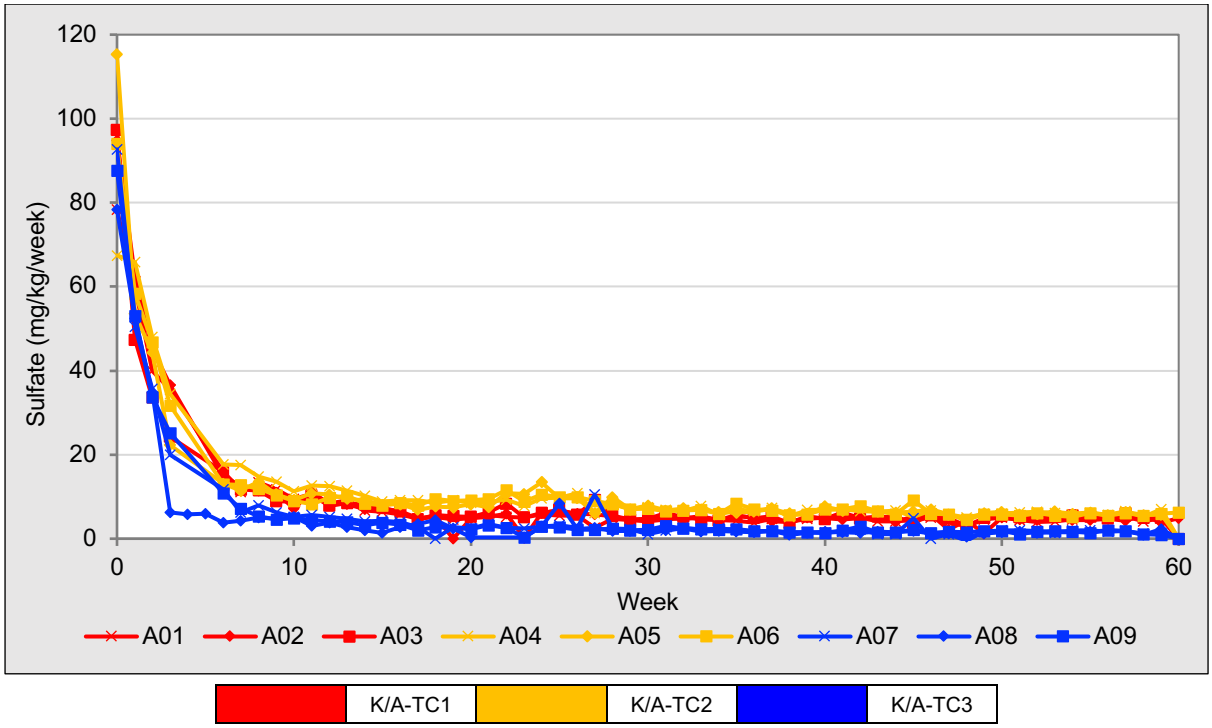


*Figure 55 – Aitik mine waste humidity cell tests (HCT) sulfate results measured from leachates collected over the 60-week testing period.*

### 5.3.3 Weekly leachate NP and AP consumption results

Within this section calculated cumulative NP and AP consumption, expressed as kg $CaCO_3$ eq/t, for Kevitsa and Aitik HCT triplicate sets are summarised. Kevitsa HCT leachate NP and AP consumption results are shown in Figures 56 and 58, respectively, while Aitik HCT NP and AP consumption results are shown in Figures 57 and 59.

NP consumption calculated within this study is based on calculations outlined in table 18.1 of the MEND 1.20.1 manual (Price 2009). NP consumption within this section represents the empirical open system NP consumption, calculated using leachate sulfate ($SO_4$), total alkalinity and acidity. AP consumption represents a measure of the reduction in a materials acidity producing potential over time as AP sources are depleted/ consumed. More details on NP/AP consumption and relevant calculations can be found in Chapter 4 of this thesis.

#### *Kevitsa HCT NP and AP consumption results*

It can be seen in Figure 56 that K-TC1 and K-TC3 cells exhibit higher cumulative NP consumption results than control K-TC2 cells, over the 60-week leaching period. After

the leaching period K-TC1 cells (K01, K02 and K03) held cumulative calculate NP consumption values of 2.02 kg $CaCO_3$ eq/t, 2.02 kg $CaCO_3$ eq/t and 1.99 kg $CaCO_3$ eq/t, respectively. These values were noticeably higher than the cumulative NP consumption values held by K-TC2 control cells (K04, K05 and K06). These cells held final values of 1.03 kg $CaCO_3$ eq/t, 1.01 kg $CaCO_3$ eq/t and 1.09 kg $CaCO_3$ eq/t over the leaching period. K-TC3 cells demonstrated higher NP consumption results than control cells but slightly lower cumulative values than the control temperature, enhanced $CO_2$ aeration cell (K-TC1). K-TC3 cells (K07, K08 and K09) reached 1.90 kg $CaCO_3$ eq/t, 1.88 kg $CaCO_3$ eq/t and 1.74 kg $CaCO_3$ eq/t during the 60-week HCT protocol.

Results demonstrated in NP consumption align to a degree with AP consumption within Kevitsa cells. It can be seen in Figure 58 that over the 60-week period K-TC1 and K-TC3 cell demonstrated reduced cumulative AP consumption totals, compared to the K-TC2 control cells. Over the first 20 weeks of leaching K-TC1 and K-TC2 cells showed similar AP consumption rates before diverging. K-TC3 cells held consistently lower AP consumption values over the leaching period. This is to be expected as sulfide oxidation, and subsequent sulfide production, would be expected to be lower at reduced temperatures, which inhibit sulfide oxidation kinetics. Over the 60-week period K-TC1, K-TC2 and K-TC3 triplicate cells held mean cumulative AP consumption values of 0.867 kg $CaCO_3$ eq/t, 1.09 kg $CaCO_3$ eq/t and 0.511 kg $CaCO_3$ eq/t, respectively.

***Aitik HCT NP and AP consumption results***

Cumulative NP consumption results for Aitik HCT cells are displayed in Figure 57. It can be seen in this figure that A-TC1 and A-TC3 cells demonstrated higher cumulative NP consumption values than A-TC2 control cells over the testing period. Cells A01 (0.915 kg $CaCO_3$ eq/t), A02 (0.987 kg $CaCO_3$ eq/t), A03 (0.970 kg $CaCO_3$ eq/t), A07 (1.02 kg $CaCO_3$ eq/t) and A09 (0.934 kg $CaCO_3$ eq/t) held closely associated cumulative NP consumption rates during the leaching period. A-TC3 cell A08 deviated slightly from other cells within its triplicate with a final value of 1.19 kg $CaCO_3$ eq/t. The average cumulative NP consumption of A-TC2 (control) cells was calculated as 0.343 kg $CaCO_3$ eq/t. Overall Aitik HCT cells held lower cumulative AP consumption rates

than Kevitsa cells, see Figures 58 and 59. These cells show similar trends demonstrated within Kevitsa cells; A-TC1 and A-TC3 cells demonstrate higher overall AP consumption rates than A-TC2 cell over the 60-week leaching period. A-TC1, A-TC2 and A-TC3 cell triplicates held mean total AP consumption values of 0.488 kg $CaCO_3$ eq/t, 0.595 kg $CaCO_3$ eq/t and 0.323 kg $CaCO_3$ eq/t, respectively. In line with Kevitsa cell results A-TC3 cells held the lowest AP production rates, which was expected due to lower experimental conditions (10$^{O}$C), compared to A-TC1 (25$^{O}$C) and A-TC2 (25$^{O}$C).

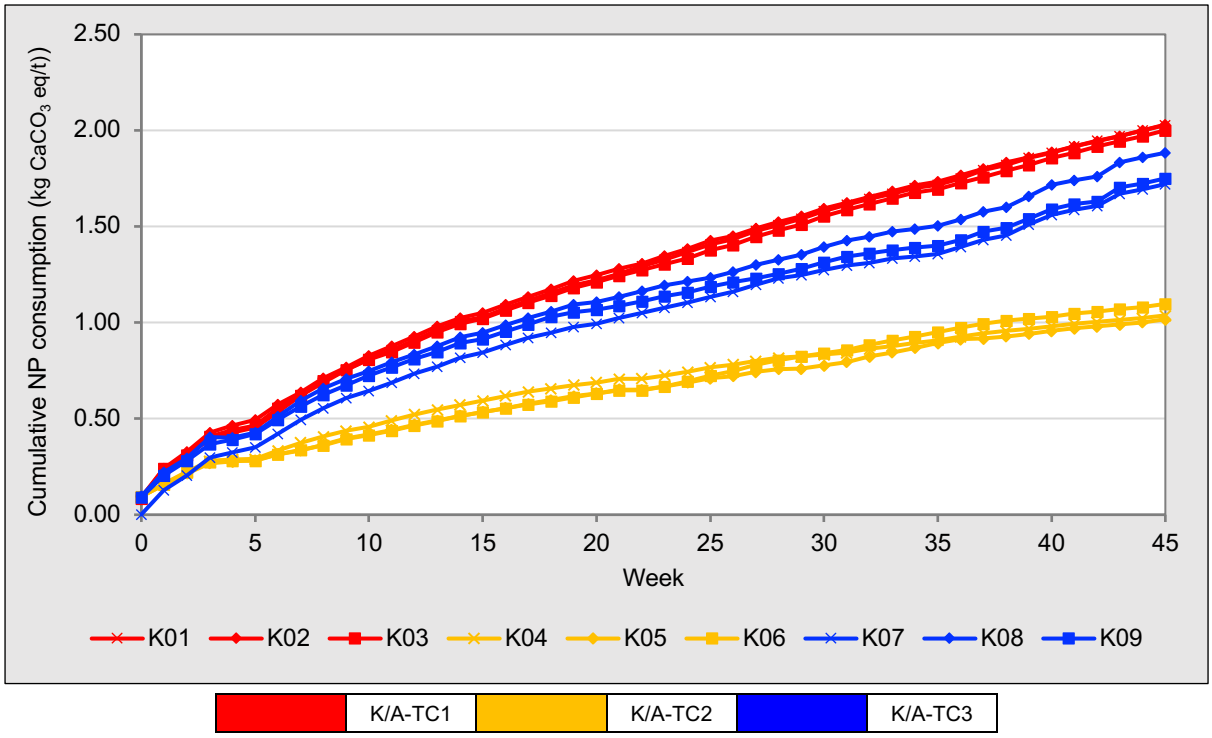


*Figure 56 – Kevitsa mine waste humidity cell tests (HCT) cumulative NP results measured from leachates collected over the 60-week testing period.*

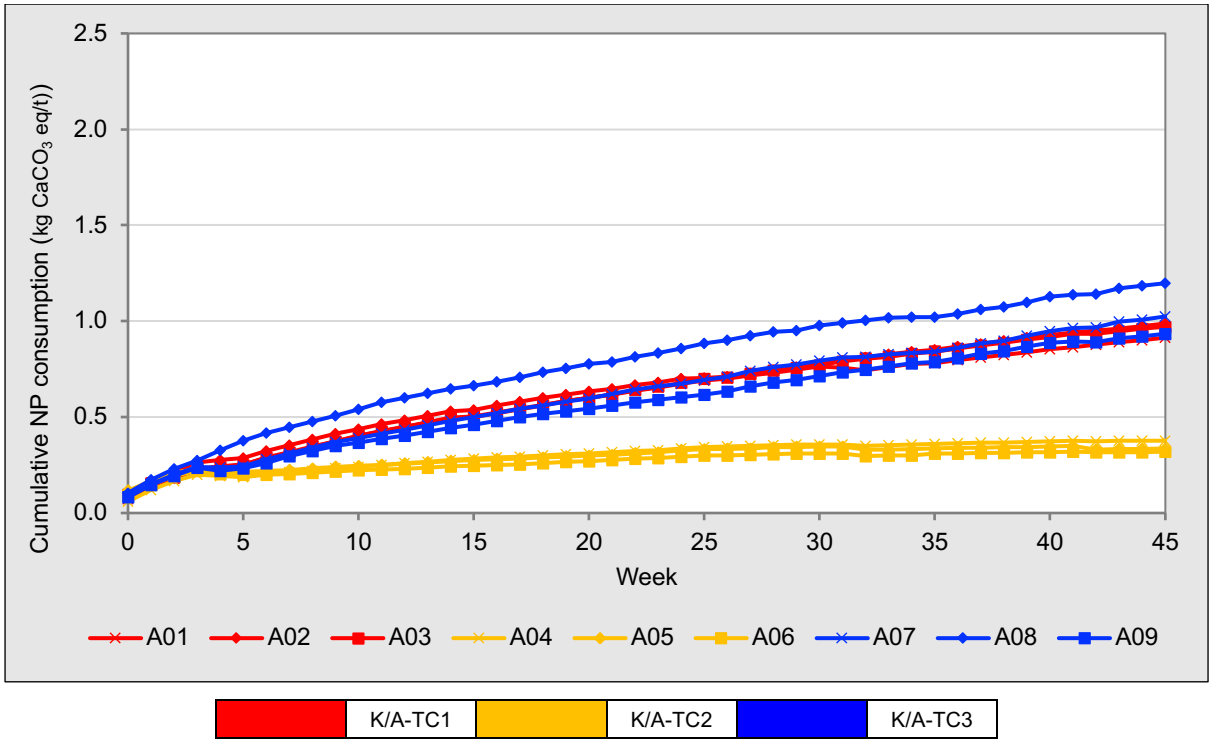


*Figure 57 – Aitik mine waste humidity cell tests (HCT) cumulative NP results measured from leachates collected over the 60-week testing period.*

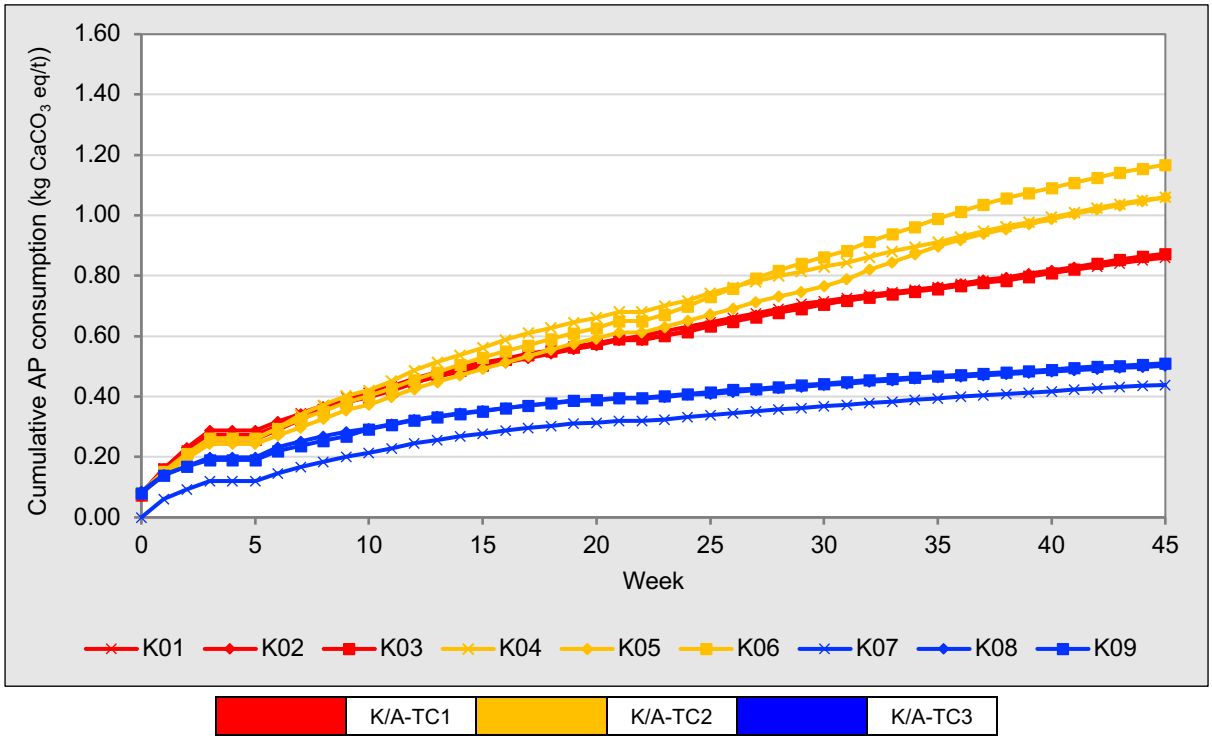


*Figure 58 – Kevitsa mine waste humidity cell tests (HCT) cumulative AP results measured from leachates collected over the 60-week testing period.*

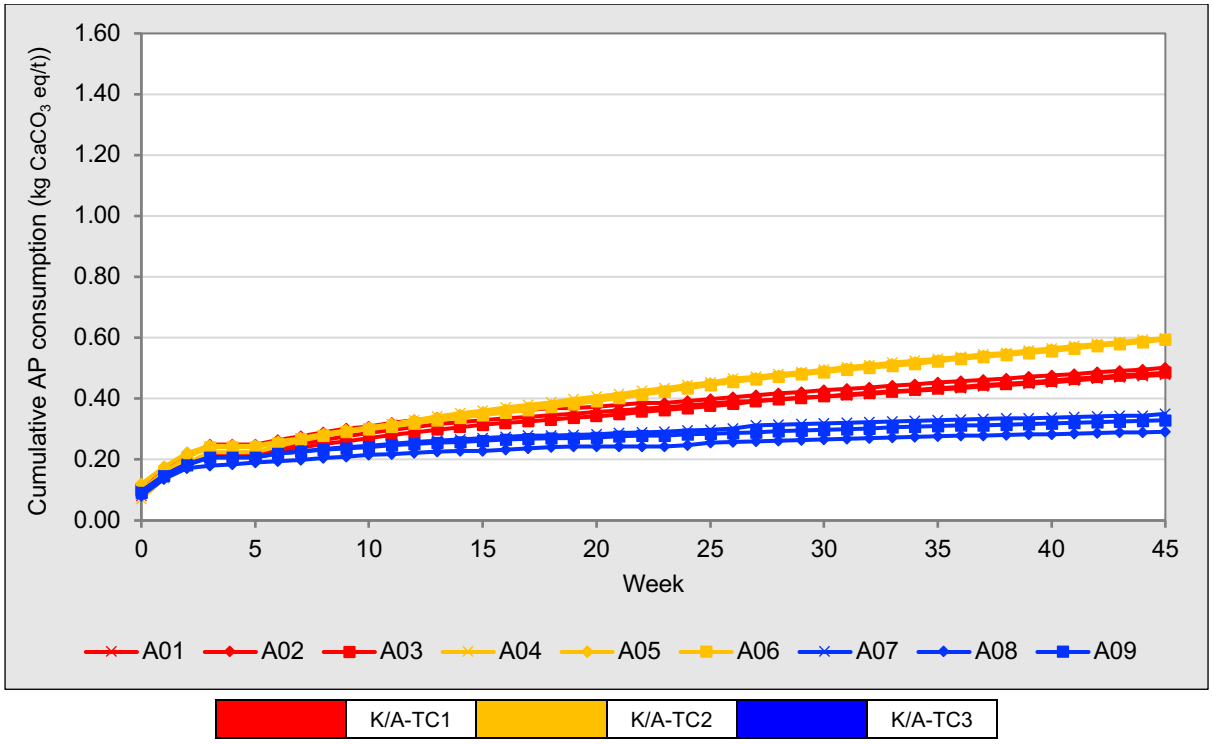


*Figure 59 – Aitik mine waste humidity cell tests (HCT) cumulative AP results measured from leachates collected over the 60-week testing period.*

### 5.3.4 Weekly HCT leachate major anions and cation results

Within this section major anion and cation leachate release results measured via ICP-OES are described. Calcium (Ca), Magnesium (Mg) and Sodium (Na) leachate concentrations are outlined for all of the Kevitsa and Aitik HCT triplicate sets, with results displayed as release over time as well as cumulative release over the 60-week leaching periods.

#### *Weekly leachate calcium results*

Leached Calcium (Ca) (mg/kg/week) release results for Kevitsa HCT's are shown in Figure 60, while Ca release results measured from Aitik HCT leachates are shown in Figure 61. Cumulative Ca release for Kevitsa and Aitik triplicate HCT sets are displayed in Figure 62 and 63, respectively.

#### *Kevitsa HCT Ca results*

Within K-TC1, cell K01 measured a minimum Ca release rate of 2.45 mg/kg/week (week 50), while this cell maximum release was measured within the initial cell leach (week 0),10.67 mg/kg/week. The mean and median Ca release rates for cell K01 were

5.97 mg/kg/week and 5.82 mg/kg/week, respectively over the 60-week leaching period. Cell K02 had a somewhat similar pattern, with its minimum Ca release of 2.41 mg/kg/week measured in week 51 and a maximum release rate of 12.10 mg/kg/week measured in week 0. The mean and median Ca release rates for this cell were calculated as 6.13 mg/kg/week and 5.83 mg/kg/week, respectively. K03, the third cell of K-TC1, exhibited its lowest value of 2.19 mg/kg/week in week 51, while its maximal release rate of 11.38 mg/kg/week was measured in week 6. The mean and median Ca release rates for this cell were 5.54 mg/kg/week and 5.29 mg/kg/week, respectively.

Cell K04 measured its minimum Ca release rate of 2.60 mg/kg/week in week 50 and peaked at 11.79 mg/kg/week during the initial leach (week 0), with a mean release rate of 5.04 mg/kg/week and a median release rate of 4.65 mg/kg/week. Cell K05 demonstrated its lowest Ca release rate of 2.71 mg/kg/week in week 50 and highest rate of 12.66 mg/kg/week in week 0. Cell K05's mean and median Ca release rates were measured as 5.09 mg/kg/week and 4.76 mg/kg/week, respectively. Cell K06, measured the lowest single week Ca release rate of the whole Kevitsa HCT cell set with a minimum release of 0.84 mg/kg/week measured in week 45. This cells maximum rate of 12.38 mg/kg/week was measured within the initial leach (week 0). The mean Ca release rate for cell K06 was calculated as 5.24 mg/kg/week, while the median rate was 4.99 mg/kg/week.

K-TC3 cells measured higher maximal Ca release readings as compared to the other Kevitsa cell sets. For cell K07, the minimum release rate value of 1.61 mg/kg/week was recorded in week 51, while the maximum Ca release of 14.86 mg/kg/week was measured in week 43. The mean and median Ca release rates for K07 were calculated as 6.55 mg/kg/week and 6.11 mg/kg/week, respectively. Cell K08 had a minimum Ca release rate of 1.83 mg/kg/week recorded in week 51 and reached its maximum of 15.59 mg/kg/week in week 40, having a calculated mean Ca release of 7.10 mg/kg/week and a median rate of 7.09 mg/kg/week. The final Kevitsa cell, K09, measured its lowest Ca release rate of 1.55 mg/kg/week in week 49 and highest of 13.70 mg/kg/week in week 43. The mean release for cell K09 was 6.03 mg/kg/week, while the median was 5.99 mg/kg/week.

While there are variations in individual readings, the triplicate sets generally show similar patterns of Ca release across the 60-week leaching period. The third triplicate (K-TC3) exhibited slightly higher maximal readings compared to the first two triplicates (K-TC1 and K-TC2). These higher maximal Ca release rates align with noted variability within the reduce temperature HCT aeration system during this period of leaching.

Cumulative Ca release for Kevitsa HCT cells over the 60-week leaching period is shown in Figure 62. K-TC1 triplicate cells, K01, K02 and K03, cumulatively released 346 mg/kg, 362 mg/kg and 327 mg/kg of calcium within this kinetic testing protocol. Competitively over this period control Kevitsa cells (K-TC2), K04, K05 and K06, released 297 mg/kg, 300 mg/kg and 309 mg/kg of Ca, respectively. Reduced temperature triplicate cells within the K-TC3 set demonstrated higher cumulative Ca release rates than control cells over the 60-week leaching period, with cells K07, K08 and K09 releasing 386 mg/kg, 419 mg/kg and 356 mg/kg, respectively.

***Aitik HCT Ca results***

Within A-TC1 cell A01 Ca release rates ranged from a minimum of 1.74 mg/kg/week (week 49) to a maximum of 24.18 mg/kg/week (week 0), with a mean release of 6.42 mg/kg/week and a median of 5.07 mg/kg/week over the 60-week leaching period. Cell A02's Ca release rates ranged from 1.98 mg/kg/week in week 51 to 25.89 mg/kg/week, measured within the initial cell leach (week 0). This cell demonstrated calculated mean and median Ca release rates of 6.57 and 5.73 mg/kg/week, respectively. Similarly to cells A01 and A02, cell maximum Ca release rate was measured within the initial cell leach (27.53 mg/kg/week). Cell A03 measured a minimal Ca release rate of 2.16 mg/kg/week (week 51), with a mean Ca release rate of 6.54 mg/kg/week and a median rate of 5.46 mg/kg/week.

It can be seen in Figure 61 that A-TC2 cells, comprises cells A04, A05, and A06, generally measured lower Ca release rates than A-TC1 and A-TC3 cell sets over the 60-week leaching period. The Ca release rates measured from cell A04 leachates ranged from a minimum of 1.75 mg/kg/week (week 50) to a maximum of 20.82 mg/kg/week (week 1), with a mean release rate of 4.32 mg/kg/week and a median of 3.247723 mg/kg/week. Cell a05 measured a minimum release rate of 2.13

mg/kg/week (week 54) and a maximal release rate of 37.59 mg/kg/week within the initial cell leach (week 0). This cell measured a mean release rate of 4.43 mg/kg/week, with a median of 3.19 mg/kg/week. Measurements recorded from cell A06 ranged from 1.85 mg/kg/week (week 54) to 25.61 mg/kg/week (week 0), with a mean Ca release rate of 4.15 mg/kg/week and a median rate of 3.09 mg/kg/week.

As was noted with Kevitsa reduced temperature cells (K-TC3), A-TC3 cells measured distinctively high Ca release rate between weeks 37 and 43. This observation falls in line with other variable analytes results within these leaching weeks, in which variable cell aeration was noted. Cell A07 Ca release rates ranged from 1.25 mg/kg/week (week 54) to a maximum of 24.04 mg/kg/week (week 0), with a mean rate of 6.71 mg/kg/week and a median rate of 6.49 mg/kg/week. Ca release rates for cell A08 ranged from 0.93 mg/kg/week (week 54) to 35.10 mg/kg/week (week 0), with a mean release of 7.90 mg/kg/week and a median release of 7.56 mg/kg/week. Cell A09 measured maximal and minimal Ca release rates within the same leaching weeks as cells A07 and A08, with a minimum release rate of 1.39 mg/kg/week in week 54 and a maximal release rate of 23.33 mg/kg/week within the initial cell leach (week 0).

Over the 60-week leaching period control cells within the A-TC2 triplicate (A04, A05 and A06) cumulatively released 259 mg/kg, 261 mg/kg and 245 mg/kg of Ca. Altered parameter Aitik triplicates, A-TC1 and A-TC3, demonstrated higher total Ca releases over the leaching period. A-TC1 cells, A01, A02 and A03, cumulatively released 385 mg/kg, 394 mg/kg and 392 mg/kg of Ca over 60 weeks. A-TC3 cells A07 and A08 measured cumulative Ca releases of 396 mg/kg and 378 mg/kg, presenting closely correlated total releases as A-TC1 triplicate cells. Cell A08 demonstrated noticeably higher cumulative Ca release over the same period with 466 mg/kg, see Figure 63.

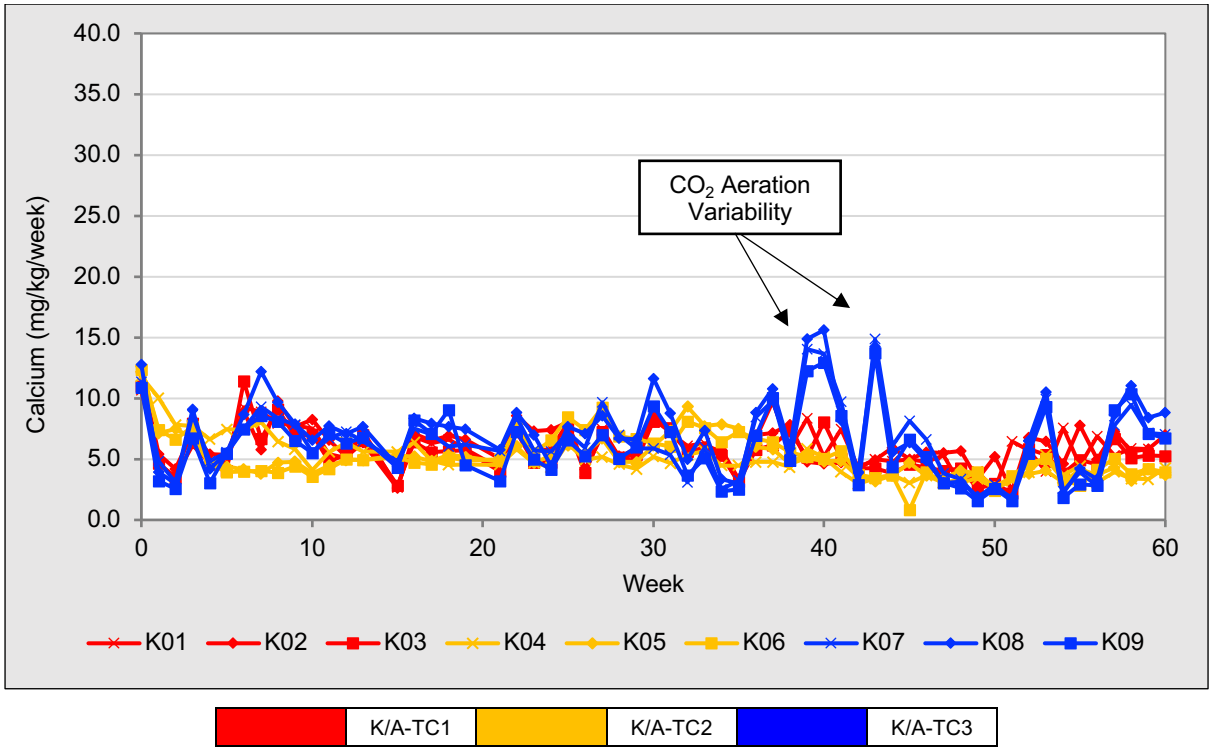


*Figure 60 – Kevitsa mine waste humidity cell tests (HCT) calcium results measured from leachates collected over the 60-week testing period.*

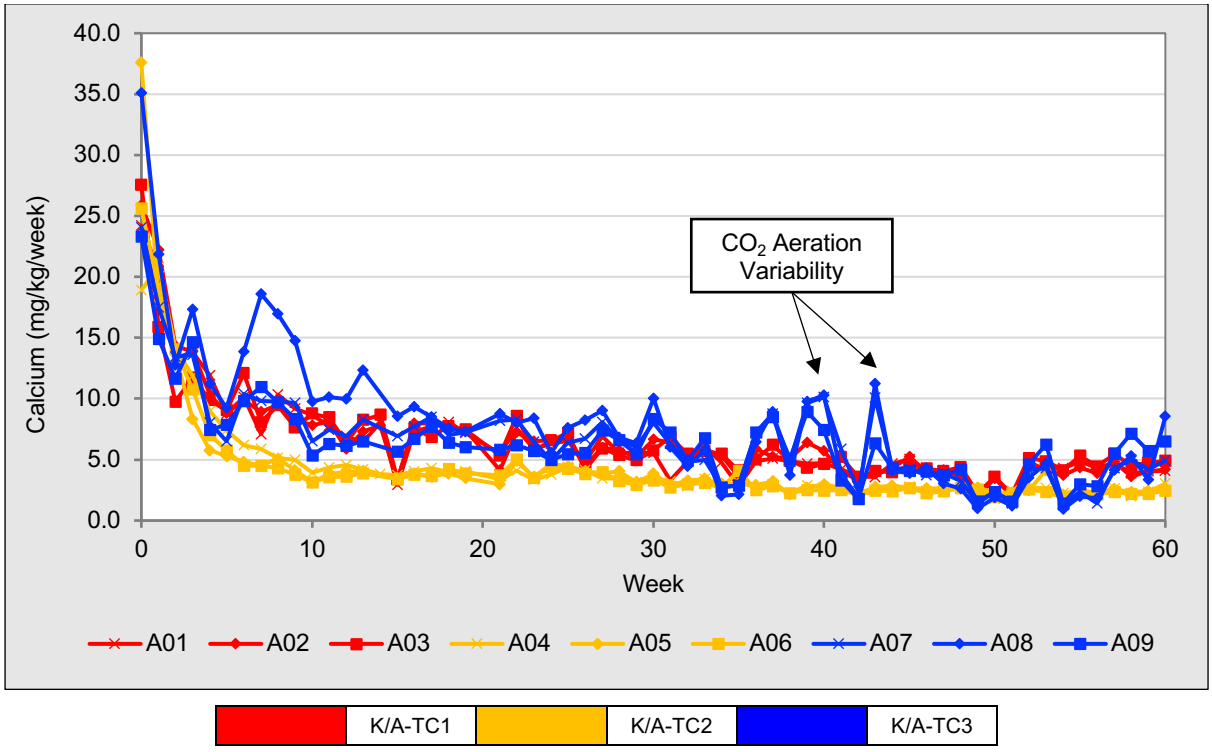


*Figure 61 – Aitik mine waste humidity cell tests (HCT) calcium results measured from leachates collected over the 60-week testing period.*

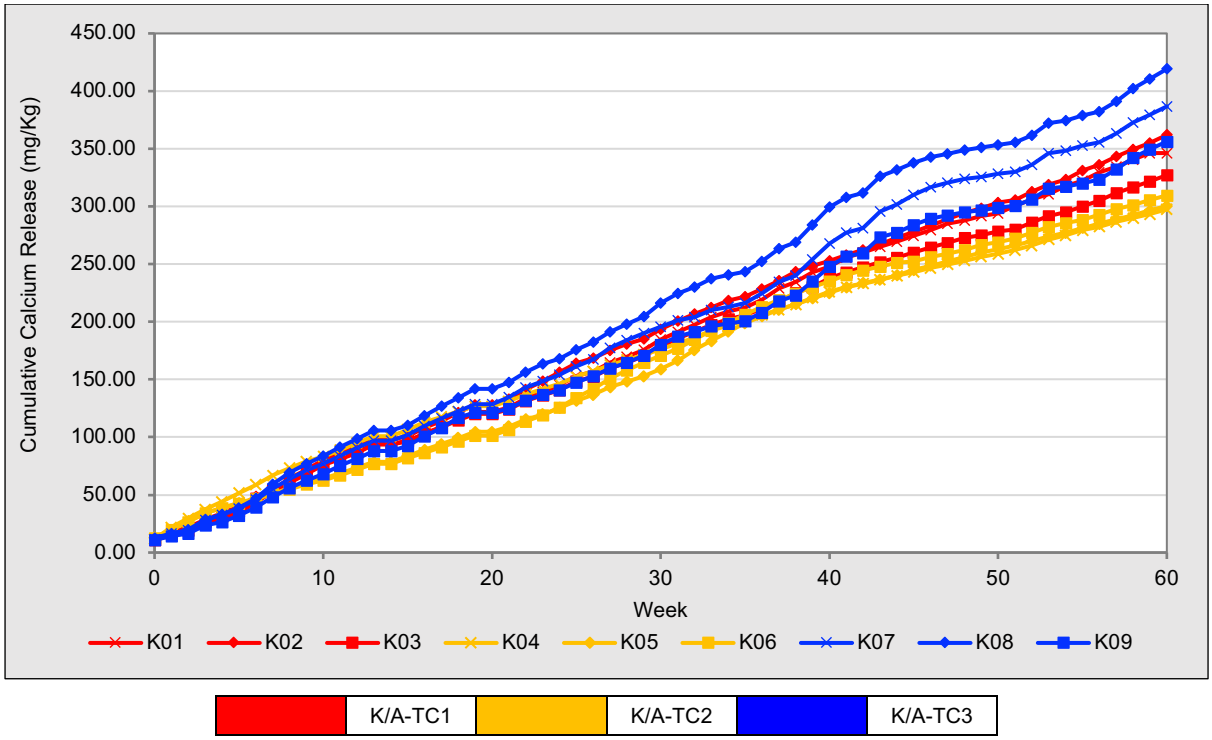


*Figure 62 – Kevitsa mine waste humidity cell tests (HCT) cumulative calcium results measured from leachates collected over the 60-week testing period.*

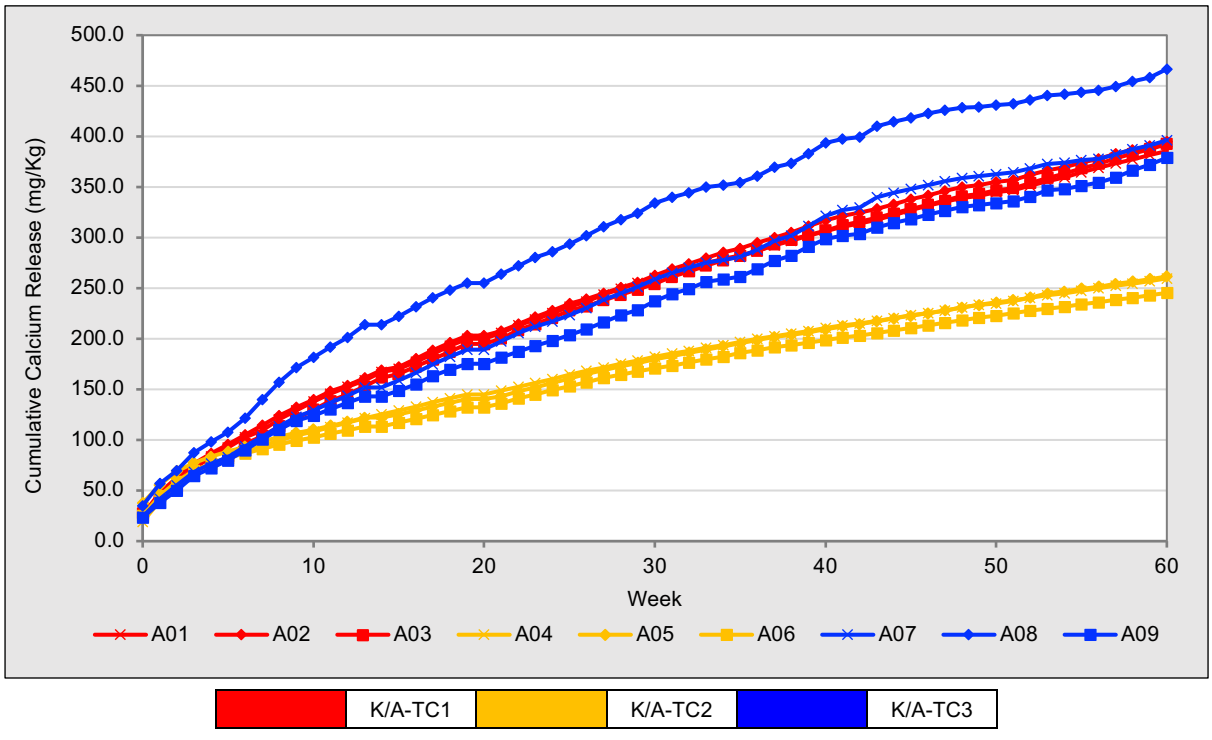


*Figure 63 – Aitik mine waste humidity cell tests (HCT) cumulative calcium results measured from leachates collected over the 60-week testing period.*

***Weekly leachate magnesium results***

Leached Magnesium (Mg) (mg/kg/week) release results for Kevitsa HCT's are shown in Figure 64, while Mg release results measured from Aitik HCT leachates are shown in Figure 65. Cumulative Mg release for Kevitsa and Aitik triplicate HCT sets are displayed in Figure 66 and 67, respectively.

***Kevitsa HCT Mg results***

It can be seen in Figure 64 that between the initial leach (week 0) and leach week 30 K-TC1 cells displayed consistently higher Mg release rates than K-TC2 and K-TC3 cells. Cell K01 measured a minimum Mg release rate of 1.28 mg/kg/week in week 48, while the maximum release rate was 34.23 mg/kg/week, recorded in week 1. The mean and median Mg release rates for K01 were 5.99 mg/kg/week and 4.15 mg/kg/week, respectively. K02 demonstrated a minimum release rate of 1.19 mg/kg/week in week 49, a maximum of 31.95 mg/kg/week in week 1. This cell had a calculated mean Mg release rate of 5.84 mg/kg/week and a median rate of 3.84 mg/kg/week. For cell K03, the Mg release rates ranged from a minimum of 1.33 mg/kg/week in week 49 to a maximum of 34.81 mg/kg/week in week 1, with mean and median release rates of 5.90 mg/kg/week and 4.18 mg/kg/week, respectively.

Cell K04 measured its minimum Mg release rate of 0.75 mg/kg/week in week 39 and its maximum rate of 15.43 mg/kg/week in week 1. The mean Mg release rate for this cell was 2.93 mg/kg/week, with a median rate of 1.90 mg/kg/week. Cell K05 recorded its lowest Mg release rate in week 50 (0.75 mg/kg/week), while the highest rate, 15.92 mg/kg/week, was recorded within the initial leach (week 0). This cell had a calculated mean Mg release rate of 2.82 mg/kg/week and a median rate of 2.02 mg/kg/week over the 60-week leaching period. K06 displayed a minimum Mg release rate of 0.80 mg/kg/week in week 50, with a maximum rate of 16.69 mg/kg/week in week 1. Cell K06 held mean and median Mg release rates of 3.09 mg/kg/week and 2.33mg/kg/week, respectively.

K-TC3 cell K07 measured its minimum Mg release rate of 0.55 mg/kg/week in week 49, and its maximum rate of 25.68 mg/kg/week in week 1. The mean and median Mg release rate values were calculated as 4.51 mg/kg/week and 3.03 mg/kg/week,

respectively. Cell K08 measured a minimum Mg value of 0.63 mg/kg/week in week 49, and a maximum of 24.44 mg/kg/week within the initial cell leach (week 0). Cell K08 had mean and median Mg release rates of 4.54 mg/kg/week and 2.97 mg/kg/week, respectively over the testing period. As was measured in cells K07 and K08, K09 demonstrated a minimum release rate value of 0.52 mg/kg/week in week 49. This cell measured maximum Mg release rate of 24.25 mg/kg/week in week 1, and over the leaching period had a mean Mg release rate of 4.52 mg/kg/week, and a median rate of 2.93 mg/kg/week.

Cumulative Mg release for Kevitsa HCT cells over the 60-week leaching period is shown in Figure 66. K-TC1 triplicate cells, K01, K02 and K03, cumulatively released 347 mg/kg, 345 mg/kg and 348 mg/kg of Mg, representing the highest cumulative release rates of Mg measured amongst Kevitsa HCT's. Control Kevitsa cells (K-TC2), K04, K05 and K06, released 173 mg/kg, 166 mg/kg and 182 mg/kg of Mg over the same period, respectively. The K-TC3 triplicate set demonstrated higher cumulative Mg release rates than control cells over the 60-week leaching period, with cells K07, K08 and K09 releasing 266 mg/kg, 268 mg/kg and 266 mg/kg, respectively.

***Aitik HCT Mg results***

A01 exhibited the maximum Mg release rate of 4.02 mg/kg/week within the initial cell leach (week 0) and a minimum Mg release of of 0.01 mg/kg/week during week 49. The mean and median Mg release rates for A01 were 0.36 mg/kg/week and 0.09 mg/kg/week respectively. Similarly, cell A02 presented its highest Mg release rate at 4.71 mg/kg/week in the first week and the lowest at 0.01 mg/kg/week in week 49. The mean and median release rates for A02 were 0.35 mg/kg/week and 0.07 mg/kg/week, respectively. Lastly, cell A03 demonstrated its maximum rate in the first week at 5.23 mg/kg/week, and its minimum in week 49 at 0.02 mg/kg/week. This cells mean and median Mg release rates were 0.34 mg/kg/week and 0.08 mg/kg/week, respectively.

Cell A04 exhibited its maximum Mg release rate of 3.25 mg/kg/week in week 0 and its minimum rate of 0.04 mg/kg/week in week 58. The mean and median Mg release rates for A04 were 0.27 mg/kg/week and 0.09 mg/kg/week, respectively. Cell A05's highest Mg release rate was 6.42 mg/kg/week (week 0), while its lowest rate was measured

as 0.04 mg/kg/week in week 56. The mean and median release rates for A05 were 0.27 mg/kg/week and 0.07 mg/kg/week, respectively. Cell A06 measured maximum release rate in week 0 at 4.58 mg/kg/week, and its minimum rate in week 50 at 0.04 mg/kg/week. The mean and median Mg release rates for A06 were 0.26 mg/kg/week and 0.08 mg/kg/week, respectively.

Cell A07 measured its maximum Mg release rate of 4.20 mg/kg/week in week 0 and its minimum release rate of 0.009 mg/kg/week during week 49. The mean and median Mg release rates for cell A07 were 0.31 and 0.10 mg/kg/week, respectively. Similarly, cell A08 measured its maximum Mg release rate at 5.85 mg/kg/week within the initial leach (week 0) and its lowest rate of 0.003 mg/kg/week in week 49. The mean and median release rates for A08 were 0.32 mg/kg/week and 0.09 mg/kg/week, respectively. Cell A09 measured its highest Mg release rate of 5.65 mg/kg/week within the initial leach, and its lowest rate of 0.008 mg/kg/week in week 49. This cells mean and median Mg release rates were calculated as 0.32 mg/kg/week and 0.09 mg/kg/week, respectively.

Over the 60-week leaching period control cells within the A-TC2 triplicate (A04, A05 and A06) cumulatively released 16.54 mg/kg, 16.51 mg/kg and 15.81 mg/kg of Mg. It can be seen in Figure 67 that altered parameter Aitik triplicates, A-TC1 and A-TC3, demonstrated marginally higher total Mg releases over the 60-week leaching period. A-TC1 cells, A01, A02 and A03, cumulatively released 21.83 mg/kg, 21.01 mg/kg and 20.78 mg/kg of Mg over 60 weeks. A-TC3 cells A07, A08 and A09 measured cumulative Mg release rates of 18.36 mg/kg, 19.42 mg/kg and 18.31 mg/kg.

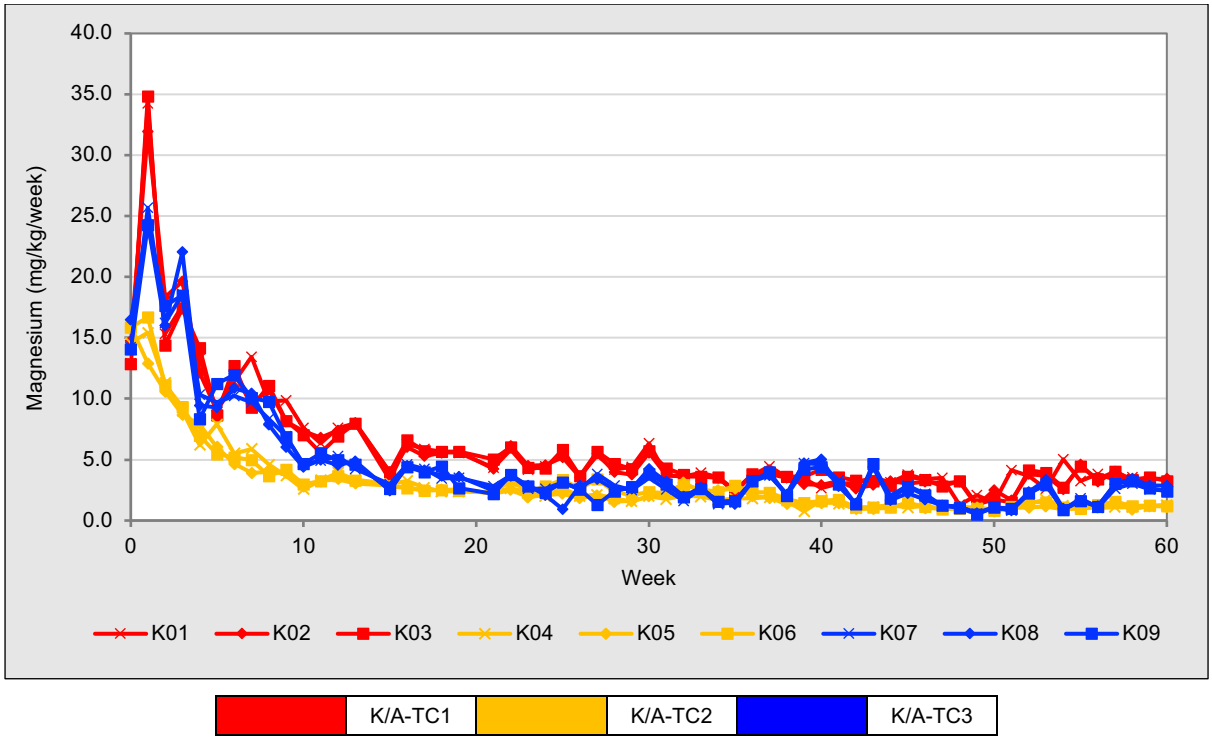


*Figure 64 – Kevitsa mine waste humidity cell tests (HCT) Magnesium results measured from leachates collected over the 60-week testing period.*

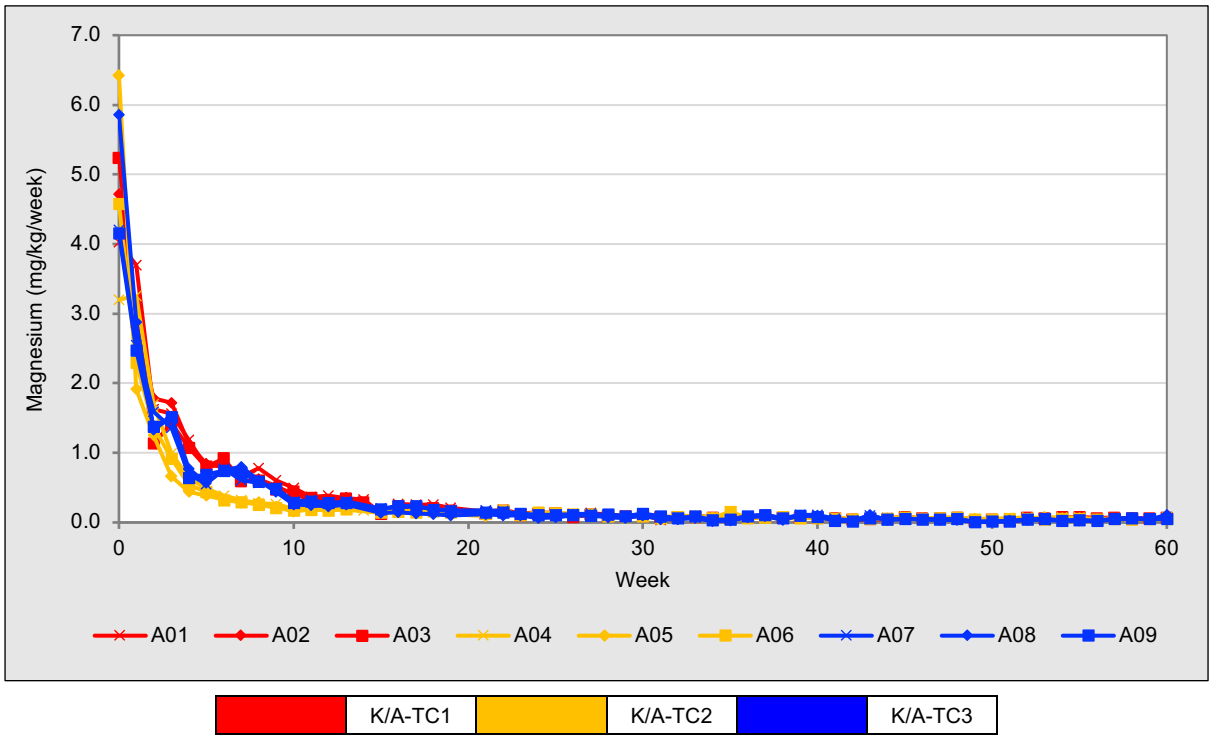


*Figure 65 – Aitik mine waste humidity cell tests (HCT) Magnesium results measured from leachates collected over the 60-week testing period.*

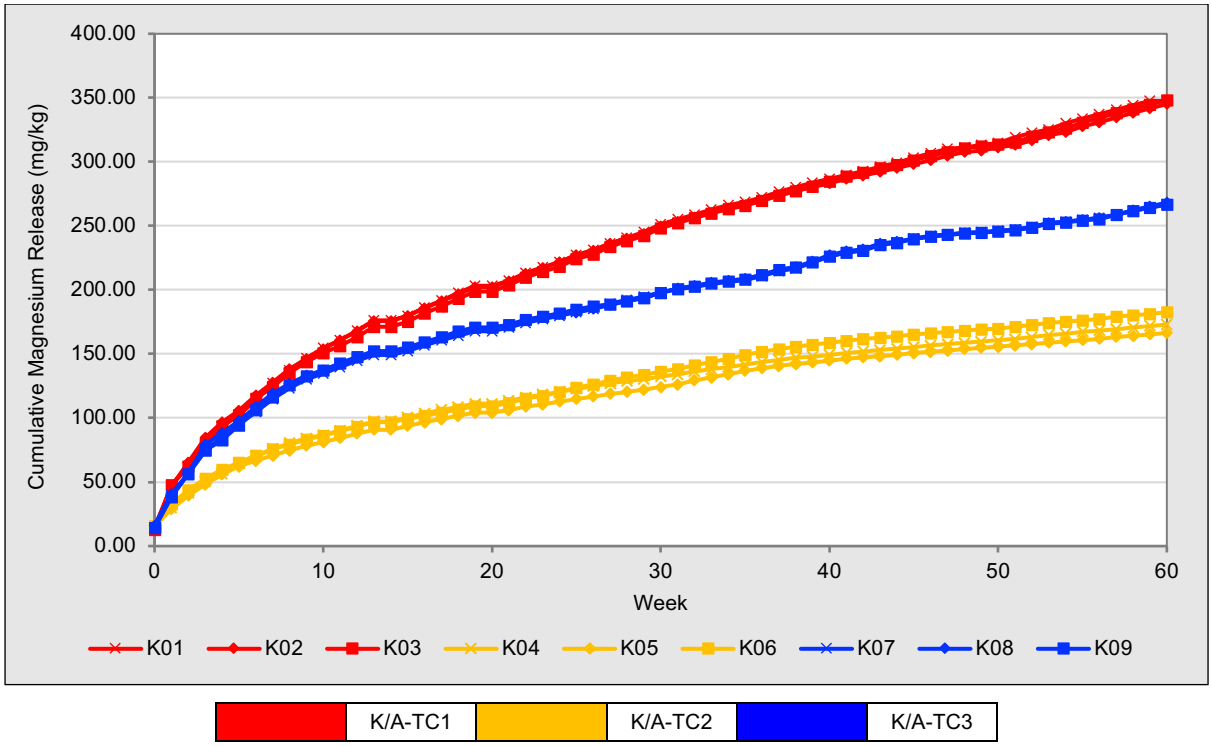


*Figure 66 – Kevitsa mine waste humidity cell tests (HCT) cumulative magnesium results measured from leachates collected over the 60-week testing period.*

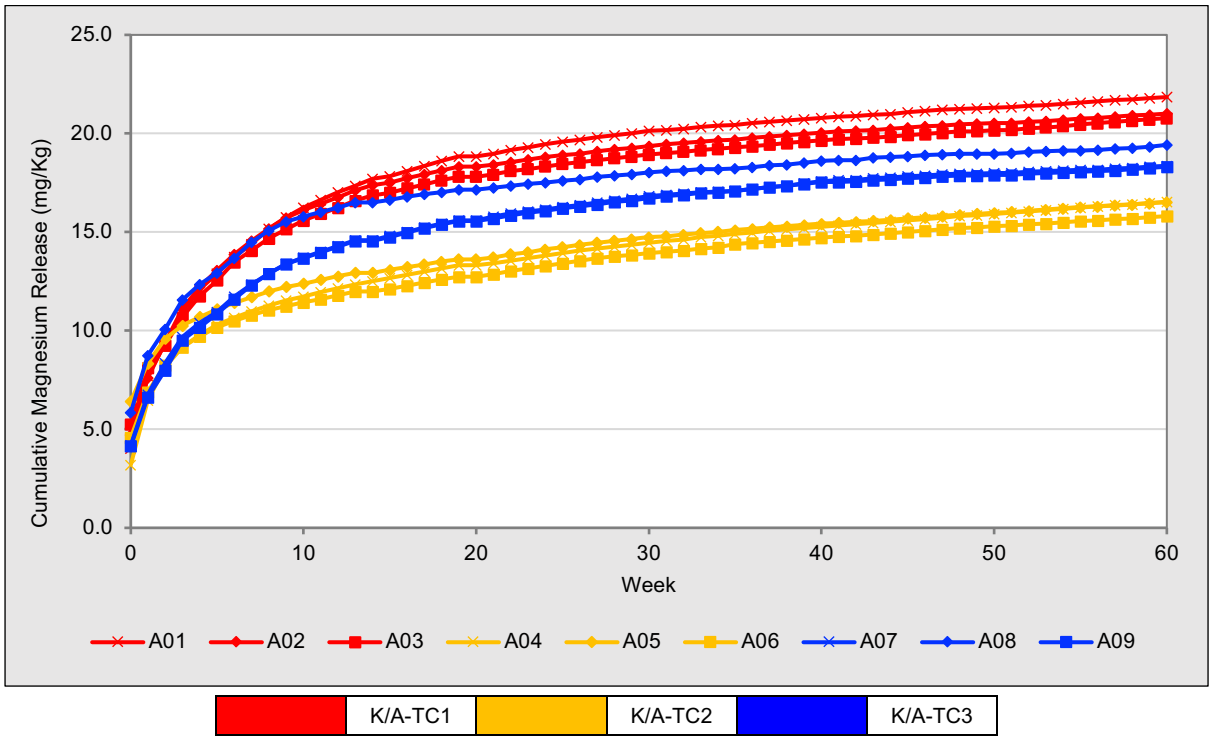


*Figure 67 - Aitik mine waste humidity cell tests (HCT) cumulative magnesium results measured from leachates collected over the 60-week testing period.*

***Weekly leachate sodium results***

Leached Sodium (Na) (mg/kg/week) release results for Kevitsa and Aitik HCT cell sets displayed minimal variations between cell triplicate sets, irrelevant of the cell conditions, over the 60-week testing period. For both Kevitsa and Aitik triplicate sets, TC3 cells were shown to leach the least Na over the 60-week period, with TC1 cells generally leaching the highest concentrations of Na. Cumulative release of Na over the testing period showed minimal differentiation between cell sets, with Kevitsa cells displaying cumulative releases ranging from a maximal value of 16.14 mg/kg (K02) to a minimal value of 14.55 mg/kg (K07).

Figures (A20.7 - A20.10) and detailed descriptions of Kevitsa and Aitik cell leached Na measurements over the 60-week leaching period can be found in Appendix 20 of this thesis.

### 5.3.5 Weekly HCT leachate trace element results

Within this section trace element leachate release results measured via ICP-OES are described. Potassium (K), Manganese (Mn) and Nickel (Ni) leachate concentrations are outlined for the Kevitsa and Aitik HCT triplicate sets, with results displayed as release over time as well as cumulative release over the 60-week leaching periods.

***Weekly leachate potassium and manganese results***

Leached Potassium (K) (mg/kg/week) release results for Kevitsa HCT's are shown in Figure 68, with cumulative K release for Kevitsa cells shown in Figure 70. Manganese (Mn) release results measured from Aitik HCT leachates are shown in Figure 69, with cumulative release results shown in Figure 71.

***Kevitsa HCT K results***

Cell K01 had an initial leach (week 0) K release rate of 3.86 mg/kg/week, with the highest release measurement of 7.88 mg/kg/week recorded in week 3, and a minimal rate of 0.71 mg/kg/week in week 48. The mean release rate for cell K01 was 2.49 mg/kg/week, while the median rate was 1.81 mg/kg/week. Cell K02's K release rate peaked at 8.49 mg/kg/week in week 3. It measured its lowest rate of 0.85 mg/kg/week in week 49. The mean release rate was 2.60 mg/kg/week, and the median was 1.80 mg/kg/week. Cell K03 had an initial measurement (week 0) of 3.87 mg/kg/week and

peaked at 7.24 mg/kg/week in week 3. The minimal cell K03 release rate was 0.69 mg/kg/week in week 50. The mean measurement for this cell was calculated as 2.56 mg/kg/week, and the median rate was 1.96 mg/kg/week.

Cell K04 measured an initial K release rate of 4.22 mg/kg/week (week 0), while this cells maximum rate of 5.66 mg/kg/week was recorded in week 2. The minimum rate of 0.66 mg/kg/week was recorded in week 42 for cell K04. The mean release rate for cell K04 was 1.87 mg/kg/week, while the median was 1.49 mg/kg/week. Cell K05 measured a peak K release rate of 5.42 mg/kg/week in week 2. The lowest rate was 0.61 mg/kg/week within week 42. For cell K05 the mean K release rate was 1.93 mg/kg/week, while the median was 1.59 mg/kg/week. Cell K06 had an initial leach (week 0) release rate of 4.29 mg/kg/week, with a peak rate of 5.57 mg/kg/week recorded in week 2. Cell K06's lowest release rate of 0.43 mg/kg/week was measured in week 45 and this cell had a mean and median release rates of 1.91 mg/kg/week and 1.64 mg/kg/week, respectively.

Over the 60-week testing period Kevitsa reduced temperature HCT cells, K-TC3, displayed the lowest potassium release rates amongst Kevitsa cells. For cell K07, the K release rates decreased over time, with the peak release rate of 5.71 mg/kg/week recorded in week 3 and the minimum release rate of 0.42 mg/kg/week in week 49. The mean and median K release rates for K07 were 1.82 mg/kg/week and 1.44 mg/kg/week, respectively. Cell K08 showed a similar trend to K07, with a peak release rate of 6.61 mg/kg/week in week 3 and a minimum release rate of 0.48 mg/kg/week recorded at week 49. The mean and median K release rates for this cell are slightly higher than cell K07, at 1.95 mg/kg/week and 1.55 mg/kg/week, respectively. Cell K09 also measured its highest K release rate in week 3, measuring 5.77 mg/kg/week. The lowest K release rate for cells K09 was observed in week 49, with a rate of 0.39 mg/kg/week. The mean and median release rates for K09 were measured as 1.82 mg/kg/week and 1.40 mg/kg/week, respectively, which are similar to the other two cells in the K-TC3 group.

The cumulative potassium (K) release for Kevitsa HCT cells over the 60-week leaching period is shown in Figure 70. K-TC1 triplicate cells, K01, K02 and K03, cumulatively released 114 mg/kg, 153 mg/kg and 151 mg/kg of K. Control Kevitsa cells (K-TC2),

K04, K05 and K06, released 110 mg/kg, 113 mg/kg and 112 mg/kg of K over the same period, respectively. K-TC3 triplicate set cells measured cumulative potassium releases within cells K07, K08 and K09 of 107 mg/kg, 115 mg/kg and 107 mg/kg.

***Aitik HCT Mn results***

It can be seen in Figure 68 that A-TC1 cells, A01, A02 and A03, demonstrated similar trends over the 60-week period with minor fluctuations in Mn release rates. The Mn release rate peaked in the initial leach (week 0) and decreased over time with smaller peaks occurring throughout. The mean Mn release rates for A01, A02, and A03 were 0.11 mg/kg/week, 0.12 mg/kg/week, and 0.11 mg/kg/week respectively. The median Mn release rates for these cells were calculated as 0.105 mg/kg/week, 0.106 mg/kg/week, and 0.103 mg/kg/week. The minimum Mn release rate for A01, A02, and A03 all occurred in week 51 with release rates of 0.020 mg/kg/week, 0.017 mg/kg/week, and 0.019 mg/kg/week, while the maximum Mn release rate all occurred within the initial leach (week 0) with release rates of 0.532 mg/kg/week, 0.577 mg/kg/week, and 0.631 mg/kg/week.

A-TC2 cells demonstrated a clear reduction in Mn release rates throughout the 60-week period, when compared to A-TC1 and A-TC3 cells. An initial peak in Mn release rates within the initial leach (week 0) was followed by a drastic reduction in weekly reduction rates, with a number of weekly concentrations below detection limits. The mean Mn release rates for cells A04, A05, and A06 were calculated as 0.019 mg/kg/week, 0.0274 mg/kg/week, and 0.025 mg/kg/week, respectively, with medians at 0.007 mg/kg/week, 0.009 mg/kg/week, and 0.0120 mg/kg/week. The large variation between mean and median release rates within this triplicate set suggests a large skewness in the average release rates. The minimum, above detection limit, release rates for cells A04 and A05 occurred in weeks 10 and 17 with release rates of 0.0005 mg/kg/week and 0.0003 mg/kg/week, respectively. The maximum release rates for these cells were all observed within the initial leach with rates of 0.35 mg/kg/week, 0.77 mg/kg/week, and 0.53 mg/kg/week, respectively for cells A04, A05 and A06.

The highest overall Mn release rates were observed within A-TC3 HCT cells over the 60-week leaching period. Cells A07, A08, and A09 held calculated mean Mn release

rates of 0.14 mg/kg/week, 0.17 mg/kg/week, and 0.13 mg/kg/week, respectively. The median Mn release rates for these cells were 0.122 mg/kg/week, 0.128 mg/kg/week, and 0.120 mg/kg/week. The minimum Mn release rates for cells A07, A08, and A09 occurred in weeks 51, 51, and 42 with release rates of 0.015 mg/kg/week, 0.013 mg/kg/week, and 0.008 mg/kg/week, respectively. The maximum release rates occurred within the initial leach (week 0), with maximal release rates of 0.523 mg/kg/week, 0.720 mg/kg/week, and 0.479 mg/kg/week.

Comparing the triplicate sets, A-TC2 generally displayed lower Mn leaching rates than A-TC1 and A-TC3 cells, both in terms of maximum, mean, and median release rates. During this kinetic testing protocol, A-TC2 triplicate cells (A04, A05 and A06) cumulatively released 1.01 mg/kg, 1.45 mg/kg and 1.43 mg/kg of Mn. A-TC1 cells, A01, A02 and A03, cumulatively released 6.90 mg/kg, 6.96 mg/kg and 6.74 mg/kg of Mn over 60 weeks. A-TC3 cells, A07, A08 and A09 measured the highest cumulative Mn releases of the Aitik HCT sets with totals of 8.63 mg/kg, 10.05 mg/kg and 8.10 mg/kg, respectively.

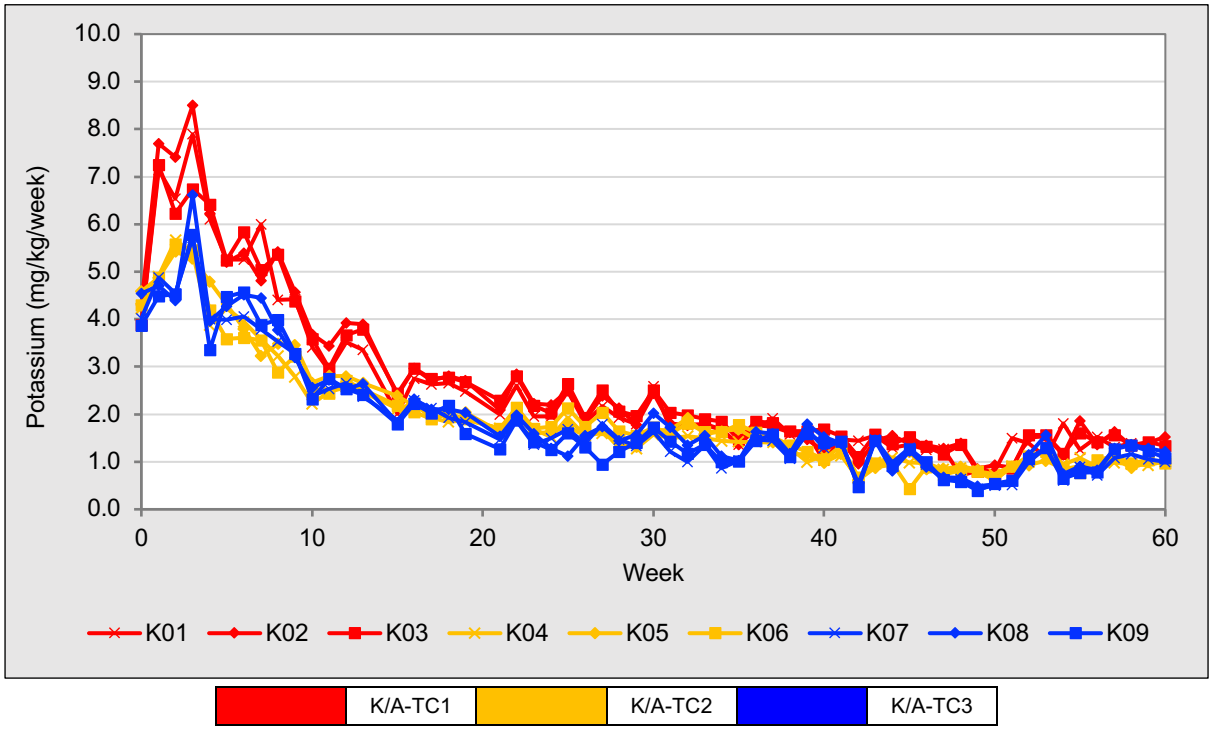


*Figure 68 – Kevitsa mine waste humidity cell tests (HCT) potassium results measured from leachates collected over the 60-week testing period.*

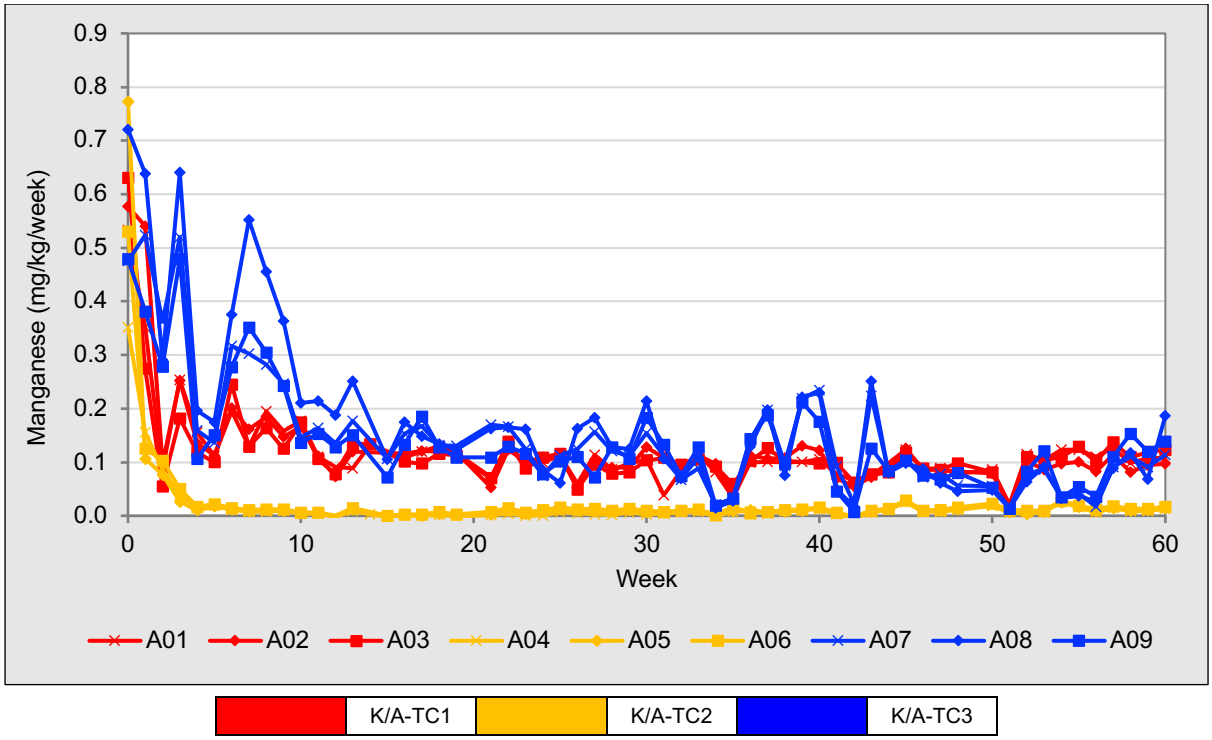


*Figure 69 – Aitik mine waste humidity cell tests (HCT) manganese results measured from leachates collected over the 60-week testing period.*

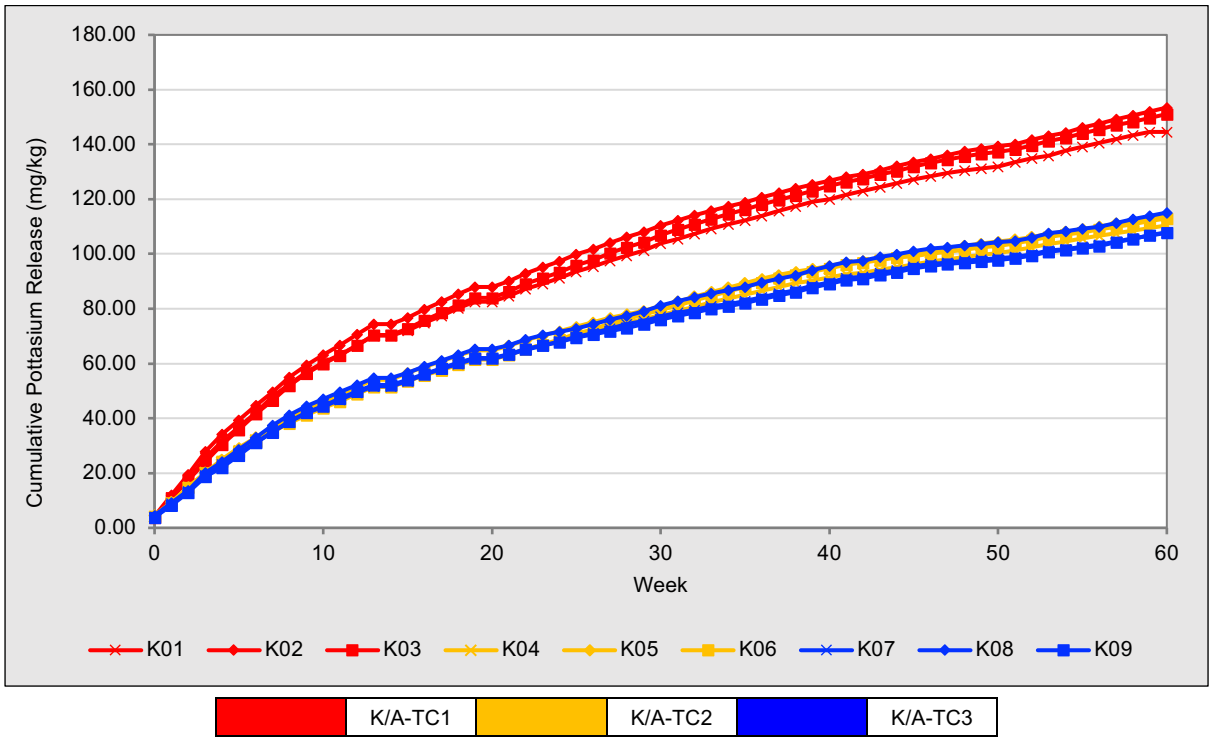


*Figure 70 – Kevitsa mine waste humidity cell tests (HCT) cumulative potassium results measured from leachates collected over the 60-week testing period.*

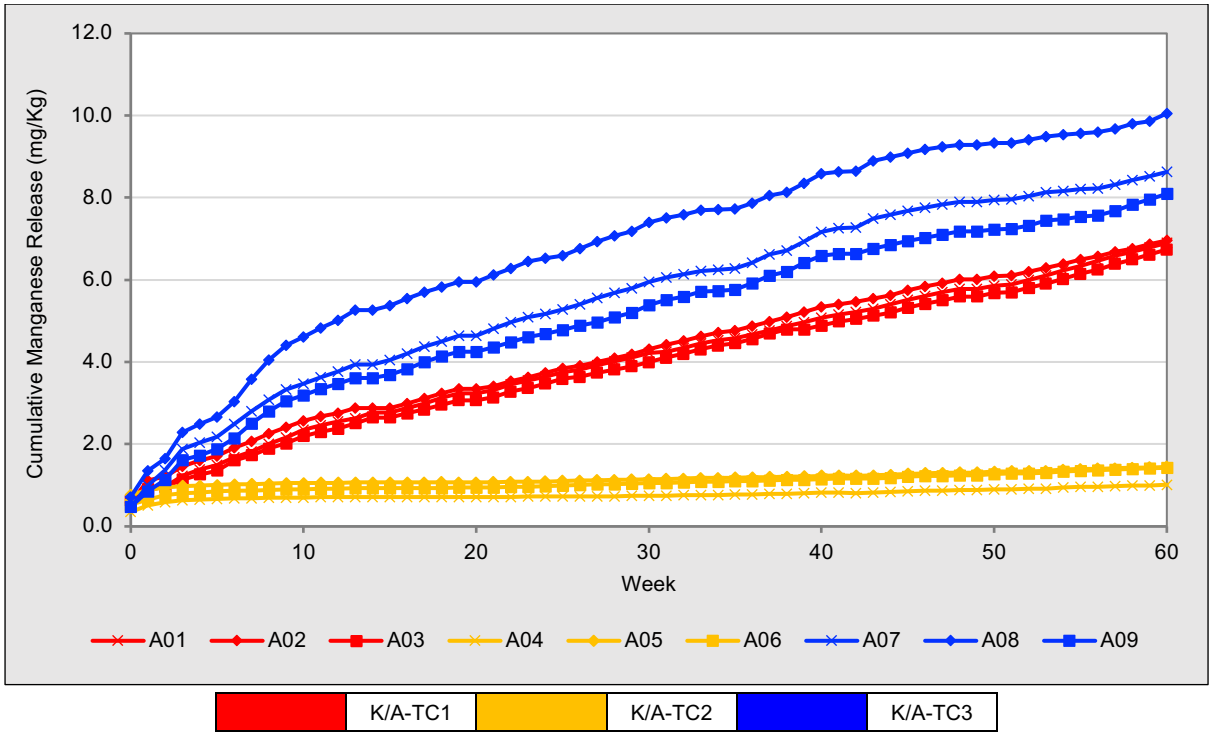


*Figure 71 – Aitik mine waste humidity cell tests (HCT) cumulative manganese results measured from leachates collected over the 60-week testing period.*

### *Weekly leachate nickel results*

Leached Nickel (Ni) (mg/kg/week) release results for Kevitsa HCT's are shown in Figure 72, with cumulative Ni release for Kevitsa cells shown in Figure 73.

### *Kevitsa HCT Ni results*

It can be seen in Figure 72 that Ni release rates were highly variable throughout the 60-week leaching periods for all Kevitsa HCT triplicate sets. Variability in nickel leaching was most prominent within K-TC3 HCT cells, displaying pronounced peaks and dips throughout the leaching period. K-TC1 cells displayed relatively less variability, although visual variability in these results is likely masked by the high variability displayed by reduced temperature HCT results.

Cell K01 measured its highest Ni release rate of 0.26 mg/kg/week in week 6, while its lowest release rate of 0.003 mg/kg/week was measured in week 2. The mean Ni release rate for K01 was 0.08 mg/kg/week, while the median was 0.06 mg/kg/week. In the case of K02, the maximum Ni release rate was 0.14 mg/kg/week recorded in week 8, while the minimum was 0.002 mg/kg/week measured in week 2. The mean Ni

release rate for K02 over this period was measured as 0.06 mg/kg/week, with a median release rate of 0.058 mg/kg/week. Cell K03 displayed a similar fluctuating pattern with a peak Ni release rate of 0.192 mg/kg/week measured in week 6 and a minimum of 0.001 mg/kg/week measured in week 2. The mean Ni release rate for this cell was 0.07 mg/kg/week, while the median was 0.06 mg/kg/week.

Cell K04's Ni release rate reaches its maximum of 0.17 mg/kg/week within the initial leach (week 0), with the minimum release rate of 0.0005 mg/kg/week occurring in week 48. The mean and median Ni release rates were calculated 0.02 mg/kg/week and 0.01 mg/kg/week, respectively for cell K04. The K05 cell displayed a general decrease in Ni release rates over time, with the highest release rate of 0.10 mg/kg/week recorded in week 0 and the lowest of 0.0001 mg/kg/week in week 23. The mean release rate for this cell was measured as 0.018 mg/kg/week, while the median is notably lower at 0.004 mg/kg/week. For cell K06, the Ni release rate peaked at 0.18 mg/kg/week in week 32. The mean and median Ni release rates for K06 were calculated as 0.03 mg/kg/week and 0.01 mg/kg/week, respectively.

K-TC3 cells, K07, K08 and K09, measured the highest mean Ni release rates across the Kevitsa triplicate sets, with mean rates of 0.175 mg/kg/week, 0.191 mg/kg/week, and 0.183 mg/kg/week respectively. These cells also measured the maximum recorded Ni release rates within the data set, with K07 peaking at 0.563 mg/kg/week in week 40, K08 peaking at 0.583 mg/kg/week in week 40, and K09 at 0.569 mg/kg/week in week 43. However, their minimum Ni release rates are still comparatively low, indicating a wide range of variation over the testing period. The minimums for cells K07, K08, and K09 occurred in week 51, with release rates of 0.004 mg/kg/week, 0.005 mg/kg/week, and 0.006 mg/kg/week respectively. The median Ni release rates for K07, K08, and K09 were 0.150 mg/kg/week, 0.172 mg/kg/week, and 0.161 mg/kg/week respectively.

Notably compared to the K-TC1 and K-TC2 cells, K-TC3 cells display sharp rises and falls in Ni release rates. Specific peaks are noted around weeks 40-43, which aligns with noted gas composition variations in reduced temperature aeration system.

The cumulative Nickel (Ni) release for Kevitsa HCT cells over the 60-week leaching period is shown in Figure 73. K-TC1 triplicate cells, K01, K02 and K03, cumulatively released 4.41 mg/kg, 3.65 mg/kg and 4.29 mg/kg of Ni. Control Kevitsa cells (K-TC2), K04, K05 and K06, released 1.16 mg/kg, 0.47 mg/kg and 1.40 mg/kg of Ni over the same period, respectively. K-TC3 triplicate set cells measured the highest cumulative nickel release rates amongst Kevitsa triplicate HCT sets. It can be seen in Figure 72 that within cells K07, K08 and K09 total Ni releases of 10.18 mg/kg, 10.91mg/kg and 10.44 mg/kg were measured over the 60-weel testing period.

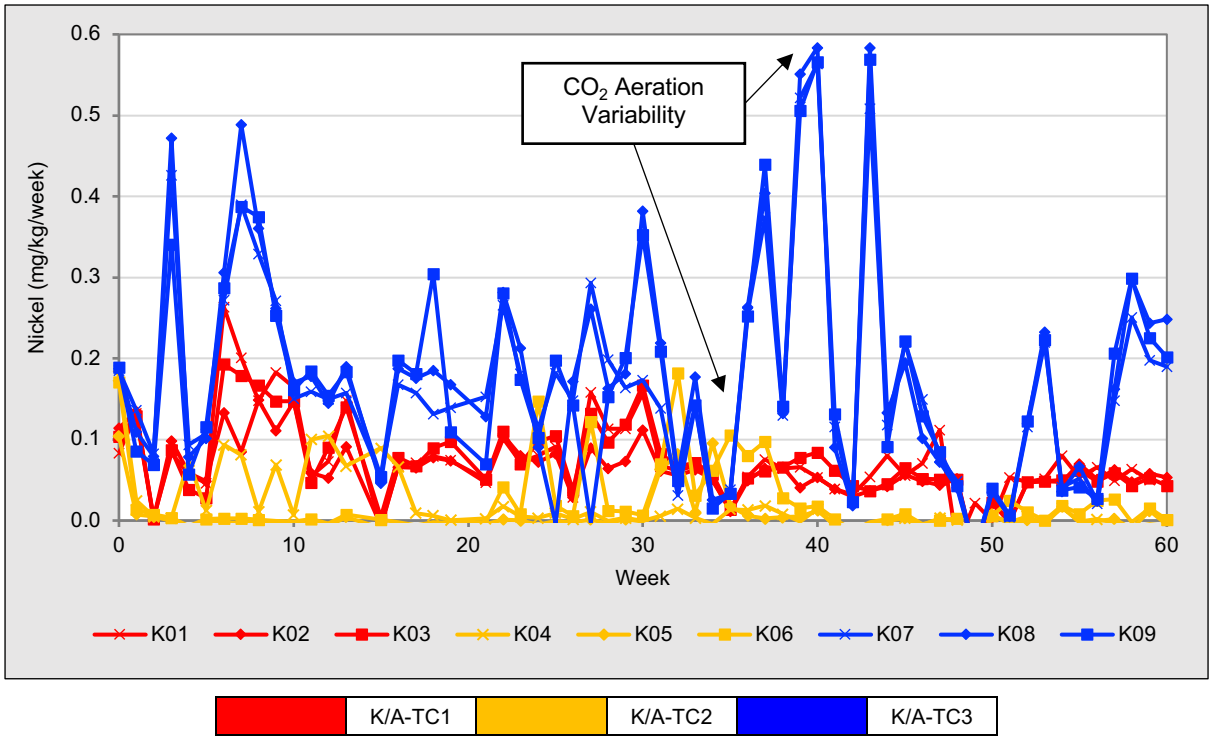


*Figure 72 – Kevitsa mine waste humidity cell tests (HCT) nickel results measured from leachates collected over the 60-week testing period.*

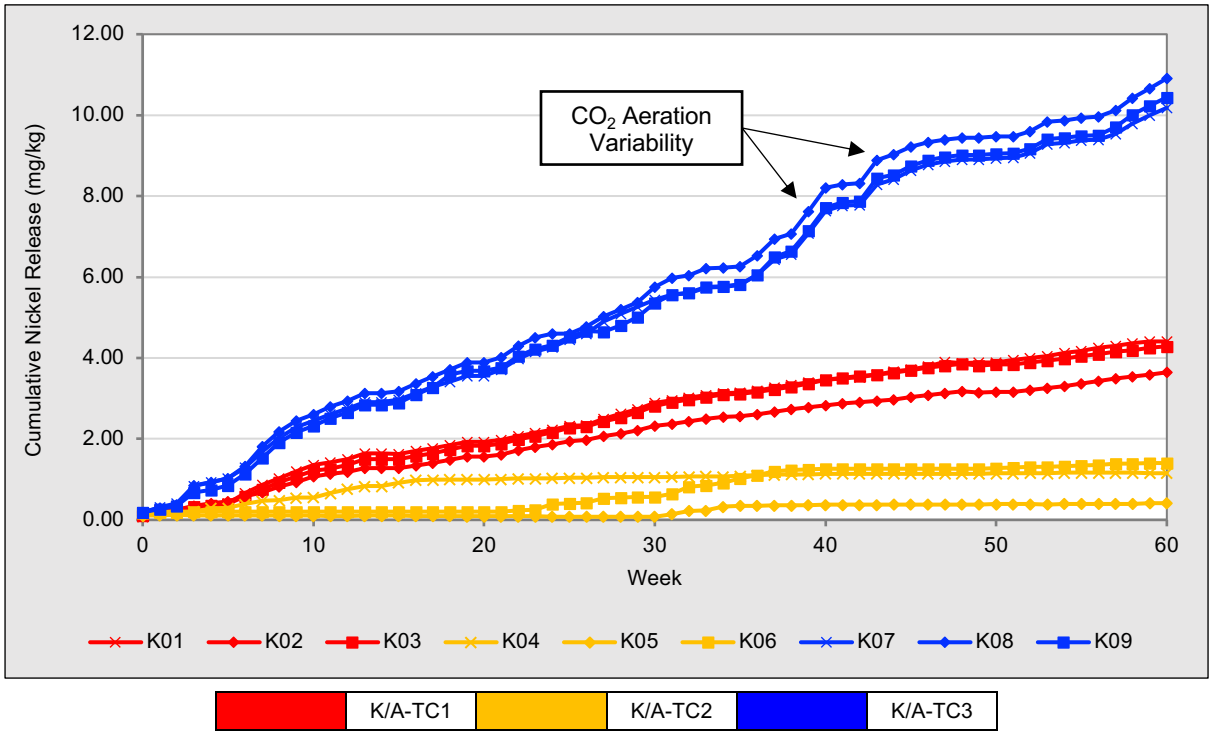


*Figure 73 – Kevitsa mine waste humidity cell tests (HCT) cumulative nickel results measured from leachates collected over the 60-week testing period.*

### 5.3.6 Triplicate cell sets QA/QC - relative percentage differences (RPD)

The cumulative release rates (mg/kg) for key analytes for Kevitsa and Aitik HCT triplicate cell sets are shown in Tables 15 and 16, respectively. Within these tables dissolved inorganic carbon (DIC), sulfate ($SO_4$), magnesium (Mn), calcium (Ca), sodium (Na) and potassium (K) cumulative releases are summarised for both wastes sets, while nickel (Ni) is shown for Kevitsa in table 15 and manganese (Mn) is shown for Aitik cells in table 16. These tables display the relative percent difference (RPD) between cells in each triplicate set, as well as the average RPD.

It can be seen in Table 15 that within K-TC1 (Enhanced $CO_2$/Standard Temperature) cells the RPD values range from a low of 0.1%, for DIC between cells K01 and K02, to a high of 18.95%, for Ni between cells K01 and K02. The average RPD is lowest for Mg (0.6%) and highest for Ni (12.64%). This indicates that the measurements for magnesium were most consistent, while the measurements for nickel showed the most variability, while still being within a statistically acceptable RPD range (<20%). None of the presented analytes presented RPD values above acceptable limits within cell triplicate set K-TC1.

Control cells, K-TC2 (Reduced $O_2$/Standard Temperature) held calculated RPD values ranging from a low of 0.93%, for sulfate between cells K04 and K05, to a high of 99.31%, for Ni between cells K05 and K06. The average RPD is lowest for K (2.08%) and notably high for nickel (67.53%). Thus, the measurements for potassium were most consistent, while the measurements for nickel had the highest degree of variability. Notably, the variability in measurements of nickel in this test condition is significantly higher than in the other two test conditions, this could be attributed to the lower concentrations within this cell set, with most weekly release rates close to or below analytical detection limits (ADL).

K-TC3 (Enhanced $CO_2$/Reduced Temperature) measured calculated RPD values ranging from a low of 0.07%, for Na between cells K07 and K09, to a high of 16.21%, for Ca between cells K08 and K09. The average RPD is lowest for Mg (0.39%) and highest for Ca (10.82%) within this triplicate set. This suggests that the measurements for magnesium were the most consistent, while the measurements for calcium showed the most variability in this test condition, although cumulative loads were still within acceptable RPD bounds between these cells.

*Table 15 – Kevitsa triplicate HCT analyte cumulative release results and triplicate RPD %*

| **K-TC1 - Kevitsa Enhanced $CO_2$ (10%) / Standard Temperature (25$^{O}$C) HCT Triplicates** | | | | | | | |
|---|---|---|---|---|---|---|---|
| Parameter | K01 | K02 | K03 | K01-K02 RPD % | K01-K03 RPD % | K02-K03 RPD % | Average RPD (%) |
| DIC (mg/kg) | 440.81 | 440.36 | 425.8 | 0.1 | 3.47 | 3.36 | 2.31 |
| Sulfate (mg/kg) | 943.42 | 975.52 | 958.94 | 3.35 | 1.63 | 1.71 | 2.23 |
| Nickel (mg/kg) | 4.41 | 3.65 | 4.29 | 18.95 | 2.73 | 16.24 | 12.64 |
| Magnesium (mg/kg) | 347.59 | 345.04 | 348.13 | 0.74 | 0.16 | 0.89 | 0.60 |
| Calcium (mg/kg) | 346.28 | 362.03 | 327.15 | 4.45 | 5.68 | 10.12 | 6.75 |
| Sodium (mg/kg) | 15.84 | 16.14 | 15.34 | 1.89 | 3.19 | 5.07 | 3.38 |
| Potassium (mg/kg) | 144.57 | 153.48 | 151.1 | 5.98 | 4.42 | 1.56 | 3.99 |
| **K-TC2 - Kevitsa Reduced $O_2$ (10% $N_2$) / Standard Temperature (25$^{O}$C) Control HCT Triplicates** | | | | | | | |
| Parameter | K04 | K05 | K06 | K04-K05 RPD % | K04-K06 RPD % | K05-K06 RPD % | Average RPD (%) |
| DIC (mg/kg) | 73.86 | 62.68 | 54.24 | 16.38 | 30.64 | 14.43 | 20.48 |
| Sulfate (mg/kg) | 1182.68 | 1193.74 | 1314.88 | 0.93 | 10.59 | 9.66 | 7.06 |
| Nickel (mg/kg) | 1.16 | 0.47 | 1.4 | 84.33 | 18.95 | 99.31 | 67.53 |
| Magnesium (mg/kg) | 173.02 | 166.52 | 182.63 | 3.82 | 5.41 | 9.23 | 6.15 |
| Calcium (mg/kg) | 297.51 | 300.33 | 309.57 | 0.94 | 3.97 | 3.03 | 2.65 |
| Sodium (mg/kg) | 15.05 | 15.43 | 16.08 | 2.46 | 6.59 | 4.14 | 4.40 |
| Potassium (mg/kg) | 110.46 | 113.95 | 112.98 | 3.11 | 2.26 | 0.86 | 2.08 |
| **K-TC3 - Kevitsa Enhanced $CO_2$ (10%) / Reduced Temperature (10$^{O}$C) HCT Triplicates** | | | | | | | |
| Parameter | K07 | K08 | K09 | K07-K08 RPD % | K07-K09 RPD % | K08-K09 RPD % | Average RPD (%) |
| DIC (mg/kg) | 554.98 | 594.04 | 533.06 | 6.8 | 4.03 | 10.82 | 7.22 |
| Sulfate (mg/kg) | 477.04 | 533.38 | 544.54 | 11.15 | 13.21 | 2.07 | 8.81 |
| Nickel (mg/kg) | 10.18 | 10.91 | 10.44 | 6.9 | 2.53 | 4.38 | 4.60 |
| Magnesium (mg/kg) | 266.61 | 268.15 | 266.82 | 0.58 | 0.08 | 0.5 | 0.39 |
| Calcium (mg/kg) | 386.73 | 419.16 | 356.3 | 8.05 | 8.19 | 16.21 | 10.82 |
| Sodium (mg/kg) | 14.55 | 14.92 | 14.56 | 2.53 | 0.07 | 2.46 | 1.69 |
| Potassium (mg/kg) | 107.78 | 115.14 | 107.91 | 6.6 | 0.12 | 6.48 | 4.40 |

Within triplicate cells within A-TC1 (Enhanced $CO_2$/Standard Temperature) the RPD values ranged from as low as 0.42%, for DIC between cells A01 and A03, to as high as 57.88%, for K between cells A01 and A02. The averaged RPD is lowest for DIC (0.99%), indicating a high level of consistency in these measurements, while it is significantly highest for potassium (38.64%), suggesting a large variability in potassium measurements under these conditions. It is noted that the RPD between cells A02 and A03 was measured as 1.83%, an acceptable RPD, but a significantly higher cumulative lead measured in cell A01 caused a skewness within the averaged RPD for potassium.

Between cells in Aitik triplicate set A-TC2 (Reduced $O_2$/Standard Temperature) the lowest RPD value was observed for sulfate, calculated as 0.17% between cells A05 and A06. The highest RPD was noted for cumulative DIC (23.72% between cells A05 and A06). The averaged RPD values show that the measurements for sulfate were the most consistent (0.40%), while the measurements for DIC had the highest degree of variability (15.84%), while still within the acceptable RPD range.

The last Aitik triplicate set, A-TC3 (Enhanced $CO_2$/Reduced Temperature) demonstrated calculated RPD values ranging from a low of 0.27%, for Mg between cells A07 and A09, to a high of 42.21%, for DIC between cells A08 and A09. The averaged RPD was lowest for sodium (4.54%), suggesting more consistent measurements, and highest for DIC (28.27%), indicating greater variability in the measurements of DIC under these conditions. It has been previously noted that cell A08 displayed DIC values above other cells within this triplicate. This may be due to aeration cycle malfunctions during various period of the testing, leading to higher than designed $CO_2$ concentrations within this cells aeration system. Comparatively cells A07 and A08 held a calculated RPD of 12.47 % for DIC over the same period, within acceptable RPD ranges in this study.

*Table 16 – Aitik triplicate HCT analyte cumulative release results and triplicate RPD %*

| **A-TC1 Aitik Enhanced $CO_2$ (10%) / Standard Temperature (25$^{O}$C) HCT Triplicate** | | | | | | | |
|---|---|---|---|---|---|---|---|
| Parameter | A01 | A02 | A03 | A01-A02 RPD % | A01-A03 RPD % | A02-A03 RPD % | Average RPD (%) |
| DIC (mg/kg) | 240.12 | 236.56 | 239.11 | 1.49 | 0.42 | 1.07 | 0.99 |
| Sulfate (mg/kg) | 522.37 | 546.48 | 537.2 | 4.51 | 2.8 | 1.71 | 3.01 |
| Manganese (mg/kg) | 6.9 | 6.96 | 6.74 | 0.9 | 2.33 | 3.24 | 2.16 |
| Magnesium (mg/kg) | 21.85 | 21.01 | 20.78 | 3.91 | 5.02 | 1.11 | 3.35 |
| Calcium (mg/kg) | 385.51 | 394.78 | 392.4 | 2.38 | 1.77 | 0.6 | 1.58 |
| Sodium (mg/kg) | 15.91 | 14.01 | 13.97 | 12.68 | 13 | 0.31 | 8.66 |
| Potassium (mg/kg) | 144.57 | 79.67 | 81.14 | 57.88 | 56.2 | 1.83 | 38.64 |
| **A-TC2 - Aitik Reduced $O_2$ (10% $N_2$) / Standard Temperature (25$^{O}$C) Control HCT Triplicates** | | | | | | | |
| Parameter | A04 | A05 | A06 | A04-A05 RPD % | A04-A06 RPD % | A05-A06 RPD % | Average RPD (%) |
| DIC (mg/kg) | 38.24 | 40.94 | 32.26 | 6.82 | 16.97 | 23.72 | 15.84 |
| Sulfate (mg/kg) | 659.08 | 655.17 | 656.26 | 0.6 | 0.43 | 0.17 | 0.40 |
| Manganese (mg/kg) | 1.02 | 1.45 | 1.43 | 35.17 | 33.62 | 1.6 | 23.46 |
| Magnesium (mg/kg) | 16.54 | 16.51 | 15.81 | 0.18 | 4.51 | 4.33 | 3.01 |
| Calcium (mg/kg) | 259.67 | 261.5 | 245.35 | 0.7 | 5.67 | 6.37 | 4.25 |
| Sodium (mg/kg) | 15.05 | 13.19 | 12.61 | 13.15 | 17.65 | 4.53 | 11.78 |
| Potassium (mg/kg) | 63.25 | 57.12 | 51.09 | 10.18 | 21.27 | 11.15 | 14.20 |
| **A-TC3 - Aitik Enhanced $CO_2$ (10%) / Reduced Temperature (10$^{O}$C) HCT Triplicates** | | | | | | | |
| Parameter | A07 | A08 | A09 | A07-A08 RPD % | A07-A09 RPD % | A08-A09 RPD % | Average RPD (%) |
| DIC (mg/kg) | 336.56 | 455.99 | 297.05 | 30.14 | 12.47 | 42.21 | 28.27 |
| Sulfate (mg/kg) | 354.9 | 301.16 | 337.25 | 16.38 | 5.1 | 11.3 | 10.93 |
| Manganese (mg/kg) | 8.63 | 10.05 | 8.1 | 15.25 | 6.37 | 21.56 | 14.39 |
| Magnesium (mg/kg) | 18.36 | 19.42 | 18.31 | 5.62 | 0.27 | 5.9 | 3.93 |
| Calcium (mg/kg) | 396.19 | 466.55 | 378.88 | 16.31 | 4.47 | 20.74 | 13.84 |
| Sodium (mg/kg) | 11.36 | 12.16 | 11.43 | 6.81 | 0.62 | 6.18 | 4.54 |
| Potassium (mg/kg) | 61.64 | 74.45 | 58.14 | 18.82 | 5.85 | 24.6 | 16.42 |

# Chapter 6 - Discussion

## Introduction

Within this Chapter the results and figures presented in Chapter 5 are discussed and interpreted in detail. The potential implications for kinetic testing procedures that implement variable gas compositions and temperature controls are discussed in the context of the research questions and aims devised in Chapter 1. The wider perspective related to mine closure planning and the implications for mine waste geochemical drainage development is also considered.

This thesis was undertaken with the overarching purpose of assessing the potential implications of enhanced $CO_2$ concentrations on mine waste geochemical development and ARD classification/ prediction. To date no standardised kinetic or static tests have been developed to assess the potential environmental implications of enhanced $CO_2$ concentrations on sulfidic mine drainage quality. Within this research project an altered humidity cell test (HCT) protocol was developed that considered site-specific conditions. The importance of this study stems from accepted perspective that the failure to predict acid rock drainage (ARD) accurately has the potential to lead to substantial environmental consequences (Parbhakar-Fox and Lottermoser 2015).

Suitable mining wastes have been touted within the scientific community as a potential feedstock for large scale carbon dioxide removal (CDR) (Hitch and Dipple 2012b; Royal Society and Royal Academy of Engineering 2018; McQueen et al. 2020). To date little research has been carried out that assesses the potential implications of these CDR strategies, such as enhanced weathering, on mine waste geochemical development and ARD prediction (Kandji et al. 2017a).

Several studies have also identified seasonally variable pore gas compositions within existing sulfidic mining waste storage facilities, with sulfide oxidation consuming $O_2$ and driving $CO_2$ concentrations above atmospheric levels (Lorca et al. 2016; Vriens et al. 2018; Vriens et al. 2019a). These seasonally variable pore gas compositions are not considered within standardised kinetic testing for sulfidic wastes with the only

comparable method designed to assess the weathering of carbonate abundant coal wastes and overburden (Hornberger et al. 2004; Perry et al. 2009; EPA 2011).

The combination of the forementioned factors outlines the need for specific kinetic testing methods that assess the weathering and metal leaching characteristics of sulfidic waste materials under variable environmental conditions. Based on these premises and the literature review outlined in Chapter 3 the following hypothesises, research aims, and research questions were developed:

**Research hypothesis:**

- The presence of enhanced carbon dioxide concentrations within mining waste facilities has an impact on waste rock weathering.
- Current kinetic testing methods, specifically humidity cell testing (HCT), produce leaching characteristics that are not representative of environments in which above atmospheric carbon dioxide concentrations are present.

**Research aims:**

- To assess the potential implications of enhanced carbon dioxide concentrations on mine waste weathering.
- To determine whether running HCT's on aluminosilicate rich waste rocks under elevated $CO_2$ concentrations and varying temperatures impacts sulfide mineral oxidation rates and the quality of recovered cell leachates.
- To determine if alterations in waste geochemical and mineralogical characteristics have occurred between pre and post experimental testing.

**Research questions:**

1. What is the relationship between predicted ARD risk and $CO_2$ concentration?
2. How does host rock mineralogy and $CO_2$ concentration impact drainage quality?
3. Are altered humidity cell tests appropriate for assessing enhanced mine waste weathering in the presence of elevated $CO_2$?

**Humidity cell tests (HCT) specific research questions:**

- How does the introduction of 10% $CO_2$ into an ASTM standard HCT aeration cycle affect the leaching rates of key analytes and metals?
- How does the reduction in test temperature impact weekly leachate chemistry compared to standard temperature cells?

## 6.1 Research Findings Summary

Based on the results outlined in Chapter 5 several research findings summary points have been developed. These points will be discussed in the context of this studies research aims and research questions in the following sections of this Chapter.

### 6.1.1 Material characterisation findings

- Mineralogical analysis in the form of bulk mineral abundance and petrographic thin sections displayed minimal distinguishable alterations to Kevitsa waste rock materials, irrespective of HCT conditions, as a result of the 60-week leaching protocols. Aitik HCT materials also displayed minimal alteration, with the exception of Anorthite, which was shown to drop in abundance from 13.3 wt% in pre HCT materials to between 6.9-8.5% in post HCT materials. Petrographic thin sections under cross polarised light displayed minimal alteration to observable silicate and sulfide minerals between pre and post HCT materials.
- Elemental analysis via ED-XRF displayed minimal alteration to elemental abundance between pre and post HCT samples for both Kevitsa and Aitik cells. A <10% variation in Mg and Ca content was observed for both HCT sets, irrelevant of experimental conditions. Al was shown to increase by 10-15% across all Aitik post HCT samples compared to A-Pre results. Aitik post HCT's also displayed consistent 10-20% increase in Si across all post HCT residues.
- Kevitsa materials were shown to have theoretical maximum CCP values of between 295-312 kg/t $CO_2$, with marginal increases in altered HCT triplicate set cells when compared to control. Aitik materials held calculated CCP values of between 73-87 kg/t $CO_2$ with minimal variation between post HCT material values.
- Physical observations taken during decommissioning noted 'cementing' of enhanced $CO_2$ cell materials, with clear agglomeration of sample particles within enhanced $CO_2$ cells. Select cells displayed distinct oxidation of particles over the 60-week period, supported by periodic photographs of the cells over the testing period.

### 6.1.2 Static testing findings

- Post HCT material total C% measurements from Kevitsa cells displayed a marginal decrease in total C% following the leaching period, with a pre HCT value of 0.09%

and post HCT values of 0.06-0.08%. Aitik materials conversely displayed a marginal increase in total C% in post HCT cells, although the margin of change is too small to make definitive comments. Within both cell sets no distinguishable variation is noted between variable experimental condition triplicate sets.

- Total S% measurements taken post kinetic testing was less than the pre HCT source material total S% measurements in all cells. The initial Aitik composite total S% measurement was 0.85%, this was shown to drop to between 0.62% and 0.818% post kinetic testing. Cells A02 and A08 displayed distinctively higher total S% contents amongst Aitik cells. The Kevitsa composite held a total S% of 0.47%. Post HCT total S% was shown to marginally decrease in all Kevitsa materials with K-TC1, K-TC2 and K-TC3 holding mean S% values of 0.43%, 0.41% and 0.42%.
- ABA testing carried out on pre and post HCT materials displayed a consistent increase in NP across all 9 Kevitsa HCTs, irrespective of experimental conditions. Similarly, Kevitsa post HCT materials displayed a marginal decrease in MPA. NNP and NPR values were consistent among Kevitsa triplicate sets with little variance between cell triplicates. Aitik cells within the A-TC1 and A-TC2 triplicates displayed similar NP values to the pre HCT NP value. A-TC3 cells displayed an increase in NP across all cells of between 23-36% over the pre HCT value. Aitik post HCT MPA values were consistently ~15-20% lower than the pre HCT measurement. A-TC1 and A-TC2 cells displayed consistent NPR values, comparable to the pre HCT NPR of ~0.29. A-TC3 cells displayed an increase in NPR to 0.41-0.44.
- Kevitsa and Aitik post HCT materials displayed consistent increases in NAG pH values within all triplicate sets, with minimal observable variation within or between triplicate sets for each operation. All Kevitsa materials were shown to have no measurable single addition total NAG. Variable total NAG values were observed within Aitik HCT materials, with no distinguishable patterns between triplicate cells and corresponding variations in test conditions.
- ABCC testing was ran in a limited capacity due to budgetary and laboratory constraints. ABCC curves generated for Kevitsa post HCT materials displayed a slight decrease in available NP within enhanced $CO_2$ cell triplicates (K-TC1 and K-TC3) compared to the pre HCT duplicates. The control HCT cell K05 displayed a greater NP availability post kinetic testing. Aitik materials showed little observable variance between post HCT and pre HCT materials.

- Minimal variation was observed between Kevitsa material pre and post HCT paste pH measurements. Aitik materials displayed an increase in paste pH within post HCT residues compared to pre HCT measurements. The greatest increase over the source material was observed in A-TC3 cells, which average a paste pH of pH 8.62, compared to the pre HCT measurement of pH 8. Paste EC was shown to drop in all post HCT materials for both operations when compared to pre HCT values. Kevitsa materials displayed minimal variations in post HCT paste EC between triplicate sets, while reduced temperature Aitik cells, A-TC3, displayed a clear reduction in paste EC when compared to other triplicate sets and the pre material values.
- 24-hour leach tests displayed minimal alterations to leaching properties between triplicate sets from both operations. Eluent pH increased in all Kevitsa post HCT materials when compared to the pre HCT material leach eluent. Aitik post HCT materials displayed a reverse trend of lower post HCT eluent pH measurements. DIC was shown to marginally increase in post HCT cells with K-TC3 cells demonstrating the most consistent increase compared to K-Pre. Aitik cells demonstrated a more pronounced decrease in DIC across all post HCT cells, with the exception of A03. Aitik post HCT cell A03 showed pronounced variations in both eluent pH and DIC, as well as elemental concentrations. Compared to other A-TC1 cells, cell A03 displayed 67% and 79% lower Mn concentrations. Generally, all enhanced $CO_2$ HCT materials displayed enhanced leaching of Mg compared to control cells. Most elemental concentrations displayed negligible differentiations between triplicate cells or triplicate sets, irrelevant of the material or test conditions.

### 6.1.3 Kinetic testing findings

- Throughout the 60-week leaching period enhanced $CO_2$ HCT triplicates in both control temperature and reduced temperatures generally demonstrated higher leachate pH measurements than control cells for both Kevitsa and Aitik HCT sets.
- EC readings fluctuated greatly, compared to control cell, in enhanced $CO_2$ Kevitsa cells over the leaching period, with K-TC3 cells demonstrating generally lower EC measurements than control cells or K-TC1. Altered HCT sets within the Aitik HCT group also displayed a degree of fluctuation over the test period, although control cells were shown to demonstrate consistently lower EC readings than altered cells.

- Weekly dissolved inorganic carbon (DIC) measurements were shown to be consistently higher in enhanced $CO_2$ cell triplicate sets within both cell groups. Issues with the aeration system 2 within cold room cells was noted between weeks 32 and 45. During these weeks DIC spikes and troughs were noted which consistently align with excess and reduced $CO_2$ availability within the HCT aeration system in reduced temperature cells. Within Kevitsa cell sets enhanced $CO_2$ triplicates, K-TC1 and K-TC3, held mean cumulative DIC release loads 590% and 788% higher than the control cell set (K-TC2) mean cumulative DIC release over the same period. Aitik cell demonstrated the same trends in DIC differentiations between cell sets. Cumulatively over the testing period control Aitik HCT cells averaged a DIC release of 36 mg/kg of DIC. Comparatively DIC load release was 905% higher in reduced temperature A-TC3 cells on average, while A-TC cells demonstrated a mean increase of 561% over control cells.
- Total alkalinity and acidity measurements were available for the first 45 weeks of testing in both cell groups. Alkalinity measurements were consistently higher in enhanced $CO_2$ cells compared to control cells for both operations. Kevitsa cells reduced temperature cells demonstrated alkalinity measurement volatility in line with aeration system variability between weeks 35 and 45. pH measurements taken post hydrogen peroxide dosing displayed a slightly higher level of resistance to acidic pH change in enhanced $CO_2$ cells compared to controls for both operations. Total acidity depression was demonstrated in enhanced $CO_2$ cells throughout the testing period, with no measurable acidity detected in the majority of measurements taken over the initial 45 weeks within Kevitsa cells.
- Sulfate release reached a relatively steady state after ~8 weeks in all Aitik cells. Kevitsa control cells demonstrated a higher level of variability with steadier state releases noted after week 40. Enhanced $CO_2$ cells from both locations demonstrated apparent $SO_4$ suppression when compared to control cells. Although this was expected within reduced temperature cells, due to reduced kinetic rates of sulfide oxidation under colder temperatures, enhanced $CO_2$ control cells, K-TC2 and A-TC2, measured consistently less sulfate release than control cell sets.
- AP and NP consumption results were available for the first 45 weeks of kinetic testing. It was demonstrated in both operations cell sets that NP consumption was between 75- 100% higher in enhanced $CO_2$ cell triplicates. Conversely, over the same testing period AP consumption was notably lower in $CO_2$ enhanced HCT's.

- Mg and Ca release rates were shown to vary considerably between enhanced $CO_2$ cell sets and control sets for Kevitsa and Aitik HCTs, respectively. Magnesium release was shown to consistently be higher within Kevitsa enhanced $CO_2$ cells, compared to control cells. This may suggest the enhanced weathering of Mg rich silicates, which the initial mineralogical analysis suggests represents a large proportion of this material, under enhanced $CO_2$ conditions. Ca release rates showed a similar trend within enhanced $CO_2$ Aitik cells over the leaching period. The potential for preferential weathering of faster reacting silicate minerals in the presence of enhanced $CO_2$ concentrations is discussed later in this Chapter.
- Trace element release rates demonstrated interesting distinctions between enhanced $CO_2$ cell triplicates and control cells. Ni and Mn were noted as the trace elements with the most prevalent release rates for Kevitsa and Aitik cell sets, respectively. Mn release rates were shown to be consistently higher within Aitik enhanced $CO_2$ cells over the 60-week period when compared to control triplicate cells. Over the leaching period Aitik control cells, A-TC2, cumulatively release between 1.02 mg/kg and 1.42 mg/kg, while A-TC1 and A-TC3 cells release >6.5 mg/kg and >8 mg/kg, respectively. Ni release rates from Kevitsa cells were erratic in nature over the 60-week period within enhanced $CO_2$ cells. Cells within K-TC1 and K-TC3 consistently measured higher Ni release rates than control cells, although no ready state was reached over the testing period. It was noted that Ni weekly release loads were noticeably sensitive to variations In the aeration system, with distinct peaks and troughs corresponding to weeks with disrupted $CO_2$ aeration supply. Over the leaching period all reduced temperature enhanced $CO_2$ Kevitsa cells cumulatively released <10 mg/kg of Ni, compared to <1.5 mg/kg within corresponding control cells.
- RPD analysis was carried out on the cumulative release loads of triplicate cells for key parameters including DIC, $SO_4$, Ni, Mg, Ca, Na and K for Kevitsa cell sets. Within K-TC1 RPD% values for these parameters were all >19% between cells, with an averaged Mg RPD value of <1%, demonstrating a close repeatability between cell leaching characteristics. K-TC3 cells demonstrated similar levels of apparent repeatability with all averaged RPD values <11% across the assessed parameters. A higher level of apparent variability was noted in K-TC2 RPD values for Ni, which demonstrated averaged RPD values <67%.

## 6.2 Interpretation of Study Findings

Within this study HCT experimental conditions were varied to assess the implications of enhanced $CO_2$ aeration gas compositions and reduced temperature on mine waste geochemical development and HCT leachate chemistry. Materials utilised were collected from two differing mining operations to account for potential result biases based on an individual deposits mineralogical characteristic. A composite material was created for both operations HCT sets which was homogenised to reduce individual sample bias, with composite samples assessed for homogeneity before the experimental protocol. 60 weeks of leachate chemistry was collected for 9 humidity cells within each operations set, with pH, ORP, EC, alkalinity, acidity and dissolved major, minor and trace elements measured on a weekly basis. 3 triplicate sets were undertaken for either operational set, summarised as follows:

- **Test Conditions 1** – Control Temperature (25$^{o}$C), Enhanced $CO_2$ HCT (10% $CO_2$ by volume)
- **Test Conditions 2** – Control Temperature (25$^{o}$C), Control Aeration HCT (10% $N_2$ to balance $CO_2$ by volume)
- **Test Conditions 3** – Reduced Temperature (10$^{o}$C), Enhanced $CO_2$ HCT (10% $CO_2$ by volume)

It was noted that over the 60-week testing period sulfate release rates were supressed within enhanced $CO_2$ cells, when compared to the control. DIC measurements were considerably higher within test condition 1 and test condition 3 cell sets, which corresponded to higher pH, alkalinity, Mg, Ca, Ni (Kevitsa) and Mn (Aitik) concentrations, when compared to corresponding control cells for each operation. Measured total acidity was reduced in enhanced $CO_2$ condition cells, irrespective of condition set. The weekly release rates and cumulative load of DIC, Ca, Mg, Ni and Mn concentrations were notably higher within test condition 3 cells for both operations. This displayed a distinct variation in leaching characteristics between test conditions in response to enhanced $CO_2$ concentration within the test aeration system and temperature alteration.

### 6.2.1 Potential mechanisms behind variations in HCT leaching characteristics

The differentiations between leaching characteristics between the 3 cells sets for either operation can broadly be explained through an understanding of temperature dependent reaction kinetics (Arrhenius equation), Henrys laws and the open system Bjerrum plot (Henry 1803; Arrhenius 1889; Stumm and Morgan 1995).

One of the key research questions of this study was identified as ***'How does the introduction of 10% $CO_2$ into an ASTM standard HCT aeration cycle affect the leaching rates of key analytes and metals?'*** To answer this research, question the weekly concentrations of key analytes measured in control cells (K-TC-2 and A-TC2) must be compared to enhanced $CO_2$ cells (K-TC1. K-TC3, A-TC1 and A-TC3) and potential mechanisms for these variations explored. The temperature alteration within test condition 3 cell sets means these cells are not directly comparable to control cells, as no reduced temperature control cells were undertaken in this study. The potential implications of temperature alteration on ML rates and waste geochemical developed are covered in the following sections of this Chapter.

To understand the potential mechanisms that cause variations in analyte values and ML rates/loads between cell testing conditions the mean cumulative release loads for DIC, $SO_4$, Ca, Mg and Ni (Kevitsa) and Mn (Aitik) for each HCT condition set have been compiled, see Figure 74. It can be seen in Figures 74 (a) and 74 (b) that a commonality was observed between the general load release trends of presented analytes within both Kevitsa and Aitik HCT sets. It was shown over the 60-week leaching period that when comparing enhanced $CO_2$ cell sets to control cells, that cumulative DIC release loads increased by 585% and 782% within K-TC1 and K-TC3 cells, respectively. This increase was similarly noted within Aitik enhanced $CO_2$ cell triplicates, A-TC1 and A-TC3, which cumulatively released, on average, 542% and 878% more DIC than the control cell set A-TC2. The potential mechanisms of these differentiations in DIC, including $CO_2$ solubility and dissolved speciation, are discussed later in this Chapter. Mg and Ca cumulative release loads were also shown to increase in enhanced $CO_2$ cells within both operational sets. Trace element release of Ni (Kevitsa) and Mn (Aitik) demonstrated increased release loads over the 60-week period, compared to control cells over the same testing period.

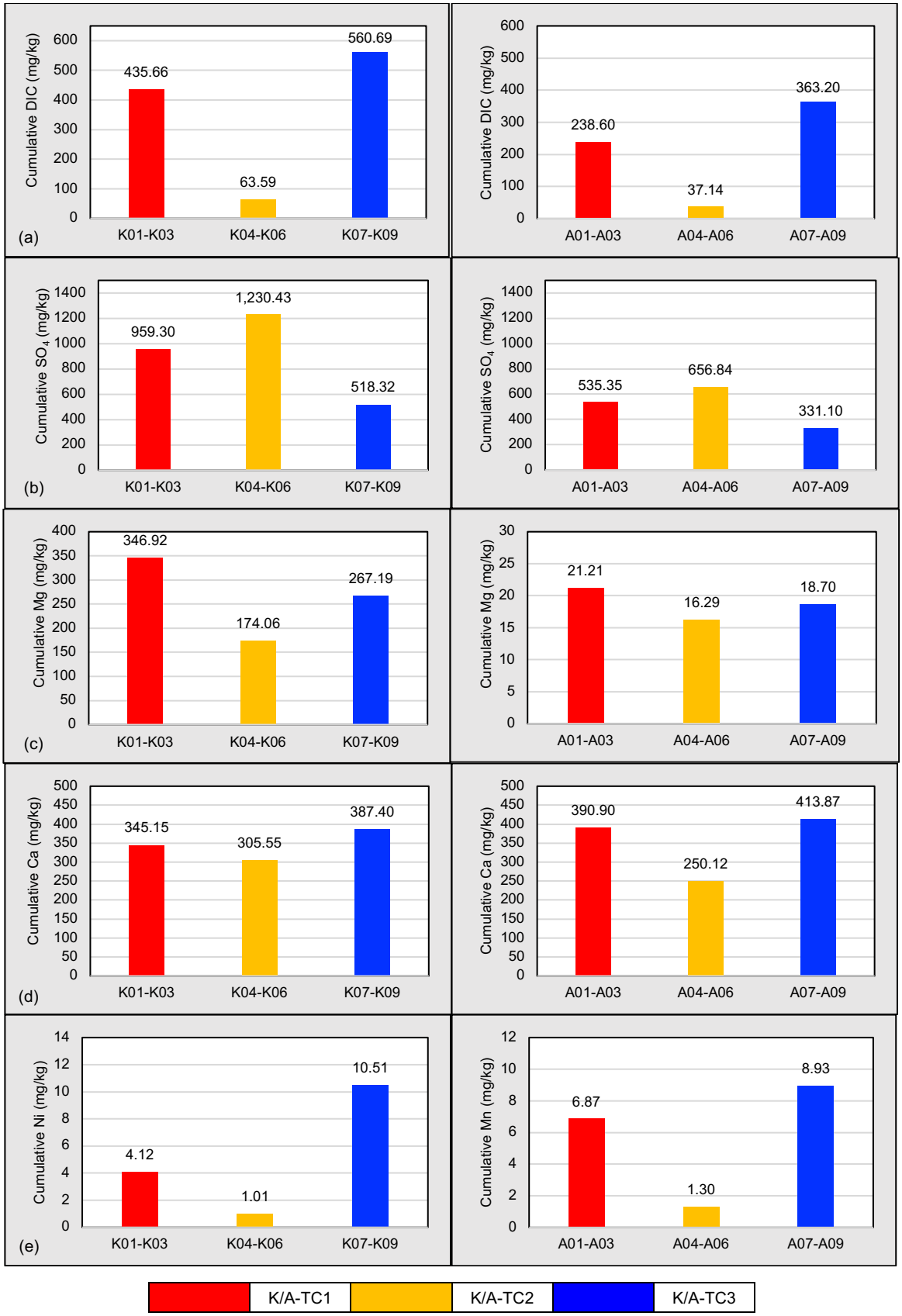


*Figure 74 - Averaged triplicate cumulative release for leached analytes from Kevitsa and Aitik HCT sets. (a) DIC, (b) SO4, (c) Mg, (d) Ca, (e) Ni (Kevitsa) / Mn (Aitik)*

### 6.2.2 Potential DIC and alkalinity differentiation mechanisms

It is noted that dissolved inorganic carbon (DIC) was measured in this research project as a standalone parameter, with an assessment of individual dissolved carbon species not possible within this study. DIC represents a direct measurement of the sum of aqueous phase carbon dioxide, bicarbonate, carbonate and carbon acid within a solution, see Equation 29 (Hanrahan 2012a; Cole and Prairie 2014).

*Equation 29 - Dissolved inorganic carbon (DIC) speciation* (Hanrahan 2012a)

$$DIC = [CO_2] + [HCO_3^-] + [CO_3^{2-}] + [H_2CO_3]$$

*Where: DIC = Dissolved Inorganic Carbon, $CO_2$ = Aqueous Phase Carbon Dioxide, $HCO_3^-$ = Bicarbonate, $CO_3^{2-}$ = Carbonate, $H_2CO_3$ = Carbonic Acid*

Equations 30 to 33 outline the basic carbonate chemistry within natural waters in an open system accounting for the constitutes of total DIC (Stumm and Morgan 1995; Appelo and Postma 2004; Velbel 2009; Fagerlund et al. 2010; Nduagu et al. 2012; Langman et al. 2014; Meysman and Montserrat 2017). Equation 30 outlines how the amount of dissolved carbon dioxide species within a solution is proportional to the gaseous counterpart within the atmosphere of a system (Henry 1803). The carbonate system can be described simply by equations 31 to 33. Within an open system carbonic ($H_2CO_3$) acid is formed through the reaction of aqueous $CO_{2\ (aq)}$ and water ($H_2O$), Equation 31. Carbonic acid can then dissociate to bicarbonate ions ($HCO_3$) and hydronium ($H^+$), which adds acidity to the system, Equation 32. Depending on the systems pH, bicarbonate can then dissociate further to carbonate ($CO_3^{2-}$) and hydronium ($H^+$). The sum of these dissolved carbon species equals the total dissolved inorganic carbon (DIC) of a solution, as shown in Equation 29.

*Equation 30 - Gas phase and aqueous phase $CO_2$ transfer*

$$CO_{2(g)} \Leftrightarrow CO_{2(aq)}$$

Where: $CO_{2\ (g)}$ = Gaseous Phase Carbon Dioxide, $CO_{2\ (aq)}$ = Aqueous Phase Carbon Dioxide

*Equation 31 - Carbonic acid formation*

$$CO_{2(aq)} + H_2O \Rightarrow H_2CO_3$$

Where: $CO_{2\,(aq)}$ = Aqueous Phase Carbon Dioxide, $H_2O$ = Water, $H_2CO_3$ = Carbonic Acid

*Equation 32 - Carbonic acid dissociation*

$$H_2CO_3 \Leftrightarrow HCO_3^- + H^+$$

Where: $H_2CO_3$ = Carbonic Acid, $HCO_3^-$ = Bicarbonate, $H^+$ = Hydronium

*Equation 33 - Bicarbonate dissociation*

$$HCO_3^- \Leftrightarrow H^+ + CO_3^{2-}$$

Where: $HCO_3^-$ = Bicarbonate, $H^+$ = Hydronium, $CO_3^{2-}$ = *Carbonate*

The differentiation in DIC between control temperature enhanced $CO_2$ cells and control cells is a function of $CO_2$ concentration. The exact carbon species present within produced weekly leachates is difficult to empirically quantify, but through assessment of pH measurements of corresponding leach weeks the relative carbon dominant species can be estimated (Stumm and Morgan 1995; Hanrahan 2012a; Cole and Prairie 2014). Humidity cell tests can be considered an open system, as they interact with an external aeration system that feeds humidified and dry air within the cells (Price 2009; ASTM 2018). This means an open system Bjerrum plot, see Figure 75, can be used to assess the potentially dominant carbon species in cell leachates at specific pH ranges (Stumm and Morgan 1995; Hanrahan 2012).

Gaseous phase $CO_{2\,(g)}$ should be proportional to aqueous phase $CO_{2\,(aq)}$ if the system is in thermodynamic equilibrium in relation to Henry's constant for $CO_2$ (Stumm and Morgan 1995; Hanrahan 2012a; Meysman and Montserrat 2017) . It is noted that within the measured leachate pH ranges of enhanced $CO_2$ cells within this study, DIC, which is composed of the total sum of dissolved $CO_{2\,(aq)}$ species, see Equation 29, would be dominated by $HCO_3^-$ ions and $CO_3^{2-}$ ions (Stumm and Morgan 1995; Hanrahan 2012; Cole and Prairie 2014). This interpretation is based on the open system Bjerrum plot, see Figure 75.

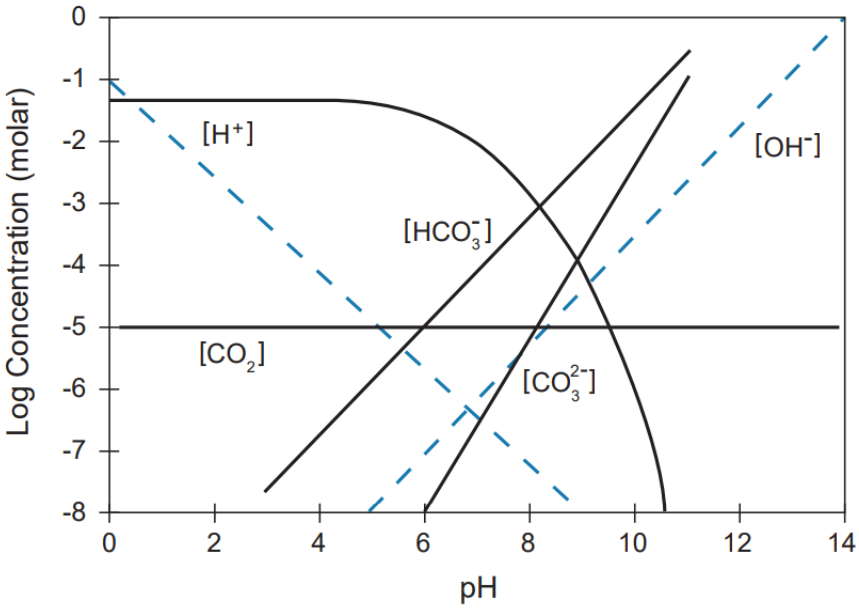


*Figure 75 - A Bjerrum plot of the log of concentrations of various inorganic carbon species as a function of pH in an open system at 25°C with $pCO_2 = 10^{-3.5}$ atm* (Hanrahan 2012a)

Weekly leachate pH measurements and corresponding DIC release rates from all HCT sets are plotted in Figure 76. Distinct clustering is noted in for enhanced $CO_2$ cells from both operational sets, with these HCT cells generally displaying higher pH measurements in line with higher DIC concentrations during corresponding weeks.

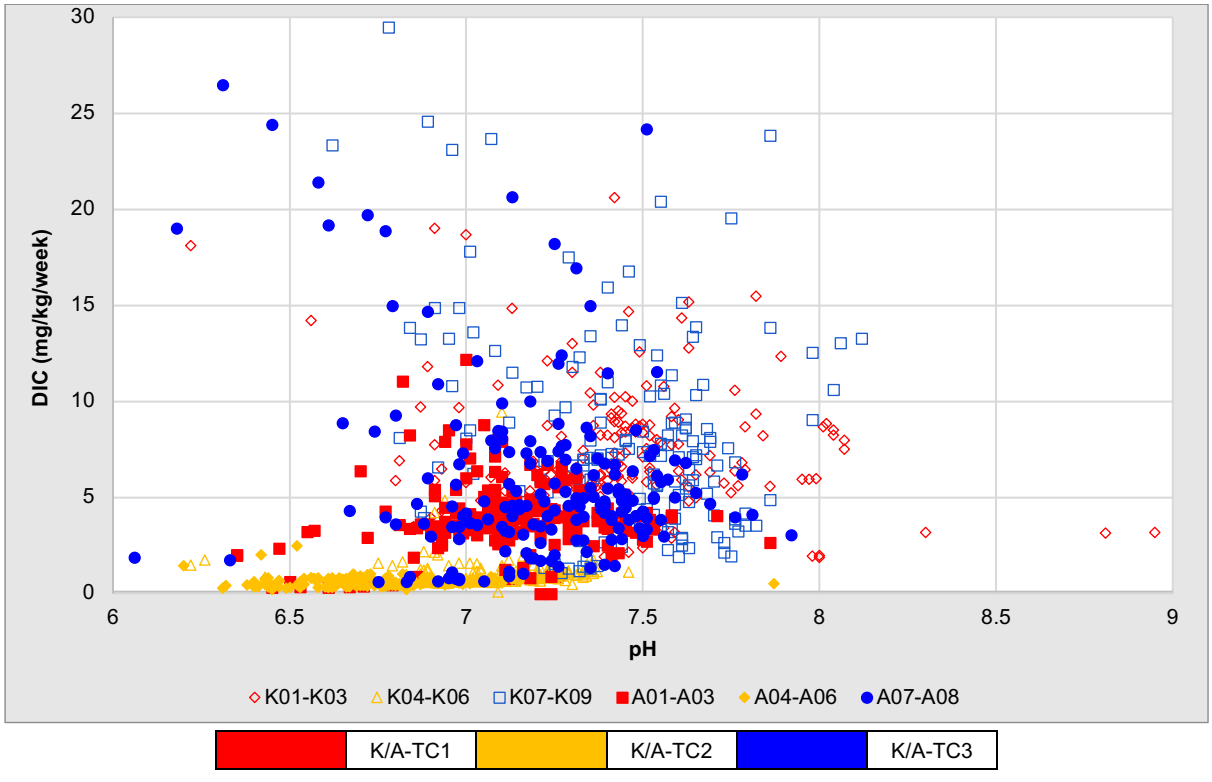


*Figure 76 – Leachate DIC plotted against pH for Kevitsa and Aitik HCT's*

Weekly alkalinity measurements demonstrated similar trends to that of DIC, with enhanced $CO_2$ cell sets from both operations demonstrating higher total alkalinity than control cells. This would be expected as alkalinity in most natural water systems is directly related to the availability of dissolved carbonate ($CO_3^{2-}$), bicarbonate ($HCO_3^-$), and hydroxyl ($OH^-$) anions (Stumm and Morgan 1995).

Enhanced silicate weathering, in the presence of carbonic acid, may also contribute to the weekly total alkalinity increases demonstrated within enhanced $CO_2$ cells (Sherlock et al. 1995; Stumm and Morgan 1995; Morin and Hutt 2001; Lu et al. 2022). This would also suggest a potential causation for enhanced concentrations of Mg and Ca cations within enhanced $CO_2$ cell weekly leachates, with Ca and Mg bearing silicates representing a large proportion of waste mineral abundance for both waste composites (Meysman and Montserrat 2017). Fast reacting silicate minerals (e.g. Olivine group and Anorthite minerals) are noted as secondary buffering sources within mine waste drainage systems, after primary carbonates (e.g. Calcite, Magnesite) (Nordstrom and Alpers 1999; Morin and Hutt 2001; Renforth et al. 2011). The potential for and mechanisms of potential enhanced silicate weathering are discussed in more detail later in this Chapter.

### 6.2.3 Carbon dioxide solubility controls

The rate that which gaseous phase $CO_{2\,(g)}$ dissolves in waste pore water is likely to have been a key mechanism for variations in leachate DIC concentrations between control temperature, test condition 1, and reduced temperature, test condition 3, cells. It is well understood that the solubility of $CO_2$ decreases with increased temperatures, see Figure 77, therefore it is hypothesized that the increase in DIC between reduced temperature cells and control temperature cells demonstrated within this study was influenced by temperature differentiation (25$^{O}$C and 10$^{O}$C) (Wiebe and Gaddy 1940; Carroll et al. 1991).

As the solubility of $CO_2$ would likely be higher within reduced temperature cells it can be theorized that the increased concentration of dissolved carbon species would be a likely factor in noted increases in alkalinity and subsequent reduced acidity within $CO_2$ enhanced cells. Although higher carbonic acid may be formed due to the increased

dissolution of $CO_2$, the ~neutral pH ranges of measured leachates suggest bicarbonate would be the dominant dissolved caron species within collected leachate solutions in these cells (Stumm and Morgan 1995).

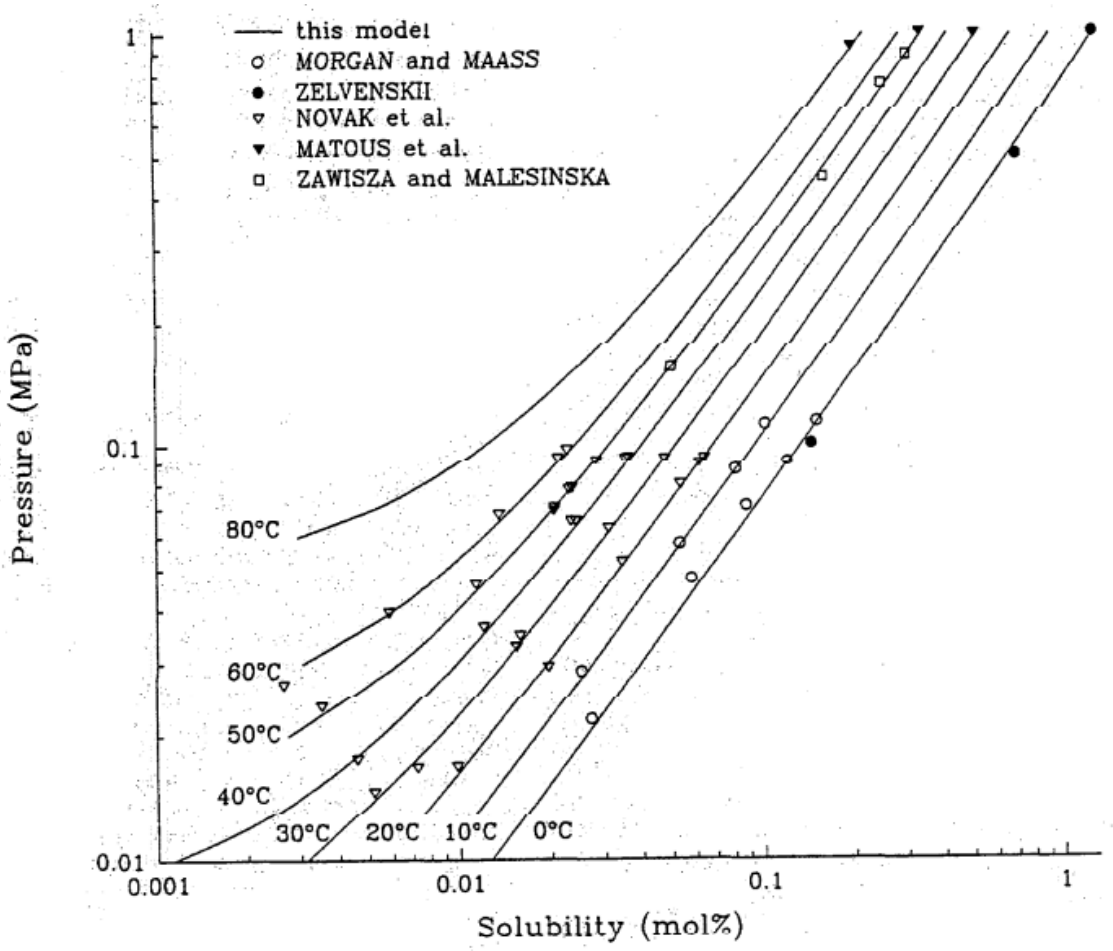


*Figure 77 – Carbon dioxide solubility in water under variable temperatures and pressures* (Carroll et al. 1991).

### 6.2.4 Potential sulfate suppression mechanisms

Sulfate release is often used as a proxy in the kinetic testing of sulfidic mine wastes to assess the oxidation of reactive sulfide minerals (Lottermoser 2010; Parbhakar-Fox and Lottermoser 2015). It is generally accepted that oxidation of sulfides, such as pyrite and pyrrhotite, in the presence of oxygen and water leads to an increased release of soluble sulfate, acidity and metal release in mine wasters (Morin and Hutt 2001).

Interestingly, it was observed that the sulfate release load was reduced within $CO_2$ enhanced cells, compared to control cell sets within both operations cell groups. Within

control temperature enhanced $CO_2$ cells, K-TC1 and A-TC1, cumulative sulfate release was suppressed by 22% and 18%, respectively, on average. This apparent suppression in sulfate suggests reduced rates of sulfide mineral oxidation. The mechanisms behind this reduction are unlikely to be due to reduced $O_2$ availability as aeration system $O_2$ contents were balanced amongst all cells to avoid preferential sulfide oxidation due to variable $O_2$ availability, see Chapter 4. Studies have demonstrated the ability of sulfate reducing bacteria (SRB) to reduce sulfate release in anaerobic conditions (Paul et al. 2017), although this was unlikely the mechanism for reduced sulfate load within this study as $O_2$ concentrations were intended to be uniform across cell sets, irrelevant of aeration system conditions. Bacterially mediated reactions were not considered as part of this study.

***Potential temperature controls on sulfate release***

Sulfate cumulative release loads within reduced temperature enhanced $CO_2$ cell sets, K-TC3 and A-TC3, were shown to be 58% and 49% lower than comparable control cell sets, K-TC2 and A-TC2, respectively. It is theorised that sulfate release suppression within reduced temperature cells is a mechanism of the reduced kinetic rate of chemical reactions under reduced temperatures. This is based on the Arrhenius equation, see Equation 34, which outlines the overall temperature dependency of general chemical reactions (Arrhenius 1889). It is theorised that sulfide mineral oxidation rates are kinetically supressed due to the temperature dependency of the reaction (Nielsen et al. 2006), leading to a reduction in sulfate release within reduced temperature HCT cell leachates.

*Equation 34 - The Arrhenius equation for temperature dependence of reaction rates*

$$k = Ae^{\frac{-E_a}{RT}}$$

Where: $k$ = Arrhenius rate constant, $A$ = pre-exponential factor, $E_a$ = Activation energy, $R$ = Universal gas constant, $T$ = Absolute Temperature

Sulfate suppression was also noted within control temperature enhanced $CO_2$ cells, when compared to control cells. The potential mechanisms behind this suppression are complex to interpret, as both cell conditions were balanced with the same concentration of $O_2$ to avoid differential oxidation due to $O_2$ availability (Sherlock et al.

1995; Birkham et al. 2003; Vriens et al. 2018). Under the assumption that $O_2$ availability was the same between cells in testing conditions 1 and 2, the differentiating parameter between these cell sets is the enhanced presence of $CO_2$ within the aeration system. Various potential geochemical mechanisms that may have caused these variations in sulfate release have been considered and evaluated within this section.

***Potential pH controls on sulfate release***

Variations in leachate pH were considered as a potential mechanism for variations in sulfate release between test condition 1 and test condition 2 cell sets. pH measurement within reduced temperature enhanced $CO_2$ cells were higher than control temperature enhanced $CO_2$ cells throughout the leaching period. The mean leachate pH measurements for cell sets K-TC1, K-TC2, A-TC1 and A-TC2 over the leaching period were pH 7.45, pH 7.08, pH, 7.10 and pH 6.70, respectively. A study carried out by Nielsen, Vollertsen and Hvitved-Jacobsen (2006) assessed the kinetic implications of changes in pH and temperature on sulfide oxidation rates in wastewater. The study demonstrated that increases in pH led to increases in sulfide oxidation rates around neutral pH (Nielsen et al. 2006), conversely to this study which suggested an opposing trend between pH and $SO_4$.

As the pH ranges between cell leachates within this study was not as wide as other studies that have investigated pH dependence on sulfide oxidation and sulfur speciation, more research would be needed to quantify this as a potential mechanism for the results presented in this research. It can be seen in Figure 78 that within Kevitsa cell sets distinct clustering of weekly sulfate release loads was noted in relation to corresponding leachate pH measurement. No statistically notable correlations were observed between pH and sulfate release, although clear clustering of testing conditions groups was demonstrated within both operations data sets. Similar clustering patterns were also observed within the corresponding Aitik cell results, see Appendix 18.

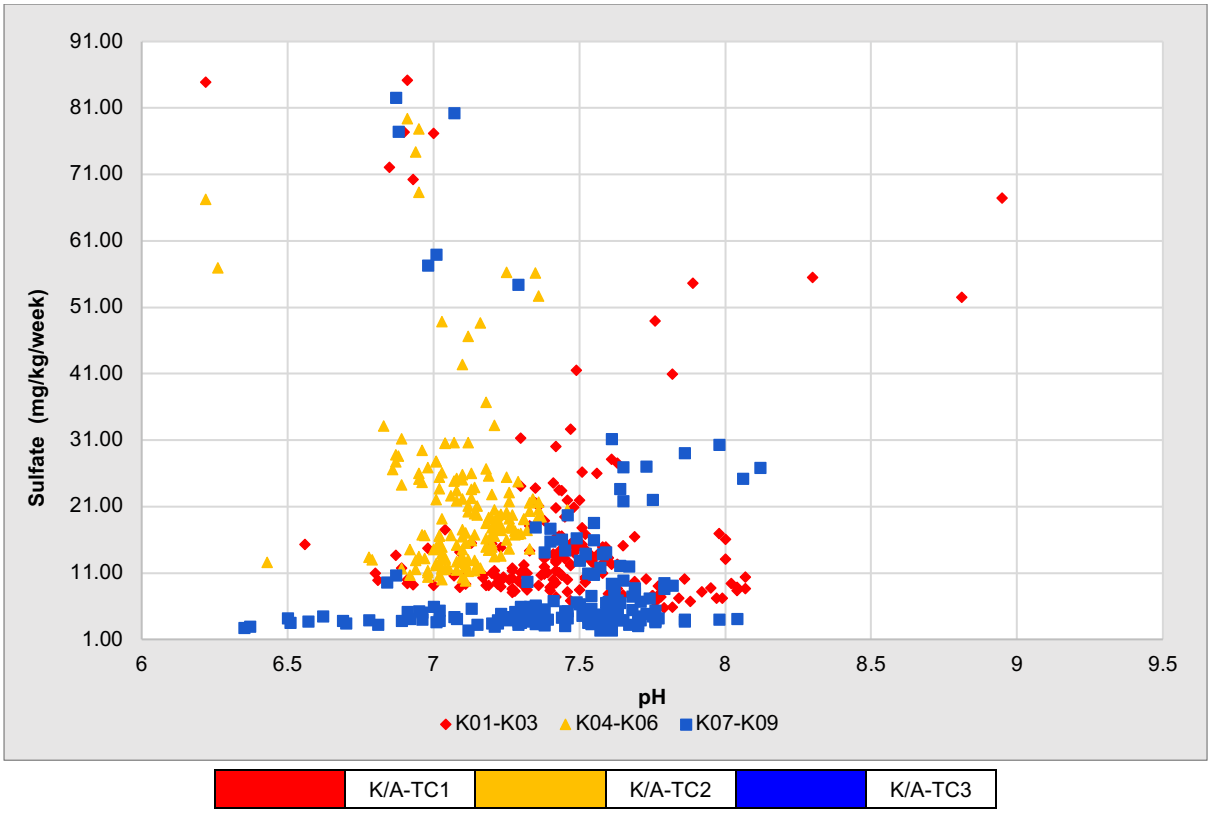


*Figure 78 - Kevitsa HCT leachate sulfate ($SO_4$) release rates plotted against corresponding leachate pH measurements.*

***Potential surface passivation controls on sulfate release***

As outlined within the previous sections of this Chapter weekly DIC release measurements were distinctly variable between experimental condition sets. DIC is therefore considered a potential mechanism for differences in sulfate release between enhanced $CO_2$ and control cell sets held at standard temperature conditions. At present there is a lack of research on the influence of $CO_2$ concentration on the rate of sulfide oxidation, with limited studies aimed at the assessment of coal wastes in which carbonate phases are abundant (Cempa-Balewicz 2015).

It was shown in Figure 74 (a) and 74 (b) that DIC was released at higher rates and cumulative loads within enhanced $CO_2$ cells. At the measured leachate pH ranges within enhanced $CO_2$ cells the dominant dissolved carbon species would be bicarbonate followed by carbonate (Stumm and Morgan 1995; Hanrahan 2012).

Multiple studies that have researched the potential for CDR using sulfidic silicate rich mine wastes have noted stable carbonate precipitation within mining waste rock and

tailings facilities (Wilson et al. 2014b; Harrison et al. 2015; McQueen et al. 2020; Power et al. 2020). The mechanisms behind enhanced silicate weathering due to carbonic acid formation and subsequent increases in metal cation release are covered in more detail later in this Chapter. Within this section the potential influence of surface passivation on sulfide oxidation and subsequent sulfate release is considered.

Studies carried out at the Mount Keith Ni mine, Australia, and Diavik diamond mine, Canada, have outlined the potential for stable carbonate precipitation as a result of enhanced weathering (EW) of reactive silicate minerals within tailings (Langman et al. 2014; Wilson et al. 2014). Similarly, studies such as Harrison et al., (2015) have demonstrated that the precipitation of secondary carbonate minerals can lead to the passivation of reactive mineral surfaces. It can therefore be theorised that potential stable secondary carbonate precipitation within enhanced $CO_2$ cell pore spaces could have caused partial surface passivation on reactive sulfide minerals. These precipitation products could have potentially inhibited the rate of sulfide oxidation. Further mineralogical analysis of post HCT residues via SEM-EDS analysis is suggested for future testing, as this mineralogical assessment method has successfully demonstrated secondary precipitation products on mineral surface at higher resolutions that other techniques, such as SEM-EDX.

The premise of this theory lies within several factors related to results and observations gathered during and after kinetic testing, static testing, and mineralogical analysis. These factors can be outlined as follows:

- Enhanced $CO_2$ HCT DIC leachate measurements suggest enhanced levels of bicarbonate and carbonate ions in solution at the pH ranges recorded.
- Multiple studies have demonstrated the presence of precipitated secondary carbonate phases on mineral surface both in-situ and within carbonation experiments carried out under enhanced $CO_2$ conditions (Wilson et al. 2014a; Kandji et al. 2017c; Hamilton et al. 2018b; McCutcheon et al. 2019).
- Post decommissioning materials within enhanced $CO_2$ cells were observed to have ‘cemented’ and clear agglomeration of particles had occurred.
- Post decommissioning static testing demonstrated that enhanced $CO_2$ Kevitsa cell materials had maintained a larger proportion of total S% than control cells.

- A distinct lack of sulfide mineral weathering was observed in post testing mineralogical analysis via petrographic thin sections.

It is noted that the very nature of the ASTM HCT protocol restricts the presence of secondary mineral products, with the test primarily focused on assessing the weathering of primary minerals (Price 2009). Therefore, it is likely that soluble precipitated secondary carbonate phases, such as magnesite or hydromagnesite, are unlikely to have remained in large abundance within cells post leach phases. This would add a precedent to both the increased DIC measurements in enhanced $CO_2$ cell leachates and provide a potential reasoning as to why no stable secondary carbonate minerals were identified within post testing mineralogical analysis. The influence of liquid to solid ratio (L:S) and flushing frequencies in kinetic testing methods is discussed in more detail later in this Chapter.

The apparent cementing of waste materials observed post testing may suggest the precipitation of secondary phases, although mineralogical characterisation displayed minimal alteration post testing. There is the potential that this secondary product could be gypsum, although more testing is required to assesses this. Post testing images for selective cells are shown in Appendix 22.

It is hypothesised that although the long-term accumulation of secondary stable carbonate phases within enhanced $CO_2$ cell materials is unlikely, such phases could have formed between leaching events. Multiple studies have demonstrated the rapid dissolution/weathering of reactive silicates, such as olivine, brucite, serpentine group and kimberlites, under both ambient and above ambient $CO_2$ concentrations (Harrison et al. 2013; Tominaga et al. 2017; Mervine et al. 2018; Wang et al. 2018). Within such studies stable carbonate has been noted through SEM-EDS analysis following exposure to $CO_2$ at varied concentrations.

The abundance of leached Mg and Ca cations within leachates of enhanced $CO_2$ cells, combined with the availability of soluble carbon species suggests that precipitation of Mg/Ca secondary carbonates may have occurred within these tests. More experimental work is required to quantify this hypothesis, with a revaluation of dominant carbon species, pore water pH conditions and the leaching frequency of

kinetic test methods. Such an assessment would allow the quantification of the potential impacts of carbonate mediated sulfide mineral surface passivation. Potential speciation and saturation indices could be modelled in programs such as PHREEQC (Appelo and Postma 2004).

***The potential influence of enhanced $CO_2$ concentration on microbially mediated sulfide oxidation reactions***

There is a distinct lack of direct research that has assessed the influence of variable $CO_2$ concentrations on microbially mediated sulfide oxidation in mining wastes. A study by Bryan et al. (2012) assessed the effects of $CO_2$ availability on Leptospirillum ferriphilum and Acidithiobacillus ferrooxidans. While not directly related to mine wastes, this study found that $CO_2$ availability did have an impact on bacterial growth patterns, with bacteria species demonstrating greater growth under below atmospheric $CO_2$ conditions (Bryan et al. 2012). This may be a potential mechanism behind the enhanced sulfate release noted within control cells within this study. Control cell set aeration systems were balanced with $N_2$ proportionally with $CO_2$ enhanced cells to avoid differentiations in $O_2$ availability. This would have led to a slight reduction in $CO_2$ availability, compared to atmospheric levels. Based on the results of Bryan et al. (2012) it could be theorised that the slight reduction in aeration system $CO_2$ within control cells, coupled with the increase in $CO_2$ within altered cells, could have been a mechanism behind apparent sulfate suppression.

It is unlikely that sulfate reducing bacteria (SRB) may have led to a reduction in sulfate release rates in enhanced $CO_2$ HCT cells, as the aeration system was still aerobic. The implications of SRB species on carbonate mineral precipitation in the presence of enhanced $CO_2$ conditions has been assessed in previous studies (Paul et al. 2017). The presence of SRB's is an unlikely influential mechanism within this study as the lack of organic matter means there is not an electron donor. It is noted that bacterially mediated sulfide oxidation was not a research consideration in this study. More research is required to fully assess the influence of varied aeration protocols within kinetic testing on sulfide mineral oxidation rates.

### 6.2.5 The impact of liquid to solid ratios and leaching frequency within HCT protocols

The high L:S of HCT leaches and the high frequency of leaching events restricts the accumulation and precipitation of stable carbonate phases in a solid form. This is a consequence of the very purpose of a HCT, which is to assess the reaction rates of primary minerals and subsequent analyte leaching rates (Price 2009; Sapsford et al. 2009b; ASTM 2018). This ultimately means that the contact time between interstitial pore water and reactive surfaces is shorter than in field conditions, where the pore water L:S ratio and water rock contact time would be governed by temperature, evaporation, precipitation and storage method (Dold 2017; Maest and Nordstrom 2017).

It has been demonstrated within several studies that variable test conditions, notably, temperature, PSD, aeration regime, liquid to solid ratio (L:S) and cell design play a large role in chemical characteristics of eluents produced in kinetic leach tests (Morin and Hutt 2000a; Sapsford et al. 2009b; Maest and Nordstrom 2017). The dilution effect caused by a high L:S and flushing frequency is likely to have diluted some soluble analytes below detection limits within this study, compared to potential in-situ drainage measurements at either operations waste storage facilities (Dent et al., 2022).

It is noted that the lack of stable secondary carbonate precipitation noted through mineralogical analysis post testing is potentially a consequence of the high flushing rates of HCT procedures as part of the ASTM standard. Studies carried out to assess the potential of silicate rich mining wastes to sequester atmospheric $CO_2$ have noted distinct stable carbonate precipitation under ambient conditions, as previously mentioned (Wilson et al. 2014b). The potential that secondary carbonate phases may have reached saturation and precipitated within enhanced $CO_2$ cells between leaching would require geochemical modelling. As previously discussed, the relative pH ranges of collected leachate and DIC concentration suggest dissolved carbon species would have been dominated by bicarbonate and carbonate ions (Stumm and Morgan 1995; Hanrahan 2012) .

Further studies would require measurement of pore water pH throughout a HCT protocol to understand the change in speciation of carbon in dissolved form. It is likely

that the flushing of cells and the relatively high L:S led to the degassing of dissolved $CO_{2\,(aq)}$ within pore water spaces, causing an increase in collected leachate pH as the solution reached equilibrium with atmospheric $CO_2$ levels between aeration cycles (Stumm and Morgan, 1999).

Interestingly reduced temperature cells consistently demonstrated lower water retention rates and higher leaching volumes than control temperature cells across the 60-week period, see Figures 42 and 43. These cells sets were observed to form condensation within the cell between leaching periods. The potential implications of reduced water retention on the concentration of analytes requires further investigation.

### 6.2.6 Potential mechanisms behind the enhanced leaching of major and minor cations and trace elements

As previously discussed, the concentration of DIC species was higher within enhanced $CO_2$ cell sets from both operations, when compared to control cells. The relative higher concentrations of DIC within reduced temperature cells is potentially related to the temperature dependent solubility controls of $CO_2$, as discussed within the previous sections (Wiebe and Gaddy 1940; Carroll et al. 1991; Lucile et al. 2012).

Although it is assumed that bicarbonate and carbonate ions would present the dominant carbon species in solution, the initial dissolution of $CO_{2(g)}$ into waste pore water would have led to the formation of carbonic acid (Stumm and Morgan 1995; Hanrahan 2012b; Meysman and Montserrat 2017; Montserrat et al. 2017; Hartmann et al. 2023). The presence of carbonic acid is likely to have weathered reactive silicate minerals within the waste materials. Acidification of pore water due to $CO_2$ ingress has been shown to be a driving mechanism behind cation concentrations in mine waste tailings utilised in carbon sequestration (Khalidy and Santos 2021).

#### *Enhanced silicate weathering mechanisms*

Silicate weathering in the presence of carbonic acid ($H_2CO_3$) and the acidity ($H^+$) produced during the dissociation of $H_2CO_3$ to $HCO_3^-$ and $H^+$, see Equation 35, is likely to have released soluble metal cations into solution. In the presence of acidity (H+),

Mg and Ca silicates react to form free cations, silicon dioxide and water, the simplified equation for Mg silicate weathering is shown in Equation 35 (Rackley 2017b).

*Equation 35 - Mg silicate weathering in the presence of acidity*

$$Mg_2SiO_4 + 4H^+ \Longrightarrow 2Mg^{2+} + SiO_2 + 2H_2O$$

Where: $Mg_2SiO_4$ = Mg Silicate, $H^+$ = Hydronium ions (Acidity), $Mg^{2+}$ = Mg Cations, $SiO_2$ = Silicon Dioxide, $2H_2O$ = Water

The free cations released within such a reaction are a function of the deportment of elements within the reactive silicate minerals. This process is a likely mechanism for the enhanced leaching of Mg and Ca cations within the leachates of enhanced $CO_2$ cells from both operations. Mineralogical analysis of composite materials used within both operations HCT sets demonstrated the abundance of Mg and Ca silicate phases in Kevitsa and Aitik waste rocks. Studies such as Cempa-Balewicz (2015) have demonstrated elevated concentrations of Mg, Ca and K within waters saturated with $CO_2$ in contact with silicate rich mining wastes. Such observations were also accompanied by reduced levels of $SO_4$, when compared to water not saturated with $CO_2$ (Cempa-Balewicz 2015). These findings align well with the results observed within this research study.

As previously discussed, bicarbonate ($HCO_3^-$) was likely the dominant carbon species within enhanced $CO_2$ HCT leachates. Under this assumption it can be theorised that the free Mg and Ca cations, measured in weekly leachates, may have combined with bicarbonate ions to form Mg/Ca carbonate species, see Equation 36 (Rackley 2017b).

*Equation 36 - Mg carbonate formation*

$$Mg^{2+} + HCO_3^- \Longrightarrow MgCO_3 + H^+$$

Where: $Mg^{2+}$ = Mg Cations, $HCO_3^-$ = Bicarbonate, $MgCO_3$ = Mg Carbonate, $H^+$ = Hydronium ion

### *Elemental mineral deportment*

Of the major, minor and trace elements analysed within weekly leachates of Kevitsa cells Ni was shown to demonstrate large variations in weekly concentrations between

cell sets and testing conditions. Over the 60-week testing period K-TC1, K-TC2 and K-TC3 cells were shown to cumulatively release Ni loads of 4.12mg, 1.01mg and 10.51mg, respectively. In order to understand the potential mechanisms behind these variations between cell sets the mineral deportment of Ni within these waste materials should be considered. Deportment analysis was not directly carried out within this study, but data previously collected by MEM Ltd, on behalf of Boliden Mines, may give an indication of the potential mineralogical sources of Ni within the waste rocks. Figure 79 shows the results of Ni deportment analysis carried out in 2018 on various waste rocks collected from the same rock facilities as the materials utilised within this study.


*Figure 79 - Mineralogical Ni deportment (% normalised) analysis for waste rock materials from the Kevitsa operation* (MEM Ltd 2018).

It can be seen in Figure 79 that within assessed waste rock samples Ni was mainly deported within pentlandite, olivine group, clinopyroxenes and serpentine group minerals (MEM Ltd 2018). It is acknowledged that due to the heterogeneous nature of waste facilities that these deportment results are not representative of wastes utilised within this study (Morin and Hutt 2001; Lottermoser 2010), but they provide a potential indication of likely sources of enhanced Ni leaching.

As it has been demonstrated that sulfide oxidation was likely supressed within $CO_2$ enhanced cell sets. Therefore, it is likely that enhanced levels of Ni leaching within

altered cell sets was unlikely to be a result of the weathering of Ni bearing sulfide minerals, such as Pentlandite. It is theorised that the enhanced Ni leaching within enhanced $CO_2$ Kevitsa cells may be the result of preferential weathering of Ni bearing silicates, this is based on the deportment analysis carried out by MEM Ltd in 2018 (MEM Ltd 2018). This hypothesis is supported by the Ni and Si weekly leaching results demonstrated in Figure 80. It can be seen in this figure that enhanced $CO_2$ cell groups demonstrated increased Ni leaching, in line with increased Si leaching.

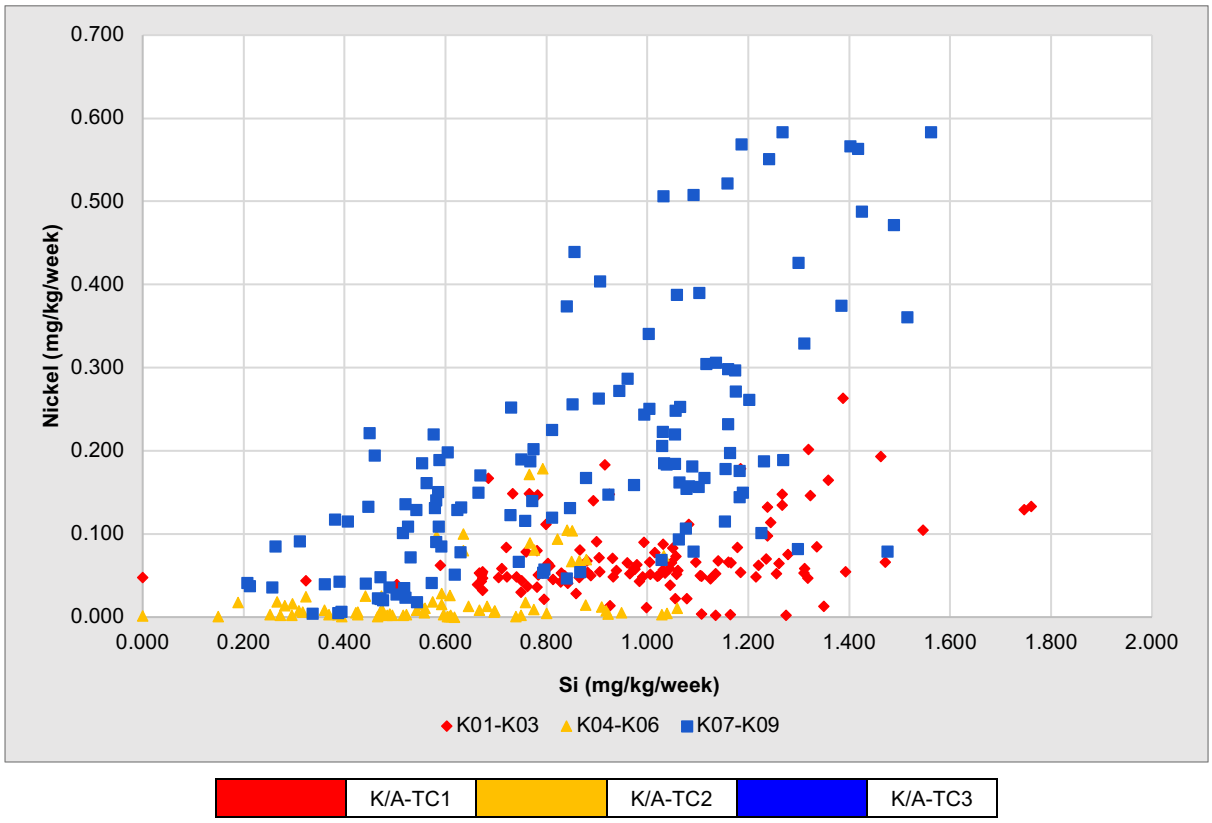


*Figure 80 – Nickel (Ni) release plotted against silica (Si) concentrations for Kevitsa HCT leachates in corresponding collection weeks.*

The theory that the presence of enhanced $CO_2$ within these kinetic tests may have led to preferential weathering of reactive silicates can be further supported by plotting Ni release against Mg release over the leaching period, see Figure 81. It was demonstrated that Ni release rates were associated with increased Mg release within enhanced $CO_2$ cell sets. Mg silicates mineral groups, including amphibole group, clinopyroxene group, olivine group and tremolite, represent over 75% of the mineral abundance of Kevitsa composite samples. It can therefore be theorised that the potential preferential weathering of these minerals may have led to increased mobility

of associated trace metals and cations (Cempa-Balewicz 2015; Hamilton et al. 2018b). Further investigations and expansions of experimental work are required to validate this theory. It is suggested that SEM-EDS analysis is carried out to assess micro-scale alterations to mineral surfaces as a result of enhanced mineral weathering.

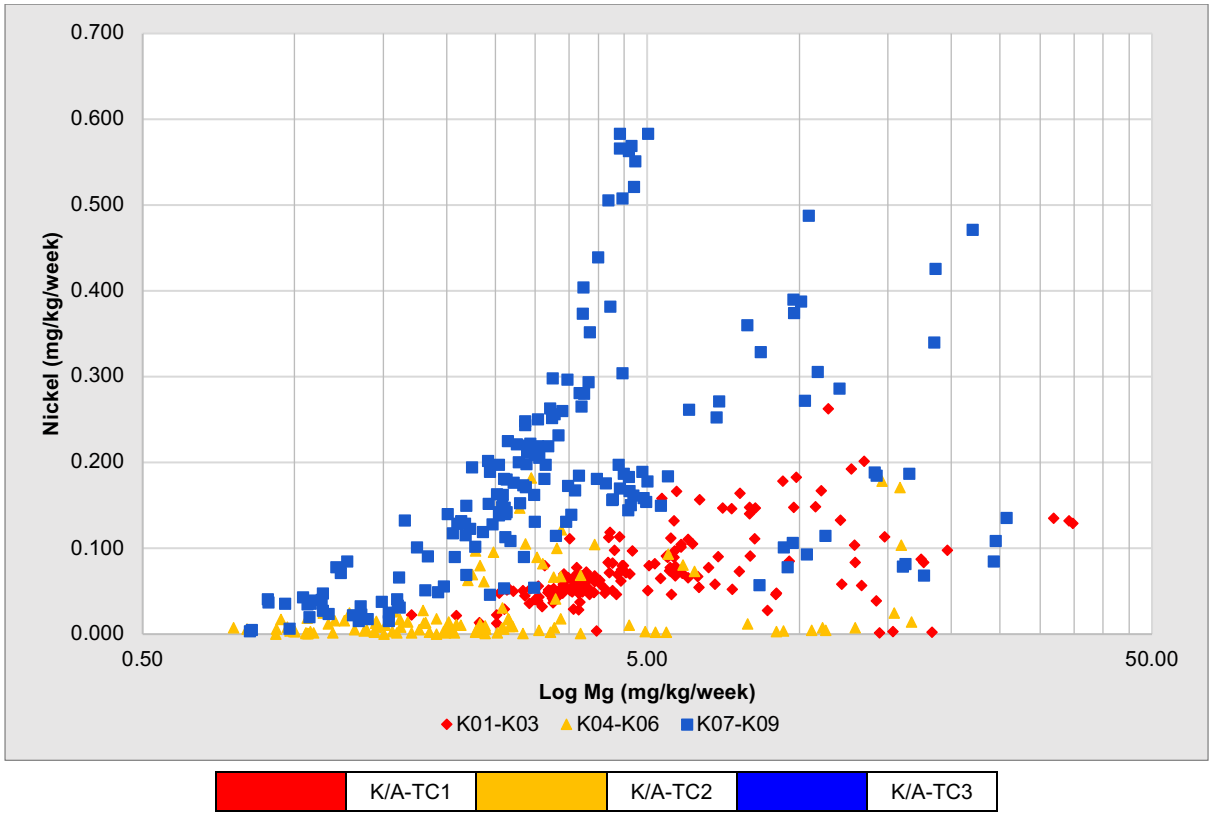


*Figure 81 – Log Magnesium (Mg) release plotted against Nickel (Ni) concentrations for Kevitsa HCT leachates in corresponding collection weeks.*

The preferential weathering of fast reacting silicates, such as olivine and anorthite, could also have been a mechanism that influenced the increased weekly alkalinity measurements noted within enhanced $CO_2$ cells within both operational sets. It is well understood that silicates provide a secondary neutralising capacity within mining wastes, after carbonate mineral (Morin and Hutt 2001). Weathering of silicates is associated with subsequent releases of deported cations, an increase in alkalinity and a potential rise in solution pH due to increased acid buffering capacity (Meysman and Montserrat 2017). All of these factors were noted within enhanced $CO_2$ cells weekly leachate analytes within this study.

### 6.2.7 The potential implications on ARD classification

The physical and geochemical properties of post HCT residues demonstrated minimal alterations in mineralogy or apparent ARD risk, classified through ABA analysis. These findings are complex to interpret as singular metrics, but in combination with kinetic testing outputs allow a better quantification of overall ARD and metalliferous drainage risk. It is widely acknowledged that static testing, kinetic testing and mineralogy is often required in tandem to assess ARD onset risk adequately (Morin and Hutt 1998; Nordstrom and Alpers 1999; Morin and Hutt 2000b; Morin and Hutt 2001; Lottermoser 2010; Parbhakar-Fox and Lottermoser 2015). Mineralogical, static and kinetic testing data/findings have therefore been considered holistically within this section.

Mineralogical abundance analysis carried out on HCT residues demonstrated minimal alteration to bulk mineral phases, while petrographic thin sections displayed similarly minor changes in mineral properties. As previously mentioned, the high L:S ratio and flushing frequency of ASTM HCT procedures likely inhibited the precipitation of secondary phases (ASTM 2018b; Dent et al. 2022)

Analysis of key ABA and NAG parameters in line with recommendations outlined in the GARD guide demonstrated little change in overall ARD classification post HCT testing, based purely on static testing results (GARD 2014). NAG pH and NPR values measured on post HCT residues demonstrated little change in ARD classification based on the guidelines of the MEND and GARD manual, see Figure 82 (Price 2009; GARD 2014). It was noted that although Aitik materials have been classed as PAF, based on ABA and other static testing, an onset of acidity conditions was not observed over the 60-week period. It is likely that longer kinetic testing procedures would be needed to fully assess the ARD risks of this waste material (Morin and Hutt 2000a; Morin and Hutt 2001; Sapsford et al. 2009b; Maest and Nordstrom 2017).

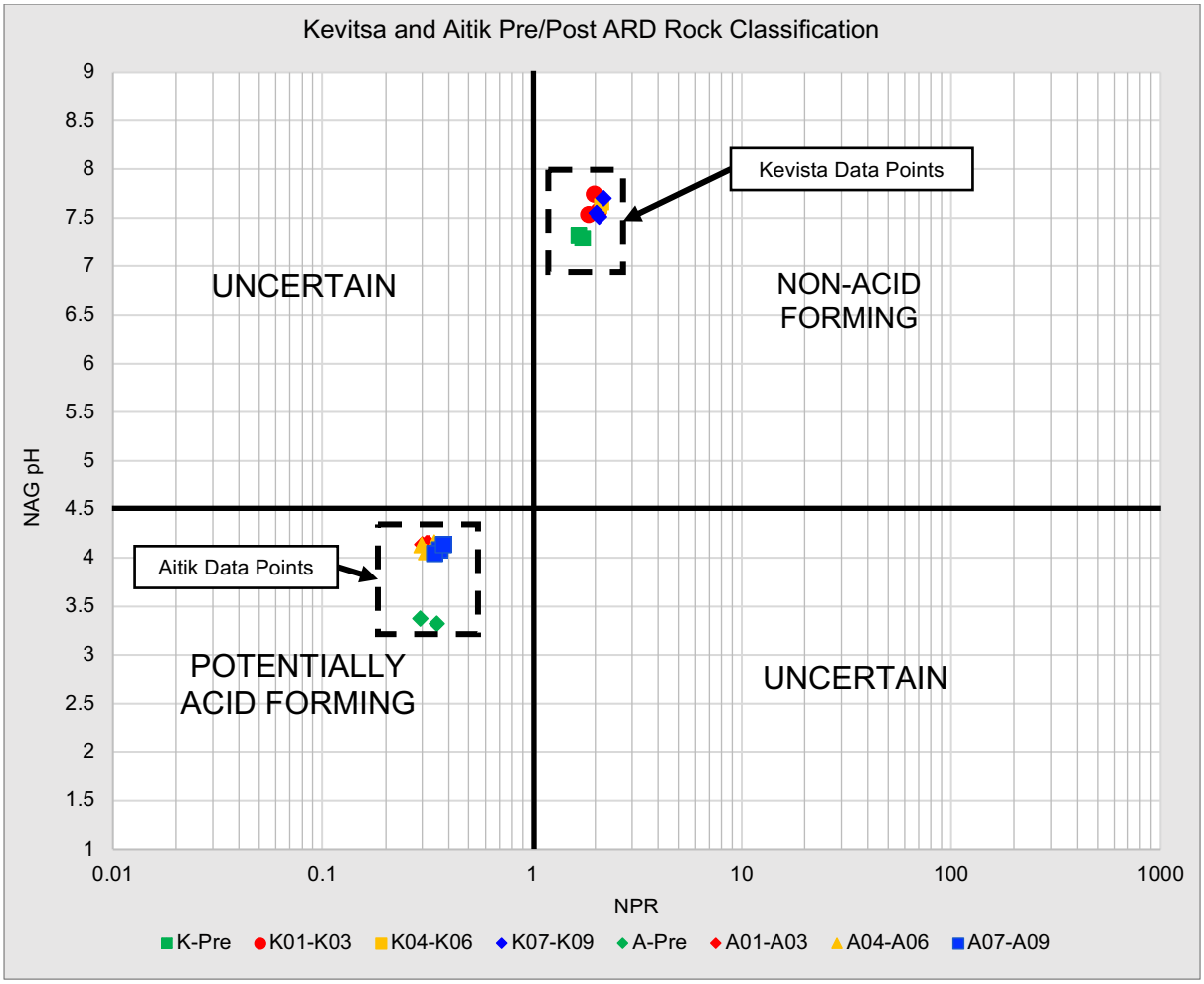


*Figure 82 – Kevitsa and Aitik Pre/Post ARD rock classifications.*

Static testing undertaken on post HCT residues displayed minimal alterations to geochemical properties of waste composites in response to varied kinetic testing conditions. As previously mentioned, the high L:S / flushing frequency of such kinetic tests restrict the precipitation and accumulation of secondary mineral phases (Dent et al. 2022). It can be theorised that the lack of distinct change in material characteristics between HCT triplicates set residues post testing is a consequence of this.

Previous studies undertaken on comparable waste rock materials from the Kevitsa mine demonstrated clear alterations in waste ABA characteristics post expose to enhanced $CO_2$ conditions over comparable time scales (Savage et al. 2019; Savage et al. 2021). These tests were carried out in the form of a carbonation reactor column experiments, refer to Chapter 2, and were not exposed to any leaching events over a comparable time scale. Post decommissioning treated materials demonstrated clear increases in NP total C% and NAG pH, with clear cementing and agglomeration of

particles. It can be theorised that the alterations observed within these previous studies were likely the result of Mg/Ca carbonate reaching saturation and subsequently precipitating within material pore spaces (Wilson et al. 2014a). The differentiations observed between characterisation results of previous studies and the results generated within this study add further premise to the proposed need for more site-specific ARD assessment methods.

Empirical open system NP consumption, in line with table 18.1 of the MEND 1.20.1 manual, was calculated using alkalinity, acidity and sulfate measurements collected over the first 45 weeks of testing (Price 2009). As it has previously been discussed, enhanced $CO_2$ aeration cells measured higher concentrations of DIC and alkalinity, which may be expected as carbonate and bicarbonate should represent the majority of carbon species at the measured pH ranges (Stumm and Morgan 1995; Kirby and Cravotta 2005; Hanrahan 2012b; Meysman and Montserrat 2017). In line with these measurements, it was shown that enhanced $CO_2$ cells displayed apparent suppression of sulfate, under both control and reduced temperature conditions, suggesting a reduced rate of sulfide mineral oxidation.

Considering the findings outlined above it can be theorised that the overall consumption of NP sources should be reduced within enhanced $CO_2$ cells, as less acidity is readily produced to be consumed. The results generated through the calculation of the empirical open-source NP consumption contradict this theory with enhanced $CO_2$ cell sets displaying calculated NP consumption rates higher than control cells within both operational sets. It is acknowledged that a portion of NP would be readily consumed due to the production and dissociation of carbonic acid during the dissolution of $CO_2$ (Stumm and Morgan 1995; Rackley 2017b), although this was not directly measurable within this system. The apparent mismatch in calculated open system NP consumption rates and increased alkalinity/reduced acidity within enhanced $CO_2$ cells requires an examination of the equation that is used to estimation NP consumption. The equation, recommended in the interpretation of HCT data sets, is displayed in Equation 37 (Price 2009).

*Equation 37 - Empirical Open System NP consumption around Neutral pH*

$$Empirical\ Open\ system\ NP\ Consumption\ around\ Neutral\ pH\ (mg\ CaCO_3/kg/week) = Theoretical\ NP\ Consumption\ (mg/kg/week) + Alkalinity\ Production\ Rate\ (mg/kg/week) - Acidity\ Production\ Rate\ (mg/kg/week)$$

Based on (1) and (2):

(1) $2H^+SO_4^{2-} + CaCO_{3(s)} \Leftrightarrow Ca^{2+} + SO_4^{2-} + H_2CO_3^0$

(2) $H_2CO_3^0 + CaCO_{3(s)} \Leftrightarrow Ca^{2+} + 2HCO_3^-$

As the theoretical NP consumption calculation outlined in Price (2009) is based on sulphate generation it is independent of any external impacts and therefore purely estimates the generation, and subsequent neutralising, of acidity generated through sulphide oxidation. The empirical open system NP consumption calculation, shown in Equation 37, considers alkalinity as well as acidity (Price 2009). This calculation is designed with the assumption that the only alkalinity source within a system comes from preexisting NP sources within a tested waste material. Within this study the addition of enhanced $CO_2$ within a kinetic test method led to an increased concentration of bicarbonate ions in cell leachates, evidenced by the increase in DIC release rates at the measured pH ranges. It is theorised that this increase in DIC was a mechanism for the distinct increased in measured total alkalinity, see Equation 38, compared to control cells.

*Equation 38 - The components of alkalinity in natural waters*

$$Alkalinity = [HCO_3^-] + 2[CO_3^{2-}] + [OH^-] - [H^+]$$

Where: $HCO_3^-$ = Bicarbonate, $CO_3^{2-}$ = Carbonate, $OH^-$ = Hydroxide, $H^+$ = Hydronium ions

The noted increases in DIC, and by default bicarbonate ions in solution, leads to an artificially high leachate total alkalinity. As the open system calculations outlined in the MEND guide are designed so that alkalinity measurements are added to the theoretical NP, the increased alkalinity within enhanced $CO_2$ cells gives an artificially high NP consumption value, even though most of the measured bicarbonate is not actually contributing to the actual NP. It can therefore be theorised that the open

system empirical NP consumption calculations outlined in current standards are not suitable for estimating NP consumption within such a system, as the impact of the bicarbonate ions cannot be assessed. The utilisation of these calculations for a system that contains elevated levels of $CO_2$, such as was demonstrated in Vriens et al., (2019), may lead to an over estimation of NP consumption and inaccurate prediction of ARD onset. It is recommended that an empirical assessment of the current NP consumption calculations should be reviewed for applicability to varied drainage and waste storage conditions.

### 6.2.8 Repeatability and QA/QC of the testing method

Although the results and interpretations presented within previous sections of this Chapter outline distinct changes in the leaching quality of altered HCT sets, when compared to control sets, the reliability and repeatability of generated results must be considered. As outlined in Chapter 4 of this thesis the repeatability of testing methods implemented were assessed through relative percentage difference (RPD) analysis (EPA 2011), and correlation co-efficient calculations between triplicate cells. RPD analysis was carried out on the cumulative release loads of key leached analytes, while correlation analysis was undertaken between individual cell leaching results. As previously noted, correlation does not demonstrate causation or statistical significance, it is rather a demonstration of correlation strength (McCarroll 2016). RPD analysis provides a baseline for assessing the representativeness of duplicate values, with a lower RPD % suggesting a greater level of repeatability (BCFSM 2013).

#### *Analysis of RPD results*

The cumulative release loads of key leached analytes, including DIC, sulfate, Ni, Mg and Ca, were used to provide baseline RPD values between cell triplicates. Using a baseline of ‘acceptable’ RPD % of 20% and an ‘unacceptable’ RPD % of 50% the relative repeatability of cells was assessed. Within both Kevitsa and Aitik enhanced $CO_2$ HCT triplicate sets, irrelevant of temperature condition, sulfate, Mg, Ca, Na and Ni/Mn al displayed averaged RPD values of <20%, with most parameters displaying RPD values <5% between cells within triplicate cells. This was the case for DIC cumulative load releases within all enhanced $CO_2$ triplicate sets, other than A-TC3. Within set A-TC3 the erroneously high DIC release rates demonstrated within cell A08

led to RPD values of 42% and 30% when compared to cells A07 and A09. Cells A07 and A09 did hold an acceptable RPD value of 12%.

Control cell sets, K-TC2 and A-TC2, displayed generally acceptable RPD values between release load values for most measured analytes. Control cells within operations cell groups displayed larger RPD % values for select analytes including DIC and trace elements Ni (Kevitsa) and Mn (Aitik). Kevitsa control cells displayed a mean Ni release load RPD % of 67.5% between triplicate cells. This was caused by the erroneous release load of Ni within cell K05 which was over 80% lower than comparable cells. Although some of the RPD % values within control cells are considered 'unacceptable' based on the testing criteria, it must be noted that release rates within control cells was often near or below the analytical detection limit (ADL). It has been noted that RPD acceptance is less reliable as a metric when values are near ADL and acceptable ranges should be expanded to account for potential analytical variation around ADL values (EPA 2011; BCFSM 2013).

The overall RPD analysis results demonstrated a clear level of repeatability between triplicate cells within this study, with key analytes well within the acceptable baseline. The low RPD % values within both operations cell triplicate groups align well with most values holding a calculated RPD of <2-5%. These results give merit to the repeatability of the designed methods. Further testing with varying materials would be required to fully assess the reproducibility of trends presented within this study. It is suggested that studies are carried within multiple laboratories and results generated compared, as is common practise in the development of new or amended standard methods (Sobek et al. 1978; Morin and Hutt 2001; BSI 2002a; Price 2009).

***Analysis of correlation co-efficient results***

Correlation analysis was carried out to assess potential relationships between measured parameters and provide an indication of potential mechanisms for variations in leachate quality. Pearsons r value was calculated between parameters as well as between triplicate groups to assess the reproducibility of results between comparable cells sets. Correlation co-efficient matrixes were created to compare multiple cells results from each location HCT set, these can be found in Appendix 17.

Figure 83 shows duplicate correlations between cells within multiple triplicate sets for pH, DIC and sulfate release rates. It can be seen in this figure that cells A02 and A01 displayed a strong correlation in pH with a correlation coefficient of r = 0.897 and an $R^2$ value of 0.806. Similar trends in strong correlations were observed between comparable cells within the same test condition and triplicate groups. As it can be seen in Table 17, correlation coefficients calculated between trends in leachate pH demonstrated strong relationships between triplicate cells, with weaker correlations demonstrated between different test conditions.

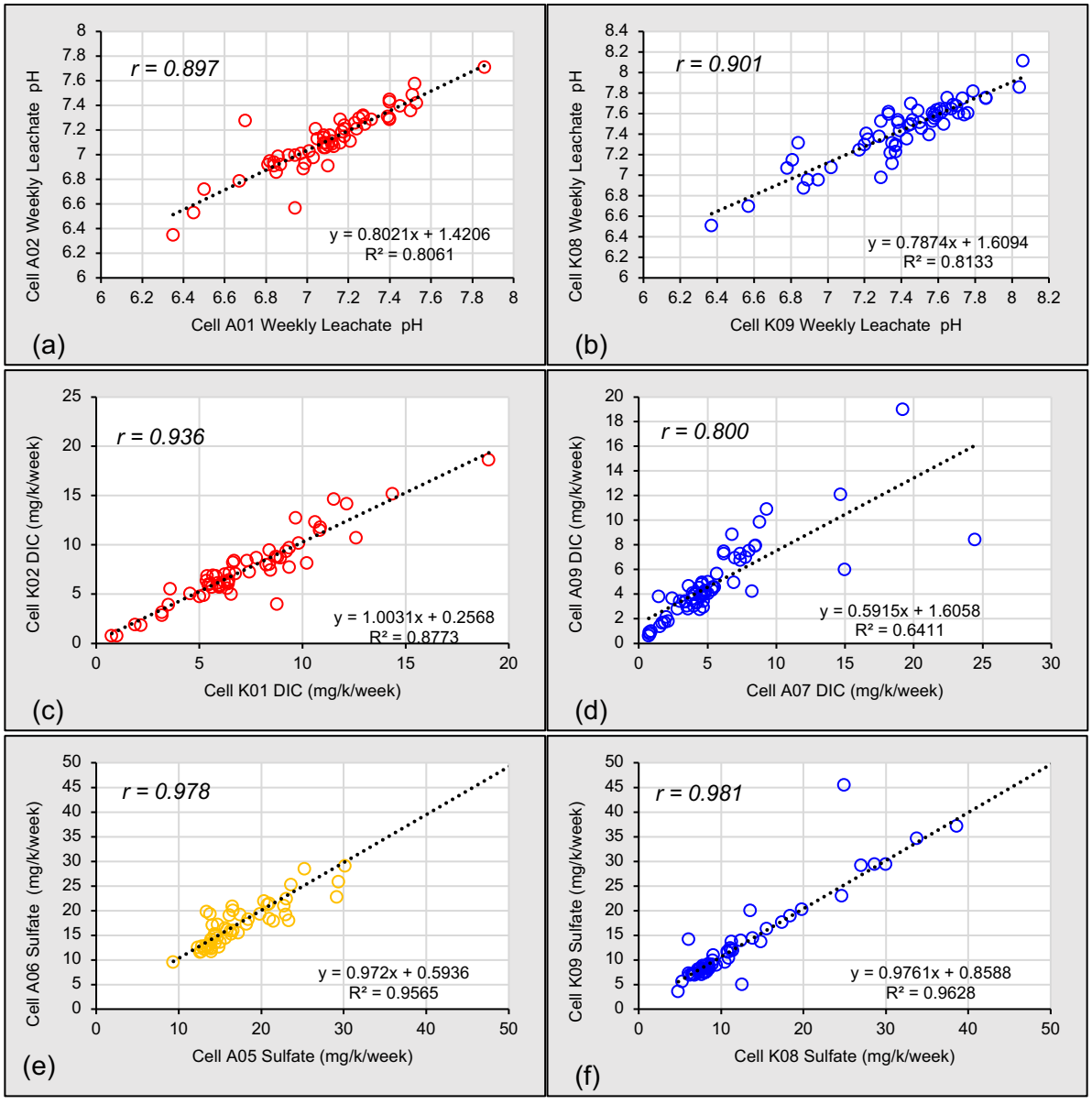


*Figure 83 - Analyte correlation plots for (a) cells A02 and A03 pH, (b) cells K08 and K09 pH, (c) cells K01 and K02 DIC, (d) cells A07 and A09 DIC, (e) cells A05 and A06 $SO_4$ and (f) cells K08 and K08 $SO_4$.*

*Table 17 - Kevitsa cell leachate pH measurement correlation coefficients (r)*

| | *K01* | *K02* | *K03* | *K04* | *K05* | *K06* | *K07* | *K08* | *K09* |
|---|---|---|---|---|---|---|---|---|---|
| *K01* | 1 | | | | | | | | |
| *K02* | 0.863 | 1 | | | | | | | |
| *K03* | 0.877 | 0.846 | 1 | | | | | | |
| *K04* | 0.215 | 0.107 | 0.138 | 1 | | | | | |
| *K05* | 0.346 | 0.175 | 0.399 | 0.712 | 1 | | | | |
| *K06* | 0.292 | 0.122 | 0.367 | 0.687 | 0.937 | 1 | | | |
| *K07* | 0.564 | 0.510 | 0.570 | 0.144 | 0.277 | 0.227 | 1 | | |
| *K08* | 0.534 | 0.516 | 0.534 | 0.179 | 0.217 | 0.148 | 0.935 | 1 | |
| *K09* | 0.618 | 0.577 | 0.633 | 0.187 | 0.321 | 0.264 | 0.892 | 0.902 | 1 |

### 6.2.9 The wider applications of this study's findings

Within this section the wider applications of this study's findings are outlines in respect to ARD prediction methods, CDR deployment and mine closure planning.

#### *ARD prediction methods*

The results produced within this study agree with the generalised suggestion within Maest and Nordstrom (2017) that there is a need for more consistent and standardised interpretation of humidity cell test data sets. The work undertaken by Keith Brady and Roger Hornberger clearly outlined the need for kinetic testing that accounted for enhanced $CO_2$ conditions as a results of carbonate dissolution in coal wastes materials. This work ultimately led to the creation of the EPA 1627 standard (Hornberger et al. 2004; Perry et al. 2009; EPA 2011). Within this study the same concept was applied to sulfidic mine wastes collected from two different mining operations in northern Europe.

This study has looked to assess the viability of utilising an industry standard kinetic test method, in the form of an altered ASTM D5744 HCT (ASTM 2018), to characterise drainage quality produced by multiple mining waste materials under variable $CO_2$ and temperature conditions. The key mechanisms that drove variations in HCT leaching quality within this study require further investigation and geochemical modelling. The results produced suggest that the increased solubility of $CO_2$ at reduced temperatures may have led to preferential weathering of metal bearing silicates. This was evidenced by increased total DIC within reduced temperature cells in line with increased Ni and Mg release rates for Kevitsa wastes and increased Mn and Ca release rates within

Aitik Wastes. The pH of weekly leachates suggested that the increase in dissolved carbon species within enhanced $CO_2$ cell sets was likely dominated by bicarbonate and carbonate ions, which ultimately provided alkalinity to the system.

The leaching variations between cell test conditions suggest that the current standard ASTM D5744 humidity cell test method may not be applicable in assessing the primary mineral reaction rates of wastes that are exposed to temporally variable pore gas compositions. This agrees with the Lapakko (2003) who suggested that temperature variations during a humidity cell test may lead to variable leaching characteristics. It has been demonstrated that both temperature and aeration system gas composition play a significant role in metal leaching and sulfate release rates.

At present most standard ARD prediction and characterisation methods are based on work of Sobek et al., (1978) (AMIRA 2002; Price 2009; GARD 2014). In the over 40 years since the publication of this report, limited advancements in estimation of NP, AP, ARD onset have been made that significantly deter or build on the work undertaken by Sobek. Calculations of AP/NP, alkalinity, acidity and AP/NP consumption are based on idealised conditions in respect to calcite as the primary constitute to neutralising reactions and pyrite as the primary sulfide mineral in consideration of acid generating potential (Sherlock et al. 1995; Morin and Hutt 2001; Price 2009). This study has demonstrated that alteration from these idealised assumptions leads to significantly variable estimations of drainage quality and metal leaching potential.

It has been discussed that the current estimation of open system NP consumption recommended in the interpretation of HCT results by Price (2009) may lead to misestimation of NP depletion, based on the assumptions of the calculation, for wastes in which alkalinity is produced from non-primary NP sources.

It is suggested that amended kinetic test methods, such as those in this study, could potentially be used in the assessment of drainage quality produced by wastes passively exposed to above atmospheric $CO_2$ conditions. Multiple studies carried out within the sulfidic waste rock facilities of the Antamina mine in Peru have demonstrated seasonally variable internal pore gas compositions (Lorca et al. 2016; Vriens et al.

2018; Vriens et al. 2019a). Pore gas within these facilities has been shown to vary seasonally with $O_2$ and $CO_2$ conditions intrinsically linked. These studies demonstrated pore gas $CO_2$ concentrations above 7%, by volume, coupled with supressed $O_2$ pore gas measurements. Cover trial systems carried out at the Kevitsa operation demonstrated similar seasonally oscillating trends in pore gas compositions, with up to 7.9% $CO_2$ measured within these trials.

The above-mentioned studies from the Antamina mine and results generated from Kevitsa trials outline the importance of assessing the implications of varied internal pore gas compositions as part of mine closure and mine drainage management. It has been outlined in previous sections of this thesis that $O_2$ availability and $CO_2$ exposure play a key role in AP and NP mineral reactions and the long-term prediction of ARD. Carbonate chemistry and the presence of solid and dissolved carbon species is a key consideration in the assessment of silicate weathering, sulfide oxidation and the metal leaching potential of mining wastes (Sherlock et al. 1995; Morin and Hutt 2001; Cempa-Balewicz 2015; Morin 2017).

***The potential environmental implications of utilising mining wastes for CDR***

Multiple studies have outlined how the enhanced weathering of reactive silicates has the potential to store $CO_2$ as stable carbonate (Wilson et al. 2011; Power et al. 2013; Power et al. 2014b; Kelemen et al. 2020; McQueen et al. 2020; Power et al. 2020). This is an interesting proposition for mine operators as, in the absence of acidic mine drainage, operational emissions may be offset through carbonate mineral precipitation and storage. It is widely speculated within the scientific research that mine wastes may play a large role in the movement towards meeting net zero emissions targets (Royal Society and Royal Academy of Engineering 2018).

It is hypothesised by the author that ultimately the large-scale viability of using suitable mine wastes as a CDR feedstock depends on a number of factors including, but not limited to; interactions with and prevalence of ARD, long-term carbon storage duration/resilience and the ability to develop and standardise the monitoring, reporting and verification (MRV) of carbon dioxide removals (Bellassen et al. 2015).

At the time of writing no internationally recognised standard exists for the accreditation and validation of carbon dioxide removal using mining wastes. Private companies such as Puro Earth have developed independent standards, known as the 'Puro Standard', for assessing carbon removals via enhanced rock weathering (Puro Earth 2023). Such private companies are attempting to create independent 'standards' that can be followed to gain carbon removal credits, and often provide a registry service for carbon removals. While the business case for this seems obvious with systems such as the European Union Trading system (EU ETS) providing an economic value for offsets (European Commission 2023), at present no standard for EW/mineral carbonation mediated carbon removal exists that is uniformly accepted by governmental and regulatory bodies.

While the economic viability of CDR utilising mine wastes is still contested within the scientific and political communities (Hitch and Dipple 2012), the push towards carbon neutrality means that ultimately, viable removal technologies will be assessed and implemented at scale. One of the important applications of this study lies in assessing the potential implications that large scale CDR deployment at mining operations may have on ARD prediction, development, and management, both during operation and post closure. This is especially the case in situations where active mineral carbonation methods may be employed to enhance the weathering of reactive silicates.

It has been outlined within the literature review conducted in this study that limited consideration has been given to the potential environmental implications of large-scale CDR using mine wastes (Kandji et al. 2017a; Kandji et al. 2017d; Savage et al. 2019a; Savage et al. 2021; Savage et al. 2022). Select studies have evaluated the fate of metal cations generated in the weathering of silicate minerals during enhanced weathering in the presence of enhanced $CO_2$ concentrations (Cempa-Balewicz 2015; Hamilton et al. 2018a). Although these studies provide a foundation to assess how large-scale CDR at mining operations may impact waste geochemistry, to date no noted research has thus far looked to assess ARD development/classification in the context of current industry standard methods.

Based on literature assessments and the results generated within this study, it is the opinion of the author that clear regulatory consideration needs to be given to the

potential environmental implications of large-scale CDR employment at mining operations. This is particularly prevalent due to number of 'suitable' mine operations globally, with mine wastes of various compositions being considered for wide scale application (Langman et al. 2014; Wilson et al. 2014a; Kandji et al. 2017c; Kandji et al. 2017d; Mervine et al. 2018; Bullock et al. 2021). With the environmental and political push towards net zero emission targets regulatory standards will be required for the large deployment of mine waste CDR technologies (Royal Society and Royal Academy of Engineering 2018).

***Holistic waste management***

The results generated within this study demonstrated the potential implications of enhanced $CO_2$ concentrations on mine drainage quality development, with enhanced metal leaching, sulfate suppression and variable NP/AP consumption rates demonstrated between altered and control kinetic tests. The findings of this study raise questions about the viability of current ARD prediction standards/manuals, such as the AMIRA handbook, ASTM D5744, MEND 1.20.1 and BS EN 15875:2011, in adequately predicting ARD potential in environments where waste materials may be exposed to variable pore-gas compositions and temperature. It is recommended that further research is carried out to assess the potential implications of enhanced $CO_2$ on mine waste geochemical development, with the goal of developing new standard testing methods that can be used to undertake site specific ARD prediction. The development of such methods will allow operators and regulators to more effectively assess the potential environmental risks associated with exposing sulfidic mine wastes to enhanced $CO_2$ environments, either as part of a CDR method or as part of closure planning.

It has been demonstrated within this study that ARD prediction, CDR, carbon neutral mining and mine closure planning are intrinsically linked. At present these factors are considered independently by mining operators and environmental regulators. It is suggested by the author that a more holistic and site-specific approach to ARD management and drainage quality prediction is required.

# Chapter 7 - Conclusions and Recommendations

## Introduction

This final Chapter looks to conclude the findings of this research study and put into perspective the potential implications for kinetic testing and mine waste management. Recommendations for further work to validate and build on the findings of this study are given.

## 7.1 Key Conclusions

Based on the results generated within this research study the following key conclusions have been drawn, considering the research questions, aims and hypothesis outlined in Chapter 1.2 of this study:

- The application of enhanced $CO_2$ concentrations within humidity cell tests (HCT) following standard ASTM- D5744 led to variable weekly leaching characteristics for both Kevitsa and Aitik HCT triplicate HCT sets. Based on the results of this study current kinetic testing standards, such as ASTM-D5744, are likely to produce unrepresentative leaching characteristics for wastes that are exposed to seasonally variable pore gas compositions.
- Cumulative leaching of major anions and cations, as well as trace elements, showed distinct increases in overall leached volumes in cells treated with enhanced $CO_2$ concentrations in both control temperature conditions (25$^{o}$C) (K-TC1 and A-TC1) and reduced temperature conditions (10$^{o}$C) (K-TC3 and A-TC3), when compared to control cells (K-TC2 and A-TC2). The increased saturation of $CO_2$ within cells exposed to enhanced humidified $CO_2$ air cycles is interpreted to have led to increased leaching of Mg, Ca and K in both Kevitsa and Aitik cell sets.
- Variability in leachate quality between reduced temperature HCTs (K-TC3 and A-TC3) and standard temperature HCT's exposed to enhanced $CO_2$ concentrations (K-TC1 and A-TC1) has been interpreted as a result of the following:

  - The solubility of $CO_2$ increases with decreasing temperatures, as such the production of carbonic acid ($H_2CO_3$) within cell pore water is likely to have increased in reduced temperature HCT's. This would explain increased rates of DIC leaching as well as the increased leaching of trace elements associated with neutralising mineral sources, both carbonate and fast reacting silicates (such as olivine or anorthite).
  - Sulfide oxidation rates are slower under reduced temperatures – This would explain the apparent reduction in measured sulfate release in reduced temperature cells in comparison to standard temperature cell sets (K-TC2 and A-TC2).
  - The potential for sulfide mineral surface passivation between leaching cycles, potentially as a result of secondary mineral precipitation at elevated pH conditions. This may lead to restricted sulfide mineral oxidation and sulfate release.
- Static testing and material characterisation pre and post HCT testing showed minimal variation in material geochemical and mineralogical composition for both test materials. This is likely to be due to high liquid to solid ratio of ASTM HCT protocols.
- Mineralogical analysis via SEM-EDX and optical microscopy showed no distinguishable changes to materials recovered from either Kevitsa or Aitik HCT's. This has been interpreted as a result of the relatively high L:S within standard HCT procedures. The weekly flushing ratio of 2:1 L:S is significantly higher than flushing rates in situ. High relative flushing rates of waste materials in these kinetic tests likely limits the precipitation of stable secondary minerals.
- The potential for carbon dioxide emissions should also be considered as part of CDR assessment and ARD management. At present no industry or regulatory standards exist within the mining industry that fully assess life cycle emissions from waste materials because of sulfide oxidation and subsequent acidity production and carbonate dissolution. Silicates weathering in the presence of enhanced $CO_2$ concentrations and subsequent storage of carbon in the form of bicarbonate and carbonate may provide long term $CO_2$ removal if these carbon species are not reemitted as gas phase $CO_2$ in the process of buffering acidity caused by sulfide oxidation.

- Cells from both Aitik and Kevitsa demonstrated a reduction in leached sulfate concentrations over the 60-week testing period. This was expected in reduced temperature cells (K-TC3 and A-TC3) due to the inverse relationship between temperature and sulfide oxidation kinetics. Standard temperature cells exposed to enhanced $CO_2$ humidified air cycles (K-TC1 and A-TC1) demonstrated reduced sulfate leaching when compared to standardised cells with the same testing materials (K-TC2 and A-TC2). $O_2$ levels within the humidified air cycles were set across all cells to reduce potential variable sulfide oxidation due to differing $O_2$ concentrations. The apparent reduction in leached sulfate therefore requires further study to assess the potential mechanism behind this variability.

## 7.2 Implications for ARD Onset Prediction and Management

Based on the outcomes of this study the potential implications for acid rock drainage prediction and kinetic testing methods have been summarised below:

- Although ARD classification following standard industry practices, such as the GARD and MEND guides, did not change significantly post kinetic testing with enhanced $CO_2$ concentrations, increased metal mobility has been demonstrated under such testing conditions.
- ABA classification parameters, such as MPA, NPR an NP, were not significantly influenced by variable testing parameters in this study. Longer term testing periods would be required to assess the potential long-term influence on ARD classification as a results of variable kinetic testing conditions.
- It is likely that current kinetic testing and material characterisation standards that are legally required by regulatory bodies misrepresent the long-term ARD potential of metal mining wastes.
- The enhanced metal leaching observed in enhanced $CO_2$ HCT's (K-TC1, K-TC3 and A-TC3, A-TC1 and A-TC3) over the 60-week testing period may provide a more representative prediction of transition metal leaching within the drainage system of waste rock facilities in which enhanced weathering is prevalent.
- Kinetic tests such as HCT and leaching columns that are used to predict long term mine drainage quality likely wrongly estimate ARD onset or metal release rates post mine closure and remediation strategies.

- The enhanced presence of $CO_2$ within waste pore spaces may have led to microbial cycling of sulfur species resulting in the retardation of sulfate. This may lead to variable sulfate release from such drainage systems.

## 7.3 Study Limitations

Limitations to this study and the experimental test work carried out in this research program have been outlined as follows:

- The storage of acidified leachate samples produced as part of this study were stored for extended periods of time before elemental analysis (after week 20). This was due to the following:
  - The closure of university facilities in line with COVID-19 regulations following lockdowns commencing in March 2020.
  - The inability to use the university ICP-OES facility following the end of COVID-19 restrictions due to the breakdown of the university analytical system. A new system was purchased and operational up to 12 months following collection from HCT's.
- Budgetary and time restrictions meant that the commencement of reduced temperature humidity cell tests with standard gas compositions was not possible. This means the overall comparison of K-TC3 and A-TC3 cell sets to their standard temperature counterparts is limited.
- The length of the testing period was likely not long enough to establish if potentially acid forming (PAF) wastes may produce acidic drainage. Longer leaching cycles are likely needed to more comprehensively assess the potential for the onset of acidity, specifically for Aitik wastes materials, which have been identified as PAF through ABA assessment.
- Due to overall waste availability only waste rocks of fraction size >22mm were available for testing. The crushing of these materials to pass a <6.3mm sieve size is likely to increased reactive surface areas, and therefore is not representative of the reactivity of unaltered <22mm particle size fractions from either Kevitsa or Aitik's waste rock facilities. Within a waste rock facility mining waste PSD varies greatly, and therefore so will the overall reactivity. This study provides an indication of the potential implications of enhanced $CO_2$ concentration on mine waste

geochemical development under specific testing protocols. It is not intended to provide input into existing or planned ARD assessment for either mining operation.

- By design secondary mineral products are unlikely to precipitate in stable form within a HCT. As a HCT following ASTM-D5744 is primarily designed to assess primary mineral reaction rates and metal leaching characteristics, the applicability of this kinetic testing protocol is limited in its ability to adequately assess precipitation of secondary minerals. This is evidenced by the lack of mineralogical variability in both mineral abundance and petrographic analysis in this study.
- Budgetary and time limitations within this study meant that some potentially beneficial characterisation could not be carried out within this research program. This includes, but is not limited to, total acid digestion, kinetic NAG tests, X-ray diffraction (XRD), carbon and sulfur speciation and carbon isotope analysis.
- It Is widely accepted within the scientific literature that bacteria and biogeochemical processes play a large role in overall ARD onset. This study did not consider the potential role that the presence of various bacterial species may play in the development of drainage quality in waste rock facilities to a great extent.

## 7.4 Study Recommendations

Following the completion of this research study and summarisation of key conclusions and study limitations the following recommendations are made for further consideration:

- The commencement and assessment of multiple kinetic testing protocols considering enhanced $CO_2$ concentrations and variable $O_2$ concentrations within mining waste pore spaces – This may include a comparison of column leaching tests, up flow percolation tests (UPT) and humidity cell tests. This sort of comparative study would allow quantification of the potential implications of variable pore gas parameters on mine waste geochemical development and ARD prediction. The results generated from such a study could then be used to inform the design of a kinetic testing protocol that considers site-specific parameters such as pore gas composition, internal waste temperature, precipitation/leaching frequency, particle size distribution and mineralogical variability.

- The use of pore water pH measurements within kinetic testing cell and column tests is recommended. It was demonstrated that the increased proportion of $CO_2$ within testing atmospheres leads to increased DIC. Leaching of treated mine wastes leads to disequilibrium of leachates with the collection atmosphere. This is likely to lead to degassing of aqueous phase $CO_2$ during leaching protocols and the wrongful estimation of pore water pH. The potential for this has been highlighted in EPA standard 1627, section 3.3.1 (EPA 2011). The addition of pore water pH probes will provide a more accurate estimation of pore water geochemistry within such kinetic testing methods.
- Further kinetic testing that assesses $CO_2$ enhanced conditions should consider the influence of bacterially mediated ARD development and the role various bacterial species may play in enhanced $CO_2$ environments.
- Application of mine waste CDR potential and operational applicability as part of mine planning and mineral exploration stages. As part of a mining operations exploration phase key elemental assay and mineralogical data is commonly collected as part of mine planning. This data contains key data that could be used to assess preliminary CDR suitability, this includes conducting carbon capture potential (CCP) assessments and waste volume projections. An assessment of CCP at this early stage of mining operation would allow integration of such data into deposit block models in programs such as LeapFrog. Such applications would allow for waste deposition that promotes CDR as part of waste management and closure planning. An assessment of CCP potential could allow active segregation of high CCP waste for utilisation in active CDR protocols. This would further the potential to utilise mine wastes as a large-scale CDR method through EW of reactive silicate portions.
- Modelling the geochemical development of wastes under variable pore gas conditions within waste facilities would allow for a more comprehensive assessment of the ARD potential of suitable wastes. It is suggested that leaching data collected from standard humidity cells and amended humidity cells within this study are modelled in programs such as PHREEQC and Geochemists Work Bench (GWB). This would allow for a better understanding of mineral saturation indices, potential leachate products and pore water development in such systems.
- An assessment of elemental deportment within minerals of wastes before such kinetic testing would be beneficial to assessing the sources of enhanced leaching

within long term kinetic testing methods. For wastes that are abundant faster reacting silicate sources, such as forsterite, this analysis would be beneficial as It would better the understanding of mineralogical sources of enhanced metal leaching under variable testing conditions.

- There is the need for the development of kinetic testing procedures that can assess the potential carbon dioxide flux within mining waste rock facilities. It is well established that the EW of reactive silicate rich mining wastes has the potential to sequester atmospheric $CO_2$, but the balance between carbon dioxide removal and carbon dioxide emitted through carbonate dissolution has not been established within the existing scientific literature to date. There is therefore the need for cross disciplinary research between researchers who specialise in ARD characterisation and prediction and researchers who's scientific focus is CDR via EW. Without a robust quantification of the balance between $CO_2$ emissions via carbonate dissolution and $CO_2$ removal via carbonate precipitation following EW a monitoring, reporting and verification (MRV) system for carbon offsets utilising mine wastes is unlikely to be accepted by regulatory bodies.
- In order to robustly quantify variability in mine waste pore gas compositions and the potential subsequent implications for waste drainage development large scale in-situ assessment are required. It is recommended that internal gas compositions within waste rock dumps that both the Kevitsa and Aitik mining operations are routinely monitored for $CO_2$ and $O_2$ variability. The application of a small-scale waste rock dump trial, such as the dumps developed at the Antamina mine, would allow site specific assessments to be carried out. Within such a trial pore gas composition could be measured in tandem with toe drainage quality via a lysimeter. Such a field scale trial would allow a quantification of the relationship between pore-gas compositional variability and ARD development within large scale waste rock dumps.

# Bibliography

AMIRA. 2002. *ARD Test Handbook Confidential Project P387A Prediction & Kinetic Control of Acid Mine Drainage*. Available at: www.amira.com.au.

Appelo, C.A.J. and Postma, D. 2004. *Geochemistry, Groundwater and Pollution*. Appelo, C. A. J. and Postma, D. eds. CRC Press. doi: 10.1201/9781439833544.

Arrhenius, S. 1889. Über die Dissociationswärme und den Einfluss der Temperatur auf den Dissociationsgrad der Elektrolyte. *Zeitschrift für Physikalische Chemie* 4U(1), pp. 96–116. doi: 10.1515/zpch-1889-0408.

ASTM. 2018. *Standard Test Method for Laboratory Weathering of Solid Materials Using a Humidity Cell 1*. Available at: www.astm.org,.

Baciocchi, R., Costa, G., Bartolomeo, E. Di, Polettini, A. and Pomi, R. 2010. Carbonation of stainless steel slag as a process for CO2 storage and slag valorization. *Waste and Biomass Valorization* 1(4), pp. 467–477. doi: 10.1007/s12649-010-9047-1.

Baird, R., Eaton, A. and Rice, E. 2015. *Standard methods for the examination of water and wastewater*. 23rd ed. Available at: https://doi.org/10.2105/SMWW.2882.216.

Baurov, A.A. 2021. Methods of Carbon Sequestration (Review). *Polymer Science - Series D* 14(4), pp. 603–605. doi: 10.1134/S1995421222010038.

BCFSM. 2013. *PART A QUALITY CONTROL AND QUALITY ASSURANCE*. Vancouver. Available at: https://www2.gov.bc.ca/assets/gov/environment/research-monitoring-and-reporting/monitoring/emre/bc_field_sampling_manual_part_a.pdf [Accessed: 12 May 2023].

Beerling, D.J. et al. 2018. Farming with crops and rocks to address global climate, food and soil security /631/449 /706/1143 /704/47 /704/106 perspective. *Nature Plants* 4(3), pp. 138–147. doi: 10.1038/s41477-018-0108-y.

Beerling, D.J. et al. 2020. Potential for large-scale CO2 removal via enhanced rock weathering with croplands. *Nature* 583(7815), pp. 242–248. doi: 10.1038/s41586-020-2448-9.

Bellassen, V. et al. 2015. Monitoring, reporting and verifying emissions in the climate economy. *Nature Climate Change* 5(4), pp. 319–328. doi: 10.1038/nclimate2544.

Berthet, L. 2020. *Boliden Summary Report Kevitsa Mine*. Available at: https://www.boliden.com/globalassets/operations/exploration/mineral-resources-and-mineral-reserves-pdf/2020/resources-and-reserves-kevitsa-2020-12-31.pdf [Accessed: 18 February 2021].

BHP. 2023. *Unlocking the potential of mineral carbonation*. Available at: https://www.bhp.com/news/articles/2020/09/unlocking-the-potential-of-mineral-carbonation [Accessed: 28 March 2023].

Birkham, T.K., Hendry, M.J., Wassenaar, L.I., Mendoza, C.A. and Seok Lee, E. 2003. Characterizing geochemical reactions in unsaturated mine waste-rock piles using gaseous O2, CO2, 12CO2, and 13CO2. *Environmental Science and Technology* 37(3), pp. 496–501. doi: 10.1021/es020587c.

Blowes, D.W., Ptacek, C.J., Jambor, J.L., Weisener, C.G., Paktunc, D., Gould, W.D. and Johnson, D.B. 2013. The Geochemistry of Acid Mine Drainage. In: *Treatise on Geochemistry: Second Edition*. Elsevier Inc., pp. 131–190. doi: 10.1016/B978-0-08-095975-7.00905-0.

Boschi, C., Dini, A., Baneschi, I., Bedini, F., Perchiazzi, N. and Cavallo, A. 2017. Brucite-driven CO2 uptake in serpentinized dunites (Ligurian Ophiolites, Montecastelli, Tuscany). *Lithos*. doi: 10.1016/j.lithos.2017.07.005.

Bouzahzah, H., Benzaazoua, M. and Bussière, B. 2010. A modified protocol of the ASTM normalized humidity cell test as laboratory weathering method of concentrator tailings.

Brady, K. and Scheetz, B. 2005. *ADTI-WP2 LEACHING COLUMN METHOD FOR OVERBURDEN ANALYSIS AND PREDICTION OF WEATHERING RATES*. Available at: https://www.researchgate.net/publication/253696079.

Brady, K.B.C. and Hornberger, R.J. 1989. *MINE DRAINAGE PREDICTION AND OVERBURDEN ANALYSIS IN PENNSYLVANIA*.

Bryan, C.G., Davis-Belmar, C.S., van Wyk, N., Fraser, M.K., Dew, D., Rautenbach, G.F. and Harrison, S.T.L. 2012. The effect of CO 2 availability on the growth, iron oxidation and CO 2-fixation rates of pure cultures of Leptospirillum ferriphilum and Acidithiobacillus ferrooxidans. *Biotechnology and Bioengineering* 109(7), pp. 1693–1703. doi: 10.1002/bit.24453.

BSI. 2001. *BS EN 13137:2001 - Characterization of waste — Determination of total organic carbon (TOC) in waste, sludges and sediments*.

BSI. 2002. *BS EN 12457-1:2002 - Characterisation of waste — Leaching — Compliance test for leaching of granular waste materials and sludges — Part 1: One stage batch test at a liquid to solid ratio of 2 l/kg for materials with high solid content and with particle size below 4 mm (without or with size reduction)*.

BSI. 2012a. *BS EN 15875:2011 - Characterization of waste — Static test for determination of acid potential and neutralisation potential of sulfidic waste*.

BSI. 2012b. *PD CEN/TR 16365:2012 Characterization of waste. Sampling of waste from extractive industries*.

BSI. 2014. *BS ISO 18227:2014 - Soil quality — Determination of elemental composition by Xray fluorescence*.

BSI. 2015. *BS EN ISO 17892-3:2015 - Geotechnical investigation and testing — Laboratory testing of soil*.

BSI. 2016a. *BS EN 14582:2016 - TC - Characterization of waste. Halogen and sulfur content. Oxygen combustion in closed systems and determination methods*.

BSI. 2016b. *BS EN ISO 17892-4:2016 Geotechnical investigation and testing. Laboratory testing of soil. Determination of particle size distribution*.

BSI. 2022. *BS 1377-2 — Methods of test for soils for civil engineering purposes*.
Buamah, R. 2009. *ADSORPTIVE REMOVAL OF MANGANESE, ARSENIC AND IRON FROM GROUNDWATER*.

Bullock, L.A., James, R.H., Matter, J., Renforth, P. and Teagle, D.A.H. 2021. Global Carbon Dioxide Removal Potential of Waste Materials From Metal and Diamond Mining. *Frontiers in Climate* 3. doi: 10.3389/fclim.2021.694175.

Carroll, J., Slupsky, J. and Mather, alan. 1991. The solubility of carbon dioxide in water at low pressure. *The Journal of Physical Chemistry* 20(6).

Cempa-Balewicz, M. 2015. Influence of the presence of carbon dioxide on chemical composition of water in contact with mining waste. *Journal of Sustainable Mining* 14(1), pp. 38–45. doi: 10.1016/j.jsm.2015.08.006.

Charles, J., Barnes, A., Declercq, J. and Warrender, R. 2015. *Difficulties of Interpretation of NAG Test Results on Net Neutralizing Mine Wastes* Available at: https://www.researchgate.net/publication/275406813.

Chmielarski, M. 2019. *An assessment of the carbon sequestration potential of ultramafic nickel mine waste rock: Investigation of impacting environmental factors*. UNPUBLISHED, Cardiff University.

Cole, J.J. and Prairie, Y.T. 2014. Dissolved CO2 in Freshwater Systems☆. In: *Reference Module in Earth Systems and Environmental Sciences*. Elsevier. doi: 10.1016/b978-0-12-409548-9.09399-4.

Cravotta, C.A. 2008. Dissolved metals and associated constituents in abandoned coal-mine discharges, Pennsylvania, USA. Part 2: Geochemical controls on constituent concentrations. *Applied Geochemistry* 23(2), pp. 203–226. doi: 10.1016/j.apgeochem.2007.10.003.

Cravotta, C.A., Dugas, D.L., Brady, K.B.C. and Kovalchuk, T.E. 1994. Effects of Selective Handling of Pyritic, Acid-Forming Materials on the Chemistry of Pore Gas and Ground Water at A Reclaimed Surface Coal Mine, Clarion County, PA, USA. *Journal American Society of Mining and Reclamation* 1994, pp. 365–374. doi: 10.21000/JASMR94010365.

Dent, J., Pearce, S., Brookshaw, D., Savage, R., Barnes B, A., Mueller, S. and Kaasalainen, H. 2022. *CASE STUDIES TO DEMONSTRATE THE IMPORTANCE OF LIQUID TO SOLID RATIOS FOR GEOCHEMICAL TESTING METHOD SELECTION AND WATER QUALITY PREDICTION*.

Diedrich, T., Schott, J. and Oelkers, E.H. 2014. An experimental study of tremolite dissolution rates as a function of pH and temperature: Implications for tremolite toxicity and its use in carbon storage. *Mineralogical Magazine* 78(6), pp. 1449–1464. doi: 10.1180/minmag.2014.078.6.12.

Dold, B. 2017. Acid rock drainage prediction: A critical review. *Journal of Geochemical Exploration* 172, pp. 120–132. doi: 10.1016/j.gexplo.2016.09.014.

Duchesne, J. et al. 2017. Passive Mineral Carbonation of Mg-rich Mine Wastes by Atmospheric CO2. *Energy Procedia*. doi: 10.1016/j.egypro.2017.03.1745.

Dunn, J.G. 1997. The oxidation of sulphide minerals. *Thermochimica Acta* 300(1–2), pp. 127–139. doi: 10.1016/S0040-6031(96)03132-2.

Elghali, A., Benzaazoua, M., Taha, Y., Amar, H., Ait-khouia, Y., Bouzahzah, H. and Hakkou, R. 2023. Prediction of acid mine drainage: Where we are. *Earth-Science Reviews* 241. doi: 10.1016/j.earscirev.2023.104421.

EPA. 1994. *Technical Document: Acid Mine Drainage Prediction*.

EPA. 2011. *Method 1627: Kinetic Test Method for the Prediction of Mine Drainage Quality Background*.

Eufrasio, R.M. et al. 2022. Environmental and health impacts of atmospheric CO2 removal by enhanced rock weathering depend on nations' energy mix. *Communications Earth and Environment* 3(1). doi: 10.1038/s43247-022-00436-3.

European Commission. 2023. *EU Emissions Trading System (EU ETS)*. Available at: https://climate.ec.europa.eu/eu-action/eu-emissions-trading-system-eu-ets_en [Accessed: 24 February 2023].

Fagerlund, J., Nduagu, E., Romão, I. and Zevenhoven, R. 2010. A stepwise process for carbon dioxide sequestration using magnesium silicates. *Frontiers of Chemical Engineering in China* 4(2), pp. 133–141. Available at: http://link.springer.com/10.1007/s11705-009-0259-5 [Accessed: 18 March 2019].

Fernández Bertos, M., Simons, S.J.R., Hills, C.D. and Carey, P.J. 2004. A review of accelerated carbonation technology in the treatment of cement-based materials and sequestration of CO2. *Journal of Hazardous Materials* 112(3), pp. 193–205. doi: 10.1016/j.jhazmat.2004.04.019.

Gadikota, G. 2021. Carbon mineralization pathways for carbon capture, storage and utilization. *Communications Chemistry* 4(1). doi: 10.1038/s42004-021-00461-x.
GARD. 2014. *Development of the Global Acid Rock Drainage Guide*.

Gerdemann, S.J., O'Connor, W.K., Dahlin, D.C., Penner, L.R. and Rush, H. 2007. Ex situ aqueous mineral carbonation. *Environmental Science and Technology* 41(7), pp. 2587–2593. doi: 10.1021/es0619253.

Gerson, A.R., Rolley, P.J., Davis, C., Feig, S.T., Doyle, S. and Smart, R.S.C. 2019. Unexpected Non-acid Drainage from Sulfidic Rock Waste. *Scientific Reports* 9(1). doi: 10.1038/s41598-019-40357-4.

GTK. 2018. *Geological Survey of Finland Bulletin 407 • Special Issue Development of the Paleoproterozoic Svecofennian orogeny: new constraints from the southeastern boundary of the Central Finland Granitoid Complex*. Available at: https://doi.org/10.30440/bt407.

Gunning, P.J., Hills, C.D. and Carey, P.J. 2010. Accelerated carbonation treatment of industrial wastes. *Waste Management* 30(6), pp. 1081–1090. doi: 10.1016/j.wasman.2010.01.005.

Hamilton, J.L. et al. 2018a. Fate of transition metals during passive carbonation of ultramafic mine tailings via air capture with potential for metal resource recovery. *International Journal of Greenhouse Gas Control* 71, pp. 155–167. doi: 10.1016/j.ijggc.2018.02.008.

Hamilton, J.L. et al. 2018b. Fate of transition metals during passive carbonation of ultramafic mine tailings via air capture with potential for metal resource recovery. *International Journal of Greenhouse Gas Control* 71, pp. 155–167. Available at: https://www.sciencedirect.com/science/article/pii/S1750583617309258 [Accessed: 18 March 2019].

Hanrahan, G. 2012a. *Key Concepts in Environmental Chemistry*. Elsevier. doi: 10.1016/C2009-0-20235-2.

Harrison, A.L., Dipple, G.M., Power, I.M. and Mayer, K.U. 2015. Influence of surface passivation and water content on mineral reactions in unsaturated porous media: Implications for brucite carbonation and CO2 sequestration. *Geochimica et Cosmochimica Acta* 148, pp. 477–495. doi: 10.1016/j.gca.2014.10.020.

Harrison, A.L., Power, I.M. and Dipple, G.M. 2013. Accelerated carbonation of brucite in mine tailings for carbon sequestration. *Environmental Science and Technology* 47(1), pp. 126–134. doi: 10.1021/es3012854.

Hartmann, J. et al. 2013. Enhanced chemical weathering as a geoengineering strategy to reduce atmospheric carbon dioxide, supply nutrients, and mitigate ocean acidification. *Reviews of Geophysics* 51(2), pp. 113–149. doi: 10.1002/rog.20004.

Hartmann, J. et al. 2023. Stability of alkalinity in ocean alkalinity enhancement (OAE) approaches - consequences for durability of CO2storage. *Biogeosciences* 20(4), pp. 781–802. doi: 10.5194/bg-20-781-2023.

Henry, W. 1803. III. Experiments on the quantity of gases absorbed by water, at different temperatures, and under different pressures. *Philosophical Transactions of the Royal Society of London* 93, pp. 29–274. doi: 10.1098/rstl.1803.0004.

Herzog, H. 2002. *Carbon Sequestration via Mineral Carbonation: Overview and Assessment Motivation and Scientific Basis*. Available at: https://sequestration.mit.edu/pdf/carbonates.pdf [Accessed: 24 October 2020].

Hills, C.D., Tripathi, N. and Carey, P.J. 2020. Mineralization Technology for Carbon Capture, Utilization, and Storage. *Frontiers in Energy Research* 8. doi: 10.3389/fenrg.2020.00142.

Hitch, M., Ballantyne, S.M. and Hindle, S.R. 2010. Revaluing mine waste rock for carbon capture and storage. *International Journal of Mining, Reclamation and Environment* 24(1), pp. 64–79. doi: 10.1080/17480930902843102.

Hitch, M. and Dipple, G.M. 2012a. Economic feasibility and sensitivity analysis of integrating industrial-scale mineral carbonation into mining operations. *Minerals Engineering* 39, pp. 268–275. doi: 10.1016/j.mineng.2012.07.007.

Hornberger, R.J. et al. 2004. REFINEMENT OF ADTI-WP2 STANDARD WEATHERING PROCEDURES, AND EVALUATION OF PARTICLE SIZE AND SURFACE AREA EFFECTS UPON LEACHING RATES: PART 1: LABORATORY EVALUATION OF METHOD PERFORMANCE. *Journal American Society of Mining and Reclamation* 2004(1), pp. 916–947. Available at: http://www.asmr.us/Publications/Conference Proceedings/2004/0916-Hornberger PA.pdf.

IPCC. 2005. *Summary for Policymakers A Special Report of Working Group III of the Intergovernmental Panel on Climate Change IPCC Special Report Carbon Dioxide Capture and Storage Summary for Policymakers*.

Jansen, K., Thauer, R.K., Widdel, F. and Fuchs, G. 1984. *Carbon assimilation pathways in sulfate reducing bacteria. Formate, carbon dioxide, carbon monoxide, and acetate assimilation by Desulfovibrio baarsii*.

Jonsson, E. et al. 2023. Critical metals and minerals in the Nordic countries of Europe: diversity of mineralization and green energy potential. *Geological Society, London, Special Publications* 526(1). doi: 10.1144/sp526-2022-55.

Kalinin, A.A. and Kudryashov, N.M. 2021. Porphyry-related metamorphosed Au-Ag and Cu-Mo deposits in the precambrian of the fennoscandian shield. *Minerals* 11(2), pp. 1–26. doi: 10.3390/min11020139.

Kandji, E.H.B., Plante, B., Bussière, B., Beaudoin, G. and Dupont, P.P. 2017a. Geochemical behavior of ultramafic waste rocks with carbon sequestration potential: a case study of the Dumont Nickel Project, Amos, Québec. *Environmental Science and Pollution Research* 24(12), pp. 11734–11751. doi: 10.1007/s11356-017-8735-9.

Kandji, E.H.B., Plante, B., Bussière, B., Beaudoin, G. and Dupont, P.P. 2017b. Kinetic testing to evaluate the mineral carbonation and metal leaching potential of ultramafic tailings: Case study of the Dumont Nickel Project, Amos, Québec. *Applied Geochemistry* 84, pp. 262–276. doi: 10.1016/j.apgeochem.2017.07.005.

Kantzas, E.P. et al. 2022. Substantial carbon drawdown potential from enhanced rock weathering in the United Kingdom. *Nature Geoscience* 15(5), pp. 382–389. doi: 10.1038/s41561-022-00925-2.

Karlsson, P. 2018. *Boliden Summary Report*.

Karlsson, Teemu. 2022. *Geochemical and Mineralogical Characterization of Waste Rocks for Preliminary Mine Drainage Quality Prediction*.

Kelemen, P., Benson, S.M., Pilorgé, H., Psarras, P. and Wilcox, J. 2019. An Overview of the Status and Challenges of CO2 Storage in Minerals and Geological Formations. *Frontiers in Climate* 1. doi: 10.3389/fclim.2019.00009.

Kelemen, P.B., McQueen, N., Wilcox, J., Renforth, P., Dipple, G. and Vankeuren, A.P. 2020. Engineered carbon mineralization in ultramafic rocks for CO2 removal from air: Review and new insights. *Chemical Geology* 550. doi: 10.1016/j.chemgeo.2020.119628.

Kemeny, P.C. et al. 2021. Sulfate sulfur isotopes and major ion chemistry reveal that pyrite oxidation counteracts CO2 drawdown from silicate weathering in the Langtang-Trisuli-Narayani River system, Nepal Himalaya. *Geochimica et Cosmochimica Acta* 294. doi: 10.1016/j.gca.2020.11.009.

Khalidy, R. and Santos, R.M. 2021. The fate of atmospheric carbon sequestrated through weathering in mine tailings. *Minerals Engineering* 163. doi: 10.1016/j.mineng.2020.106767.

Kirby, C.S. and Cravotta, C.A. 2005. Net alkalinity and net acidity 2: Practical considerations. *Applied Geochemistry* 20(10), pp. 1941–1964. doi: 10.1016/j.apgeochem.2005.07.003.

Kohler, P., Hartmann, J. and Wolf-Gladrow, D.A. 2010. Geoengineering potential of artificially enhanced silicate weathering of olivine. *Proceedings of the National Academy of Sciences*. doi: 10.1073/pnas.1000545107.

Langman, J.B., Moore, M.L., Ptacek, C.J., Smith, L., Sego, D. and Blowes, D.W. 2014. Diavik waste rock project: Evolution of mineral weathering, element release, and acid generation and neutralization during a five-year humidity cell experiment. *Minerals* 4(2), pp. 257–278. doi: 10.3390/min4020257.

Lapakko, K. 1988. Prediction of Acid Mine Drainage from Duluth Complex Mining Wastes in Northeastern Minnesota. *Journal American Society of Mining and Reclamation* 1988(1), pp. 180–190. doi: 10.21000/jasmr88010180.

Lapakko, K. 2000. *Modification of the ASTM 5744-96 Kinetic Test*. Available at: https://www.researchgate.net/publication/284026261.

Lapakko, K.A. 2003. *Developments in humidity-cell tests and their application*. Available at: https://www.researchgate.net/publication/284026337.

Lapakko, K.A. and Antonson, D.A. 2006. PYRITE OXIDATION RATES FROM HUMIDITY CELL TESTING OF GREENSTONE ROCK. *Journal American Society of Mining and Reclamation* 2006(2), pp. 1007–1025. doi: 10.21000/JASMR06021007.

Lapakko, K.A., Engstrom, J.N. and Antonson, D.A. 2006. EFFECTS OF PARTICLE SIZE ON DRAINAGE QUALITY FROM THREE LITHOLOGIES 1.

Li, J. and Hitch, M. 2016. Carbon dioxide adsorption isotherm study on mine waste for integrated CO2 capture and sequestration processes. *Powder Technology* 291, pp. 408–413. doi: 10.1016/j.powtec.2015.12.011.

Li, J. and Hitch, M. 2018. Economic analysis on the application of mechanical activation in an integrated mineral carbonation process. *International Biodeterioration and Biodegradation*. doi: 10.1016/j.ibiod.2016.08.026.

Li, J., Jacobs, A.D. and Hitch, M. 2022. The effect of mineral composition on direct aqueous carbonation of ultramafic mine waste rock for CO2 sequestration, a case study of Turnagain ultramafic complex in British Columbia, Canada. *International Journal of Mining, Reclamation and Environment* 36(4), pp. 267–286. doi: 10.1080/17480930.2022.2041340.

Lindvall, M. 2005. *Strategies for remediation of very large deposits of mine waste; the Aitik mine, Northern Sweden*.

Lorca, M.E., Mayer, K.U., Pedretti, D., Smith, L. and Beckie, R.D. 2016. Spatial and Temporal Fluctuations of Pore-Gas Composition in Sulfidic Mine Waste Rock. *Vadose Zone Journal* 15(10), p. vzj2016.05.0039. doi: 10.2136/vzj2016.05.0039.

Lottermoser, B. 2010. *Mine Wastes*. 3rd ed. Springer. doi: 10.1007/978-3-642-12419-8.

Lu, X., Carroll, K.J., Turvey, C.C. and Dipple, G.M. 2022. Rate and capacity of cation release from ultramafic mine tailings for carbon capture and storage. *Applied Geochemistry* 140. doi: 10.1016/j.apgeochem.2022.105285.

Lucile, F., Cézac, P., Contamine, F., Serin, J.P., Houssin, D. and Arpentinier, P. 2012. Solubility of carbon dioxide in water and aqueous solution containing sodium hydroxide at temperatures from (293.15 to 393.15) K and pressure up to 5 MPa: Experimental measurements. *Journal of Chemical and Engineering Data* 57(3), pp. 784–789. doi: 10.1021/je200991x.

Luolavirta, K., Hanski, E., Maier, W., Lahaye, Y., O'Brien, H. and Santaguida, F. 2018a. In situ strontium and sulfur isotope investigation of the Ni-Cu-(PGE) sulfide ore-bearing Kevitsa intrusion, northern Finland. *Mineralium Deposita* 53(7), pp. 1019–1038. doi: 10.1007/s00126-018-0792-6.

Luolavirta, K., Hanski, E., Maier, W. and Santaguida, F. 2018b. Whole-rock and mineral compositional constraints on the magmatic evolution of the Ni-Cu-(PGE) sulfide ore-bearing Kevitsa intrusion, northern Finland. *Lithos* 296–299, pp. 37–53. doi: 10.1016/j.lithos.2017.10.015.

Maest, A.S. and Nordstrom, D.K. 2017. A geochemical examination of humidity cell tests. *Applied Geochemistry* 81, pp. 109–131. doi: 10.1016/j.apgeochem.2017.03.016.

Maier, W.D., Barnes, S.J. and Groves, D.I. 2013. The Bushveld Complex, South Africa: Formation of platinum-palladium, chrome- and vanadium-rich layers via hydrodynamic sorting of a mobilized cumulate slurry in a large, relatively slowly cooling, subsiding magma chamber. *Mineralium Deposita* 48(1), pp. 1–56. doi: 10.1007/s00126-012-0436-1.

Makkonen, H. V., Halkoaho, T., Konnunaho, J., Rasilainen, K., Kontinen, A. and Eilu, P. 2017. Ni-(Cu-PGE) deposits in Finland – Geology and exploration potential. *Ore Geology Reviews* 90, pp. 667–696. doi: 10.1016/j.oregeorev.2017.06.008.

Manning, D.A.C. 2001. Calcite precipitation in landfills: an essential product of waste stabilization. *Mineralogical Magazine* 65(5), pp. 603–610. doi: 10.1180/002646101317018424.

Matter, J.M. et al. 2016. Rapid carbon mineralization for permanent disposal of anthropogenic carbon dioxide emissions. *Science* 352(6291), pp. 1312–1314. doi: 10.1126/science.aad8132.

Mayes, W.M., Riley, A.L., Gomes, H.I., Brabham, P., Hamlyn, J., Pullin, H. and Renforth, P. 2018. Atmospheric CO2 Sequestration in Iron and Steel Slag: Consett, County Durham, United Kingdom. *Environmental Science and Technology*. doi: 10.1021/acs.est.8b01883.

Mayes, W.M., Younger, P.L. and Aumônier, J. 2008. Hydrogeochemistry of alkaline steel slag leachates in the UK. *Water, Air, and Soil Pollution* 195(1–4), pp. 35–50. doi: 10.1007/s11270-008-9725-9.

McCarroll, D. 2016. *Simple Statistical Tests for Geography*. Chapman and Hall/CRC. doi: 10.1201/9781315380438.

McCutcheon, J., Power, I.M., Shuster, J., Harrison, A.L., Dipple, G.M. and Southam, G. 2019. Carbon Sequestration in Biogenic Magnesite and Other Magnesium Carbonate Minerals. *Environmental Science and Technology* 53(6), pp. 3225–3237. doi: 10.1021/acs.est.8b07055.

McQueen, N., Kelemen, P., Dipple, G., Renforth, P. and Wilcox, J. 2020. Ambient weathering of magnesium oxide for CO2 removal from air. *Nature Communications* 11(1). doi: 10.1038/s41467-020-16510-3.

MEM. 2019. *Detailed Geochemistry and Waste Characterisation Report*.

MEM Ltd. 2018. *Ni-Cu WRD Mineralogy*.

Mervine, E.M. et al. 2018. Potential for offsetting diamond mine carbon emissions through mineral carbonation of processed kimberlite: an assessment of De Beers mine sites in South Africa and Canada. *Mineralogy and Petrology* 112, pp. 755–765. doi: 10.1007/s00710-018-0589-4.

Meysman, F.J.R. and Montserrat, F. 2017. Negative CO2 emissions via enhanced silicate weathering in coastal environments. *Biology Letters* 13(4). doi: 10.1098/rsbl.2016.0905.

Montserrat, F., Renforth, P., Hartmann, J., Leermakers, M., Knops, P. and Meysman, F.J.R. 2017. Olivine Dissolution in Seawater: Implications for CO2 Sequestration through Enhanced Weathering in Coastal Environments. *Environmental Science and Technology* 51(7), pp. 3960–3972. doi: 10.1021/acs.est.6b05942.

Moodley, I., Sheridan, C.M., Kappelmeyer, U. and Akcil, A. 2018. Environmentally sustainable acid mine drainage remediation: Research developments with a focus on waste/by-products. *Minerals Engineering* 126, pp. 207–220. Available at: https://www.sciencedirect.com/science/article/pii/S0892687517302169 [Accessed: 3 April 2019].

Morin, K.A. 2017. *Explanations of Poregas CO2 Variability Relative to O2 in the Equity Silver Waste-Rock Pile MDAG.com Internet Case Study 50 Explanations for Poregas CO 2 Variability Relative to O 2 in the Equity Silver Waste-Rock Pile*. Available at: www.mdag.com/case_studies/cs50.html.

Morin, K.A. and Hutt, N.M. 1998. *KINETIC TESTS AND RISK ASSESSMENT FOR ARD*. Available at: http://home1.gte.net/mdag/index.htm.

Morin, K.A. and Hutt, N.M. 2000. *Lessons learned from long-term and large-batch humidity cells*. Metallurgy, and Exploration, Inc. Available at: www.mdag.com.

Morin, K.A. and Hutt, N.M. 2001. *Environmental geochemistry of minesite drainage practical theory and case studies*. MDAG Pub.

Moyo, A., Parbhakar-Fox, A., Meffre, S. and Cooke, D.R. 2023. Alkaline industrial wastes – Characteristics, environmental risks, and potential for mine waste management. *Environmental Pollution* 323, p. 121292. doi: 10.1016/j.envpol.2023.121292.

NASA. 2023. *Vital signs - Carbon dioxide* . Available at: https://climate.nasa.gov/vital-signs/carbon-dioxide/ [Accessed: 26 April 2023].

National Academy of Sciences. 2019. *Negative Emissions Technologies and Reliable Sequestration*. Washington, D.C.: National Academies Press. Available at: https://www.nap.edu/catalog/25259.

Nduagu, E., Björklöf, T., Fagerlund, J., Mäkilä, E., Salonen, J., Geerlings, H. and Zevenhoven, R. 2012. Production of magnesium hydroxide from magnesium silicate for the purpose of CO2 mineralization – Part 2: Mg extraction modeling and application to different Mg silicate rocks. *Minerals Engineering* 30, pp. 87–94. Available at: https://linkinghub.elsevier.com/retrieve/pii/S0892687511004286 [Accessed: 18 March 2019].

Nielsen, A.H., Vollertsen, J. and Hvitved-Jacobsen, T. 2006. Kinetics and Stoichiometry of Aerobic Sulfide Oxidation in Wastewater from Sewers-Effects of pH and Temperature. *Water Environment Research* 78(3), pp. 275–283. doi: 10.2175/106143005x94367.

Nordstrom, D.K. and Alpers, C.N. 1999. *Chapter 6 - Geochemistry of acid mine waters*. Oelkers, E.H. and Schott, J. 1995. *Experimental study of anorthite dissolution and the relative mechanism of feldspar hydrolysis*.

Ojala, V.J. and Iljina, M. 2008. *Metallogeny and tectonic evolution of the Northern Fennoscandian Shield*. O'Kane Consultants Ltd. 2018a. *Aitik Drilling Project – Drilling Works Factual Report (FR)*.

O'Kane Consultants Ltd. 2018b. *Kevitsa Sonic Drilling Project-Factual Report*.

Olajire, A.A. 2013. A review of mineral carbonation technology in sequestration of CO2. *Journal of Petroleum Science and Engineering* 109, pp. 364–392. Available at: https://www.sciencedirect.com/science/article/pii/S0920410513000673 [Accessed: 15 March 2019].

Oskierski, H.C., Turvey, C.C., Wilson, S.A., Dlugogorski, B.Z., Altarawneh, M. and Mavromatis, V. 2021. Mineralisation of atmospheric CO2 in hydromagnesite in ultramafic mine tailings – Insights from Mg isotopes. *Geochimica et Cosmochimica Acta* 309, pp. 191–208. doi: 10.1016/j.gca.2021.06.020.

Parbhakar-Fox, A., Fox, N., Hill, R., Ferguson, T. and Maynard, B. 2018a. Improved mine waste characterisation through static blended test work. *Minerals Engineering* 116, pp. 132–142. doi: 10.1016/j.mineng.2017.09.011.

Parbhakar-Fox, A., Fox, N., Jackson, L. and Cornelius, R. 2018b. Forecasting geoenvironmental risks: Integrated applications of mineralogical and chemical data. *Minerals* 8(12). doi: 10.3390/min8120541.

Parbhakar-Fox, A., Lottermoser, B. and Bradshaw, D. 2013. Evaluating waste rock mineralogy and microtexture during kinetic testing for improved acid rock drainage prediction. *Minerals Engineering* 52, pp. 111–124. doi: 10.1016/j.mineng.2013.04.022.

Parbhakar-Fox, A. and Lottermoser, B.G. 2015. A critical review of acid rock drainage prediction methods and practices. *Minerals Engineering* 82, pp. 107–124. doi: 10.1016/j.mineng.2015.03.015.

Park, A.-H.A., Jadhav, R. and Fan, L.-S. 2008. CO2 Mineral Sequestration: Chemically Enhanced Aqueous Carbonation of Serpentine. *The Canadian Journal of Chemical Engineering* 81(3–4), pp. 885–890. Available at: http://doi.wiley.com/10.1002/cjce.5450810373 [Accessed: 18 March 2019].

Paul, V.G., Wronkiewicz, D.J. and Mormile, M.R. 2017. Impact of elevated CO2 concentrations on carbonate mineral precipitation ability of sulfate-reducing bacteria and implications for CO2 sequestration. *Applied Geochemistry* 78, pp. 250–271. doi: 10.1016/j.apgeochem.2017.01.010.

Paulo, C., Power, I.M., Stubbs, A.R., Wang, B., Zeyen, N. and Wilson, S.A. 2021a. Evaluating feedstocks for carbon dioxide removal by enhanced rock weathering and CO2 mineralization. *Applied Geochemistry* 129. doi: 10.1016/j.apgeochem.2021.104955.

Paulo, C., Power, I.M., Stubbs, A.R., Wang, B., Zeyen, N. and Wilson, S.A. 2021b. Evaluating feedstocks for carbon dioxide removal by enhanced rock weathering and CO2 mineralization. *Applied Geochemistry* 129. doi: 10.1016/j.apgeochem.2021.104955.

Perry, E.F. and Brady, K. 2009. *Simulated Weathering of Coal Overburden With the Kinetic Test Procedure for the Prediction of Mine Drainage Quality*. Available at: https://www.researchgate.net/publication/277202077.

Perry, E.F., Brady, K., Perry, E.F., Brady, K.B.C. and Hornberger, R.J. 2009. *A standard column weathering test to estimate coal overburden leachate quality*. Available at: https://www.researchgate.net/publication/289429069.

Pieretti, M., Karlsson, T., Arvilommi, S. and Muniruzzaman, M. 2022. Challenges in predicting the reactivity of mine waste rocks based on kinetic testing: Humidity cell tests and reactive transport modeling. *Journal of Geochemical Exploration* 237. doi: 10.1016/j.gexplo.2022.106996.

Pogge von Strandmann, P.A.E. et al. 2019. Rapid CO 2 mineralisation into calcite at the CarbFix storage site quantified using calcium isotopes. *Nature Communications* 10(1). doi: 10.1038/s41467-019-10003-8.

Power, I.M. et al. 2014. Strategizing carbon-neutral mines: A case for pilot projects. *Minerals* 4(2), pp. 399–436. doi: 10.3390/min4020399.

Power, I.M., Dipple, G.M., Bradshaw, P.M.D. and Harrison, A.L. 2020. Prospects for CO2 mineralization and enhanced weathering of ultramafic mine tailings from the Baptiste nickel deposit in British Columbia, Canada. *International Journal of Greenhouse Gas Control* 94. doi: 10.1016/j.ijggc.2019.102895.

Power, I.M., Harrison, A.L., Dipple, G.M., Wilson, S.A., Kelemen, P.B., Hitch, M. and Southam, G. 2013. Carbon mineralization: From natural analogues to engineered systems. *Reviews in Mineralogy and Geochemistry* 77(1), pp. 305–360. doi: 10.2138/rmg.2013.77.9.

Price, W.A. 2009. *Mining and Mineral Sciences Laboratories Prediction Manual for Drainage Chemistry from Sulphidic Geologic Materials Work performed for: MEND Program*.

Prigiobbe, V., Hänchen, M., Werner, M., Baciocchi, R. and Mazzotti, M. 2009. Mineral carbonation process for CO2 sequestration. In: *Energy Procedia*. pp. 4885–4890. doi: 10.1016/j.egypro.2009.02.318.

Puro Earth. 2023. *Puro Standard General Rules*. Available at: https://puro.earth/puro-standard-carbon-removal-credits/ [Accessed: 24 March 2023].

Puthiya Veetil, S.K., Rebane, K., Yörük, C.R., Lopp, M., Trikkel, A. and Hitch, M. 2021. Aqueous mineral carbonation of oil shale mine waste (limestone): A feasibility study to develop a CO2 capture sorbent. *Energy* 221. doi: 10.1016/j.energy.2021.119895.

Rackley, S.A. 2017a. *Carbon capture and storage*. Elsevier. doi: 10.1016/B978-0-12-812041-5.00002-7.

Rackley, S.A. 2017b. Mineral carbonation. In: *Carbon Capture and Storage*. Elsevier, pp. 253–282. doi: 10.1016/B978-0-12-812041-5.00010-6.

Raza, A., Gholami, R., Rezaee, R., Rasouli, V. and Rabiei, M. 2019. Significant aspects of carbon capture and storage – A review. *Petroleum* 5(4), pp. 335–340. doi: 10.1016/j.petlm.2018.12.007.

Reichle, D.E., Houghton, J.C. and Kane, R.L. 1997. *A REVIEW OF CARBON SEQUESTRATION SCIENCE AND TECHNOLOGY OPPORTUNITIES BY THE U.S. DEPARTMENT OF ENERGY*. Socolow. Available at: http://cdiac2.esd.ornl.gov/index.html.

Renforth, P. 2012. The potential of enhanced weathering in the UK. *International Journal of Greenhouse Gas Control* 10, pp. 229–243. doi: 10.1016/j.ijggc.2012.06.011.

Renforth, P. 2019. The negative emission potential of alkaline materials. *Nature Communications* 10(1). doi: 10.1038/s41467-019-09475-5.

Renforth, P., Washbourne, C.L., Taylder, J. and Manning, D.A.C. 2011a. Silicate production and availability for mineral carbonation. *Environmental Science and Technology*. doi: 10.1021/es103241w.

Romanov, V., Soong, Y., Carney, C., Rush, G.E., Nielsen, B. and O'Connor, W. 2015. Mineralization of Carbon Dioxide: A Literature Review. *ChemBioEng Reviews* 2(4), pp. 231–256. doi: 10.1002/cben.201500002.

Royal Society and Royal Academy of Engineering. 2018. *Greenhouse gas removal.* Available at: https://royalsociety.org/-/media/policy/projects/greenhouse-gas-removal/royal-society-greenhouse-gas-removal-report-2018.pdf [Accessed: 18 January 2021].

Sammelin, M. 2011. *The Nature of Gold in the Aitik Cu-Au Deposit Implications for Mineral Processing and Mine Planning*.

Sanna, A., Uibu, M., Caramanna, G., Kuusik, R. and Maroto-Valer, M.M. 2014. A review of mineral carbonation technologies to sequester CO2. *Chemical Society Reviews* 43(23), pp. 8049–8080. doi: 10.1039/c4cs00035h.

Santos, R.M., van Audenaerde, A., Chiang, Y.W., Iacobescu, R.I., Knops, P. and van Gerven, T. 2015. Nickel extraction from olivine: Effect of carbonation pre-treatment. *Metals* 5(3), pp. 1620–1644. doi: 10.3390/met5031620.

Sapsford, D., Bowell, R., Williams, C. and Williams, K. 2008. A Comparison of Kinetic NAG tests with Static and Humidity Cell Tests for the Prediction of ARD.

Sapsford, D.J., Bowell, R.J., Dey, M. and Williams, K.P. 2009. Humidity cell tests for the prediction of acid rock drainage. *Minerals Engineering* 22(1), pp. 25–36. doi: 10.1016/j.mineng.2008.03.008.

Savage, R., Barnes, A., Pearce, S., Roberts, M., Renforth, P., Chmielarski, M., Mueller, S., & Sapsford, D. (2022). Quantification Of Methods To Assess Carbonation In Mine Wastes-Potential Implications For Long-Term Mine Waste Drainage Quality And Acid Rock Drainage (ARD) Prediction. Proceedings of the ICARD 2022 Conference. https://www.researchgate.net/publication/365650808

Savage, R., Barnes, A., Pearce, S. and Roberts, M. 2021. Carbonation of Magnesium Silicate Minerals in Mine Waste: Practical Laboratory Testing Methods to Assess the Dual Opportunity for Carbon Capture and AMD Mitigation. In: *Proceedings of the IMWA 2021 conference – "Mine Water Management for Future Generations."* Available at: https://www.researchgate.net/publication/358802944.

Savage, R., Pearce, S., Mueller, S., Barnes, A., Renforth, P. and Sapsford, D. 2019. Methods for assessing acid and metalliferous drainage mitigation and carbon sequestration in mine waste: A case study from Kevitsa mine, Finland. In: *Proceedings of the International Conference on Mine Closure*. Australian Centre for Geomechanics, pp. 1073–1086. doi: 10.36487/ACG_rep/1915_86_Savage.

Sherlock, E.J., Lawrence, R.W. and Poulin, R. 1995. *On the neutralization of acid rock drainage by carbonate and silicate minerals*. Springer-Verlag.

Siegrist, M., Southam, C., Bowman, G., Wilson, S.A. and Southam, G. 2017. Analysis of the Potential for Negative CO2Emission Mine Sites through Bacteria-mediated Carbon Mineralisation: Evidence from Australia. In: *Energy Procedia*. doi: 10.1016/j.egypro.2017.03.1749.

Simate, G.S. and Ndlovu, S. 2014. Acid mine drainage: Challenges and opportunities. *Journal of Environmental Chemical Engineering* 2(3), pp. 1785–1803. doi: 10.1016/j.jece.2014.07.021.

Snæbjörnsdóttir, S., Sigfússon, B., Marieni, C., Goldberg, D., Gislason, S.R. and Oelkers, E.H. 2020. Carbon dioxide storage through mineral carbonation. *Nature Reviews Earth and Environment* 1(2), pp. 90–102. doi: 10.1038/s43017-019-0011-8.

Sobek, A., Freeman, J., Smith, R. and Grim, E. 1978. *Field and laboratory methods applicable to overburdens and minesoils*.

Sood, A. and Vyas, S. 2017. Carbon Capture and Sequestration- A Review. In: *IOP Conference Series: Earth and Environmental Science*. Institute of Physics Publishing. doi: 10.1088/1755-1315/83/1/012024.

SRK. 2019. *TECHNICAL REPORT FOR THE KEVITSA CU-NI-PGE MINE, FINLAND Boliden Kevitsa Mining Oy*.

Stewart, W.A., Miller, S.D. and Smart, R. 2006. Advances in acid rock drainage (ARD) characterisation of mine wastes. In: *7th International Conference on Acid Rock Drainage 2006, ICARD - Also Serves as the 23rd Annual Meetings of the American Society of Mining and Reclamation*. American Society of Mining and Reclamation, pp. 2098–2119. doi: 10.21000/jasmr06022098.

Stromberg, B. and Banwart, S. 1994. *Kinetic modelling of geochemical processes at the Aitik mining waste rock site in northern Sweden*.

Stubbs, A.R., Paulo, C., Power, I.M., Wang, B., Zeyen, N. and Wilson, S.A. 2022. Direct measurement of CO2 drawdown in mine wastes and rock powders: Implications for enhanced rock weathering. *International Journal of Greenhouse Gas Control* 113. doi: 10.1016/j.ijggc.2021.103554.

Stumm, W. and Morgan, J.J. 1995. *Aquatic Chemistry: Chemical Equilibria and Rates in Natural Waters, 3rd Edition*. 3rd ed. Wiley.

Tominaga, M., Beinlich, A., Lima, E.A., Tivey, M.A., Hampton, B.A., Weiss, B. and Harigane, Y. 2017. Multi-scale magnetic mapping of serpentinite carbonation. *Nature Communications*. doi: 10.1038/s41467-017-01610-4.

USGS. 2023. *What is carbon sequestration?* Available at: https://www.usgs.gov/faqs/what-carbon-sequestration?qt - news_science_products=0#qt-news_science_products [Accessed: 18 February 2023].

Vaasjoki, M. 2001. *Radiometric age determinations from Finnish Lapland and their bearing on the timing of Precambrian volcano-sedimentary sequences Edited U-Pb GEOCHRONOLOGY OF THE PEURASUVANTO AREA, NORTHERN FINLAND*.

Veetil, S.P. and Hitch, M. 2020. Recent developments and challenges of aqueous mineral carbonation: a review. *International Journal of Environmental Science and Technology* 17(10), pp. 4359–4380. doi: 10.1007/s13762-020-02776-z.

Velbel, M.A. 2009. Dissolution of olivine during natural weathering. *Geochimica et Cosmochimica Acta* 73(20), pp. 6098–6113. doi: 10.1016/j.gca.2009.07.024.

Vriens, B., Arnault, M. St., Laurenzi, L., Smith, L., Mayer, K.U. and Beckie, R.D. 2018. Localized Sulfide Oxidation Limited by Oxygen Supply in a Full-Scale Waste-Rock Pile. *Vadose Zone Journal* 17(1), pp. 1–14. doi: 10.2136/vzj2018.06.0119.

Vriens, B., Smith, L., Mayer, K.U. and Beckie, R.D. 2019. Poregas distributions in waste-rock piles affected by climate seasonality and physicochemical heterogeneity. *Applied Geochemistry* 100, pp. 305–315. doi: 10.1016/j.apgeochem.2018.12.009.

Wang, B. et al. 2018. *Migration of transition metals and potential for mineral carbonation during acid leaching of kimberlite mine tailings*.

Wanhainen, C., Broman, C. and Martinsson, O. 2003. The Aitik Cu-Au-Ag deposit in northern Sweden: A product of high salinity fluids. *Mineralium Deposita* 38(6), pp. 715–726. doi: 10.1007/s00126-003-0363-2.

Wiebe, R. and Gaddy, V.L. 1940. *Solubility of Carbon Dioxide in Water The Solubility of Carbon Dioxide in Water at Various Temperatures from 12 to 40° and at Pressures to 500 Atmospheres. Critical Phenomena**. Available at: https://pubs.acs.org/sharingguidelines.

Wilberforce, T., Olabi, A.G., Sayed, E.T., Elsaid, K. and Abdelkareem, M.A. 2021. Progress in carbon capture technologies. *Science of the Total Environment* 761. doi: 10.1016/j.scitotenv.2020.143203.

Wilcox, J., Kolosz, B. and Freeman, J. 2021. *CDR Primer*. Available at: https://cdrprimer.org/read [Accessed: 28 February 2023].

Wilson, S.A. et al. 2014a. Offsetting of CO2 emissions by air capture in mine tailings at the Mount Keith Nickel Mine, Western Australia: Rates, controls and prospects for carbon neutral mining. *International Journal of Greenhouse Gas Control* 25, pp. 121–140. doi: 10.1016/j.ijggc.2014.04.002.

Wilson, S.A., Dipple, G.M., Power, I.M., Barker, S.L.L., Fallon, S.J. and Southam, G. 2011. Subarctic weathering of mineral wastes provides a sink for atmospheric CO 2. *Environmental Science and Technology* 45(18), pp. 7727–7736. doi: 10.1021/es202112y.

# Appendix

## List of Appendices

# Appendix 1 – HCT RAMS

This appendix contains the university risk assessment and method statement (RAMS) used within this research study.

| Rhys Savage HCT Set up | Method Statement |
|---|---|

| Contract: | **Geochemic Ltd/KESS 2 Funded PhD Project** |
|---|---|

| Title: PhD Humidity cell experiments | Issue: 1 |
|---|---|
| Ref: | Page 251 of 4 |

| Prepared by: Rhys Savage | Date: 17/10/2019 | Reviewed by | Date: |
|---|---|---|---|

**WORK DESCRIPTION:**

This Method Statement covers the following:

- Safe procedure for entry to a temperature-controlled room for experimental periods
- Experimental procedures in temperature-controlled rooms
- Geochemical testing

A comprehensive Risk Assessment is attached to this Method Statement.

Prior to any work commencing on these site activities, all operatives must have access permission from company management and must be made aware of the requirements of this Method Statement and the appropriate Risk Assessments.

**The methods detailed in this Method Statement will only be deviated from if authorised by Devin Sapsford, after consultation with Andrew Barnes, managing director of Geochemic ltd if necessary, and in such circumstances any variations must be recorded in writing and appended to this Method Statement.**

| AUTHORISATION | Date | Name (Print) | Signature |
|---|---|---|---|
| Prepared by: | 17/10/2019 | RHYS SAVAGE | |
| Revised by: | | | |
| Received by: | 20/10/2019 | DEVIN SAPSFORD | |

## 1.0 Brief Description of Works

Work within this project includes leaching of altered humidity cell tests on waste rock materials at Geochemic Ltd, Pontypool. The procedures in the test follow a novel altered version of standard ASTM D5744 − 18 (Standard Test Method for Laboratory Weathering of Solid Materials Using a Humidity Cell). Within the experiments, which will predominantly be carried out in temperature-controlled rooms and a geochemical laboratory, a 2 day testing cycling on a weekly basis will be carried out. Day 1 will include leaching of the humidity cells using de-ionised water, while day 2 will include collection of leachates, weighing of cells and analysis of cell leachates using standard geochemical testing methods.

## 2.0 Location of Works

Geochemic Ltd, Lower Race, Pontypool, Torfaen, Wales, NP4 5UH

## 3.0 Programme

Humidity cells will follow the humid and dry air cycles described in ASTM D5744 – 18 with the addition of $CO_2$ and $N_2$ to the compressed air supply. The air cycle will include 3 days of dry air followed by 3 days of humid air and a day for leaching. Leaching and collection of leachates will be carried out over 2 day periods (Monday and Tuesday) on a weekly basis over/ up to 18 months. The programme for days 1 and 2 are described below:

Day 1:

- Calibrate all equipment including scales and lab apparatus.
- Read and follow safe procedure protocols for entry to the warm and cold rooms for testing (See appendix 5)
- The gas supply, both $CO_2$ and $N_2$ will be switched off and checked by company operatives before leaching procedures.
- Once safe procedures have been followed weighing and leaching of the humidity cells will be carried out using a separatory funnel containing de-ionised water.
- The cells will be allowed to leach overnight.

Day 2:

- Calibrate all equipment including scales and lab apparatus.
- Read and follow safe procedure protocols for entry to the warm and cold rooms for testing (See appendix 5)
- The gas supply, both CO2 and N2 will be switched off and checked by company operatives before leaching procedures.
- Once safe procedures have been followed the leachates from the cells will be collected and weighed before being transferred to the geochemical lab for geochemical analysis.
- The cells will then be individually weighed and replaced in their rack position.
- Following collection of leachates, the cells will be replaced in their position in the rack (See appendix 1 and 2), before checks are carried out on gas seals and cell plumbing.
- Once the plumbing has been inspected the dry air cycle will resume and operatives will leave the temperature-controlled rooms.
- Geochemical analysis will then be carried out on the test leachates.

## 4.0 Special Conditions or Constraints

The carrying out of weekly procedures is dependent on safe $CO_2$ and $O_2$ levels within the warm and cold room environments (see risk assessment). If the safe levels specified within the risk assessment are not met then experimental procedures will not be carried out until deems safe by company supervisors.

CO2 sensors will be calibrated on a monthly time scale following company internal procedures.

## 5.0 Personal Protective Equipment (PPE).

**Minimum Site PPE Required**

- Steel toed boots / wellie (with steel midsole)
- Hand protection (Nitrile gloves or red nitrile dipped rigger gauntlets)
- Laboratory coat
- Eye protection
- Handheld $CO_2$ alarm

## 6.0 Supervision

The supervisor's onsite are: Andrew Barnes and Mark Roberts (Geochemic Ltd)

The works will be supervised by the Site Supervisor, and all communications must be relayed through the Site Supervisor, to the operatives (Rhys Savage). During experimental procedures in the warm and cold room there will be no lone working with 2 operatives needed to carry out work safely.

## 7.0 Training

No training will be required for this test work. At least one of the operatives will be first aid trained.

## 8.0 Inventory and Equipment

- Humidity cells
- $CO_2$/$N_2$ gases (Industrial grade)
- Nitrite gloves
- Acidified sample bottles
- De-ionised water supply.
- Humidity cell rack and plumbing.
- $CO_2$ and $O_2$ sensor.
- Calibrated scales
- 0.45 um syringe filters
- Syringes
- 1 litre collection bottles

**Full set up inventory can be found in standard ASTM D5744 – 18**

## 9.0 Working Methods/ Sequence of Work

9.1 Checks and pre commencement requirements

- Ensure all people involved in working on site have adequate PPE and have undergone the necessary inductions
- Read and follow safe procedure protocols for entry to the warm and cold rooms for testing (See appendix 5)
- The gas supply, both CO2 and N2 will be switched off and checked by company operatives before leaching procedures.
- Once safe procedures have been followed weighing and leaching of the humidity cells will be carried out using a separatory funnel containing de-ionised water.

9.2 Site establishment

The site is located within Geochemic Ltd.

9.3 Site Operations

Day 1:

- Calibrate all equipment including scales and lab apparatus.
- Read and follow safe procedure protocols for entry to the warm and cold rooms for testing (See appendix 5)
- The gas supply, both CO2 and N2 will be switched off and checked by company operatives before leaching procedures.
- Once safe procedures have been followed weighing and leaching of the humidity cells will be carried out using a separatory funnel containing de-ionised water.
- The cells will be allowed to leach overnight.

Day 2:

- Calibrate all equipment including scales and lab apparatus.
- Read and follow safe procedure protocols for entry to the warm and cold rooms for testing (See appendix 5)
- The gas supply, both CO2 and N2 will be switched off and checked by company operatives before leaching procedures.
- Once safe procedures have been followed the leachates from the cells will be collected and weighed before being transferred to the geochemical lab
- The cells will then be individually weighed and replaced in their rack position.
- Following collection of leachates, the cells will be replaced in their position in the rack (See appendix 1 and 2), before checks are carried out on gas seals and cell plumbing.
- Once the plumbing has been inspected the dry air cycle will resume and operatives will leave the temperature-controlled rooms.
- Geochemical analysis will then be carried out on the test leachates.

## 10 Health, Safety and Welfare

- All personnel will receive an induction. Records will be maintained on site.
- All site personnel will then be familiarised with the site and made aware of any hazards.

- All personnel involved in the works will be briefed in accordance with this method statement and the associated risk assessments.
- All operatives should follow the safe procedures for entry list that will be located on the door of each temperature controlled room (see appendix 4)
- All personnel will be equipped with appropriate PPE & RPE (if required).
- No eating or drinking on site. No smoking on site – use designated points, outside of the gate.
- No mobile phone use while working – move to a safe area.
- Welfare facilities are available for workers in the site, including:
    - Toilets
    - Washing facilities
    - Drinking water
    - Rest facilities

## 11 Emergency procedures

All the existing site emergency procedures will be reviewed and ensure that all of them are followed, and that relevant information is given to the people on site at time of induction or when changes are made to procedures.

The closest accident and emergency department: Royal Gwent Hospital

Royal Gwent Hospital Address and contact number:

Royal Gwent Hospital
Cardiff Road
Newport
NP20 2UB
Tel: 01633 23423

# Appendix 2 – Mineralogical Classification Scheme and Notes

This appendix contains the mineralogical classification notes and typical mineralogical compositions of target and gangue phases reported in this study. Analysis was undertaken at the Petrolab Ltd laboratory, Cornwall, UK.

**Classification Notes:**

- Traces of galena and sphalerite were identified using SEM-EDX analysis however no grains were observed optically.
- Identified albite also contains traces of orthoclase.
- Amphiboles in Sample A are generally composed of hornblende and form euhedral crystals as supported by optical petrography.
- Amphiboles in sample K are mostly fine grained, intergrown actinolite and tremolite which are altered from abundant clinopyroxenes in the sample to produce heavily altered gabbroic textures.
- Where individual crystals of temolite have been identified not as part of this alteration texture, a separate tremolite classification has been used.
- No sulfates were identified optically but traces grains fitting a gypsum classification were identified using SEM.
- Clinopyroxene is mostly composed of diopside with traces of hedenbergite.
- Chrome-magnetite is of magnetite composition and contains 10-20% Cr.

Table A2.1 – Mineral classification and group mineral compositions

| | **Minerals** | **SG** | **Group minerals / Typical composition** |
|---|---|---|---|
| **Target** | Pyrrhotite | 4.6 | $Fe_{(1-x)}S$ (x=0-0.17) |
| | Pyrite | 5.01 | $FeS_2$ |
| | Chalcopyrite | 4.19 | $CuFeS_2$ |
| | Pentlandite | 5.01 | $(Fe,Ni)_9S_8$ |
| | Calcite | 2.71 | $CaCO_3$ |
| | Dolomite | 2.85 | $CaMg(CO_3)_2$ |
| | Ankerite | 3.1 | $Ca(Fe,Mg)(CO_3)_2$ |
| | Galena | 7.4 | PbS |
| | Sphalerite | 4.08 | (Zn,Fe)S |
| **Gangue** | Clinopyroxene | 3.3 | $CaMgSi_2O_6$ |
| | Amphibole | 3.01 | See classification notes |
| | Orthopyroxene | 3.2 | $(Fe^{+},Mg)_2Si_2O_6$ |
| | Tremolite | 3.18 | $Ca_2Mg_5(Si_8O_{22})(OH)_2$ |
| | Chlorite | 2.8 | $(Mg,Al,Fe^{++})_{12}(Si,Al)_8O_{20}(OH)_8$ |
| | Albite | 2.6 | $NaAlSi_3O_8$ |
| | Goethite | 4.27 | FeOOH |

| | | | |
|---|---|---|---|
| | Serpentine | 2.65 | $Mg_3Si_2O_5(OH)_4$ |
| | Magnetite | 5.3 | $Fe_3O_4$ |
| | Biotite | 3 | $K(Fe,Mg)_3(AlSi_3O_{10})(OH)_2$ |
| | Anorthite | 2.76 | $CaAl_2Si_2O_8$ |
| | Hematite | 5.3 | $Fe_2O_3$ |
| | Quartz | 2.65 | $SiO_2$ |
| | Chrome-magnetite | 5.3 | $CrFe_3O_4$ |
| | Sulfates | 1.90 - 3.10 | See classification notes |
| | Olivine | 3.2 | $(Mg,Fe)_2SiO_4$ |
| | Ilmenite | 4.27 | $Fe^{++}TiO_3$ |
| | Accessory Phases | 2.80 - 5.15 | See classification notes |
| | Titanomagnetite | 5.3 | $Fe^{2+}(Fe^{+},Ti)_2O_4$ |
| | Muscovite | 2.83 | $KAl_2(Si_3Al)O_{10}(OH,F)_2$ |
| | Kaolinite_Illite | 2.63 | Fine-grained clays |
| | Arsenopyrite | 6.07 | FeAsS |

# Appendix 3 – Mineralogical and petrographic images

This appendix contains images collected as part of the mineralogical and petrographic analysis carried out by Petrolab Ltd. Further details on the methods used within this analysis can be found in Chapter 4 of this thesis. Selective detailed descriptions of petrographic observations are given for select samples from each composite material. Petrographic observations were carried out for samples K-Pre, A-Pre, K02, A02, K05, A05, K08 and A08.

Images in this appendix for all assessed samples include:

- A photo of the sample as received.
- A low magnification image (10mm)
- A general view image thin section (1mm)
- A cross polarised thin section image (1mm)
- A reflective light thin section image (1mm)

**Pre HCT-Composite Waste Rock Observations – Kevitsa**

The K-Pre sample presented for petrographic mineralogical assessment is shown as received in Figure A3.6, while a low magnification view of sample thin section can be seen in Figure A3.7. This sample is predominantly composed of gabbroic fragments (websterite to olivine websterite in composition) containing abundant clinopyroxene which is readily altered to amphiboles intergrown with clays (illite) and tremolite/actinolite which falls under the amphibole group as alteration from clinopyroxene. Orthopyroxene is also observed as well as traces of olivine which is readily altered to serpentine, iddingsite and chlorite down their abundant irregular fracture planes. Thin veinlets of goethite and magnetite also form along the olivine fracture planes, and fragments readily spall down these planes breaking the gabbroic fragments apart. Traces of biotite were also observed locked in gabbroic fragments, and very rare diorite fragments were identified.

Sulphides include pyrrhotite, pyrite, chalcopyrite and traces of pentlandite which are all variably distributed throughout the gabbroic texture. They may preferentially occur interstitially between pyroxene and olivine junctions but are also observed peppered throughout the texture possibly as an overprint texture. Rarely sulphides occur in a similar

fashion to iron oxides down olivine fracture planes. One occurrence of covellite was observed as an oxidation surrounding a liberated chalcopyrite fragment. Pentlandite is rare and usually forms acicular elongate crystals hosted within pyrrhotite. The sample contains more sulphides than carbonates and therefore may be potentially acid generating.

It can be seen in Figures A3.7 and A3.8 that this sample was abundant in fragments of gabbro, composed of clinopyroxene (cpx) and orthopyroxene (opx). Fractures in weathered pyroxenes and residual olivine are infilled with limonite (lm) and chlorite (chl) respectively. The reflected light image shown in Figure A3.9 displays commonly locked grains of pyrrhotite (po) with rarer intergrown chalcopyrite (cpy).

**Pre HCT-Composite Waste Rock Images – Aitik**

Fragments in this sample include primarily quartz-mica schists with rare garnet-mica schists which are all heavily foliated showing high degrees of metamorphism. Minerals present include quartz, feldspars (~27% albite and 13% anorthite as determined using SEM-EDX analysis), muscovite, biotite, and amphiboles. Foliations are peppered with epidote and clinozoisite evidencing hydrothermal calcic replacement of the schists. Traces of high-grade amphibolite were also present. Diorite fragments were also present composed of feldspars, amphiboles, quartz and biotite.

Sulphides include pyrite and pyrrhotite which are commonly coarse, euhedral and liberated. These are mainly derived from diorite fragments. The majority of schists are peppered with magnetite which forms subhedral grains usually elongate parallel to foliation. Figures A3.1 and A3.2 display a general view of the sample showing diorite and schist fragments. The schist contains abundant platy muscovite (ms) which is strongly foliated and folded, with rarer biotite (bt). The presence of garnets (grt) also indicates a high degree of metamorphism. The reflected light image shown in Figure A3.5 displays coarse liberated pyrite (py) and magnetite (mag), with rare, locked chalcopyrite (cpy) within composite fragments.

### *Post HCT Composite Waste Rock Observations – Kevitsa*

**Post HCT Sample K02**

Materials recovered from Kevitsa HCT cell K02 are predominantly composed of gabbroic fragments (websterite to olivine websterite in composition) containing abundant clinopyroxene which is readily altered to amphiboles (actinolite/tremolite) intergrown with clays (illite). Orthopyroxene is also observed as well as traces of olivine which is readily altered to serpentine, iddingsite and chlorite down their abundant irregular fracture planes. Thin veinlets of goethite and magnetite also form along the olivine fracture planes, and fragments readily spall down these planes breaking the gabbroic fragments apart. Rare feldspars are observed forming an ophitic texture surrounding smaller clinopyroxenes. Traces of biotite were also observed locked in gabbroic fragments, and very rare diorite fragments were identified.

Sulphides include pyrrhotite, pyrite, chalcopyrite, and traces of pentlandite which are all variably distributed throughout the gabbroic texture. They may preferentially occur interstitially between pyroxene and olivine junctions but are also observed peppered throughout the texture possibly as an overprint texture. Rarely sulphides occur in a similar fashion to iron oxides down olivine fracture planes. One occurrence of covellite was observed as an oxidation surrounding a liberated chalcopyrite fragment. Pentlandite is rare and usually forms acicular elongate crystals hosted within pyrrhotite. Magnetite was observed surrounding several grains of pyrrhotite and chalcopyrite which may be from oxidation of the original sulphides. It can be seen in the cross polarised thin section image shown in Figure A3.14 that sample K02 displays gabbroic fragments composed of clinopyroxene (cpx), orthopyroxene (opx) and partly serpentinised olivine's (ol). Multiple fractures in the olivine's are infilled by iron oxides. Identified sulfide minerals can be seen in Figure A3.15. This reflected light thin section identified a composite mass of magnetite (mag) with residual pyrrhotite (po) cores and finer grained chalcopyrite (cpy). Finely disseminated pentlandite (pn) was also observed.

**Post HCT Sample K05**

Similarly to samples K-Pre and K02, materials recovered from HCT K02 was predominantly composed of gabbroic fragments (websterite to olivine websterite in composition) containing abundant clinopyroxene which are heavily altered to amphiboles (actinolite/tremolite). Orthopyroxene is also observed as well as traces of olivine which is readily altered to serpentine, iddingsite and chlorite down their abundant irregular fracture planes. Thin veinlets of goethite and magnetite also form along the olivine fracture planes. Traces of biotite were also observed locked in gabbroic fragments.

Sulphides include pyrrhotite, pyrite, chalcopyrite and traces of pentlandite which are all variably distributed throughout the gabbroic texture. The majority of sulphides appear clean and unaltered, mostly occurring near serpentinised olivine's. It is shown in Figure A3.20 that numerous locked grains of pyrrhotite (po) with intergrown finer grained chalcopyrite (cpy) was observed. Fine needles of pentlandite (pn) were also observed intergrown in the pyrrhotite Pentlandite is rare and usually forms acicular elongate crystals hosted within pyrrhotite. Magnetite was observed surrounding several grains of pyrrhotite and chalcopyrite which may be from oxidation of the original sulphides. The cross polarised thin section of sample K05, shown in Figure A3.19, showing gabbroic fragments composed of clinopyroxene (cpx) and heavily fractured partly serpentinised olivine's (ol) with fractures infilled by iron oxides (FeO).

**Post HCT Sample K08**

K-TC3 sample K08 showed minimal observable mineralogical alteration compared to K-Pre, with this sample also predominantly composed of gabbroic fragments (websterite to olivine websterite in composition) containing abundant clinopyroxene. These clinopyroxenes are readily altered to amphiboles intergrown with clays (illite) and tremolite/actinolite which falls under the amphibole group as alteration from clinopyroxene. Orthopyroxene is also observed as well as traces of olivine which is readily altered to serpentine, iddingsite and chlorite down their abundant irregular fracture planes.

Clear gabbroic fragments composed of clinopyroxene (cpx), orthopyroxene (opx) and partly serpentinised olivine's (ol), can be seen in the cross polarised thin section of sample K08, see Figure A3.24. Multiple fractures in the olivines are infilled by iron oxides

and altered to green clays of iddingsite (idd). Patches of alteration to clays/tremolite were also observed in multiple fragments. Thin veinlets of goethite and magnetite also form along the olivine fracture planes, and fragments readily spall down these planes breaking the gabbroic fragments apart. Traces of biotite were also observed locked in gabbroic fragments, and very rare diorite fragments were identified.

Sulphides include pyrrhotite, pyrite, chalcopyrite and traces of pentlandite which are all variably distributed throughout the gabbroic texture. They may preferentially occur interstitially between pyroxene and olivine junctions but are also observed peppered throughout the texture possibly as an overprint texture. Pentlandite is rare and usually forms acicular elongate crystals hosted within pyrrhotite. The reflected light image of sample K08, see Figure A3.25, displayed heavily cleaved pyrrhotite (po) with abundant fractures, patches of oxidation to pyrite (py) and rare goethite (gt) oxide rims. It is likely that this alteration of pyrrhotite has derived from the leaching process.

**Post HCT Composite Waste Rock Observations – Aitik**

Petrographic mineralogical observations are provided for post HCT samples A02, A05 and A07 within this section. Cross polarised thin section and reflected light thin section images are presented.

**Post HCT Sample A02**

Sample A02 included primarily quartz-mica schists with rare garnet-mica schists which are all heavily foliated showing high degrees of metamorphism. Minerals present included quartz, feldspars (~32% albite and 7% anorthite as determined using SEM-EDX analysis), muscovite, biotite, and amphiboles. This sample contained notably less anorthite than the pre HCT Aitik sample A-Pre. Foliations are peppered with epidote and clinozoisite evidencing hydrothermal calcic replacement of the schists. Traces of high-grade amphibolite were also present. Diorite fragments were also present composed of feldspars, amphiboles, quartz and biotite. The cross polarised image of this sample, see Figure A3.29, showed abundant garnet-mica schist fragments. The schist contains abundant platy biotite (bt) which is strongly foliated, and coarse garnets (grt). Rare fragments of diorite were observed containing amphiboles (amph).

Sulphides include pyrite and pyrrhotite which are commonly coarse, euhedral and liberated. These are mainly derived from diorite fragments. Rare magnetite is observed rimming chalcopyrite and some pyrite grains show mottled textures and patches of oxidation. Reflective light thin sections of this sample, see Figure A3.30, identified liberated pyrite (py) and magnetite (mag). The pyrite contains rare finely disseminated blebs of chalcopyrite (cpy). Most schists within this sample are peppered with magnetite which forms subhedral grains usually elongate parallel to foliation. One diorite fragment observed contained a portion of calcite vein suggesting there is later stage crosscutting carbonate veins which may raise the potential for acid neutralisation. However, the sample still contains more sulphides than carbonates and therefore may be potentially acid generating, purely based on mineralogical characterisation.

**Post HCT Sample A05**

Sample K05 include primarily quartz-mica schists with rare garnet-mica schists which are all heavily foliated showing high degrees of metamorphism. Minerals present included quartz, feldspars (~27% albite and 8% anorthite as determined using SEM-EDX analysis), muscovite, biotite, and amphiboles. Foliations are peppered with epidote and clinozoisite evidencing hydrothermal calcic replacement of the schists. The cross polarised image shown in Figure A3.34 cleared demonstrated diorite and schist fragments. The schist contains abundant platy biotite (bt) which is strongly foliated. Some fragments contain coarse euhedral crystals of magnetite (mag). Some feldspar fragments are very coarse (< 4 mm) and are possibly derived from coarser granites of pegmatites. Diorite fragments were also present composed of feldspars, amphiboles, quartz and biotite. Sulphides include coarse euhedral pyrite found in both schist and diorite fragments. Chalcopyrite is commonly observed surrounding the coarser pyrite crystals. The reflected light image shown in Figure A3.35 shows subhedral grains of pyrite (py) and chalcopyrite (cpy) within schist fragments.

**Post HCT Sample A08**

As was noted in other Aitik samples, sample A08 displays fragments that include primarily quartz-mica schists with rare garnet-mica schists which are all heavily foliated showing high degrees of metamorphism. Minerals present include quartz, feldspars (~27% albite and 8% anorthite as determined using SEM-EDX analysis), muscovite, biotite, and amphiboles. It can be seen in Figure A3.39 that observed schists contain abundant platy

muscovite (ms) which is strongly foliated and folded, biotite (bt) containing inclusions of magnetite. Diorite fragments contain abundant amphiboles (amph). Foliations are peppered with epidote and clinozoisite evidencing hydrothermal calcic replacement of the schists. Rare fragments of higher-grade amphibolite's were also observed. Diorite fragments were also present composed of feldspars, amphiboles, quartz and biotite. Sulphides include coarse euhedral pyrite found in both schist and diorite fragments. Chalcopyrite is commonly observed surrounding the coarser pyrite crystals. Figure A3.40 displays an abundance of subhedral grains of magnetite (mag) with small rims of haematite (hm). Schist fragments typically contain a high abundance of magnetite which are coarse and elongate parallel to foliation. These coarse grains appear to have very thin rims and small exsolutions of haematite.

Figure A3.1 - Sample GCL0100-A-PRE - Photograph of sample as received (scale in cm).

Figure A3.2 - Sample GCL0100-A-PRE - Low magnification view of sample thin section.

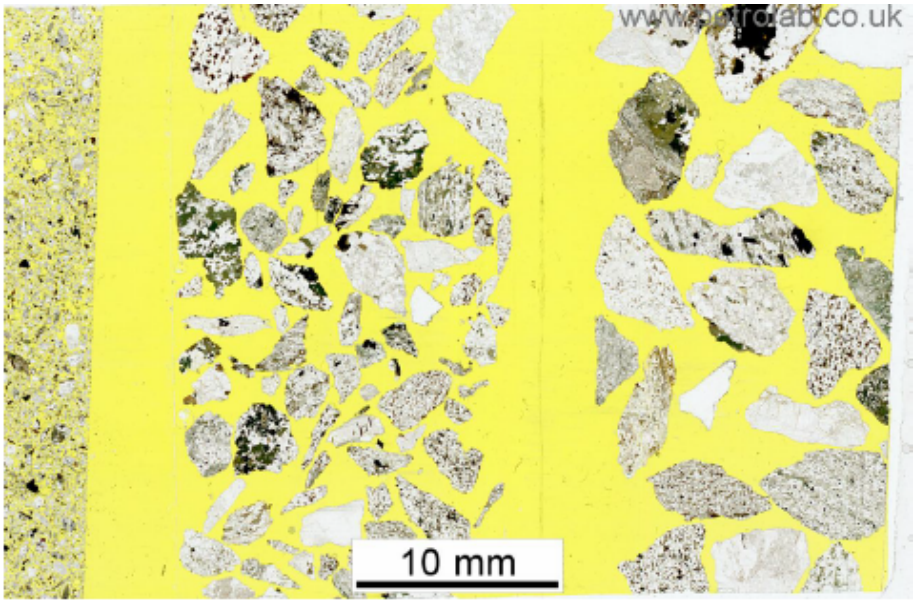


Figure A3.3 - Sample GCL0100-A-PRE - General view of sampe.

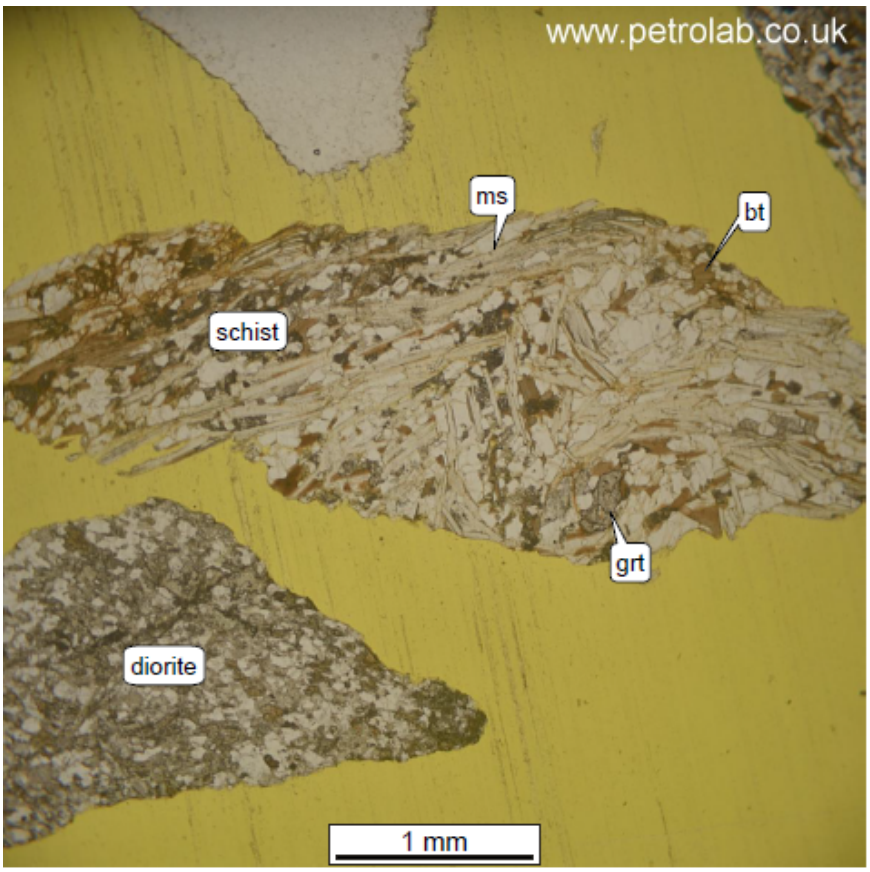

Figure A3.4 - Sample GCL0100-A-PRE - Cross polarised light image of previous photo.

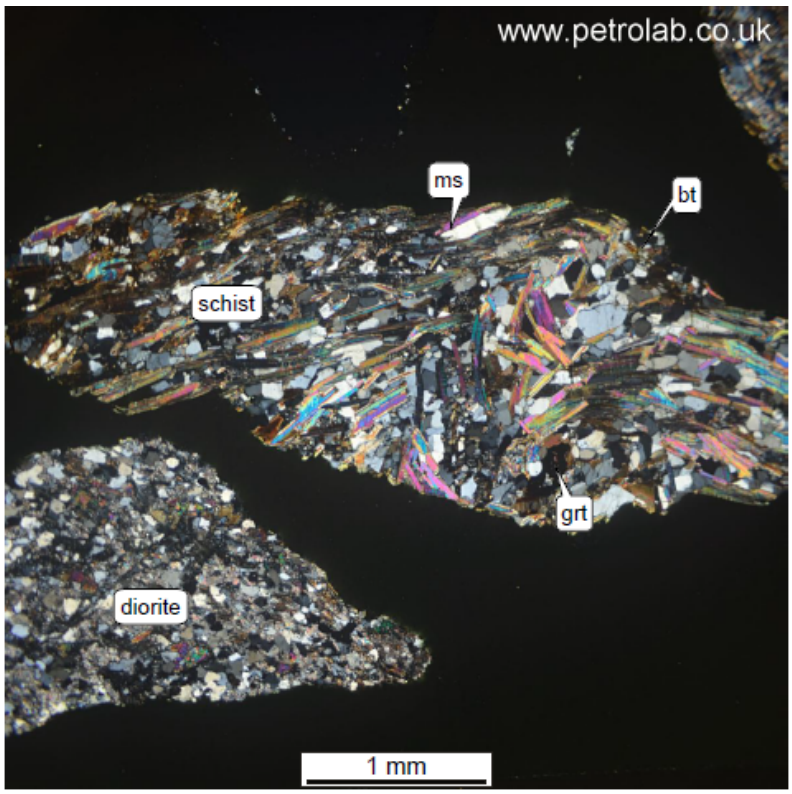


Figure A3.5 - Sample GCL0100-A-PRE - Reflected light image.

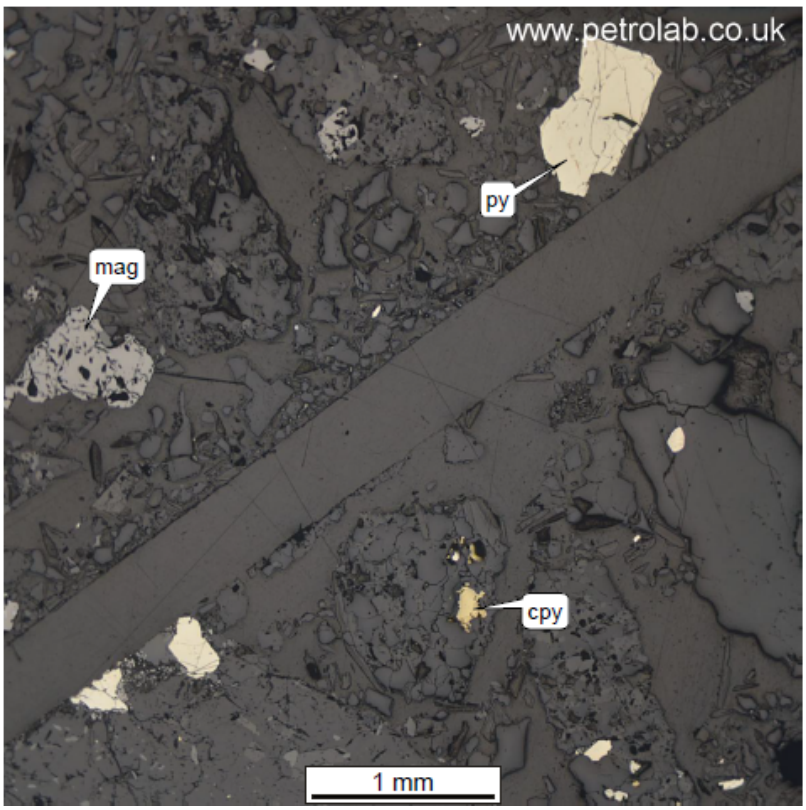

Figure A3.6 - Sample GCL0100-K-PRE - Photograph of sample as received (scale in cm).


Figure A3.7 - Sample GCL0100-K-PRE - Low magnification view of sample thin section.

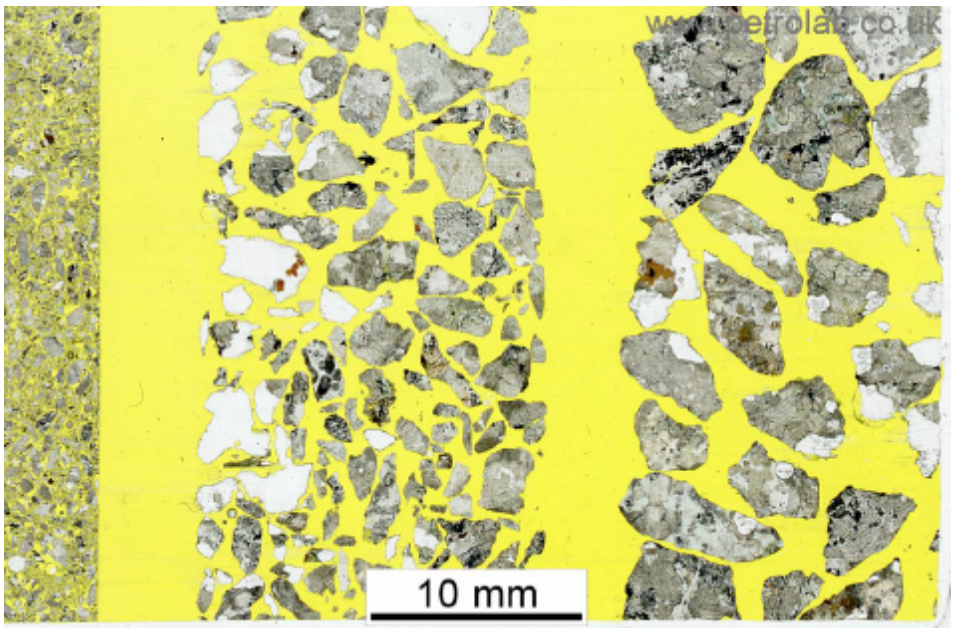

Figure A3.8 - Sample GCL0100-K-PRE - General view of sample.

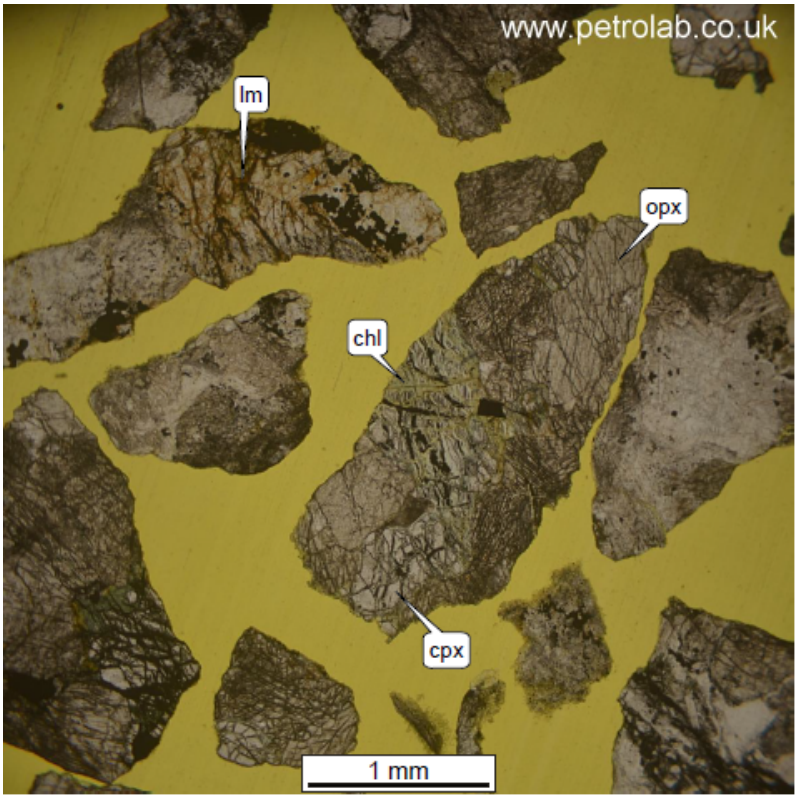


Figure A3.9 - Sample GCL0100-K-PRE - Cross polarised light image of previous photo.

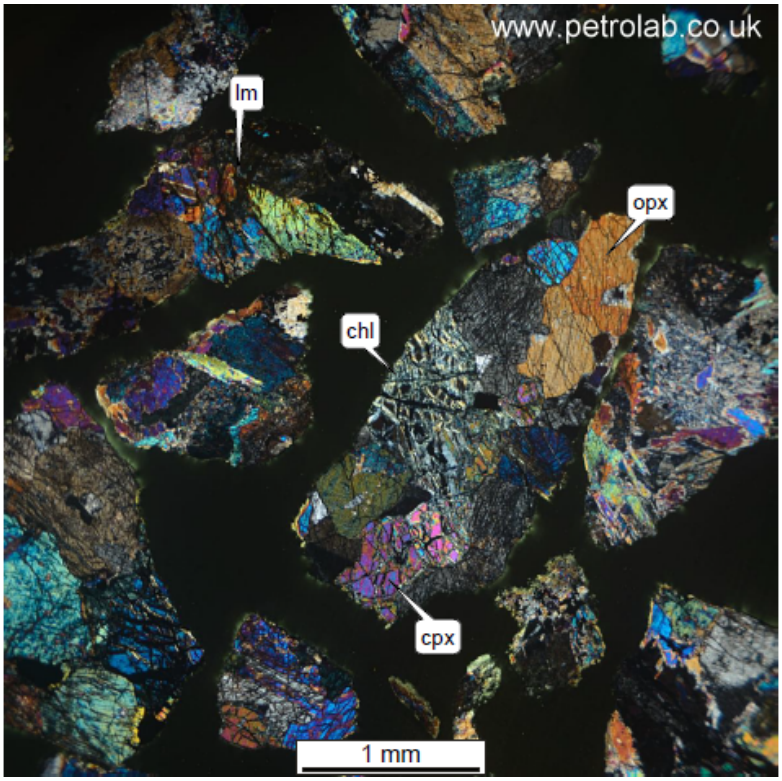

Figure A3.10 - Sample GCL0100-K-PRE - Reflected light image.

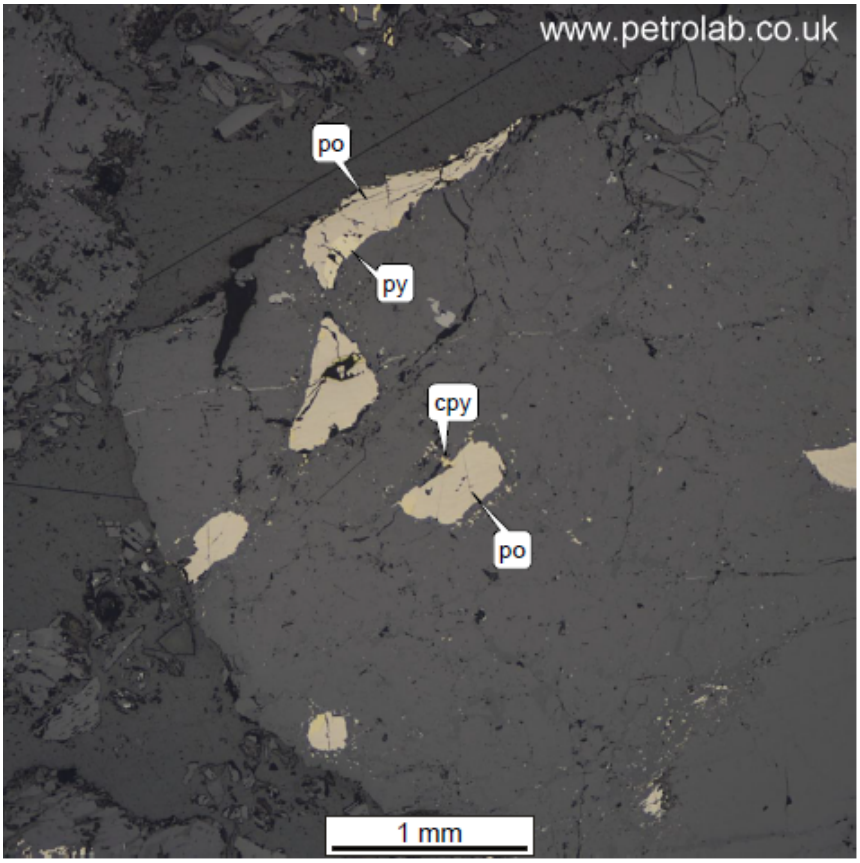


Figure A3.11 - Sample GCL0100-K02-Post - Photograph of sample as received (scale in cm).

Figure A3.12 - Sample GCL0100-K02-Post - Low magnification view of sample thin section.

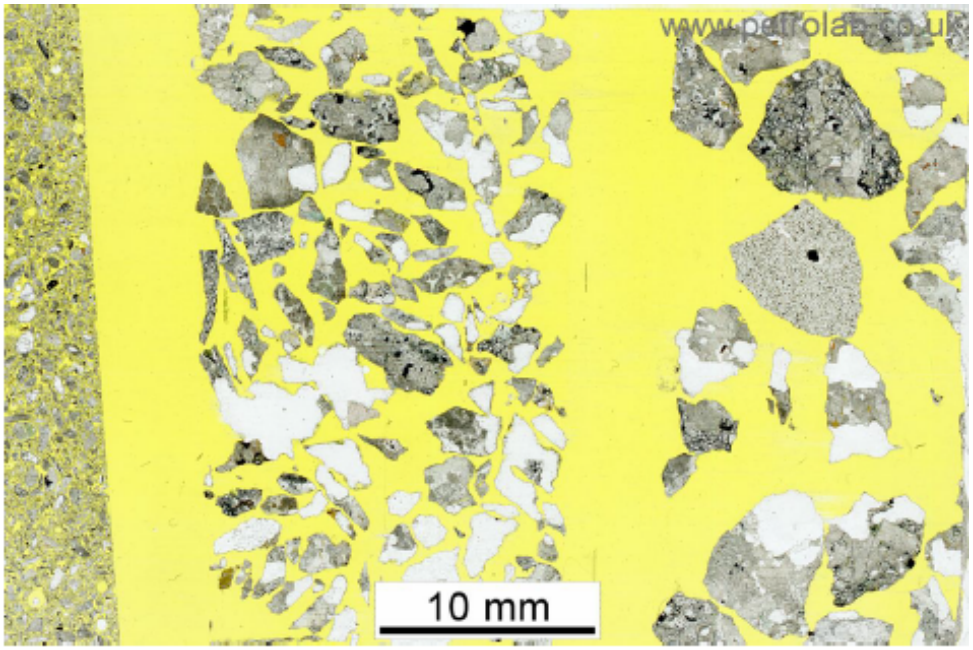


Figure A3.13 - Sample GCL0100- K02-Post - General view of sample.

Figure A3.14 - Sample GCL0100- K02-Post - Cross polarised light image of previous photo.


Figure A3.15 - Sample GCL0100- K02-Post - Reflected light image.

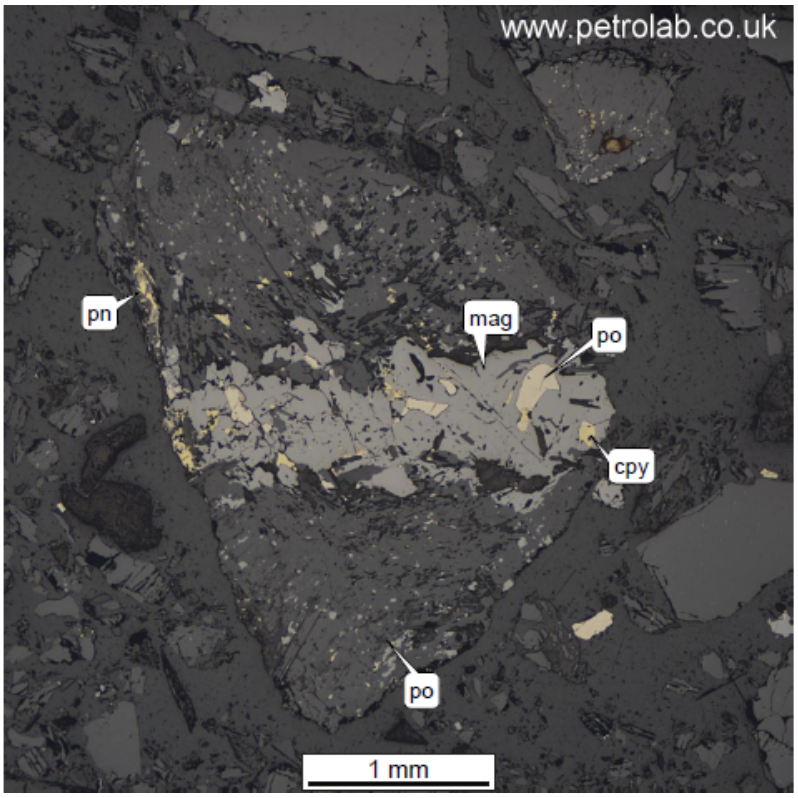

Figure A3.16 - Sample GCL0100-K05-Post - Photograph of sample as received (scale in cm).

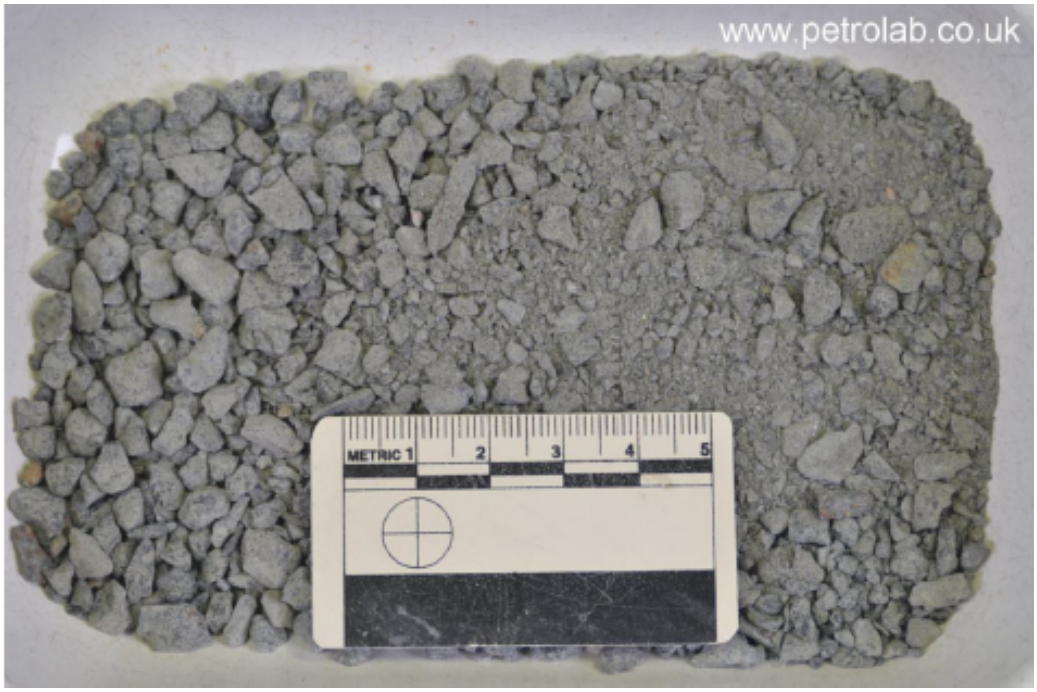


Figure A3.17 - Sample GCL0100-K05-Post - Low magnification view of sample thin section.

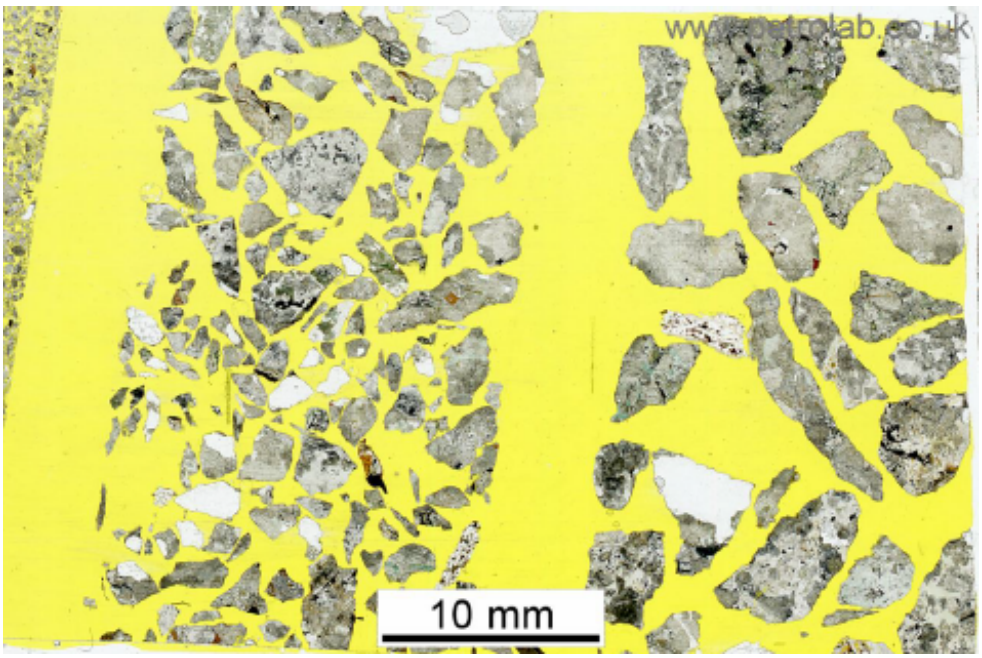

Figure A3.18 - Sample GCL0100- K05-Post - General view of sample.


Figure A3.19 - Sample GCL0100- K05-Post - Cross polarised light image of previous photo.

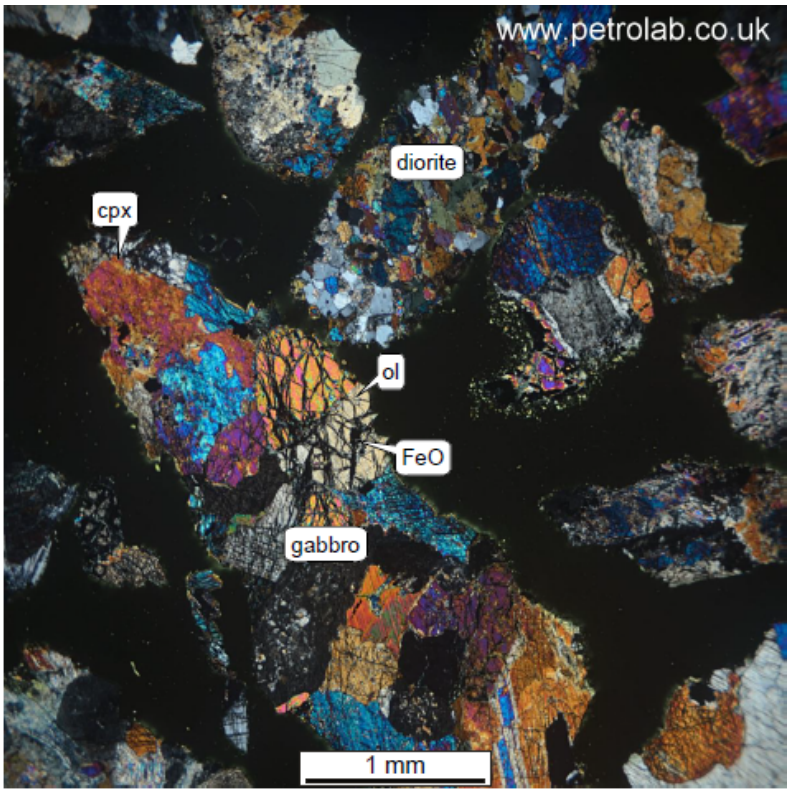

Figure A3.20 - Sample GCL0100- K05-Post - Reflected light image.

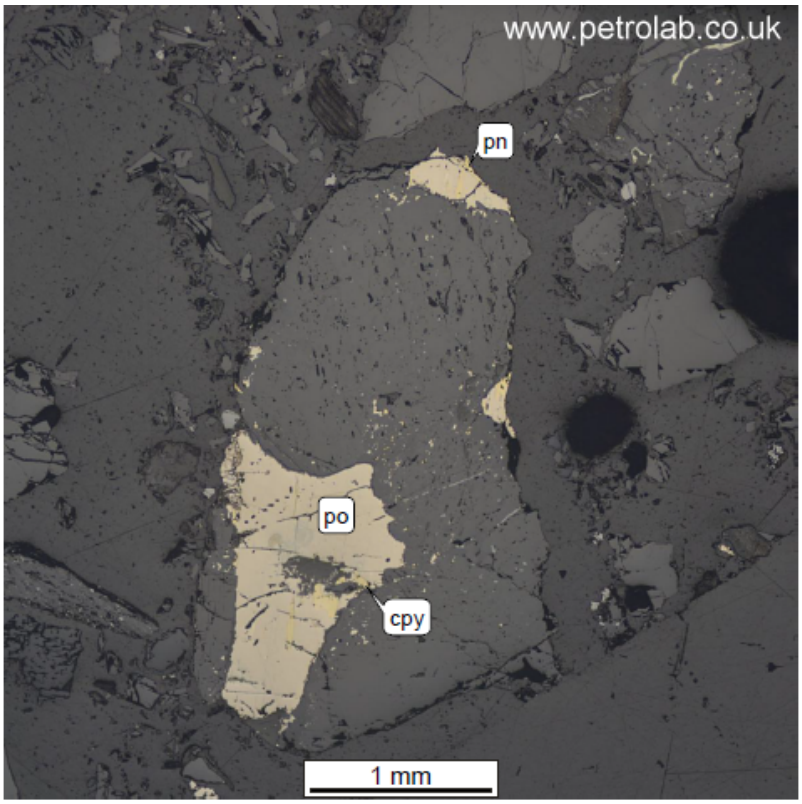


Figure A3.21 - Sample GCL0100-K08-Post - Photograph of sample as received (scale in cm).

Figure A3.22 - Sample GCL0100-K08-Post - Low magnification view of sample thin section.

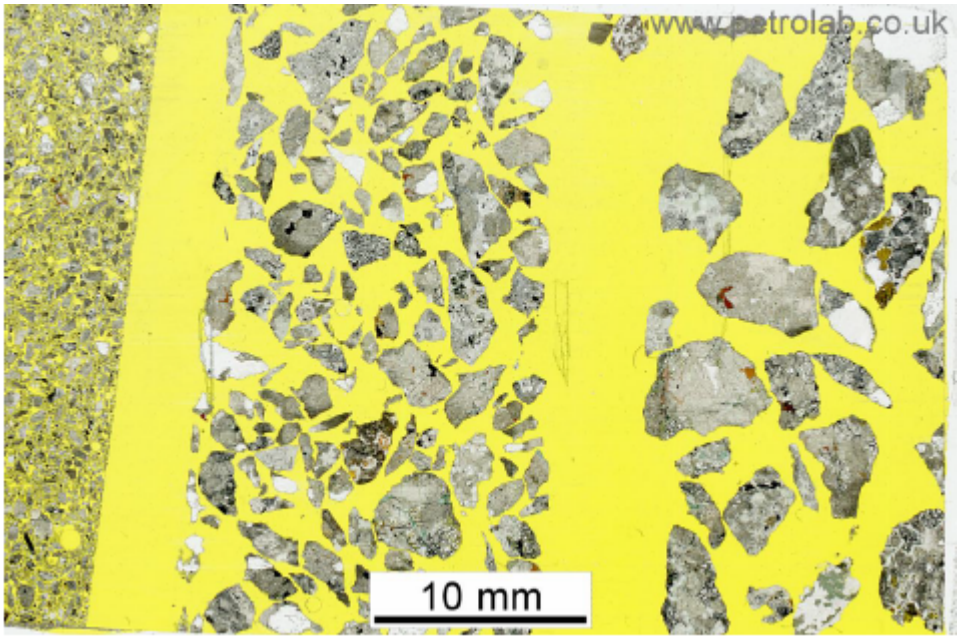


Figure A3.23 - Sample GCL0100- K08-Post - General view of sample.

Figure A3.24 - Sample GCL0100- K08-Post - Cross polarised light image of previous photo.

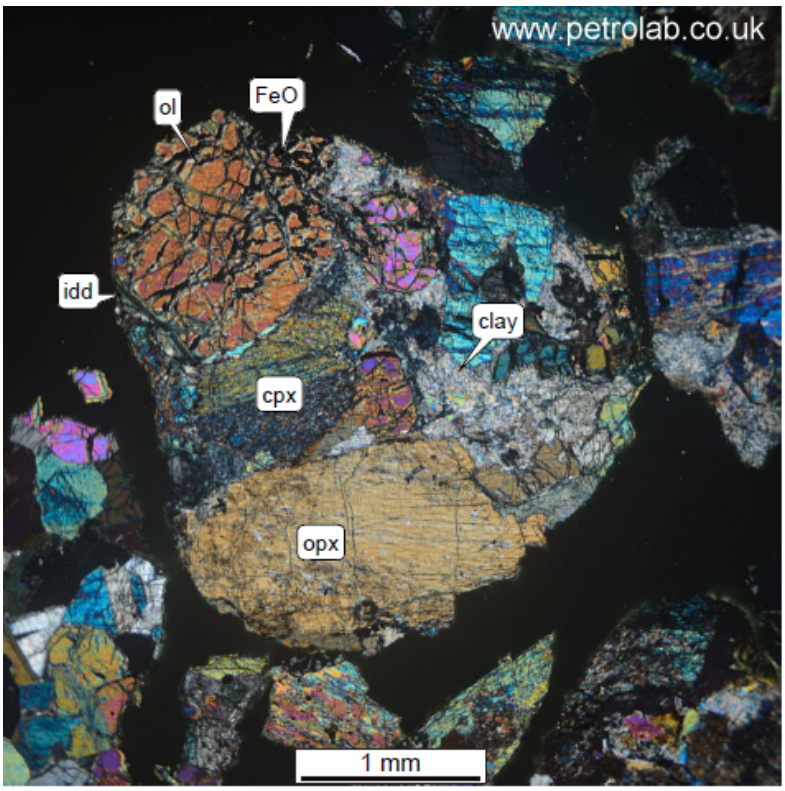


Figure A3.25 - Sample GCL0100- K08-Post - Reflected light image.

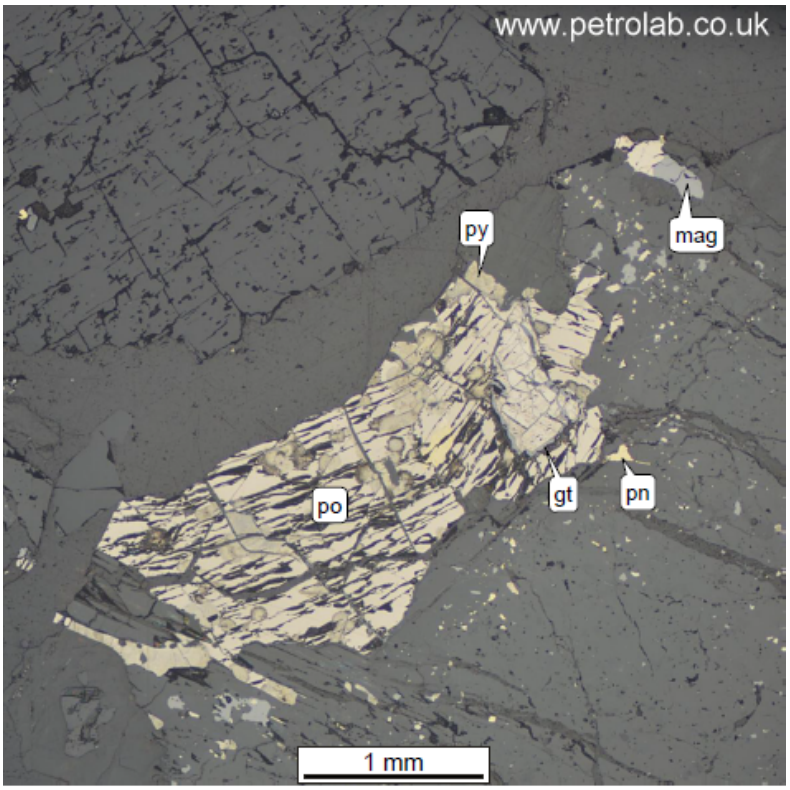

Figure A3.26 - Sample GCL0100-A02-Post - Photograph of sample as received (scale in cm).


Figure A3.27 - Sample GCL0100-A02-Post - Low magnification view of sample thin section.

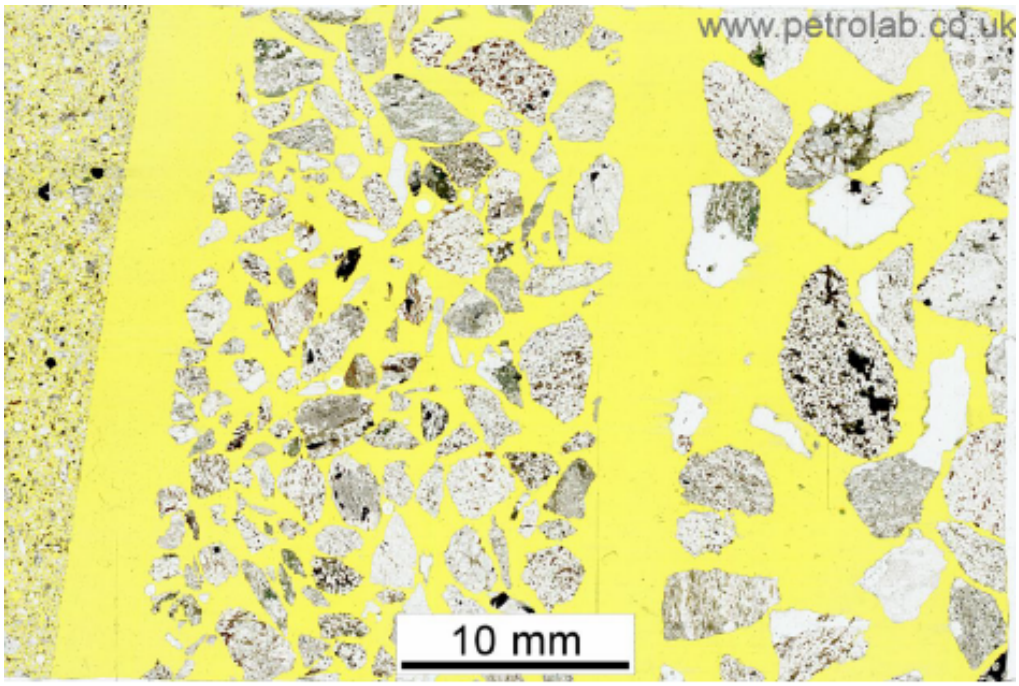

Figure A3.28 - Sample GCL0100- A02-Post - General view of sample.

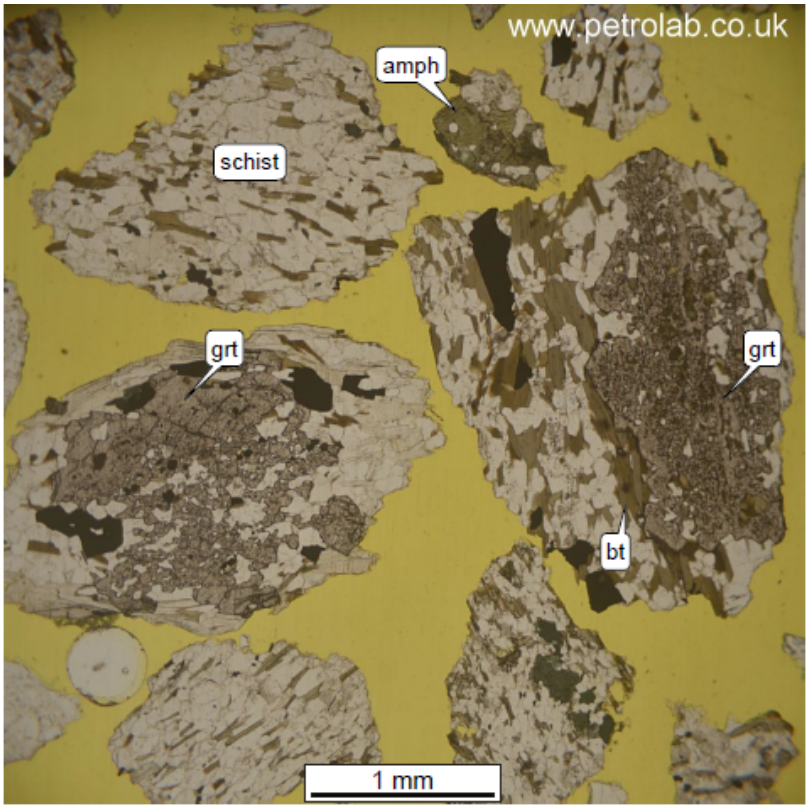


Figure A3.29 - Sample GCL0100- A02-Post - Cross polarised light image of previous photo.

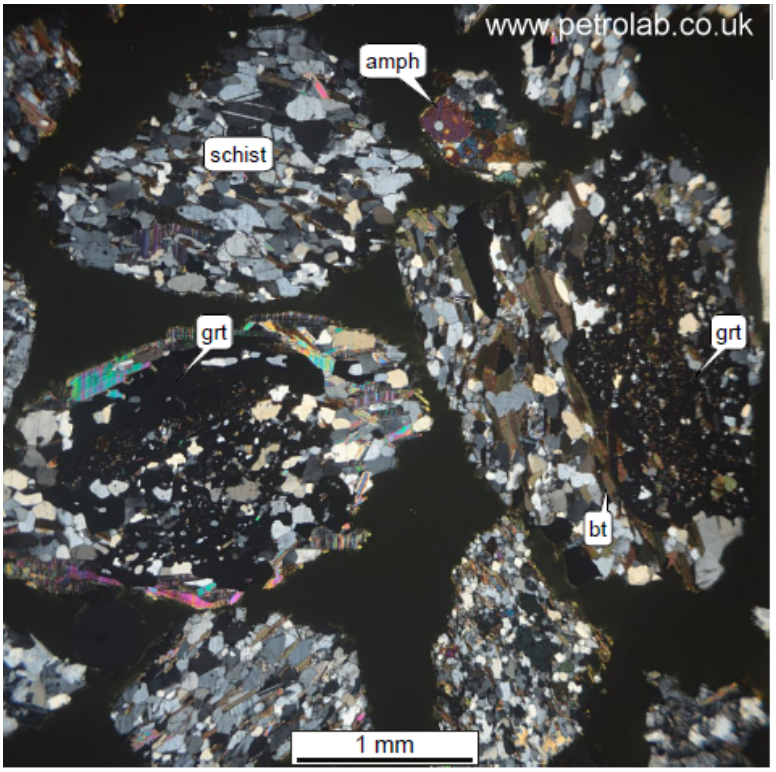

Figure A3.30 - Sample GCL0100- A02-Post - Reflected light image.

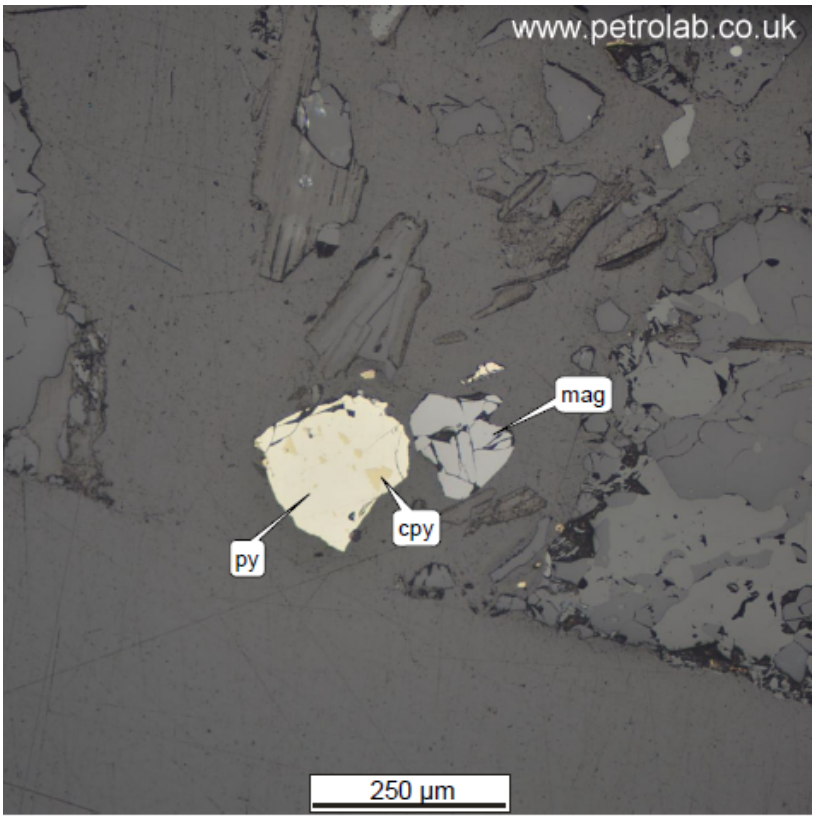


Figure A3.31 - Sample GCL0100-A05-Post - Photograph of sample as received.

Figure A3.32 - Sample GCL0100-A05-Post - Low magnification view of sample thin section.

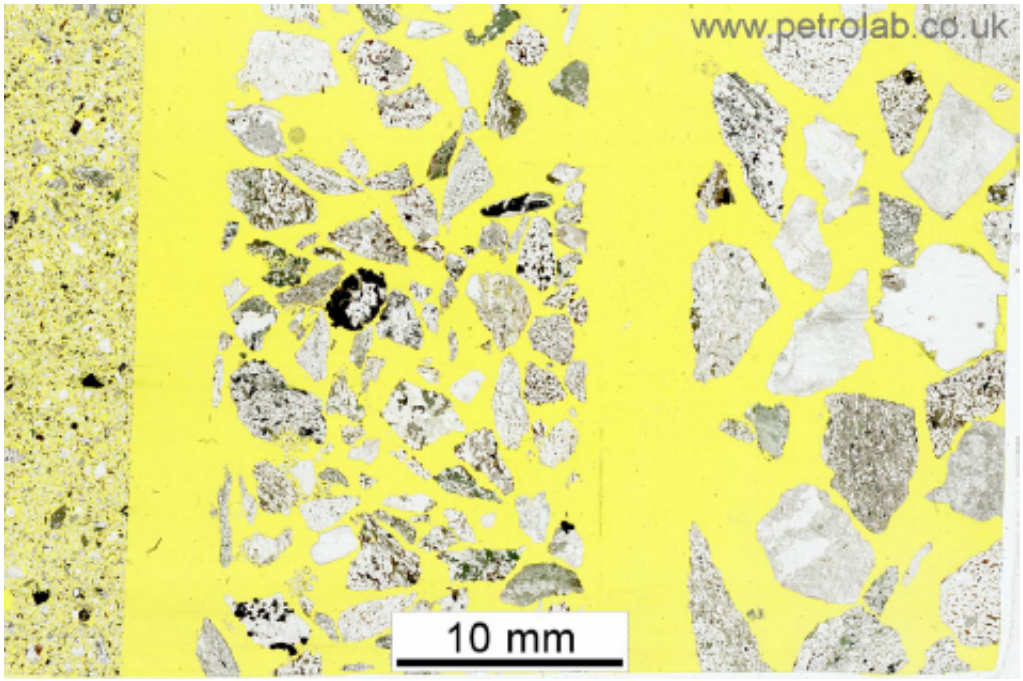


Figure A3.33 - Sample GCL0100- A05-Post - General view of sample

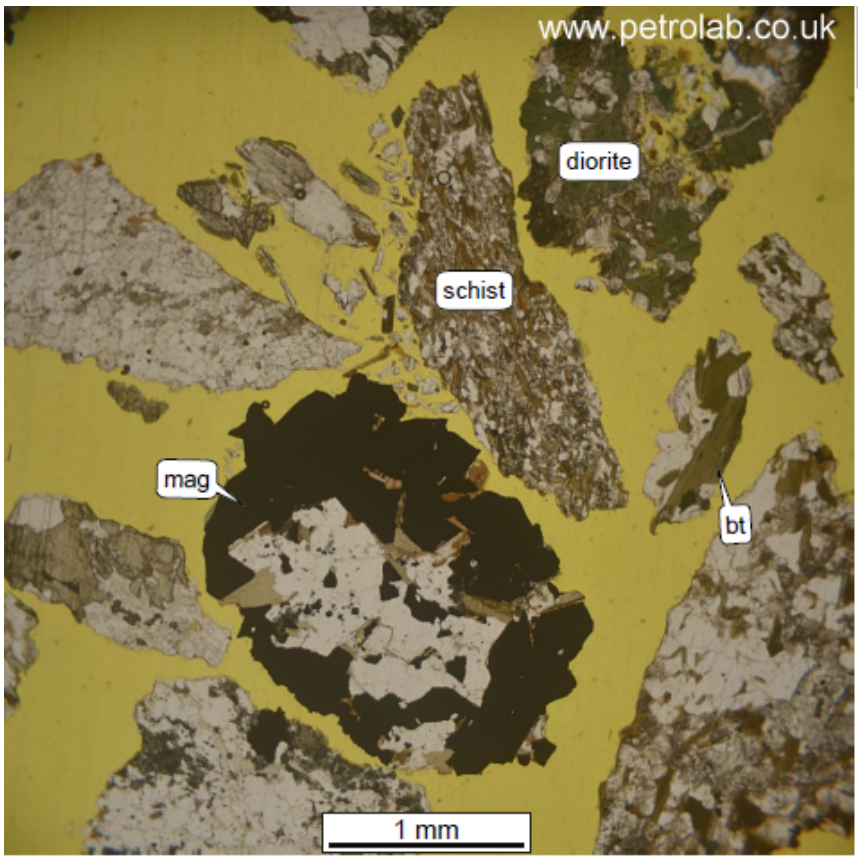

Figure A3.34 - Sample GCL0100- A05-Post - Cross polarised light image of previous photo.

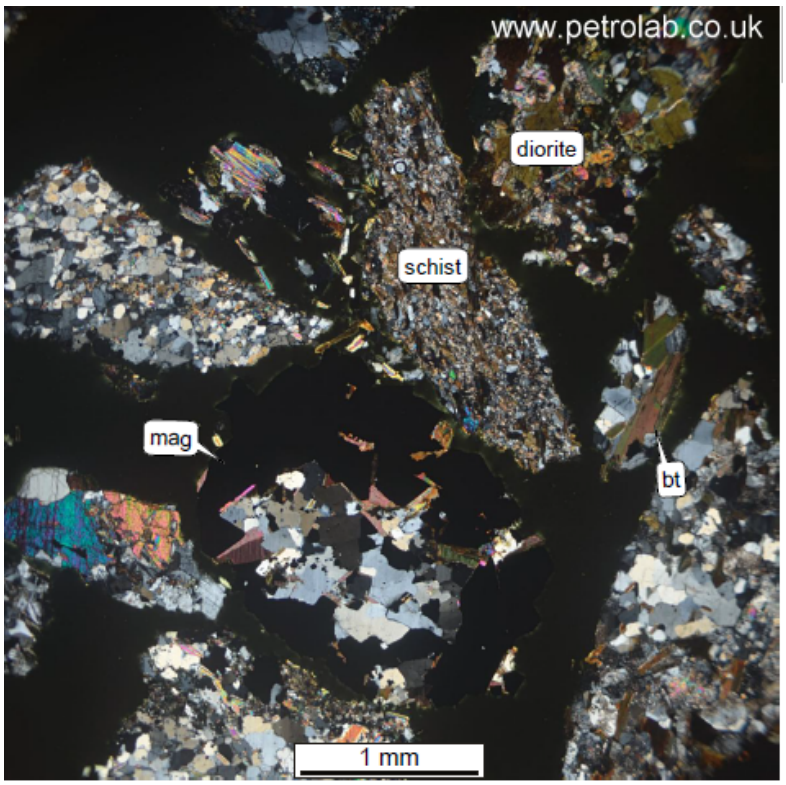


Figure A3.35 - Sample GCL0100- A05-Post - Reflected light

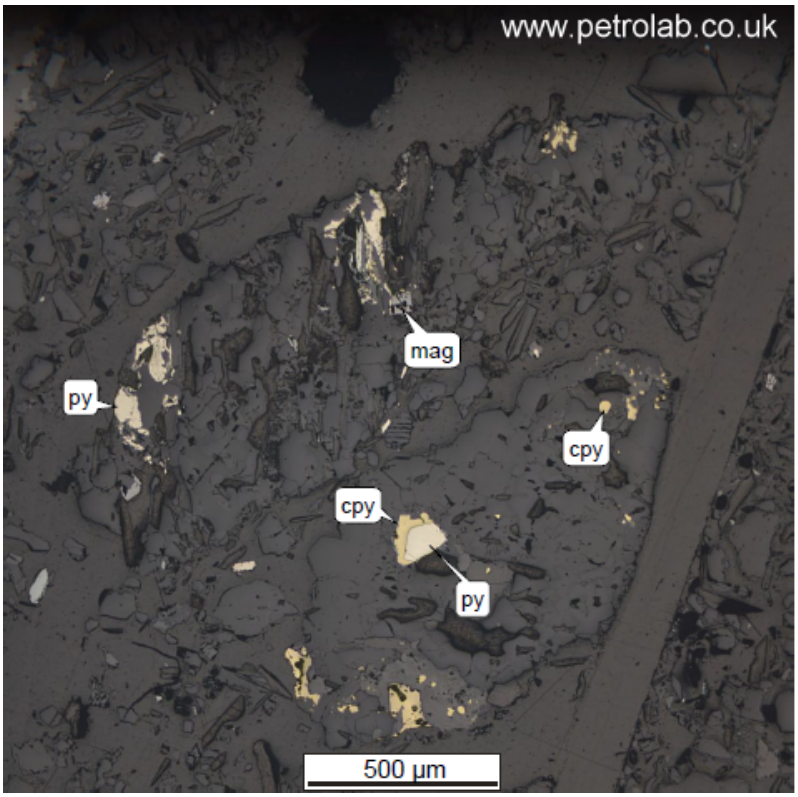

Figure A3.36 - Sample GCL0100-A08-Post - Photograph of sample as received (scale in cm).


Figure A3.37 - Sample GCL0100-A08-Post - Low magnification view of sample thin section.

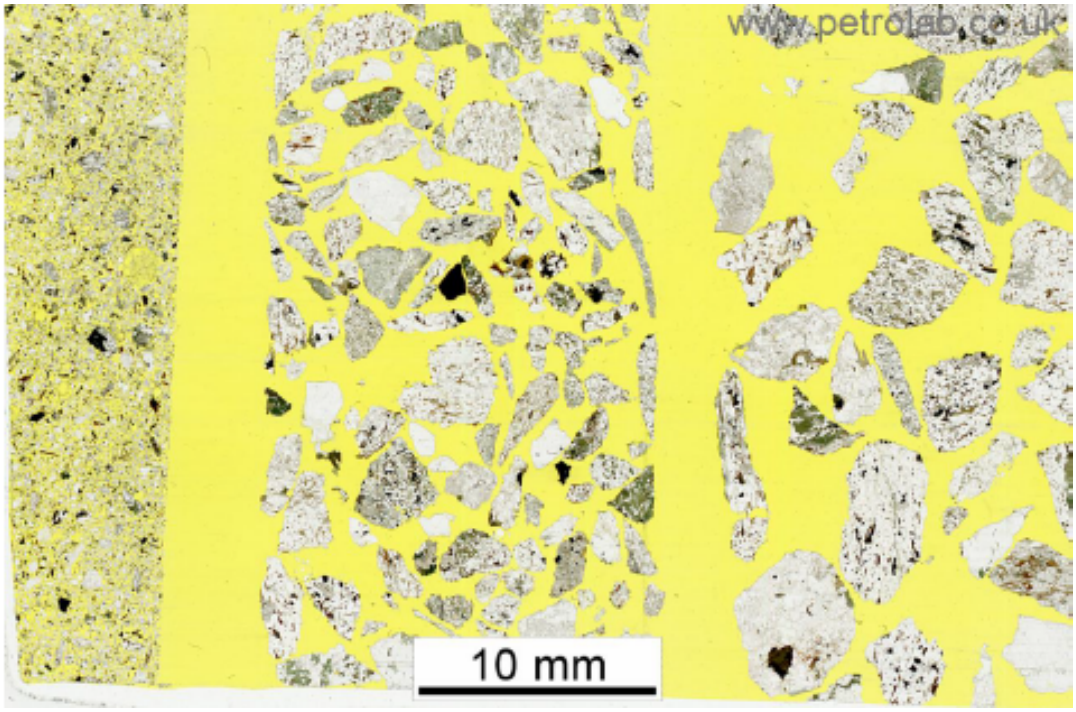

Figure A3.38 - Sample GCL0100- A08-Post - General view of sample.

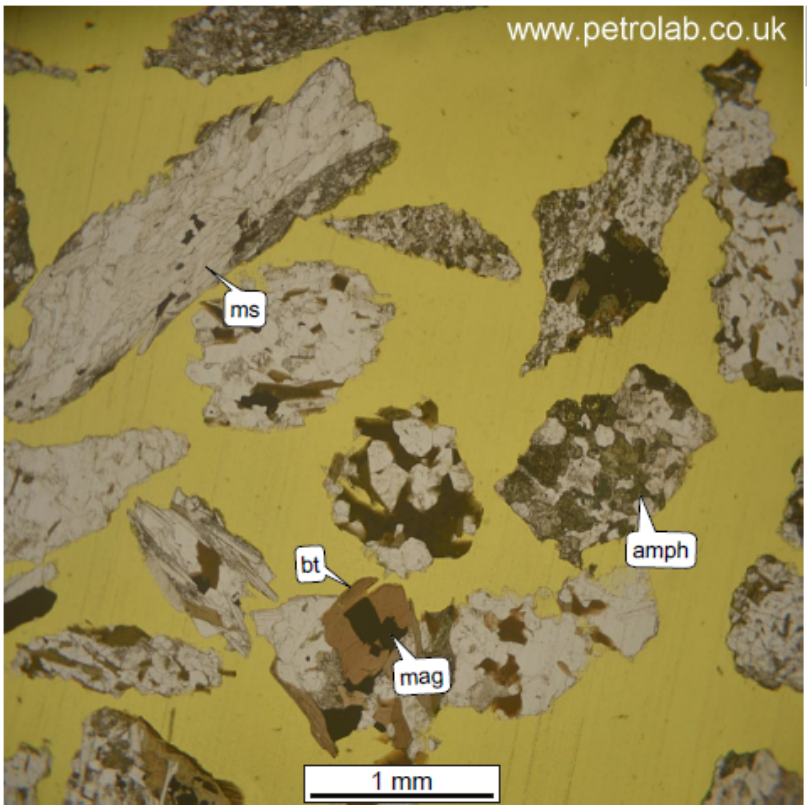


Figure A3.39 - Sample GCL0100- A08-Post - Cross polarised light image of previous photo

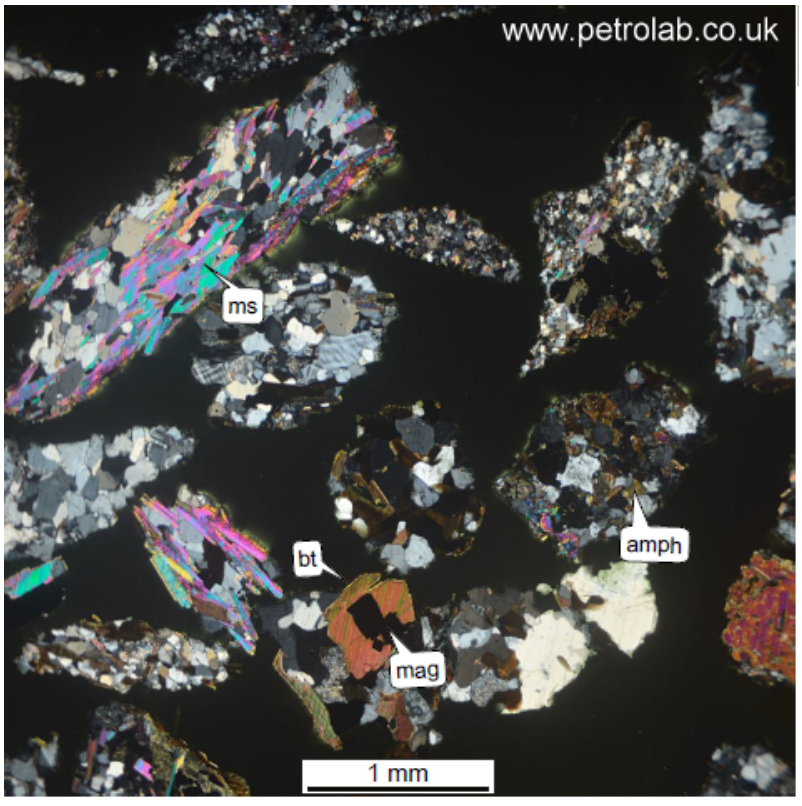

Figure A3.40 - Sample GCL0100- A08-Post - Reflected light image.

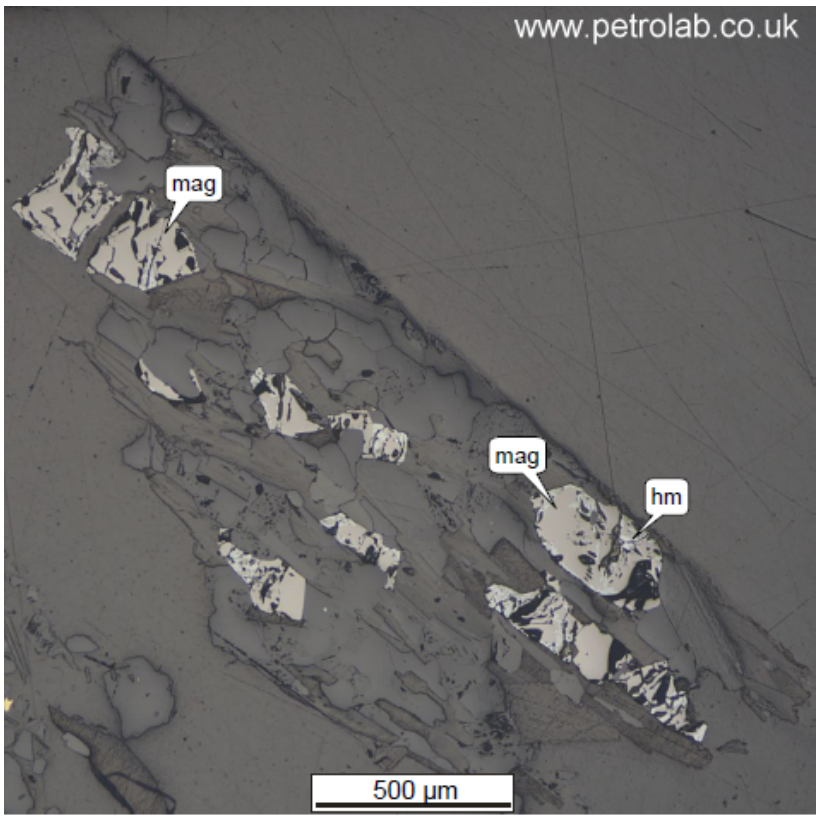

# Appendix 4 – Bulk Mineralogy Data Tables

Table A3.1 – Sample A-Pre bulk mineralogy data

| Sample GCL0100-A-PRE | | |
|---|---|---|
| Mineral / Phase | Vol% | Wt% |
| Feldspar group, fsp | 40.90% | 38.80% |
| Quartz, qtz | 22.90% | 22.20% |
| Amphibole group, amph | 10.80% | 12.60% |
| Muscovite, ms | 9.60% | 9.90% |
| Biotite, bt | 5.40% | 6.10% |
| Chlorite, chl | 3.30% | 3.20% |
| Magnetite, mag | 1.40% | 2.60% |
| Garnet group, grt | 1.10% | 1.50% |
| Pyrite, py | 0.80% | 1.50% |
| Goethite, Gt | 0.50% | 0.80% |
| Calcite, cal | 0.50% | 0.50% |
| Pyrrhotite, po | 0.10% | 0.20% |
| Clinopyroxene group, cpx | 0.10% | 0.10% |
| Chalcopyrite, cp | Trace | Trace |
| Ilmenite, ilm | Trace | Trace |

Table A3.2 – Sample K-Pre bulk mineralogy data

| Sample GCL0100-K-PRE | | |
|---|---|---|
| Mineral / Phase | Vol% | Wt% |
| Clinopyroxene group, cpx | 35.80% | 38.40% |
| Amphibole group, amph | 30.60% | 30.90% |
| Orthopyroxene group, opx | 12.60% | 14.10% |
| Tremolite, trm | 7.50% | 7.10% |
| Chlorite, chl | 4.80% | 4.00% |
| Feldspar group, fsp | 2.20% | 1.80% |
| Goethite, Gt | 1.30% | 1.70% |
| Magnetite, mag | 0.90% | 1.50% |
| Pyrrhotite, po | 0.70% | 0.90% |
| Calcite, cal | 0.40% | 0.30% |
| Pyrite, py | 0.20% | 0.30% |
| Chalcopyrite, cp | 0.10% | 0.20% |
| Pentlandite, pn | 0.10% | 0.20% |
| Olivine, ol | 0.10% | 0.10% |

Table A3.3 – Sample K02-Post bulk mineralogy data

| Sample GCL0100-K02-POST | | |
|---|---|---|
| Mineral / Phase | Vol% | Wt% |
| Amphibole group, amph | 32.50% | 31.30% |
| Clinopyroxene group, cpx | 29.60% | 30.30% |

| | | |
|---|---|---|
| Orthopyroxene group, opx | 15.90% | 17.00% |
| Tremolite, trm | 8.80% | 7.90% |
| Magnetite, mag | 1.80% | 2.80% |
| Chlorite, chl | 3.40% | 2.70% |
| Goethite, Gt | 1.60% | 2.10% |
| Pyrrhotite, po | 1.40% | 1.90% |
| Feldspar group, fsp | 1.50% | 1.20% |
| Serpentine group, srp | 1.00% | 0.90% |
| Haematite, hm | 0.50% | 0.80% |
| Chalcopyrite, cp | 0.40% | 0.50% |
| Pentlandite, pn | 0.20% | 0.30% |
| Pyrite, py | 0.10% | 0.20% |
| Olivine, ol | 0.10% | 0.10% |
| Covellite, cv | Trace | Trace |

Table A3.4 – Sample K05-Post bulk mineralogy data

| Sample GCL0100-K05-POST | | |
|---|---|---|
| Mineral / Phase | Vol% | Wt% |
| Clinopyroxene group, cpx | 32.40% | 33.90% |
| Amphibole group, amph | 32.40% | 31.90% |
| Orthopyroxene group, opx | 12.10% | 13.20% |
| Tremolite, trm | 9.80% | 9.00% |
| Chlorite, chl | 4.10% | 3.30% |
| Magnetite, mag | 1.50% | 2.40% |
| Goethite, Gt | 1.30% | 1.70% |
| Pyrrhotite, po | 1.20% | 1.70% |
| Feldspar group, fsp | 1.50% | 1.20% |
| Serpentine group, srp | 1.00% | 0.90% |
| Chalcopyrite, cp | 0.30% | 0.40% |
| Pentlandite, pn | 0.20% | 0.30% |
| Olivine, ol | 0.20% | 0.20% |

Table A3.5 – Sample K08-Post bulk mineralogy data

| Sample GCL0100-K08-POST | | |
|---|---|---|
| Mineral / Phase | Vol% | Wt% |
| Clinopyroxene group, cpx | 32.90% | 34.20% |
| Amphibole group, amph | 32.40% | 31.70% |
| Orthopyroxene group, opx | 13.70% | 14.90% |
| Tremolite, trm | 7.60% | 7.00% |
| Chlorite, chl | 4.00% | 3.20% |
| Magnetite, mag | 1.30% | 2.00% |
| Goethite, Gt | 1.50% | 2.00% |
| Feldspar group, fsp | 2.30% | 1.80% |
| Pyrrhotite, po | 1.00% | 1.40% |
| Serpentine group, srp | 0.90% | 0.80% |
| Pyrite, py | 0.30% | 0.50% |

| | | |
|---|---|---|
| Pentlandite, pn | 0.20% | 0.30% |
| Olivine, ol | 0.20% | 0.20% |

Table A3.6 – Sample A02-Post bulk mineralogy data

| Sample GCL0100-A02-POST | | |
|---|---|---|
| Mineral / Phase | Vol% | Wt% |
| Feldspar group, fsp | 39.30% | 36.60% |
| Quartz, qtz | 20.90% | 19.90% |
| Amphibole group, amph | 13.20% | 15.20% |
| Muscovite, ms | 11.60% | 11.80% |
| Biotite, bt | 6.70% | 7.40% |
| Magnetite, mag | 1.30% | 2.40% |
| Garnet group, grt | 1.10% | 1.50% |
| Chlorite, chl | 1.50% | 1.40% |
| Pyrite, py | 0.70% | 1.30% |
| Goethite, Gt | 0.60% | 0.90% |
| Chalcopyrite, cp | 0.40% | 0.60% |
| Calcite, cal | 0.60% | 0.60% |
| Ilmenite, ilm | 0.10% | 0.20% |
| Pyrrhotite, po | 0.10% | 0.20% |
| Clinopyroxene group, cpx | 0.10% | 0.10% |

Table A3.7 – Sample A05-Post bulk mineralogy data

| Sample GCL0100-A05-POST | | |
|---|---|---|
| Mineral / Phase | Vol% | Wt% |
| Feldspar group, fsp | 34.70% | 32.50% |
| Quartz, qtz | 19.70% | 18.90% |
| Amphibole group, amph | 11.90% | 13.80% |
| Muscovite, ms | 11.20% | 11.40% |
| Biotite, bt | 8.30% | 9.30% |
| Garnet group, grt | 2.90% | 3.90% |
| Chlorite, chl | 2.60% | 2.50% |
| Pyrite, py | 1.30% | 2.40% |
| Magnetite, mag | 1.00% | 1.90% |
| Clinopyroxene group, cpx | 0.90% | 1.10% |
| Calcite, cal | 0.80% | 0.80% |
| Chalcopyrite, cp | 0.50% | 0.80% |
| Goethite, Gt | 0.40% | 0.60% |
| Pyrrhotite, po | 0.20% | 0.30% |

Table A3.8 – Sample A08-Post bulk mineralogy data

| Sample GCL0100-A08-POST | | |
|---|---|---|
| Mineral / Phase | Vol% | Wt% |
| Feldspar group, fsp | 35.50% | 33.10% |
| Quartz, qtz | 22.20% | 21.10% |

| | | |
|---|---|---|
| Amphibole group, amph | 13.30% | 15.30% |
| Muscovite, ms | 10.90% | 11.10% |
| Biotite, bt | 6.60% | 7.30% |
| Magnetite, mag | 2.40% | 4.50% |
| Chlorite, chl | 2.60% | 2.50% |
| Garnet group, grt | 1.40% | 1.90% |
| Goethite, Gt | 0.70% | 1.10% |
| Pyrite, py | 0.50% | 0.90% |
| Calcite, cal | 0.60% | 0.60% |
| Chalcopyrite, cp | 0.20% | 0.30% |
| Pyrrhotite, po | 0.10% | 0.20% |
| Clinopyroxene group, cpx | 0.10% | 0.10% |

# Appendix 5 – Kevitsa Borehole Parameter Table

PSD and moisture data received from Kevitsa boreholes (O'Kane Consultants Ltd 2018b).

Table A5.1 – Borehole average PSD data recovered from the Kevitsa waste rock facilities.

| Location / Borehole | Average % fines (<2.3 mm) | Average % gravel 2.3 mm to 22 mm | Average % Cobble >22 mm | Average Moisture % |
|---|---|---|---|---|
| K_BH01 | 16 | 25 | 59 | 3.3 |
| K_BH02 | 13 | 23 | 66 | 2.5 |
| K_BH03 | 8 | 24 | 68 | 1.9 |
| K_BH04 | 12 | 18 | 69 | 2 |

# Appendix 6 – Post HCT PSD Data

This appendix contains the raw PSD data generated in this study.

Table A6.1 – Raw post HCT PSD data outputs

| | | Sieve sizes and collected sample mass (g) | | | | | | | | | |
|---|---|---|---|---|---|---|---|---|---|---|---|
| Sample | Initial mass (g) | >6.3mm | >4mm | >2.36mm | >2mm | >1mm | >500 um | >250 um | >125 um | >63 um | <63 um |
| GCL0100-K01 (Post) | 502.95 | 0 | 27.44806 | 24.43583 | 5.358386 | 14.94184 | 8.947211 | 6.014514 | 4.294661 | 3.260762 | 4.841436 |
| GCL0100-K02 (Post) | 489.95 | 0 | 25.17604 | 24.41595 | 5.119793 | 16.14475 | 9.15598 | 5.805746 | 4.155483 | 3.61865 | 4.35431 |
| GCL0100-K03 (Post) | 492.25 | 0 | 25.04825 | 24.18729 | 5.338503 | 15.9658 | 9.265335 | 5.98469 | 4.244955 | 3.370116 | 5.010438 |
| GCL0100-K04 (Post) | 501.2 | 0 | 24.07223 | 24.08788 | 5.418034 | 16.6617 | 9.702754 | 6.302813 | 4.592902 | 4.046128 | 4.771846 |
| GCL0100-K05 (Post) | 505.3 | 0 | 21.96715 | 24.50542 | 5.249031 | 16.55234 | 10.339 | 6.809822 | 4.881201 | 3.906949 | 4.50343 |
| GCL0100-K06 (Post) | 493.05 | 0 | 22.21884 | 22.81539 | 5.050204 | 16.26404 | 10.30918 | 6.909236 | 5.149617 | 5.135699 | 4.404016 |
| GCL0100-K07 (Post) | 492.6 | 0 | 22.5538 | 24.58495 | 5.089969 | 16.31375 | 9.861815 | 6.372403 | 4.553136 | 3.588826 | 5.219207 |
| GCL0100-K08 (Post) | 489 | 0 | 24.45808 | 24.08788 | 5.199324 | 15.83656 | 9.15598 | 6.193459 | 4.413958 | 3.549061 | 4.940849 |
| GCL0100-K09 (Post) | 501.65 | 0 | 24.19017 | 23.4914 | 5.199324 | 15.94592 | 10.0507 | 6.750174 | 4.821553 | 4.115717 | 5.199324 |
| GCL0100-A01 (Post) | 496.2 | 0 | 29.71584 | 20.39964 | 4.165424 | 10.75654 | 5.756039 | 6.233224 | 9.931405 | 7.625012 | 4.115717 |
| GCL0100-A02 (Post) | 369.6 | 0 | 22.34848 | 14.23601 | 3.290586 | 8.56944 | 4.87126 | 5.010438 | 8.549558 | 6.839646 | 3.807536 |
| GCL0100-A03 (Post) | 501.95 | 0 | 29.28579 | 22.18908 | 4.473606 | 11.63137 | 5.557212 | 5.487623 | 9.653047 | 7.287007 | 4.145541 |
| GCL0100-A04 (Post) | 500.95 | 0 | 29.51392 | 21.26454 | 4.274779 | 11.42261 | 5.775922 | 5.756039 | 9.782285 | 7.465951 | 4.254896 |
| GCL0100-A05 (Post) | 510.9 | 0 | 30.47563 | 21.37389 | 4.384134 | 11.92962 | 5.925042 | 5.626802 | 9.782285 | 7.326772 | 4.095835 |
| GCL0100-A06 (Post) | 508.85 | 0 | 33.17284 | 21.63237 | 4.095835 | 10.98519 | 5.348444 | 5.437916 | 9.00686 | 6.978825 | 3.83736 |
| GCL0100-A07 (Post) | 495.55 | 0 | 33.43759 | 20.28035 | 3.718063 | 10.72671 | 5.487623 | 5.487623 | 9.08639 | 7.197535 | 3.76777 |
| GCL0100-A08 (Post) | 484.1 | 0 | 29.0126 | 19.9324 | 3.83736 | 10.6273 | 5.716274 | 5.825629 | 9.921463 | 7.833781 | 4.35431 |
| GCL0100-A09 (Post) | 506.1 | 0 | 30.78443 | 21.35401 | 4.036186 | 11.33313 | 5.716274 | 5.676509 | 9.593399 | 7.505716 | 3.936773 |

# Appendix 7 – Additional Post HCT ABCC Data

Within this appendix the raw data and ABCC graphs from all samples presented as well as preminary runs ran on samples K01-K08 are shown. Prelimianry sample runs were ran in triplicate run sets. The prelimianry data for sample K01-K08 are additional to the data presented within the thesis document. Preliminary runs were undertaken to assess the appropriate HCl dosing volumes and molar strength required. Test methodology is outlined in Chapter 4.

Table A7.1 – ABCC test raw data outputs – Preliminary Results K01-K08

| Sample | Time (min) | HCL Added (mL) | $H_2SO_4$ added (kg/t) | Run 1 pH | Run 2 pH | Run 3 pH |
|---|---|---|---|---|---|---|
| GCL0100-K01-POST-ABCC-0.5 | 0 | 0 | 0 | 9.22 | 9.19 | 9.12 |
| | 15 | 0.5 | 6.125 | 8.63 | 8.46 | 8.35 |
| | 30 | 1 | 12.25 | 8.21 | 7.86 | 7.7 |
| | 45 | 1.5 | 18.375 | 7.85 | 7.4 | 7.21 |
| | 60 | 2 | 24.5 | 7.48 | 6.98 | 6.79 |
| | 75 | 2.5 | 30.625 | 7.02 | 6.46 | 6.33 |
| | 90 | 3 | 36.75 | 6.31 | 5.91 | 5.86 |
| | 105 | 3.5 | 42.875 | 5.64 | 5.29 | 5.3 |
| | 120 | 4 | 49 | 4.98 | 4.68 | 4.72 |
| | 135 | 4.5 | 55.125 | 4.51 | 4.32 | 4.35 |
| | 150 | 5 | 61.25 | 4.23 | 4.06 | 4.1 |
| | 165 | 5.5 | 67.375 | 3.99 | 3.83 | 3.89 |
| | 180 | 6 | 73.5 | 3.79 | 3.62 | 3.69 |
| | 195 | 6.5 | 79.625 | 3.6 | 3.43 | 3.51 |
| | 210 | 7 | 85.75 | 3.43 | 3.27 | 3.35 |
| | 225 | 7.5 | 91.875 | 3.29 | 3.12 | 3.21 |
| | 240 | 8 | 98 | 3.16 | 3.01 | 3.1 |
| | 255 | 8.5 | 104.125 | 3.06 | 2.91 | 3 |
| | 270 | 9 | 110.25 | 2.97 | 2.82 | 2.91 |
| | 285 | 9.5 | 116.375 | 2.88 | 2.74 | 2.83 |
| | 300 | 10 | 122.5 | 2.82 | 2.67 | 2.77 |
| | 315 | 10.5 | 128.625 | 2.75 | 2.61 | 2.71 |
| | 330 | 11 | 134.75 | 2.7 | 2.56 | 2.66 |
| | 345 | 11.5 | 140.875 | 2.65 | 2.52 | 2.61 |
| | 360 | 12 | 147 | 2.61 | 2.48 | 2.57 |
| | 375 | 12.5 | 153.125 | 2.57 | | 2.53 |
| | 390 | 13 | 159.25 | 2.54 | | 2.5 |

| | | | | | | |
|---|---|---|---|---|---|---|
| | 405 | 13.5 | 165.375 | 2.51 | | |
| | 420 | 14 | 171.5 | 2.48 | | |
| GCL0100-K02-POST-ABCC-0.5 | 0 | 0 | 0 | 9.21 | 9.34 | 9.26 |
| | 15 | 0.5 | 6.125 | 8.56 | 8.76 | 8.66 |
| | 30 | 1 | 12.25 | 8.02 | 8.35 | 8.05 |
| | 45 | 1.5 | 18.375 | 7.54 | 7.89 | 7.5 |
| | 60 | 2 | 24.5 | 7.14 | 7.4 | 7.04 |
| | 75 | 2.5 | 30.625 | 6.72 | 6.97 | 6.63 |
| | 90 | 3 | 36.75 | 6.18 | 6.43 | 6.13 |
| | 105 | 3.5 | 42.875 | 5.6 | 5.85 | 5.6 |
| | 120 | 4 | 49 | 4.95 | 5.24 | 4.98 |
| | 135 | 4.5 | 55.125 | 4.48 | 4.66 | 4.5 |
| | 150 | 5 | 61.25 | 4.19 | 4.29 | 4.21 |
| | 165 | 5.5 | 67.375 | 3.96 | 4.03 | 3.97 |
| | 180 | 6 | 73.5 | 3.75 | 3.81 | 3.76 |
| | 195 | 6.5 | 79.625 | 3.55 | 3.61 | 3.57 |
| | 210 | 7 | 85.75 | 3.38 | 3.43 | 3.39 |
| | 225 | 7.5 | 91.875 | 3.23 | 3.28 | 3.24 |
| | 240 | 8 | 98 | 3.1 | 3.15 | 3.11 |
| | 255 | 8.5 | 104.125 | 3 | 3.04 | 3.01 |
| | 270 | 9 | 110.25 | 2.9 | 2.94 | 2.91 |
| | 285 | 9.5 | 116.375 | 2.83 | 2.85 | 2.83 |
| | 300 | 10 | 122.5 | 2.76 | 2.78 | 2.76 |
| | 315 | 10.5 | 128.625 | 2.7 | 2.72 | 2.7 |
| | 330 | 11 | 134.75 | 2.64 | 2.67 | 2.65 |
| | 345 | 11.5 | 140.875 | 2.59 | 2.62 | 2.6 |
| | 360 | 12 | 147 | 2.55 | 2.58 | 2.56 |
| | 375 | 12.5 | 153.125 | 2.52 | 2.54 | 2.52 |
| | 390 | 13 | 159.25 | 2.48 | 2.51 | 2.49 |
| | 395 | 13.5 | 165.375 | | 2.48 | |
| GCL0100-K03-POST-ABCC-0.5 | 0 | 0 | 0 | 8.91 | 9.21 | 9.06 |
| | 15 | 0.5 | 6.125 | 8.05 | 8.49 | 8.22 |
| | 30 | 1 | 12.25 | 7.48 | 7.92 | 7.47 |
| | 45 | 1.5 | 18.375 | 7.01 | 7.47 | 6.93 |
| | 60 | 2 | 24.5 | 6.46 | 6.98 | 6.39 |
| | 75 | 2.5 | 30.625 | 5.83 | 6.36 | 5.8 |
| | 90 | 3 | 36.75 | 5.13 | 5.71 | 5.1 |
| | 105 | 3.5 | 42.875 | 4.57 | 5.04 | 4.51 |
| | 120 | 4 | 49 | 4.23 | 4.48 | 4.15 |
| | 135 | 4.5 | 55.125 | 3.95 | 4.15 | 3.88 |
| | 150 | 5 | 61.25 | 3.72 | 3.88 | 3.64 |
| | 165 | 5.5 | 67.375 | 3.51 | 3.64 | 3.44 |
| | 180 | 6 | 73.5 | 3.34 | 3.44 | 3.28 |

| | | | | | | |
|---|---|---|---|---|---|---|
| | 195 | 6.5 | 79.625 | 3.2 | 3.27 | 3.14 |
| | 210 | 7 | 85.75 | 3.08 | 3.12 | 3.03 |
| | 225 | 7.5 | 91.875 | 2.98 | 3.01 | 2.93 |
| | 240 | 8 | 98 | 2.89 | 2.91 | 2.85 |
| | 255 | 8.5 | 104.125 | 2.82 | 2.82 | 2.78 |
| | 270 | 9 | 110.25 | 2.76 | 2.75 | 2.71 |
| | 285 | 9.5 | 116.375 | 2.7 | 2.68 | 2.66 |
| | 300 | 10 | 122.5 | 2.66 | 2.63 | 2.62 |
| | 315 | 10.5 | 128.625 | 2.61 | 2.58 | 2.58 |
| | 330 | 11 | 134.75 | 2.58 | 2.54 | 2.54 |
| | 345 | 11.5 | 140.875 | 2.54 | 2.5 | 2.51 |
| | 360 | 12 | 147 | 2.51 | | 2.48 |
| | 375 | 12.5 | 153.125 | 2.48 | | |
| GCL0100-K04-ABCC-POST-0.5 | 0 | 0 | 0 | 9.19 | 9.14 | 9.1 |
| | 15 | 0.5 | 6.125 | 8.4 | 8.34 | 8.34 |
| | 30 | 1 | 12.25 | 7.75 | 7.63 | 7.76 |
| | 45 | 1.5 | 18.375 | 7.26 | 7.13 | 7.32 |
| | 60 | 2 | 24.5 | 6.83 | 6.67 | 6.82 |
| | 75 | 2.5 | 30.625 | 6.23 | 6.11 | 6.12 |
| | 90 | 3 | 36.75 | 5.59 | 5.5 | 5.4 |
| | 105 | 3.5 | 42.875 | 4.9 | 4.83 | 4.72 |
| | 120 | 4 | 49 | 4.41 | 4.38 | 4.3 |
| | 135 | 4.5 | 55.125 | 4.1 | 4.08 | 3.99 |
| | 150 | 5 | 61.25 | 3.84 | 3.82 | 3.74 |
| | 165 | 5.5 | 67.375 | 3.63 | 3.6 | 3.52 |
| | 180 | 6 | 73.5 | 3.43 | 3.41 | 3.33 |
| | 195 | 6.5 | 79.625 | 3.27 | 3.25 | 3.17 |
| | 210 | 7 | 85.75 | 3.14 | 3.12 | 3.04 |
| | 225 | 7.5 | 91.875 | 3.02 | 3.01 | 2.94 |
| | 240 | 8 | 98 | 2.93 | 2.92 | 2.84 |
| | 255 | 8.5 | 104.125 | 2.85 | 2.84 | 2.77 |
| | 270 | 9 | 110.25 | 2.78 | 2.77 | 2.7 |
| | 285 | 9.5 | 116.375 | 2.72 | 2.72 | 2.64 |
| | 300 | 10 | 122.5 | 2.66 | 2.66 | 2.59 |
| | 315 | 10.5 | 128.625 | 2.62 | 2.62 | 2.55 |
| | 330 | 11 | 134.75 | 2.58 | 2.58 | 2.51 |
| | 345 | 11.5 | 140.875 | 2.54 | 2.55 | 2.47 |
| | 360 | 12 | 147 | 2.51 | 2.51 | |
| | 375 | 12.5 | 153.125 | 2.48 | 2.48 | |
| GCL0100-K05-ABCC-POST-0.5 | 0 | 0 | 0 | 9.28 | 9.11 | 9.13 |
| | 15 | 0.5 | 6.125 | 8.52 | 8.14 | 8.08 |
| | 30 | 1 | 12.25 | 7.83 | 7.5 | 7.39 |
| | 45 | 1.5 | 18.375 | 7.29 | 7.01 | 6.9 |

| | | | | | | |
|---|---|---|---|---|---|---|
| | 60 | 2 | 24.5 | 6.77 | 6.45 | 6.38 |
| | 75 | 2.5 | 30.625 | 6.1 | 5.77 | 5.79 |
| | 90 | 3 | 36.75 | 5.33 | 4.94 | 5.04 |
| | 105 | 3.5 | 42.875 | 4.6 | 4.37 | 4.46 |
| | 120 | 4 | 49 | 4.2 | 4.03 | 4.12 |
| | 135 | 4.5 | 55.125 | 3.92 | 3.74 | 3.84 |
| | 150 | 5 | 61.25 | 3.67 | 3.5 | 3.6 |
| | 165 | 5.5 | 67.375 | 3.45 | 3.29 | 3.39 |
| | 180 | 6 | 73.5 | 3.27 | 3.13 | 3.22 |
| | 195 | 6.5 | 79.625 | 3.12 | 2.99 | 3.08 |
| | 210 | 7 | 85.75 | 3 | 2.87 | 2.96 |
| | 225 | 7.5 | 91.875 | 2.89 | 2.78 | 2.85 |
| | 240 | 8 | 98 | 2.81 | 2.69 | 2.77 |
| | 255 | 8.5 | 104.125 | 2.73 | 2.62 | 2.69 |
| | 270 | 9 | 110.25 | 2.67 | 2.56 | 2.63 |
| | 285 | 9.5 | 116.375 | 2.61 | 2.51 | 2.57 |
| | 300 | 10 | 122.5 | 2.56 | 2.46 | 2.52 |
| | 315 | 10.5 | 128.625 | 2.52 | | 2.47 |
| | 330 | 11 | 134.75 | 2.48 | | |
| GCL0100-K06-POST-ABCC-1 | 0 | 0 | 0 | 9.09 | 9.15 | 9.11 |
| | 15 | 0.5 | 6.125 | 8.14 | 8.16 | 8.25 |
| | 30 | 1 | 12.25 | 7.46 | 7.43 | 7.49 |
| | 45 | 1.5 | 18.375 | 6.95 | 6.93 | 6.94 |
| | 60 | 2 | 24.5 | 6.43 | 6.39 | 6.43 |
| | 75 | 2.5 | 30.625 | 5.82 | 5.77 | 5.85 |
| | 90 | 3 | 36.75 | 5.1 | 5.03 | 5.17 |
| | 105 | 3.5 | 42.875 | 4.51 | 4.48 | 4.54 |
| | 120 | 4 | 49 | 4.15 | 4.14 | 4.16 |
| | 135 | 4.5 | 55.125 | 3.87 | 3.86 | 3.88 |
| | 150 | 5 | 61.25 | 3.63 | 3.62 | 3.63 |
| | 165 | 5.5 | 67.375 | 3.42 | 3.41 | 3.42 |
| | 180 | 6 | 73.5 | 3.24 | 3.24 | 3.25 |
| | 195 | 6.5 | 79.625 | 3.1 | 3.1 | 3.1 |
| | 210 | 7 | 85.75 | 2.98 | 2.98 | 2.98 |
| | 225 | 7.5 | 91.875 | 2.88 | 2.89 | 2.88 |
| | 240 | 8 | 98 | 2.79 | 2.8 | 2.79 |
| | 255 | 8.5 | 104.125 | 2.71 | 2.73 | 2.71 |
| | 270 | 9 | 110.25 | 2.65 | 2.66 | 2.65 |
| | 285 | 9.5 | 116.375 | 2.6 | 2.61 | 2.59 |
| | 300 | 10 | 122.5 | 2.55 | 2.56 | 2.54 |
| | 315 | 10.5 | 128.625 | 2.5 | 2.52 | 2.5 |
| | 330 | 11 | 134.75 | 2.46 | 2.47 | 2.46 |
| | 0 | 0 | 0 | 8.97 | 9.07 | 8.92 |

| | | | | | | |
|---|---|---|---|---|---|---|
| GCL0100-K07-ABCC-0.5-1 | 15 | 0.5 | 6.125 | 8.18 | 7.99 | 7.92 |
| | 30 | 1 | 12.25 | 7.75 | 7.3 | 7.41 |
| | 45 | 1.5 | 18.375 | 7.32 | 6.83 | 7.01 |
| | 60 | 2 | 24.5 | 6.73 | 6.34 | 6.42 |
| | 75 | 2.5 | 30.625 | 5.96 | 5.8 | 5.72 |
| | 90 | 3 | 36.75 | 5.18 | 5.13 | 5 |
| | 105 | 3.5 | 42.875 | 4.57 | 4.56 | 4.49 |
| | 120 | 4 | 49 | 4.21 | 4.2 | 4.15 |
| | 135 | 4.5 | 55.125 | 3.93 | 3.93 | 3.88 |
| | 150 | 5 | 61.25 | 3.69 | 3.69 | 3.64 |
| | 165 | 5.5 | 67.375 | 3.48 | 3.48 | 3.45 |
| | 180 | 6 | 73.5 | 3.3 | 3.31 | 3.28 |
| | 195 | 6.5 | 79.625 | 3.15 | 3.17 | 3.15 |
| | 210 | 7 | 85.75 | 3.03 | 3.05 | 3.04 |
| | 225 | 7.5 | 91.875 | 2.93 | 2.95 | 2.94 |
| | 240 | 8 | 98 | 2.85 | 2.87 | 2.86 |
| | 255 | 8.5 | 104.125 | 2.77 | 2.79 | 2.8 |
| | 270 | 9 | 110.25 | 2.7 | 2.73 | 2.74 |
| | 285 | 9.5 | 116.375 | 2.65 | 2.68 | 2.68 |
| | 300 | 10 | 122.5 | 2.6 | 2.63 | 2.63 |
| | 315 | 10.5 | 128.625 | 2.55 | 2.59 | 2.59 |
| | 330 | 11 | 134.75 | 2.51 | 2.55 | 2.55 |
| | 345 | 11.5 | 140.875 | 2.48 | 2.52 | 2.52 |
| | 360 | 12 | 147 | | 2.49 | 2.49 |
| GCL0100-K08-ABCC-POST-0.5-1 | 0 | 0 | 0 | 8.87 | 8.75 | |
| | 15 | 0.5 | 6.125 | 7.87 | 7.77 | |
| | 30 | 1 | 12.25 | 7.33 | 7.16 | |
| | 45 | 1.5 | 18.375 | 6.85 | 6.65 | |
| | 60 | 2 | 24.5 | 6.21 | 6.08 | |
| | 75 | 2.5 | 30.625 | 5.49 | 5.44 | |
| | 90 | 3 | 36.75 | 4.72 | 4.8 | |
| | 105 | 3.5 | 42.875 | 4.29 | 4.36 | |
| | 120 | 4 | 49 | 3.98 | 4.05 | |
| | 135 | 4.5 | 55.125 | 3.71 | 3.8 | |
| | 150 | 5 | 61.25 | 3.49 | 3.58 | |
| | 165 | 5.5 | 67.375 | 3.31 | 3.41 | |
| | 180 | 6 | 73.5 | 3.16 | 3.26 | |
| | 195 | 6.5 | 79.625 | 3.04 | 3.13 | |
| | 210 | 7 | 85.75 | 2.93 | 3.03 | |
| | 225 | 7.5 | 91.875 | 2.85 | 2.93 | |
| | 240 | 8 | 98 | 2.77 | 2.85 | |
| | 255 | 8.5 | 104.125 | 2.71 | 2.78 | |
| | 270 | 9 | 110.25 | 2.65 | 2.72 | |
| | 285 | 9.5 | 116.375 | 2.6 | 2.67 | |

| | | | | | | |
|---|---|---|---|---|---|---|
| | 300 | 10 | 122.5 | 2.55 | 2.63 | |
| | 315 | 10.5 | 128.625 | 2.51 | 2.59 | |
| | 330 | 11 | 134.75 | 2.48 | 2.55 | |
| | 345 | 11.5 | 140.875 | | 2.52 | |
| | 360 | 12 | 147 | | 2.49 | |

**Preliminary ABCC output graphs**

Figure A7.1 – K01 ABCC Curve

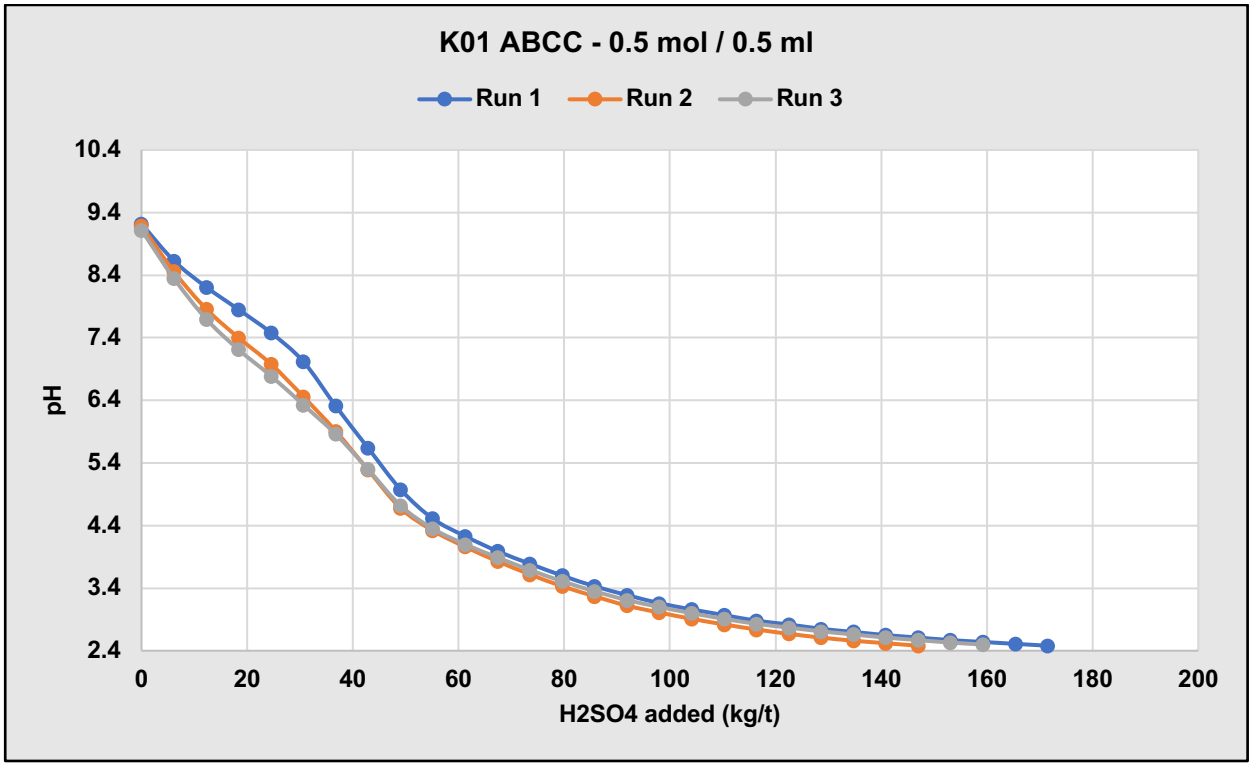

Figure A7.2 – K02 ABCC Curve

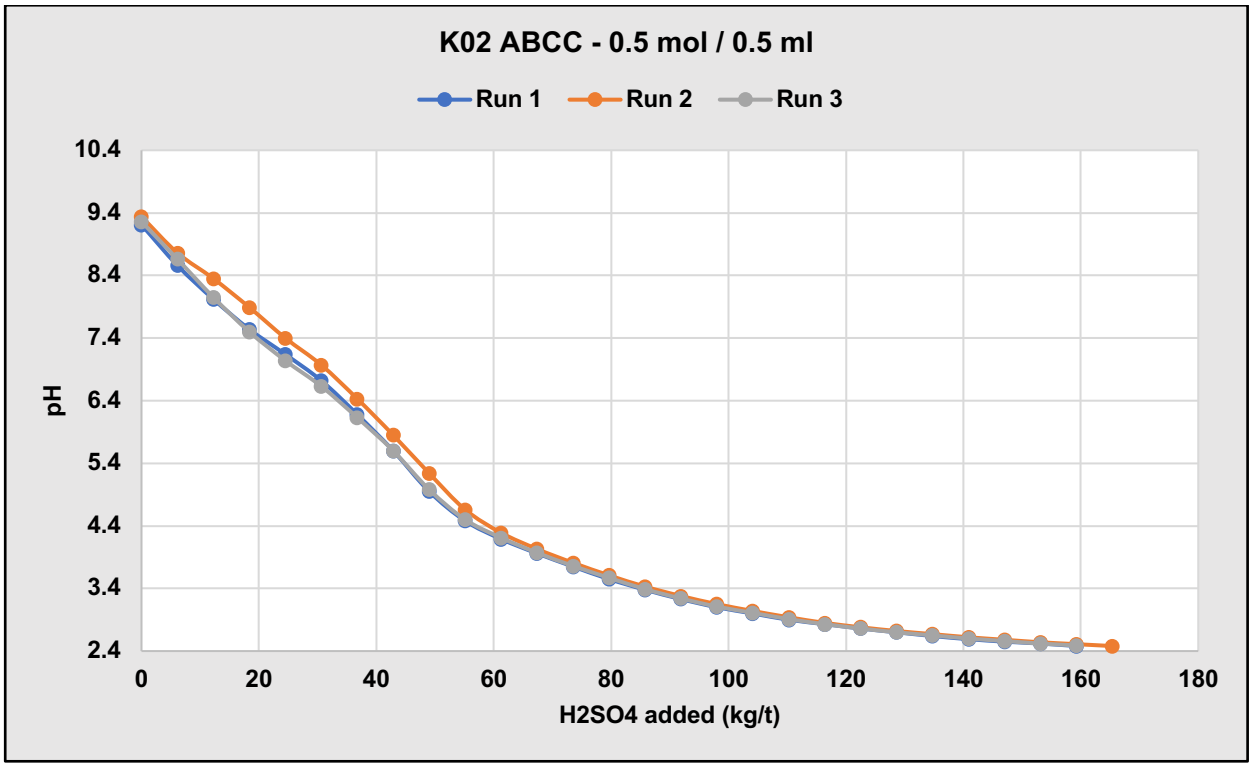


Figure A7.3 – K03 ABCC Curve

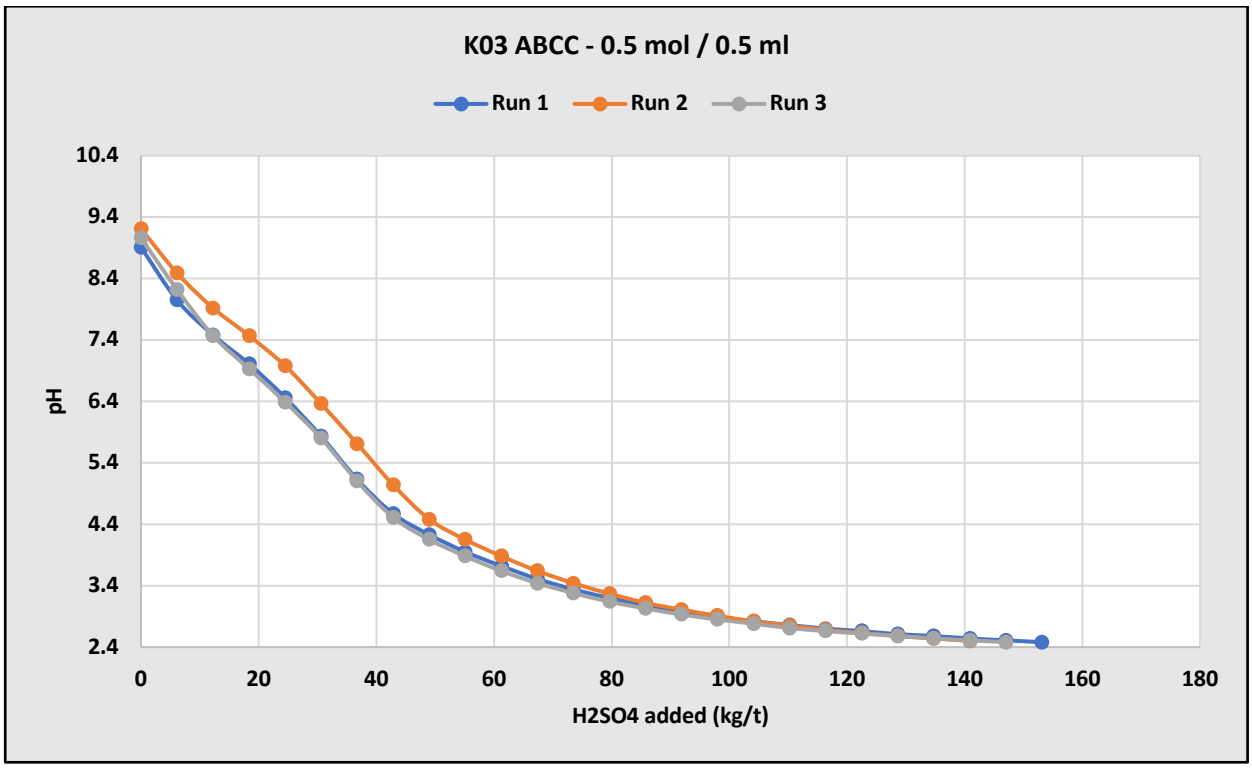

Figure A7.4 – K04 ABCC Curve

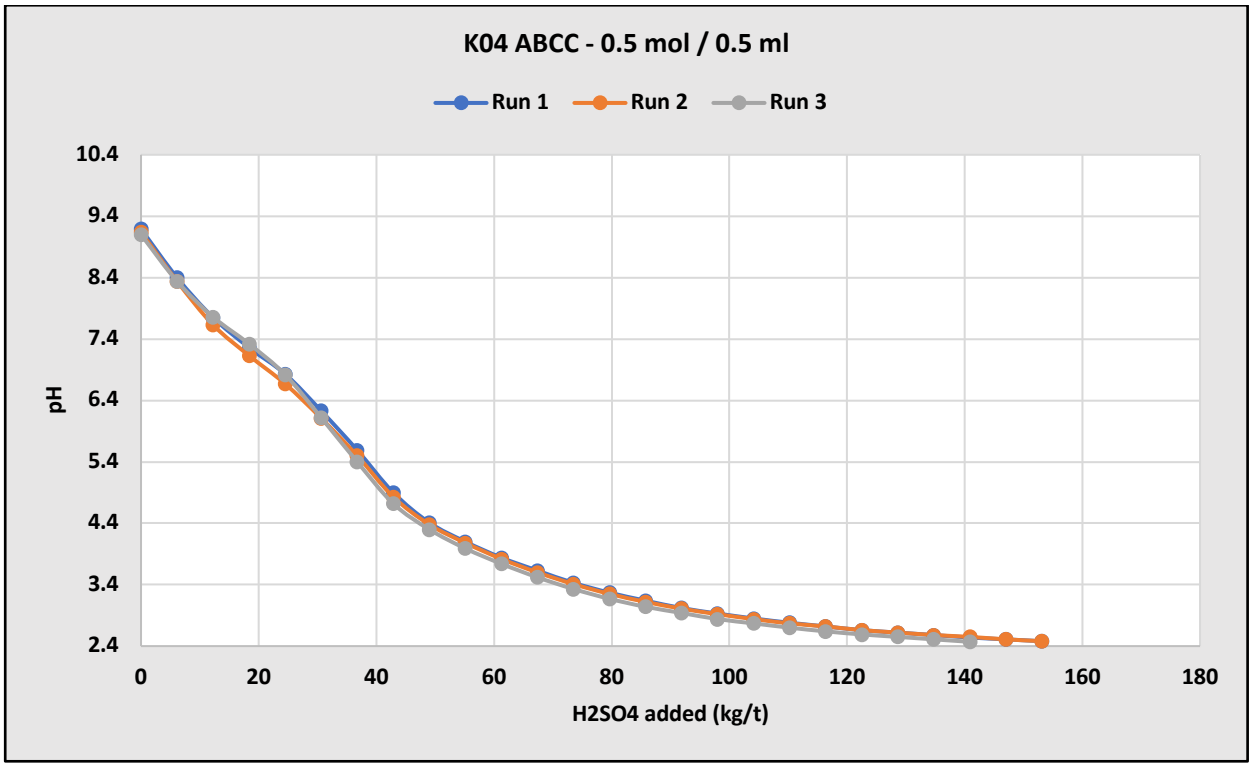


Figure A7.5 – K05 ABCC Curve

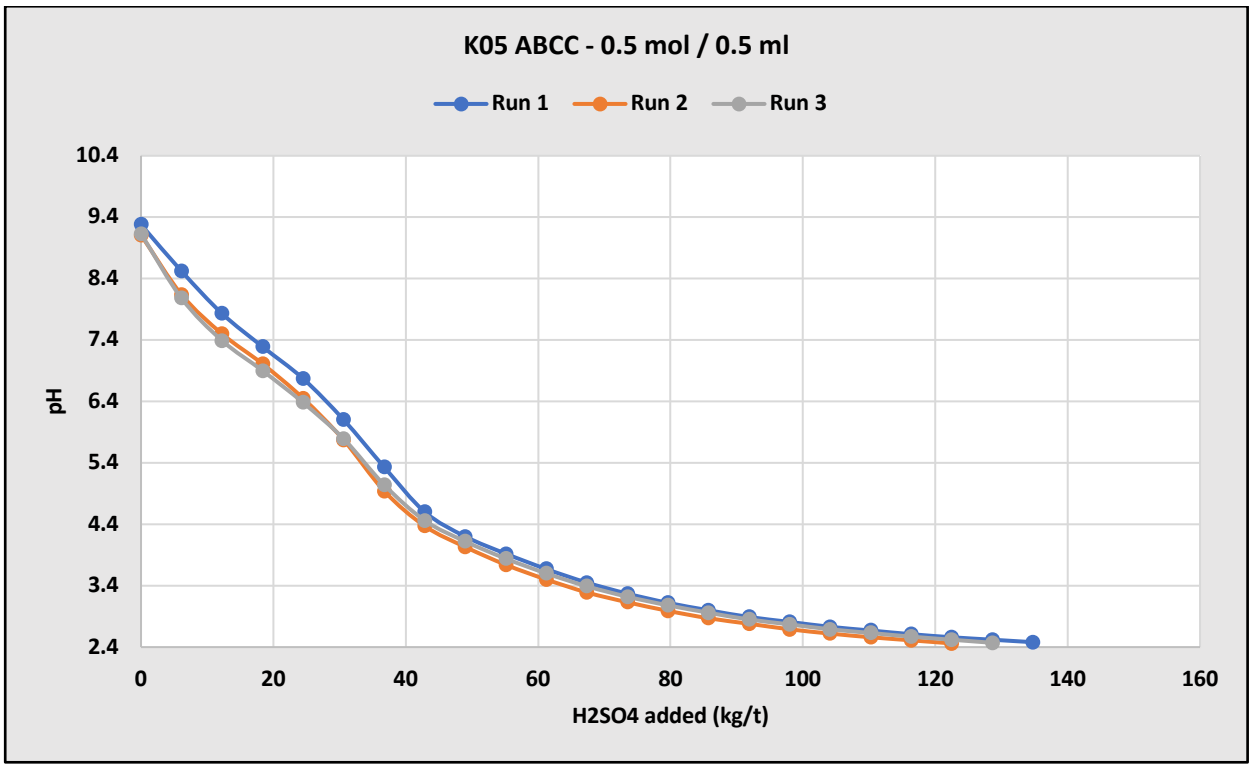

Figure A7.6 – K06 ABCC Curve

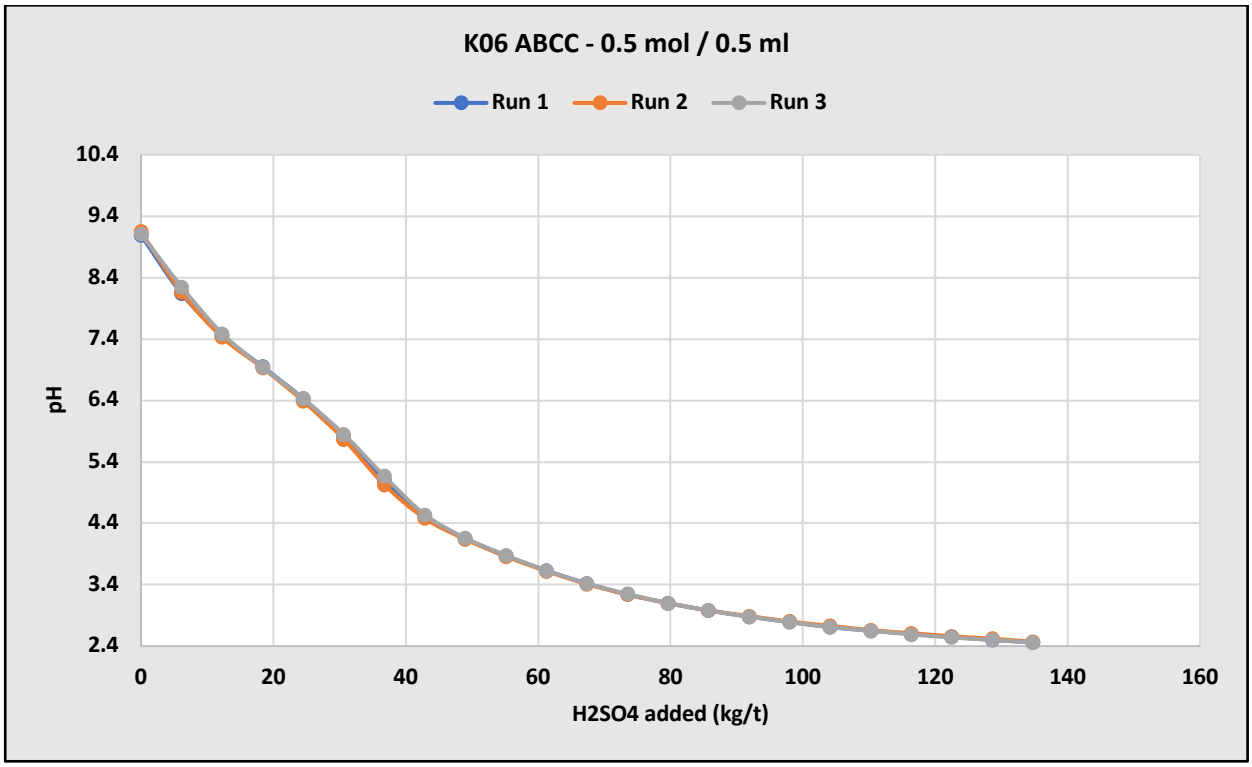


Figure A7.7 – K07 ABCC Curve

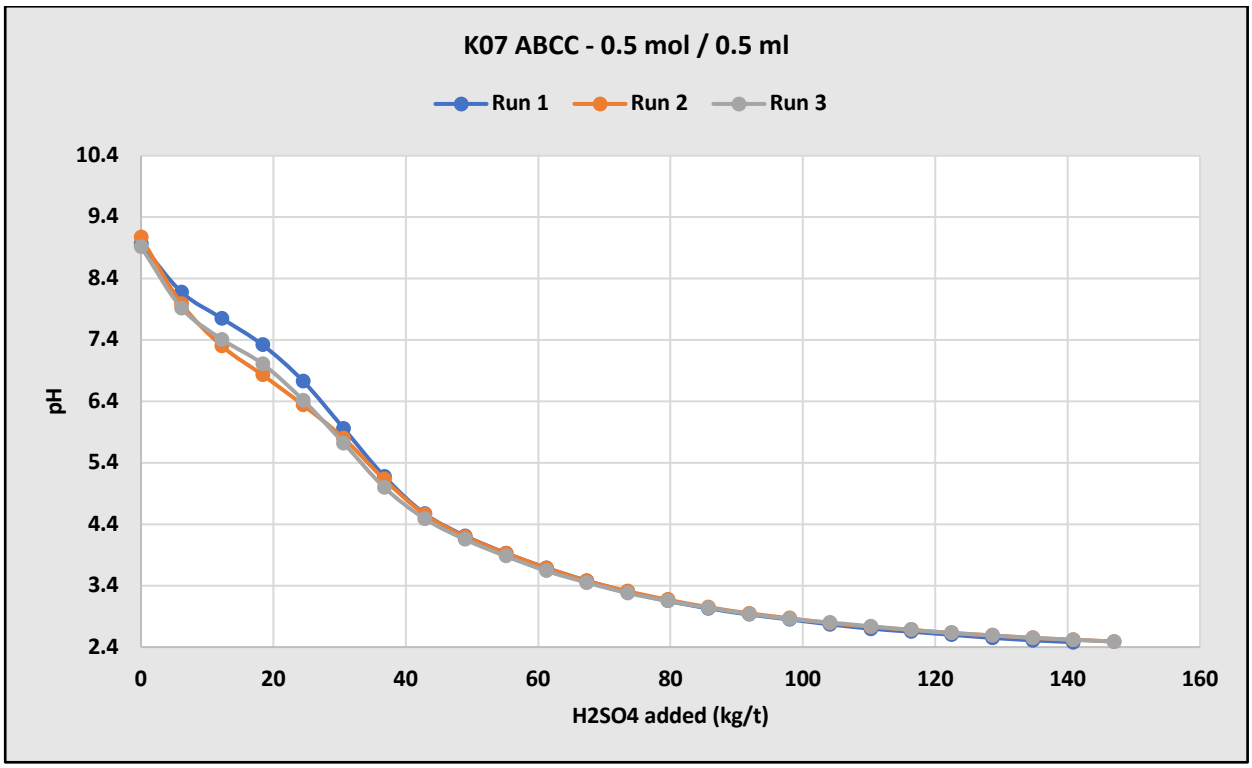

Figure A7.8 – K08 ABCC Curve

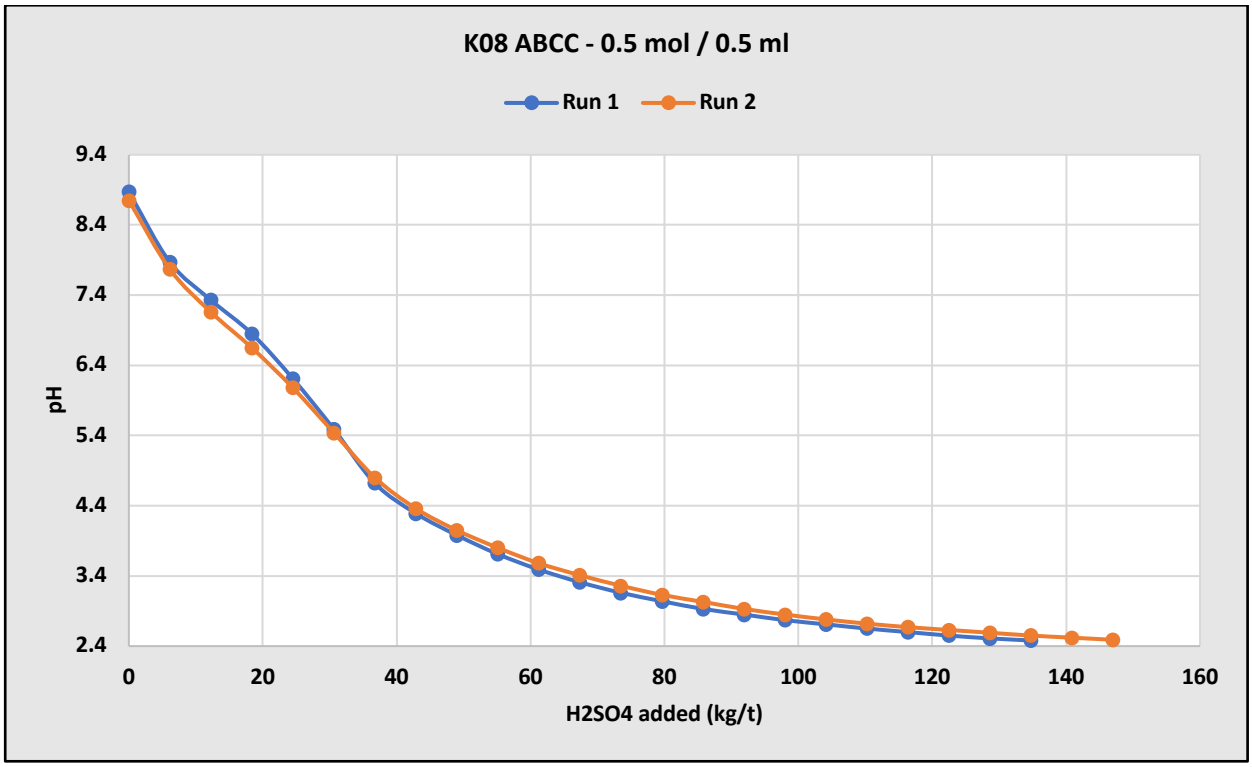


Table A7.2 – Sample K-Pre raw ABCC outputs from results presented in this thesis.

| **Sample ID** | **GCL0100-K-PRE** | | |
|---|---|---|---|
| **Parameters** | Addition Volume per step (mL) | Acid Strength (N) | Sample Mass (g) |
| | **0.202** | **0.1** | **2.0001** |
| **step** | pH | HCl Added (mL) | H2SO4 added (kg/t) |
| 0 (Start) | 9.49 | 0.00 | 0.00 |
| 1 | 9.13 | 0.20 | 0.49 |
| 2 | 8.46 | 0.40 | 0.99 |
| 3 | 7.6 | 0.61 | 1.48 |
| 4 | 7.16 | 0.81 | 1.98 |
| 5 | 6.85 | 1.01 | 2.47 |
| 6 | 6.54 | 1.21 | 2.97 |
| 7 | 6.23 | 1.41 | 3.46 |
| 8 | 5.92 | 1.62 | 3.96 |
| 9 | 5.6 | 1.82 | 4.45 |
| 10 | 5.27 | 2.02 | 4.95 |
| 11 | 4.94 | 2.22 | 5.44 |
| 12 | 4.68 | 2.42 | 5.94 |
| 13 | 4.47 | 2.63 | 6.43 |
| 14 | 4.27 | 2.83 | 6.93 |
| 15 | 4.11 | 3.03 | 7.42 |

| | | | |
|---|---|---|---|
| 16 | 3.96 | 3.23 | 7.92 |
| 17 | 3.83 | 3.43 | 8.41 |
| 18 | 3.71 | 3.64 | 8.91 |
| 19 | 3.6 | 3.84 | 9.40 |
| 20 | 3.5 | 4.04 | 9.90 |
| 21 | 3.41 | 4.24 | 10.39 |
| 22 | 3.32 | 4.44 | 10.89 |
| 23 | 3.25 | 4.65 | 11.38 |
| 24 | 3.18 | 4.85 | 11.88 |
| 25 | 3.12 | 5.05 | 12.37 |
| 26 | 3.07 | 5.25 | 12.87 |
| 27 | 3.01 | 5.45 | 13.36 |
| 28 | 2.97 | 5.66 | 13.86 |
| 29 | 2.92 | 5.86 | 14.35 |
| 30 | 2.88 | 6.06 | 14.85 |
| 31 | 2.85 | 6.26 | 15.34 |
| 32 | 2.81 | 6.46 | 15.84 |
| 33 | 2.78 | 6.67 | 16.33 |
| 34 | 2.75 | 6.87 | 16.83 |
| 35 | 2.72 | 7.07 | 17.32 |
| 36 | 2.7 | 7.27 | 17.82 |
| 37 | 2.68 | 7.47 | 18.31 |
| 38 | 2.65 | 7.68 | 18.81 |
| 39 | 2.63 | 7.88 | 19.30 |
| 40 | 2.61 | 8.08 | 19.80 |
| 41 | 2.59 | 8.28 | 20.29 |
| 42 | 2.58 | 8.48 | 20.78 |
| 43 | 2.56 | 8.69 | 21.28 |
| 44 | 2.54 | 8.89 | 21.77 |
| 45 | 2.53 | 9.09 | 22.27 |
| 46 | 2.51 | 9.29 | 22.76 |

Table A7.3 – Sample K-Pre-DUP raw ABCC outputs from results presented in this thesis.

| **Sample ID** | **GCL0100-K-PRE-DUP-RR** | | |
|---|---|---|---|
| **Parameters** | Addition Volume per step (mL) | Acid Strength (N) | Sample Mass (g) |
| | **0.202** | **0.1** | **2.0003** |
| **step** | pH | HCl Added (mL) | H2SO4 added (kg/t) |
| 0 (Start) | 9.51 | 0.00 | 0.00 |
| 1 | 9.19 | 0.20 | 0.49 |
| 2 | 8.75 | 0.40 | 0.99 |
| 3 | 7.99 | 0.61 | 1.48 |

| | | | |
|---|---|---|---|
| 4 | 7.52 | 0.81 | 1.98 |
| 5 | 7.22 | 1.01 | 2.47 |
| 6 | 6.98 | 1.21 | 2.97 |
| 7 | 6.74 | 1.41 | 3.46 |
| 8 | 6.47 | 1.62 | 3.96 |
| 9 | 6.19 | 1.82 | 4.45 |
| 10 | 5.89 | 2.02 | 4.95 |
| 11 | 5.62 | 2.22 | 5.44 |
| 12 | 5.32 | 2.42 | 5.94 |
| 13 | 5.01 | 2.63 | 6.43 |
| 14 | 4.75 | 2.83 | 6.93 |
| 15 | 4.55 | 3.03 | 7.42 |
| 16 | 4.37 | 3.23 | 7.92 |
| 17 | 4.21 | 3.43 | 8.41 |
| 18 | 4.07 | 3.64 | 8.91 |
| 19 | 3.95 | 3.84 | 9.40 |
| 20 | 3.83 | 4.04 | 9.90 |
| 21 | 3.73 | 4.24 | 10.39 |
| 22 | 3.63 | 4.44 | 10.89 |
| 23 | 3.54 | 4.65 | 11.38 |
| 24 | 3.46 | 4.85 | 11.88 |
| 25 | 3.38 | 5.05 | 12.37 |
| 26 | 3.31 | 5.25 | 12.87 |
| 27 | 3.25 | 5.45 | 13.36 |
| 28 | 3.19 | 5.66 | 13.86 |
| 29 | 3.13 | 5.86 | 14.35 |
| 30 | 3.08 | 6.06 | 14.84 |
| 31 | 3.03 | 6.26 | 15.34 |
| 32 | 2.99 | 6.46 | 15.83 |
| 33 | 2.94 | 6.67 | 16.33 |
| 34 | 2.91 | 6.87 | 16.82 |
| 35 | 2.87 | 7.07 | 17.32 |
| 36 | 2.84 | 7.27 | 17.81 |
| 37 | 2.81 | 7.47 | 18.31 |
| 38 | 2.78 | 7.68 | 18.80 |
| 39 | 2.76 | 7.88 | 19.30 |
| 40 | 2.73 | 8.08 | 19.79 |
| 41 | 2.71 | 8.28 | 20.29 |
| 42 | 2.69 | 8.48 | 20.78 |
| 43 | 2.67 | 8.69 | 21.28 |
| 44 | 2.65 | 8.89 | 21.77 |
| 45 | 2.63 | 9.09 | 22.27 |
| 46 | 2.61 | 9.29 | 22.76 |
| 47 | 2.6 | 9.49 | 23.26 |
| 48 | 2.58 | 9.70 | 23.75 |
| 49 | 2.56 | 9.90 | 24.25 |

| | | | |
|---|---|---|---|
| 50 | 2.54 | 10.10 | 24.74 |
| 51 | 2.53 | 10.30 | 25.24 |
| 52 | 2.51 | 10.50 | 25.73 |
| 53 | 2.5 | 10.71 | 26.23 |

Table A7.4 – Sample K02 raw ABCC outputs from results presented in this thesis.

| **Sample ID** | **GCL0100-K02-POST** | | |
|---|---|---|---|
| **Parameters** | Addition Volume per step (mL) | Acid Strength (N) | Sample Mass (g) |
| | **0.212** | **0.1** | **2.0031** |
| **step** | pH | HCl Added (mL) | H2SO4 added (kg/t) |
| 0 (Start) | 9.69 | 0.00 | 0.00 |
| 1 | 9.33 | 0.21 | 0.52 |
| 2 | 8.45 | 0.42 | 1.04 |
| 3 | 7.69 | 0.64 | 1.56 |
| 4 | 7.24 | 0.85 | 2.07 |
| 5 | 6.85 | 1.06 | 2.59 |
| 6 | 6.44 | 1.27 | 3.11 |
| 7 | 6.01 | 1.48 | 3.63 |
| 8 | 5.56 | 1.70 | 4.15 |
| 9 | 5.08 | 1.91 | 4.67 |
| 10 | 4.7 | 2.12 | 5.19 |
| 11 | 4.42 | 2.33 | 5.70 |
| 12 | 4.21 | 2.54 | 6.22 |
| 13 | 4 | 2.76 | 6.74 |
| 14 | 3.83 | 2.97 | 7.26 |
| 15 | 3.68 | 3.18 | 7.78 |
| 16 | 3.55 | 3.39 | 8.30 |
| 17 | 3.45 | 3.60 | 8.82 |
| 18 | 3.35 | 3.82 | 9.33 |
| 19 | 3.27 | 4.03 | 9.85 |
| 20 | 3.2 | 4.24 | 10.37 |
| 21 | 3.13 | 4.45 | 10.89 |
| 22 | 3.07 | 4.66 | 11.41 |
| 23 | 3.02 | 4.88 | 11.93 |
| 24 | 2.97 | 5.09 | 12.45 |
| 25 | 2.93 | 5.30 | 12.96 |
| 26 | 2.89 | 5.51 | 13.48 |
| 27 | 2.85 | 5.72 | 14.00 |
| 28 | 2.81 | 5.94 | 14.52 |
| 29 | 2.78 | 6.15 | 15.04 |
| 30 | 2.75 | 6.36 | 15.56 |
| 31 | 2.72 | 6.57 | 16.08 |

| | | | |
|---|---|---|---|
| 32 | 2.69 | 6.78 | 16.60 |
| 33 | 2.67 | 7.00 | 17.11 |
| 34 | 2.65 | 7.21 | 17.63 |
| 35 | 2.62 | 7.42 | 18.15 |
| 36 | 2.6 | 7.63 | 18.67 |
| 37 | 2.58 | 7.84 | 19.19 |
| 38 | 2.56 | 8.06 | 19.71 |
| 39 | 2.54 | 8.27 | 20.23 |
| 40 | 2.52 | 8.48 | 20.74 |
| 41 | 2.51 | 8.69 | 21.26 |
| 42 | 2.49 | 8.90 | 21.78 |

Table A7.5 – Sample K05 raw ABCC outputs from results presented in this thesis.

| **Sample ID** | **GCL0100-K05-POST-RR** | | |
|---|---|---|---|
| **Parameters** | Addition Volume per step (mL) | Acid Strength (N) | Sample Mass (g) |
| | **0.265** | **0.1** | **2.0001** |
| **step** | pH | HCl Added (mL) | H2SO4 added (kg/t) |
| 0 (Start) | 9.46 | 0.00 | 0.00 |
| 1 | 9.27 | 0.27 | 0.65 |
| 2 | 8.87 | 0.53 | 1.30 |
| 3 | 8.4 | 0.80 | 1.95 |
| 4 | 7.84 | 1.06 | 2.60 |
| 5 | 7.47 | 1.33 | 3.25 |
| 6 | 7.21 | 1.59 | 3.90 |
| 7 | 7 | 1.86 | 4.54 |
| 8 | 6.82 | 2.12 | 5.19 |
| 9 | 6.63 | 2.39 | 5.84 |
| 10 | 6.42 | 2.65 | 6.49 |
| 11 | 6.2 | 2.92 | 7.14 |
| 12 | 5.97 | 3.18 | 7.79 |
| 13 | 5.72 | 3.45 | 8.44 |
| 14 | 5.46 | 3.71 | 9.09 |
| 15 | 5.18 | 3.98 | 9.74 |
| 16 | 4.92 | 4.24 | 10.39 |
| 17 | 4.69 | 4.51 | 11.04 |
| 18 | 4.5 | 4.77 | 11.69 |
| 19 | 4.35 | 5.04 | 12.34 |
| 20 | 4.21 | 5.30 | 12.98 |
| 21 | 4.09 | 5.57 | 13.63 |
| 22 | 3.99 | 5.83 | 14.28 |
| 23 | 3.89 | 6.10 | 14.93 |
| 24 | 3.8 | 6.36 | 15.58 |

| | | | |
|---|---|---|---|
| 25 | 3.71 | 6.63 | 16.23 |
| 26 | 3.63 | 6.89 | 16.88 |
| 27 | 3.56 | 7.16 | 17.53 |
| 28 | 3.49 | 7.42 | 18.18 |
| 29 | 3.42 | 7.69 | 18.83 |
| 30 | 3.36 | 7.95 | 19.48 |
| 31 | 3.31 | 8.22 | 20.13 |
| 32 | 3.25 | 8.48 | 20.77 |
| 33 | 3.2 | 8.75 | 21.42 |
| 34 | 3.16 | 9.01 | 22.07 |
| 35 | 3.11 | 9.28 | 22.72 |
| 36 | 3.07 | 9.54 | 23.37 |
| 37 | 3.03 | 9.81 | 24.02 |
| 38 | 3 | 10.07 | 24.67 |
| 39 | 2.97 | 10.34 | 25.32 |
| 40 | 2.94 | 10.60 | 25.97 |
| 41 | 2.91 | 10.87 | 26.62 |
| 42 | 2.88 | 11.13 | 27.27 |
| 43 | 2.86 | 11.40 | 27.92 |
| 44 | 2.84 | 11.66 | 28.57 |
| 45 | 2.82 | 11.93 | 29.21 |
| 46 | 2.8 | 12.19 | 29.86 |

Table A7.6 – Sample K08 raw ABCC outputs from results presented in this thesis.

| **Sample ID** | **GCL0100-K08-POST** | | |
|---|---|---|---|
| **Parameters** | Addition Volume per step (mL) | Acid Strength (N) | Sample Mass (g) |
| | **0.2008** | **0.1** | **2.0021** |
| **step** | pH | HCl Added (mL) | H2SO4 added (kg/t) |
| 0 (Start) | 9.5 | 0.00 | 0.00 |
| 1 | 9.15 | 0.20 | 0.49 |
| 2 | 8.07 | 0.40 | 0.98 |
| 3 | 7.31 | 0.60 | 1.47 |
| 4 | 6.88 | 0.80 | 1.97 |
| 5 | 6.5 | 1.00 | 2.46 |
| 6 | 6.08 | 1.20 | 2.95 |
| 7 | 5.68 | 1.41 | 3.44 |
| 8 | 5.33 | 1.61 | 3.93 |
| 9 | 4.88 | 1.81 | 4.42 |
| 10 | 4.53 | 2.01 | 4.91 |
| 11 | 4.26 | 2.21 | 5.41 |
| 12 | 4.05 | 2.41 | 5.90 |
| 13 | 3.87 | 2.61 | 6.39 |

| | | | |
|---|---|---|---|
| 14 | 3.72 | 2.81 | 6.88 |
| 15 | 3.6 | 3.01 | 7.37 |
| 16 | 3.48 | 3.21 | 7.86 |
| 17 | 3.38 | 3.41 | 8.35 |
| 18 | 3.29 | 3.61 | 8.85 |
| 19 | 3.21 | 3.82 | 9.34 |
| 20 | 3.14 | 4.02 | 9.83 |
| 21 | 3.08 | 4.22 | 10.32 |
| 22 | 3.02 | 4.42 | 10.81 |
| 23 | 2.97 | 4.62 | 11.30 |
| 24 | 2.92 | 4.82 | 11.79 |
| 25 | 2.88 | 5.02 | 12.29 |
| 26 | 2.84 | 5.22 | 12.78 |
| 27 | 2.8 | 5.42 | 13.27 |
| 28 | 2.77 | 5.62 | 13.76 |
| 29 | 2.74 | 5.82 | 14.25 |
| 30 | 2.71 | 6.02 | 14.74 |
| 31 | 2.68 | 6.22 | 15.23 |
| 32 | 2.65 | 6.43 | 15.73 |
| 33 | 2.63 | 6.63 | 16.22 |
| 34 | 2.61 | 6.83 | 16.71 |
| 35 | 2.59 | 7.03 | 17.20 |
| 36 | 2.57 | 7.23 | 17.69 |
| 37 | 2.55 | 7.43 | 18.18 |
| 38 | 2.53 | 7.63 | 18.67 |
| 39 | 2.51 | 7.83 | 19.17 |
| 40 | 2.49 | 8.03 | 19.66 |

Table A7.7 – Sample A-Pre raw ABCC outputs from results presented in this thesis.

| **Sample ID** | **GCL0100-A-PRE** | | |
|---|---|---|---|
| **Parameters** | Addition Volume per step (mL) | Acid Strength (N) | Sample Mass (g) |
| | **0.202** | **0.1** | **2.0014** |
| **step** | pH | HCl Added (mL) | H2SO4 added (kg/t) |
| 0 (Start) | 8.67 | 0.00 | 0.00 |
| 1 | 6.55 | 0.20 | 0.49 |
| 2 | 5.81 | 0.40 | 0.99 |
| 3 | 5.38 | 0.61 | 1.48 |
| 4 | 5.02 | 0.81 | 1.98 |
| 5 | 4.68 | 1.01 | 2.47 |
| 6 | 4.43 | 1.21 | 2.97 |
| 7 | 4.20 | 1.41 | 3.46 |
| 8 | 4.00 | 1.62 | 3.96 |

| | | | |
|---|---|---|---|
| 9 | 3.82 | 1.82 | 4.45 |
| 10 | 3.67 | 2.02 | 4.95 |
| 11 | 3.53 | 2.22 | 5.44 |
| 12 | 3.41 | 2.42 | 5.93 |
| 13 | 3.31 | 2.63 | 6.43 |
| 14 | 3.22 | 2.83 | 6.92 |
| 15 | 3.14 | 3.03 | 7.42 |
| 16 | 3.06 | 3.23 | 7.91 |
| 17 | 3.00 | 3.43 | 8.41 |
| 18 | 2.94 | 3.64 | 8.90 |
| 19 | 2.89 | 3.84 | 9.40 |
| 20 | 2.84 | 4.04 | 9.89 |
| 21 | 2.79 | 4.24 | 10.39 |
| 22 | 2.75 | 4.44 | 10.88 |
| 23 | 2.71 | 4.65 | 11.37 |
| 24 | 2.67 | 4.85 | 11.87 |
| 25 | 2.64 | 5.05 | 12.36 |
| 26 | 2.61 | 5.25 | 12.86 |
| 27 | 2.58 | 5.45 | 13.35 |
| 28 | 2.55 | 5.66 | 13.85 |
| 29 | 2.52 | 5.86 | 14.34 |
| 30 | 2.49 | 6.06 | 14.84 |

Table A7.8 – Sample A-Pre-DUP raw ABCC outputs from results presented in this thesis.

| **Sample ID** | **GCL0100-A-PRE-DUP-RR** | | |
|---|---|---|---|
| **Parameters** | Addition Volume per step (mL) | Acid Strength (N) | Sample Mass (g) |
| | **0.212** | **0.1** | **2.0001** |
| **step** | pH | HCl Added (mL) | H2SO4 added (kg/t) |
| 0 (Start) | 9.04 | 0.00 | 0.00 |
| 1 | 6.61 | 0.21 | 0.52 |
| 2 | 5.82 | 0.42 | 1.04 |
| 3 | 5.41 | 0.64 | 1.56 |
| 4 | 5.09 | 0.85 | 2.08 |
| 5 | 4.77 | 1.06 | 2.60 |
| 6 | 4.49 | 1.27 | 3.12 |
| 7 | 4.27 | 1.48 | 3.64 |
| 8 | 4.09 | 1.70 | 4.15 |
| 9 | 3.93 | 1.91 | 4.67 |
| 10 | 3.8 | 2.12 | 5.19 |
| 11 | 3.67 | 2.33 | 5.71 |
| 12 | 3.55 | 2.54 | 6.23 |

| | | | |
|---|---|---|---|
| 13 | 3.45 | 2.76 | 6.75 |
| 14 | 3.35 | 2.97 | 7.27 |
| 15 | 3.26 | 3.18 | 7.79 |
| 16 | 3.19 | 3.39 | 8.31 |
| 17 | 3.12 | 3.60 | 8.83 |
| 18 | 3.06 | 3.82 | 9.35 |
| 19 | 3.01 | 4.03 | 9.87 |
| 20 | 2.96 | 4.24 | 10.39 |
| 21 | 2.91 | 4.45 | 10.91 |
| 22 | 2.87 | 4.66 | 11.43 |
| 23 | 2.83 | 4.88 | 11.95 |
| 24 | 2.8 | 5.09 | 12.46 |
| 25 | 2.76 | 5.30 | 12.98 |
| 26 | 2.73 | 5.51 | 13.50 |
| 27 | 2.7 | 5.72 | 14.02 |
| 28 | 2.67 | 5.94 | 14.54 |
| 29 | 2.64 | 6.15 | 15.06 |
| 30 | 2.62 | 6.36 | 15.58 |
| 31 | 2.59 | 6.57 | 16.10 |
| 32 | 2.57 | 6.78 | 16.62 |
| 33 | 2.55 | 7.00 | 17.14 |
| 34 | 2.52 | 7.21 | 17.66 |
| 35 | 2.5 | 7.42 | 18.18 |
| 36 | 2.48 | 7.63 | 18.70 |

Table A7.9 – Sample A02 raw ABCC outputs from results presented in this thesis.

| **Sample ID** | **GCL0100-A02-POST** | | |
|---|---|---|---|
| **Parameters** | Addition Volume per step (mL) | Acid Strength (N) | Sample Mass (g) |
| | **0.2008** | **0.1** | **2.0003** |
| **step** | pH | HCl Added (mL) | H2SO4 added (kg/t) |
| 0 (Start) | 8.89 | 0.00 | 0.00 |
| 1 | 7.08 | 0.20 | 0.49 |
| 2 | 6.16 | 0.40 | 0.98 |
| 3 | 5.64 | 0.60 | 1.48 |
| 4 | 5.26 | 0.80 | 1.97 |
| 5 | 4.86 | 1.00 | 2.46 |
| 6 | 4.58 | 1.20 | 2.95 |
| 7 | 4.4 | 1.41 | 3.44 |
| 8 | 4.28 | 1.61 | 3.94 |
| 9 | 4.16 | 1.81 | 4.43 |
| 10 | 4.07 | 2.01 | 4.92 |
| 11 | 3.97 | 2.21 | 5.41 |

| | | | |
|---|---|---|---|
| 12 | 3.88 | 2.41 | 5.90 |
| 13 | 3.8 | 2.61 | 6.39 |
| 14 | 3.72 | 2.81 | 6.89 |
| 15 | 3.64 | 3.01 | 7.38 |
| 16 | 3.58 | 3.21 | 7.87 |
| 17 | 3.51 | 3.41 | 8.36 |
| 18 | 3.46 | 3.61 | 8.85 |
| 19 | 3.4 | 3.82 | 9.35 |
| 20 | 3.34 | 4.02 | 9.84 |
| 21 | 3.29 | 4.22 | 10.33 |
| 22 | 3.23 | 4.42 | 10.82 |
| 23 | 3.18 | 4.62 | 11.31 |
| 24 | 3.14 | 4.82 | 11.81 |
| 25 | 3.09 | 5.02 | 12.30 |
| 26 | 3.05 | 5.22 | 12.79 |
| 27 | 3.02 | 5.42 | 13.28 |
| 28 | 2.99 | 5.62 | 13.77 |
| 29 | 2.95 | 5.82 | 14.26 |
| 30 | 2.92 | 6.02 | 14.76 |
| 31 | 2.89 | 6.22 | 15.25 |
| 32 | 2.86 | 6.43 | 15.74 |
| 33 | 2.84 | 6.63 | 16.23 |
| 34 | 2.81 | 6.83 | 16.72 |
| 35 | 2.79 | 7.03 | 17.22 |
| 36 | 2.76 | 7.23 | 17.71 |
| 37 | 2.74 | 7.43 | 18.20 |
| 38 | 2.72 | 7.63 | 18.69 |
| 39 | 2.69 | 7.83 | 19.18 |
| 40 | 2.67 | 8.03 | 19.68 |
| 41 | 2.65 | 8.23 | 20.17 |
| 42 | 2.63 | 8.43 | 20.66 |
| 43 | 2.61 | 8.63 | 21.15 |
| 44 | 2.59 | 8.84 | 21.64 |
| 45 | 2.57 | 9.04 | 22.13 |
| 46 | 2.55 | 9.24 | 22.63 |
| 47 | 2.53 | 9.44 | 23.12 |
| 48 | 2.52 | 9.64 | 23.61 |
| 49 | 2.5 | 9.84 | 24.10 |

Table A7.10 – Sample A05 raw ABCC outputs from results presented in this thesis.

| **Sample ID** | **GCL0100-A05-POST** | | |
|---|---|---|---|
| **Parameters** | Addition Volume per step (mL) | Acid Strength (N) | Sample Mass (g) |
| | **0.212** | **0.1** | **2.000** |
| **step** | pH | HCl Added (mL) | H2SO4 added (kg/t) |
| 0 (Start) | 8.46 | 0.00 | 0.00 |
| 1 | 7.01 | 0.21 | 0.52 |
| 2 | 5.89 | 0.42 | 1.04 |
| 3 | 5.29 | 0.64 | 1.56 |
| 4 | 4.76 | 0.85 | 2.08 |
| 5 | 4.45 | 1.06 | 2.60 |
| 6 | 4.25 | 1.27 | 3.12 |
| 7 | 4.1 | 1.48 | 3.64 |
| 8 | 3.96 | 1.70 | 4.16 |
| 9 | 3.84 | 1.91 | 4.67 |
| 10 | 3.72 | 2.12 | 5.19 |
| 11 | 3.62 | 2.33 | 5.71 |
| 12 | 3.52 | 2.54 | 6.23 |
| 13 | 3.42 | 2.76 | 6.75 |
| 14 | 3.34 | 2.97 | 7.27 |
| 15 | 3.26 | 3.18 | 7.79 |
| 16 | 3.19 | 3.39 | 8.31 |
| 17 | 3.12 | 3.60 | 8.83 |
| 18 | 3.06 | 3.82 | 9.35 |
| 19 | 3 | 4.03 | 9.87 |
| 20 | 2.95 | 4.24 | 10.39 |
| 21 | 2.9 | 4.45 | 10.91 |
| 22 | 2.86 | 4.66 | 11.43 |
| 23 | 2.82 | 4.88 | 11.95 |
| 24 | 2.78 | 5.09 | 12.47 |
| 25 | 2.74 | 5.30 | 12.99 |
| 26 | 2.71 | 5.51 | 13.50 |
| 27 | 2.68 | 5.72 | 14.02 |
| 28 | 2.65 | 5.94 | 14.54 |
| 29 | 2.62 | 6.15 | 15.06 |
| 30 | 2.59 | 6.36 | 15.58 |
| 31 | 2.57 | 6.57 | 16.10 |
| 32 | 2.54 | 6.78 | 16.62 |
| 33 | 2.52 | 7.00 | 17.14 |
| 34 | 2.49 | 7.21 | 17.66 |

Table A7.10 – Sample A08 raw ABCC outputs from results presented in this thesis.

| **Sample ID** | **GCL0100-A08-POST** | | |
|---|---|---|---|
| **Parameters** | Addition Volume per step (mL) | Acid Strength (N) | Sample Mass (g) |
| | **0.2008** | **0.1** | **2.0011** |
| **step** | pH | HCl Added (mL) | H2SO4 added (kg/t) |
| 0 (Start) | 9.5 | 0.00 | 0.00 |
| 1 | 8.18 | 0.20 | 0.49 |
| 2 | 6.76 | 0.40 | 0.98 |
| 3 | 6.01 | 0.60 | 1.48 |
| 4 | 5.48 | 0.80 | 1.97 |
| 5 | 5 | 1.00 | 2.46 |
| 6 | 4.67 | 1.20 | 2.95 |
| 7 | 4.45 | 1.41 | 3.44 |
| 8 | 4.29 | 1.61 | 3.93 |
| 9 | 4.15 | 1.81 | 4.43 |
| 10 | 4.03 | 2.01 | 4.92 |
| 11 | 3.92 | 2.21 | 5.41 |
| 12 | 3.82 | 2.41 | 5.90 |
| 13 | 3.73 | 2.61 | 6.39 |
| 14 | 3.64 | 2.81 | 6.88 |
| 15 | 3.56 | 3.01 | 7.38 |
| 16 | 3.48 | 3.21 | 7.87 |
| 17 | 3.41 | 3.41 | 8.36 |
| 18 | 3.35 | 3.61 | 8.85 |
| 19 | 3.28 | 3.82 | 9.34 |
| 20 | 3.22 | 4.02 | 9.83 |
| 21 | 3.17 | 4.22 | 10.33 |
| 22 | 3.11 | 4.42 | 10.82 |
| 23 | 3.07 | 4.62 | 11.31 |
| 24 | 3.02 | 4.82 | 11.80 |
| 25 | 2.98 | 5.02 | 12.29 |
| 26 | 2.94 | 5.22 | 12.78 |
| 27 | 2.9 | 5.42 | 13.28 |
| 28 | 2.87 | 5.62 | 13.77 |
| 29 | 2.83 | 5.82 | 14.26 |
| 30 | 2.8 | 6.02 | 14.75 |
| 31 | 2.77 | 6.22 | 15.24 |
| 32 | 2.74 | 6.43 | 15.73 |
| 33 | 2.71 | 6.63 | 16.23 |
| 34 | 2.69 | 6.83 | 16.72 |
| 35 | 2.66 | 7.03 | 17.21 |
| 36 | 2.64 | 7.23 | 17.70 |
| 37 | 2.61 | 7.43 | 18.19 |

| | | | |
|---|---|---|---|
| 38 | 2.59 | 7.63 | 18.68 |
| 39 | 2.57 | 7.83 | 19.18 |
| 40 | 2.55 | 8.03 | 19.67 |
| 41 | 2.53 | 8.23 | 20.16 |
| 42 | 2.51 | 8.43 | 20.65 |
| 43 | 2.49 | 8.63 | 21.14 |

# Appendix 8 – 24 hour 2:1 Leach test data

This appendix contains the raw data collected from 24 hour 2:1 leach tests undertaken in this study. Red values indicate the analytical detection limit (ADL).

Table A8.1a – Raw data outputs for 24 hours 2:1 (L:S) leach tests

| | | | | | | Alkalinity | | | Acidity | | | | | | | |
|---|---|---|---|---|---|---|---|---|---|---|---|---|---|---|---|---|
| Sample | Sample Volume (ml) | T ($^{O}$C) | pH | EC (µS/cm) | ORP (mV) | Alk 8.3 (ml) | Alk 8.3 (mg CaCO3/L) | Alk 4.5 (ml) | Alk 4.5 (mg CaCO3/L) | pH | Acid 4.5 (ml) | Acid 4.5 (mg CaCO3/L) | Acid 8.3 (ml) | Acid 8.3 (mg CaCO3/L) | Sulfate (mg/L) | IC (ppm) |
| A-PRE-LEACH | 50 | 20.89 | 8.07 | 341.3 | 230.79 | 0 | 0 | 0.82 | 2040 | 4.17 | 0.02 | 2.2 | 0.16 | 15.6 | 98.9 | 9.24 |
| A-PRE-LEACH-DUP | 50 | 20.68 | 8.13 | 344.5 | 224.46 | 0 | 0 | 0.83 | 2080 | 4.13 | 0.02 | 2.4 | 0.16 | 16 | 98.8 | 9.22 |
| A01-LEACH | 50 | 20.41 | 7.76 | 106 | 253.97 | 0 | 0 | 0.34 | 845 | 4.06 | 0.03 | 2.8 | 0.16 | 15.6 | 19.8 | 4.3 |
| A02-LEACH | 50 | 20.16 | 7.88 | 115.8 | 245.7 | 0 | 0 | 0.44 | 1100 | 4.05 | 0.03 | 2.6 | 0.15 | 15.2 | 18.9 | 5.11 |
| A03-LEACH | 50 | 20.23 | 7.95 | 116.7 | 229.09 | 0 | 0 | 0.57 | 1415 | 3.96 | 0.04 | 4 | 0.18 | 17.6 | 17.1 | 5.95 |
| A04-LEACH | 50 | 20.69 | 8.08 | 148.9 | 223.85 | 0 | 0 | 0.82 | 2050 | 3.89 | 0.04 | 4.4 | 0.18 | 18 | 18.7 | 8.65 |
| A05-LEACH | 50 | 20.42 | 8.06 | 119.5 | 222.92 | 0 | 0 | 0.56 | 1390 | 3.84 | 0.05 | 4.6 | 0.19 | 18.8 | 16.7 | 6.09 |
| A05-LEACH-DUP | 50 | 20.15 | 8.08 | 120.4 | 222.08 | 0 | 0 | 0.54 | 1360 | 3.83 | 0.05 | 4.8 | 0.18 | 18 | 16.5 | 5.98 |
| A06-LEACH | 50 | 20.27 | 7.99 | 118.3 | 225.95 | 0 | 0 | 0.5 | 1240 | 3.86 | 0.04 | 4.4 | 0.18 | 17.6 | 18.3 | 5.32 |
| A07-LEACH | 50 | 20.64 | 7.88 | 96.7 | 257.33 | 0 | 0 | 0.39 | 965 | 3.98 | 0.04 | 4 | 0.18 | 17.6 | 17.2 | 3.56 |
| A08-LEACH | 50 | 20.55 | 7.87 | 106 | 236.58 | 0 | 0 | 0.44 | 1110 | 3.95 | 0.04 | 4 | 0.17 | 17.2 | 16.1 | 4.42 |
| A09-LEACH | 50 | 20.27 | 7.9 | 102.9 | 236.5 | 0 | 0 | 0.43 | 1070 | 3.99 | 0.04 | 3.6 | 0.18 | 17.6 | 15.9 | 4.28 |
| K-PRE-LEACH | 50 | 20.99 | 9.62 | 386.6 | 146.08 | 0.14 | 360 | 0.57 | 1420 | 3.37 | 0.18 | 17.8 | 0.31 | 31.2 | 106.8 | 5.92 |
| K-PRE-LEACH-DUP | 50 | 20.79 | 9.6 | 387.6 | 138.5 | 0.15 | 365 | 0.59 | 1485 | 3.39 | 0.18 | 18.2 | 0.32 | 31.8 | 106.1 | 6.01 |
| K01-LEACH | 50 | 22.53 | 9.78 | 231.2 | 161.51 | 0.2 | 10 | 0.56 | 27.75 | 3.39 | 0.26 | 26 | 0.41 | 40.8 | 39.0 | 6.54 |
| K01-LEACH-DUP | 50 | 23.46 | 9.59 | 231.1 | 138.47 | 0.18 | 9 | 0.62 | 30.75 | 3.36 | 0.26 | 25.8 | 0.4 | 40 | 39.2 | 7.78 |
| K02--LEACH | 50 | 22.37 | 9.73 | 285.8 | 145.27 | 0.2 | 9.75 | 0.56 | 28 | 3.24 | 0.33 | 33.4 | 0.48 | 48.2 | 57.8 | 5.55 |
| K03-LEACH | 50 | 22.6 | 9.82 | 217.7 | 138.87 | 0.22 | 11.25 | 0.56 | 28.25 | 3.41 | 0.26 | 26 | 0.41 | 40.6 | 34.6 | 5.1 |

| | | | | | | | | | | | | | | | |
|---|---|---|---|---|---|---|---|---|---|---|---|---|---|---|---|
| K04-LEACH | 50 | 22.39 | 9.88 | 206.2 | 132.68 | 0.22 | 10.75 | 0.5 | 24.75 | 3.39 | 0.26 | 26 | 0.41 | 40.8 | 31.7 | 5.73 |
| K05-LEACH | 50 | 22.68 | 9.93 | 230.3 | 126.34 | 0.25 | 12.25 | 0.5 | 25.25 | 3.33 | 0.22 | 22 | 0.39 | 39.4 | 37.1 | 6.53 |
| K06-LEACH | 50 | 24.05 | 9.86 | 215.3 | 130.5 | 0.22 | 11.25 | 0.52 | 26.25 | 3.39 | 0.26 | 26 | 0.41 | 41 | 35.7 | 6.76 |
| K07-LEACH | 50 | 23.61 | 9.73 | 295.1 | 129.17 | 0.2 | 9.75 | 0.52 | 26 | 3.24 | 0.33 | 33.4 | 0.48 | 48.2 | 61.6 | 6.94 |
| K08-LEACH | 50 | 23.43 | 9.75 | 279.2 | 128.26 | 0.2 | 10.25 | 0.55 | 27.25 | 3.27 | 0.26 | 26.2 | 0.48 | 48.2 | 55.6 | 6.2 |
| K09-LEACH | 50 | 23.42 | 9.73 | 279.5 | 128.57 | 0.2 | 10 | 0.54 | 26.75 | 3.3 | 0.26 | 26 | 0.48 | 48 | 56.8 | 6.08 |

## Table A8.1b – Raw data outputs for 24 hours 2:1 (L:S) leach tests

| | Ca | Fe | K | Mg | Na | S | Si | Ag | Al | As | B | Ba | Be | Bi | Cd | Co | Cr | Cu | Hg | Li |
|---|---|---|---|---|---|---|---|---|---|---|---|---|---|---|---|---|---|---|---|---|
| | ppm | ppm | ppm | ppm | ppm | ppm | ppm | ppb | ppb | ppb | ppb | ppb | ppb | ppb | ppb | ppb | ppb | ppb | ppb | ppb |
| Sample I DL -> | 0.1 | 0.1 | 0.1 | 0.1 | 0.1 | 1 | 0.1 | 1 | 10 | 0.1 | 10 | 1 | 1 | 1 | 0.1 | 1 | 1 | 1 | 0.05 | 10 |
| A-PRE-LEACH | 37.45 | ***0.1*** | 32.19 | 5.823 | 6.893 | 35.24 | 2.21 | ***1*** | 148.6 | 0.408 | 26 | 40.55 | ***1*** | ***1*** | ***0.1*** | ***1*** | ***1*** | ***1*** | ***0.05*** | 11.42 |
| A-PRE-LEACH-DUP | 37.96 | ***0.1*** | 32.69 | 6.015 | 7.141 | 34.92 | 2.231 | ***1*** | 150.3 | 0.44 | 22.47 | 40.96 | ***1*** | ***1*** | ***0.1*** | ***1*** | ***1*** | ***1*** | ***0.05*** | ***10*** |
| A01-LEACH | 5.2 | 0.979 | 21.62 | 0.827 | 3.56 | 8.751 | 3.973 | ***1*** | 2229 | 0.408 | 20.99 | 66.51 | ***1*** | ***1*** | ***0.1*** | ***1*** | ***1*** | 13.16 | ***0.05*** | ***10*** |
| A02-LEACH | 7.204 | 0.339 | 20.99 | 0.77 | 3.058 | 8.379 | 2.833 | ***1*** | 703.9 | 0.279 | 16.1 | 52.14 | ***1*** | ***1*** | ***0.1*** | ***1*** | ***1*** | 5.436 | ***0.05*** | ***10*** |
| A03-LEACH | 7.74 | 0.167 | 22.16 | 0.717 | 3.263 | 8.683 | 2.228 | ***1*** | 800.2 | 0.403 | 21.87 | 37.59 | ***1*** | ***1*** | ***0.1*** | ***1*** | ***1*** | 3.48 | ***0.05*** | ***10*** |
| A04-LEACH | 12.55 | ***0.1*** | 23.18 | 0.849 | 3.433 | 9.085 | 2.088 | ***1*** | 496.5 | 0.357 | 20.76 | 40.13 | ***1*** | ***1*** | ***0.1*** | ***1*** | ***1*** | ***1*** | ***0.05*** | ***10*** |
| A06-LEACH | 7.136 | 0.43 | 22.64 | 0.75 | 4.244 | 9.318 | 2.933 | ***1*** | 1369 | 0.527 | 23.46 | 64.47 | ***1*** | ***1*** | ***0.1*** | ***1*** | ***1*** | 7.993 | ***0.05*** | ***10*** |
| A07-LEACH | 3.854 | 1.342 | 21.65 | 0.77 | 4.2 | 8.346 | 4.858 | ***1*** | ***10*** | 0.557 | 21.7 | 93.05 | ***1*** | ***1*** | ***0.1*** | ***1*** | 1.156 | 15.56 | ***0.05*** | ***10*** |
| A08-LEACH | 5.075 | 0.673 | 21.37 | 0.686 | 4.184 | 8.214 | 3.56 | ***1*** | 848.4 | 0.388 | 21.94 | 55.06 | ***1*** | ***1*** | ***0.1*** | ***1*** | ***1*** | 7.931 | ***0.05*** | ***10*** |
| A09-LEACH | 4.883 | 1.153 | 21.53 | 0.69 | 3.618 | 9.218 | 4.525 | ***1*** | 6692 | 0.493 | 24.27 | 76.87 | ***1*** | ***1*** | ***0.1*** | ***1*** | 1.063 | 14.43 | ***0.05*** | ***10*** |
| K-PRE-LEACH | 23.22 | ***0.1*** | 19.33 | 25.56 | 6.779 | 49.41 | 9.193 | ***1*** | ***10*** | 2.34 | ***10*** | 23.47 | ***1*** | ***1*** | ***0.1*** | ***1*** | ***1*** | ***1*** | ***0.05*** | ***10*** |
| K-PRE-LEACH-DUP | 23.09 | ***0.1*** | 19.35 | 25.38 | 6.738 | 49.62 | 9.169 | ***1*** | ***10*** | 2.283 | ***10*** | 23.22 | ***1*** | ***1*** | ***0.1*** | ***1*** | ***1*** | ***1*** | ***0.05*** | ***10*** |
| K01-LEACH | 21.22 | ***0.1*** | 9.592 | 12.13 | 3.038 | 27.51 | 16.93 | ***1*** | ***10*** | 4.337 | 56.37 | 17.87 | ***1*** | ***1*** | ***0.1*** | ***1*** | ***1*** | 1.625 | ***0.05*** | ***10*** |
| K01-LEACH-DUP | 16.62 | ***0.1*** | 6.823 | 10.01 | 2.431 | 22.52 | 13.5 | ***1*** | ***10*** | 2.342 | ***10*** | 14.74 | ***1*** | ***1*** | ***0.1*** | ***1*** | ***1*** | 1.298 | ***0.05*** | ***10*** |
| K02--LEACH | 26.44 | ***0.1*** | 10.55 | 16.68 | 3.299 | 41.29 | 17.81 | ***1*** | 18.17 | 4.13 | 42.55 | 23.24 | ***1*** | ***1*** | ***0.1*** | ***1*** | ***1*** | 2.015 | ***0.05*** | ***10*** |
| K03-LEACH | 16.28 | ***0.1*** | 6.412 | 9.616 | 2.519 | 21.24 | 15.14 | ***1*** | ***10*** | 1.991 | ***10*** | 14.16 | ***1*** | ***1*** | ***0.1*** | ***1*** | ***1*** | 2.018 | 0.058 | ***10*** |

| | | | | | | | | | | | | | | | | | | | |
|---|---|---|---|---|---|---|---|---|---|---|---|---|---|---|---|---|---|---|---|
| K04-LEACH | 16.5 | 0.1 | 8.571 | 7.22 | 2.643 | 18.43 | 12.8 | 1 | 10 | 1.828 | 10 | 11.59 | 1 | 1 | 0.1 | 1 | 1 | 1.553 | 0.05 | 10 |
| K05-LEACH | 18.94 | 0.1 | 7.484 | 7.724 | 2.946 | 28.5 | 13.09 | 1 | 10 | 1.265 | 10 | 13.83 | 1 | 1 | 0.1 | 1 | 1 | 1 | 0.05 | 10 |
| K06-LEACH | 17.31 | 0.1 | 6.977 | 7.934 | 2.458 | 24.2 | 12.56 | 1 | 10 | 1.366 | 10 | 12.57 | 1 | 1 | 0.1 | 1 | 1 | 1.225 | 0.05 | 10 |
| K07-LEACH | 23.07 | 0.1 | 7.602 | 12.92 | 2.435 | 43.12 | 12.53 | 1 | 10 | 2.371 | 10 | 15.65 | 1 | 1 | 0.1 | 1 | 1 | 1.058 | 0.051 | 10 |
| K08-LEACH | 21.84 | 0.1 | 8.086 | 11.83 | 2.317 | 28.73 | 14.08 | 1 | 10 | 2.521 | 10 | 16.41 | 1 | 1 | 0.1 | 1 | 1 | 1 | 0.05 | 10 |
| K09-LEACH | 21.18 | 0.1 | 8.538 | 11.69 | 2.262 | 35.62 | 12.84 | 1 | 10 | 2.141 | 10 | 15.67 | 1 | 1 | 0.1 | 1 | 1 | 1.103 | 0.05 | 10 |

Table A8.1c – Raw data outputs for 24 hours 2:1 (L:S) leach tests

| | Mn | Mo | Ni | P | Pb | Rb | Sb | Se | Sn | Sr | Th | Ti | Tl | U | V | W | Zn |
|---|---|---|---|---|---|---|---|---|---|---|---|---|---|---|---|---|---|
| | ppb | ppb | ppb | ppb | ppb | ppb | ppb | ppb | ppb | ppb | ppb | ppb | ppb | ppb | ppb | ppb | ppb |
| Sample | 1 | 0.5 | 1 | 50 | 0.1 | 1 | 0.5 | 0.1 | 0.5 | 1 | 0.5 | 1 | 0.5 | 0.1 | 0.5 | 5 | 1 |
| A-PRE-LEACH | 112.5 | 2.4 | 1 | 50 | 0.1 | 10.4 | 1.982 | 1.867 | 0.5 | 202.4 | 0.5 | 2.116 | 0.5 | 1.516 | 0.517 | 5 | 1 |
| A-PRE-LEACH-DUP | 114 | 2.451 | 1 | 50 | 0.1 | 10.45 | 2.003 | 1.955 | 0.5 | 204 | 0.5 | 1.896 | 0.5 | 1.588 | 0.533 | 5 | 1 |
| A01-LEACH | 50.99 | 1.64 | 1 | 50 | 3.019 | 10.09 | 1.357 | 0.989 | 0.568 | 29.18 | 0.5 | 80.93 | 0.5 | 0.309 | 2.865 | 5 | 3.05 |
| A02-LEACH | 32.49 | 1.59 | 1 | 50 | 1.246 | 8.573 | 1.331 | 0.853 | 0.5 | 34.56 | 0.5 | 27.67 | 0.5 | 0.244 | 1.53 | 5 | 1.122 |
| A03-LEACH | 16.98 | 1.761 | 1 | 50 | 0.708 | 7.026 | 1.411 | 0.748 | 0.5 | 38 | 0.5 | 14.38 | 0.5 | 0.3 | 2.246 | 5 | 1 |
| A04-LEACH | 10.78 | 2.359 | 1 | 50 | 0.104 | 8.144 | 1.568 | 0.9 | 0.5 | 50.42 | 0.5 | 2.629 | 0.5 | 0.491 | 1.479 | 5 | 1 |
| A06-LEACH | 24.41 | 1.193 | 1 | 50 | 2.034 | 8.119 | 1.518 | 0.856 | 0.5 | 42.53 | 0.5 | 33.88 | 0.5 | 0.336 | 3.412 | 5 | 1.517 |
| A07-LEACH | 54.44 | 1.355 | 1 | 50 | 3.839 | 11.51 | 1.55 | 0.915 | 0.5 | 26.45 | 0.613 | 104.9 | 0.5 | 0.354 | 4.11 | 5 | 5.274 |
| A08-LEACH | 30.56 | 1.445 | 1 | 50 | 1.586 | 9.997 | 1.522 | 0.835 | 0.5 | 29.61 | 0.5 | 53.58 | 0.5 | 0.284 | 2.824 | 5 | 2.073 |
| A09-LEACH | 44.41 | 1.705 | 1 | 50 | 3.319 | 11.05 | 1.818 | 0.784 | 0.5 | 27.71 | 0.521 | 100.3 | 0.5 | 0.376 | 4.171 | 5 | 3.339 |
| K-PRE-LEACH | 1 | 0.903 | 4.014 | 50 | 0.1 | 43.21 | 0.668 | 1.803 | 0.5 | 37.83 | 0.5 | 2.921 | 0.5 | 0.1 | 1.998 | 5 | 1 |
| K-PRE-LEACH-DUP | 1 | 0.893 | 3.886 | 50 | 0.1 | 42.88 | 0.667 | 1.859 | 0.5 | 37.47 | 0.5 | 3.083 | 0.5 | 0.1 | 2.006 | 5 | 1 |
| K01-LEACH | 1 | 0.511 | 1.442 | 50 | 0.1 | 18.18 | 0.5 | 2.512 | 0.5 | 17.09 | 0.5 | 2.178 | 0.5 | 0.1 | 6.481 | 5 | 1 |
| K01-LEACH-DUP | 1 | 0.5 | 2.127 | 50 | 0.1 | 15.65 | 0.5 | 1.425 | 0.5 | 14.64 | 0.5 | 1.151 | 0.5 | 0.1 | 3.209 | 5 | 1 |
| K02--LEACH | 1.229 | 0.666 | 2.074 | 50 | 0.1 | 25.17 | 0.5 | 2.794 | 0.5 | 20.79 | 0.5 | 3.174 | 0.5 | 0.1 | 5.591 | 6.009 | 1 |
| K03-LEACH | 1 | 0.5 | 1.876 | 50 | 0.1 | 18.76 | 0.5 | 1.823 | 0.5 | 13.77 | 0.5 | 1.079 | 0.5 | 0.1 | 3.253 | 5 | 1 |

| | | | | | | | | | | | | | | | | |
|---|---|---|---|---|---|---|---|---|---|---|---|---|---|---|---|---|
| K04-LEACH | 1 | 0.5 | 1.943 | 50 | 0.1 | 23.73 | 0.5 | 2.013 | 0.5 | 14.87 | 0.5 | 1.064 | 0.5 | 0.1 | 3.369 | 5 | 1 |
| K05-LEACH | 1 | 0.5 | 1.495 | 50 | 0.1 | 18.93 | 0.5 | 2.155 | 0.5 | 17.59 | 0.5 | 1.155 | 0.5 | 0.1 | 3.447 | 5 | 1 |
| K06-LEACH | 1 | 0.5 | 1.884 | 50 | 0.1 | 19.55 | 0.5 | 2.706 | 0.5 | 15.33 | 0.5 | 1.046 | 0.5 | 0.1 | 3.066 | 5 | 1.334 |
| K07-LEACH | 1 | 0.5 | 2.14 | 50 | 0.1 | 22.32 | 0.5 | 2.822 | 0.5 | 18.55 | 0.5 | 1.735 | 0.5 | 0.1 | 2.752 | 9.231 | 1 |
| K08-LEACH | 1 | 0.5 | 1.911 | 50 | 0.1 | 23.41 | 0.5 | 2.706 | 0.5 | 17.5 | 0.5 | 1.438 | 0.5 | 0.1 | 2.983 | 5 | 1 |
| K09-LEACH | 1 | 0.5 | 2.48 | 50 | 0.1 | 24.6 | 0.5 | 2.567 | 0.5 | 16.96 | 0.5 | 1.571 | 0.5 | 0.1 | 2.982 | 5 | 1 |

# Appendix 9 – Raw Kevitsa Cover Trial System data

This appendix contains the raw cover trial pore gas compositional data collected from the Boliden Kevitsa mine.

Table A9.1 – Raw waste cover trial pore gas data from the Kevitsa mine

| | | Date | | | | | | | | | | | | | | | |
|---|---|---|---|---|---|---|---|---|---|---|---|---|---|---|---|---|---|
| | | 23/04/2019 | | | 17/07/2019 | | | 11/09/2019 | | | 30/12/2019 | | | 02/04/2020 | | | |
| **Location** | **Port** | **O2 %** | **CO2 %** | **CH4** | **O2 %** | **CO2 %** | **CH4** | **O2 %** | **CO2 %** | **CH4** | **O2 %** | **CO2 %** | **CH4** | **O2 %** | **CO2 %** | **CH4** | **DP** |
| **CST 1** | 1 | 20.7 | 0 | 0 | 20.6 | 0.1 | 0 | 21.4 | 0 | 0 | 20.2 | 0 | 0 | 19.9 | 0 | 0 | No reading |
| | 2 | 20.8 | 0 | 0 | 20.8 | 0.1 | 0 | 21.4 | 0 | 0 | 20.2 | 0 | 0 | 19.9 | 0 | 0 | No reading |
| | 3 | 20.9 | 0 | 0 | 20.6 | 0.1 | 0 | 21.3 | 0.1 | 0 | 20.1 | 0 | 0 | 19.8 | 0 | 0 | No reading |
| | 4 | 15.9 | 0.7 | 0 | 20.1 | 1.5 | 0 | 21.5 | 0 | 0 | 20.1 | 0 | 0 | 20 | 0 | 0 | No reading |
| | 5 | 20.8 | 0 | 0 | 20.1 | 1.3 | 0 | 21.1 | 0.4 | 0 | 19.6 | 0.2 | 0 | 18.7 | 1 | 0 | No reading |
| | 6 | 20.8 | 0 | 0 | 20.9 | 0 | 0 | 21.5 | 0 | 0 | 20 | 0 | 0 | 19.7 | 0.3 | 0.7 | No reading |
| **CST 2** | 1 | 18.7 | 0.6 | 0 | 19.6 | 0.8 | 0 | 19.9 | 0.8 | 0 | 20.1 | 0.4 | 0 | 19.8 | 0.3 | -29.08 | No reading |
| | 2 | 19.1 | 0.5 | 0 | 19.7 | 0.8 | 0 | 19.8 | 0.7 | 0 | 20.1 | 0.4 | 0 | 19.9 | 0.3 | -29.08 | No reading |
| | 3 | 10.5 | 4.1 | -0.1 | 18.3 | 1.6 | 0 | 15.3 | 5.6 | 0 | 20.6 | 0 | 0 | 19.9 | 0.3 | -29.08 | No reading |
| | 4 | 7.8 | 5.6 | -0.1 | 6.8 | 6.3 | 0 | 12.8 | 7.5 | 0 | 14.1 | 3.3 | 0 | 19.9 | 0.3 | -29.08 | No reading |
| | 5 | 7.7 | 6.2 | -0.1 | 5.7 | 7.9 | 0 | 11.6 | 7.9 | 0 | 17.5 | 1.4 | 0 | 19.8 | 0.3 | -29.08 | No reading |

# Appendix 10 – Paste pH raw data sheets

This appendix contains the raw paste pH and EC data collected within this study.

Table A10.1 – Aitik paste pH and EC data.

| Sample | Sample Mass (g) | De-ion Mass (g) | Start (T) | Measurement (T) | pH | EC (µS/cm) |
|---|---|---|---|---|---|---|
| A-Pre | 10.00 | 10.01 | 15:15 | 15:30 | 7.994 | 986 |
| A-Pre-DUP | 10.00 | 10.03 | 15:20 | 15:35 | 8.001 | 986 |
| A01-Post | 10.00 | 10.01 | 15:25 | 15:40 | 8.306 | 754 |
| A02-Post | 10.00 | 9.99 | 15:30 | 15:45 | 8.322 | 787 |
| A03-Post | 10.00 | 10.03 | 15:40 | 15:55 | 8.229 | 795 |
| A04-Post | 10.00 | 10.02 | 15:35 | 15:50 | 8.442 | 625 |
| A05-Post | 9.95 | 10.00 | 15:45 | 16:00 | 8.44 | 630 |
| A06-Post | 9.95 | 10.01 | 15:50 | 16:05 | 8.503 | 610 |
| A07-Post | 9.95 | 9.98 | 15:55 | 16:10 | 8.48 | 608 |
| A08-Post | 9.98 | 10.00 | 16:00 | 16:15 | 8.734 | 524 |
| A09-Post | 9.97 | 10.01 | 16:05 | 16:20 | 8.655 | 565 |
| | | | | | | |

Table A10.2 – Kevitsa paste pH and EC data.

| Sample | Sample Mass (g) | De-ion Mass (g) | Start (T) | Measurement (T) | pH | EC (µS/cm) |
|---|---|---|---|---|---|---|
| K-Pre | 9.97 | 10.02 | 16:10 | 16:25 | 8.907 | 712 |
| K-Pre-Dup | 9.98 | 10.01 | 16:15 | 16:30 | 8.901 | 735 |
| K01-Post | 9.98 | 10.00 | 16:20 | 16:35 | 8.833 | 689 |
| K02-Post | 10.00 | 9.99 | 16:25 | 16:40 | 8.914 | 673 |
| K03-Post | 9.98 | 9.97 | 16:30 | 16:45 | 8.865 | 669 |
| K04-Post | 10.00 | 10.02 | 16:35 | 16:50 | 8.823 | 727 |
| K05-Post | 10.01 | 10.02 | 16:40 | 16:55 | 8.875 | 679 |
| K06-Post | 9.95 | 9.99 | 16:45 | 17:00 | 8.859 | 690 |
| K07-Post | 9.95 | 10.00 | 16:50 | 17:05 | 8.91 | 613 |
| K08-Post | 10.04 | 10.01 | 16:55 | 17:10 | 8.845 | 698 |
| K09-Post | 10.02 | 10.01 | 17:00 | 17:15 | 8.867 | 649 |

# Appendix 11 – Boliden Kevitsa operational emissions data

This appendix contains the operational emissions data for the mill and mine from the Kevitsa mine collected between Ausgust 2016 and August 2018. Data provided by Boliden mines with permissions.

Table A11.1 – Kevitsa mine emissions data

| Month | Total direct $CO_2$ emissions, tonnes (ETS + non-ETS) | |
|---|---|---|
| | Mill | Mine |
| Aug'16 | 777 | 5116 |
| Sep'16 | 773 | 5259 |
| Oct'16 | 736 | 5498 |
| Nov'16 | 678 | 4903 |
| Dec'16 | 617 | 5119 |
| Jan'17 | 229 | 5160 |
| Feb'17 | 207 | 5365 |
| Mar'17 | 194 | 5384 |
| Apr'17 | 328 | 5416 |
| May'17 | 328 | 5416 |
| Jun'17 | 484 | 5180 |
| Jul'17 | 508 | 5425 |
| Aug'17 | 544 | 5561 |
| Sep'17 | 449 | 5871 |
| Oct'17 | 619 | 5348 |
| Nov'17 | 462 | 5676 |
| Dec'17 | 788 | 5611 |
| Jan'18 | 531 | 5405 |
| Feb'18 | 462 | 5358 |
| Mar'18 | 425 | 6193 |
| Apr'18 | 497 | 5430 |
| May'18 | 458 | 5883 |
| Jun'18 | 491 | 6189 |
| Jul'17 | 457 | 5747 |
| Aug'18 | 797 | 6377 |
| | Sources | |
| | -diesel and fuel oil for transportation<br>-wood chip for heat production<br>-purchased electricity<br>-purchased heat | -diesel and fuel oil for transportation<br>-usage of explosives |

# Appendix 12 – Raw NAG Test Data Outputs

This appendix contains the raw NAG data collected within this study

Table A12.1 – Raw NAG test data outputs

| **Project Name:** | GCL0100 | | | **Pre Boil** | | | **Post Boil** | | | | | | | | | |
|---|---|---|---|---|---|---|---|---|---|---|---|---|---|---|---|---|
| **Sample No.** | **Mass of Sample** | **Mass $H_2O$** | **Mass $H_2O_2$** | **Temp** | **pH** | **EC** | **Temp** | **pH** | **EC** | **Volume Back Titrated** | **Vol NaOH to pH 4.5 (ml)** | **Vol NaOH to pH 7.0 (ml)** | **Total Vol (ml)** | **pH 4.5 NAG** | **pH 7.0 NAG** | **Total NAG** |
| | **g** | | | **˚C** | | **µS/cm** | **˚C** | | **µS/cm** | **mL** | **mL** | | | **kg $H_2SO_4$ eq/t** | | |
| GCL0100-K-Pre | 1.5003 | 75 | 75 | 23.1 | 7.278 | 187.9 | 21.77 | 7.29 | 184.4 | 50 | 0 | 0 | 0 | 0 | 0 | 0 |
| GCL0100-K-Pre-Dup | 1.5003 | 75 | 75 | 22.9 | 7.137 | 189.2 | 21.69 | 7.32 | 174.8 | 50 | 0 | 0 | 0 | 0 | 0 | 0 |
| K01-HCT-POST-NAG | 1.5008 | 75 | 75 | | | | 21.8 | 7.53 | 222.2 | 50 | 0 | 0 | 0 | 0 | 0 | 0 |
| K01-HCT-POST-NAG-DUP | 1.5001 | 75 | 75 | | | | 21.88 | 7.59 | 219 | 50 | 0 | 0 | 0 | 0 | 0 | 0 |
| K02-HCT-POST-NAG | 1.5002 | 75 | 75 | | | | 22.27 | 7.74 | 226.6 | 50 | 0 | 0 | 0 | 0 | 0 | 0 |
| K03-HCT-POST-NAG | 1.4999 | 75 | 75 | | | | 22.26 | 7.57 | 193.2 | 50 | 0 | 0 | 0 | 0 | 0 | 0 |
| K04-HCT-POST-NAG | 1.5018 | 75 | 75 | | | | 22.36 | 7.64 | 195.1 | 50 | 0 | 0 | 0 | 0 | 0 | 0 |
| K05-HCT-POST-NAG | 1.501 | 75 | 75 | | | | 22.05 | 7.64 | 196.5 | 50 | 0 | 0 | 0 | 0 | 0 | 0 |
| K06-HCT-POST-NAG | 1.501 | 75 | 75 | | | | 22.22 | 7.61 | 190.1 | 50 | 0 | 0 | 0 | 0 | 0 | 0 |
| K07-HCT-POST-NAG | 1.501 | 75 | 75 | | | | 22.31 | 7.7 | 194.5 | 50 | 0 | 0 | 0 | 0 | 0 | 0 |
| K08-HCT-POST-NAG | 1.501 | 75 | 75 | | | | 21.81 | 7.55 | 187.3 | 50 | 0 | 0 | 0 | 0 | 0 | 0 |
| K09-HCT-POST-NAG | 1.501 | 75 | 75 | | | | 21.62 | 7.51 | 193.7 | 50 | 0 | 0 | 0 | 0 | 0 | 0 |
| GCL0100-A-Pre | 1.5019 | 75 | 75 | 21.3 | 3.459 | 345 | 21.71 | 3.37 | 327.1 | 50 | 0.29 | 0.67 | 0.96 | 2.83840469 | 3.7192889 | 6.55769359 |
| GCL0100-A-Pre-Dup | 1.5021 | 75 | 75 | 21.5 | 3.411 | 363 | 21.6 | 3.32 | 354.7 | 50 | 0.31 | 0.69 | 1 | 3.03375275 | 3.71879369 | 6.75254643 |
| A01-HCT-POST-NAG | 1.501 | 75 | 75 | | | | 21.68 | 4.15 | 208.6 | 50 | 0.08 | 0.46 | 0.54 | 0.78347768 | 4.50499667 | 5.28847435 |

| | | | | | | | | | | | | | | | | |
|---|---|---|---|---|---|---|---|---|---|---|---|---|---|---|---|---|
| A01-HCT-POST-NAG-DUP | 1.501 | 75 | 75 | | | | 21.5 | 4.14 | 210.4 | 50 | 0.08 | 0.47 | 0.55 | 0.78347768 | 4.60293138 | 5.38640906 |
| A02-HCT-POST-NAG | 1.501 | 75 | 75 | | | | 21.51 | 4.15 | 226.5 | 50 | 0.1 | 0.54 | 0.64 | 0.9793471 | 5.28847435 | 6.26782145 |
| A03-HCT-POST-NAG | 1.501 | 75 | 75 | | | | 21.57 | 4.14 | 209.3 | 50 | 0.09 | 0.51 | 0.6 | 0.88141239 | 4.99467022 | 5.87608261 |
| A04-HCT-POST-NAG | 1.501 | 75 | 75 | | | | 21.54 | 4.06 | 227.6 | 50 | 0.12 | 0.56 | 0.68 | 1.17521652 | 5.48434377 | 6.65956029 |
| A05-HCT-POST-NAG | 1.501 | 75 | 75 | | | | 21.56 | 4.16 | 212.4 | 50 | 0.07 | 0.47 | 0.54 | 0.68554297 | 4.60293138 | 5.28847435 |
| A06-HCT-POST-NAG | 1.501 | 75 | 75 | | | | 21.45 | 4.13 | 222.7 | 50 | 0.07 | 0.49 | 0.56 | 0.68554297 | 4.7988008 | 5.48434377 |
| A07-HCT-POST-NAG | 1.501 | 75 | 75 | | | | 21.39 | 4.08 | 222.6 | 50 | 0.1 | 0.57 | 0.67 | 0.9793471 | 5.58227848 | 6.56162558 |
| A08-HCT-POST-NAG | 1.501 | 75 | 75 | | | | 21.37 | 4.04 | 244.4 | 50 | 0.12 | 0.6 | 0.72 | 1.17521652 | 5.87608261 | 7.05129913 |
| A09-HCT-POST-NAG | 1.501 | 75 | 75 | | | | 21.31 | 4.13 | 223.3 | 50 | 0.09 | 0.51 | 0.6 | 0.88141239 | 4.99467022 | 5.87608261 |
| **RPD (A Duplicates)** | 0% | 0% | 0% | -1% | 1% | -5% | 1% | 1% | -8% | 0% | -7% | -3% | -4% | -7% | 0% | -3% |

# Appendix 13 – Initial HCT Cell Characteristics

| Geochemic ID | Drill Hole | Material Type | Mass Empty Cell (g) | Mass Cell, + Filter + Tubing (g) | Mass Cell, + Filter + Tubing + Sample (g) | Mass Cell, + Filter + Tubing + Sample + Water (g) | Cell Charge (g) | Initial Water Added (mL) | Calculation of actual cell charge added and initial water added | | | |
|---|---|---|---|---|---|---|---|---|---|---|---|---|
| | | | | | | | | | Actual Wet Cell Charge (g) | Calculated Dry Cell Charge Equivalent (g) | Initial Water Added | Total Water Added including pore water (g) |
| K01 | N/A | Waste rock (>22mm crushed) | 552.65 | 572.2 | 1572.2 | 2570.75 | 1000.0 | 998.6 | 1000.00 | 1000.00 | 998.60 | 998.60 |
| K02 | N/A | Waste rock (>22mm crushed) | 528.25 | 547.7 | 1547.6 | 2547 | 1000.0 | 999.4 | 999.95 | 999.95 | 999.40 | 999.40 |
| K03 | N/A | Waste rock (>22mm crushed) | 565 | 584.1 | 1584.2 | 2579.85 | 1000.1 | 995.7 | 1000.05 | 1000.05 | 995.70 | 995.70 |
| K04 | N/A | Waste rock (>22mm crushed) | 550.85 | 570.2 | 1570.2 | 2570.65 | 1000.0 | 1000.5 | 1000.00 | 1000.00 | 1000.45 | 1000.45 |
| K05 | N/A | Waste rock (>22mm crushed) | 509 | 528.3 | 1528.3 | 2527.05 | 1000.1 | 998.8 | 1000.05 | 1000.05 | 998.75 | 998.75 |
| K06 | N/A | Waste rock (>22mm crushed) | 542.2 | 561.8 | 1561.9 | 2560.6 | 1000.1 | 998.8 | 1000.05 | 1000.05 | 998.75 | 998.75 |

| | | | | | | | | | | | | |
|---|---|---|---|---|---|---|---|---|---|---|---|---|
| K07 | N/A | Waste rock (>22mm crushed) | 562.85 | 582.2 | 1582.3 | 2582.35 | 1000.1 | 1000.1 | 1000.05 | 1000.05 | 1000.10 | 1000.10 |
| K08 | N/A | Waste rock (>22mm crushed) | 521.1 | 540.1 | 1540.2 | 2537.05 | 1000.1 | 996.9 | 1000.05 | 1000.05 | 996.90 | 996.90 |
| K09 | N/A | Waste rock (>22mm crushed) | 532.8 | 552.4 | 1552.3 | 2548.6 | 1000.0 | 996.3 | 999.95 | 999.95 | 996.30 | 996.30 |
| **A01** | N/A | Waste rock (>22mm crushed) | 613 | 632.7 | 1632.7 | 2632.15 | 1000.1 | 999.5 | 1000.05 | 1000.05 | 999.45 | 999.45 |
| **A02** | N/A | Waste rock (>22mm crushed) | 569.5 | 588.8 | 1588.8 | 2585.3 | 1000.1 | 996.5 | 1000.05 | 1000.05 | 996.50 | 996.50 |
| **A03** | N/A | Waste rock (>22mm crushed) | 559.05 | 572.9 | 1574.9 | 2574.9 | 1002.1 | 1000.0 | 1002.05 | 1002.05 | 1000.00 | 1000.00 |
| **A04** | N/A | Waste rock (>22mm crushed) | 567.05 | 586.4 | 1586.3 | 2583.15 | 1000.0 | 996.9 | 999.95 | 999.95 | 996.85 | 996.85 |
| **A05** | N/A | Waste rock (>22mm crushed) | 570.2 | 588.9 | 1588.9 | 2588.85 | 1000.0 | 1000.0 | 1000.00 | 1000.00 | 1000.00 | 1000.00 |
| **A06** | N/A | Waste rock (>22mm crushed) | 581.8 | 600.3 | 1600.3 | 2592.9 | 1000.1 | 992.6 | 1000.05 | 1000.05 | 992.60 | 992.60 |

| | | | | | | | | | | | | |
|---|---|---|---|---|---|---|---|---|---|---|---|---|
| **A07** | N/A | Waste rock (>22mm crushed) | 569.55 | 588.9 | 1588.9 | 2585.7 | 1000.0 | 996.9 | 1000.00 | 1000.00 | 996.85 | 996.85 |
| **A08** | N/A | Waste rock (>22mm crushed) | 578 | 596.7 | 1596.7 | 2593.2 | 1000.0 | 996.5 | 1000.00 | 1000.00 | 996.50 | 996.50 |
| **A09** | N/A | Waste rock (>22mm crushed) | 565.25 | 584.3 | 1584.3 | 2583.1 | 1000.1 | 998.8 | 1000.05 | 1000.05 | 998.80 | 998.80 |

# Appendix 14 – Weekly HCT data outputs

Due to the size of the data tables produced within the 18 HCT cells within this study, raw data produced from weekly HCT leachates is not presented within the pdf version of this thesis submission. Raw data outputs are available in electronically formatted data sheets separate to this document. These documents contain data related to weekly outputs for the parameters:

- Produced leachate volumes.
- Cell water retention.
- Cell weights.
- Weekly aqueous analysis (pH, EC, ORP, DIC, sulfate, alkalinity, acidity, Eh)
- Weekly leachate elemental analysis
- Calibration Records

A summary of the weekly analytical outputs for the analytes pH, EC, DIC and sulfate are shown within this appendix for Kevitsa and Aitik cells. Blank cells indicate values that were either not available/measured during the protocol or where measurements were below ADL.

Table A14.1 – Kevitsa cell weekly leachate pH measurements

| pH | | | | | | | | | |
|---|---|---|---|---|---|---|---|---|---|
| **Week** | **K01** | **K02** | **K03** | **K04** | **K05** | **K06** | **K07** | **K08** | **K09** |
| 0 | 6.85 | 6.9 | 6.93 | 6.94 | 6.95 | 6.91 | 7.07 | 6.87 | 6.88 |
| 1 | 6.91 | 7 | 6.22 | 6.95 | 6.26 | 6.22 | 7.01 | 7.29 | 6.98 |
| 2 | 8.3 | 8.95 | 8.81 | 7.35 | 7.36 | 7.25 | 7.98 | 8.06 | 8.12 |
| 3 | 7.76 | 7.89 | 7.82 | 7.16 | 7.12 | 7.03 | 7.73 | 7.86 | 7.75 |
| 4 | 7.59 | 7.63 | 7.6 | 6.88 | 6.91 | 6.75 | 7.41 | 7.43 | 7.36 |
| 5 | 7.45 | 7.48 | 7.41 | 6.82 | 6.92 | 6.79 | 7.38 | 7.45 | 7.5 |
| 6 | 7.61 | 7.63 | 7.42 | 7.18 | 7.18 | 7.04 | 7.64 | 7.61 | 7.65 |
| 7 | 7.49 | 7.56 | 7.47 | 7.1 | 7.19 | 7.04 | 7.46 | 7.55 | 7.4 |
| 8 | 7.3 | 7.46 | 7.3 | 6.89 | 6.98 | 6.89 | 7.35 | 7.44 | 7.49 |
| 9 | 7.51 | 7.38 | 7.35 | 6.87 | 7.01 | 6.88 | 7.4 | 7.38 | 7.52 |
| 10 | 7.23 | 6.56 | 7.13 | 7.21 | 7.27 | 7.15 | 7.64 | 7.67 | 7.65 |
| 11 | 7.42 | 7.48 | 7.35 | 6.96 | 7.1 | 6.95 | 7.45 | 7.58 | 7.59 |
| 12 | 7.43 | 7.5 | 7.44 | 6.83 | 6.96 | 6.87 | 7.55 | 7.5 | 7.52 |
| 13 | 7.36 | 7.45 | 7.41 | 7.03 | 7.1 | 7.02 | 7.55 | 7.57 | 7.53 |
| 14 | 7.44 | 7.43 | 7.52 | 7.2 | 7.36 | 7.29 | 6.87 | 6.84 | 7.32 |
| 15 | 8 | 8 | 7.98 | 7.26 | 7.46 | 7.34 | 7.79 | 7.79 | 7.82 |
| 16 | 7.41 | 6.87 | 7.43 | 7.25 | 7.33 | 7.26 | 7.61 | 7.62 | 7.62 |
| 17 | 7.52 | 7.48 | 7.09 | 7.33 | 7.36 | 7.27 | 7.69 | 7.68 | 7.69 |

| | | | | | | | | | |
|---|---|---|---|---|---|---|---|---|---|
| 18 | 7.58 | 7.44 | 7.55 | 7.29 | 7.37 | 7.31 | 7.62 | 7.64 | 7.65 |
| 19 | 7.58 | 7.45 | 7.54 | 7.32 | 7.36 | 7.31 | 7.71 | 7.74 | 7.59 |
| 20 | 7.52 | 7.54 | 7.63 | 7.19 | 7.21 | 7.28 | 7.7 | 7.57 | 7.61 |
| 21 | 7.61 | 7.51 | 7.6 | 7.2 | 7.22 | 7.15 | 7.6 | 7.63 | 7.5 |
| 22 | 7.42 | 7.36 | 7.5 | 7.29 | 7.26 | 7.15 | 7.2 | 7.17 | 7.25 |
| 23 | 7.38 | 7.33 | 7.44 | 7.18 | 7.2 | 7.12 | 7.33 | 7.46 | 7.54 |
| 24 | 7.65 | 7.69 | 7.47 | 7.14 | 7.14 | 6.86 | 7.54 | 7.49 | 7.63 |
| 25 | 7.45 | 7.33 | 7.51 | 7.14 | 7.23 | 7.12 | 7.35 | 7.21 | 7.41 |
| 26 | 7.59 | 7.58 | 7.56 | 7.22 | 7.21 | 7.1 | 7.53 | 7.33 | 7.6 |
| 27 | 7.5 | 7.42 | 7.49 | 7.23 | 7.26 | 7.21 | 7.3 | 7.35 | 7.12 |
| 28 | 7.39 | 7.42 | 7.47 | 7.1 | 7.02 | 7.02 | 7 | 7.33 | 7.62 |
| 29 | 7.2 | 7.11 | 7.38 | 7.03 | 7.11 | 7.01 | 7.02 | 7.37 | 7.3 |
| 30 | 7.09 | 6.89 | 6.98 | 7.2 | 7.28 | 7.25 | 7.13 | 6.95 | 6.96 |
| 31 | 7.22 | 7.43 | 7.42 | 7.23 | 7.13 | 7.12 | 7.23 | 7.28 | 7.38 |
| 32 | 7.46 | 7.32 | 7.37 | 7.2 | 7.07 | 7.01 | 7.63 | 7.76 | 7.61 |
| 33 | 7.27 | 7.26 | 7.31 | 7.26 | 7.13 | 7.07 | 7.31 | 7.37 | 7.23 |
| 34 | 7 | 7.27 | 6.93 | 7.33 | 7.08 | 7.08 | 7.6 | 7.73 | 7.75 |
| 35 | 7.46 | 7.39 | 7.5 | 7.2 | 7.13 | 6.95 | 7.32 | 7.39 | 7.44 |
| 36 | 7.52 | 7.42 | 7.41 | 7.3 | 7.21 | 7.08 | 6.91 | 7.02 | 7.08 |
| 37 | 7.42 | 7.27 | 6.91 | 7.23 | 7.19 | 7.06 | 6.62 | 6.89 | 6.96 |
| 38 | 7.42 | 7.4 | 7.47 | 7.25 | 7.26 | 7.03 | 7.53 | 7.59 | 7.64 |
| 39 | 7.23 | 7.27 | 6.8 | 7.12 | 7.02 | 6.97 | 6.5 | 6.57 | 6.7 |
| 40 | 7.4 | 7.24 | 7.38 | 7.13 | 7.1 | 7.06 | 6.69 | 6.78 | 7.07 |
| 41 | 7.52 | 7.38 | 7.39 | 7.18 | 7.18 | 7.11 | 7.63 | 7.7 | 7.68 |
| 42 | 7.31 | 7.07 | 7.04 | 7 | 7.01 | 6.96 | 7.45 | 7.51 | 7.46 |
| 43 | 7.29 | 7.22 | 7.21 | 7.08 | 7.04 | 7.03 | 6.35 | 6.37 | 6.51 |
| 44 | 7.36 | 6.81 | 6.91 | 7.16 | 7.1 | 7.1 | 6.92 | 6.81 | 7.15 |
| 45 | 7.18 | 7.19 | 7.28 | 7.03 | 7.02 | 7.01 | 7.01 | 7.22 | 7.35 |
| 46 | | | | | | | | | |
| 47 | 7.11 | 7.22 | 7.32 | 6.43 | 6.79 | 6.78 | 7.32 | 7.2 | 7.3 |
| 48 | | | | | | | | | |
| 49 | 7.2 | 7.17 | 7.27 | 7.11 | 7.11 | 7.08 | 7.33 | 7.37 | 7.29 |
| 50 | 7.47 | 7.31 | 7.3 | 7.12 | 7.11 | 7.09 | 7.53 | 7.59 | 7.58 |
| 51 | 7.23 | 7.17 | 7.27 | 7.03 | 7.05 | 6.94 | 7.27 | 7.35 | 7.32 |
| 52 | 7.86 | 7.73 | 7.77 | 7.1 | 7.14 | 7.08 | 7.55 | 7.58 | 7.56 |
| 53 | 7.79 | 7.69 | 7.78 | 7.1 | 7.1 | 7.04 | 7.57 | 7.65 | 7.76 |
| 54 | 7.65 | 7.63 | 7.75 | 6.98 | 6.98 | 6.89 | 7.25 | 7.34 | 7.22 |
| 55 | 8.04 | 8.07 | 8.07 | 7.1 | 7.11 | 7.14 | 7.77 | 7.86 | 7.76 |
| 56 | 7.97 | 7.95 | 7.99 | 7.02 | 7.02 | 6.92 | 7.57 | 7.71 | 7.61 |
| 57 | 8.01 | 8.02 | 8.04 | 7.21 | 7.15 | 7.02 | 7.98 | 8.04 | 7.86 |
| 58 | 7.84 | 7.92 | 7.78 | 6.98 | 6.97 | 6.95 | 7.61 | 7.45 | 7.7 |
| 59 | 7.79 | 7.75 | 7.88 | 7.01 | 6.92 | 6.94 | 7.35 | 7.29 | 7.53 |
| 60 | 7.82 | 7.6 | 7.76 | 7.03 | 7.03 | 7.04 | 7.67 | 7.38 | 7.54 |
| Minimum | 6.85 | 6.56 | 6.22 | 6.43 | 6.26 | 6.22 | 6.35 | 6.37 | 6.51 |
| Maximum | 8.3 | 8.95 | 8.81 | 7.35 | 7.46 | 7.34 | 7.98 | 8.06 | 8.12 |
| Mean | 7.48 | 7.44 | 7.44 | 7.11 | 7.12 | 7.04 | 7.37 | 7.41 | 7.44 |
| Median | 7.45 | 7.42 | 7.43 | 7.14 | 7.11 | 7.04 | 7.45 | 7.45 | 7.52 |

Table A14.2 – Aitik cell weekly leachate pH measurements

| pH | | | | | | | | | |
|---|---|---|---|---|---|---|---|---|---|
| **Week** | **A01** | **A02** | **A03** | **A04** | **A05** | **A06** | **A07** | **A08** | **A09** |
| 0 | 6.35 | 6.35 | 6.47 | 6.2 | 6.52 | 6.42 | 6.06 | 7.51 | 6.33 |

| | | | | | | | | | |
|---|---|---|---|---|---|---|---|---|---|
| 1 | 7.86 | 7.71 | 6.91 | 7.87 | 6.96 | 6.92 | 7.76 | 7.42 | 7.92 |
| 2 | 6.5 | 6.72 | 6.72 | 6.43 | 6.72 | 6.58 | 7.21 | 7.25 | 7.16 |
| 3 | 7.12 | 7.11 | 7.15 | 6.44 | 6.57 | 6.4 | 7.1 | 7.54 | 7.18 |
| 4 | 6.97 | 7.01 | 7.06 | 6.47 | 6.61 | 6.45 | 7.03 | 7.31 | 6.98 |
| 5 | 6.86 | 6.99 | 6.95 | 6.43 | 6.57 | 6.44 | 6.9 | 7.35 | 6.98 |
| 6 | 7.08 | 7.1 | 7 | 6.73 | 6.82 | 6.66 | 7.28 | 7.4 | 7.37 |
| 7 | 6.91 | 7 | 6.97 | 6.64 | 6.73 | 6.58 | 6.97 | 7.52 | 7.1 |
| 8 | 6.84 | 6.94 | 7 | 6.56 | 6.68 | 6.56 | 7.09 | 7.27 | 7.07 |
| 9 | 7.01 | 7.03 | 7.06 | 6.7 | 6.72 | 6.62 | 7.21 | 7.39 | 7.18 |
| 10 | 6.82 | 6.95 | 7.05 | 6.89 | 6.9 | 6.83 | 7.32 | 7.48 | 7.31 |
| 11 | 7.08 | 7.06 | 7.14 | 6.71 | 6.88 | 6.61 | 7.14 | 7.27 | 7.13 |
| 12 | 6.98 | 6.89 | 7.09 | 6.64 | 6.65 | 6.53 | 7.11 | 7.65 | 7.13 |
| 13 | 7.1 | 7.08 | 7.08 | 6.77 | 6.78 | 6.69 | 7.28 | 7.47 | 7.25 |
| 14 | 7.1 | 6.91 | 7.22 | 7.05 | 7.05 | 6.95 | 7.1 | 7.57 | 7.08 |
| 15 | 7.18 | 7.24 | 7.13 | 7.15 | 7.07 | 6.96 | 7.44 | 7.45 | 7.51 |
| 16 | 6.7 | 7.28 | 7.13 | 7.13 | 7.04 | 6.94 | 7.35 | 7.53 | 7.38 |
| 17 | 7.23 | 7.26 | 7.24 | 7.14 | 7.07 | 6.9 | 7.36 | 7.78 | 6.99 |
| 18 | 7.27 | 7.32 | 7.35 | 7.14 | 7.07 | 6.91 | 7.44 | 7.62 | 7.5 |
| 19 | 7.27 | 7.31 | 7.35 | 7.13 | 7.04 | 6.88 | 7.53 | 7.26 | 7.48 |
| 20 | 7.31 | 7.29 | 7.37 | 7.09 | 7.07 | 6.93 | 7.69 | 7.54 | 7.56 |
| 21 | 7.4 | 7.29 | 7.33 | 7.06 | 6.9 | 6.79 | 7.35 | 7.55 | 7.5 |
| 22 | 7.18 | 7.21 | 7.2 | 7.02 | 6.98 | 6.83 | 7.23 | 7.55 | 7.33 |
| 23 | 7.25 | 7.3 | 7.32 | 7.05 | 6.92 | 6.81 | 7.47 | 7.31 | 7.39 |
| 24 | 7.52 | 7.58 | 7.58 | 6.96 | 6.92 | 6.79 | 7.49 | 7.26 | 7.43 |
| 25 | 7.51 | 7.49 | 7.44 | 7.04 | 6.9 | 6.79 | 7.45 | 7.43 | 7.41 |
| 26 | 7.4 | 7.43 | 7.41 | 7.13 | 6.97 | 6.84 | 7.39 | 7.21 | 7.41 |
| 27 | 7.4 | 7.45 | 7.37 | 7.02 | 6.91 | 6.85 | 7.28 | 7.26 | 7.59 |
| 28 | 7.39 | 7.31 | 7.15 | 7.05 | 6.94 | 6.76 | 7.36 | 7.43 | 7.59 |
| 29 | 7.4 | 7.3 | 7.03 | 6.99 | 6.98 | 6.81 | 7.29 | 7.21 | 7.33 |
| 30 | 7.09 | 7.1 | 7.17 | 7.1 | 7 | 6.87 | 6.98 | 6.67 | 6.65 |
| 31 | 7.08 | 7.14 | 7.22 | 6.89 | 6.83 | 6.77 | 6.97 | 7.12 | 7.12 |
| 32 | 7.09 | 7.06 | 7.13 | 7.03 | 6.86 | 6.74 | 7.41 | 7.35 | 7.44 |
| 33 | 7.05 | 7.13 | 7.08 | 7.01 | 6.96 | 6.81 | 7.19 | 7.34 | 7.39 |
| 34 | 7.16 | 7.1 | 7.11 | 7.01 | 6.87 | 6.76 | 7.39 | 7.25 | 7.26 |
| 35 | 7.11 | 7.16 | 7.18 | 6.99 | 6.93 | 7.07 | 7.21 | 7.12 | 7.24 |
| 36 | 7.16 | 7.29 | 7.19 | 6.94 | 6.92 | 6.78 | 7.12 | 7.13 | 7.17 |
| 37 | 7.17 | 7.19 | 7.18 | 6.95 | 6.95 | 6.76 | 6.89 | 6.77 | 7.03 |
| 38 | 7.08 | 7.16 | 7.25 | 6.97 | 6.98 | 6.79 | 7.42 | 7.24 | 7.46 |
| 39 | 7.04 | 7.21 | 6.77 | 6.89 | 6.83 | 6.72 | 6.61 | 6.58 | 6.18 |
| 40 | 7.18 | 7.15 | 6.72 | 6.87 | 6.89 | 6.69 | 6.79 | 6.72 | 6.89 |
| 41 | 7.12 | 7.09 | 7.02 | 6.94 | 6.85 | 6.7 | 7.38 | 7.33 | 7.31 |
| 42 | 6.81 | 6.92 | 6.9 | 6.82 | 6.81 | 6.66 | 7.17 | 7.11 | 7.18 |
| 43 | 6.99 | 6.93 | 6.93 | 6.8 | 6.84 | 6.67 | 6.45 | 6.31 | 6.74 |
| 44 | 6.94 | 6.57 | 6.55 | 6.88 | 6.8 | 6.69 | 7.06 | 6.77 | 6.88 |
| 45 | 6.94 | 7 | 7 | 6.79 | 6.76 | 6.67 | 7.15 | 7.05 | 7.15 |
| 46 | | | | | | | | | |
| 47 | 6.84 | 6.91 | 6.94 | 6.63 | 6.64 | 6.47 | 7 | 6.96 | 7.11 |
| 48 | | | | | | | | | |
| 49 | 6.45 | 6.53 | 6.61 | 6.71 | 6.63 | 6.44 | 6.95 | 6.75 | 6.98 |
| 50 | 6.85 | 6.86 | 6.92 | 6.85 | 6.74 | 6.61 | 7.25 | 7.19 | 7.34 |
| 51 | 6.67 | 6.79 | 6.71 | 6.83 | 6.62 | 6.5 | 6.98 | 6.92 | 7.05 |
| 52 | 7.53 | 7.42 | 7.29 | 6.77 | 6.63 | 6.61 | 7.42 | 7.4 | 7.53 |
| 53 | 7.45 | 7.4 | 7.48 | 6.78 | 6.63 | 6.58 | 7.51 | 7.5 | 7.81 |

| | | | | | | | | | |
|---|---|---|---|---|---|---|---|---|---|
| 54 | 7.5 | 7.36 | 7.51 | 6.8 | 6.6 | 6.49 | 6.97 | 6.83 | 7.12 |
| 55 | 6.87 | 6.92 | 6.98 | 6.68 | 6.54 | 6.47 | 6.99 | 7.01 | 7.23 |
| 56 | 7.03 | 6.98 | 7.08 | 6.32 | 6.41 | 6.31 | 6.84 | 6.96 | 7.16 |
| 57 | 7.28 | 7.25 | 7.31 | 6.79 | 6.63 | 6.53 | 7.17 | 7.39 | 7.31 |
| 58 | 7.24 | 7.21 | 7.23 | 6.52 | 6.38 | 6.46 | 6.96 | 7.15 | 7.22 |
| 59 | 7.21 | 7.11 | 7.11 | 6.53 | 6.54 | 6.4 | 6.86 | 6.8 | 7.1 |
| 60 | 7.13 | 7.07 | 7.23 | 6.78 | 6.67 | 6.62 | 6.8 | 7.18 | 6.92 |
| Minimum | 6.35 | 6.35 | 6.47 | 6.2 | 6.38 | 6.31 | 6.06 | 6.31 | 6.18 |
| Maximum | 7.86 | 7.71 | 7.58 | 7.87 | 7.07 | 7.07 | 7.76 | 7.78 | 7.92 |
| Mean | 7.10 | 7.12 | 7.10 | 6.86 | 6.81 | 6.69 | 7.16 | 7.23 | 7.21 |
| Median | 7.1 | 7.11 | 7.13 | 6.88 | 6.84 | 6.69 | 7.19 | 7.27 | 7.22 |

Table A14.3 – Kevitsa cell weekly leachate EC measurements

| EC @ 25ºC (µS/cm) | | | | | | | | | |
|---|---|---|---|---|---|---|---|---|---|
| **Week** | **K01** | **K02** | **K03** | **K04** | **K05** | **K06** | **K07** | **K08** | **K09** |
| 0 | 199.72 | 222.75 | 200.26 | 217.65 | 233.15 | 228.58 | 134.54 | 238.19 | 220.14 |
| 1 | 662.16 | 595.85 | 657.24 | 421.71 | 320.61 | 395.55 | 452.26 | 456.99 | 444.91 |
| 2 | 323.96 | 386.86 | 317.66 | 303.27 | 290.85 | 289.63 | 276.84 | 273.15 | 278 |
| 3 | 299.47 | 334.49 | 283.77 | 227.89 | 211.62 | 227.91 | 287.56 | 332.08 | 281.06 |
| 4 | 295.82 | 270.36 | 311.42 | 201.55 | 209.39 | 199.74 | 218.24 | 202.83 | 178.36 |
| 5 | 187.2 | 173.71 | 177.89 | 201.31 | 142.71 | 133.36 | 178.06 | 175.96 | 192.21 |
| 6 | 357.4 | 349.6 | 391.63 | 223.78 | 171.51 | 192.36 | 269.19 | 291.34 | 287.75 |
| 7 | 325.85 | 280.89 | 303.43 | 258.37 | 158.82 | 186.4 | 280.4 | 328.12 | 286.43 |
| 8 | 305.79 | 313.16 | 333.6 | 195 | 164.77 | 151.32 | 247.37 | 254.02 | 254.11 |
| 9 | 300.63 | 245.94 | 265.58 | 173.44 | 159.31 | 163.75 | 210.82 | 200.45 | 201.11 |
| 10 | 241.1 | 246.96 | 235.3 | 125.69 | 116.61 | 130.12 | 151.16 | 157.82 | 151.12 |
| 11 | 119.62 | 219.01 | 190.33 | 167.01 | 145.89 | 145.95 | 168.98 | 183.19 | 184.73 |
| 12 | 222.65 | 236.39 | 228.48 | 191.73 | 156.61 | 165.69 | 181.41 | 169.02 | 172.59 |
| 13 | 510.86 | 282.72 | 504.25 | 319.07 | 229.97 | 299.99 | 301.56 | 354.16 | 322.33 |
| 14 | 198.96 | 194.82 | 201.39 | 149.25 | 136.46 | 151.25 | 189.31 | 194.79 | 183.66 |
| 15 | 114.24 | 137.97 | 140.06 | 155.12 | 134.99 | 147.87 | 115.36 | 106.09 | 106.02 |
| 16 | 201.38 | 199.31 | 207.3 | 164.96 | 137.03 | 132.86 | 163.99 | 168.29 | 162.21 |
| 17 | 195.14 | 184.16 | 189.24 | 136.01 | 123.62 | 126.4 | 150.07 | 163.45 | 151.21 |
| 18 | 187.48 | 187.02 | 185.72 | 116.46 | 131.65 | 127.81 | 128.37 | 149.76 | 161.16 |
| 19 | 185.55 | 192.76 | 186.81 | 124.17 | 125.56 | 127.81 | 135.72 | 145.01 | 108.28 |
| 20 | 136.02 | 134.84 | 135.53 | 96.82 | 101.22 | 127.72 | 75.92 | 61.4 | 62.44 |
| 21 | 155.25 | 154.9 | 160.31 | 131.43 | 129.22 | 104.96 | 121.35 | 117.38 | 91.19 |
| 22 | 189.63 | 205.14 | 196.65 | 137.44 | 129.6 | 135.81 | 143.63 | 142.68 | 135.64 |
| 23 | 153.5 | 170.61 | 148.58 | 123.4 | 107.84 | 165.08 | 108.72 | 124.92 | 109.13 |
| 24 | 166.18 | 176.23 | 154.12 | 116.3 | 126.2 | 168.54 | 114.28 | 92.62 | 94.18 |
| 25 | 161.7 | 158.76 | 164.82 | 126.48 | 111.13 | 155.73 | 105.84 | 70.66 | 104.35 |
| 26 | 130.14 | 133.84 | 132.28 | 119.24 | 116.1 | 152.48 | 106.98 | 127.91 | 106.79 |
| 27 | 211.88 | 197.63 | 196.4 | 124.26 | 139.35 | 204.47 | 156.35 | 147.28 | 81.81 |
| 28 | 164.69 | 147.88 | 19.07 | 115.89 | 108.33 | 153.14 | 127.01 | 126.37 | 102.92 |
| 29 | 135.66 | 122.08 | 132.93 | 86.8 | 87.53 | 111.89 | 91.26 | 100.99 | 96.38 |
| 30 | 210.43 | 188.4 | 205.16 | 113.07 | 116.62 | 135.14 | 122.79 | 168.55 | 141.97 |
| 31 | 145.92 | 149.65 | 170.06 | 104.26 | 148.71 | 137.89 | 104.49 | 135.43 | 127.09 |
| 32 | 140.99 | 138.13 | 147.41 | 100.58 | 196.93 | 182.49 | 65.52 | 92.12 | 80.67 |
| 33 | 140.7 | 132.32 | 138.21 | 116.12 | 138.26 | 147.89 | 100.38 | 115.27 | 93.3 |
| 34 | 127.75 | 134.58 | 131.07 | 102.3 | 152.9 | 138.21 | 57.85 | 68.16 | 57.36 |
| 35 | 55.91 | 58.96 | 51.25 | 62.45 | 89.12 | 92.48 | 39.29 | 36.79 | 36.73 |
| 36 | 166.46 | 141.29 | 134.38 | 106.39 | 123.66 | 139.69 | 132.45 | 137.2 | 125.05 |

| | | | | | | | | | |
|---|---|---|---|---|---|---|---|---|---|
| 37 | 170.93 | 145.92 | 135.3 | 109.63 | 126.45 | 168.2 | 167.98 | 171.51 | 161.92 |
| 38 | 135.32 | 144.98 | 142.66 | 100.12 | 93.95 | 117.6 | 97.73 | 100.14 | 91.6 |
| 39 | 153.67 | 212.91 | 146.07 | 99.36 | 105.08 | 111.01 | 213.27 | 223.92 | 196.24 |
| 40 | 118.29 | 126.7 | 154.72 | 92.55 | 92.14 | 94.85 | 196.4 | 222.31 | 200.06 |
| 41 | 155.64 | 130.93 | 145.58 | 96.84 | 103.75 | 107.26 | 105.23 | 108.24 | 102.09 |
| 42 | 132.45 | 130.11 | 159.63 | 86.77 | 91.6 | 98.25 | 80.47 | 88.01 | 77.22 |
| 43 | 172.54 | 161.28 | 176.48 | 121.13 | 121.13 | 124.67 | 333.57 | 384.3 | 385.02 |
| 44 | 70.25 | 64.56 | 62.04 | 38.07 | 42.02 | 39.68 | 44.76 | 50.42 | 41.46 |
| 45 | 132.04 | 131.24 | 135.91 | 78.16 | 87.95 | 88.81 | 118.9 | 106.37 | 113.11 |
| 46 | | | | | | | | | |
| 47 | 127.1 | 100.8 | 106.6 | 65.3 | 63.3 | 61.4 | 63.2 | 51.1 | 48.7 |
| 48 | | | | | | | | | |
| 49 | 86.2 | 79.2 | 76.6 | 80.2 | 88.2 | 89.7 | 51.9 | 52 | 50.4 |
| 50 | 129.7 | 146.1 | 133.5 | 86.6 | 87 | 93.4 | 86.5 | 86.5 | 79.6 |
| 51 | 73.3 | 77 | 70.1 | 84.6 | 81.1 | 91.4 | 45 | 46.9 | 47.1 |
| 52 | 162.8 | 160.1 | 156.8 | 103.1 | 88.8 | 115.6 | 118.4 | 126.8 | 111.3 |
| 53 | 135.5 | 137 | 132.5 | 96.3 | 80.9 | 93.4 | 137.2 | 145.2 | 131.5 |
| 54 | 120.9 | 122.2 | 126.4 | 89.6 | 76.4 | 87 | 53.3 | 57 | 52 |
| 55 | 157.3 | 154.7 | 140.4 | 88.5 | 68.6 | 94.9 | 42.2 | 71.2 | 43 |
| 56 | 95 | 110.8 | 128.5 | 77.3 | 75.6 | 91.4 | 57.4 | 60 | 31.6 |
| 57 | 161.4 | 161.4 | 159.6 | 98.7 | 82.2 | 108 | 143.5 | 89.2 | 126.7 |
| 58 | 130.2 | 131.9 | 127.9 | 82.8 | 72.1 | 87.9 | 160.9 | 181.3 | 169.1 |
| 59 | 141.8 | 139.2 | 135.8 | 80.8 | 88 | 92.5 | 125.8 | 144.3 | 124.2 |
| 60 | 135 | 143.3 | 127.4 | 90.8 | 78.7 | 82.7 | 124.1 | 151.1 | 123.8 |
| Minimum | 55.91 | 58.96 | 19.07 | 38.07 | 42.02 | 39.68 | 39.29 | 36.79 | 31.6 |
| Maximum | 662.16 | 595.85 | 657.24 | 421.71 | 320.61 | 395.55 | 452.26 | 456.99 | 444.91 |
| Mean | 185.17 | 181.56 | 183.22 | 133.96 | 127.44 | 140.98 | 145.48 | 154.72 | 143.76 |
| Median | 157.3 | 154.9 | 154.72 | 115.89 | 121.13 | 132.86 | 127.01 | 142.68 | 124.2 |

Table A14.4 – Aitik cell weekly leachate EC measurements

| EC at 25°C (µS/cm) | | | | | | | | | |
|---|---|---|---|---|---|---|---|---|---|
| **Week** | **A01** | **A02** | **A03** | **A04** | **A05** | **A06** | **A07** | **A08** | **A09** |
| 0 | 196.14 | 235.13 | 253.34 | 172.83 | 308.2 | 243.71 | 234.36 | 160.49 | 225.64 |
| 1 | 300.19 | 263.89 | 251.57 | 309.86 | 237.6 | 251.91 | 238.11 | 127.6 | 214.71 |
| 2 | 185.26 | 211.53 | 155.32 | 233.48 | 183.64 | 202.94 | 179 | 86.23 | 163 |
| 3 | 171.88 | 178.61 | 141.97 | 146.09 | 103.73 | 128.97 | 134.9 | 172.99 | 144.44 |
| 4 | 160.87 | 148.91 | 139.4 | 150.13 | 91.23 | 103.31 | 101.63 | 226.5 | 101.92 |
| 5 | 103.6 | 107.86 | 104.21 | 90.55 | 66.09 | 72.75 | 70.92 | 200.98 | 83.62 |
| 6 | 156.24 | 149.44 | 180.47 | 110.47 | 86.63 | 79.13 | 136.59 | 176.38 | 131.75 |
| 7 | 120.89 | 146.01 | 133.94 | 134 | 78.27 | 78.29 | 132.89 | 119.31 | 144.62 |
| 8 | 149 | 145.22 | 140.25 | 89.65 | 80.91 | 73.92 | 167.99 | 124.12 | 120.8 |
| 9 | 128.37 | 133.75 | 127.14 | 90.71 | 73.48 | 66.52 | 146.08 | 121.96 | 109.7 |
| 10 | 125.92 | 113.13 | 126.49 | 67.89 | 54.71 | 53.21 | 86.35 | 179.85 | 72.75 |
| 11 | 105.23 | 115.25 | 118.39 | 80.93 | 64.66 | 61.3 | 97.09 | 163.14 | 82.53 |
| 12 | 108.59 | 99.63 | 104.97 | 85.88 | 69.17 | 63.73 | 93.68 | 101.54 | 80.85 |
| 13 | 203.61 | 230.48 | 244.87 | 153.72 | 133.15 | 125.59 | 198.49 | 107.91 | 161.37 |
| 14 | 105.65 | 108.24 | 116.45 | 73.13 | 61.73 | 56.95 | 109.48 | 99.48 | 97.71 |
| 15 | 54.91 | 60.84 | 61.33 | 71.83 | 62.08 | 59.62 | 86.31 | 91.66 | 71.74 |
| 16 | 104.43 | 112.33 | 107.1 | 73.82 | 65.6 | 62.19 | 94.38 | 88.37 | 84.65 |

| | | | | | | | | | |
|---|---|---|---|---|---|---|---|---|---|
| 17 | 103.17 | 106.88 | 95.09 | 73.66 | 59.24 | 61.08 | 101.94 | 96.03 | 90.25 |
| 18 | 104.7 | 104.98 | 105.01 | 71.81 | 62.88 | 68.6 | 90.59 | 110.87 | 78.77 |
| 19 | 100.59 | 104.93 | 97.43 | 71.69 | 59.31 | 61.78 | 88.8 | 88.09 | 74.37 |
| 20 | 71.18 | 76 | 77.07 | 57.59 | 54.78 | 56.94 | 74.78 | 100.26 | 53.55 |
| 21 | 87.38 | 73.77 | 82.54 | 65.2 | 56.69 | 63.3 | 102.11 | 72.5 | 79.12 |
| 22 | 95.17 | 97.43 | 107.53 | 69.89 | 72.7 | 72.17 | 91.35 | 117.25 | 74.11 |
| 23 | 81.99 | 93.39 | 81.28 | 59.94 | 59.91 | 58.91 | 79.52 | 96.39 | 68.71 |
| 24 | 95.28 | 97.24 | 99.15 | 76.29 | 78.96 | 75.5 | 69.63 | 102.77 | 67.72 |
| 25 | 76.6 | 63.31 | 85.81 | 63.31 | 59.69 | 58.05 | 65.63 | 83.4 | 54.91 |
| 26 | 69.57 | 68.98 | 67.69 | 67.89 | 67.15 | 61.97 | 82.66 | 65.17 | 69.5 |
| 27 | 98.98 | 91.62 | 91.51 | 65.71 | 65.85 | 68.14 | 95.59 | 102.77 | 142.33 |
| 28 | 77.17 | 84.15 | 81.07 | 64.89 | 67.4 | 56.72 | 83.14 | 83.4 | 79.07 |
| 29 | 68.46 | 65.36 | 62.39 | 48.41 | 49.54 | 45.5 | 63.66 | 65.17 | 57.08 |
| 30 | 83.33 | 92.44 | 84.69 | 61.66 | 58.4 | 54.15 | 90.11 | 105.21 | 91.48 |
| 31 | 133.08 | 86.08 | 90.49 | 59.49 | 56.16 | 55.02 | 78.14 | 72.49 | 82.7 |
| 32 | 73.94 | 75.88 | 79.65 | 65.14 | 59.24 | 52.23 | 58.5 | 57.32 | 57.58 |
| 33 | 84.03 | 79.72 | 76.93 | 60.44 | 54.72 | 49.1 | 61.68 | 67.65 | 72.93 |
| 34 | 71.96 | 69.03 | 72.66 | 52.32 | 50.27 | 47.82 | 39.16 | 30.43 | 30.7 |
| 35 | 26.32 | 31.16 | 34.76 | 32.92 | 29.72 | 37.62 | 24.02 | 19.05 | 23.5 |
| 36 | 65.35 | 77.82 | 71.56 | 51.9 | 51.01 | 43.62 | 81.75 | 74.56 | 78.62 |
| 37 | 71.09 | 73.45 | 83.26 | 59.37 | 53.87 | 47.66 | 102.11 | 103.18 | 96.54 |
| 38 | 68.22 | 69.95 | 66.72 | 44.02 | 40.74 | 42.41 | 59.99 | 49.45 | 61.01 |
| 39 | 73.69 | 84.26 | 81.04 | 54.9 | 51.61 | 47.92 | 109.68 | 110.74 | 103.03 |
| 40 | 65.79 | 75.52 | 69.77 | 52.29 | 53.73 | 45.42 | 115.24 | 112.24 | 85.84 |
| 41 | 88.3 | 64.52 | 75.89 | 54.01 | 51.78 | 48.17 | 74.18 | 52.14 | 44.53 |
| 42 | 66.84 | 63.04 | 59.9 | 47.21 | 46.78 | 42.8 | 38.1 | 31.57 | 29.76 |
| 43 | 82.07 | 77.87 | 85.61 | 69.62 | 67.3 | 61.62 | 155.21 | 175.04 | 101.98 |
| 44 | 36.31 | 28.43 | 29.24 | 24.03 | 23.44 | 21.74 | 26.67 | 27.4 | 26.88 |
| 45 | 69.21 | 71.98 | 65.73 | 51.03 | 51.83 | 47.99 | 58.85 | 57.83 | 60.49 |
| 46 | | | | | | | | | |
| 47 | 49.2 | 42.5 | 47.1 | 35 | 31.6 | 34.5 | 34.9 | 34.1 | 36 |
| 48 | | | | | | | | | |
| 49 | 39.3 | 40.4 | 43.1 | 54.5 | 51.3 | 47.4 | 26.1 | 23 | 28.5 |
| 50 | 61.3 | 58 | 65 | 52.8 | 48.4 | 42.9 | 41 | 37.5 | 43 |
| 51 | 39.5 | 39.1 | 42.8 | 55.4 | 47.3 | 45.1 | 29.2 | 26.9 | 31.4 |
| 52 | 65.2 | 67.7 | 71.8 | 50.9 | 45.7 | 45 | 54.3 | 46.1 | 57.7 |
| 53 | 58.2 | 54.7 | 65 | 44.9 | 43.9 | 38.7 | 50.3 | 51.2 | 66.5 |
| 54 | 59.9 | 56.7 | 66.4 | 48 | 46.5 | 38.8 | 23.4 | 18.2 | 25 |
| 55 | 75.8 | 70.4 | 78.1 | 55.1 | 53.1 | 49.3 | 42.3 | 38.2 | 44.6 |
| 56 | 72.6 | 65.1 | 72.8 | 45.9 | 51 | 50.6 | 32.9 | 39.1 | 47.7 |
| 57 | 84.4 | 82.8 | 89.9 | 60.1 | 59.3 | 56.6 | 68.3 | 66.5 | 76 |
| 58 | 126.6 | 122 | 149.3 | 91 | 102.6 | 88.4 | 139.1 | 144.9 | 178.2 |
| 59 | 64.4 | 63.7 | 71.8 | 47.4 | 46.8 | 42.4 | 57.9 | 48.5 | 74.4 |
| 60 | 65.4 | 64.5 | 73.5 | 57.1 | 48.4 | 46.7 | 65.8 | 106.5 | 79.6 |
| Minimum | 26.32 | 28.43 | 29.24 | 24.03 | 23.44 | 21.74 | 23.4 | 18.2 | 23.5 |
| Maximum | 300.19 | 263.89 | 253.34 | 309.86 | 308.2 | 251.91 | 238.11 | 226.5 | 225.64 |
| Mean | 95.46 | 95.54 | 96.69 | 76.77 | 69.68 | 67.19 | 88.75 | 90.84 | 83.34 |
| Median | 82.07 | 79.72 | 82.54 | 63.31 | 59.24 | 56.72 | 82.66 | 88.37 | 76 |

Table A14.5 – Kevitsa cell weekly leachate DIC measurements

| DIC (mg/kg/week) | | | | | | | | | |
|---|---|---|---|---|---|---|---|---|---|
| **Week** | **K01** | **K02** | **K03** | **K04** | **K05** | **K06** | **K07** | **K08** | **K09** |
| 0 | 3.50 | 3.97 | 4.31 | 4.85 | 4.45 | 4.22 | 3.95 | 4.30 | 3.97 |
| 1 | 19.04 | 18.70 | 18.12 | 1.46 | 1.76 | 1.51 | 17.82 | 17.53 | 14.89 |
| 2 | 3.19 | 3.18 | 3.15 | 1.85 | 1.77 | 1.62 | 12.56 | 13.04 | 13.28 |
| 3 | 10.60 | 12.34 | 15.48 | 1.95 | 1.76 | 1.56 | 2.15 | 23.86 | 19.56 |
| 4 | 9.66 | 12.78 | 9.06 | 2.18 | 2.15 | 1.58 | 7.28 | 7.24 | 6.04 |
| 5 | 7.31 | 8.42 | 6.44 | 1.66 | 2.01 | 1.46 | 7.21 | 7.95 | 8.47 |
| 6 | 14.35 | 15.20 | 20.64 | 2.10 | 1.83 | 1.33 | 13.41 | 15.16 | 13.90 |
| 7 | 12.60 | 10.78 | 10.01 | 1.47 | 1.51 | 1.20 | 16.79 | 20.42 | 15.96 |
| 8 | 11.53 | 14.68 | 13.02 | 1.34 | 1.58 | 1.18 | 13.41 | 13.99 | 12.96 |
| 9 | 10.83 | 11.52 | 10.45 | 1.26 | 1.60 | 1.23 | 11.01 | 10.12 | 10.28 |
| 10 | 12.13 | 14.24 | 14.85 | 1.32 | 1.33 | 1.08 | 7.13 | 7.54 | 7.22 |
| 11 | 6.69 | 8.44 | 5.70 | 1.02 | 1.27 | 0.93 | 8.02 | 8.88 | 8.91 |
| 12 | 6.75 | 7.14 | 6.62 | 1.00 | 1.19 | 1.04 | 7.84 | 7.40 | 7.20 |
| 13 | 9.82 | 10.25 | 9.15 | 1.15 | 1.25 | 1.09 | 7.19 | 8.27 | 7.46 |
| 14 | 8.39 | 9.51 | 8.21 | 1.07 | 1.16 | 1.02 | 13.26 | 13.84 | 12.32 |
| 15 | 1.89 | 1.98 | 1.97 | 0.97 | 1.12 | 0.91 | 4.19 | 3.56 | 3.56 |
| 16 | 9.36 | 9.73 | 8.92 | 1.13 | 1.16 | 1.09 | 8.27 | 9.09 | 8.62 |
| 17 | 8.79 | 8.82 | 8.29 | 0.86 | 1.19 | 0.92 | 8.13 | 8.58 | 7.91 |
| 18 | 9.22 | 9.38 | 7.88 | 1.11 | 1.14 | 1.01 | 8.67 | 7.96 | 10.36 |
| 19 | 7.77 | 8.74 | 8.02 | 1.08 | 1.06 | 0.96 | 6.68 | 7.60 | 4.67 |
| 20 | 6.35 | 5.67 | 5.56 | 0.78 | 0.81 | 0.69 | 4.10 | 3.22 | 2.94 |
| 21 | 5.94 | 5.82 | 6.38 | 0.98 | 0.89 | 0.82 | 7.14 | 6.51 | 3.66 |
| 22 | 8.94 | 8.75 | 8.83 | 1.18 | 1.02 | 0.93 | 10.78 | 10.75 | 9.29 |
| 23 | 6.23 | 7.05 | 5.86 | 0.94 | 1.00 | 0.80 | 6.70 | 7.55 | 5.63 |
| 24 | 6.21 | 6.32 | 6.19 | 1.00 | 0.88 | 0.70 | 5.69 | 4.96 | 4.79 |
| 25 | 8.44 | 7.47 | 7.57 | 1.21 | 1.10 | 0.98 | 7.98 | 5.95 | 7.08 |
| 26 | 3.20 | 2.88 | 3.44 | 0.91 | 0.96 | 0.89 | 6.23 | 7.01 | 5.17 |
| 27 | 8.38 | 8.11 | 8.73 | 1.15 | 1.03 | 0.91 | 11.83 | 5.96 | 8.92 |
| 28 | 5.54 | 6.15 | 6.03 | 0.82 | 0.82 | 0.69 | 8.10 | 6.99 | 5.49 |
| 29 | 6.38 | 6.30 | 6.14 | 0.86 | 0.82 | 0.75 | 6.27 | 7.00 | 6.68 |
| 30 | 10.86 | 11.82 | 9.69 | 1.23 | 1.09 | 0.98 | 11.52 | 13.30 | 10.82 |
| 31 | 6.40 | 6.14 | 6.73 | 1.22 | 1.04 | 0.94 | 6.94 | 9.72 | 8.94 |
| 32 | 5.21 | 4.92 | 5.61 | 0.95 | 0.71 | 0.62 | 2.38 | 3.91 | 2.87 |
| 33 | 6.44 | 6.46 | 6.58 | 0.80 | 0.67 | 0.59 | 6.06 | 7.06 | 5.30 |
| 34 | 5.81 | 6.88 | 6.49 | 1.04 | 0.71 | 0.69 | 1.93 | 2.64 | 1.95 |
| 35 | 2.17 | 1.92 | 2.39 | 0.86 | 0.65 | 0.57 | 2.75 | 2.68 | 2.47 |
| 36 | 7.42 | 7.33 | 6.75 | 0.48 | 0.66 | 0.67 | 14.90 | 13.64 | 12.65 |
| 37 | 10.23 | 8.19 | 7.75 | 0.83 | 0.68 | 0.62 | 23.37 | 24.59 | 23.12 |
| 38 | 6.64 | 8.24 | 8.62 | 0.83 | 0.79 | 0.71 | 5.76 | 5.87 | 5.92 |
| 39 | 8.76 | 4.06 | 5.90 | 1.17 | 0.65 | 0.63 | 40.10 | 42.50 | 31.05 |
| 40 | 5.88 | 6.18 | 8.25 | 0.80 | 0.68 | 0.72 | 31.89 | 29.47 | 23.69 |
| 41 | 6.55 | 5.05 | 4.63 | 0.81 | 0.73 | 0.70 | 5.64 | 5.85 | 5.21 |
| 42 | 5.45 | 6.07 | 4.86 | 0.78 | 0.65 | 0.66 | 3.83 | 4.43 | 3.44 |
| 43 | 4.56 | 5.12 | 4.76 | 0.83 | 0.70 | 0.68 | 54.59 | 63.08 | 56.33 |
| 44 | 5.66 | 6.94 | 5.90 | 0.88 | 0.71 | 0.67 | 6.59 | 8.13 | 5.34 |
| 45 | 5.37 | 6.91 | 6.25 | 0.78 | 0.66 | 0.65 | 8.53 | 6.92 | 7.08 |
| 46 | 5.44 | 6.01 | 5.65 | 0.83 | 0.69 | 0.65 | 7.39 | 5.26 | 5.45 |
| 47 | 5.35 | 6.39 | 6.09 | 0.87 | 0.74 | 0.72 | 5.43 | 4.05 | 4.47 |
| 48 | 5.99 | 5.77 | 5.31 | 0.84 | 0.74 | 0.71 | 3.27 | 3.19 | 2.68 |

| | | | | | | | | | |
|---|---|---|---|---|---|---|---|---|---|
| 49 | 0.76 | 0.81 | 0.81 | 0.70 | 0.70 | 0.64 | 1.43 | 1.48 | 1.34 |
| 50 | 3.58 | 5.60 | 4.56 | 0.76 | 0.70 | 0.09 | 4.12 | 3.93 | 3.39 |
| 51 | 1.01 | 0.83 | 1.01 | 0.62 | 0.63 | 0.56 | 1.10 | 1.31 | 1.20 |
| 52 | 5.60 | 5.77 | 5.64 | 0.72 | 0.67 | 0.60 | 10.86 | 11.41 | 10.42 |
| 53 | 6.47 | 7.19 | 6.84 | 0.85 | 0.69 | 0.66 | 7.74 | 7.01 | 6.87 |
| 54 | 5.00 | 4.83 | 5.26 | 0.66 | 0.67 | 0.60 | 1.56 | 1.74 | 1.38 |
| 55 | 8.26 | 8.00 | 7.52 | 9.45 | 0.83 | 0.84 | 3.26 | 4.89 | 3.68 |
| 56 | 5.97 | 5.97 | 6.00 | 0.77 | 0.68 | 0.58 | 2.31 | 2.95 | 2.53 |
| 57 | 8.70 | 8.87 | 8.51 | 1.00 | 0.79 | 0.74 | 9.05 | 10.63 | 13.84 |
| 58 | 8.22 | | | | | | | | |
| 59 | 8.68 | | | | | | | | |
| 60 | 9.35 | 7.78 | 6.39 | 0.82 | 0.77 | 0.67 | 10.88 | 10.17 | 12.44 |
| Minimum | 0.76 | 0.81 | 0.81 | 0.48 | 0.63 | 0.09 | 1.10 | 1.31 | 1.20 |
| Maximum | 19.04 | 18.70 | 20.64 | 9.45 | 4.45 | 4.22 | 54.59 | 63.08 | 56.33 |
| Mean | 7.23 | 7.46 | 7.22 | 1.25 | 1.06 | 0.92 | 9.41 | 10.07 | 9.03 |
| Median | 6.55 | 6.94 | 6.44 | 0.97 | 0.83 | 0.75 | 7.21 | 7.40 | 7.08 |

Table A14.6 – Aitik cell weekly leachate DIC measurements

| DIC (mg/kg/week) | | | | | | | | | |
|---|---|---|---|---|---|---|---|---|---|
| **Week** | **A01** | **A02** | **A03** | **A04** | **A05** | **A06** | **A07** | **A08** | **A09** |
| 0 | 1.99 | 2.04 | 2.35 | 1.45 | 2.51 | 2.03 | 1.90 | 24.19 | 1.76 |
| 1 | 2.66 | 4.05 | 3.51 | 0.53 | 0.65 | 0.64 | 4.01 | 6.72 | 3.07 |
| 2 | 0.62 | 0.73 | 0.78 | 0.48 | 0.90 | 0.70 | 3.51 | 5.77 | 3.09 |
| 3 | 4.66 | 4.62 | 3.90 | 0.61 | 0.77 | 0.63 | 8.47 | 11.55 | 7.96 |
| 4 | 4.21 | 4.17 | 4.51 | 0.67 | 0.80 | 0.23 | 3.60 | 16.97 | 2.86 |
| 5 | 3.42 | 3.60 | 3.57 | 0.78 | 0.80 | 0.82 | 2.98 | 15.00 | 3.49 |
| 6 | 7.16 | 7.92 | 12.18 | 0.85 | 1.04 | 0.79 | 7.75 | 11.50 | 7.06 |
| 7 | 5.09 | 6.03 | 5.44 | 0.81 | 1.04 | 0.82 | 8.78 | 7.19 | 9.92 |
| 8 | 8.27 | 7.93 | 7.81 | 0.82 | 1.02 | 0.83 | 8.50 | 7.69 | 8.00 |
| 9 | 7.07 | 6.40 | 5.39 | 0.92 | 0.99 | 0.81 | 7.38 | 6.80 | 6.78 |
| 10 | 11.06 | 8.52 | 8.79 | 0.86 | 0.90 | 0.76 | 4.57 | 8.54 | 3.87 |
| 11 | 4.96 | 5.09 | 4.83 | 0.74 | 0.86 | 0.70 | 5.37 | 12.41 | 4.59 |
| 12 | 4.48 | 3.62 | 3.77 | 0.75 | 0.77 | 0.64 | 4.54 | 5.28 | 4.05 |
| 13 | 3.92 | 5.42 | 6.36 | 0.78 | 0.92 | 0.77 | 5.34 | 6.38 | 4.36 |
| 14 | 6.08 | 5.43 | 5.71 | 0.66 | 0.70 | 0.61 | 8.04 | 5.96 | 7.58 |
| 15 | 0.83 | 0.89 | 0.78 | 0.65 | 0.65 | 0.57 | 4.30 | 5.19 | 3.35 |
| 16 | 6.38 | 5.93 | 5.30 | 0.80 | 0.78 | 0.68 | 5.51 | 4.97 | 4.64 |
| 17 | 6.72 | 5.56 | 4.43 | 0.86 | 0.82 | 0.61 | 6.19 | 6.22 | 7.32 |
| 18 | 6.09 | 5.39 | 5.38 | 0.73 | 0.77 | 0.59 | 4.84 | 6.83 | 4.30 |
| 19 | 6.64 | 6.05 | 5.43 | 0.81 | 0.73 | 0.58 | 5.03 | 7.44 | 4.08 |
| 20 | 4.03 | 4.37 | 4.24 | 0.62 | 0.72 | 0.56 | 4.69 | 6.16 | 2.98 |
| 21 | 3.89 | 2.85 | 3.78 | 0.61 | 0.56 | 0.45 | 8.24 | 3.87 | 4.26 |
| 22 | 6.72 | 5.82 | 6.19 | 0.63 | 0.71 | 0.53 | 6.92 | 5.84 | 5.00 |
| 23 | 4.37 | 4.35 | 3.82 | 0.67 | 0.65 | 0.46 | 4.86 | 6.52 | 4.21 |
| 24 | 3.86 | 4.09 | 4.00 | 0.60 | 0.63 | 0.45 | 3.42 | 8.85 | 3.41 |
| 25 | 4.21 | 4.05 | 4.18 | 0.80 | 0.74 | 0.57 | 4.50 | 5.45 | 3.87 |
| 26 | 2.51 | 2.14 | 2.00 | 0.76 | 0.59 | 0.45 | 4.84 | 5.18 | 4.07 |
| 27 | 4.45 | 3.74 | 3.81 | 0.63 | 0.54 | 0.46 | 7.00 | 12.00 | 6.98 |
| 28 | 3.46 | 3.38 | 3.23 | 0.62 | 0.58 | 0.40 | 5.05 | 5.25 | 5.03 |
| 29 | 3.80 | 3.61 | 3.50 | 0.75 | 0.69 | 0.47 | 4.60 | 2.65 | 4.02 |
| 30 | 4.33 | 4.77 | 3.83 | 0.56 | 0.66 | 0.49 | 6.77 | 4.34 | 8.90 |
| 31 | 3.76 | 4.06 | 4.31 | 0.63 | 0.48 | 0.41 | 5.70 | 1.15 | 5.72 |

| | | | | | | | | | |
|---|---|---|---|---|---|---|---|---|---|
| 32 | 3.07 | 3.41 | 3.14 | 0.64 | 0.55 | 0.48 | 2.84 | 1.37 | 2.85 |
| 33 | 5.06 | 4.55 | 4.33 | 0.55 | 0.62 | 0.43 | 3.62 | 8.64 | 4.69 |
| 34 | 4.18 | 3.80 | 3.60 | 0.52 | 0.52 | 0.37 | 1.53 | 18.21 | 1.42 |
| 35 | 1.26 | 1.37 | 2.02 | 0.49 | 0.52 | 0.90 | 1.74 | 3.23 | 1.72 |
| 36 | 4.35 | 4.19 | 3.65 | 0.47 | 0.53 | 0.42 | 7.38 | 20.65 | 7.32 |
| 37 | 4.42 | 4.33 | 4.92 | 0.52 | 0.59 | 0.38 | 14.68 | 18.90 | 12.12 |
| 38 | 4.42 | 4.35 | 3.97 | 0.69 | 0.57 | 0.51 | 1.46 | 3.34 | 3.87 |
| 39 | 4.00 | 4.62 | 4.29 | 0.60 | 0.50 | 0.40 | 19.19 | 21.44 | 19.04 |
| 40 | 3.52 | 4.16 | 2.92 | 0.50 | 0.59 | 0.41 | 14.98 | 19.72 | 6.03 |
| 41 | 2.78 | 2.58 | 3.52 | 0.53 | 0.61 | 0.42 | 4.43 | 2.79 | 2.79 |
| 42 | 3.60 | 3.21 | 3.15 | 0.50 | 0.54 | 0.37 | 2.13 | 2.22 | 1.87 |
| 43 | 3.14 | 2.63 | 2.52 | 0.53 | 0.54 | 0.40 | 24.43 | 26.49 | 8.46 |
| 44 | 4.48 | 3.28 | 3.23 | 0.54 | 0.60 | 0.40 | 3.90 | 4.00 | 3.65 |
| 45 | 3.75 | 3.86 | 3.32 | 0.52 | 0.54 | 0.36 | 4.41 | 4.84 | 4.55 |
| 46 | 3.31 | 3.32 | 3.16 | 0.49 | 0.58 | 0.37 | 3.39 | 4.82 | 3.47 |
| 47 | 3.38 | 3.25 | 3.20 | 0.48 | 0.54 | 0.35 | 4.20 | 3.49 | 3.30 |
| 48 | 3.18 | 3.44 | 3.55 | 0.54 | 0.57 | 0.40 | 2.46 | 2.00 | 3.73 |
| 49 | 0.33 | 0.36 | 0.34 | 0.41 | 0.42 | 0.35 | 0.81 | 0.63 | 0.80 |
| 50 | 1.89 | 0.90 | 2.40 | 0.42 | 0.43 | 0.34 | 2.02 | 1.87 | 2.21 |
| 51 | 0.37 | 0.45 | 0.39 | 0.21 | 0.33 | 0.31 | 0.73 | 0.65 | 0.68 |
| 52 | 3.35 | 3.53 | 3.45 | 0.52 | 0.41 | 0.33 | 6.21 | 5.51 | 7.50 |
| 53 | 3.29 | 3.39 | 3.20 | 0.52 | 0.42 | 0.33 | 3.94 | 3.03 | 4.13 |
| 54 | 2.82 | 2.50 | 2.73 | 0.42 | 0.36 | 0.28 | 0.79 | 0.62 | 0.94 |
| 55 | 3.62 | 3.34 | 3.56 | 0.53 | 0.80 | 0.70 | 4.05 | 3.70 | 4.05 |
| 56 | 3.07 | 3.03 | 2.80 | 0.43 | 0.36 | 0.28 | 0.90 | 1.12 | 1.05 |
| 57 | 4.00 | 2.57 | 3.77 | 0.57 | 0.46 | 0.33 | 4.60 | 4.54 | 4.98 |
| 58 | | 3.07 | 3.56 | 0.47 | 0.45 | 0.39 | 4.56 | 4.62 | 4.83 |
| 59 | | 3.03 | 3.66 | 0.58 | 0.50 | 0.37 | 4.69 | 3.62 | 3.49 |
| 60 | 3.78 | 3.50 | 3.64 | 0.60 | 0.50 | 0.37 | 9.29 | 10.03 | 10.94 |
| Minimum | 0.33 | 0.36 | 0.34 | 0.21 | 0.33 | 0.23 | 0.73 | 0.62 | 0.68 |
| Maximum | 11.06 | 8.52 | 12.18 | 1.45 | 2.51 | 2.03 | 24.43 | 26.49 | 19.04 |
| Mean | 4.07 | 3.88 | 3.92 | 0.63 | 0.67 | 0.53 | 5.52 | 7.48 | 4.87 |
| Median | 3.89 | 3.74 | 3.65 | 0.60 | 0.60 | 0.45 | 4.60 | 5.51 | 4.08 |

Table A14.7 – Kevitsa cell weekly leachate sulfate measurements

| Sulfate (mg/kg/week) | | | | | | | | | |
|---|---|---|---|---|---|---|---|---|---|
| **Week** | **K01** | **K02** | **K03** | **K04** | **K05** | **K06** | **K07** | **K08** | **K09** |
| 0 | 80.22 | 86.37 | 77.92 | 80.73 | 88.93 | 89.18 | 88.93 | 92.44 | 86.53 |
| 1 | 211.63 | 178.37 | 207.55 | 163.58 | 127.87 | 158.37 | 129.26 | 123.51 | 131.33 |
| 2 | 134.18 | 155.21 | 121.42 | 125.68 | 117.93 | 128.37 | 63.09 | 53.76 | 56.65 |
| 3 | 112.67 | 123.42 | 83.77 | 109.93 | 102.34 | 111.14 | 56.08 | 61.50 | 47.63 |
| 4 | | | | | | | | | |
| 5 | | | | | | | | | |
| 6 | 67.99 | 63.00 | 70.90 | 84.61 | 58.20 | 71.67 | 49.39 | 66.29 | 56.65 |
| 7 | 79.37 | 59.02 | 77.24 | 98.24 | 56.89 | 70.13 | 40.36 | 38.58 | 37.17 |
| 8 | 55.36 | 48.24 | 72.44 | 69.02 | 57.87 | 53.84 | 37.38 | 33.72 | 34.63 |
| 9 | 61.75 | 42.16 | 55.68 | 65.79 | 59.59 | 64.10 | 32.45 | 29.97 | 29.39 |
| 10 | 33.30 | 34.00 | 35.27 | 39.57 | 38.44 | 43.91 | 24.72 | 24.95 | 45.46 |
| 11 | 47.48 | 46.06 | 49.93 | 68.08 | 54.64 | 57.95 | 29.68 | 28.60 | 29.39 |
| 12 | 55.76 | 49.08 | 55.44 | 76.38 | 55.76 | 63.09 | 32.66 | 26.98 | 29.17 |
| 13 | 50.39 | 44.87 | 57.63 | 59.43 | 48.47 | 54.00 | 22.19 | 24.64 | 22.99 |
| 14 | 37.87 | 31.32 | 38.23 | 52.18 | 47.71 | 56.57 | 21.62 | 19.78 | 20.29 |

| | | | | | | | | | |
|---|---|---|---|---|---|---|---|---|---|
| 15 | 29.18 | 36.60 | 39.26 | 53.25 | 43.79 | 50.75 | 19.39 | 18.35 | 18.91 |
| 16 | 30.85 | 29.88 | 37.19 | 57.93 | 45.08 | 43.17 | 19.28 | 17.40 | 17.68 |
| 17 | 32.98 | 30.60 | 32.18 | 48.42 | 43.15 | 44.55 | 17.80 | 15.54 | 16.38 |
| 18 | 24.52 | 29.60 | 28.71 | 38.14 | 42.55 | 42.09 | 13.82 | 13.57 | 20.03 |
| 19 | 28.91 | 31.89 | 31.90 | 39.32 | 42.95 | 42.90 | 13.87 | 14.84 | 13.77 |
| 20 | 22.50 | 27.81 | 27.95 | 34.08 | 36.21 | 37.82 | 7.01 | 5.29 | 5.60 |
| 21 | 28.13 | 32.82 | 29.87 | 44.00 | 44.03 | 47.77 | 11.42 | 11.27 | 13.73 |
| 22 | 28.92 | | | | | | | | |
| 23 | 29.67 | 30.79 | 24.23 | 41.97 | 35.72 | 47.99 | 9.92 | 10.73 | 11.70 |
| 24 | 34.73 | 34.99 | 28.34 | 39.74 | 44.51 | 63.66 | 15.51 | 13.84 | 14.37 |
| 25 | 30.02 | 40.12 | 40.22 | 55.91 | 45.63 | 69.90 | 12.60 | 6.09 | 14.23 |
| 26 | 34.28 | 33.22 | 30.75 | 41.82 | 39.08 | 55.42 | 11.40 | 12.39 | 13.98 |
| 27 | 35.59 | 37.37 | 34.11 | 42.81 | 49.12 | 79.42 | 11.81 | 12.57 | 5.00 |
| 28 | 32.92 | 28.46 | 35.86 | 40.85 | 37.16 | 58.47 | 12.26 | 11.43 | 11.90 |
| 29 | 34.22 | 26.00 | 25.34 | 32.33 | 33.76 | 47.67 | 11.09 | 11.16 | 12.08 |
| 30 | 20.39 | 25.95 | 35.02 | 35.49 | 38.25 | 46.08 | 12.47 | 10.89 | 10.40 |
| 31 | 21.33 | 24.21 | 28.33 | 31.74 | 52.65 | 47.96 | 10.34 | 10.83 | 11.51 |
| 32 | 22.15 | 24.43 | 24.18 | 42.18 | 74.60 | 69.06 | 11.23 | 11.15 | 12.42 |
| 33 | 18.25 | 21.41 | 19.99 | 39.77 | 51.43 | 55.56 | 9.97 | 8.92 | 9.11 |
| 34 | 20.21 | 21.95 | 20.72 | 33.59 | 58.71 | 51.30 | 10.58 | 10.46 | 9.56 |
| 35 | 18.36 | 23.59 | 18.36 | 34.73 | 59.27 | 61.00 | 9.90 | 8.50 | 9.19 |
| 36 | 20.55 | 23.67 | 22.07 | 39.21 | 47.64 | 54.56 | 10.66 | 8.02 | 8.70 |
| 37 | 18.92 | 23.82 | 20.46 | 40.43 | 44.39 | 52.87 | 9.24 | 8.09 | 8.24 |
| 38 | 16.19 | 17.98 | 13.99 | 35.87 | 31.00 | 42.42 | 9.57 | 7.37 | 8.17 |
| 39 | 18.09 | 25.88 | 25.96 | 30.37 | 35.30 | 37.85 | 8.52 | 7.61 | 6.99 |
| 40 | 18.09 | 22.45 | 24.38 | 34.41 | 35.70 | 36.21 | 7.61 | 7.81 | 8.85 |
| 41 | 21.41 | 23.81 | 32.83 | 33.04 | 35.22 | 37.35 | 10.60 | 9.07 | 11.01 |
| 42 | 24.73 | 22.50 | 40.69 | 32.60 | 33.06 | 36.73 | 10.94 | 9.43 | 8.90 |
| 43 | 22.86 | 19.95 | 25.54 | 27.99 | 29.21 | 32.92 | 5.53 | 6.09 | 7.26 |
| 44 | 21.06 | 21.01 | 22.59 | 25.87 | 29.35 | 27.92 | 8.53 | 6.75 | 6.88 |
| 45 | 21.76 | 19.51 | 18.49 | 22.58 | 26.72 | 26.53 | 7.57 | 7.17 | 8.14 |
| 46 | 24.97 | 19.79 | 19.91 | 25.03 | 29.15 | 28.47 | 8.37 | 7.49 | 8.24 |
| 47 | 21.80 | 21.88 | 19.27 | 28.10 | 28.48 | 29.42 | 7.61 | 7.34 | 7.41 |
| 48 | 19.40 | 15.91 | 15.30 | 19.26 | 21.12 | 22.20 | 8.16 | 4.82 | 3.54 |
| 49 | 24.25 | 21.34 | 19.35 | 22.01 | 26.10 | 25.57 | 8.26 | 8.29 | 7.65 |
| 50 | 27.16 | 25.41 | 24.95 | 25.79 | 27.37 | 29.43 | 8.82 | 8.96 | 9.87 |
| 51 | 20.55 | 22.94 | 18.37 | 26.54 | 25.99 | 30.10 | 9.44 | 8.59 | 8.64 |
| 52 | 22.14 | 21.61 | 19.72 | 30.52 | 25.24 | 34.96 | 8.08 | 8.10 | 7.34 |
| 53 | 18.45 | 20.56 | 18.61 | 30.34 | 23.71 | 29.06 | 8.07 | 7.96 | 7.43 |
| 54 | 16.83 | 18.52 | 16.58 | 25.57 | 22.24 | 26.55 | 8.25 | 8.32 | 8.39 |
| 55 | 19.94 | 22.63 | 19.66 | 30.59 | 26.65 | 30.40 | 8.81 | 7.86 | 8.23 |
| 56 | 16.07 | 19.08 | 15.79 | 24.31 | 28.00 | 33.73 | 8.20 | 8.09 | 7.56 |
| 57 | 0.68 | 20.31 | 18.63 | 31.38 | 27.77 | 38.97 | 9.19 | 8.53 | 8.27 |
| 58 | 15.86 | 17.69 | 16.16 | 25.41 | 28.99 | 30.02 | 6.99 | 6.25 | 6.94 |
| 59 | 12.82 | 16.34 | 14.70 | 28.40 | 23.65 | 25.72 | 6.93 | 6.62 | 7.06 |
| 60 | 12.73 | 16.57 | 14.24 | 28.73 | 24.97 | 24.76 | 6.83 | 6.46 | 7.14 |
| Minimum | 0.68 | 15.91 | 13.99 | 19.26 | 21.12 | 22.20 | 5.53 | 4.82 | 3.54 |
| Maximum | 211.63 | 178.37 | 207.55 | 163.58 | 127.87 | 158.37 | 129.26 | 123.51 | 131.33 |
| Mean | 35.31 | 35.76 | 36.45 | 45.61 | 44.30 | 50.16 | 18.80 | 18.12 | 18.55 |
| Median | 24.52 | 25.64 | 26.96 | 37.00 | 38.76 | 45.31 | 10.63 | 9.95 | 10.13 |

Table A14.8 – Aitik cell weekly leachate sulfate measurements

| Sulfate (mg/kg/week) | | | | | | | | | |
|---|---|---|---|---|---|---|---|---|---|
| **Week** | **A01** | **A02** | **A03** | **A04** | **A05** | **A06** | **A07** | **A08** | **A09** |
| 0 | 89.51 | 108.34 | 110.76 | 77.58 | 131.54 | 108.19 | 106.07 | 88.35 | 100.41 |
| 1 | 142.01 | 126.15 | 113.91 | 161.52 | 120.07 | 129.16 | 110.31 | 113.85 | 115.39 |
| 2 | 88.93 | 101.95 | 75.27 | 115.47 | 92.28 | 98.47 | 74.07 | 72.45 | 70.38 |
| 3 | 77.83 | 80.90 | 56.00 | 79.54 | 51.01 | 69.36 | 41.22 | 13.15 | 51.95 |
| 4 | | | | | | | | 12.22 | |
| 5 | | | | | | | | 12.43 | |
| 6 | 35.62 | 33.16 | 36.25 | 42.09 | 30.18 | 29.10 | 23.94 | 8.01 | 22.51 |
| 7 | 25.18 | 28.89 | 27.50 | 41.15 | 25.25 | 28.45 | 13.26 | 8.82 | 14.75 |
| 8 | 30.47 | 25.86 | 25.78 | 33.51 | 29.39 | 25.86 | 16.38 | 10.51 | 11.16 |
| 9 | 26.01 | 25.40 | 21.87 | 31.39 | 23.07 | 22.35 | 12.95 | 9.84 | 9.28 |
| 10 | 20.96 | 15.72 | 19.43 | 25.25 | 19.86 | 19.26 | 10.62 | 10.62 | 9.73 |
| 11 | 22.67 | 24.17 | 22.51 | 30.25 | 23.31 | 17.93 | 11.59 | 6.45 | 9.17 |
| 12 | 18.82 | 19.08 | 17.84 | 29.61 | 22.75 | 20.96 | 10.62 | 7.93 | 8.59 |
| 13 | 20.79 | 19.95 | 19.86 | 27.79 | 20.37 | 21.87 | 9.51 | 6.07 | 8.25 |
| 14 | 14.46 | 15.62 | 17.57 | 25.25 | 20.96 | 18.38 | 8.71 | 4.13 | 6.58 |
| 15 | 14.46 | 16.14 | 16.57 | 21.51 | 18.21 | 17.31 | 8.62 | 2.86 | 7.77 |
| 16 | 12.58 | 14.44 | 14.38 | 22.05 | 18.40 | 18.27 | 8.17 | 5.58 | 7.08 |
| 17 | 10.17 | 10.50 | 10.22 | 20.58 | 14.75 | 17.21 | 5.64 | 7.18 | 4.02 |
| 18 | 11.43 | 11.88 | 12.16 | 20.18 | 16.61 | 20.04 | | 9.27 | 5.68 |
| 19 | 10.00 | | 11.47 | 20.62 | 16.15 | 19.01 | 5.73 | 4.91 | |
| 20 | 10.55 | 10.83 | 11.44 | 18.89 | 17.46 | 19.24 | 5.08 | 0.75 | 4.71 |
| 21 | 12.92 | 12.15 | 13.50 | 20.60 | 16.50 | 20.80 | 7.22 | | 6.67 |
| 22 | 11.05 | 13.13 | 18.28 | 22.23 | 23.63 | 25.25 | 5.31 | | 5.52 |
| 23 | 10.94 | 0.42 | 11.12 | 17.81 | 22.96 | 19.24 | 4.94 | 0.75 | 0.58 |
| 24 | 13.72 | 13.64 | 13.70 | 23.49 | 29.14 | 22.71 | 6.23 | 6.01 | 5.99 |
| 25 | 12.28 | 15.24 | 15.55 | 22.41 | 20.97 | 21.42 | 6.63 | 17.12 | 5.62 |
| 26 | 12.01 | 13.37 | 12.99 | 23.49 | 20.80 | 21.17 | 5.28 | 4.57 | 4.24 |
| 27 | 6.09 | 13.64 | 21.74 | 14.99 | 13.37 | 19.80 | 21.78 | 5.39 | 4.38 |
| 28 | 10.48 | 12.42 | 12.60 | 19.88 | 21.50 | 17.84 | 4.99 | 3.72 | 5.15 |
| 29 | 9.91 | 9.81 | 10.23 | 16.39 | 15.86 | 16.12 | 4.65 | 3.85 | 4.23 |
| 30 | 9.59 | 10.88 | 11.17 | 17.21 | 17.21 | 15.50 | 2.16 | 4.00 | 4.19 |
| 31 | 9.79 | 11.40 | 13.08 | 17.04 | 16.57 | 15.95 | 4.14 | 4.00 | 6.34 |
| 32 | 10.93 | 10.02 | 11.82 | 18.36 | 16.32 | 15.82 | 5.28 | 4.98 | 5.01 |
| 33 | 11.76 | 11.07 | 10.08 | 17.75 | 14.63 | 14.44 | 4.40 | 3.63 | 4.70 |
| 34 | 9.72 | 9.41 | 9.49 | 14.53 | 13.95 | 14.18 | 5.05 | 3.80 | 4.36 |
| 35 | 9.34 | 11.57 | 12.17 | 16.59 | 14.10 | 17.08 | 4.61 | 3.57 | 4.72 |
| 36 | 8.20 | 10.92 | 10.88 | 16.38 | 14.38 | 15.24 | 3.54 | 3.21 | 3.81 |
| 37 | 10.30 | 8.91 | 11.31 | 17.21 | 15.64 | 14.38 | 3.67 | 3.65 | 3.81 |
| 38 | 8.42 | 8.35 | 7.91 | 11.46 | 13.60 | 12.38 | 3.18 | 1.81 | 3.14 |
| 39 | 10.29 | 10.22 | 10.95 | 15.52 | 13.67 | 13.01 | 2.99 | 2.80 | 3.20 |
| 40 | 10.63 | 10.11 | 10.46 | 16.63 | 16.37 | 15.25 | 2.67 | 3.35 | 2.91 |
| 41 | 12.27 | 10.11 | 12.81 | 16.12 | 14.45 | 15.01 | 3.52 | 3.31 | 3.97 |
| 42 | 10.83 | 10.70 | 10.67 | 14.86 | 15.64 | 16.46 | 4.40 | 2.92 | 5.78 |
| 43 | 9.24 | 11.33 | 11.31 | 14.67 | 13.98 | 14.06 | 2.10 | 3.50 | 3.17 |
| 44 | 8.96 | 8.70 | 11.36 | 15.39 | 13.22 | 12.22 | 2.35 | 3.27 | 3.09 |
| 45 | 9.69 | 11.38 | 8.19 | 11.72 | 13.80 | 19.32 | 10.04 | 3.79 | 4.42 |
| 46 | 10.97 | 12.38 | 12.03 | 15.35 | 14.89 | 12.69 | 0.00 | 2.61 | 2.75 |
| 47 | 8.85 | 4.59 | 10.56 | 13.34 | 12.31 | 12.53 | 2.26 | 2.60 | 3.56 |
| 48 | 6.51 | 9.62 | 6.73 | 11.67 | 9.36 | 9.50 | | 1.05 | 3.13 |

| | | | | | | | | | |
|---|---|---|---|---|---|---|---|---|---|
| 49 | 9.99 | 2.53 | 10.80 | 13.92 | 13.10 | 12.12 | 3.55 | 2.49 | 3.55 |
| 50 | 10.97 | 10.87 | 11.93 | 14.78 | 13.94 | 12.27 | 4.12 | 3.23 | 3.73 |
| 51 | 9.56 | 9.74 | 10.78 | 14.64 | 12.74 | 11.66 | 4.25 | 3.43 | 2.13 |
| 52 | 8.27 | 9.40 | 11.28 | 14.88 | 13.72 | 13.25 | 3.88 | 2.77 | 3.42 |
| 53 | 8.94 | 10.63 | 11.41 | 13.52 | 13.95 | 12.36 | 2.77 | 3.26 | 3.65 |
| 54 | 9.45 | 9.22 | 11.54 | 13.44 | 13.93 | 11.73 | 4.05 | 3.15 | 3.33 |
| 55 | 11.34 | 9.63 | 11.56 | 14.61 | 14.45 | 13.48 | 4.25 | 3.71 | 3.06 |
| 56 | 10.92 | 10.53 | 10.57 | 11.19 | 13.32 | 12.90 | 3.72 | 4.19 | 3.96 |
| 57 | 11.46 | 9.40 | 12.93 | 14.31 | 15.03 | 13.53 | 3.82 | 3.68 | 3.70 |
| 58 | 8.88 | 11.93 | 10.55 | 12.22 | 12.60 | 11.60 | 2.58 | 1.85 | 2.29 |
| 59 | 10.39 | 8.29 | 10.72 | 15.44 | 12.78 | 12.72 | 2.41 | 4.73 | 2.00 |
| 60 | | 10.43 | | | | 12.72 | | | |
| Minimum | 6.09 | 0.42 | 6.73 | 11.19 | 9.36 | 9.50 | 0.00 | 0.75 | 0.58 |
| Maximum | 142.01 | 126.15 | 113.91 | 161.52 | 131.54 | 129.16 | 110.31 | 113.85 | 115.39 |
| Mean | 18.59 | 18.91 | 18.92 | 25.35 | 22.76 | 22.54 | 11.70 | 9.57 | 10.89 |
| Median | 10.92 | 11.20 | 11.88 | 17.21 | 16.01 | 16.46 | 4.97 | 3.82 | 4.38 |

# Appendix 15 – CCP Raw Data and Conversion Factors

Within this appendix the raw data outputs of CCP calculations are displayed as well as the element-to-stoichiometric oxide conversion factors and molar mass values used in this study.

Table A15.1 – CCP calculation output values for Kevitsa and Aitik pre and post HCT samples.

| SAMPLE ID | CCP |
|---|---|
| | kg/t (CO2) |
| A-PRE | 72.65814308 |
| A01-POST | 80.00048951 |
| A02-POST | 82.92379657 |
| A03-POST | 81.57370649 |
| A04-POST | 81.93134602 |
| A05-POST | 80.07202863 |
| A06-POST | 83.86391186 |
| A07-POST | 87.11304639 |
| A08-POST | 79.72415678 |
| A09-POST | 85.37985323 |
| K-PRE | 295.1019577 |
| K01-POST | 299.5710059 |
| K02-POST | 308.1112963 |
| K03-POST | 307.1591204 |
| K04-POST | 295.4685781 |
| K05-POST | 295.4870918 |
| K06-POST | 301.4364738 |
| K07-POST | 309.2786589 |
| K08-POST | 311.5464974 |
| K09-POST | 303.0725694 |

Table A15.2 – Oxide and element molecular masses used within conversion in this study.

| Molecular Mass | |
|---|---|
| Oxide/element | Molecular mass (Kg/Mole) |
| CaO | 56.0774 |
| MgO | 40.3044 |
| $Na_2O$ | 61.97894 |
| $K_2O$ | 94.196 |
| $SO_3$ | 80.0632 |
| $P_2O5$ | 141.945 |
| $CO_2$ | 44.01 |
| S | 32.065 |
| $SO_4$ | 96.06 |

Table A15.3 – Element-to-stoichiometric oxide conversion factors used in this study.

Factors were based on:

https://www.jcu.edu.au/advanced-analytical-centre/resources/element-to-stoichiometric-oxide-conversion-factors

| **Element-to-stoichiometric oxide conversion factors** | | | |
|---|---|---|---|
| Element | Element | Oxide | Conversion Factor |
| Silver | Ag | Ag2O | 1.0741 |
| Aluminium | Al | Al2O3 | 1.8895 |
| Arsenic | As | As2O3 | 1.5339 |
| Gold | Au | Au2O | 1.0406 |
| Boron | B | B2O3 | 3.2202 |
| Barium | Ba | BaO | 1.1165 |
| Beryllium | Be | BeO | 2.7758 |
| Bismuth | Bi | Bi2O5 | 1.1914 |
| Carbon | C | CO2 | 3.6644 |
| Calcium | Ca | CaO | 1.3992 |
| Cadmium | Cd | CdO | 1.1423 |
| Cerium | Ce | Ce2O3 | 1.1713 |
| Cerium | Ce | CeO2 | 1.2284 |
| Cobalt | Co | CoO | 1.2715 |
| Chromium | Cr | Cr2O3 | 1.4615 |
| Caesium | Cs | Cs2O | 1.0602 |
| Copper | Cu | CuO | 1.2518 |
| Dysprosium | Dy | Dy2O3 | 1.1477 |
| Erbium | Er | Er2O3 | 1.1435 |
| Europium | Eu | Eu2O3 | 1.1579 |

| Iron | Fe | FeO | 1.2865 |
|---|---|---|---|
| Iron | Fe2 | Fe2O3 | 1.4297 |
| Gallium | Ga | Ga2O3 | 1.3442 |
| Gadolinium | Gd | Gd2O3 | 1.1526 |
| Germanium | Ge | GeO2 | 1.4408 |
| Hafnium | Hf | HfO2 | 1.1793 |
| Mercury | Hg | HgO | 1.0798 |
| Holmium | Ho | Ho2O3 | 1.1455 |
| Indium | In | In2O3 | 1.2091 |
| Iridium | Ir | IrO | 1.0832 |
| Potassium | K | K2O | 1.2046 |
| Lanthanum | La | La2O3 | 1.1728 |
| Lithium | Li | Li2O | 2.1527 |
| Lutetium | Lu | Lu2O3 | 1.1371 |
| Magnesium | Mg | MgO | 1.6582 |
| Manganese | Mn | MnO | 1.2912 |
| Manganese | Mn | MnO2 | 1.5825 |
| Molybdenum | Mo | MoO3 | 1.5003 |
| Nitrogen | N | N2O5 | 3.8551 |
| Sodium | Na | Na2O | 1.348 |
| Niobium | Nb | Nb2O5 | 1.4305 |
| Neodymium | Nd | Nd2O3 | 1.1664 |
| Nickel | Ni | NiO | 1.2725 |
| **Osmium** | **Os** | OsO | 1.0841 |
| Phosphorus | P | P2O5 | 2.2916 |
| Lead | Pb | PbO | 1.0772 |
| Lead | Pb | PbO2 | 1.1544 |
| Palladium | Pd | PdO | 1.1504 |
| Praseodymium | Pr | Pr2O3 | 1.1703 |
| Praseodymium | Pr | Pr6O11 | 1.2082 |
| Platinum | Pt | PtO | 1.082 |
| Rubidium | Rb | Rb2O | 1.0936 |
| Rhenium | Re | ReO | 1.0859 |
| Rhodium | Rh | RhO | 1.5555 |
| Ruthenium | Ru | RuO | 1.1583 |
| Sulfur | S | SO3 | 2.4972 |
| Antimony | Sb | Sb2O5 | 1.3284 |
| Scandium | Sc | Sc2O3 | 1.5338 |
| Selenium | Se | SeO3 | 1.6079 |
| Silicon | Si | SiO2 | 2.1392 |
| Samarium | Sm | Sm2O3 | 1.1596 |
| Tin | Sn | SnO2 | 1.2696 |
| Strontium | Sr | SrO | 1.1826 |
| Tantalum | Ta | Ta2O5 | 1.2211 |
| Terbium | Tb | Tb2O3 | 1.151 |
| Terbium | Tb | Tb4O7 | 1.1762 |

| | | | |
|---|---|---|---|
| Tellurium | Te | TeO3 | 1.3762 |
| Thorium | Th | ThO2 | 1.1379 |
| Titanium | Ti | TiO2 | 1.6681 |
| Thallium | Tl | Tl2O3 | 1.1174 |
| Thulium | Tm | Tm2O3 | 1.1421 |
| Uranium | U | UO2 | 1.1344 |
| Uranium | U | UO3 | 1.2017 |
| Uranium | U | U3O8 | 1.1792 |
| Vanadium | V | V2O5 | 1.7852 |
| Tungsten | W | WO3 | 1.261 |
| Yttrium | Y | Y2O3 | 1.2699 |
| Ytterbium | Yb | Yb2O3 | 1.1387 |
| Zinc | Zn | ZnO | 1.2448 |
| Zirconium | Zr | ZrO2 | 1.3508 |

# Appendix 16 – Static Testing Parameter Graphs

Within this appendix the graphs created comparing ABA and other static test results outputs are presented, in line with recommendations within the MEND 1.20.1 manual (Price, 2009) and the GARD guide (GARD, 2014). It is noted that NPR is a ratio.

## Aitik Static Testing Parameter Graphs

Figure A16.1 – Aitik pre/post HCT NAG pH vs S%

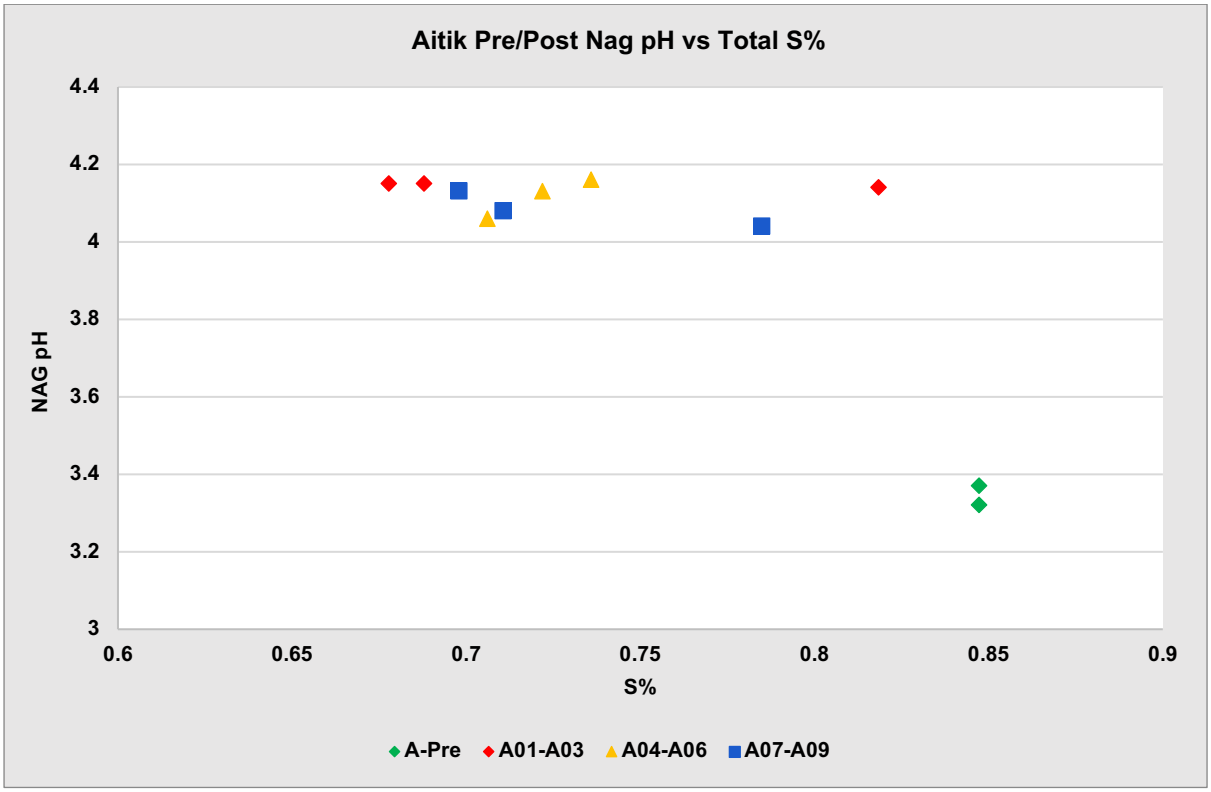

Figure A16.2 – Aitik pre/post HCT MPA vs NP

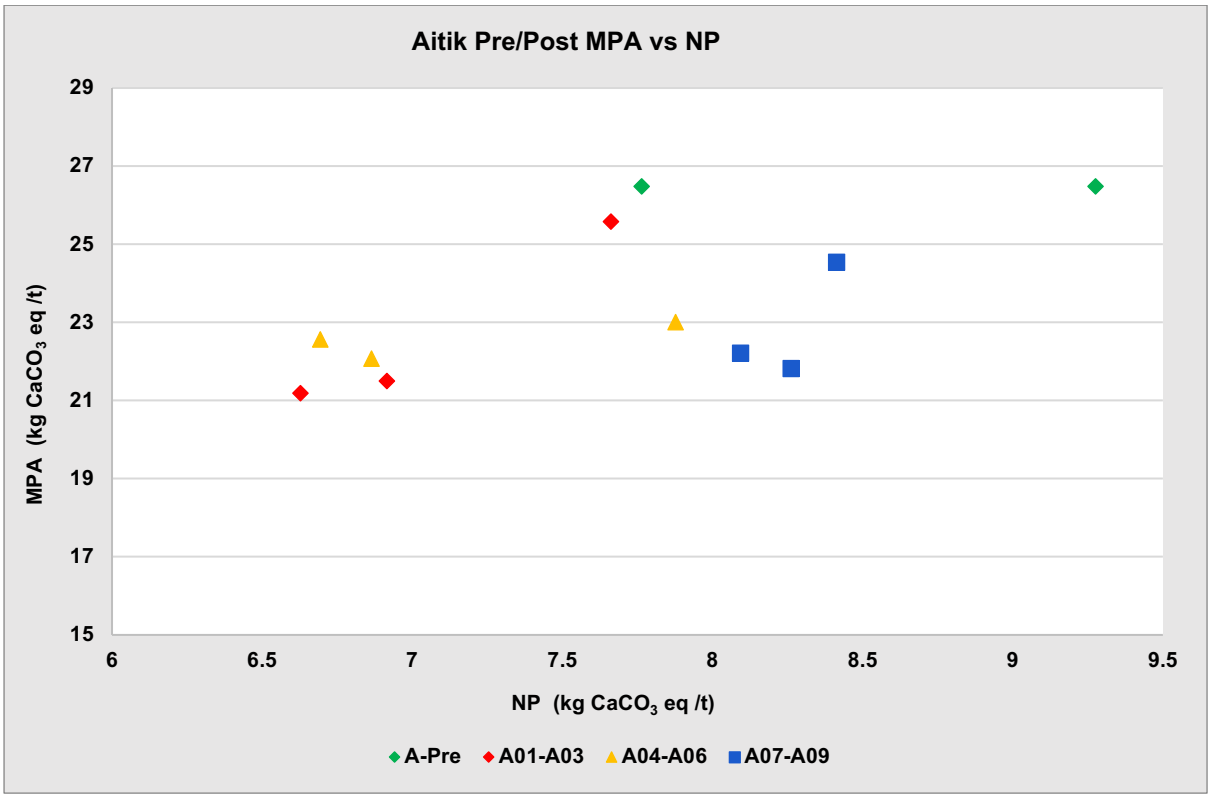


Figure A16.3 – Aitik pre/post HCT NPR vs S%

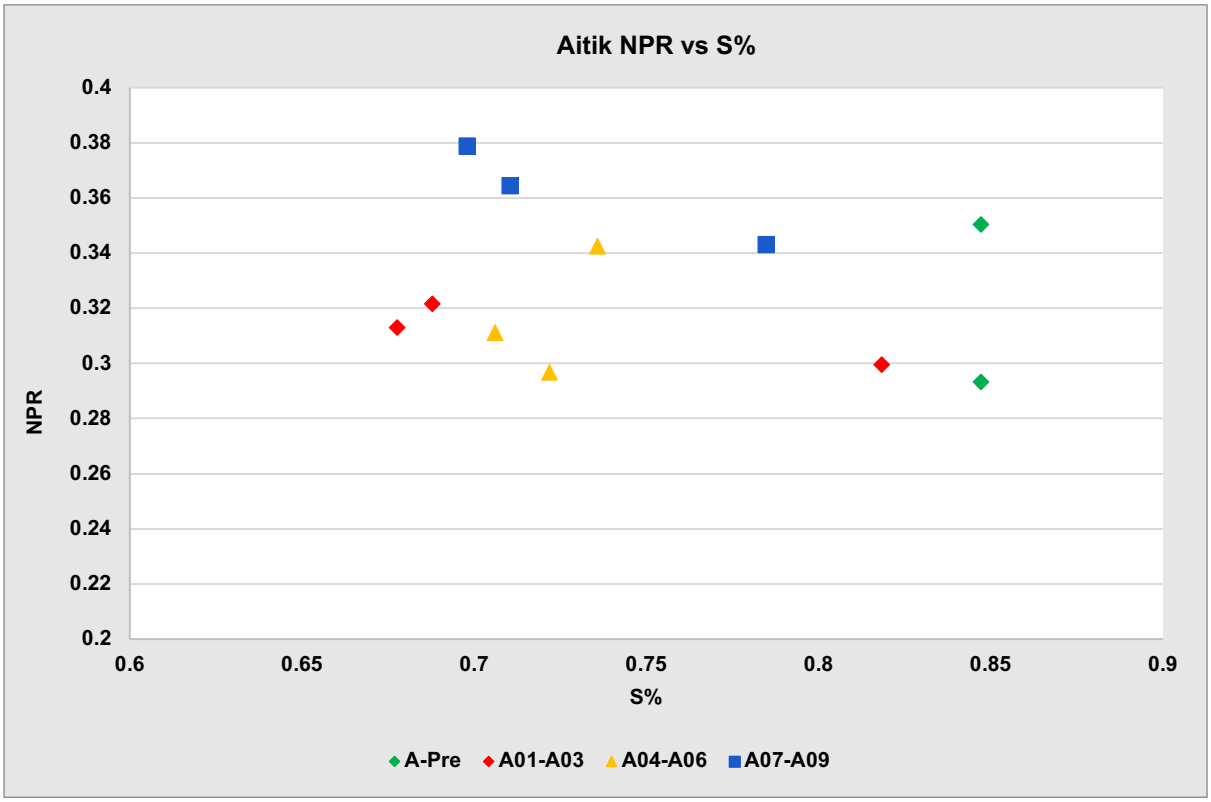

Figure A16.4 – Aitik pre/post HCT MPA vs S%

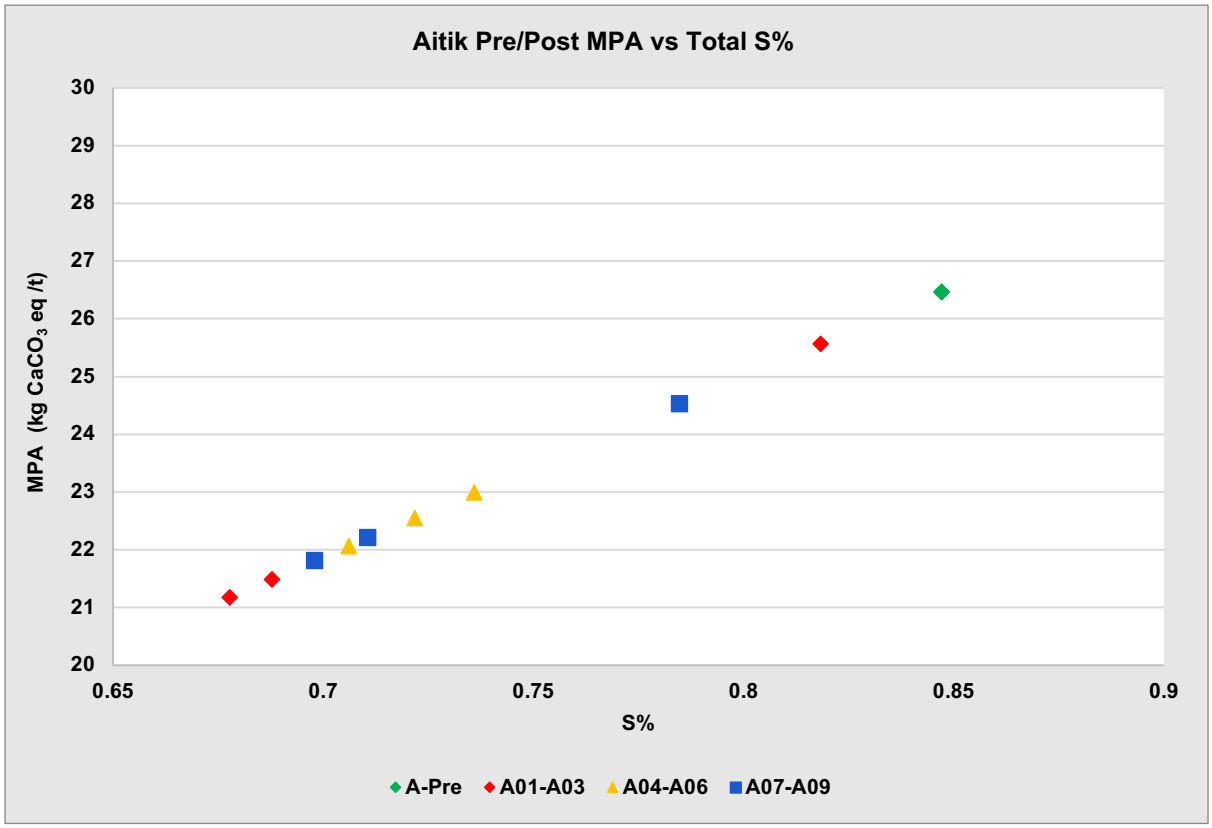


Figure A16.5 – Aitik pre/post HCT MPA vs NP

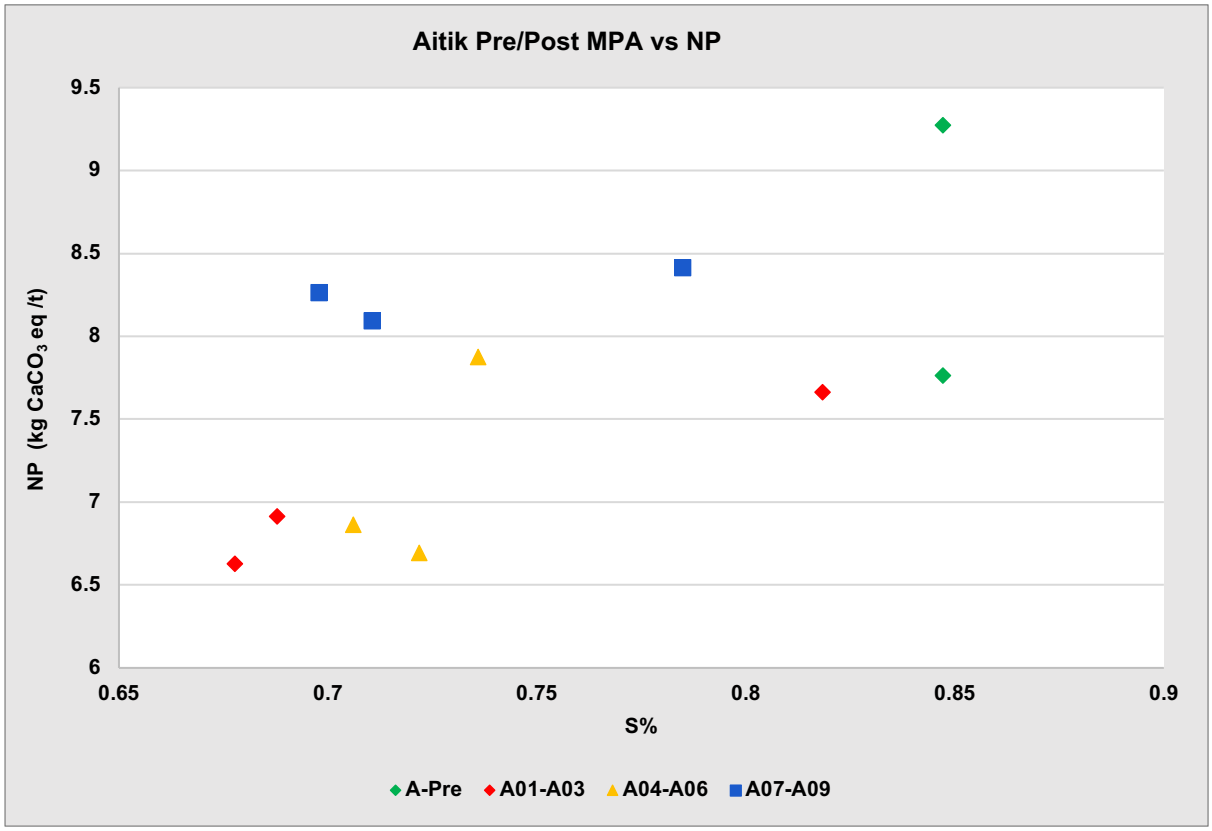

Figure A16.6 – Aitik pre/post HCT NNP vs S%

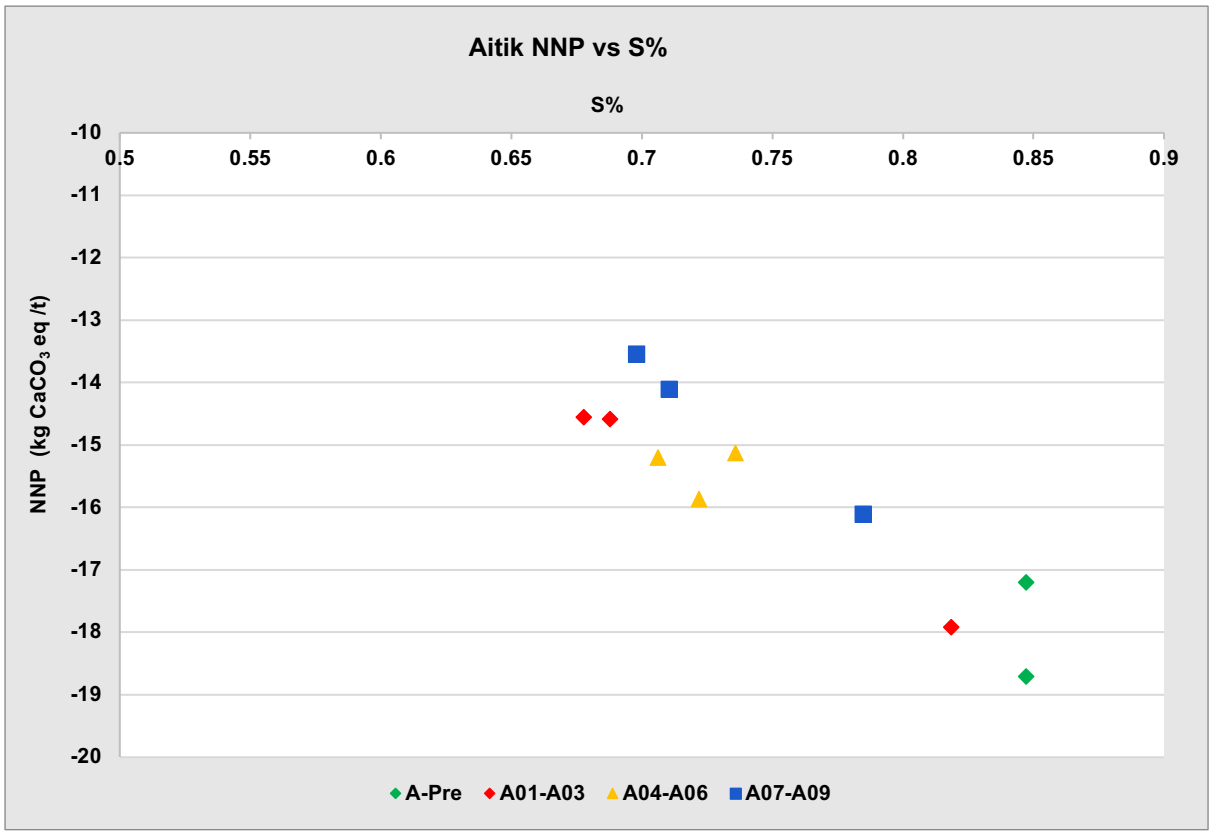


Figure A16.7 – Aitik pre/post HCT Paste EC vs S%

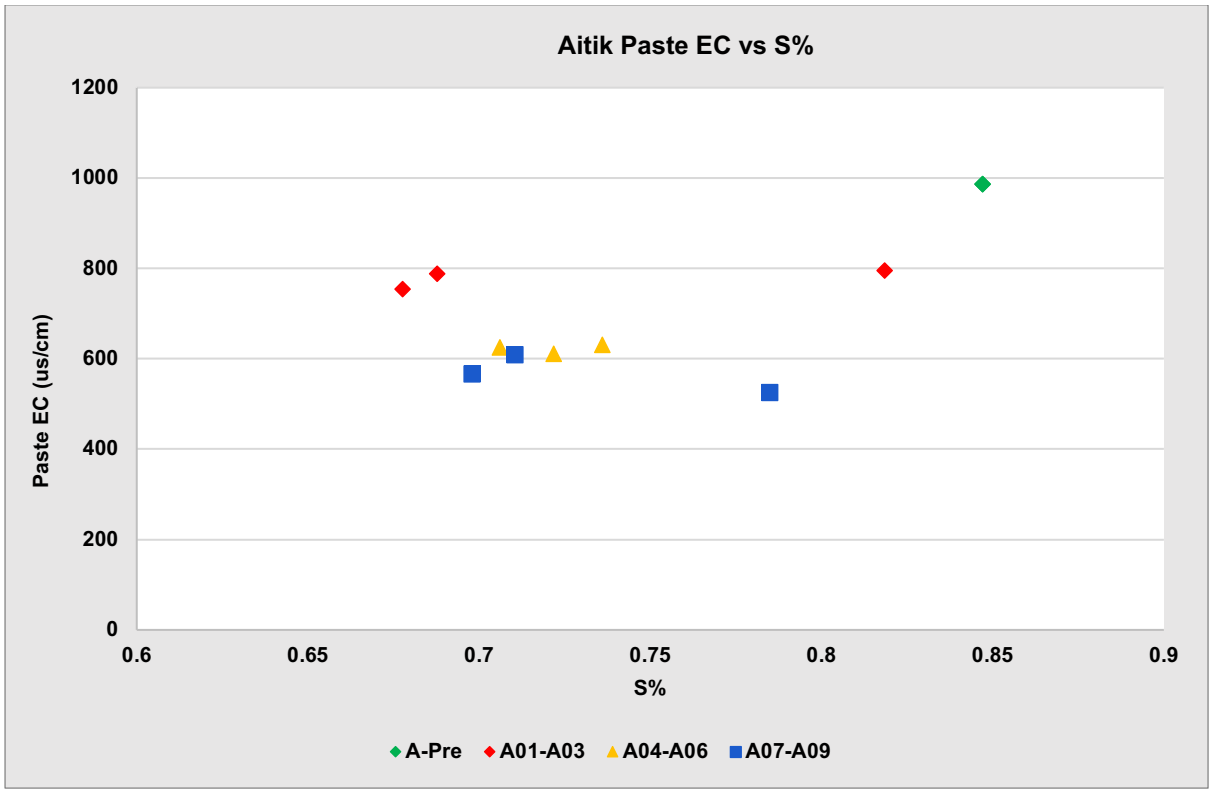

Figure A16.8 – Aitik pre/post HCT Paste pH vs S%

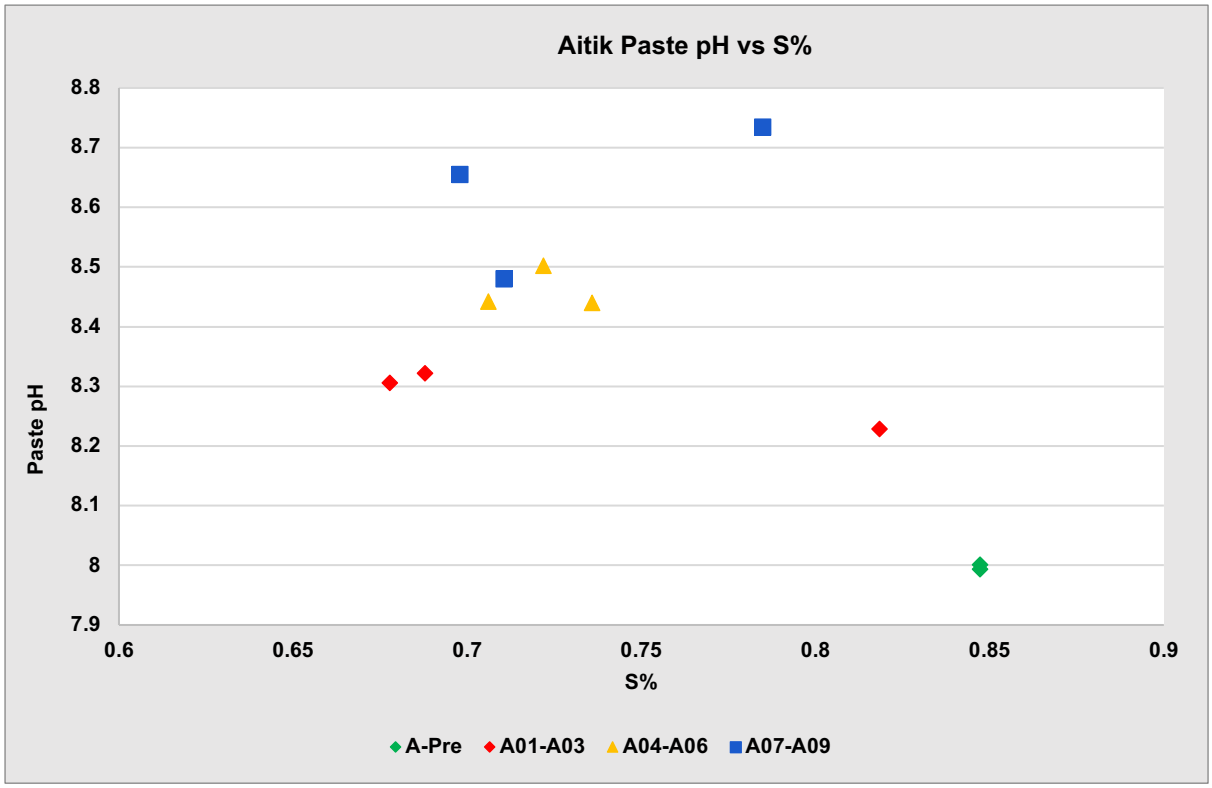


Figure A16.9 – Aitik pre/post HCT ED-XRF Mg vs NP

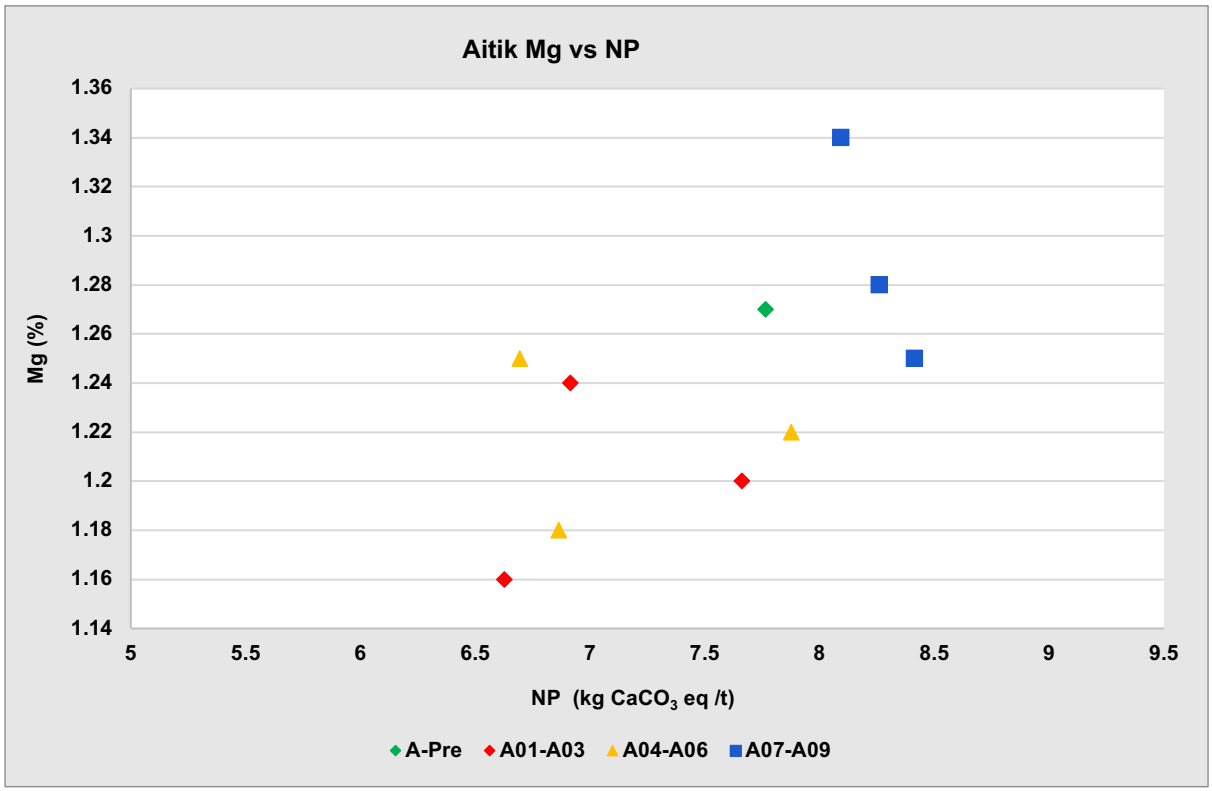

Figure A16.10 – Aitik pre/post HCT ED-XRF Ca vs NP

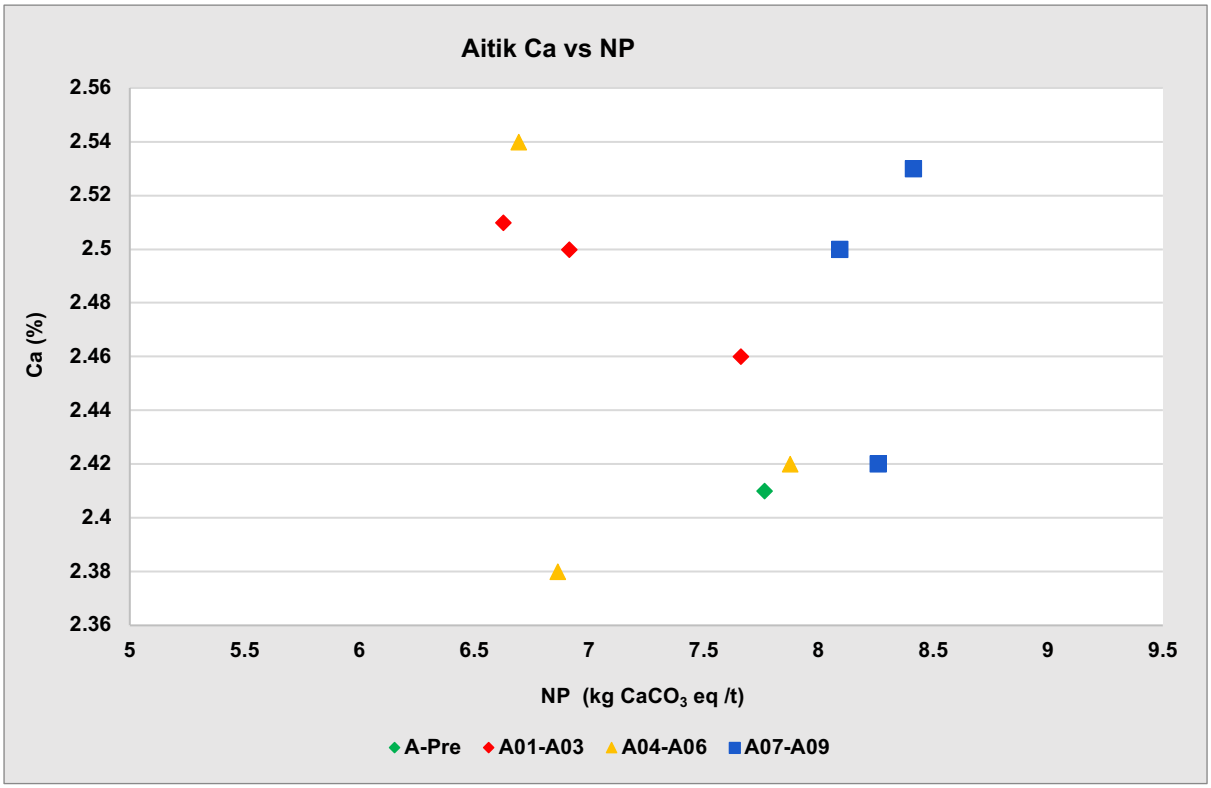


## Kevitsa Static Testing Parameter Graphs

Figure A16.11 – Kevitsa pre/post HCT NAG pH vs S%

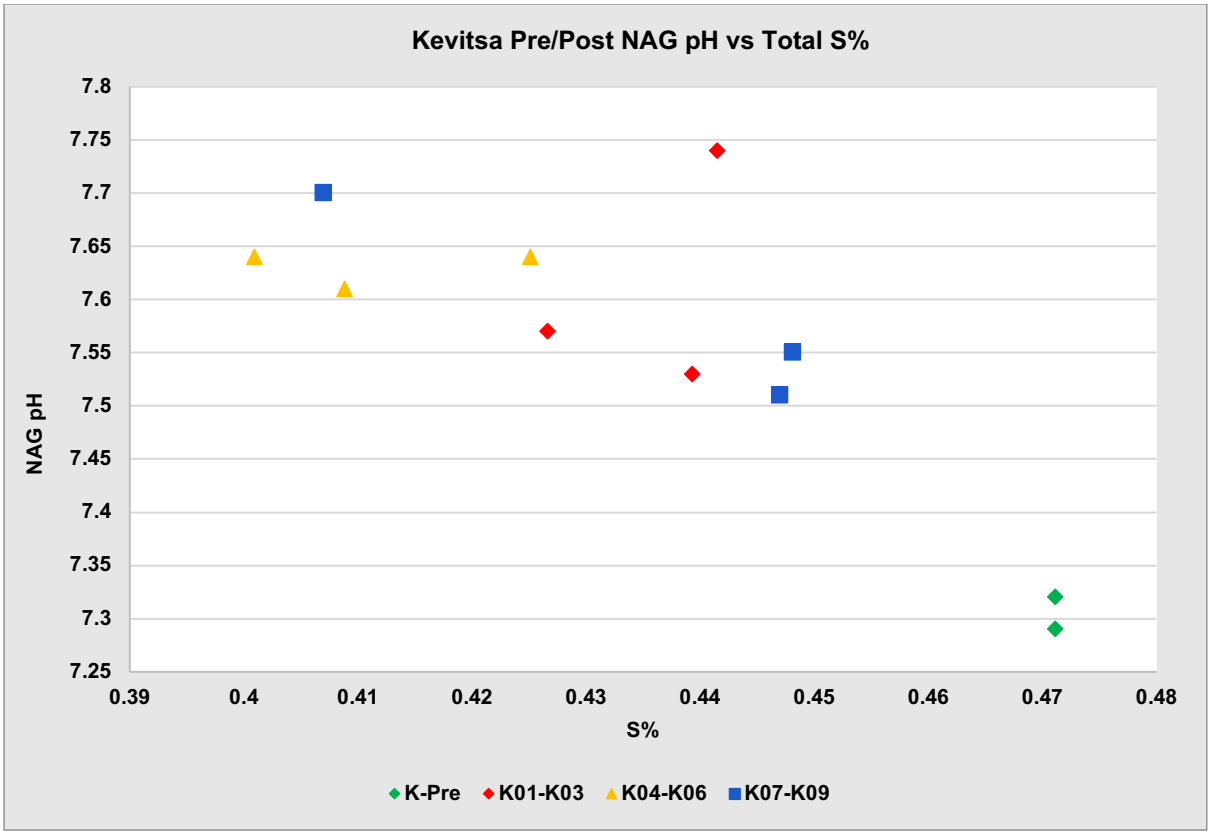

Figure A16.12 – Kevitsa pre/post HCT NAG pH vs S%

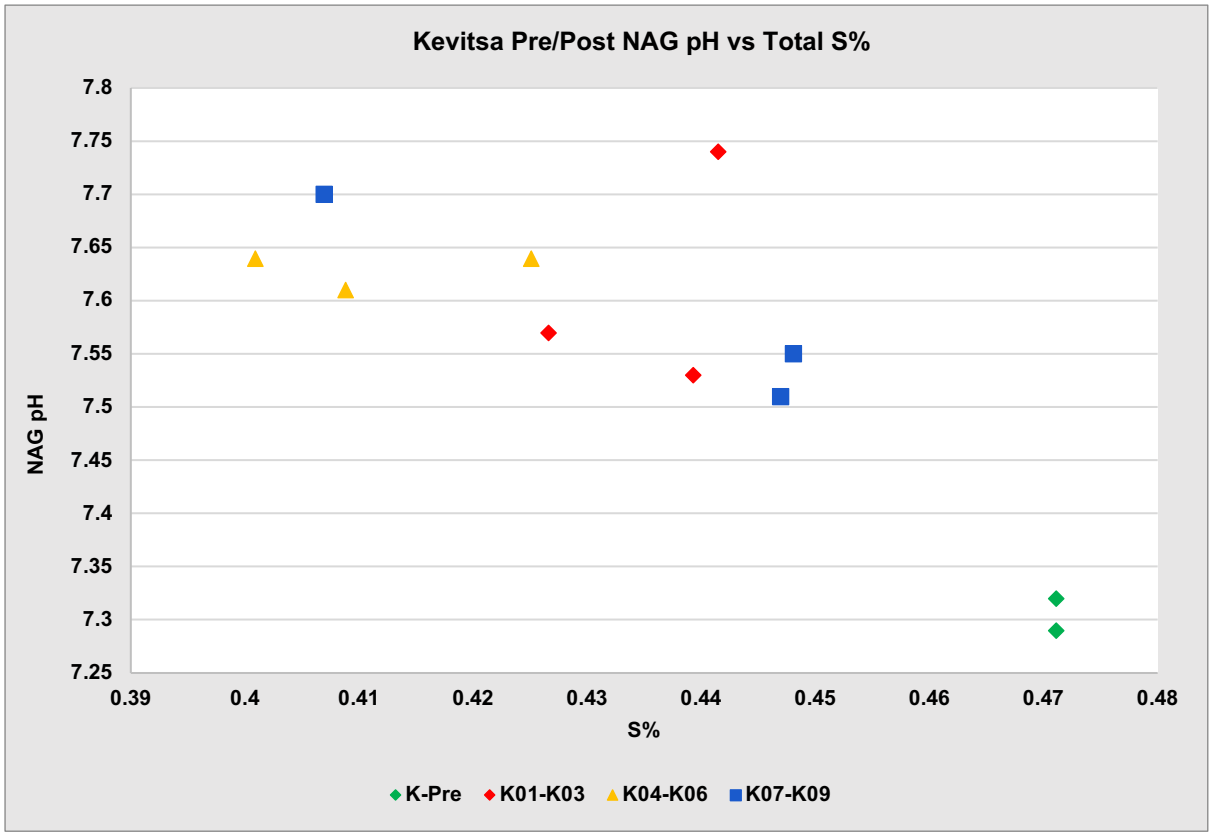


Figure A16.13 – Kevitsa pre/post HCT MPA vs S%

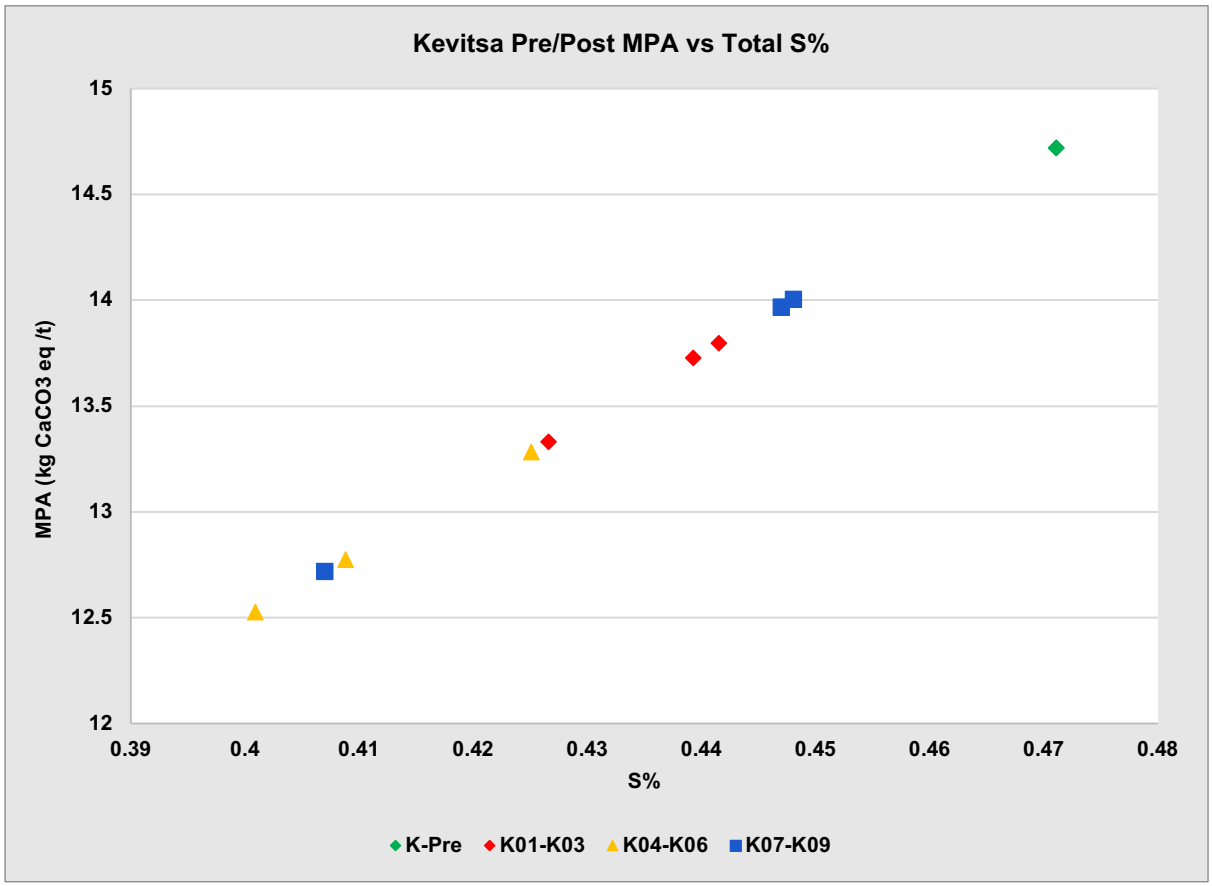

Figure A16.14 – Kevitsa pre/post HCT MPA vs NP

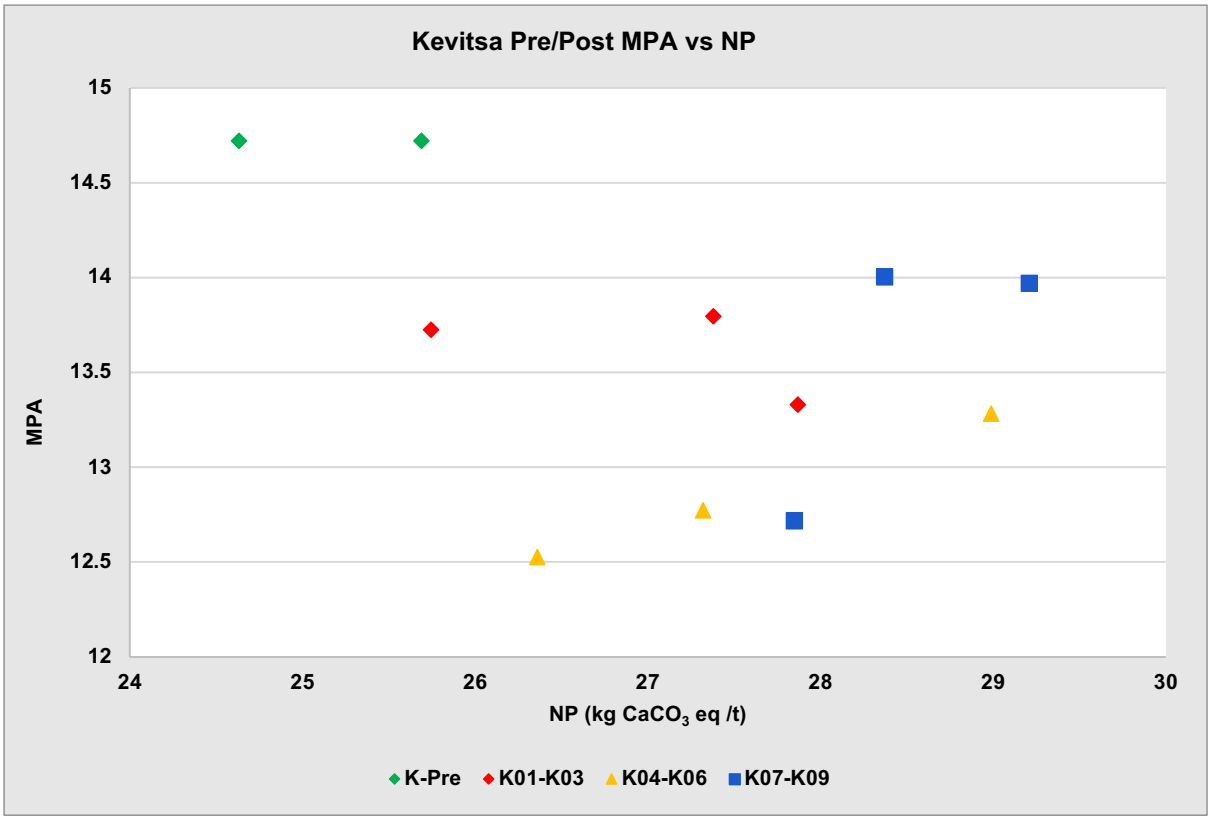


Figure A16.15 – Kevitsa pre/post HCT MPA vs NP

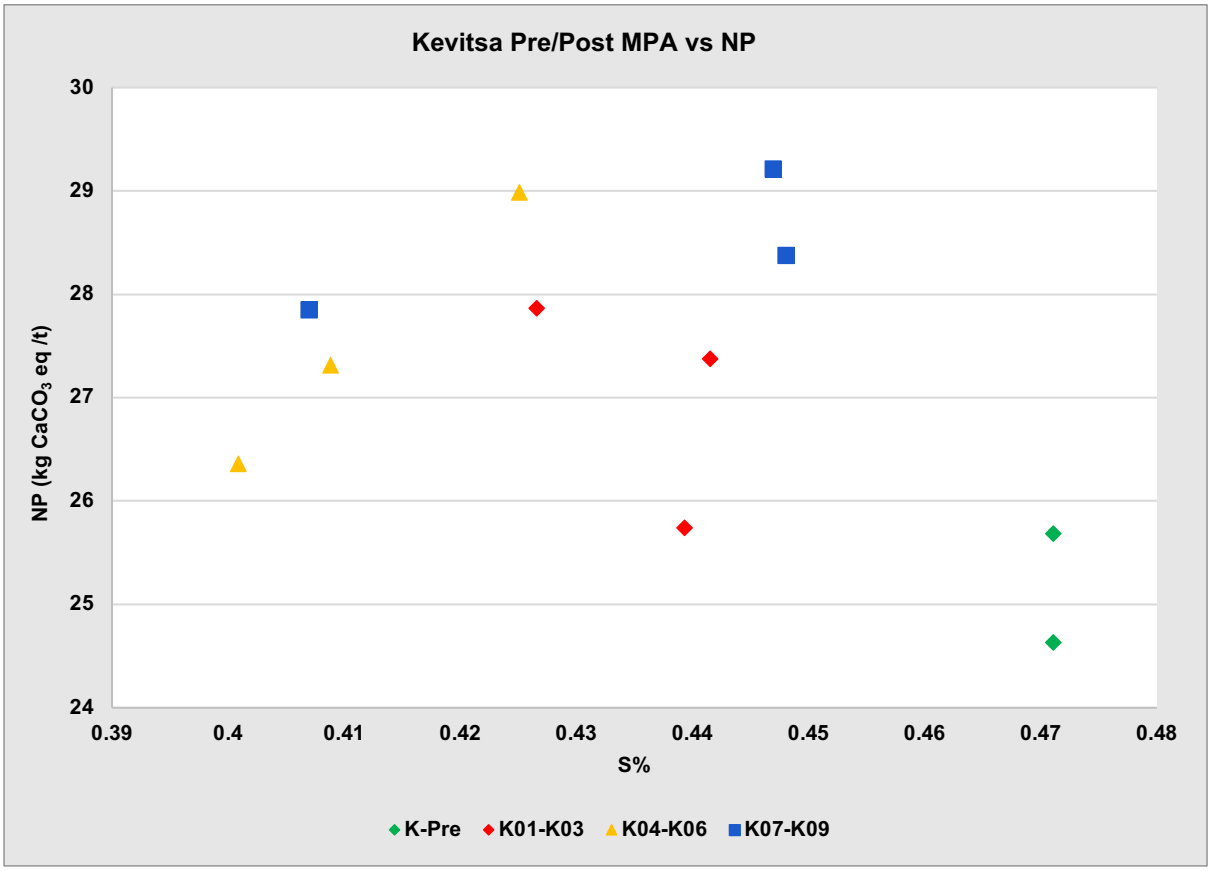

Figure A16.16 – Kevitsa pre/post HCT NPR vs S%

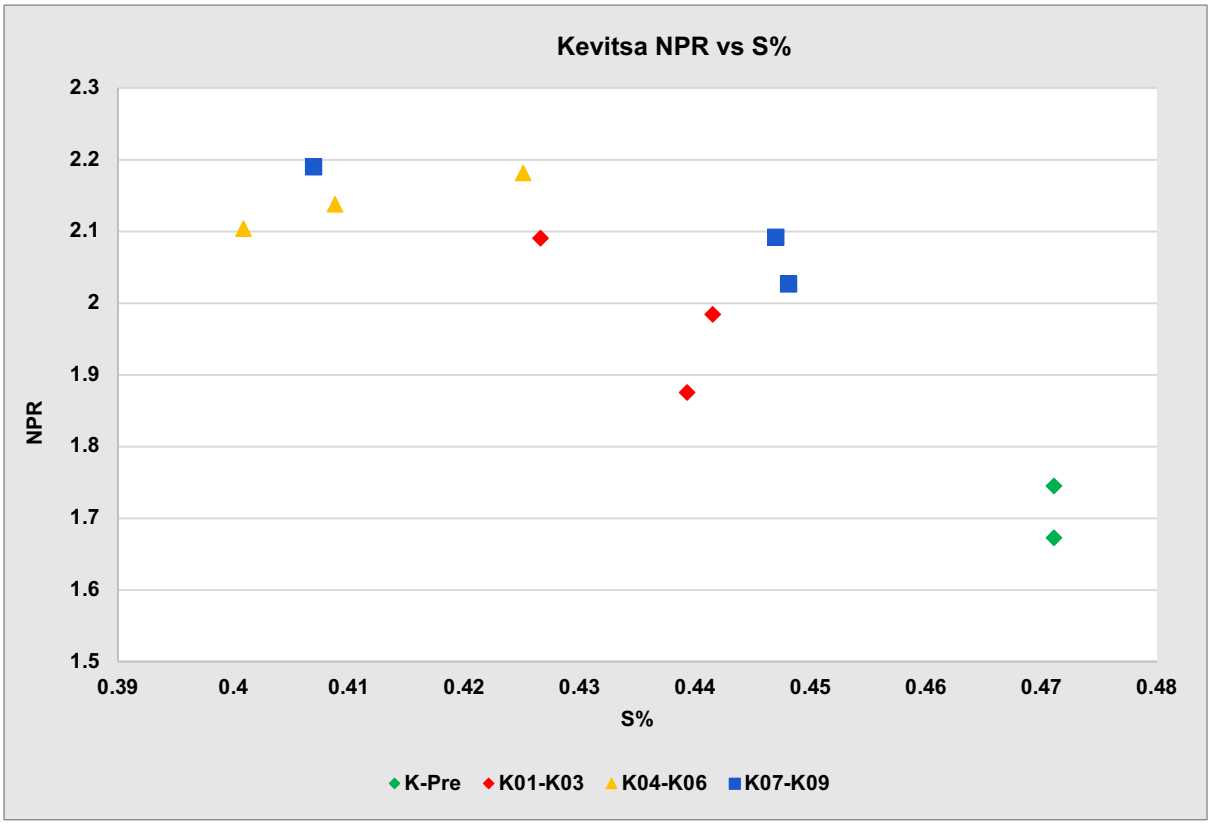


Figure A16.17 – Kevitsa pre/post HCT NNP vs S%

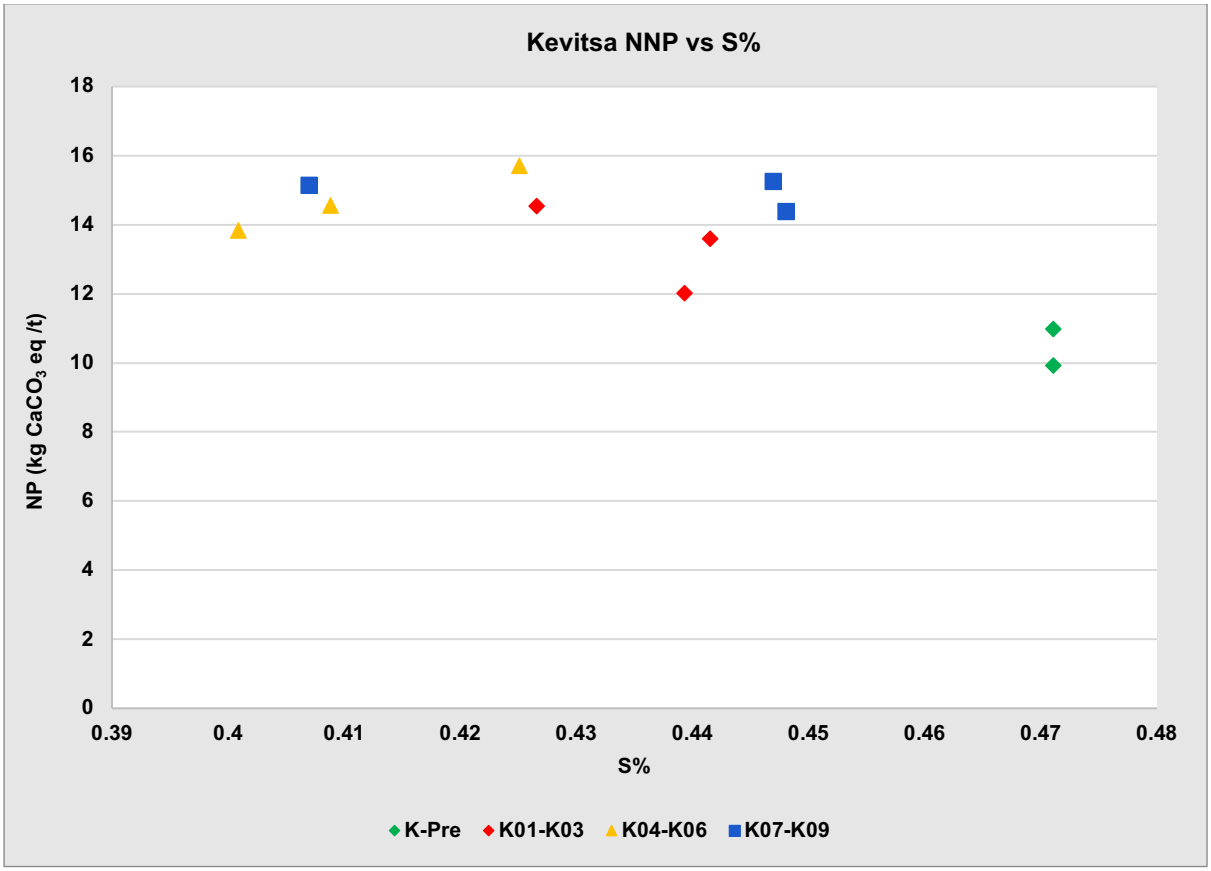

Figure A16.18 – Kevitsa pre/post HCT Paste EC vs S%

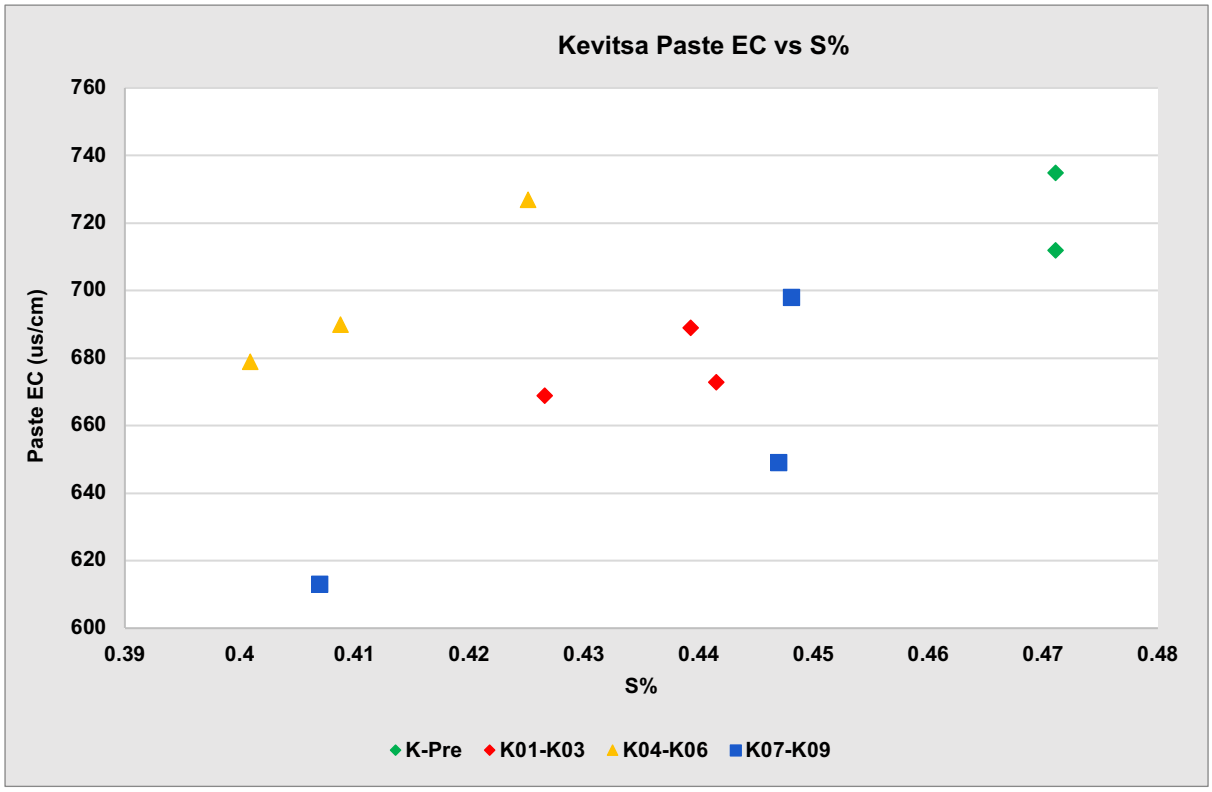


Figure A16.19 – Kevitsa pre/post HCT Paste pH vs S%

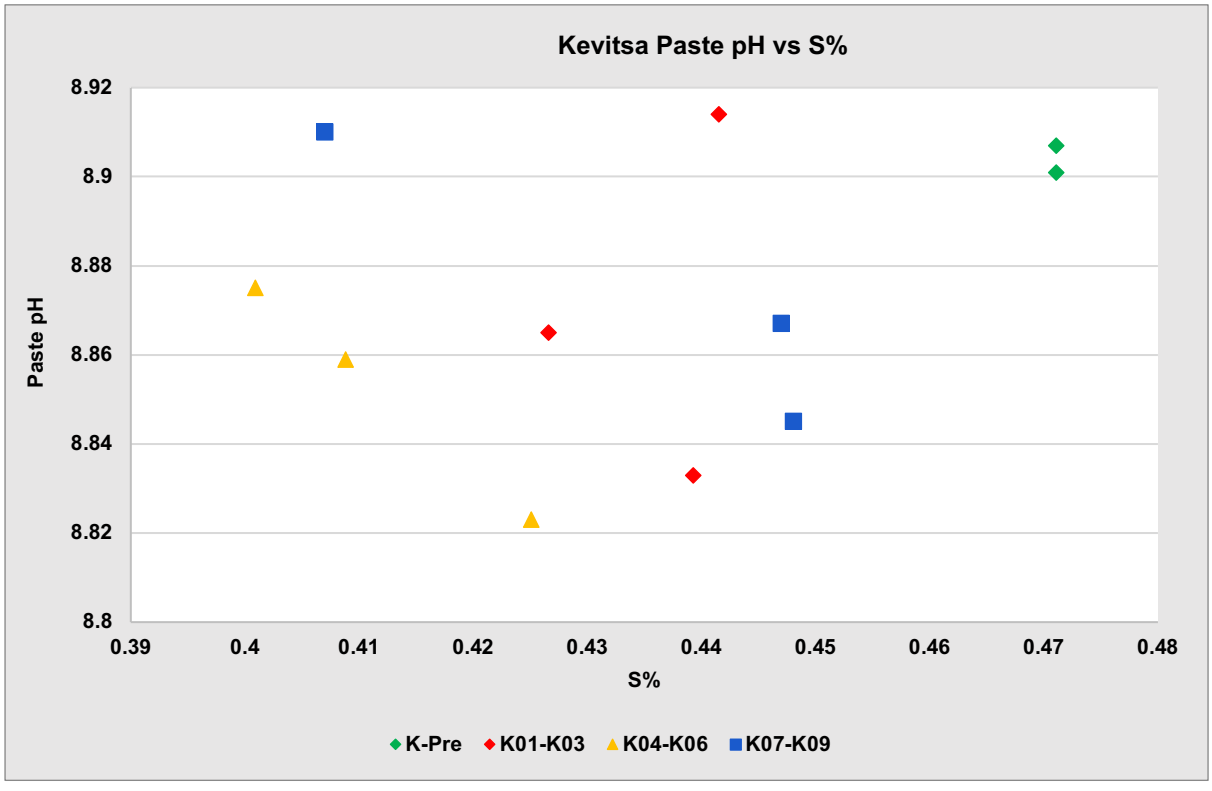

Figure A16.20 – Kevitsa pre/post HCT ED-XRF Mg vs NP

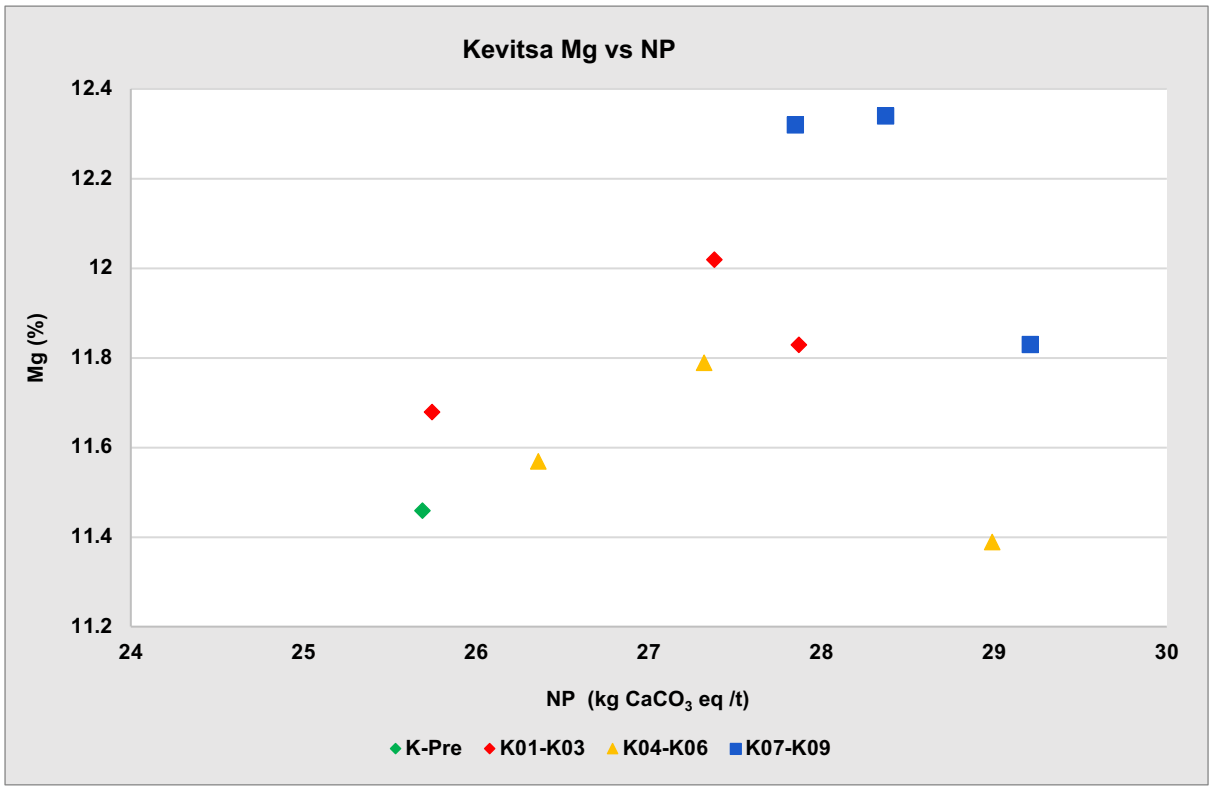


Figure A16.21 – Kevitsa pre/post HCT ED-XRF Ca vs NP

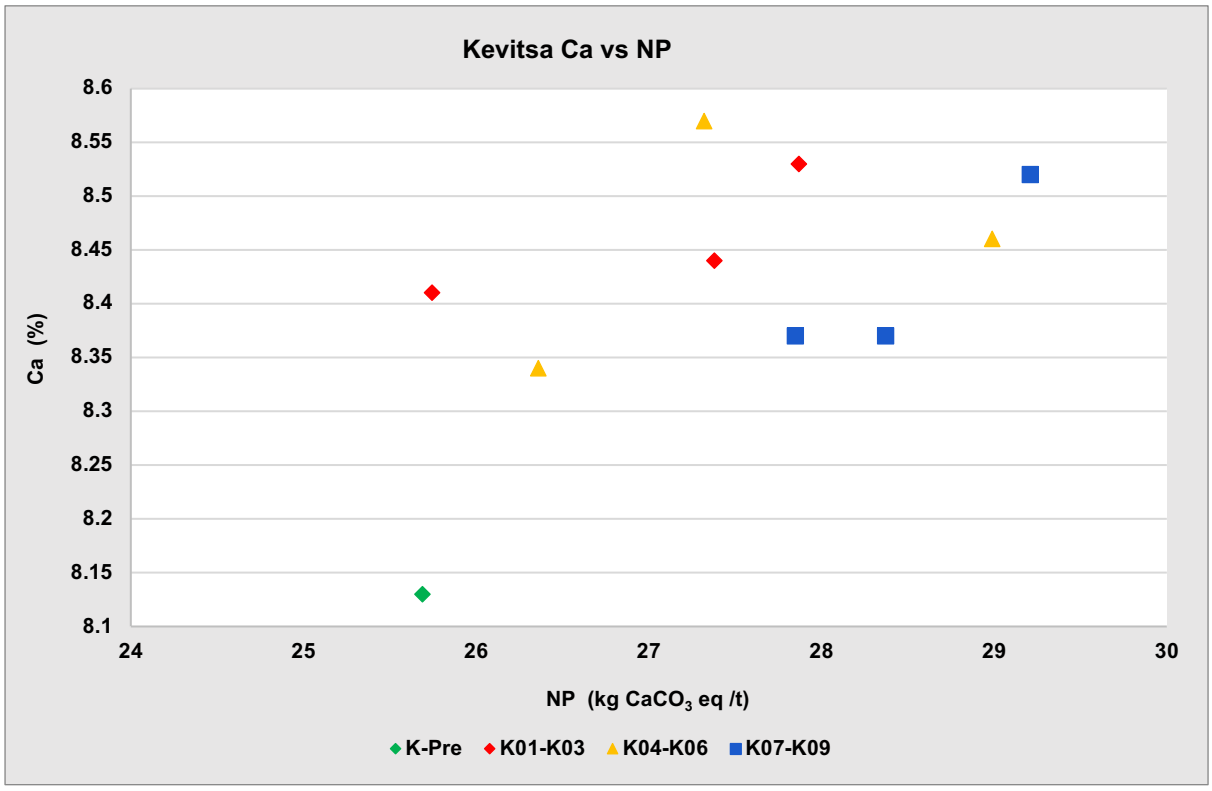

# Appendix 17 – Correlation Coefficients

This appendix contains the outputs of correlation analysis carried out om the form of Pearsons ‘r’. Methods related to this analysis is outlined in Chapter 4 of this thesis.

Table A17.1 – Weekly Kevitsa leachate pH correlation co-efficient matrix

| Kevitsa pH Correlation Co-Efficient | | | | | | | | | |
|---|---|---|---|---|---|---|---|---|---|
| Cell | K01 | K02 | K03 | K04 | K05 | K06 | K07 | K08 | K09 |
| K01 | 1 | | | | | | | | |
| K02 | 0.863 | 1 | | | | | | | |
| K03 | 0.877 | 0.846 | 1 | | | | | | |
| K04 | 0.215 | 0.107 | 0.138 | 1 | | | | | |
| K05 | 0.346 | 0.175 | 0.399 | 0.712 | 1 | | | | |
| K06 | 0.292 | 0.122 | 0.367 | 0.687 | 0.937 | 1 | | | |
| K07 | 0.564 | 0.510 | 0.570 | 0.144 | 0.277 | 0.227 | 1 | | |
| K08 | 0.534 | 0.516 | 0.534 | 0.179 | 0.217 | 0.148 | 0.935 | 1 | |
| K09 | 0.618 | 0.577 | 0.633 | 0.187 | 0.321 | 0.264 | 0.892 | 0.902 | 1 |

Table A17.2 – Weekly Kevitsa leachate EC correlation co-efficient matrix

| Kevitsa EC Correlation Co-Efficient | | | | | | | | | |
|---|---|---|---|---|---|---|---|---|---|
| Cell | K01 | K02 | K03 | K04 | K05 | K06 | K07 | K08 | K09 |
| K01 | 1 | | | | | | | | |
| K02 | 0.863 | 1 | | | | | | | |
| K03 | 0.877 | 0.846 | 1 | | | | | | |
| K04 | 0.215 | 0.107 | 0.138 | 1 | | | | | |
| K05 | 0.346 | 0.175 | 0.399 | 0.712 | 1 | | | | |
| K06 | 0.292 | 0.122 | 0.367 | 0.687 | 0.937 | 1 | | | |
| K07 | 0.564 | 0.510 | 0.570 | 0.144 | 0.277 | 0.227 | 1 | | |
| K08 | 0.534 | 0.516 | 0.534 | 0.179 | 0.217 | 0.148 | 0.935 | 1 | |
| K09 | 0.618 | 0.577 | 0.633 | 0.187 | 0.321 | 0.264 | 0.892 | 0.902 | 1 |

Table A17.3 – Weekly Kevitsa leachate DIC correlation co-efficient matrix

| Kevitsa DIC Correlation Co-Efficient | | | | | | | | | |
|---|---|---|---|---|---|---|---|---|---|
| Cell | K01 | K02 | K03 | K04 | K05 | K06 | K07 | K08 | K09 |
| K01 | 1 | | | | | | | | |
| K02 | 0.937 | 1 | | | | | | | |
| K03 | 0.907 | 0.932 | 1 | | | | | | |
| K04 | 0.132 | 0.131 | 0.140 | 1 | | | | | |
| K05 | 0.256 | 0.325 | 0.308 | 0.420 | 1 | | | | |
| K06 | 0.194 | 0.236 | 0.239 | 0.450 | 0.972 | 1 | | | |
| K07 | 0.242 | 0.117 | 0.157 | -0.093 | -0.062 | -0.040 | 1 | | |
| K08 | 0.267 | 0.163 | 0.230 | -0.041 | -0.007 | 0.013 | 0.946 | 1 | |
| K09 | 0.281 | 0.187 | 0.240 | -0.054 | 0.005 | 0.022 | 0.940 | 0.984 | 1 |

Table A17.4 – Weekly Kevitsa leachate Alkalinity correlation co-efficient matrix

| Kevitsa HCT Alkalinity Correlation Co-Efficient | | | | | | | | | |
|---|---|---|---|---|---|---|---|---|---|
| Cell | K01 | K02 | K03 | K04 | K05 | K06 | K07 | K08 | K09 |
| K01 | 1 | | | | | | | | |
| K02 | 0.967 | 1 | | | | | | | |
| K03 | 0.957 | 0.965 | 1 | | | | | | |
| K04 | 0.338 | 0.395 | 0.395 | 1 | | | | | |
| K05 | 0.451 | 0.526 | 0.468 | 0.885 | 1 | | | | |
| K06 | 0.414 | 0.479 | 0.437 | 0.884 | 0.969 | 1 | | | |
| K07 | 0.615 | 0.593 | 0.632 | 0.202 | 0.292 | 0.299 | 1 | | |
| K08 | 0.554 | 0.54 | 0.584 | 0.17 | 0.223 | 0.255 | 0.949 | 1 | |
| K09 | 0.568 | 0.564 | 0.58 | 0.255 | 0.336 | 0.345 | 0.955 | 0.953 | 1 |

Table A17.5 – Weekly Kevitsa leachate sulfate correlation co-efficient matrix

| Kevitsa Sulfate Correlation Co-Efficient | | | | | | | | | |
|---|---|---|---|---|---|---|---|---|---|
| Cell | K01 | K02 | K03 | K04 | K05 | K06 | K07 | K08 | K09 |
| K01 | 1 | | | | | | | | |
| K02 | 0.971 | 1 | | | | | | | |
| K03 | 0.977 | 0.945 | 1 | | | | | | |
| K04 | 0.951 | 0.943 | 0.95 | 1 | | | | | |
| K05 | 0.869 | 0.903 | 0.854 | 0.897 | 1 | | | | |
| K06 | 0.894 | 0.916 | 0.877 | 0.915 | 0.953 | 1 | | | |
| K07 | 0.941 | 0.918 | 0.944 | 0.916 | 0.853 | 0.851 | 1 | | |
| K08 | 0.916 | 0.893 | 0.915 | 0.894 | 0.83 | 0.826 | 0.989 | 1 | |
| K09 | 0.913 | 0.885 | 0.924 | 0.884 | 0.815 | 0.814 | 0.985 | 0.981 | 1 |

Table A17.6 – Weekly Kevitsa leachate Ca correlation co-efficient matrix

| Kevitsa Ca Correlation Co-Efficient | | | | | | | | | |
|---|---|---|---|---|---|---|---|---|---|
| Cell | K01 | K02 | K03 | K04 | K05 | K06 | K07 | K08 | K09 |
| K01 | 1 | | | | | | | | |
| K02 | 0.631 | 1 | | | | | | | |
| K03 | 0.729 | 0.823 | 1 | | | | | | |
| K04 | 0.365 | 0.415 | 0.514 | 1 | | | | | |
| K05 | 0.286 | 0.338 | 0.395 | 0.627 | 1 | | | | |
| K06 | 0.325 | 0.326 | 0.401 | 0.575 | 0.848 | 1 | | | |
| K07 | 0.421 | 0.321 | 0.484 | 0.271 | 0.075 | 0.179 | 1 | | |
| K08 | 0.543 | 0.415 | 0.608 | 0.306 | 0.147 | 0.222 | 0.924 | 1 | |
| K09 | 0.505 | 0.381 | 0.552 | 0.236 | 0.09 | 0.152 | 0.924 | 0.959 | 1 |

Table A17.7 – Weekly Kevitsa leachate Mg correlation co-efficient matrix

| Kevitsa Mg Correlation Co-Efficient | | | | | | | | | |
|---|---|---|---|---|---|---|---|---|---|
| Cell | K01 | K02 | K03 | K04 | K05 | K06 | K07 | K08 | K09 |
| K01 | 1 | | | | | | | | |
| K02 | 0.977 | 1 | | | | | | | |
| K03 | 0.982 | 0.985 | 1 | | | | | | |
| K04 | 0.892 | 0.926 | 0.887 | 1 | | | | | |
| K05 | 0.832 | 0.878 | 0.835 | 0.977 | 1 | | | | |
| K06 | 0.886 | 0.919 | 0.886 | 0.982 | 0.983 | 1 | | | |
| K07 | 0.95 | 0.973 | 0.951 | 0.938 | 0.892 | 0.92 | 1 | | |
| K08 | 0.921 | 0.952 | 0.92 | 0.929 | 0.893 | 0.912 | 0.989 | 1 | |
| K09 | 0.929 | 0.958 | 0.926 | 0.933 | 0.881 | 0.902 | 0.989 | 0.983 | 1 |

Table A17.8 – Weekly Kevitsa leachate Na correlation co-efficient matrix

| Kevitsa Na Correlation Co-Efficient | | | | | | | | | |
|---|---|---|---|---|---|---|---|---|---|
| Cell | K01 | K02 | K03 | K04 | K05 | K06 | K07 | K08 | K09 |
| K01 | 1 | | | | | | | | |
| K02 | 0.997 | 1 | | | | | | | |
| K03 | 0.997 | 0.992 | 1 | | | | | | |
| K04 | 0.993 | 0.994 | 0.99 | 1 | | | | | |
| K05 | 0.974 | 0.986 | 0.966 | 0.986 | 1 | | | | |
| K06 | 0.996 | 0.997 | 0.993 | 0.998 | 0.988 | 1 | | | |
| K07 | 0.981 | 0.99 | 0.976 | 0.987 | 0.996 | 0.992 | 1 | | |
| K08 | 0.959 | 0.976 | 0.946 | 0.966 | 0.992 | 0.973 | 0.991 | 1 | |
| K09 | 0.984 | 0.993 | 0.977 | 0.988 | 0.994 | 0.992 | 0.999 | 0.991 | 1 |

Table A17.9 – Weekly Kevitsa leachate Ni correlation co-efficient matrix

| Kevitsa Ni Correlation Co-Efficient | | | | | | | | | |
|---|---|---|---|---|---|---|---|---|---|
| Cell | K01 | K02 | K03 | K04 | K05 | K06 | K07 | K08 | K09 |
| K01 | 1 | | | | | | | | |
| K02 | 0.79 | 1 | | | | | | | |
| K03 | 0.914 | 0.871 | 1 | | | | | | |
| K04 | 0.314 | 0.292 | 0.242 | 1 | | | | | |
| K05 | -0.15 | 0.127 | 0.049 | 0.638 | 1 | | | | |
| K06 | -0.11 | 0.042 | 0.034 | 0.169 | 0.666 | 1 | | | |
| K07 | 0.283 | 0.253 | 0.366 | 0.095 | -0.28 | -0.07 | 1 | | |
| K08 | 0.322 | 0.286 | 0.416 | 0.095 | -0.23 | -0.1 | 0.966 | 1 | |
| K09 | 0.289 | 0.27 | 0.394 | 0.1 | -0.23 | -0.1 | 0.945 | 0.97 | 1 |

Table A17.10 – Weekly Kevitsa leachate Si correlation co-efficient matrix

| Kevitsa Si Correlation Co-Efficient | | | | | | | | | |
|---|---|---|---|---|---|---|---|---|---|
| Cell | K01 | K02 | K03 | K04 | K05 | K06 | K07 | K08 | K09 |
| K01 | 1 | | | | | | | | |
| K02 | 0.798 | 1 | | | | | | | |
| K03 | 0.761 | 0.713 | 1 | | | | | | |
| K04 | 0.694 | 0.686 | 0.777 | 1 | | | | | |
| K05 | 0.586 | 0.781 | 0.663 | 0.883 | 1 | | | | |
| K06 | 0.674 | 0.82 | 0.739 | 0.819 | 0.862 | 1 | | | |
| K07 | 0.663 | 0.62 | 0.733 | 0.812 | 0.676 | 0.653 | 1 | | |
| K08 | 0.661 | 0.551 | 0.71 | 0.8 | 0.647 | 0.602 | 0.957 | 1 | |
| K09 | 0.65 | 0.583 | 0.64 | 0.72 | 0.587 | 0.565 | 0.924 | 0.941 | 1 |

Table A17.11 – Weekly Aitik leachate pH correlation co-efficient matrix

| Aitik pH Correlation Co-Efficient | | | | | | | | | |
|---|---|---|---|---|---|---|---|---|---|
| Cell | A01 | A02 | A03 | A04 | A05 | A06 | A07 | A08 | A09 |
| A01 | 1 | | | | | | | | |
| A02 | 0.898 | 1 | | | | | | | |
| A03 | 0.719 | 0.775 | 1 | | | | | | |
| A04 | 0.584 | 0.624 | 0.342 | 1 | | | | | |
| A05 | 0.332 | 0.433 | 0.298 | 0.810 | 1 | | | | |
| A06 | 0.398 | 0.498 | 0.363 | 0.843 | 0.938 | 1 | | | |
| A07 | 0.554 | 0.622 | 0.546 | 0.642 | 0.526 | 0.556 | 1 | | |
| A08 | 0.178 | 0.241 | 0.349 | 0.147 | 0.218 | 0.250 | 0.540 | 1 | |
| A09 | 0.572 | 0.612 | 0.562 | 0.495 | 0.299 | 0.357 | 0.866 | 0.519 | 1 |

Table A17.12 – Weekly Aitik leachate EC correlation co-efficient matrix

| Aitik EC Correlation Co-Efficient | | | | | | | | | |
|---|---|---|---|---|---|---|---|---|---|
| Cell | A01 | A02 | A03 | A04 | A05 | A06 | A07 | A08 | A09 |
| A01 | 1 | | | | | | | | |
| A02 | 0.898 | 1 | | | | | | | |
| A03 | 0.719 | 0.775 | 1 | | | | | | |
| A04 | 0.584 | 0.624 | 0.342 | 1 | | | | | |
| A05 | 0.332 | 0.433 | 0.298 | 0.810 | 1 | | | | |
| A06 | 0.398 | 0.498 | 0.363 | 0.843 | 0.938 | 1 | | | |
| A07 | 0.554 | 0.622 | 0.546 | 0.642 | 0.526 | 0.556 | 1 | | |
| A08 | 0.178 | 0.241 | 0.349 | 0.147 | 0.218 | 0.250 | 0.540 | 1 | |
| A09 | 0.572 | 0.612 | 0.562 | 0.495 | 0.299 | 0.357 | 0.866 | 0.519 | 1 |

Table A17.13 – Weekly Aitik leachate DIC correlation co-efficient matrix

| Aitik DIC Correlation Co-Efficient | | | | | | | | | |
|---|---|---|---|---|---|---|---|---|---|
| Cell | A01 | A02 | A03 | A04 | A05 | A06 | A07 | A08 | A09 |
| A01 | 1 | | | | | | | | |
| A02 | 0.939 | 1 | | | | | | | |
| A03 | 0.860 | 0.911 | 1 | | | | | | |
| A04 | 0.463 | 0.482 | 0.454 | 1 | | | | | |
| A05 | 0.225 | 0.277 | 0.284 | 0.859 | 1 | | | | |
| A06 | 0.152 | 0.209 | 0.221 | 0.803 | 0.927 | 1 | | | |
| A07 | 0.231 | 0.279 | 0.224 | 0.044 | -0.013 | -0.059 | 1 | | |
| A08 | 0.140 | 0.196 | 0.152 | 0.307 | 0.388 | 0.295 | 0.629 | 1 | |
| A09 | 0.339 | 0.417 | 0.342 | 0.119 | 0.003 | -0.033 | 0.801 | 0.463 | 1 |

Table A17.14 – Weekly Aitik leachate Alkalinity correlation co-efficient matrix

| Aitik HCT Alkalinity Correlation Co-Efficient | | | | | | | | | |
|---|---|---|---|---|---|---|---|---|---|
| Cell | A01 | A02 | A03 | A04 | A05 | A06 | A07 | A08 | A09 |
| A01 | 1 | | | | | | | | |
| A02 | 0.885 | 1 | | | | | | | |
| A03 | 0.926 | 0.884 | 1 | | | | | | |
| A04 | 0.599 | 0.573 | 0.621 | 1 | | | | | |
| A05 | 0.27 | 0.349 | 0.394 | 0.669 | 1 | | | | |
| A06 | 0.213 | 0.28 | 0.35 | 0.684 | 0.897 | 1 | | | |
| A07 | 0.462 | 0.493 | 0.459 | 0.265 | 0.082 | -0.02 | 1 | | |
| A08 | 0.423 | 0.473 | 0.508 | 0.423 | 0.544 | 0.405 | 0.463 | 1 | |
| A09 | 0.537 | 0.583 | 0.515 | 0.351 | 0.136 | 0.058 | 0.783 | 0.352 | 1 |

Table A17.15 – Weekly Aitik leachate sulfate correlation co-efficient matrix

| Aitik Sulfate Correlation Co-Efficient | | | | | | | | | |
|---|---|---|---|---|---|---|---|---|---|
| Cell | A01 | A02 | A03 | A04 | A05 | A06 | A07 | A08 | A09 |
| A01 | 1 | | | | | | | | |
| A02 | 0.982 | 1 | | | | | | | |
| A03 | 0.967 | 0.979 | 1 | | | | | | |
| A04 | 0.982 | 0.96 | 0.932 | 1 | | | | | |
| A05 | 0.941 | 0.96 | 0.982 | 0.907 | 1 | | | | |
| A06 | 0.976 | 0.985 | 0.98 | 0.96 | 0.978 | 1 | | | |
| A07 | 0.955 | 0.969 | 0.991 | 0.921 | 0.982 | 0.98 | 1 | | |

| | | | | | | | | | |
|---|---|---|---|---|---|---|---|---|---|
| A08 | 0.927 | 0.927 | 0.95 | 0.913 | 0.963 | 0.956 | 0.964 | 1 | |
| A09 | 0.976 | 0.982 | 0.99 | 0.943 | 0.98 | 0.988 | 0.988 | 0.961 | 1 |

Table A17.16 – Weekly Aitik leachate Ca correlation co-efficient matrix

| Aitik Ca Correlation Co-Efficient | | | | | | | | | |
|---|---|---|---|---|---|---|---|---|---|
| Cell | A01 | A02 | A03 | A04 | A05 | A06 | A07 | A08 | A09 |
| A01 | 1 | | | | | | | | |
| A02 | 0.981 | 1 | | | | | | | |
| A03 | 0.947 | 0.95 | 1 | | | | | | |
| A04 | 0.936 | 0.949 | 0.856 | 1 | | | | | |
| A05 | 0.868 | 0.892 | 0.903 | 0.869 | 1 | | | | |
| A06 | 0.924 | 0.943 | 0.896 | 0.964 | 0.961 | 1 | | | |
| A07 | 0.864 | 0.891 | 0.852 | 0.828 | 0.805 | 0.834 | 1 | | |
| A08 | 0.864 | 0.879 | 0.875 | 0.802 | 0.794 | 0.801 | 0.952 | 1 | |
| A09 | 0.865 | 0.898 | 0.873 | 0.828 | 0.822 | 0.837 | 0.95 | 0.938 | 1 |

Table A17.17 – Weekly Aitik leachate Mg correlation co-efficient matrix

| Aitik Mg Correlation Co-Efficient | | | | | | | | | |
|---|---|---|---|---|---|---|---|---|---|
| Cell | A01 | A02 | A03 | A04 | A05 | A06 | A07 | A08 | A09 |
| A01 | 1 | | | | | | | | |
| A02 | 0.981 | 1 | | | | | | | |
| A03 | 0.966 | 0.989 | 1 | | | | | | |
| A04 | 0.981 | 0.958 | 0.937 | 1 | | | | | |
| A05 | 0.862 | 0.925 | 0.954 | 0.856 | 1 | | | | |
| A06 | 0.941 | 0.975 | 0.983 | 0.942 | 0.979 | 1 | | | |
| A07 | 0.978 | 0.996 | 0.988 | 0.961 | 0.936 | 0.982 | 1 | | |
| A08 | 0.95 | 0.983 | 0.994 | 0.93 | 0.97 | 0.99 | 0.988 | 1 | |
| A09 | 0.975 | 0.996 | 0.99 | 0.952 | 0.934 | 0.977 | 0.998 | 0.99 | 1 |

Table A17.18 – Weekly Aitik leachate Na correlation co-efficient matrix

| Aitik Na Correlation Co-Efficient | | | | | | | | | |
|---|---|---|---|---|---|---|---|---|---|
| Cell | A01 | A02 | A03 | A04 | A05 | A06 | A07 | A08 | A09 |
| A01 | 1 | | | | | | | | |
| A02 | 0.971 | 1 | | | | | | | |
| A03 | 0.971 | 0.992 | 1 | | | | | | |

| | | | | | | | | | |
|---|---|---|---|---|---|---|---|---|---|
| A04 | 0.988 | 0.95 | 0.944 | 1 | | | | | |
| A05 | 0.911 | 0.969 | 0.978 | 0.87 | 1 | | | | |
| A06 | 0.967 | 0.99 | 0.996 | 0.945 | 0.979 | 1 | | | |
| A07 | 0.963 | 0.993 | 0.997 | 0.937 | 0.983 | 0.995 | 1 | | |
| A08 | 0.938 | 0.977 | 0.991 | 0.9 | 0.995 | 0.989 | 0.991 | 1 | |
| A09 | 0.964 | 0.994 | 0.998 | 0.936 | 0.98 | 0.994 | 0.998 | 0.99 | 1 |

Table A17.19 – Weekly Aitik leachate Mn correlation co-efficient matrix

| Aitik Mn Correlation Co-Efficient | | | | | | | | | |
|---|---|---|---|---|---|---|---|---|---|
| Cell | A01 | A02 | A03 | A04 | A05 | A06 | A07 | A08 | A09 |
| A01 | 1 | | | | | | | | |
| A02 | 0.954 | 1 | | | | | | | |
| A03 | 0.942 | 0.896 | 1 | | | | | | |
| A04 | 0.854 | 0.855 | 0.876 | 1 | | | | | |
| A05 | 0.798 | 0.743 | 0.888 | 0.951 | 1 | | | | |
| A06 | 0.823 | 0.783 | 0.885 | 0.98 | 0.991 | 1 | | | |
| A07 | 0.738 | 0.779 | 0.626 | 0.608 | 0.471 | 0.54 | 1 | | |
| A08 | 0.784 | 0.805 | 0.688 | 0.621 | 0.527 | 0.576 | 0.955 | 1 | |
| A09 | 0.757 | 0.773 | 0.677 | 0.612 | 0.516 | 0.567 | 0.951 | 0.957 | 1 |

Table A17.20 – Weekly Aitik leachate Si correlation co-efficient matrix

| Aitik Si Correlations | | | | | | | | | |
|---|---|---|---|---|---|---|---|---|---|
| Cell | A01 | A02 | A03 | A04 | A05 | A06 | A07 | A08 | A09 |
| A01 | 1 | | | | | | | | |
| A02 | 0.717 | 1 | | | | | | | |
| A03 | 0.677 | 0.847 | 1 | | | | | | |
| A04 | 0.551 | 0.759 | 0.875 | 1 | | | | | |
| A05 | 0.591 | 0.781 | 0.787 | 0.791 | 1 | | | | |
| A06 | 0.667 | 0.573 | 0.604 | 0.549 | 0.811 | 1 | | | |
| A07 | 0.683 | 0.553 | 0.499 | 0.385 | 0.545 | 0.727 | 1 | | |
| A08 | 0.734 | 0.669 | 0.585 | 0.47 | 0.727 | 0.791 | 0.853 | 1 | |
| A09 | 0.686 | 0.566 | 0.502 | 0.391 | 0.543 | 0.759 | 0.948 | 0.853 | 1 |

# Appendix 18 – HCT Weekly Leachate Analyte Graphs

Within this appendix graphs comparing key weekly leached analyte results from the Kevitsa and Aitik HCT cells are presented.

### Kevitsa HCT parameter comparison graphs

Figure A18.1 – Kevitsa HCT cell sets weekly leachate Eh vs pH.

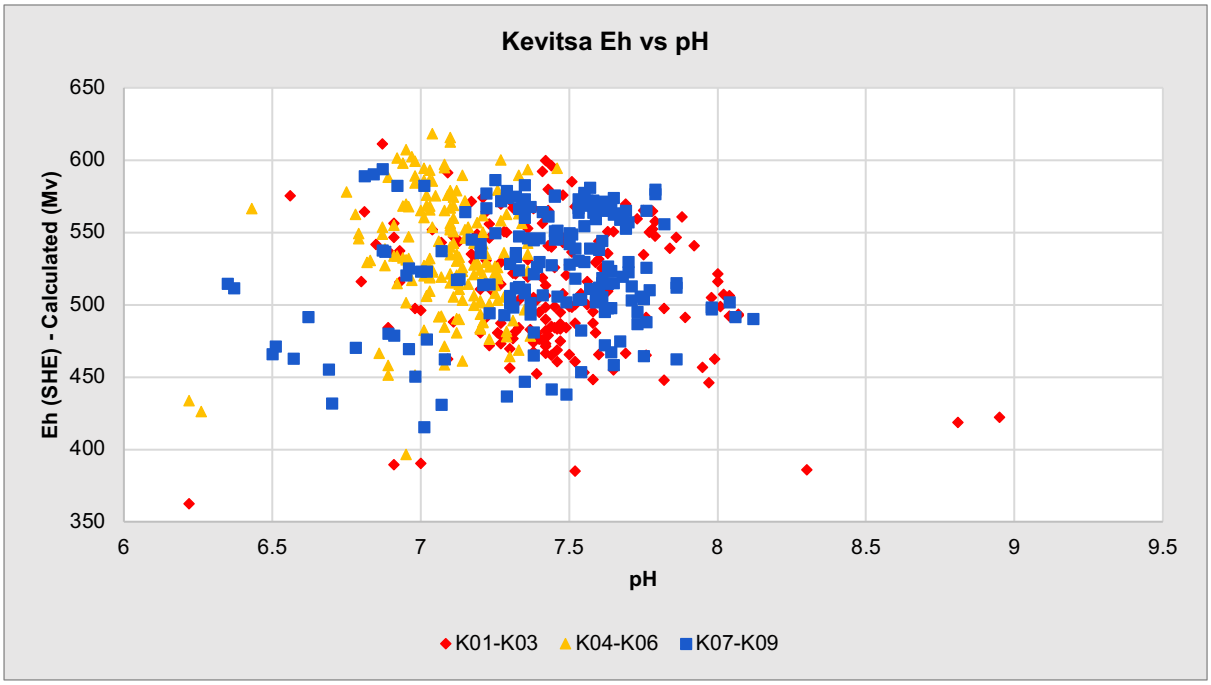


Figure A18.2 – Kevitsa HCT cell sets weekly leachate Si vs pH.

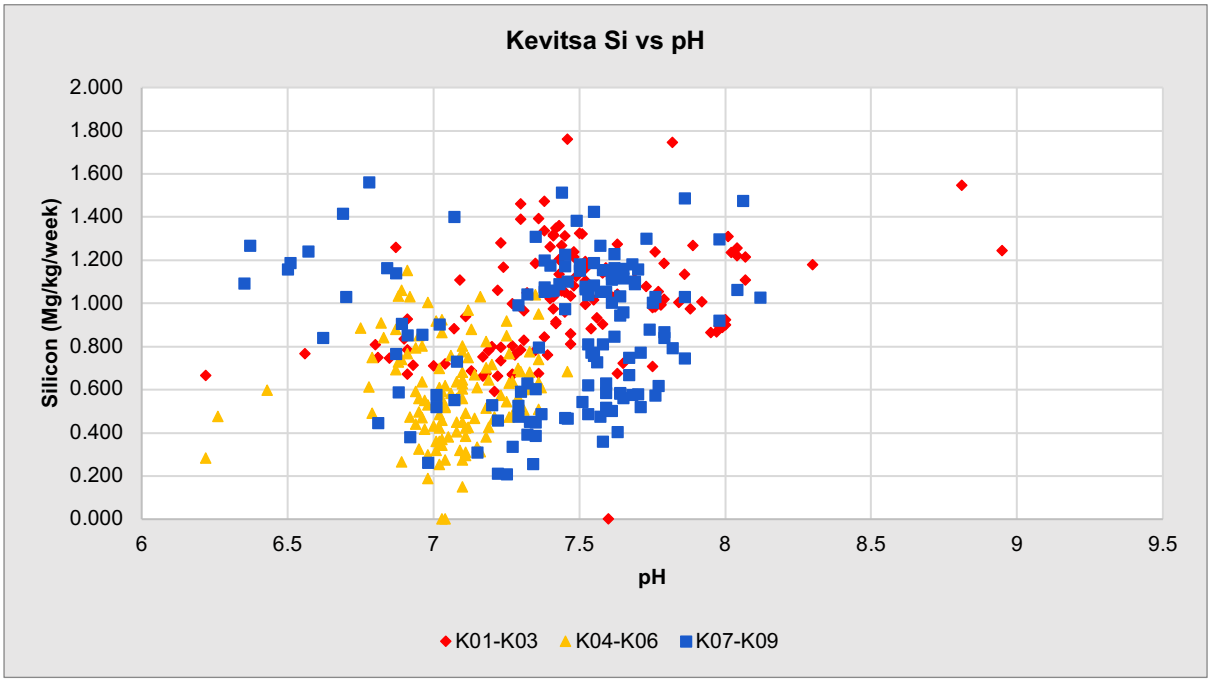

Figure A18.3 – Kevitsa HCT cell sets weekly leachate Ni vs pH.

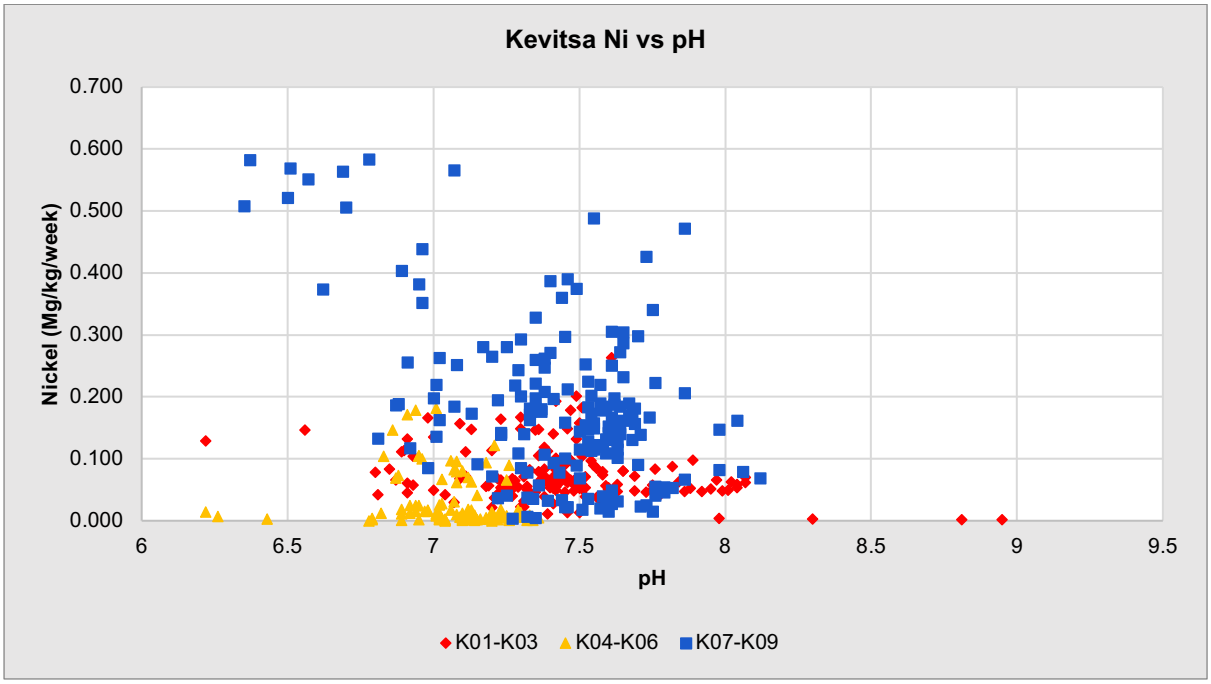


Figure A18.4 – Kevitsa HCT cell sets weekly leachate Mg vs pH.

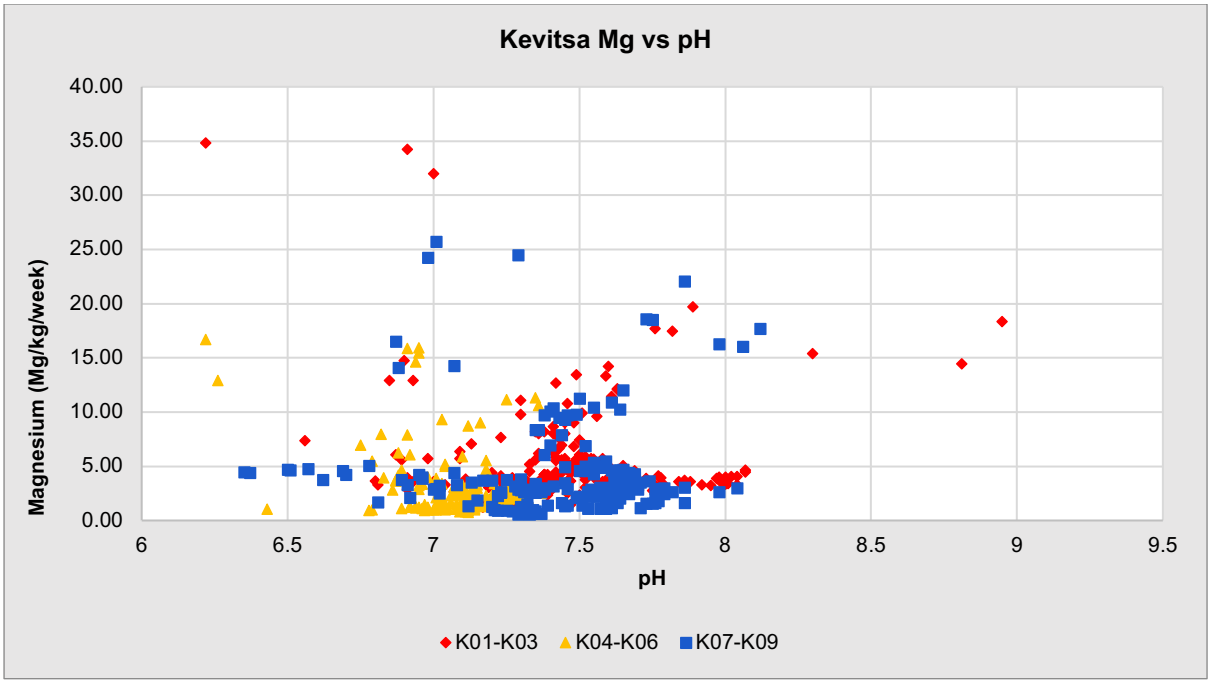

Figure A18.5 – Kevitsa HCT cell sets weekly leachate Ca vs pH.

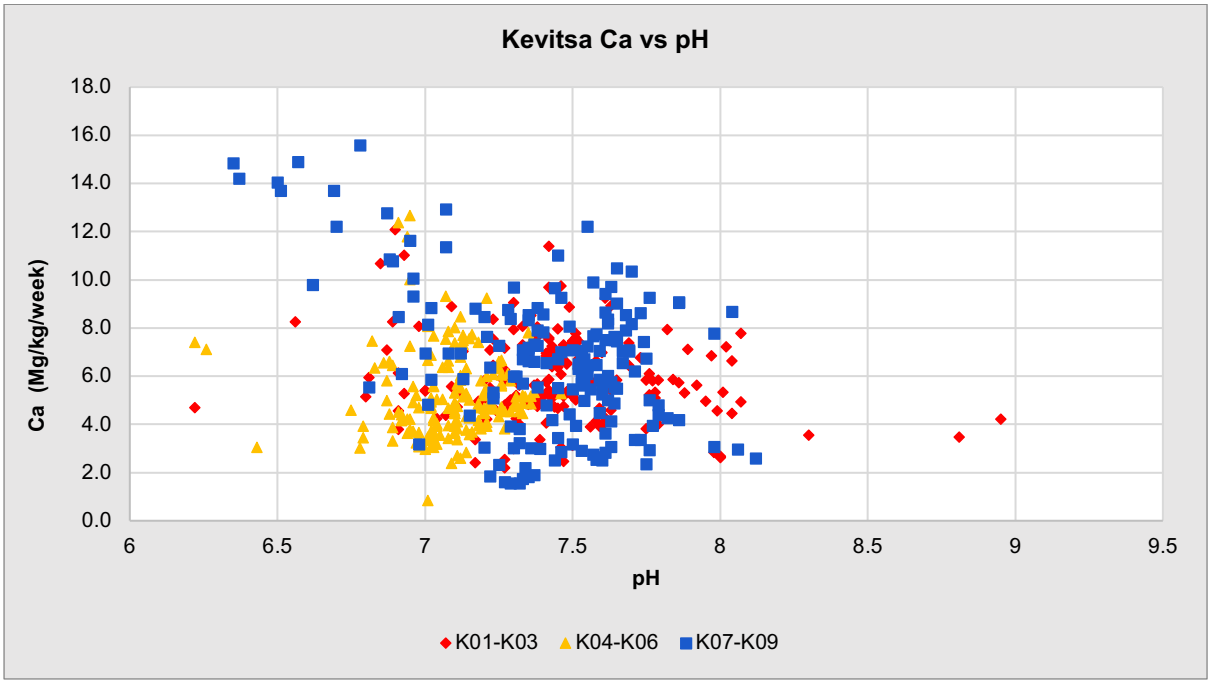


Figure A18.6 – Kevitsa HCT cell sets weekly leachate DIC vs pH.

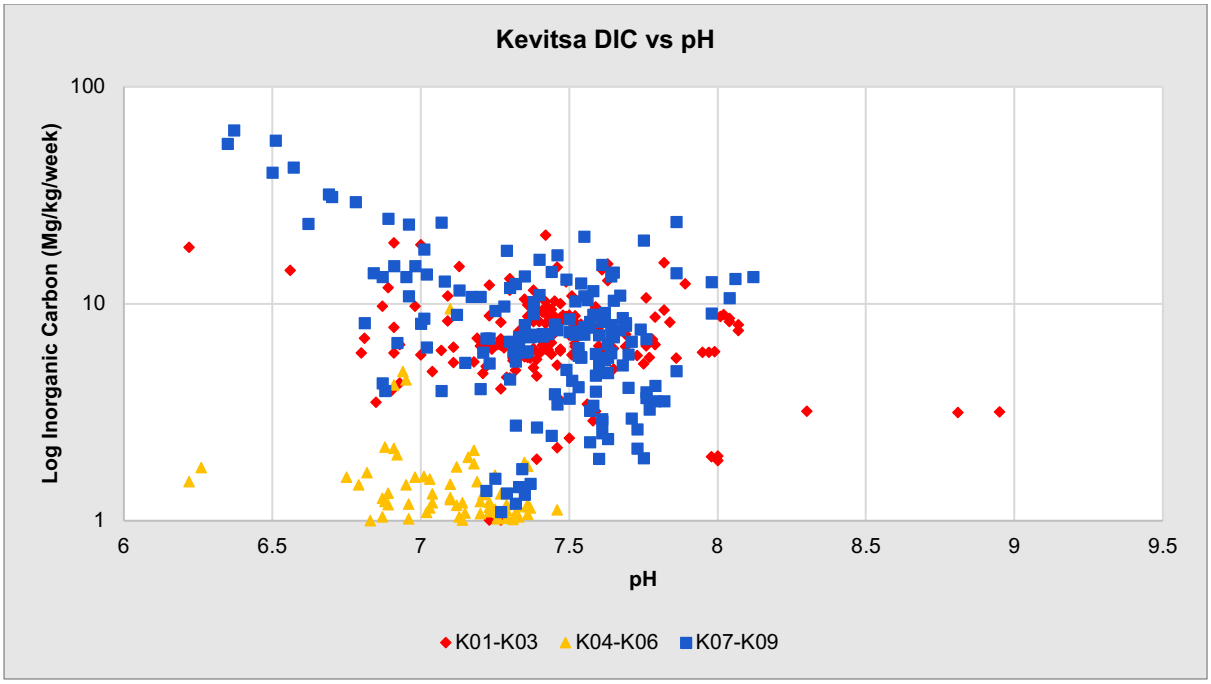

Figure A18.7 – Kevitsa HCT cell sets weekly leachate Si vs pH.

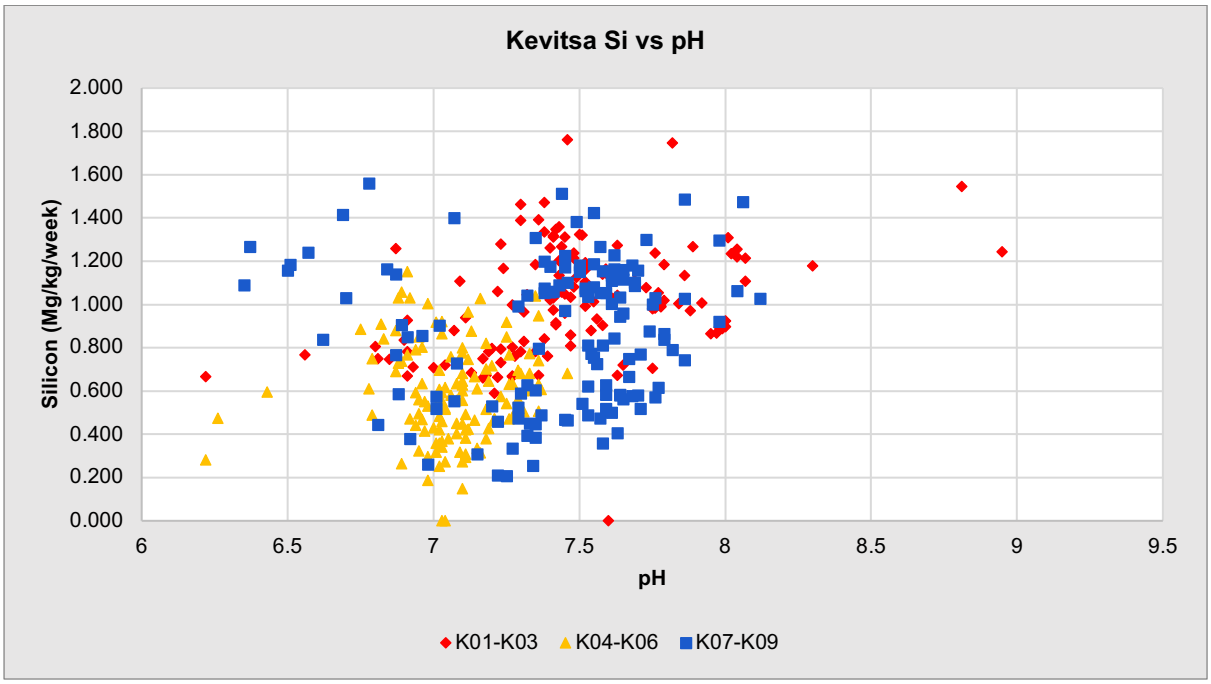


Figure A18.8 – Kevitsa HCT cell sets weekly leachate Na vs pH.

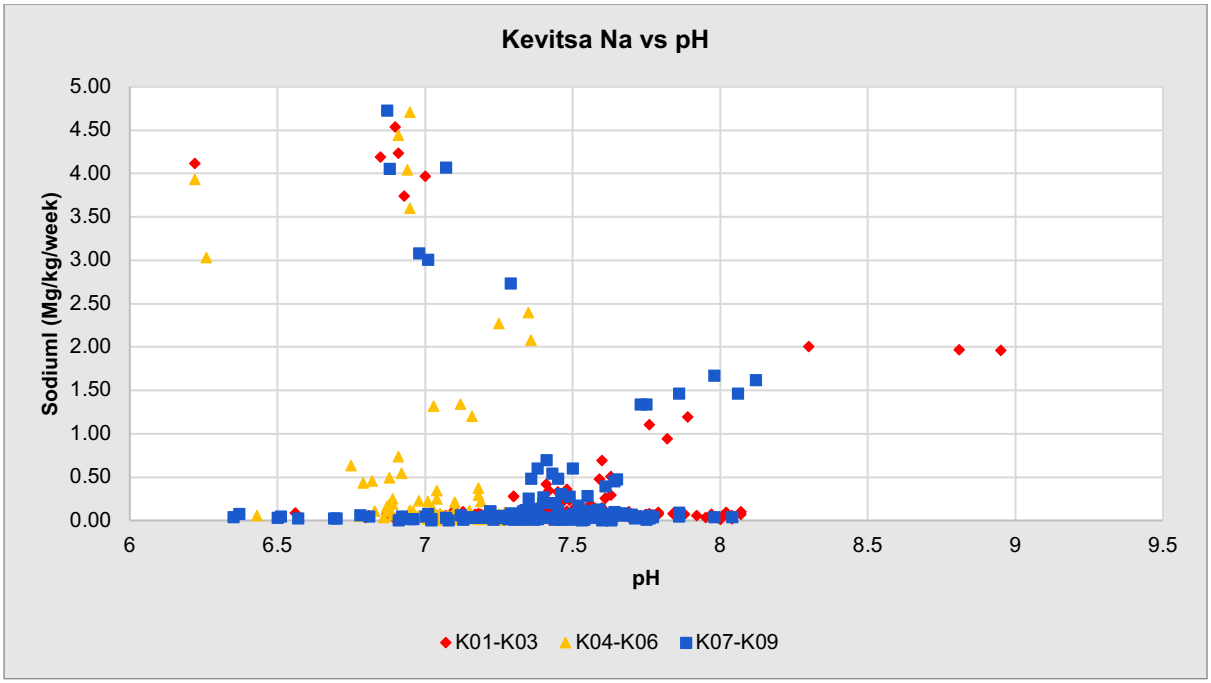

Figure A18.9 – Kevitsa HCT cell sets weekly leachate K vs pH.

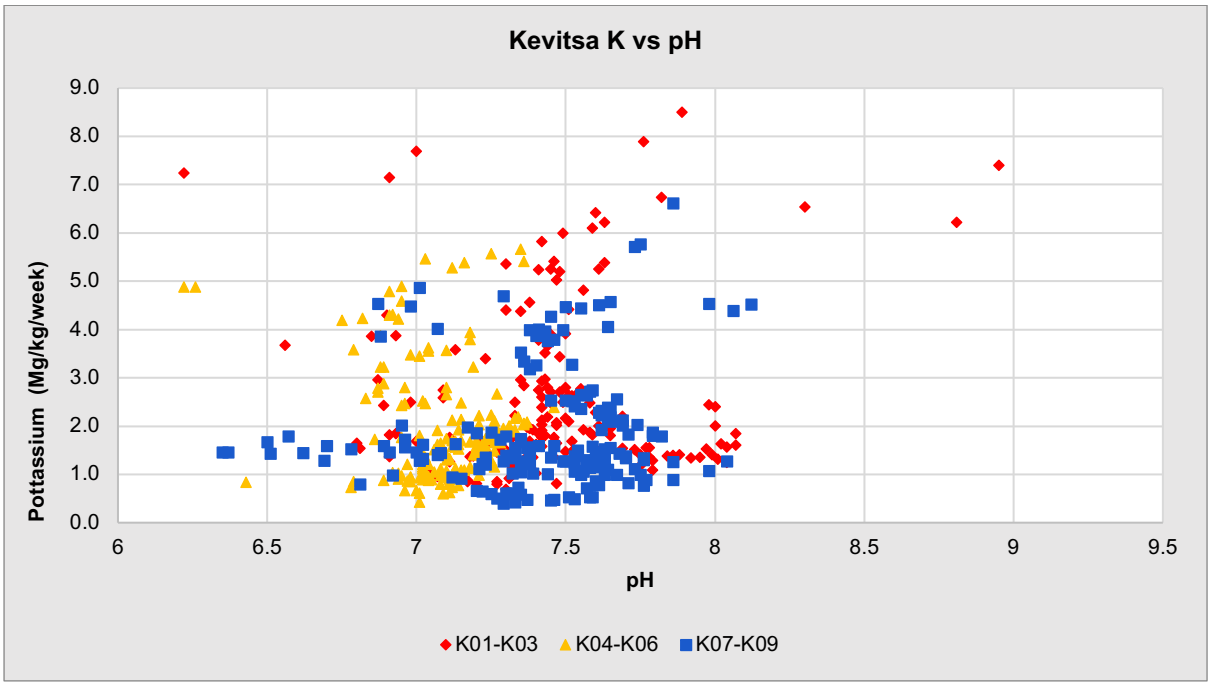


Figure A18.10 – Kevitsa HCT cell sets weekly leachate Sulfate vs pH

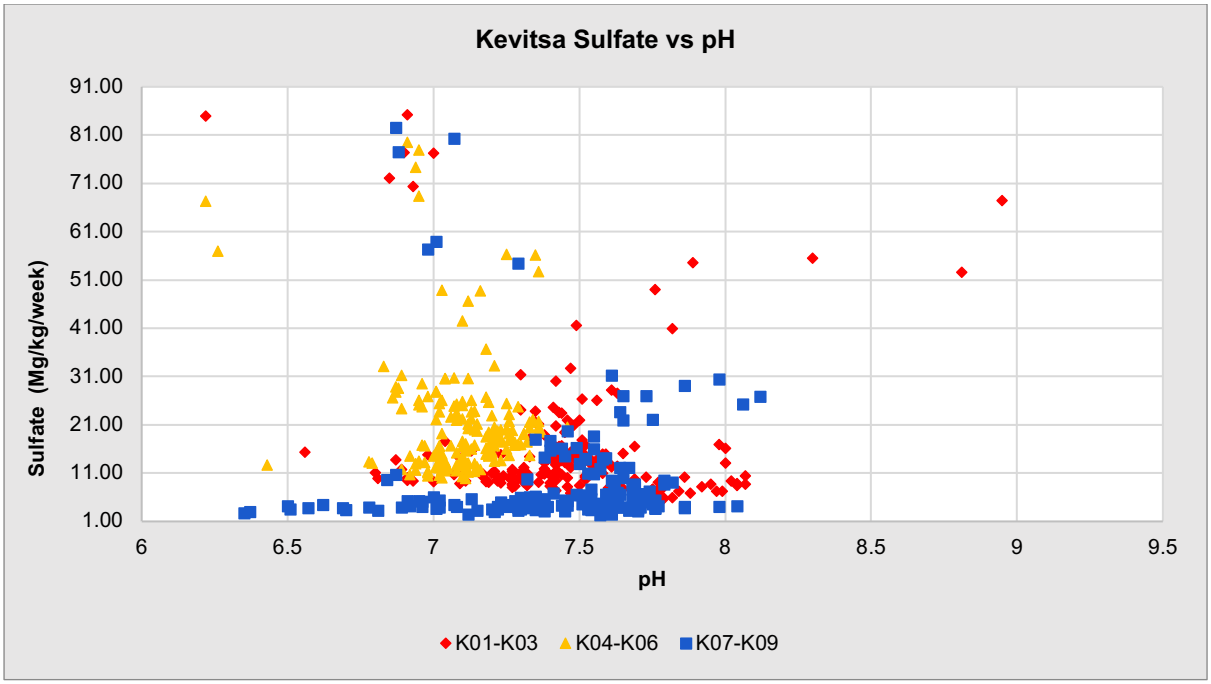

Figure A18.11 – Kevitsa HCT cell sets weekly leachate Sulfate vs DIC.

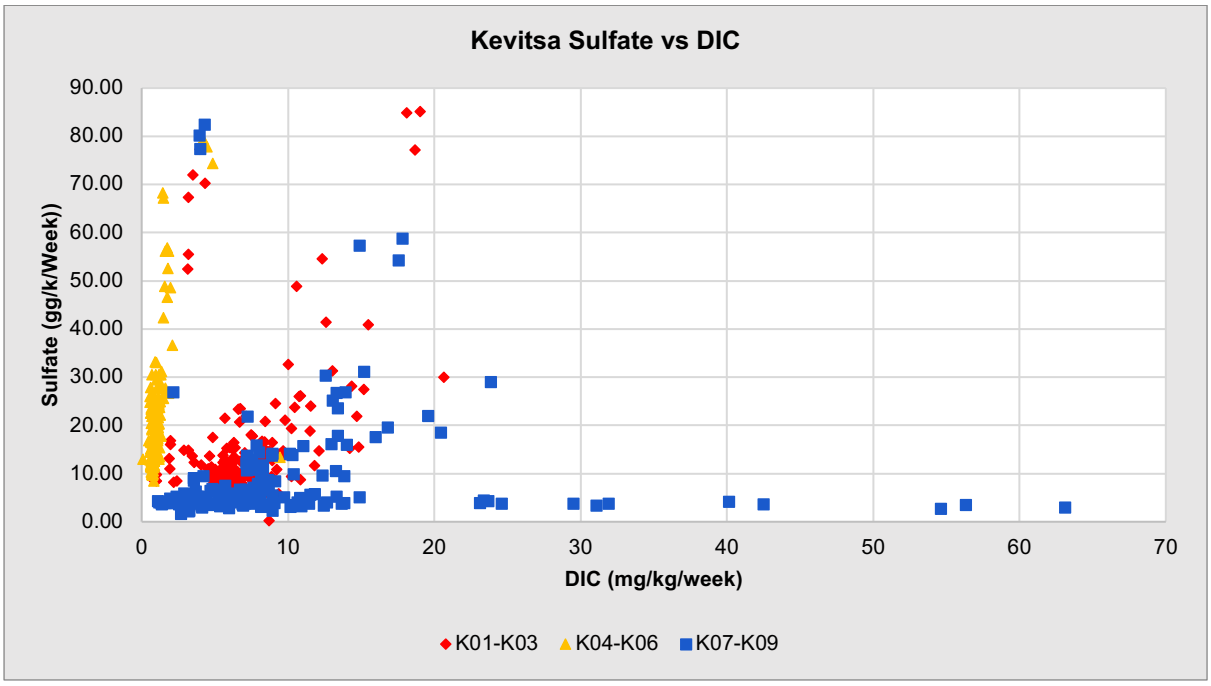


Figure A18.12 – Kevitsa HCT cell sets weekly leachate Mg vs DIC.

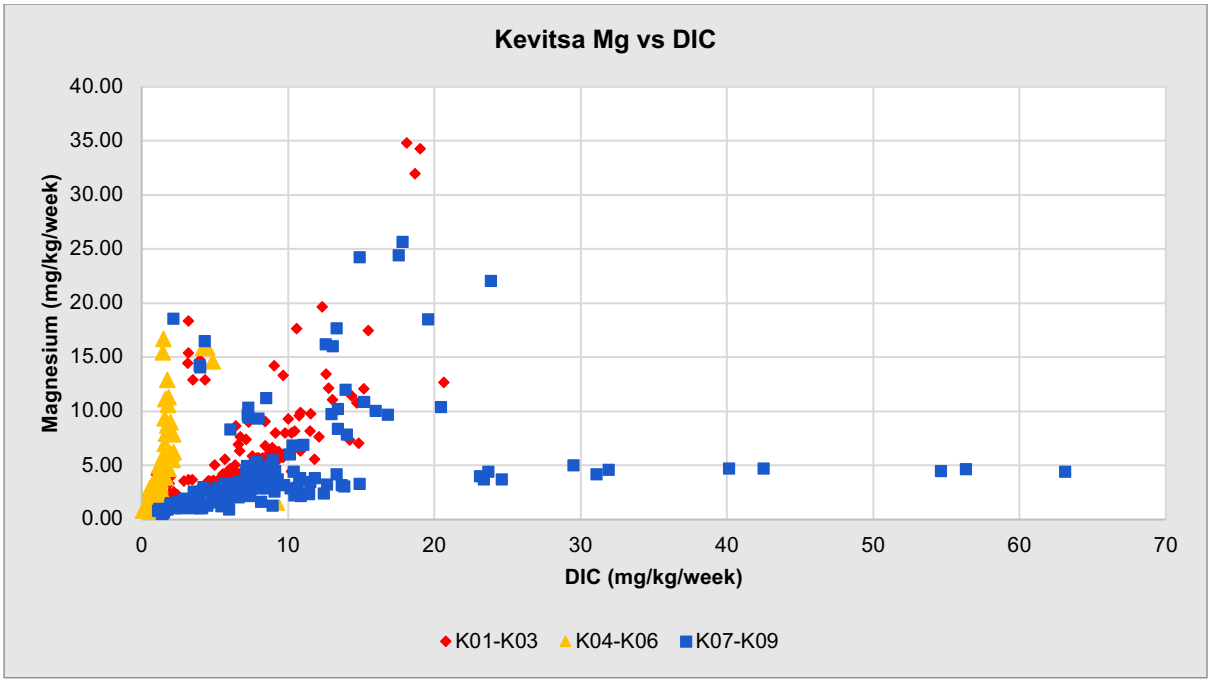

Figure A18.13 – Kevitsa HCT cell sets weekly leachate Mg vs Sulfate.

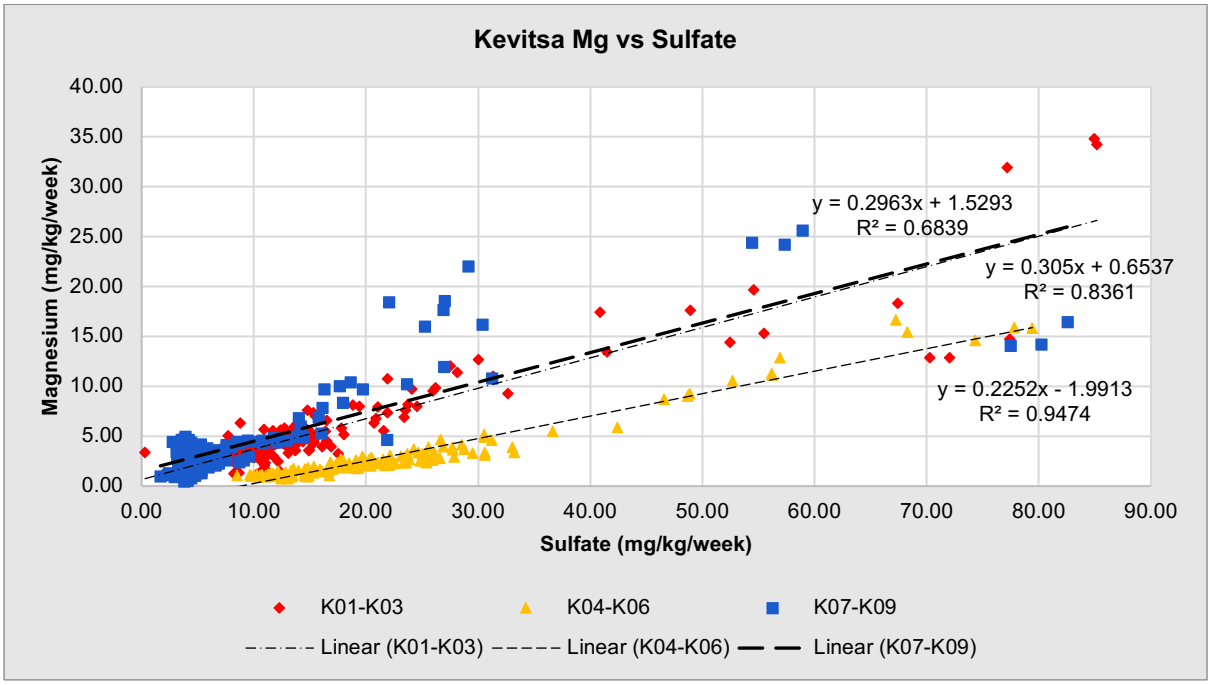


Figure A18.14 – Kevitsa HCT cell sets weekly leachate Ca vs Sulfate.

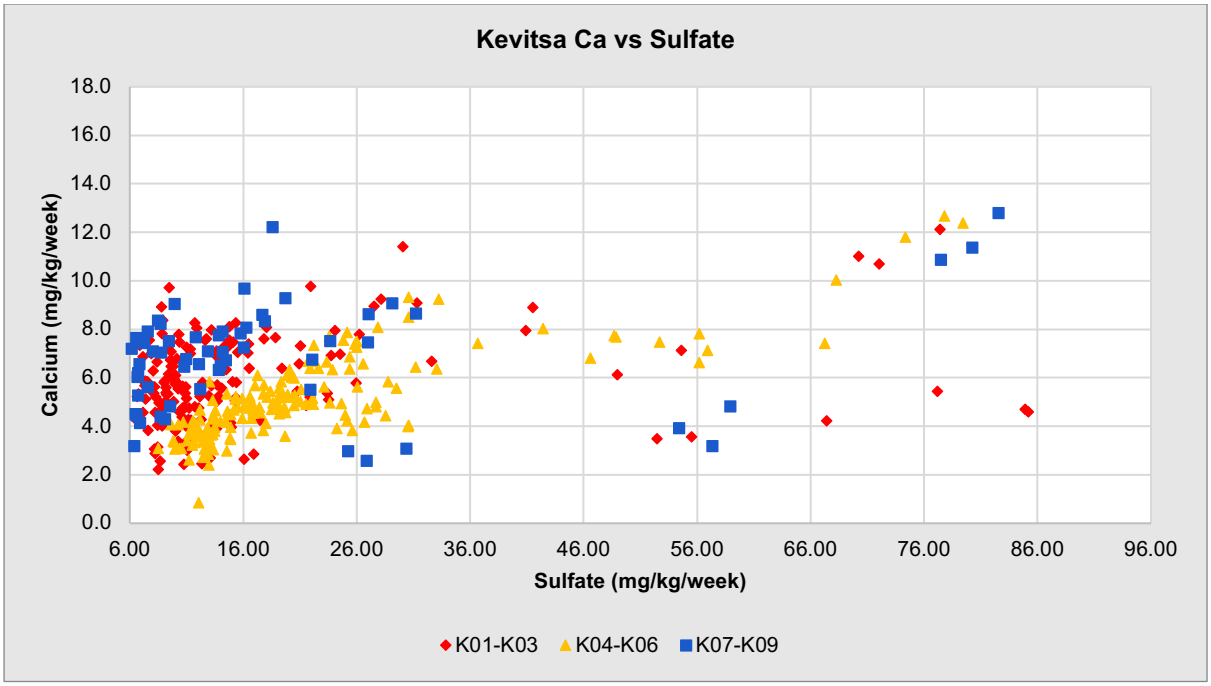

Figure A18.15 – Kevitsa HCT cell sets weekly leachate Ni vs Si.

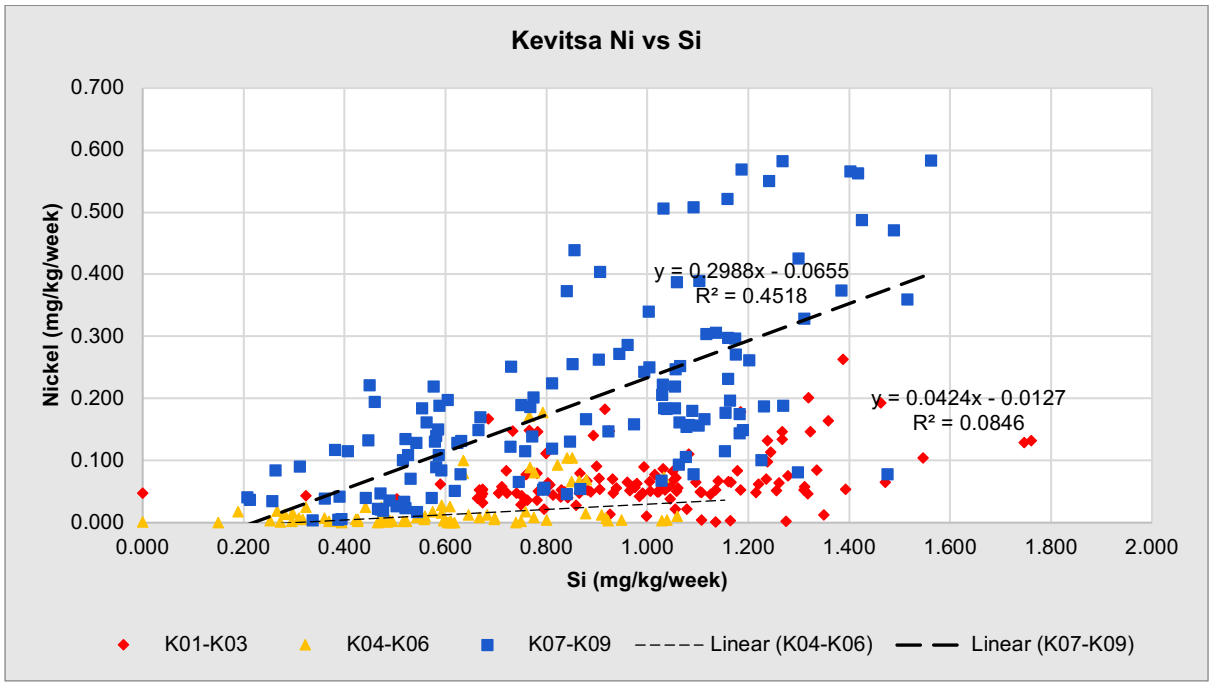


## Aitik HCT parameter comparison graphs

Figure A18.16 – Aitik HCT cell sets weekly leachate Eh vs pH.

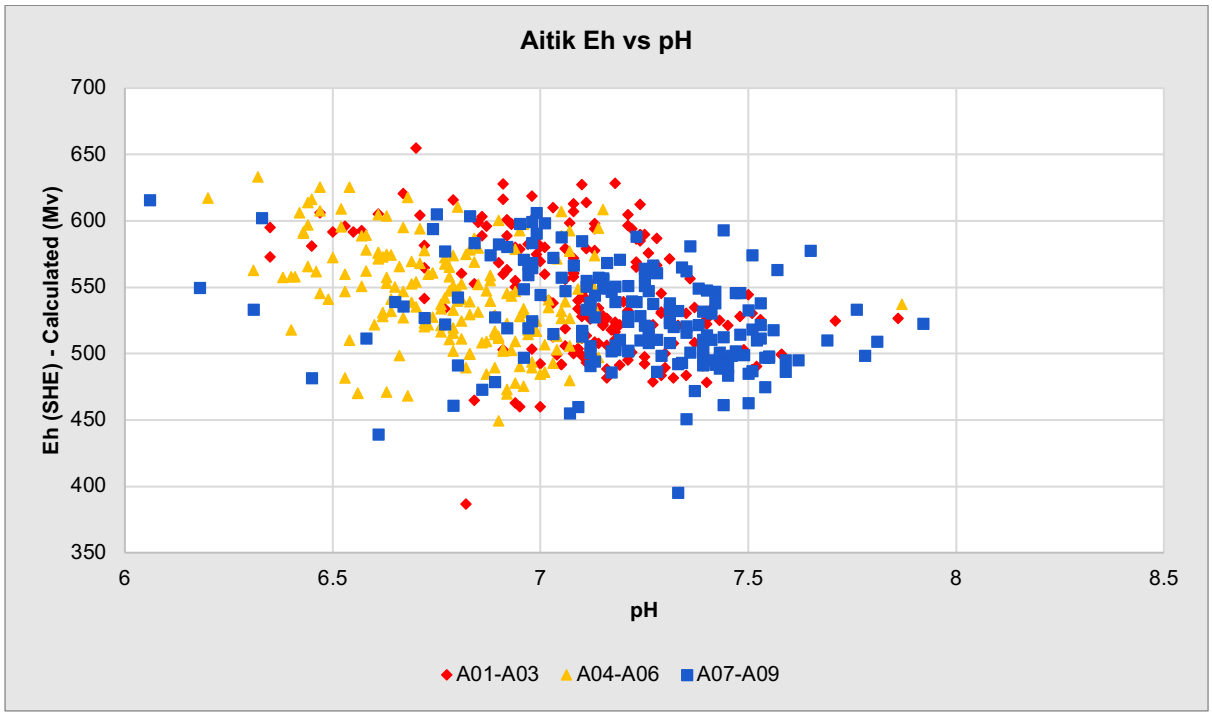

Figure A18.17 – Aitik HCT cell sets weekly leachate Si vs pH.

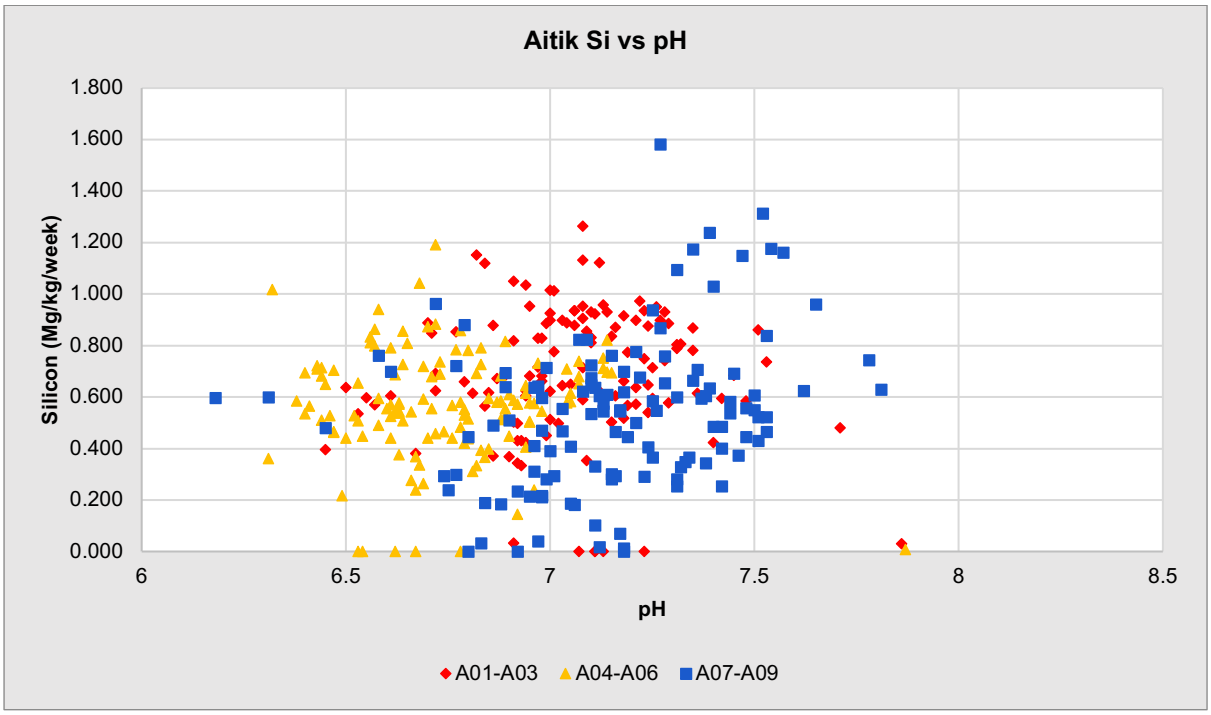


Figure A18.18 – Aitik HCT cell sets weekly leachate Mn vs pH.

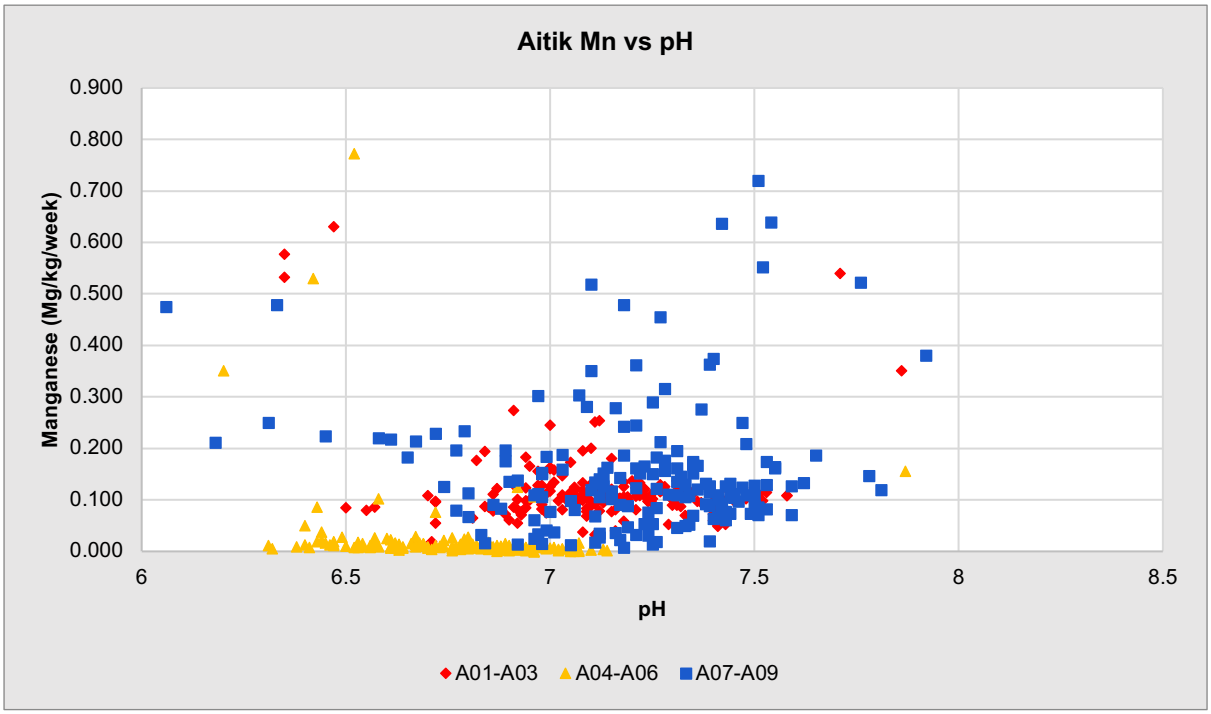

Figure A18.19 – Aitik HCT cell sets weekly leachate Mg vs pH.

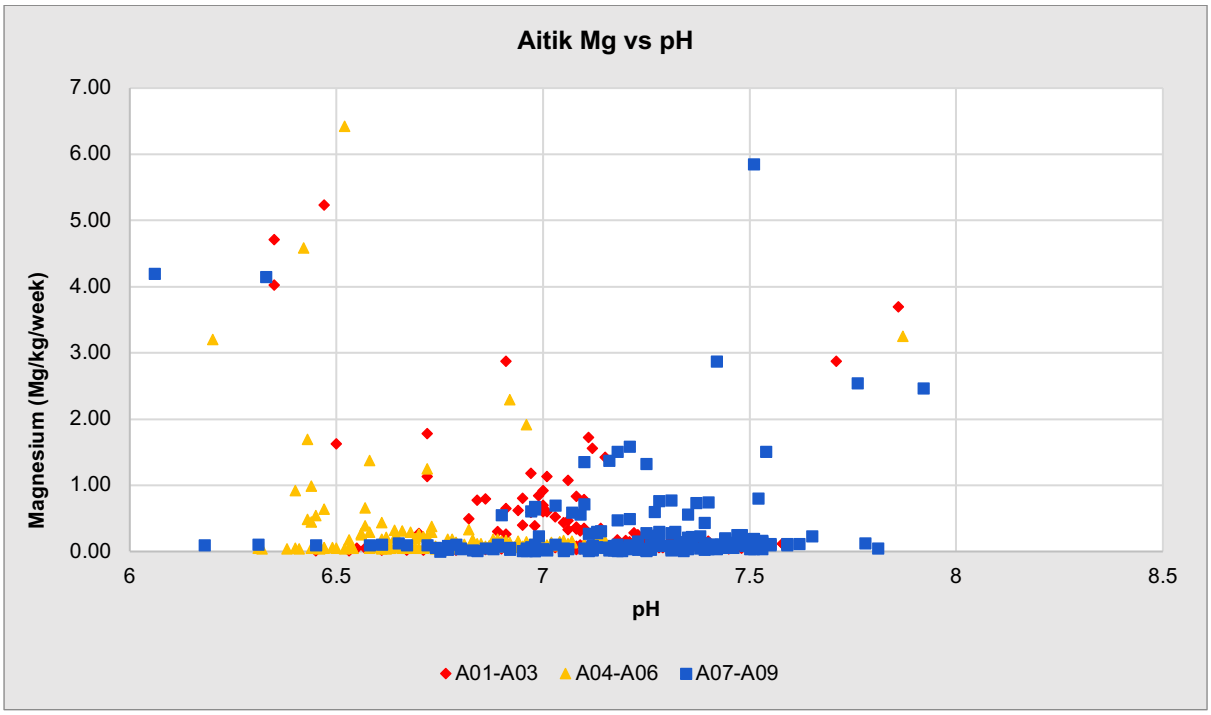


Figure A18.20 – Aitik HCT cell sets weekly leachate Ca vs pH.

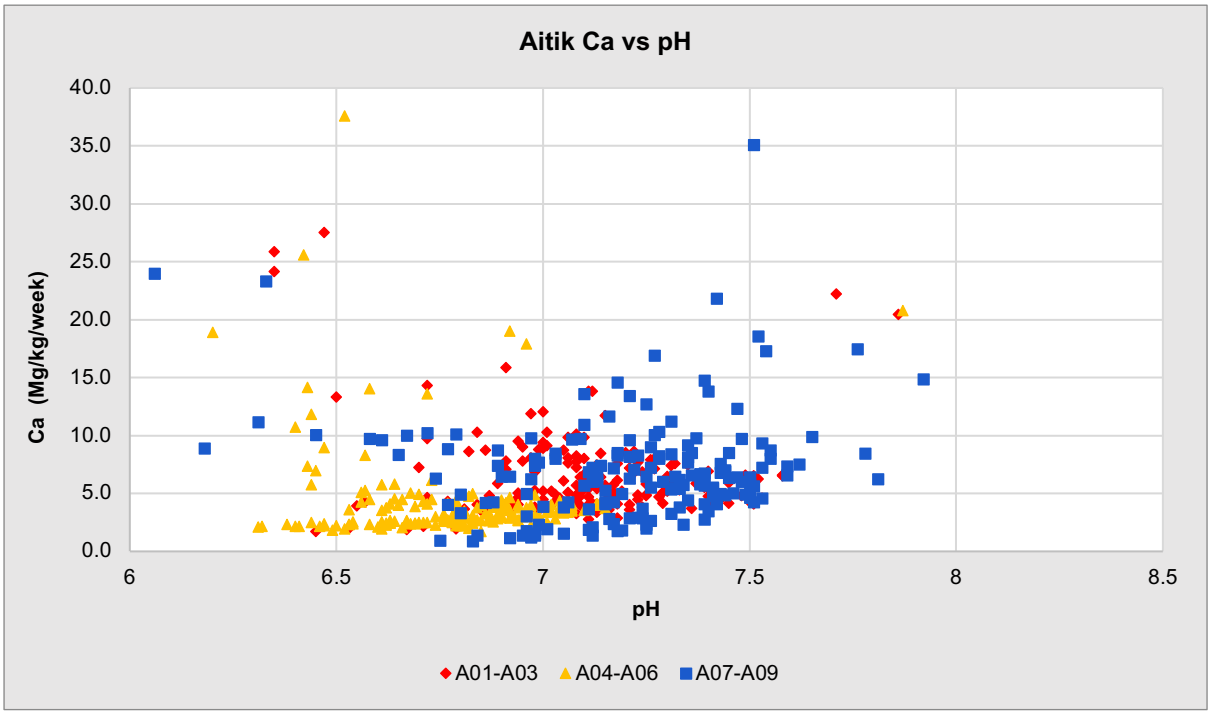

Figure A18.21 – Aitik HCT cell sets weekly leachate DIC vs pH

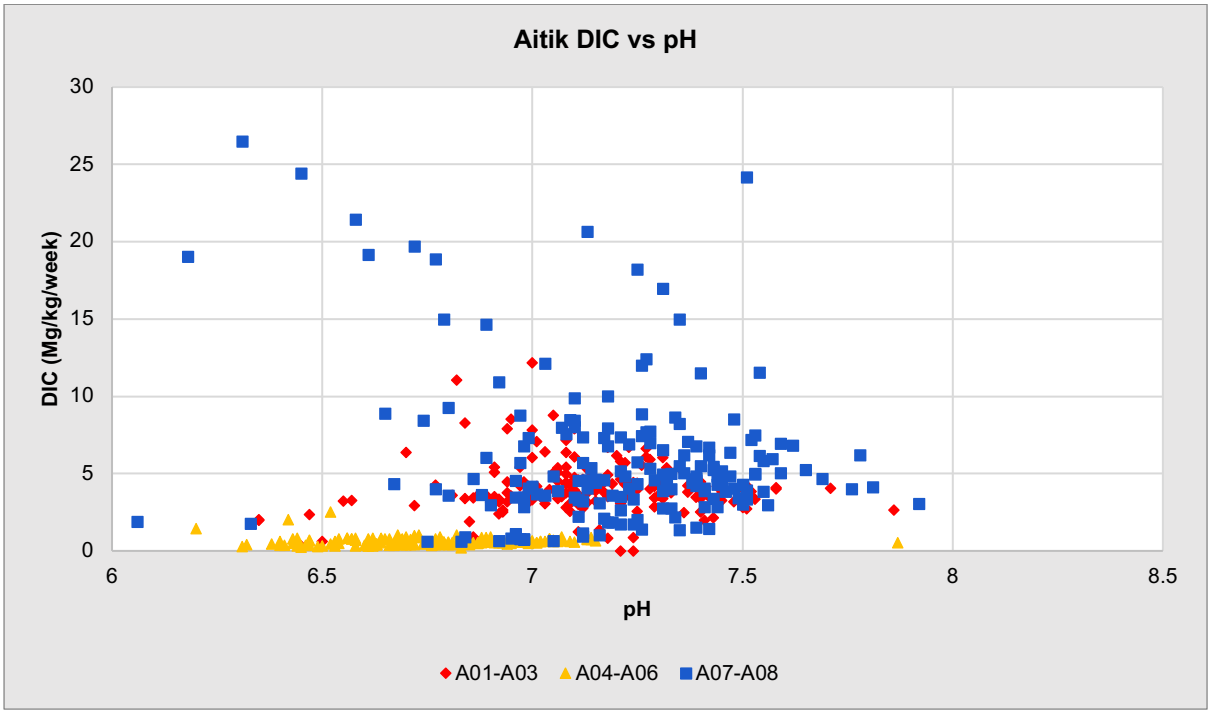


Figure A18.22 – Aitik HCT cell sets weekly leachate Si vs pH

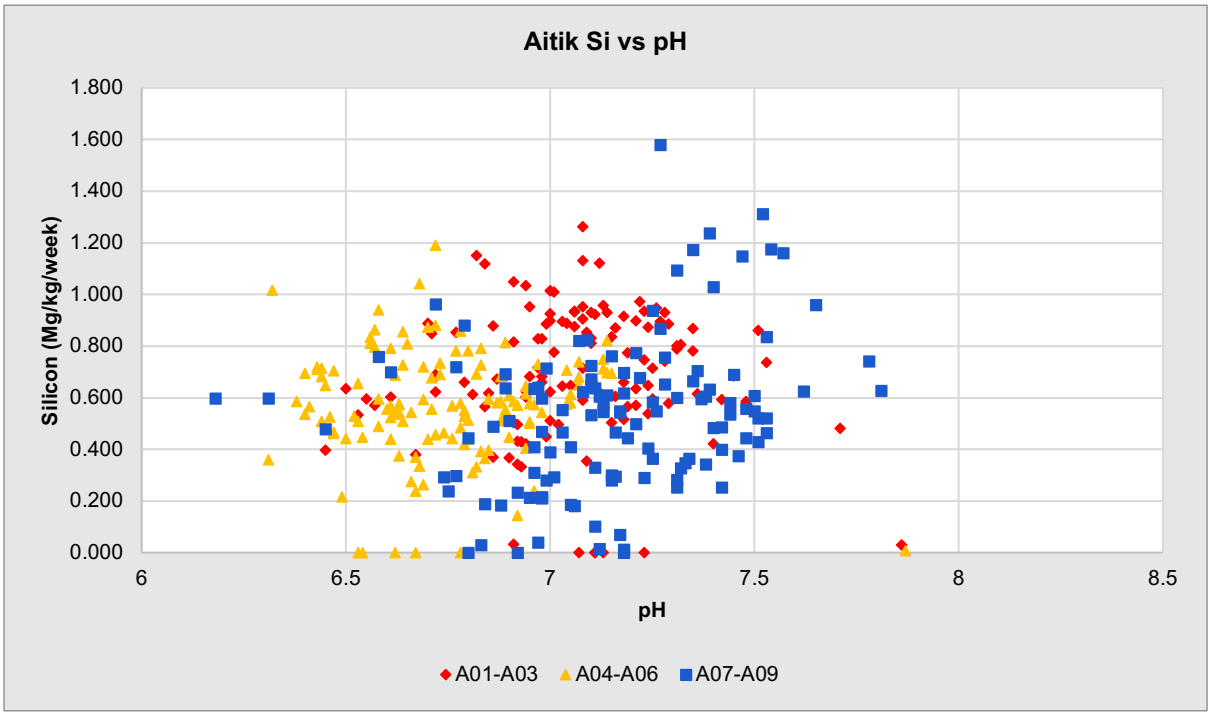

Figure A18.23 – Aitik HCT cell sets weekly leachate Na vs pH

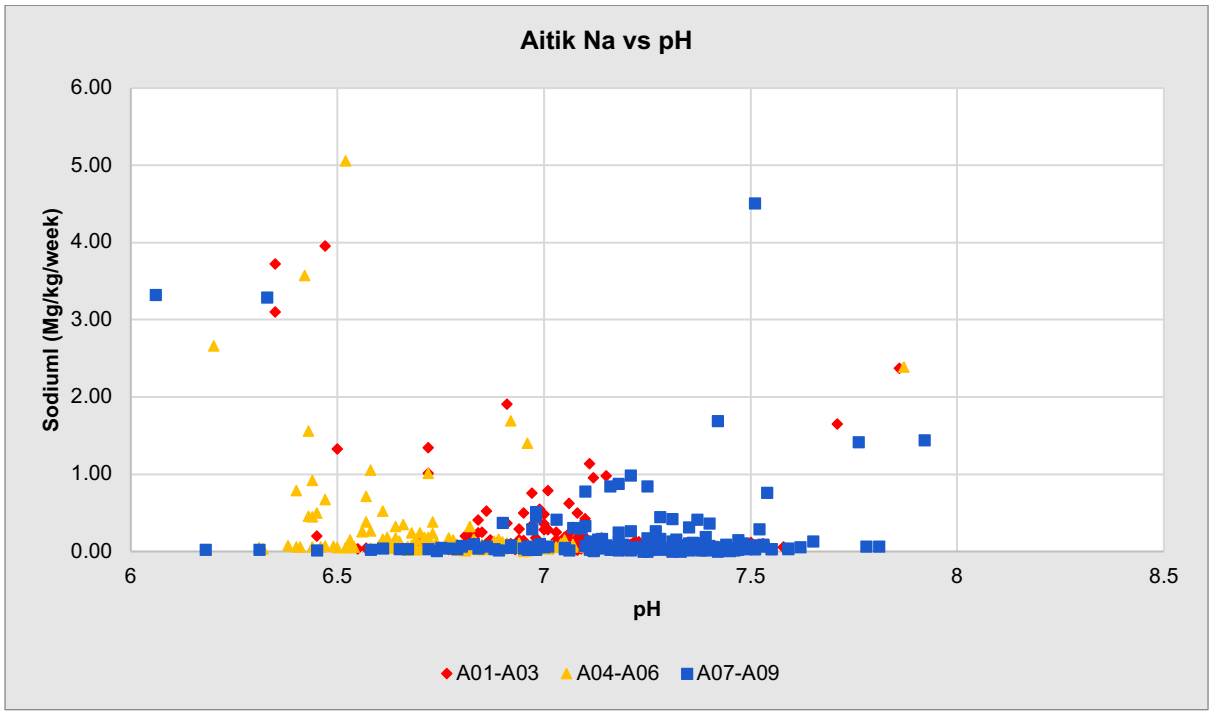


Figure A18.24 – Aitik HCT cell sets weekly leachate K vs pH

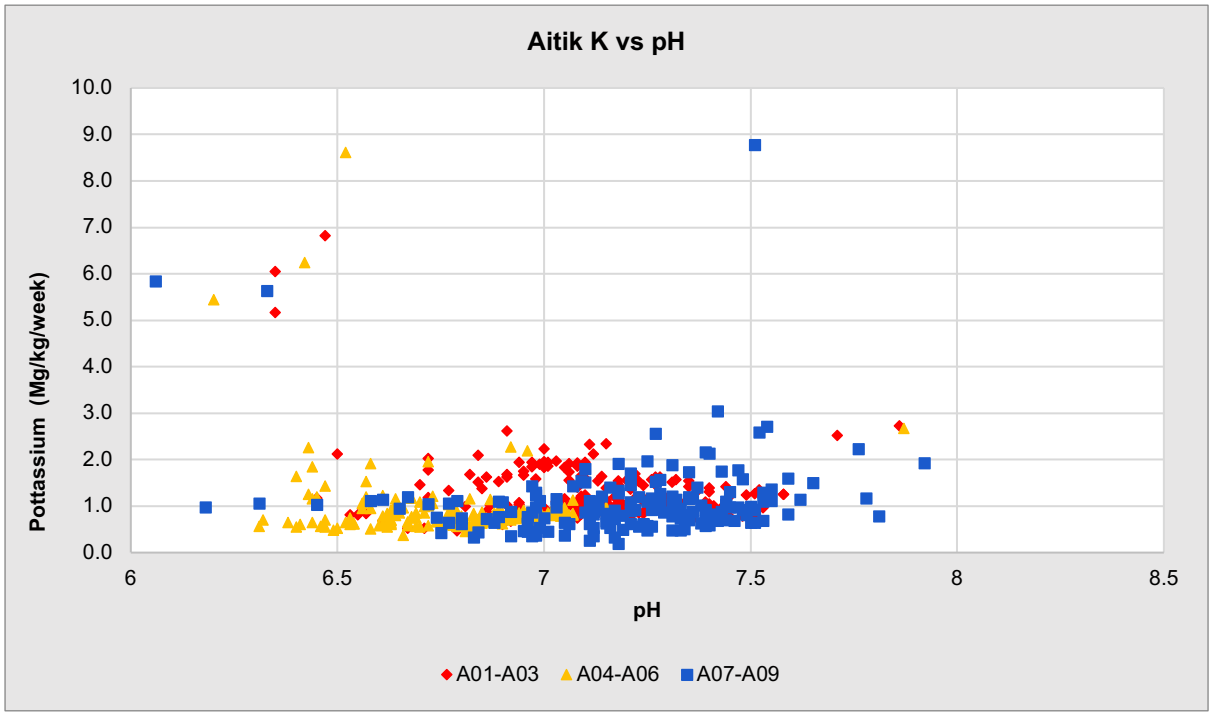

Figure A18.25 – Aitik HCT cell sets weekly leachate Sulfate vs pH

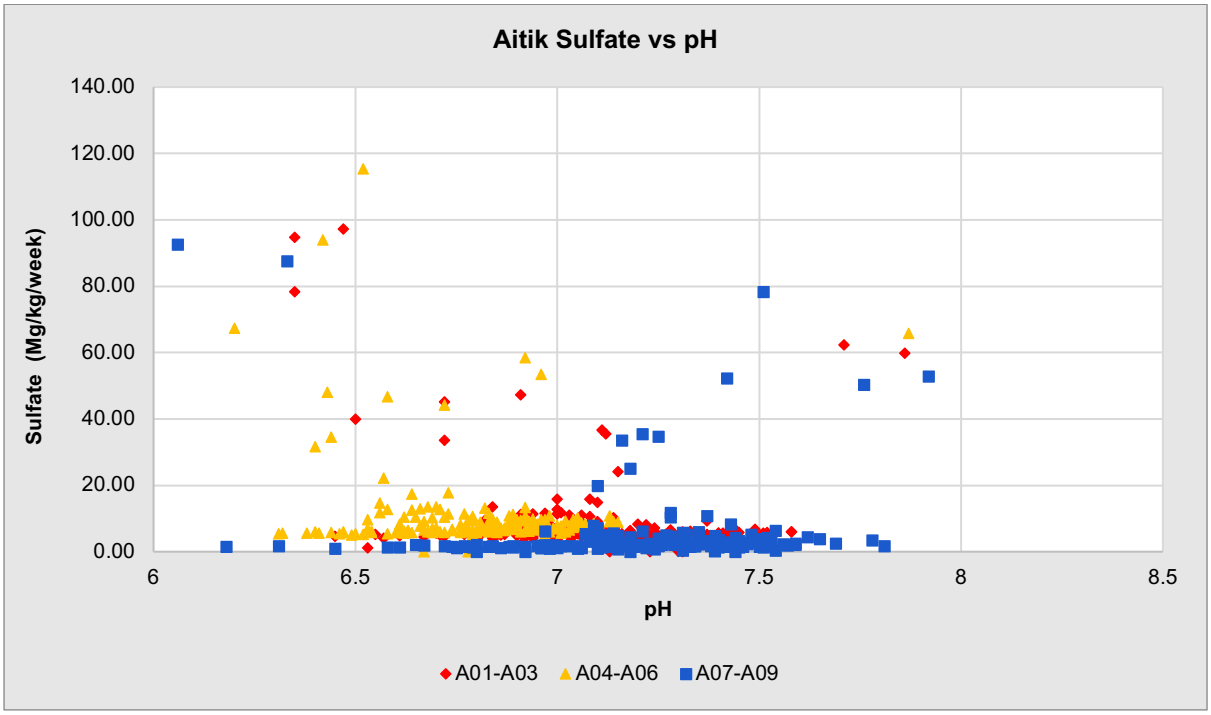


Figure A18.26 – Aitik HCT cell sets weekly leachate Mg vs Ca.

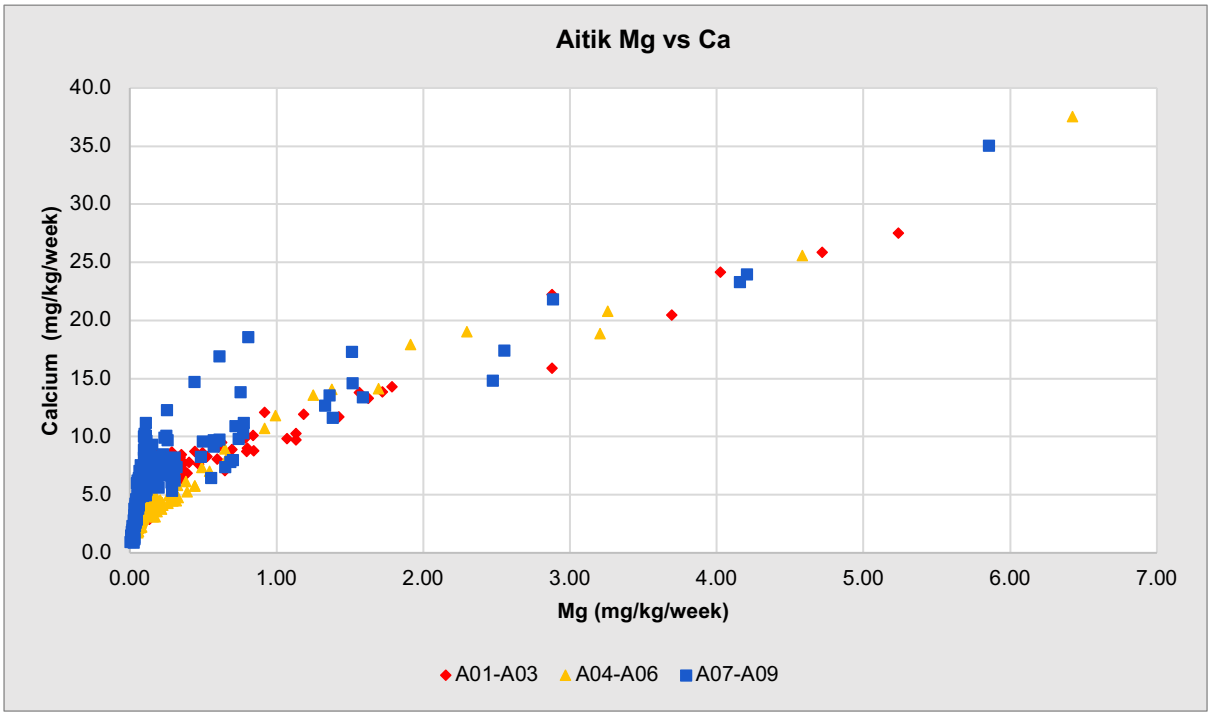

Figure A18.27 – Aitik HCT cell sets weekly leachate Sulfate vs DIC

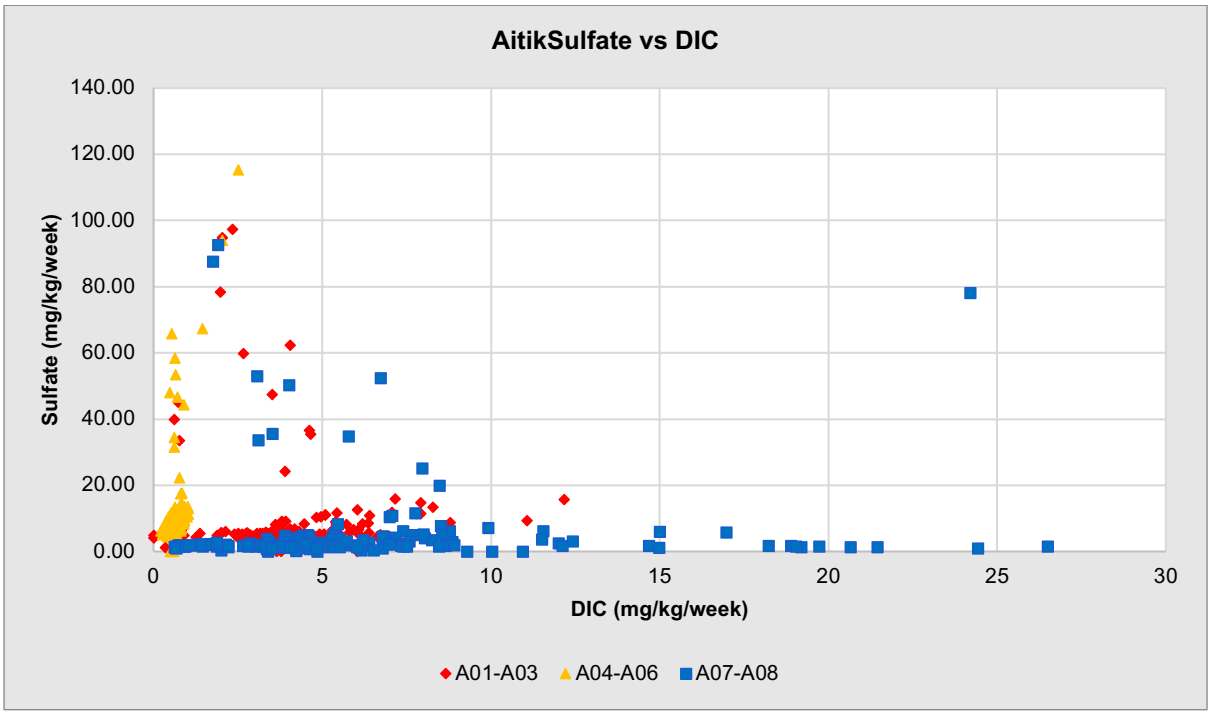


Figure A18.28 – Aitik HCT cell sets weekly leachate Mg vs DIC.

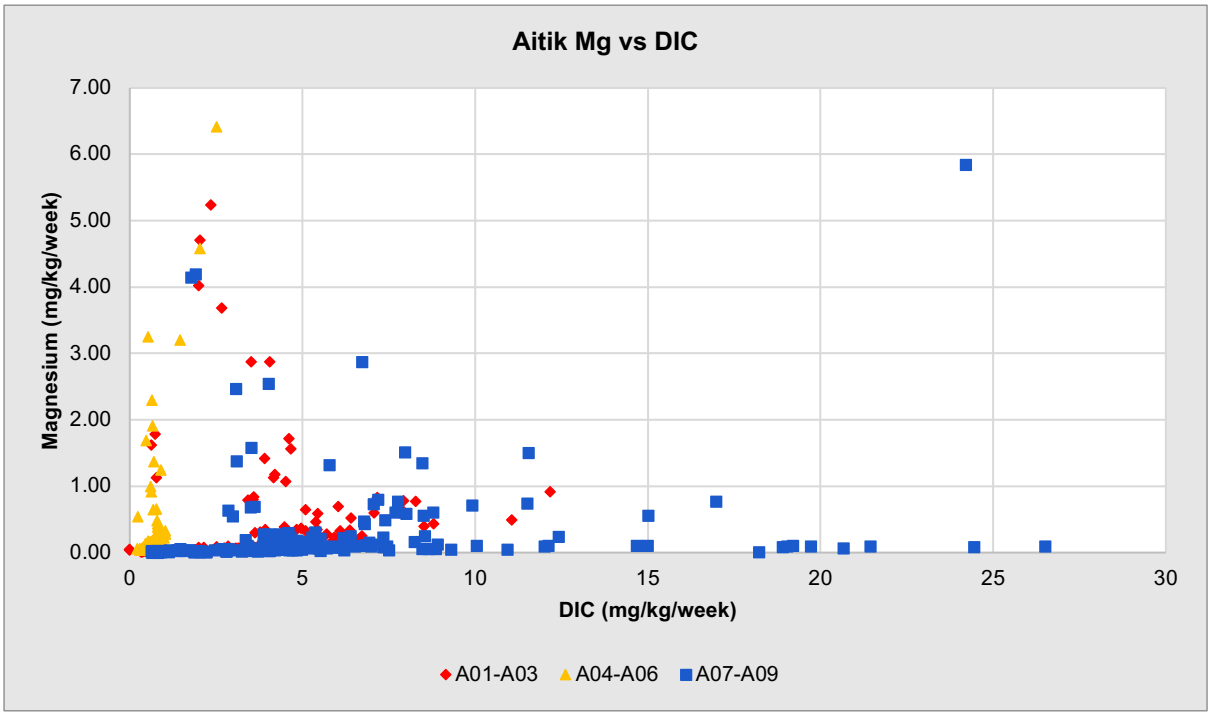

Figure A18.29 – Aitik HCT cell sets weekly leachate Mg vs Sulfate.

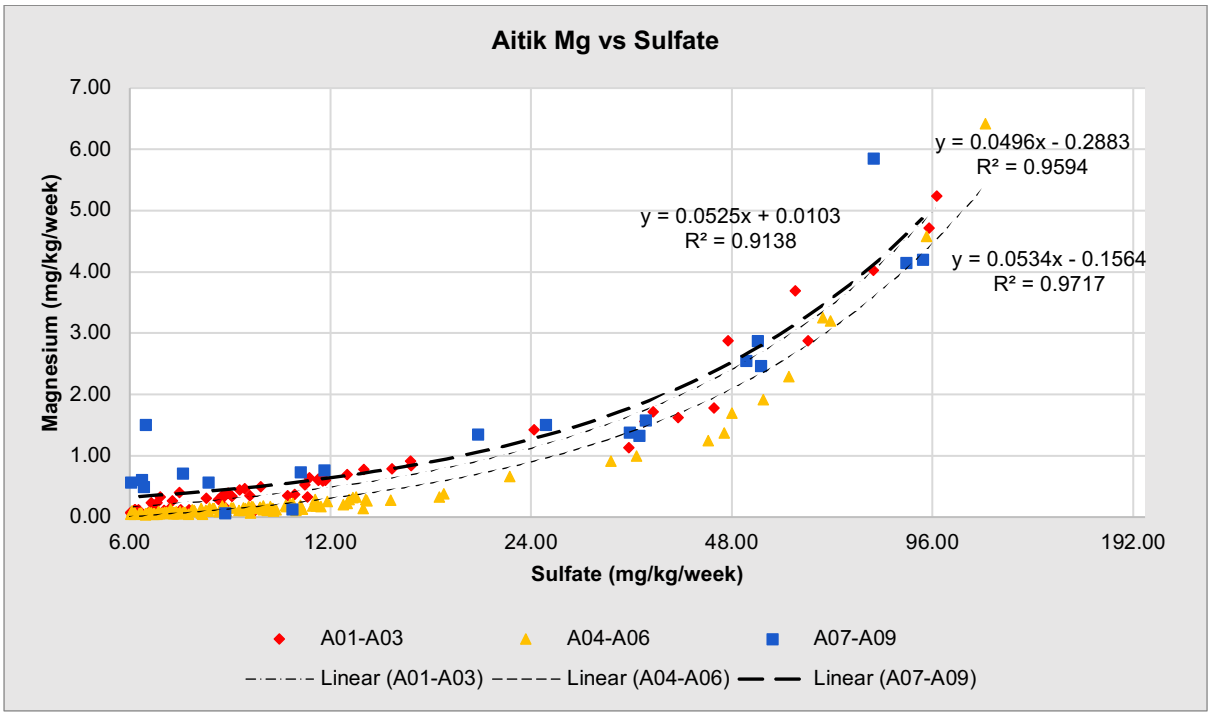


Figure A18.30 – Aitik HCT cell sets weekly leachate Ca vs Sulfate.

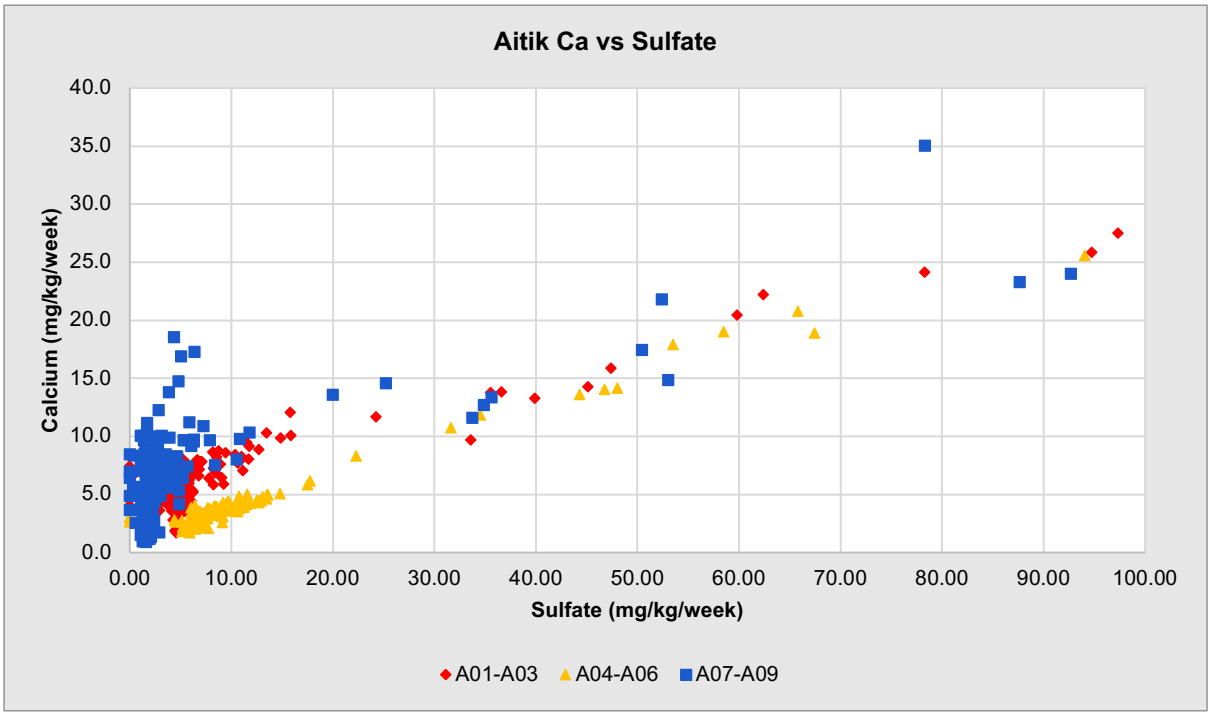

Figure A18.31 – Aitik HCT cell sets weekly leachate Mn vs Si.

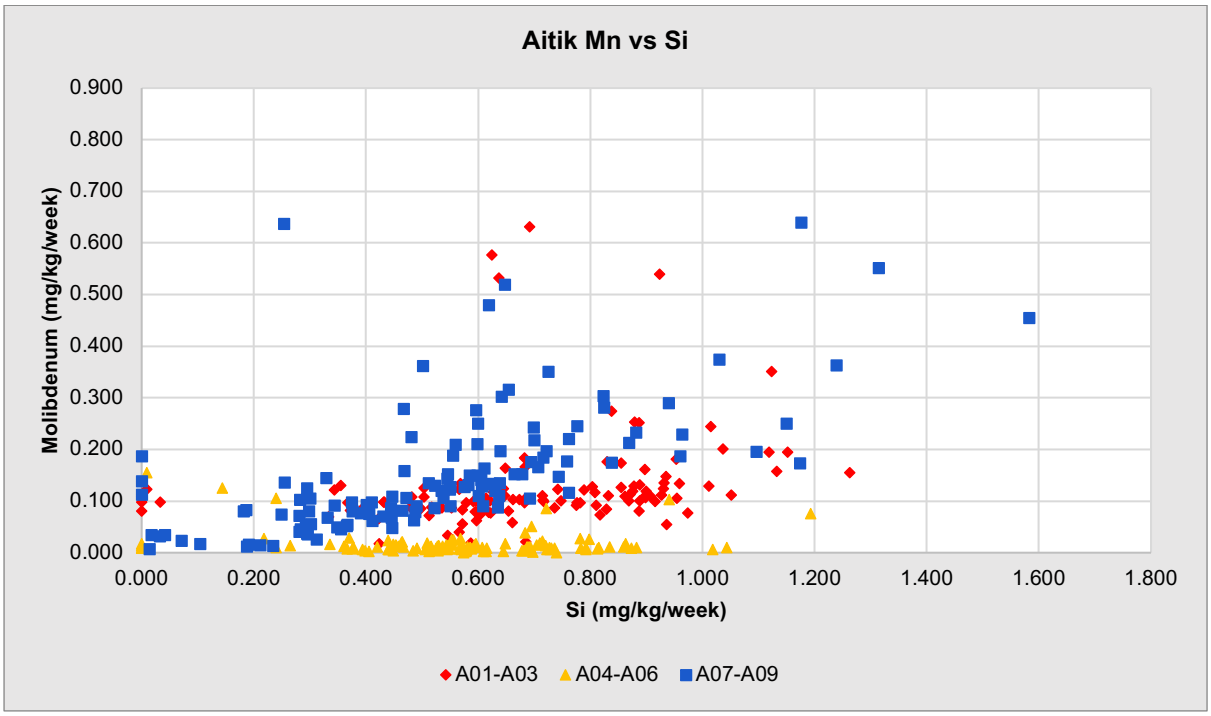


Figure A18.32 – Aitik HCT cell sets weekly leachate Mg vs Mn.

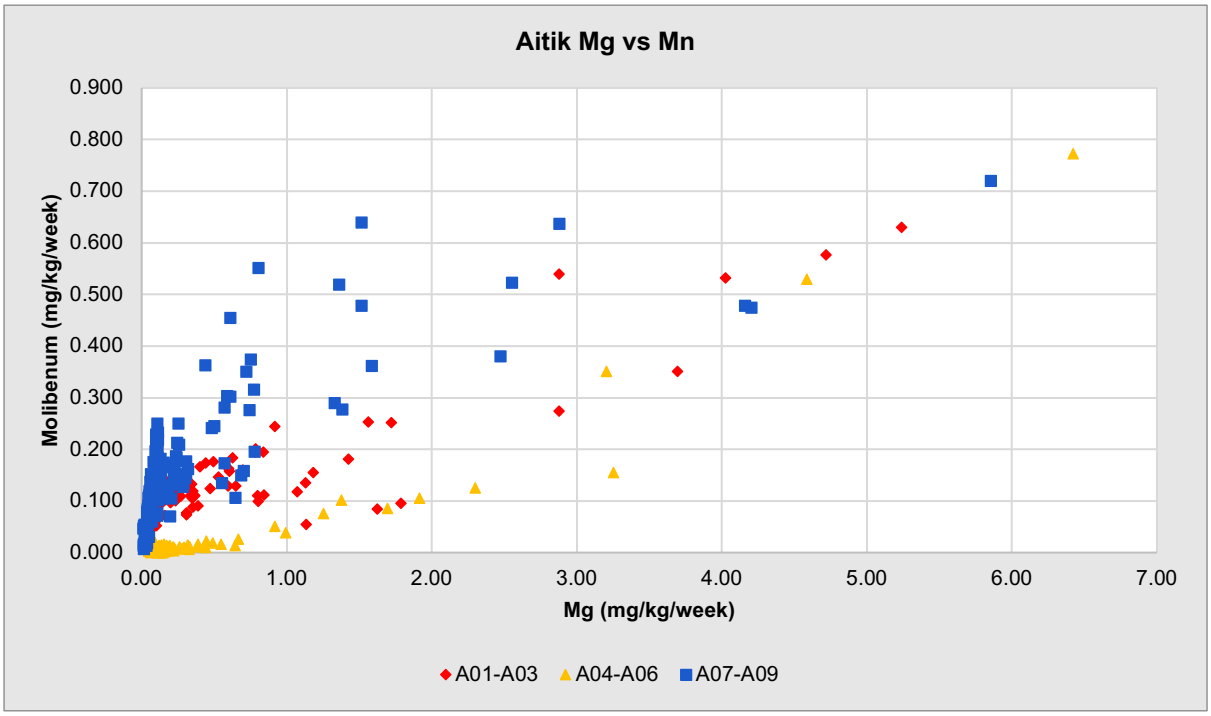

# Appendix 19 – Raw elemental anlaysis data

Within this appendix the raw results of Ed-XRF elemental analysis of pre and post HCT residues are displayed.

Table A19.1a – Raw elemental analysis results for Al, Ca, Fe, K, Mg, Na, S, Si, Ti, As, Ba, Cd and Co

| | Al | Ca | Fe | K | Mg | Na | S | Si | Ti | As | Ba | Cd | Co |
|---|---|---|---|---|---|---|---|---|---|---|---|---|---|
| Unit -> | % | % | % | % | % | % | % | % | % | mg/kg | mg/kg | mg/kg | mg/kg |
| Detection Limit | 0.3 | 1 | 0.1 | 0.2 | 0.5 | 1 | 0.2 | 1.5 | 0.01 | 50 | 300 | 50 | 200 |
| A-PRE | 6.73 | 2.41 | 4.26 | 3.33 | 1.27 | 1.18 | 0.44 | 23.66 | 0.36 | 11.208 | 2427.5 | 15.967 | 5.1 |
| A01-POST | 7.17 | 2.51 | 4.23 | 3.24 | 1.16 | 1.96 | 0.36 | 25.41 | 0.33 | 10.368 | 2359 | 17.274 | 4 |
| A02-POST | 7.64 | 2.5 | 4.41 | 3.22 | 1.24 | 2.2 | 0.4 | 27.61 | 0.33 | 8.715 | 2198.4 | 11.717 | 28.6 |
| A03-POST | 7.58 | 2.46 | 4.4 | 3.42 | 1.2 | 2.01 | 0.36 | 26.75 | 0.34 | 8.048 | 2781.9 | 24.362 | 93.4 |
| A04-POST | 7.54 | 2.38 | 4.41 | 3.34 | 1.18 | 2.37 | 0.47 | 27.16 | 0.32 | 9.408 | 2437.8 | 20.791 | -6.8 |
| A05-POST | 7.62 | 2.42 | 4.32 | 3.32 | 1.22 | 1.97 | 0.4 | 27.1 | 0.33 | 6.306 | 2552.1 | 22.124 | 56.1 |
| A06-POST | 7.76 | 2.54 | 4.24 | 3.24 | 1.25 | 2.26 | 0.43 | 27.23 | 0.33 | 9.405 | 2292.6 | 16.294 | -15.5 |
| A07-POST | 7.85 | 2.5 | 4.36 | 3.23 | 1.34 | 2.52 | 0.45 | 27.66 | 0.35 | 8.253 | 2353.1 | 12.322 | 17 |
| A08-POST | 7.54 | 2.53 | 4.41 | 3.23 | 1.25 | 1.87 | 0.44 | 26.82 | 0.32 | 7.938 | 2749.1 | 16.591 | 58.5 |
| A09-POST | 7.73 | 2.42 | 4.3 | 3.29 | 1.28 | 2.43 | 0.4 | 27.67 | 0.31 | 7.911 | 2542.6 | 17.834 | 26.6 |
| K-PRE | 1.55 | 8.13 | 7.16 | 0.09 | 11.46 | 0.19 | 0.28 | 19.23 | 0.17 | 3.915 | -24.6 | -5.689 | -30.1 |
| K01-POST | 1.83 | 8.41 | 7.11 | 0.14 | 11.68 | -0.05 | 0.32 | 20.7 | 0.18 | 3.656 | 31.7 | -5.13 | 26.6 |
| K02-POST | 1.66 | 8.44 | 7.11 | 0.08 | 12.02 | 0.19 | 0.32 | 20.48 | 0.18 | 3.712 | -93.8 | -5.764 | -1.6 |
| K03-POST | 1.62 | 8.53 | 7.14 | 0.07 | 11.83 | 0.29 | 0.27 | 20.37 | 0.17 | 3.383 | -73.6 | -4.063 | 47.1 |
| K04-POST | 1.54 | 8.46 | 7.06 | 0.07 | 11.39 | 0.01 | 0.29 | 19.64 | 0.17 | 1.115 | -38 | 0.238 | -43.9 |
| K05-POST | 1.68 | 8.34 | 6.84 | 0.11 | 11.57 | -0.26 | 0.26 | 20.18 | 0.18 | 3.988 | 17.7 | -8.465 | 69.6 |
| K06-POST | 1.58 | 8.57 | 7.17 | 0.07 | 11.79 | -0.19 | 0.33 | 20.26 | 0.18 | 2.003 | -46.6 | 1.949 | -35.9 |
| K07-POST | 1.71 | 8.37 | 7.17 | 0.09 | 12.32 | -0.19 | 0.31 | 20.97 | 0.17 | 3.01 | -8.7 | -7.627 | 68.8 |
| K08-POST | 1.64 | 8.37 | 7.06 | 0.07 | 12.34 | 0.05 | 0.33 | 20.41 | 0.17 | 2.981 | -77.6 | -10.692 | 94.8 |
| K09-POST | 1.59 | 8.52 | 6.99 | 0.06 | 11.83 | -0.11 | 0.28 | 20.75 | 0.18 | 3.408 | -31.3 | 11.731 | -5.1 |

Table A19.1b – Raw elemental analysis results for Cr, Cu, Mn, Mo, Ni, P, Pb, Se, Sr, V, Zn, Zr, U and Rb

| | Cr | Cu | Mn | Mo | Ni | P | Pb | Se | Sr | V | Zn | Zr | U | Rb |
|---|---|---|---|---|---|---|---|---|---|---|---|---|---|---|
| Unit -> | mg/kg | mg/kg | mg/kg | mg/kg | mg/kg | mg/kg | mg/kg | mg/kg | mg/kg | mg/kg | mg/kg | mg/kg | mg/kg | mg/kg |
| Detection Limit -> | 200 | 50 | 150 | 20 | 200 | 500 | 100 | 20 | 10 | 100 | 25 | 40 | 10 | 5 |
| A-PRE | 17 | 738 | 2252 | 7.643 | 10.9 | 1124.2 | -1.4 | 1.29 | 350.6 | 65.6 | 70.8 | 122.669 | 3.18 | 146.251 |
| A01-POST | 19.7 | 738.1 | 2119 | 4.696 | 15.5 | 873.1 | -0.6 | 1.918 | 355.1 | 63.4 | 73 | 115.243 | 1.711 | 142.364 |
| A02-POST | 22.5 | 867.2 | 2084 | 6.823 | 13.4 | 945 | -2.6 | 0.523 | 350.2 | 73.5 | 63.7 | 125.181 | 1.633 | 140.516 |
| A03-POST | 20.5 | 897.6 | 2066 | 14.536 | 20.4 | 1004.9 | 0.4 | 0.285 | 383.4 | 59.1 | 70 | 114.568 | 0.975 | 150.444 |
| A04-POST | 22.3 | 848.6 | 2412 | 7.841 | 13.7 | 846.7 | -2.5 | 0.886 | 348.1 | 67.1 | 64.9 | 117.785 | 1.753 | 140.935 |
| A05-POST | 20.6 | 969.1 | 2182 | 11.632 | 15.4 | 906.2 | 4.5 | 0.503 | 349.2 | 59.7 | 71.3 | 110.714 | 2.866 | 144.539 |
| A06-POST | 11.3 | 915.4 | 2037 | 3.027 | 11.1 | 882.1 | -3.8 | 1.804 | 335.3 | 71.2 | 68 | 115.304 | 2.922 | 139.873 |
| A07-POST | 21.3 | 901.2 | 2111 | 5.742 | 13.6 | 1021.6 | -0.7 | 0.273 | 327.1 | 61.4 | 64.4 | 120.928 | 10.134 | 136.741 |
| A08-POST | 12.2 | 906.2 | 2382 | 7.773 | 10.1 | 1027.6 | -1.1 | 0.11 | 361.5 | 61.3 | 69.5 | 129.037 | 3.269 | 137.876 |
| A09-POST | 8.1 | 786 | 2311 | 3.616 | 11.8 | 924.2 | 1.8 | 2.281 | 356.1 | 63.9 | 72.1 | 128.262 | 4.637 | 143.578 |
| K-PRE | 2281 | 756.4 | 1282 | 3.849 | 920.4 | 221.1 | -5 | 1.895 | 15.1 | 120 | 46 | 26.817 | 2.838 | 4.413 |
| K01-POST | 2342.1 | 747.3 | 1294 | 1.154 | 856.9 | 255.2 | -3.3 | 1.83 | 24.9 | 123.1 | 49.6 | 24.824 | 1.642 | 5.865 |
| K02-POST | 2395.3 | 763.9 | 1269 | 0.903 | 899.6 | 121.4 | -3.8 | 2.546 | 16.3 | 124.8 | 42.3 | 39.777 | 3.604 | 4.137 |
| K03-POST | 2393.3 | 738.4 | 1300 | 1.558 | 910.3 | 244.4 | -4.9 | 1.899 | 13.3 | 120.5 | 47.2 | 25.544 | 2.461 | 3.339 |
| K04-POST | 2389.4 | 704.6 | 1251 | 0.368 | 864.6 | 244.9 | -0.6 | 1.237 | 15.6 | 136.1 | 51.5 | 29.242 | 1.495 | 3.51 |
| K05-POST | 2291.2 | 687.8 | 1275 | 0.095 | 843.3 | 210.3 | -2.8 | 1.572 | 20.2 | 116.7 | 48.7 | 25.516 | 3.073 | 5.26 |
| K06-POST | 2441.9 | 790.2 | 1284 | 1.152 | 879.1 | 272 | -0.4 | 2.582 | 18.6 | 128 | 48.5 | 23.966 | 1.619 | 5.05 |
| K07-POST | 2382.7 | 727.6 | 1287 | 1.101 | 846.7 | 194.8 | -3.5 | 1.389 | 15.8 | 124.5 | 48.4 | 29.651 | 2.124 | 4.288 |
| K08-POST | 2350.2 | 789.4 | 1234 | -1.44 | 852.2 | 201.1 | -3.7 | 2.306 | 13.9 | 124.2 | 46.1 | 32.69 | 2.206 | 4.431 |
| K09-POST | 2400.4 | 706.6 | 1256 | 2.763 | 856 | 180.3 | -2.7 | 1.484 | 14.7 | 128.9 | 44.6 | 27.142 | 2.061 | 6.174 |

# Appendix 20 – Additional HCT Result Descriptions

Within this appendix additional descriptions of select leachate parameter results are outlined. Cell leachate EC, Eh, post $H_2O_2$ pH and Na results are described within this appendix.

### HCT Weekly Leachate EC Results

Kevitsa and Aitik HCT leachate EC measurements over the 60-week leaching period are shown in Figures A20.1 and A20.2, respectively. Methods utilised for aqueous sample analysis can be found in Chapter 4, section 4.6.

### Kevitsa HCT EC Results

EC readings from K-TC1 cell leachates fluctuated considerably throughout the initial leaching weeks (weeks 1-15), followed by a general stabilisation of EC throughout the rest of the leaching weeks. Cell K01 measured a maximum EC reading of 662.16 µS/cm within week 1, and a minimum of 55.91 µS/cm at week 35, with an mean leachate EC of 185.1715 µS/cm and a median of 157.3 µS/cm. Cell K02 reached a peak EC of 595.85 µS/cm in week 1 and hits its lowest point of 58.96 µS/cm at week 35. The mean leachate EC for cell K02 is 181.5644 µS/cm, with a median of 154.9 µS/cm. Cell K03 had its maximum leachate EC, 657.24 µS/cm during week 1, a trend that is demonstrated in all HCT's within this research project. The lowest K03 EC reading was 19.07 µS/cm at week 28, which represents the lowest EC reading of any cell in this program. The mean of measured leachate EC readings for K03 is 183.2217 µS/cm, while the median is 154.72 µS/cm.

K-TC2 cells demonstrated less pronounced EC fluctuations within cell leachates. The maximum EC reading for cell K04 was 421.71 µS/cm (week 1), while the minimum was 38.07 µS/cm in week 44. The mean of measured EC readings for K04 is 133.9644 µS/cm, while the median is 115.89 µS/cm. Cell K05's maximum and minimum readings are 320.61 µS/cm (week 1) and 42.02 µS/cm (week 44), respectively, with a mean of measured readings of 127.4376 µS/cm and a median of 121.13 µS/cm. The maximal EC reading for cell K06 was 395.55 µS/cm (week 1), with the lowest reading, 39.68 µS/cm, in week 44. The mean and median of measured K06 readings were 140.9761 µS/cm and 132.86 µS/cm, respectively.

Similarly to K-TC1 cells, K-TC3 demonstrated noticeable fluctuations in EC throughout the initial leaching weeks, followed by a general stabilisation of readings. All cells within this set demonstrated a distinct peak in EC readings in week 43, which aligns with an observed dip in pH values during the same leaching week, see Figure 44. Cell K07 measured it maximal EC reading of 452.26 µS/cm in week 1 while its minimum reading was at 39.29 µS/cm, measured in week 35. The mean of measured EC readings from this cell is 145.4751 µS/cm, while the median is 127.01 µS/cm. Cell K08 measured its highest EC reading of 456.99 µS/cm in week 1, with its lowest reading was 36.79 µS/cm in week 35. The mean EC for K08 is 154.7163 µS/cm, while the median of readings is 142.68 µS/cm. The lowest EC reading of K09 leachates was measured in week 56, 31.6 µS/cm, while its maximal reading was measured in week 1, 444.91 µS/cm, similarly to all cells in this study.

**Aitik HCT EC Results**

A-TC1 cells displayed a gradual decreasing trend in EC readings over the leaching period. Cell A01 achieved its peak leachate EC reading in week 1 with 300.19 µS/cm. The minimum EC reading for this cell was measured as 26.32 µS/cm in week 35. The mean and median of measured EC values for A01 are 95.46 µS/cm and 82.07 µS/cm, respectively. Cell A02 held a maximal EC reading of 263.89 µS/cm in week 1 and a minimum value of 28.43 µS/cm in week 44. The mean and median of recorded values are 95.54 µS/cm and 79.72 µS/cm, respectively. Within cell A03, the maximal EC was observed in week 0 with 253.34 µS/cm, while the minimum was measured in week 44 with 29.24 µS/cm. The mean and median value of measured EC within cell A03 leachates are 96.70 µS/cm and 82.54 µS/cm.

The control Aitik triplicate set, A-TC2 exhibited a declining trend in EC readings. Cell A04 reached its maximum EC in week 1 with 309.86 µS/cm, and its minimum EC in week 44 with 24.03 µS/cm. The mean and median EC values for A04 were 76.77 µS/cm and 63.31 µS/cm, respectively. The maximum and minimum EC readings for cell A05 were recorded in week 0 (308.2 µS/cm) and week 44 (23.44 µS/cm) respectively, with mean and median values of 69.69 µS/cm and 59.24 µS/cm. For cell A06, the maximum reading was 251.91 µS/cm in week 0, while the minimum EC reading was 21.74 µS/cm at week 44. The mean and median EC values for cell A06 are 67.19 µS/cm and 56.72 µS/cm.

Over the leaching period the A-TC3 triplicate cells demonstrated a more fluctuating trend in electrical conductivity than A-TC1 and A-TC2 cell sets. The maximum EC reading for cell A07 was recorded in week 1 with 238.11 µS/cm, while the minimum reading was in week 44 with 23.4 µS/cm. The mean and median EC values for A07 were 88.75 µS/cm and 82.66 µS/cm, respectively. Cell A08 recorded its maximum EC reading in week 4 with 226.5 µS/cm and its minimum reading in week 44 with 18.2 µS/cm. This cell has mean and median EC values of 90.84 µS/cm and 88.37 µS/cm, respectively. Cell A09 EC readings peaked in the initial leach (week 0) with 225.64 µS/cm, while the minimum EC value was recorded in week 35 with 23.5 µS/cm. The mean and median values were 83.35 µS/cm and 76 µS/cm, respectively for cell A09.

This comparison of the triplicate sets indicates that A-TC2 generally had lower EC measurements than A-TC1 and A-TC3. A-TC1 and A-TC3 displayed similar ranges of EC, but A-TC1 generally had higher values. Dips and peaks in EC readings generally align with similar anomalous readings for pH during corresponding leaching weeks.

Figure A20.1 - Kevitsa mine waste humidity cell tests (HCT) electrical conductivity (EC) results measured from leachates collected over the 60-week testing period

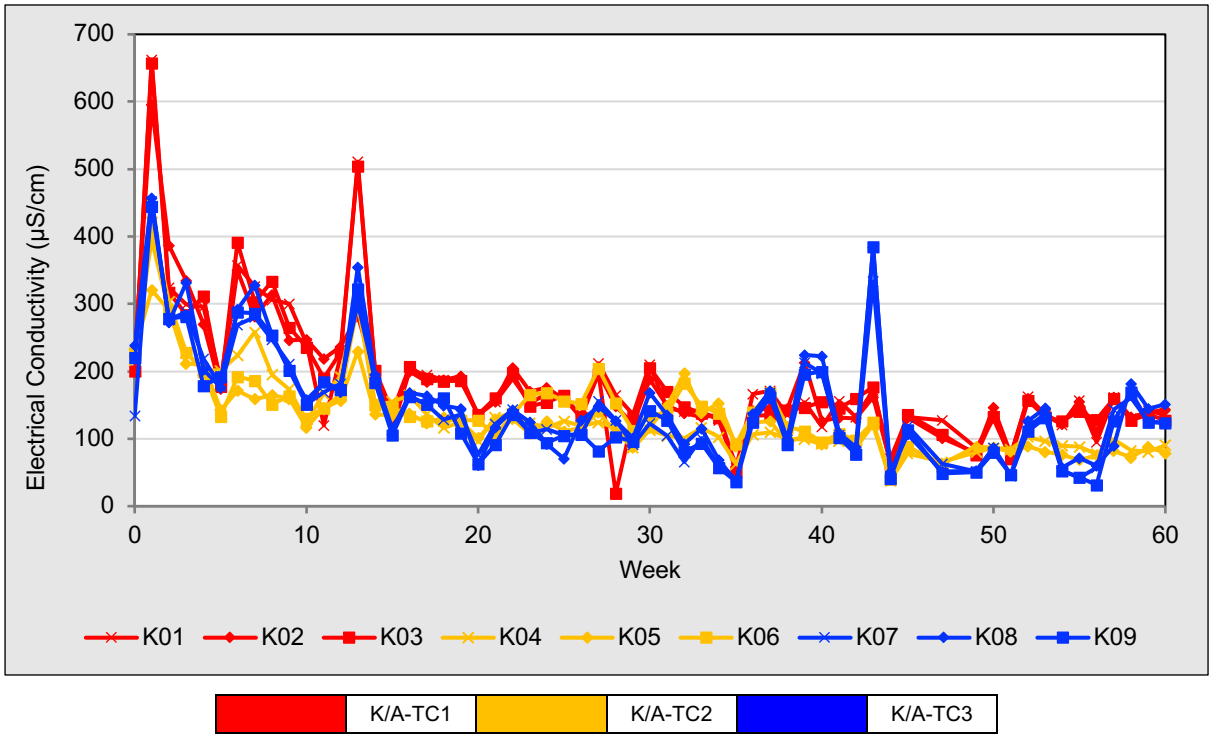

Figure A20.2 - Aitik mine waste humidity cell tests (HCT) electrical conductivity (EC) results measured from leachates collected over the 60-week testing period.

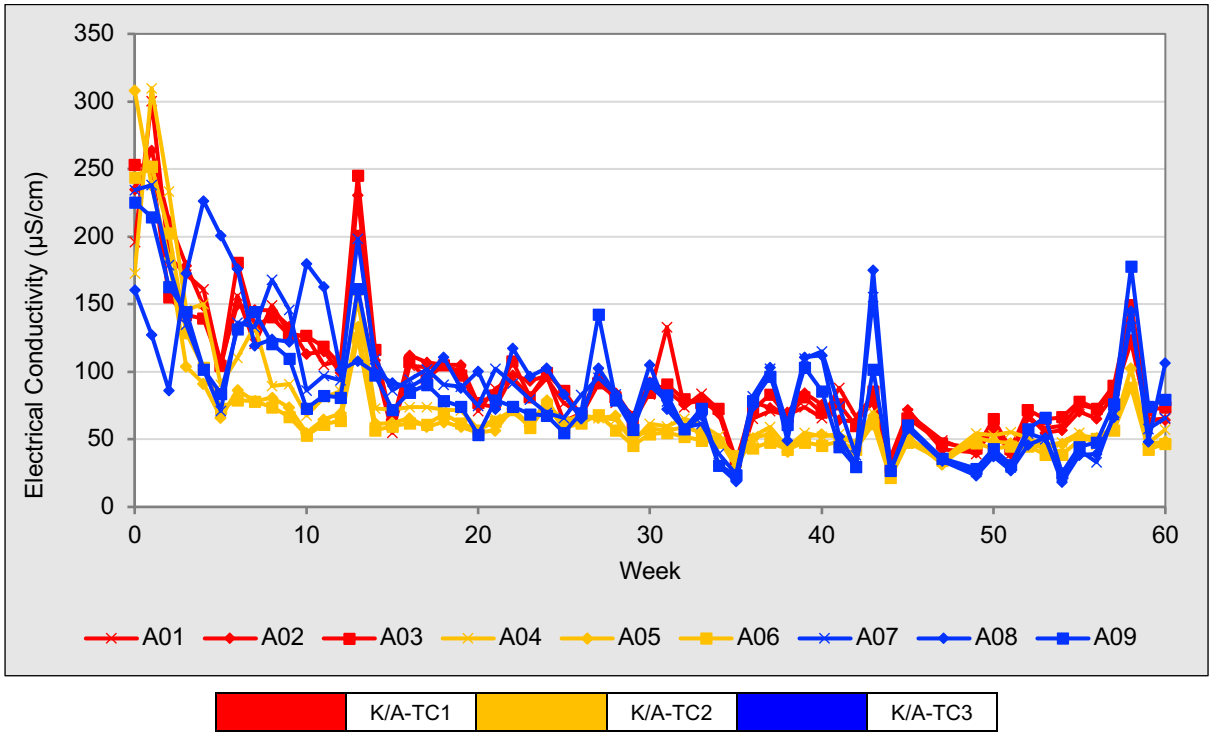


**HCT Weekly Leachate Eh Results**

Kevitsa and Aitik HCT leachate Eh measurements over the 60-week leaching period are shown in Figures A20.3 and A20.4, respectively. Methods utilised for aqueous sample analysis can be found in Chapter 4, section 4.6.

**Kevitsa HCT Eh Results**

It can be seen in Figure A20.3 that Eh values were highly variable throughout the leaching period for all triplicate HCT sets. Within K-TC1 the Eh values for K01 vary from 384.98 mV to 599.86 mV, with a mean value of 503.23 mV and a median of 498.95 mV. K02, on the other hand, displays readings that range between 390.59 mV and 611.31 mV, with mean and median values of 515.35 mV and 510.12 mV, respectively. Within cell K03 the readings range from a minimum of 362.69 mV to a maximum of 591.28 mV. The mean for K03 is 514.60 mV, while the median value is 511.32 mV. Each of these individual cells in K-TC1 shows a fluctuating trend throughout the 60-week protocol.

A-TC2 cells present slightly different Eh dynamics over the leaching period. The Eh values for cell K04 fluctuate between 396.69 mV and 612.89 mV, with a mean of 526.67 mV and a median value of 526.01 mV. Cell K05 readings range from a minimum of 426.29 mV to a maximum of 615.98 mV, with mean and median values of 536.36 mV and 532.36 mV, respectively. Lastly, K06 exhibits readings that range from 433.99 mV to 618.61 mV, with a mean of 538.61 mV and a median of 536.02 mV. Similarly to K-TC1, each cell in K-TC2 shows a fluctuating trend throughout the testing period.

The Eh values for cell K07 range from 415.79 mV to 594.16 mV, with the mean and median values being 528.32 mV and 526.8 mV respectively. Cell K08 readings span between 436.99 mV and 590.66 mV, with a mean of 525.77 mV and a median value of 522.9 mV. Cell K09 recorded values ranging from 431.42 mV to 577.41 mV. The mean for K09 was calculated as 520.88 mV, with a median of 525.71 mV.

When comparing the trends and variations between the three triplicate sets, K-TC1 demonstrated the lowest mean and median Eh (mV) values. K-TC2 displayed the highest Eh (mV) values overall, with the maximum mean and median values. K-TC3 maintained relatively consistent mean and median values, slightly lower than K-TC2 but higher than K-TC1. There were noticeable fluctuations in the readings throughout the 60-week period, with a distinct ‘consistent’ period of lower Eh values between weeks 18 and 40, demonstrated for all three triplicate sets in this study.

**Aitik HCT Eh Results**

Cell A01 held a mean Eh value of 544.8192 mV and a median value of 545.92 mV over the leaching period. The minimum Eh value for A01 was 386.64 mV (week 10) and the maximum was 655.01 (week 16). Cell A02 had a mean Eh value of 546.0466 mV and a median Eh of 536.962 mV, with the minimal Eh value measured as 459.94 mV in week 10, this cell held a maximal Eh reading of 627.86 mV in week 14. The last A-TC1 cell, A03, held a mean Eh of 543.4968 mV with a median of 539.06 mV. Its Eh values ranged from a minimum of 459.97 mV to a maximum of 607.3907 mV.

A-TC2 cells, A04, A05 an A06, held mean Eh values of 552.3576 mV, 531.9699 mV and 550.1847 mV, respectively. Cell A04 held a median Eh value of 548.4613 mV,

while its Eh values ranged from a minimum of 470.27 mV to a maximum of 633.0507 mV at week 56. For cell A05, the median Eh was 527.3093 mV, with values ranging from 449.41 mV to 625.596 mV. The last cell of this set, A06, held a median Eh of 545.69 mV. The minimum and maximum Eh values for this cell were 470.07 mV and 625.686 mV, respectively.

Within the A-TC3 triplicate A07 held a mean Eh value of 529.6392 mV and a median of 524.18 mV over the leaching period. The values ranged between 439.27 mV to 616 mV for A07 over the 60 weeks. Cell A08 held a mean Eh of 529.8722 mV, while the median was 532.4 mV. The minimum was 450.71 mV in week 5, with a maximum Eh of 605.298 mV in week 49. Cell A09 held mean and median Eh values of 530.0353 mV and 527.56 mV, respectively. The lowest recorded Eh value was 395.26 mV in week 22, with a maximal Eh of 602.6 mV in the initial leach, week 0.

Comparing the three triplicate sets, A-TC1 showed a tendency for higher maximum values while A-TC2 showed the highest variability of the triplicate sets. Less variable Eh values are demonstrated within the middle third of the experimental period.

Figure A20.3 - Kevitsa mine waste humidity cell tests (HCT) Eh results measured from leachates collected over the 60-week testing period.

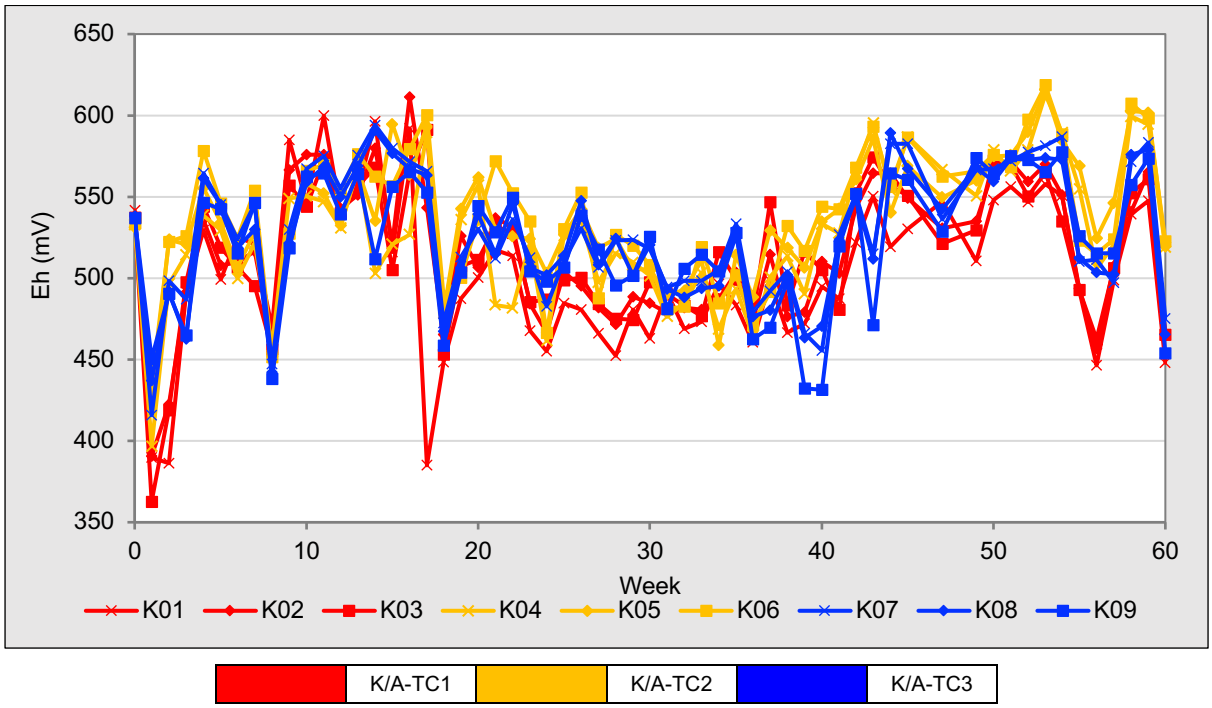

Figure A20.4 - Aitik mine waste humidity cell tests (HCT) Eh results measured from leachates collected over the 60-week testing period.

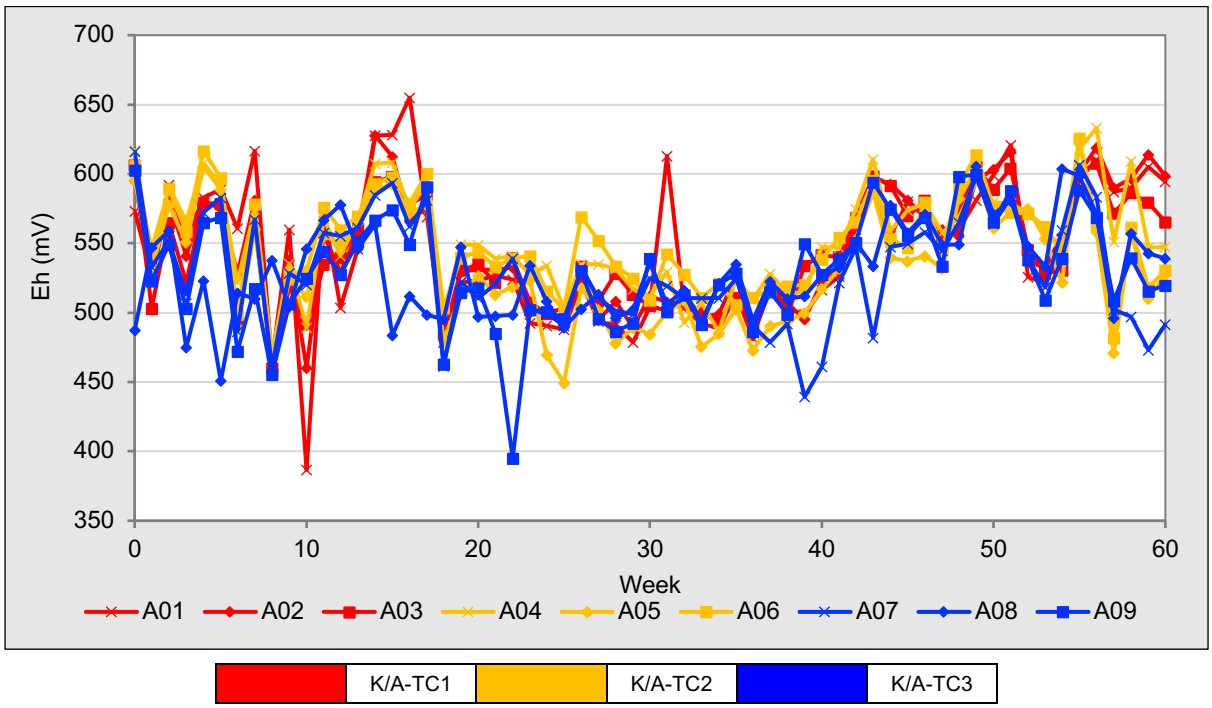


**HCT Weekly Leachate Post Hydrogen Peroxide ($H_2O_2$) pH Results**

Kevitsa and Aitik HCT leachate Post Hydrogen Peroxide ($H_2O_2$) pH Results measurements over the 60-week leaching period are shown in Figures A20.1 and A20.2, respectively. Methods utilised for aqueous sample analysis can be found in Chapter 4, section 4.6.

**Kevitsa Post Hydrogen Peroxide ($H_2O_2$) pH Results**

It can be seen in Figure A20.5 that the pH measurements taken post hydrogen peroxide addition within Kevitsa HCT leachates generally followed similar trends amongst all cells during the 45-week period. During initial leaching weeks post $H_2O_2$ pH measurements generally demonstrated suppression below pH 4.5, which may be expected due to initial dissolution of highly soluble sulfur mineral species during early leaching weeks. After week 7 general stabilisation of post $H_2O_2$ pH measurements are noted through to week 45, with the exception of week 40, in which district peaks above pH 5 are noted for Kevitsa cells from all three triplicate sets. Cell K01 exhibits a minimum post $H_2O_2$ pH measurement of pH 2.94 in week 1 and a maximum post $H_2O_2$ pH measurement of pH 4.76 in week 23, with a mean pH of pH 4.37. All Kevitsa cells, irrelevant of set and conditions, demonstrated minimal post $H_2O_2$ pH measurements

in week 1, with all measurements below pH 3.5. Cell K02 measured a maximum post $H_2O_2$ pH of pH 5.15 in week 40, while cell K03 reported a maximal pH of pH 4.73 in week 12.

K-TC2 cells demonstrate generally lower post $H_2O_2$ pH measurements throughout the 45-week period than K-TC1 and K-TC3 HCT cells. K-TC2 cells (K04, K05 and K06) held mean post $H_2O_2$ pH measurements of pH 4.25, pH 4.32 and pH 4.32, respectively. This is compared to comparable K-TC3 cells (K07, K08 and K09), which held mean post $H_2O_2$ pH measurements of pH 4.44, pH 4.44 and pH 4.39, respectively. Comparatively, all three triplicate sets follow a similar trend of increasing post $H_2O_2$ pH measurements values over the 45-week period. In terms of fluctuations, K-TC1 and K-TC3 show lesser variability compared to K-TC2.

Figure A20.5 - Kevitsa mine waste humidity cell tests (HCT) post $H_2O_2$ pH results measured from leachates collected over the 60-week testing period.

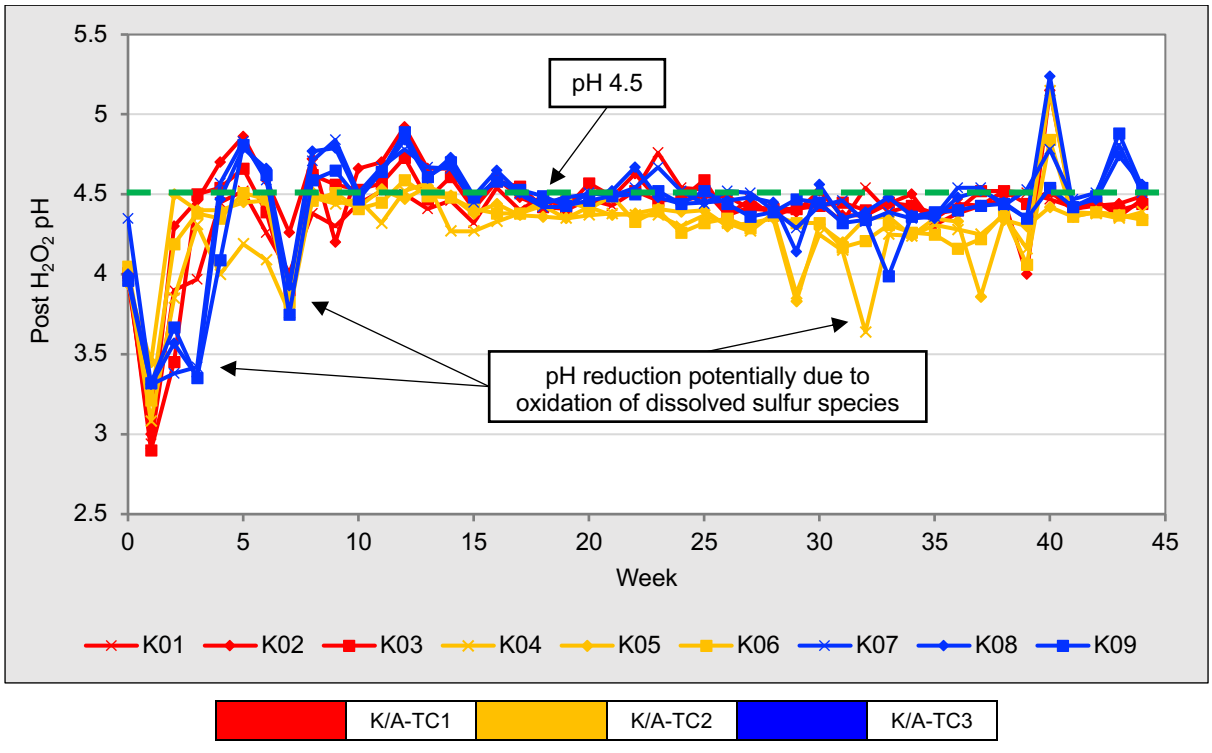


### Aitik Post Hydrogen Peroxide ($H_2O_2$) pH Results

Aitik HCT triplicate sets generally show a similar trend in post $H_2O_2$ pH measurements as Kevitsa counterparts. Higher variability in post $H_2O_2$ pH measurements are noted between the initial leach (week 0) and week 7, with a relative stabilisation of

measurements for the rest of the measurement period. Cell A01 had a minimum pH value of pH 3.98 in week 1, a maximum pH of pH 4.56 in week 5, a mean post $H_2O_2$ pH of pH 4.36. Comparably, cell A02 had a minimum post $H_2O_2$ pH measurement of pH 4.19 in week 7, a maximum of pH 4.76 in week 12, with mean and median post $H_2O_2$ pH measurements of pH 4.43 and pH 4.41, respectively. Cell A03 demonstrated the lowest minimum post $H_2O_2$ pH measurement of this triplicate set with a pH of pH 3.89 in week 2. This cells maximum measured pH post hydrogen peroxide addition was pH 4.62 in week 14, while its mean pH was pH 4.32.

Aitik control triplicate cells, A-TC2, generally measured lower post $H_2O_2$ pH measurements after week 7 than A-TC1 and A-TC3 cells. Cell A04 held the lowest post $H_2O_2$ pH measurement of pH 3.66 in week 31 and a maximum of pH 4.68 in week 12, with a mean post $H_2O_2$ pH measurement of pH 4.29. Cell A05's post $H_2O_2$ pH measurements ranged from a minimum of pH 3.97 in week 37 to a maximum of pH 4.69 in week 12, with a mean pH of pH 4.28 and a median pH of pH 4.27. Cell A06 held minimum and maximum post $H_2O_2$ pH measurements of at pH 3.72 (week 29) pH 4.67 (week 12), respectively.

Generally, A-TC3 triplicate cells demonstrated the highest post $H_2O_2$ pH measurements throughout the 45-week period, while also demonstrating more variability that other Aitik triplicates. Cell A07 held a minimum post $H_2O_2$ pH measurement of pH 3.59 in week 4, a maximum of pH 4.8 in week 30, a mean of pH 4.41. Cell A08 held the lowest minimum and highest maximum post $H_2O_2$ pH within A-TC3 cells with pH's of pH 3.45 in week 1 and the pH 4.74 in week 9. Cell A09 measured a minimum post $H_2O_2$ pH of pH 3.61 in week 4, a maximum of pH 4.75 in week 12, with mean and median pH's of pH 4.38 and pH 4.41, respectively.

Figure A20.6 - Aitik mine waste humidity cell tests (HCT) post $H_2O_2$ pH results measured from leachates collected over the 60-week testing period.

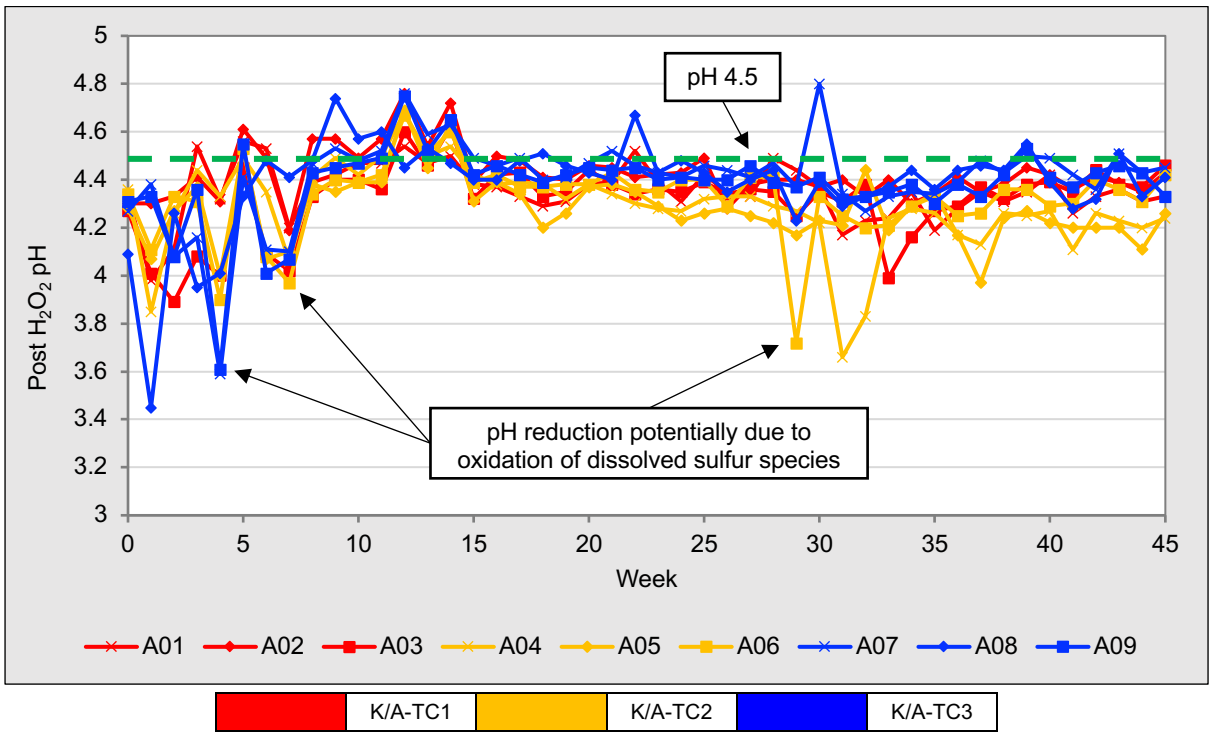


**HCT Weekly Leachate Sodium (Na) Results**

Kevitsa and Aitik HCT leachate Sodium concentrations over the 60-week leaching period are shown in Figures A20.7 and A20.9, respectively. Cumulative Na release over time is shown in Figures A20.8 and A20.9 for Kevitsa and Aitik cells. Methods utilised for aqueous sample analysis can be found in Chapter 4, section 4.6.

**Kevitsa HCT Na Results**

Cell K01 measured a maximum Na release rate of 4.22 mg/kg/week in week 1, while its minimum rate was 0.0004 mg/kg/week in week 33. The mean Na rate for K01 over the test period was 0.27 mg/kg/week, with a median rate of 0.058 mg/kg/week. The Na rate for cell K02 peaked at 4.53 mg/kg/week during the initial leach (week 0) and measured a minimal rate of 0.007 mg/kg/week in week 38. The mean rate for cell K02 was 0.28 mg/kg/week, with a median of 0.06 mg/kg/week. Within cell K03 leachates the maximum Na release rate was 4.11 mg/kg/week in week 1, while the lowest rate was 0.012 mg/kg/week in week 38. The mean Na release rate for cell K03 was 0.26 mg/kg/week and the median was 0.058 mg/kg/week.

K-TC2 cell K04 exhibited a peak Na release rate of 4.03 mg/kg/week within the initial leach (week 0) and its lowest rate of 0.002 mg/kg/week in week 38. The mean release rate for K04 was 0.26 mg/kg/week with a median of 0.045 mg/kg/week. For cell K05, the maximum Na rate was 4.70 mg/kg/week in week 0, while the minimum was 0.0045 mg/kg/week in week 43. Cell K05's mean and median rates were 0.27 mg/kg/week and 0.046 mg/kg/week, respectively. Na release rates peaked for cell K06 at 4.43 mg/kg/week in week 0 and measured a minimum of 0.0015 mg/kg/week in week 15. The mean and median Na rates for K06 were 0.28 mg/kg/week and 0.046 mg/kg/week, respectively.

In the final triplicate set, K-TC3, cell K07 recorded a maximum Na release rate of 4.06 mg/kg/week in week 0 and a minimum of 0.0013 mg/kg/week in week 36. The mean and median rates for cell K07 were 0.26 mg/kg/week and 0.046 mg/kg/week, respectively. For cell K08, the peak rate was 4.72 mg/kg/week in week 0, while the lowest rate recorded was 0.0033 mg/kg/week in week 47. The mean Na rate for cell K08 was 0.27 mg/kg/week, and the median rate was 0.048 mg/kg/week. Finally, for cell K09, the Na rate peaked at 4.36 mg/kg/week in week 0, while the lowest rate of 0.0029 mg/kg/week was measured in week 44. The mean Na rate for cell K09 over the test period was 0.27 mg/kg/week with a median rate of 0.04 mg/kg/week.

The cumulative Na (Na) release for Kevitsa HCT cells over the 60-week leaching period is shown in Figure A20.8. K-TC1 triplicate cells, K01, K02 and K03, cumulatively released 15.84 mg/kg, 16.14 mg/kg and 15.34 mg/kg of Na. Control Kevitsa cells (K-TC2), K04, K05 and K06, released 15.05 mg/kg, 15.43 mg/kg and 16.08 mg/kg of Na over the same period, respectively. K-TC3 triplicate set cells measured cumulative Na releases within cells K07, K08 and K09 of 14.55 mg/kg, 14.92 mg/kg and 14.56 mg/kg.

Figure A20.7 - Kevitsa mine waste humidity cell tests (HCT) sodium results measured from leachates collected over the 60-week testing period.

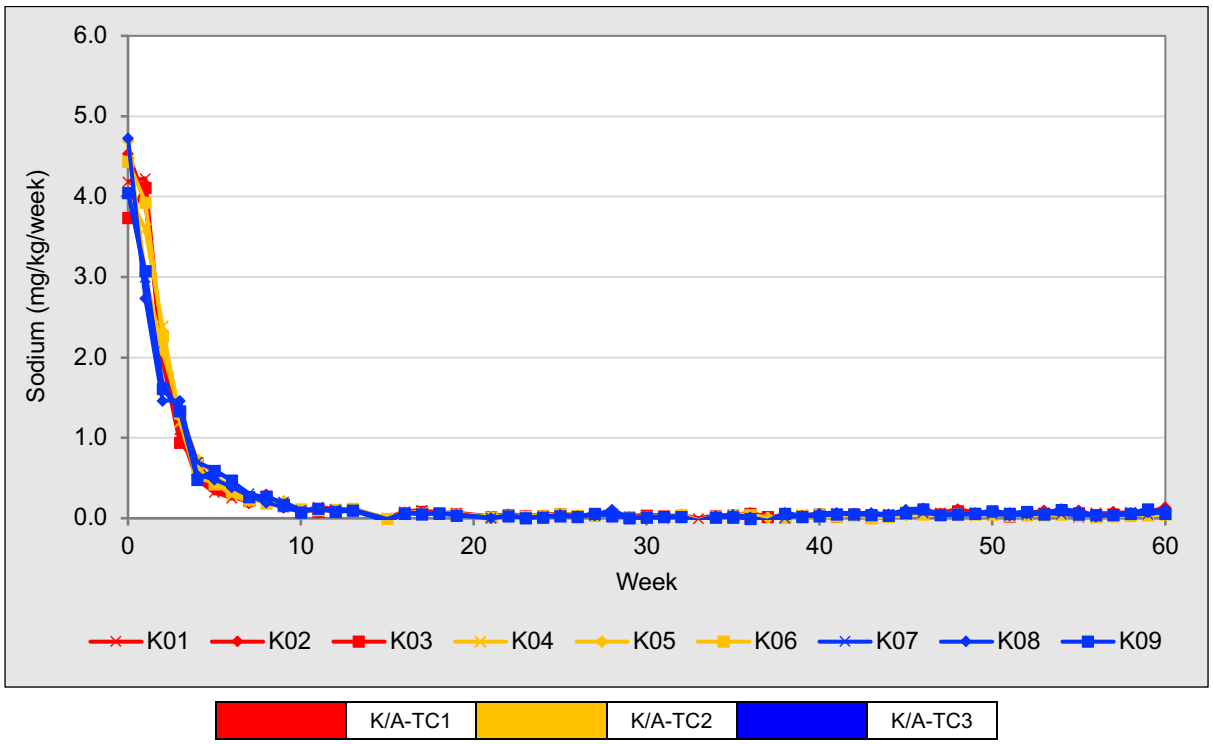


Figure A20.8 - Kevitsa mine waste humidity cell tests (HCT) cumulative sodium results measured from leachates collected over the 60-week testing period.

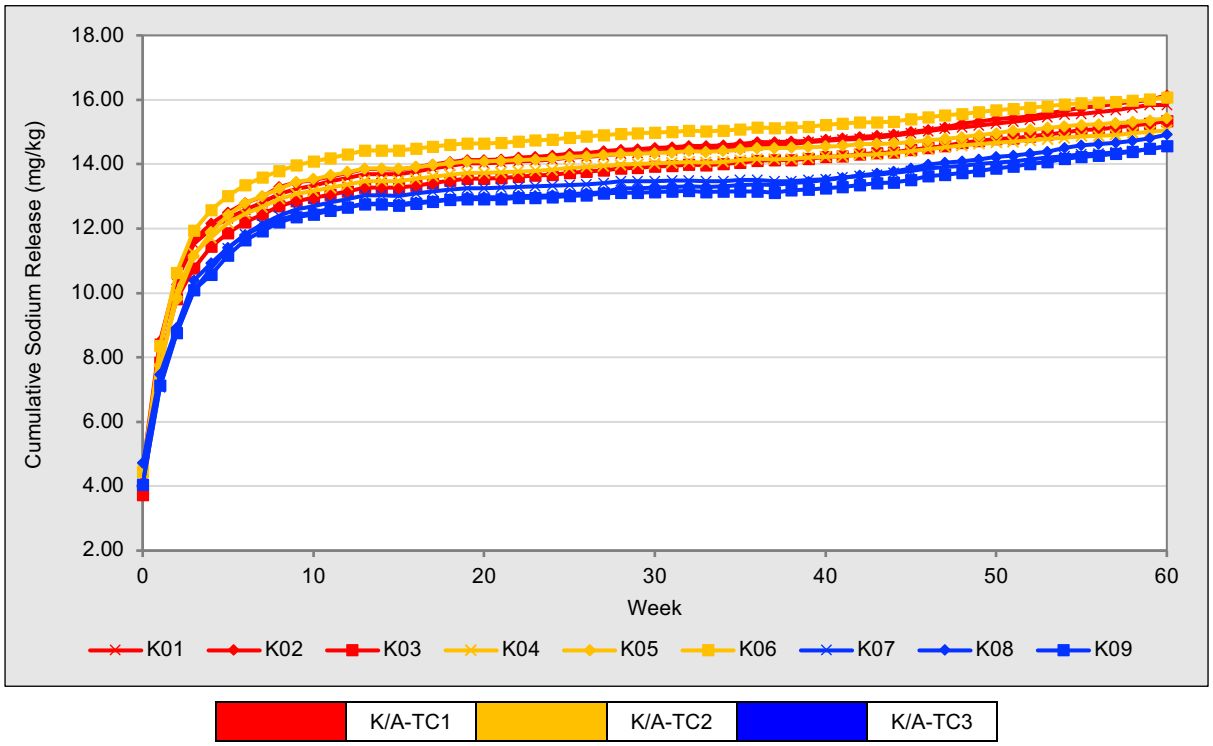

**Aitik HCT Na Results**

The maximum rates of Na release were recorded in week 0 with 3.10 mg/kg/week for cell A01, 3.72 mg/kg/week for cell A02, and 3.96 mg/kg/week for cell A03. The minimum release rates for cells A01, A02, and A03 were measured in week 37 with rates of 0.015 mg/kg/week, 0.009 mg/kg/week, and 0.020 mg/kg/week respectively. The mean release rates for cells A01, A02, A03 were calculated as 0.27 mg/kg/week, 0.24 mg/kg/week, and 0.23 mg/kg/week respectively. The median rates for these cells were 0.10 mg/kg/week, 0.07 mg/kg/week, and 0.07 mg/kg/week respectively over the 60 week leaching period.

All cells within A-TC2 measured their maximal Na release rates within the initial cell leach (week 0). These measurements were 2.66 mg/kg/week for cell A04, 5.06 mg/kg/week for cell A05, and 3.57 mg/kg/week for cell A06. The minimum rates for cells A04, A05, and A06 occurred in weeks 38, 37 and 35 respectively, with rates of 0.02 mg/kg/week, 0.005 mg/kg/week and 0.01 mg/kg/week. The mean calculated sodium release rates for cells A04, A05, A06 were 0.23 mg/kg/week, 0.22 mg/kg/week, and 0.21 mg/kg/week respectively. The corresponding median Na release rates for these cells were 0.07 mg/kg/week, 0.06 mg/kg/week, and 0.06 mg/kg/week respectively.

The maximum Na release rates for A-TC3 cells were recorded in week 0 with 3.32 mg/kg/week for cell A07, 4.51 mg/kg/week for cell A08, and 3.29 mg/kg/week for cell A09. The minimum rates for cells A07, A08, and A09 occurred in week 38 with rates of 0.002 mg/kg/week, 0.003 mg/kg/week, and 0.006 mg/kg/week respectively. The mean Na release rates for cells A07, A08, and A09 were 0.19 mg/kg/week, 0.21 mg/kg/week, and 0.20 mg/kg/week respectively. The median release rates for cells in A-TC3 were calculated as 0.05 mg/kg/week, 0.06 mg/kg/week, and 0.05 mg/kg/week over the 60-week leaching period.

A-TC2 triplicate cells (A04, A05 and A06) cumulatively released 15.05 mg/kg, 13.19 mg/kg and 12.61 mg/kg of Na. A-TC1 cells, A01, A02 and A03, cumulatively released 15.91 mg/kg, 14.01 mg/kg and 13.97 mg/kg of Na over 60 weeks. A-TC3 cells, A07, A08 and A09 measured cumulative Na release rates of 11.36 mg/kg, 12.16 mg/kg and 11.43 mg/kg.

Figure A20.9 - Aitik mine waste humidity cell tests (HCT) sodium results measured from leachates collected over the 60-week testing period.

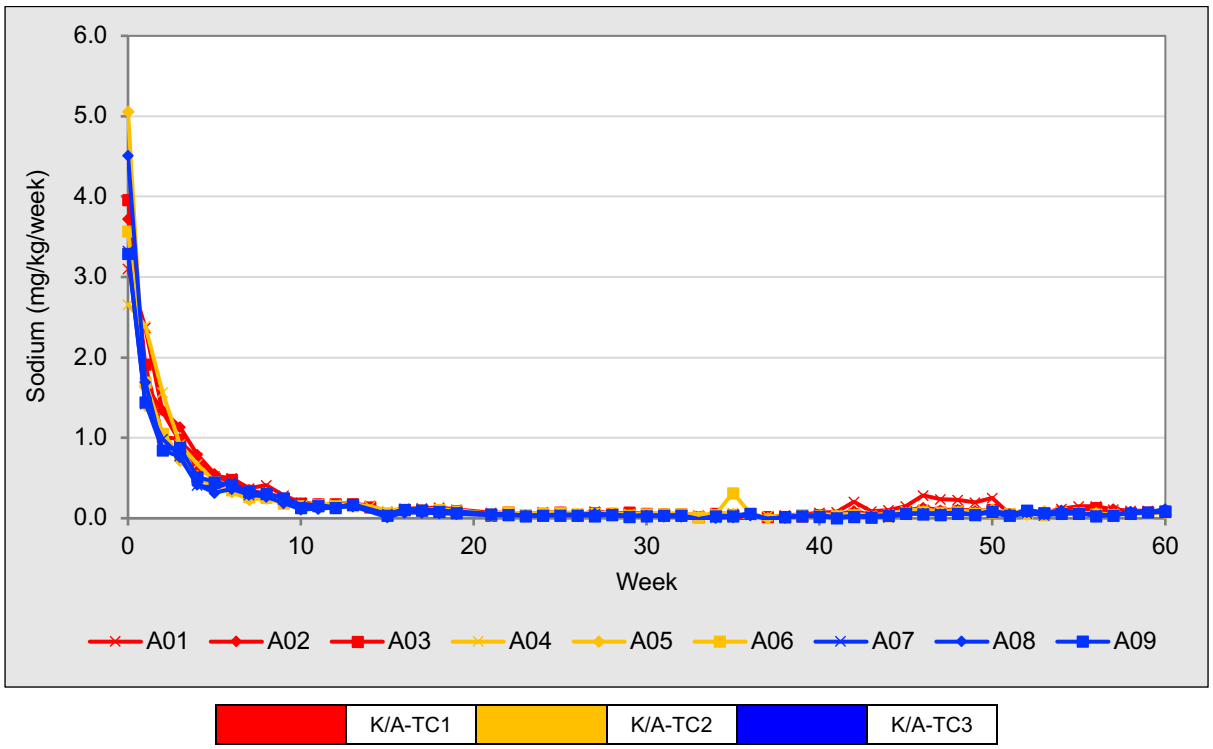


Figure A20.10 - Aitik mine waste humidity cell tests (HCT) cumulative sodium results measured from leachates collected over the 60-week testing period.

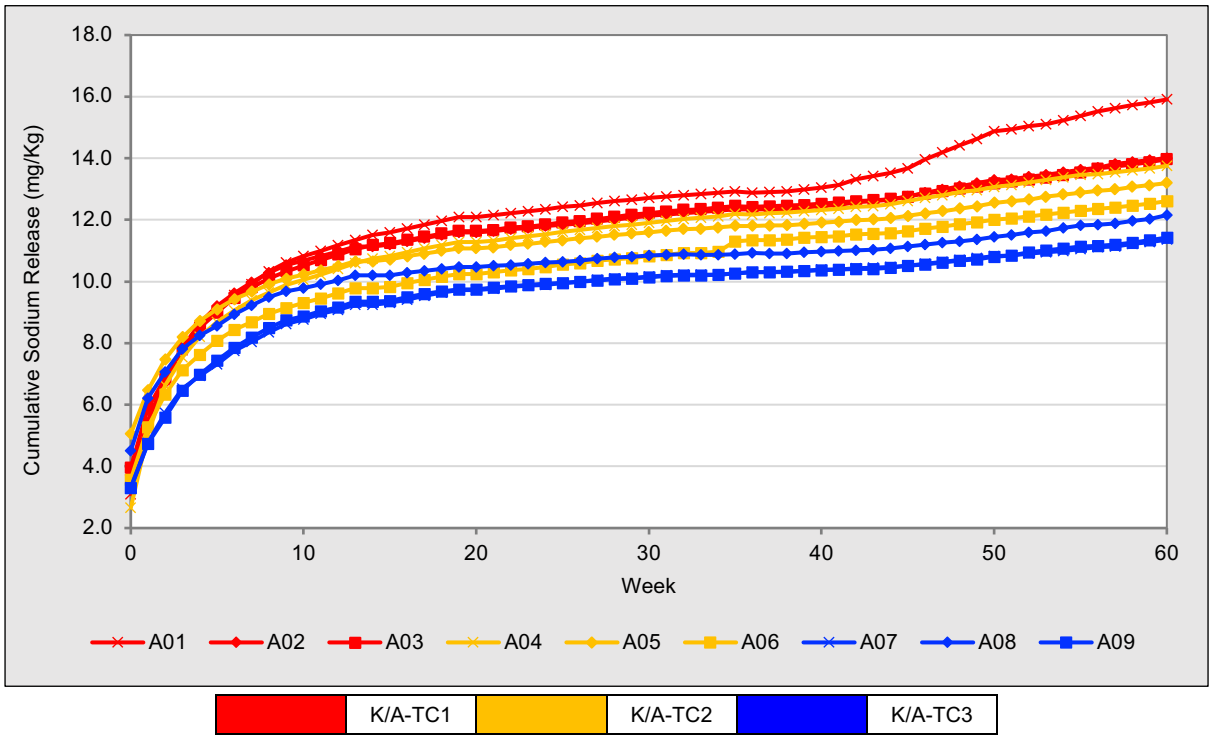

# Appendix 21 – List of Publications

This appendix includes publications authored by the candidate during the PhD research study.

**Conference Papers:**

1. Savage, RJ, Pearce, S, Mueller, S, Barnes, A, Renforth, P & Sapsford, D 2019, 'Methods for assessing acid and metalliferous drainage mitigation and carbon sequestration in mine waste: a case study from Kevitsa mine, Finland', in AB Fourie & M Tibbett (eds), *Mine Closure 2019: Proceedings of the 13th International Conference on Mine Closure*, Australian Centre for Geomechanics, Perth, pp. 1073-1086, https://doi.org/10.36487/ACG_rep/1915_86_Savage
2. Savage, R., Barnes, A., Pearce, S. and Roberts, M. 2021. Carbonation of Magnesium Silicate Minerals in Mine Waste: Practical Laboratory Testing Methods to Assess the Dual Opportunity for Carbon Capture and AMD Mitigation. In: Proceedings of the IMWA 2021 conference – "Mine Water Management for Future Generations." Available at: https://www.researchgate.net/publication/358802944.
3. Savage, R., Barnes, A., Pearce, S., Roberts, M., Renforth, P., Chmielarski, M., Mueller, S., & Sapsford, D. (2022). Quantification Of Methods To Assess Carbonation In Mine Wastes-Potential Implications For Long-Term Mine Waste Drainage Quality And Acid Rock Drainage (ARD) Prediction. Proceedings of the ICARD 2022 Conference. https://www.researchgate.net/publication/365650808

# Appendix 22 – Additional Images

Within this appendix selective images taken of the humidity cell tests at various points of the leaching protocol are shown.

The physcial properties of wastes within all cells was noted and photographed at various stages of the test protocol. Upon decomissioning photos were taken of the waste material, pre removal, once the HCT lid was removed. It was noted that enhanced $CO_2$ cells demonstrated apparent aglomeration and cemeting of materials upon abstraction. While attmpeting to remove the materials post drying, enhanaced $CO_2$ cells within sets K-TC1 and K-TC2 demonstrated distinct cementing with a distinct conglomerated nature, see Figure A22.1 and A22.2. This apparent cementing of the waste materials within these cells could be the result of a number of mechnisms.

Figure A22.1 - Cell K01 week 60 image taken inside cell post decommissioning

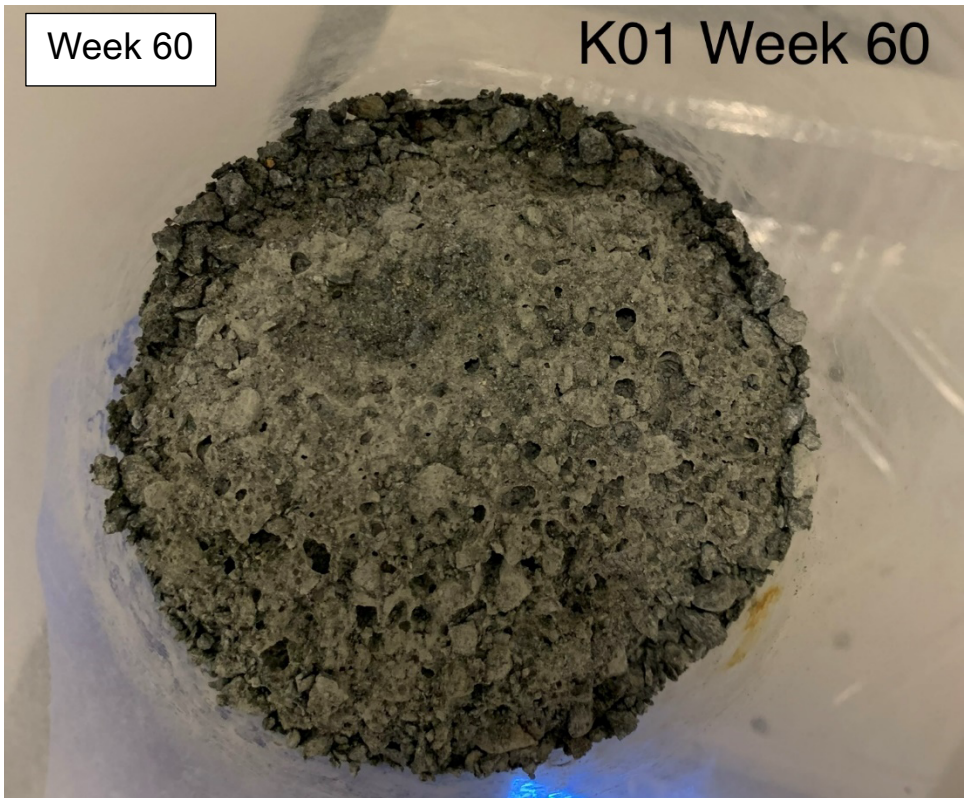

Figure A22.2 - Cell K03 (a) and K07 (b) week 60 images taken inside cell post decommissioning.

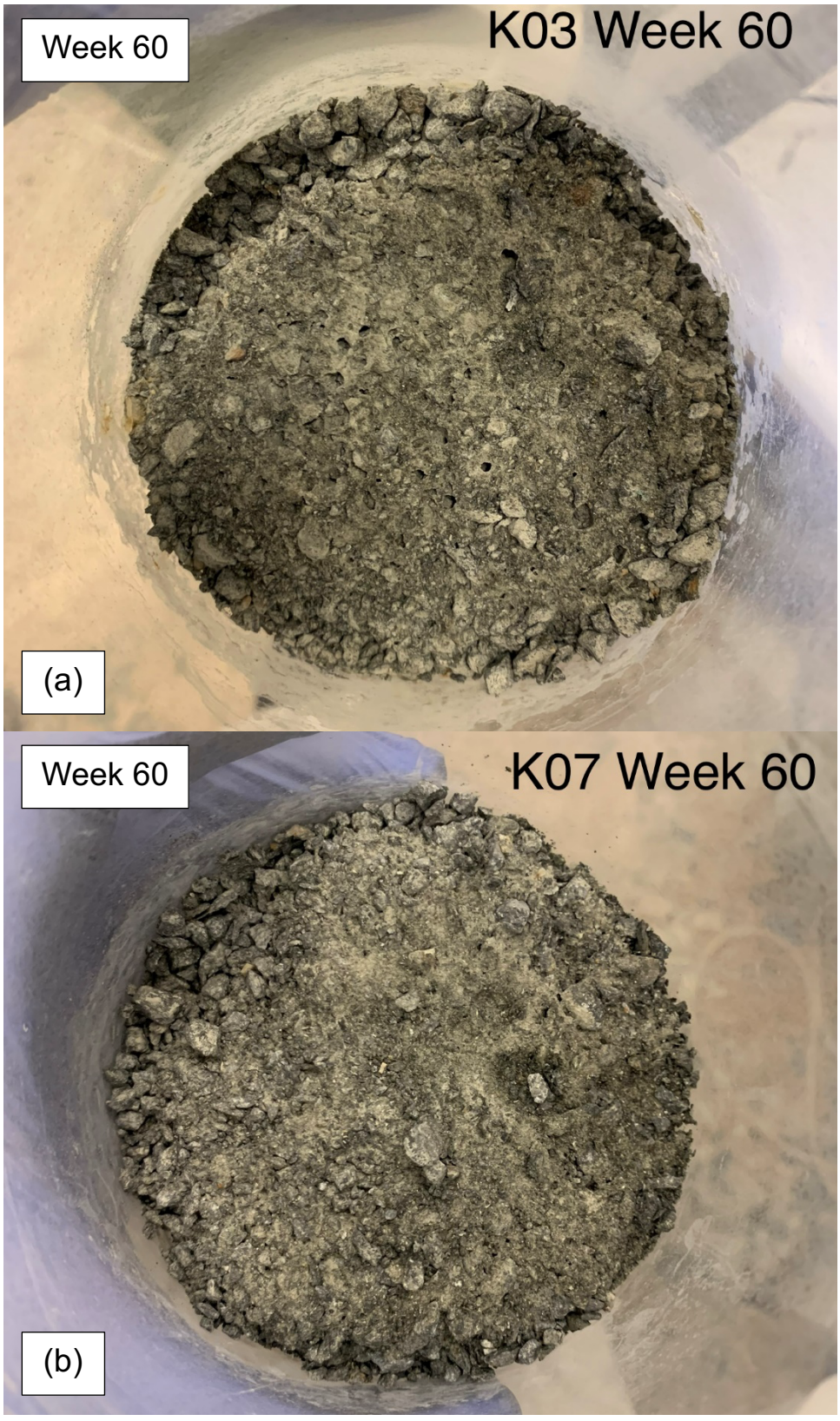

Figure A22.3 - Cell K09 week 60 image taken inside cell post decommissioning.

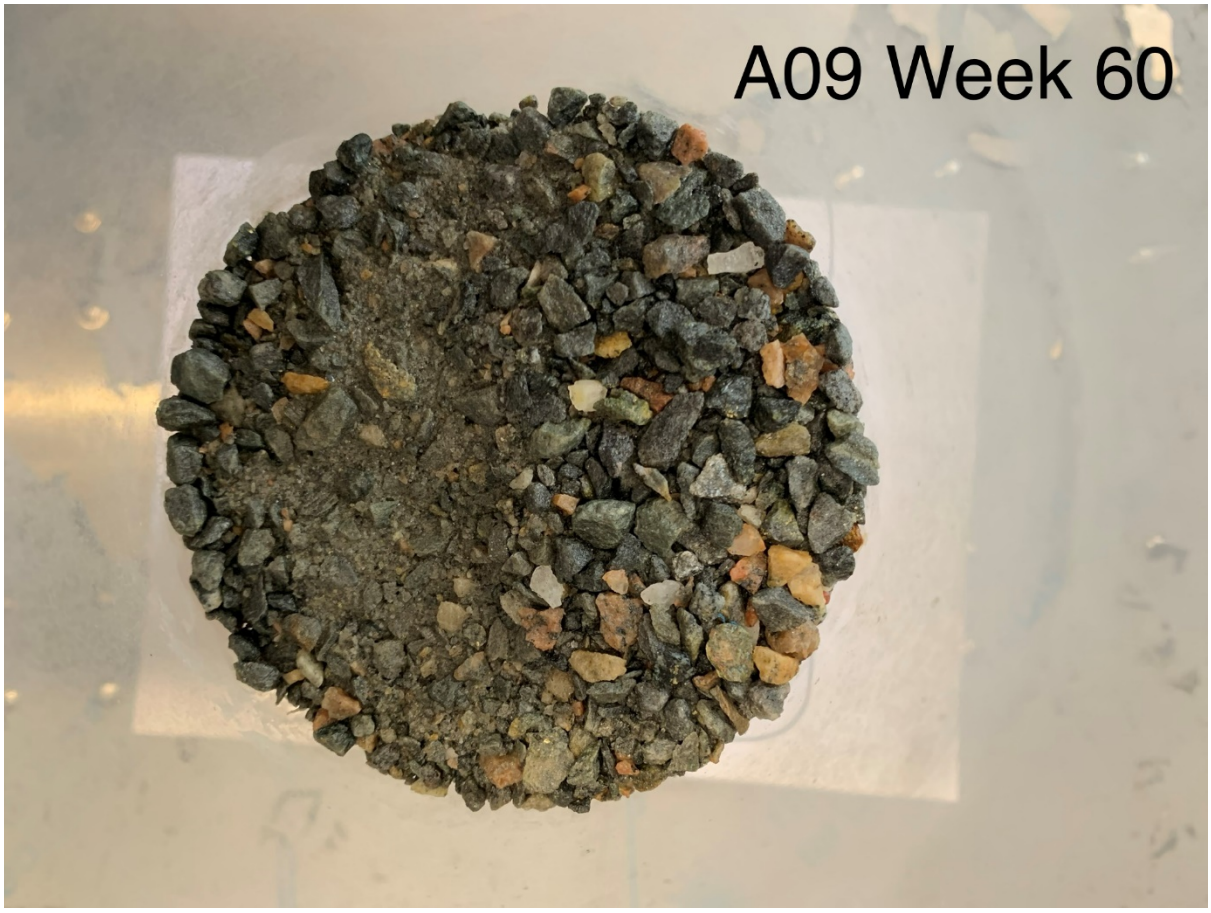

Figure A22.4 - Cell K01 image taken outside of cell in week 3. Potential signs of oxidation of irion bearing minerals.

Figure A22.5 - Cell K01 image taken outside of cell in week 60. Displaying apprent oxidation of irion bearing minerals.

Figure A22.6 - Cell K01 at weeks 1, 3 and 26. Images taken between leaching cycles